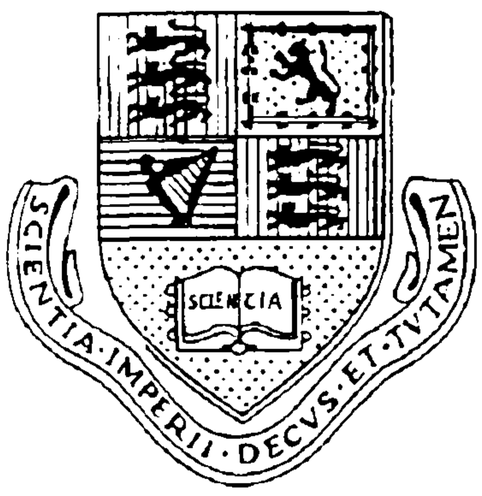


Phase Interactions in Transient Stratified Flow

by

Jonathan Shaha

Dipl. Chem.-Ing. ETH

A thesis submitted in partial fulfilment of the requirements for the degree of

Doctor of Philosophy of the University of London

and for the

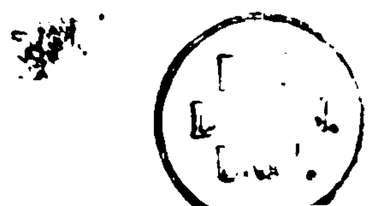
Diploma of Membership of Imperial College

Department of Chemical Engineering & Chemical Technology

Imperial College of Science, Technology and Medicine

London SW7 2BY

August 1999



The Lord says:

I am the Alpha and the Omega,

the First and the Last,

the Beginning and the End.

The Bible, Revelation 22, 13

Abstract

This thesis reports a detailed investigation of the steady state and transient behaviour of stratified gas-liquid flow, which is one of the flow patterns that can appear in a two-phase flow through a horizontal pipeline. In this flow pattern the liquid flows at the bottom of the pipe and the gas flows above it. Operational activities, such as changes in the valve openings for the inlet flow rates, disturb the flow which then becomes transient.

Stratified flow is commonly described using a one-dimensional model. Very significant terms in the equations of this model are the shear stresses between the two fluids and between the wall and the fluids. In closing the system of equations methods must be specified to calculate these shear stresses. A large range of relationships for shear stresses has been proposed in the literature for steady state stratified flow. The present research project addressed the closure issue associated with the prediction of shear stresses, including both the steady state case and the transient case.

In order to achieve this aim an experimental setup was designed for simultaneously measuring liquid holdup, pressure drop, phase velocities, and wall shear stresses in stratified flow. Experiments were carried out on two experimental flow facilities: a low pressure rig which operates at atmospheric conditions and a high pressure rig which allows studying flows at pressures above atmospheric.

The steady state and transient data were reduced through the medium of the one-dimensional model to deduce information on the shear stresses. The data was compared with published relationships for the shear stresses developed for steady state stratified flow. The investigations showed that these relationships differed greatly between themselves and, in general, with the experimental data (though some of the relationships performed fairly well). In the transient tests, significant differences occurred to the steady state relationships (which are used commercially to predict the transients).

Beside the experimental work modelling studies were undertaken using commercial software packages designed for calculating pipeline flows. The results from these simulations were compared with the experimental data.

Acknowledgments

I would like to express my sincere thanks to my supervisor, Prof. G.F. Hewitt, for his guidance, support and encouragement during the course of this study.

I am grateful to the members, past and present, of the Multiphase Fluid Systems Group at Imperial College for their friendship and the good time we had. Above all, I would like to thank Colin Hale for all his help, mainly in the experimental programme of this study. Without his support the experiments on the WASP facility at Imperial College would not have been quite so successful, if not impossible.

I appreciate the many efforts of the Mechanical and Electronics Workshops of the Department of Chemical Engineering & Chemical Technology at Imperial College which have been important for the success of this mainly experimental study. The support of the Computational Services of the Department is also greatly appreciated.

Without the many social contacts outside the College, especially at the Swiss Church, my time in London would not have been as enjoyable as it was.

I express my deepest gratitude to mum, dad and Maya for their love and support, which made me overcome so many obstacles.

This work has been undertaken within the Transient Multiphase Flows' Co-ordinated Research Project. I wish to acknowledge the contributions made to this project by the Engineering and Physical Sciences Research Council (EPSRC) and to the following industrial organisations: - AEA Technology; Amerada Hess; BG Technology; BP Amoco Exploration; CALtec; Conoco; Elf Exploration; Exxon Production Research; Institutt for Energiteknikk; Institut Francais du Petrole; Mobil North Sea; Norsk Hydro; Scandpower; Texaco Britain; Total Oil Marine. I wish to express my sincere gratitude for this support.

Table of Contents

Chapter 1: Introduction.....18

Chapter 2: Literature Review.....22

2.1 Flow Patterns in Horizontal Two-Phase Flow.....23
2.2 Experimental Studies.....24
2.2.1 Steady State Stratified Flow.....24
2.2.1.1 Characterization of the Interface.....24
2.2.1.2 Flow Fields.....27
2.2.1.3 Wall Shear Stresses.....28
2.2.2 Transient Stratified Flow.....29
2.3 1D Models.....35
2.3.1 Steady State Stratified Flow.....36
2.3.2 Transient Stratified Flow.....47
2.4 1D Codes.....53
2.4.1 Commercial Codes.....54
2.4.1.1 PLAC (Version 5.3).....54
2.4.1.2 OLGA (Version 3.4).....55
2.4.1.3 TACITE (Version 4.097).....56
2.4.2 PRESBAL Code.....57
2.4.3 TRIOMPH Code.....57

Chapter 3: Experimental Methods.....60

3.1 Introduction.....60
3.2 Review.....61
3.2.1 Wall Shear Stress.....61
3.2.2 Phase Velocity.....63
3.2.3 Pressure Drop.....65
3.2.4 Liquid Height and Interfacial Structure.....67
3.3 Instrumentation.....69
3.3.1 Hot-Wire Anemometry.....69
3.3.1.1 Operation.....70
3.3.1.2 The Probes.....70
3.3.1.3 The Anemometers.....71
3.3.2 Pressure Transmitter.....72
3.3.3 Twin-Wire Conductivity Probes.....73
3.3.4 Pitot Tube.....74
3.3.5 Data Acquisition.....75
3.4 Design of Test Spool.....76
3.5 Flow Facilities.....79
3.5.1 Low Pressure Rig.....79
3.5.1.1 Experimental Setup.....79
3.5.1.2 Operation.....81

3.5.2 WASP Facility 82
3.5.2.1 Experimental Setup 82
3.5.2.2 Operation 83
3.6 Fluid Properties 84
3.6.1 Air Density 84
3.6.2 Air Viscosity 85
3.6.3 Water Density 85
3.6.4 Water Viscosity 85
3.7 Operation of Hot-Wire Anemometry 85
3.7.1 Mounting of Glue-on Probes 85
3.7.2 Preparation of Velocity Probes 86
3.7.3 Probe Heating 87
3.7.4 Probe Setup 88
3.7.5 Grounding 89
3.7.6 Correction for Temperature 90
3.7.7 Damaged Probes and Probe Repair 90
3.8 Experimental Matrix 92
3.9 Calibration and Validation 92
3.9.1 Pressure Drop Measurement 93
3.9.1.1 Pressure Drop in Air 93
3.9.1.1.1 Pressure Drop in Air: Low Pressure Rig 93
3.9.1.1.2 Pressure Drop in Air: WASP Rig 95
3.9.1.2 Pressure Drop in Water 95
3.9.1.2.1 Pressure Drop in Water: Low Pressure Rig 95
3.9.1.2.2 Pressure Drop in Water: WASP Rig 96
3.9.2 Pitot Tube 96
3.9.2.1 Pitot Tube in Air 98
3.9.2.1.1 Pitot Tube in Air on the Low Pressure Rig 98
3.9.2.1.2 Pitot Tube in Air on the WASP Rig 98
3.9.2.2 Pitot Tube in Water 99
3.9.2.2.1 Pitot Tube in Water on the Low Pressure Rig 99
3.9.2.2.2 Pitot Tube in Water on the WASP Rig 100
3.9.3 Hot-wire and Hot-film Probes 100
3.9.3.1 Calibration of Glue-On Probes 101
3.9.3.1.1 Calibration of Glue-on Probe in Air 103
3.9.3.1.1.1 Calibration of Glue-on Probe in Air on Low Pressure Rig 103
3.9.3.1.1.2 Calibration of Glue-on Probe in Air on WASP Rig 103
3.9.3.1.2 Calibration of Glue-on Probe in Water 104
3.9.3.1.2.1 Calibration of Glue-on Probe in Water on Low Pressure Rig 104
3.9.3.1.2.2 Calibration of Glue-on Probe in Water on WASP Rig 105
3.9.3.2 Calibration of Velocity Probes 105
3.9.3.2.1 Calibration of Velocity Probe in Air 106
3.9.3.2.1.1 Calibration of Velocity Probe in Air on Low Pressure Rig 106
3.9.3.2.1.2 Calibration of Velocity Probe in Air on WASP Rig 107
3.9.3.2.2 Calibration of Velocity Probe in Water 107

3.9.3.2.2.1 Calibration of Velocity Probe in Water on Low Pressure Rig 107
3.9.3.2.2.2 Calibration of Velocity Probe in Water on WASP Rig 108
3.9.4 Thermocouples 109
3.9.5 Conductivity Probes 109
3.9.5.1 Calibration of Conductivity Probes on Low Pressure Rig 109
3.9.5.2 Calibration of Conductivity Probes on WASP Rig 110
3.10 Transformation of Local Measurements into Phase Average Parameters 112
3.10.1 Liquid Holdup 112
3.10.2 Phase Average Velocities 112
3.10.2.1 Phase Average Velocities in Gas Phase 114
3.10.2.2 Phase Average Velocities in Liquid Phase 115
3.11 Performance of Instrumentation Methods in Two-Phase Flow 116

Chapter 4: Steady State Data 143

4.1 Introduction 143
4.2 Sample Results 144
4.2.1 Results from the Low Pressure Rig 144
4.2.1.1 Transient Tests 144
4.2.1.2 Steady State Tests 146
4.2.2 Results from the WASP Rig 147
4.3 Velocities 149
4.3.1 Liquid Velocities 149
4.3.2 Gas Velocities 150
4.4 Pressure Gradient 151
4.4.1 Pressure Gradient: Qualitative Discussion 151
4.4.2 Pressure Gradient: Quantitative Discussion 152
4.5 Holdup 153
4.5.1 Holdup: Qualitative Discussion 153
4.5.2 Holdup: Quantitative Discussion 154
4.6 Hydraulic Gradient 155
4.6.1 Hydraulic Gradient: Low Pressure Rig 157
4.6.2 Hydraulic Gradient: WASP Rig 158
4.7 Wall Shear Stress 159
4.7.1 Variation with Position 159
4.7.2 Gas Wall Shear Stress 160
4.7.3 Liquid Wall Shear Stress 162
4.8 Interfacial Shear Stress 164
4.9 Interfacial Structure 167
4.9.1 Qualitative Behaviour 167
4.9.1.1 Interfacial Structure in Three Dimensions 167
4.9.1.1.1 Interfacial Structure at Atmospheric Pressure 168
4.9.1.1.2 Interfacial Structure at High Pressure 169
4.9.1.2 Axial View Pictures 170
4.9.2 Quantitative Analysis 171
4.9.2.1 A New Model for Interfacial Shear Stress for the Low Pressure Rig 172
4.9.2.2 A New Model for Interfacial Shear Stress for the WASP Rig 174

4.10 Conclusions 177

Chapter 5: Transient Data 208

5.1 Introduction 208
5.2 Experimental Programme 209
5.2.1 Experimental Programme on the Low Pressure Rig 210
5.2.2 Experimental Programme on the WASP Rig 212
5.3 Presentation of Data 215
5.3.1 Data for Low Pressure Rig 215
5.3.1.1 Case `lc` (For conditions see Table 5.1) 216
5.3.1.2 Case `lf` (For conditions see Table 5.1) 219
5.3.2 Data for WASP Rig 220
5.3.2.1 Case `wb`: 1.06 bar (For conditions see Table 5.2) 221
5.3.2.2 Case `wd`: 6.03 bar (For conditions see Table 5.2) 223
5.3.3 Discussion of Data 224
5.4 Wall Shear Stress 226
5.5 Interfacial Shear Stress 228
5.6 Interfacial Structure 232
5.6.1 Qualitative Discussion 232
5.6.2 Quantitative Discussion 234
5.6.2.1 Low Pressure Rig 235
5.6.2.2 WASP Rig 237
5.7 Comparisons with Code Predictions 239
5.7.1 Predictions from Commercial Codes 239
5.7.2 Investigations of the One-Dimensional Modelling Approach 241
5.7.3 Multi-Dimensional Effects 245
5.8 Conclusions 246

Chapter 6: Conclusions and Recommendations 278

6.1 Conclusions 278
6.1.1 Conclusions from Steady State Data 278
6.1.2 Conclusions from Transient Data 280
6.2 Recommendations for Future Work 281
6.2.1 Experimental Work 282
6.2.2 Improvement of Models 283

References 285

Nomenclature 294

Appendix A: Feasible Experimental Matrix 298

Appendix B: Experimental Procedure for Low Pressure Rig 300

Appendix C: Experimental Procedure for WASP Rig 302

List of Figures

Figure 2.1 Flow patterns in horizontal flow 59
Figure 2.2 Stratified flow in a horizontal pipe 59

Figure 3.1 Measured parameters 121
Figure 3.2 Srichai's (1994) conductivity probe section (to scale) 121
Figure 3.3 Dantec 55R47 glue-on probe (not to scale) 122
Figure 3.4 Dantec 55R42 conical hot-film probe (not to scale) 122
Figure 3.5 Dantec 55P11 miniature wire probe (not to scale) 123
Figure 3.6 Arrangement for measuring pressure drop 123
Figure 3.7 Length section through a Pitot tube with a DP cell connected (not to scale) 124
Figure 3.8 Length section through test spool (not to scale) 125
Figure 3.9 Glue-on probe on the inside tube wall (to scale) 126
Figure 3.10 Representation of conductivity probes in the cross section facing the flow (to scale) 126
Figure 3.11 Length section through conductivity probe section (to scale) 127
Figure 3.12 Velocity probe held by a slide on a mounting block and partly inserted in the test spool (not to scale) 127
Figure 3.13 Schematic of low pressure facility (with test spool inserted) 128
Figure 3.14 Length section through transition flange used for inserting test spool on the low pressure rig (not to scale) 128
Figure 3.15 View of low pressure rig from inlet section 129
Figure 3.16 Test spool inserted in low pressure rig 129
Figure 3.17 Acquisition system and electronics boxes 130
Figure 3.18 Schematic of WASP rig 130
Figure 3.19 Detailed schematic of downstream end of WASP test section with test spool inserted (not to scale) 131
Figure 3.20 Test spool inserted in WASP test section 131
Figure 3.21 Pressure drop in single phase air flow across test spool on the low pressure rig 132
Figure 3.22 Pressure drop in single phase air flow in test spool upstream of probe inserts on the low pressure rig 132
Figure 3.23 Test section on the low pressure rig modified with inclined pipe section at exit 133
Figure 3.24 Pressure drop in single phase water flow in test spool upstream of probe inserts on the low pressure rig 133
Figure 3.25 Pressure drop in single phase water flow in test spool upstream of probe inserts on the WASP rig 134
Figure 3.26 Velocity profile for air (U_G=8.2 m/s) measured with Pitot tube on the low pressure rig 134
Figure 3.27 Discrepancy between flow rate measured with Pitot and rig flow rate acquisition for air on the low pressure rig 135
Figure 3.28 Velocity profile for water (U_L=0.2 m/s) measured with Pitot tube on the low pressure rig 135

Figure 3.29 Discrepancy between flow rate measured with Pitot and water rotameter on the low pressure rig 136
Figure 3.30 Discrepancy between flow rate measured with Pitot and water rotameter on the low pressure rig for traverses of the Pitot from the tube bottom 136
Figure 3.31 Calibration curve for glue-on probe for measurement of gas wall shear stress on the low pressure rig 137
Figure 3.32 Calibration curve for glue-on probe for measurement of liquid wall shear stress on the low pressure rig 137
Figure 3.33 Calibration curve for hot-wire probe for measurement of gas velocity on the low pressure rig 138
Figure 3.34 Calibration curve for hot-film probe for measurement of liquid velocity on the low pressure rig 138
Figure 3.35 Calibration curve for thermocouple for gas temperature for experiments on the low pressure rig 139
Figure 3.36 Typical calibration curves for conductivity probes in test spool on the low pressure rig 139
Figure 3.37 Typical calibration curves for conductivity probes upstream and downstream of test spool on the low pressure rig 140
Figure 3.38 Determination of liquid holdup in the test spool from measurement of liquid height at three positions in half a cross section, assuming symmetry with respect to tube centre 140
Figure 3.39 Obtaining phase average velocity from three local measurements of velocity in the gas phase 141
Figure 3.40 Agreement of phase average velocity in gas phase obtained from measurements with hot-wire probe (u_G(hot-wire probe)) with phase average velocity obtained from rig flow rate acquisition (u_G(rig acquisition)) on the low pressure rig 141
Figure 3.41 Obtaining phase average velocity from three local measurements of velocities in liquid phase 142
Figure 3.42 Agreement of phase average velocity in liquid phase obtained from measurements with hot-film probe (u_L(hot-film probe)) with phase average velocity obtained from rig flow rate acquisition (u_L(rig acquisition)) on the low pressure rig 142

Figure 4.1 Measured pressure gradient *(dp dx)* for initial steady state of transient case 1c of the low pressure rig (U_L=0.039 m/s, U_G=7.39 m/s, atmospheric pressure) 180
Figure 4.2 Measured liquid wall shear stress τ_{wL} for initial steady state of transient case 1c of the low pressure rig (U_L=0.039 m/s, U_G=7.39 m/s, atmospheric pressure) 180
Figure 4.3 Measured gas wall shear stress τ_{wG} for initial steady state of transient case 1c of the low pressure rig (U_L=0.039 m/s, U_G=7.39 m/s, atmospheric pressure) 181
Figure 4.4 Measured liquid holdup ε_L for initial steady state of transient case 1c of the low pressure rig (U_L=0.039 m/s, U_G=7.39 m/s, atmospheric pressure) 181
Figure 4.5 Measured liquid phase average velocity u_L for initial steady state of transient case 1c of the low pressure rig (U_L=0.039 m/s, U_G=7.39 m/s, atmospheric pressure) 182

Figure 4.6 Measured gas phase average velocity u_G for initial steady state of transient case 1c of the low pressure rig (U_L=0.039 m/s, U_G=7.39 m/s, atmospheric pressure) 182
Figure 4.7 Interfacial fluctuation h_L' for initial steady state of transient case 1c of the low pressure rig (U_L=0.039 m/s, U_G=7.39 m/s, atmospheric pressure) 183
Figure 4.8 Measured liquid holdup ε_L for initial steady state of transient case wb of the WASP rig (U_L=0.038 m/s, U_G=5.33 m/s, atmospheric pressure) 184
Figure 4.9 Measured liquid phase average velocity u_L for initial steady state of transient case wb of the WASP rig (U_L=0.038 m/s, U_G=5.33 m/s, atmospheric pressure) 185
Figure 4.10 Measured gas phase average velocity u_G for initial steady state of transient case wb of the WASP rig (U_L=0.038 m/s, U_G=5.33 m/s, atmospheric pressure) 185
Figure 4.11 Interfacial fluctuation h_L' for initial steady state of transient case wb of the WASP rig (U_L=0.038 m/s, U_G=5.33 m/s, atmospheric pressure) 186
Figure 4.12 Velocity profiles in the liquid phase $u_L(y)$ for a given liquid superficial velocity of U_L=0.04 m/s and a range of gas superficial velocities U_G (see legend) on the low pressure rig 187
Figure 4.13 Velocity profiles in the liquid phase $u_L(y)$ for a given liquid superficial velocity of U_L=0.08 m/s and a range of gas superficial velocities U_G (see legend) on the low pressure rig 188
Figure 4.14 Profiles of fluctuations of liquid velocities $u_L'(y)$ for a given liquid superficial velocity of U_L=0.04 m/s and a range of gas superficial velocities U_G (see legend) on the low pressure rig 188
Figure 4.15 Profiles of fluctuations of liquid velocities $u_L'(y)$ for a given liquid superficial velocity of U_L=0.08 m/s and a range of gas superficial velocities U_G (see legend) on the low pressure rig 189
Figure 4.16 Velocity profiles in the gas phase $u_G(y)$ for a given liquid superficial velocity of U_L=0.04 m/s and a range of gas superficial velocities U_G (see legend) on the low pressure rig 189
Figure 4.17 Velocity profiles in the gas phase $u_G(y)$ for a given liquid superficial velocity of U_L=0.08 m/s and a range of gas superficial velocities U_G (see legend) on the low pressure rig 190
Figure 4.18 Profiles of fluctuations of gas velocities $u_G'(y)$ for a given liquid superficial velocity of U_L=0.04 m/s and a range of gas superficial velocities U_G (see legend) on the low pressure rig 190
Figure 4.19 Profiles of fluctuations of gas velocities $u_G'(y)$ for a given liquid superficial velocity of U_L=0.08 m/s and a range of gas superficial velocities U_G (see legend) on the low pressure rig 191
Figure 4.20 Pressure drop (dp/dx) as a function of gas superficial velocity for a given liquid superficial velocity of U_L =0.04 m/s on the low pressure rig 191
Figure 4.21 Pressure drop (dp/dx) as a function of gas superficial velocity for a given liquid superficial velocity of U_L =0.08 m/s on the low pressure rig 192
Figure 4.22 Comparison of pressure gradient calculated with PRESBAL with experimental data for U_L=0.04 m/s on the low pressure rig 192
Figure 4.23 Mean liquid height in test spool, h_L(test spool), as a function of gas superficial velocity for a given liquid superficial velocity of U_L =0.04 m/s on the low pressure rig 193

Figure 4.24 Mean liquid height in test spool, h_L(test spool), as a function of gas superficial velocity for a given liquid superficial velocity of U_L =0.08 m/s on the low pressure rig 193
Figure 4.25 Comparison of liquid holdup calculated with one-dimensional codes with experimental data for U_L=0.04 m/s on the low pressure rig 194
Figure 4.26 Comparison of liquid holdup calculated with one-dimensional codes with experimental data for 1 bar and 6 bar from the WASP rig 194
Figure 4.27 Comparison of mean liquid height in test spool, h_L(test spool), with mean liquid height upstream of test spool, h_L(upstream) on the low pressure rig..... 195
Figure 4.28 Comparison of mean liquid height in test spool, h_L(test spool), with mean liquid height downstream of test spool, h_L(downstream) on the low pressure rig 195
Figure 4.29 Comparison of mean liquid height in test spool, h_L(test spool), with mean liquid height downstream of test spool, h_L(downstream) on WASP 196
Figure 4.30 Circumferential variation of liquid wall shear stress measurement..... 196
Figure 4.31 Circumferential variation of liquid wall shear stress over a range of gas flow rates at U_L=0.08 m/s on the low pressure rig..... 197
Figure 4.32 Comparison of gas wall friction factor f_G from experiments on the low pressure rig with different models 197
Figure 4.33 Comparison of liquid wall friction factor f_L from experiments on the low pressure rig with different models 198
Figure 4.34 Comparison of interfacial friction factor f_i derived from experiments on the low pressure rig with different models..... 198
Figure 4.35 Interfacial structure for initial steady state of transient case `1a` on the low pressure rig (U_L=0.039 m/s, U_G=5.01 m/s, p=1.00 bar) 199
Figure 4.36 Interfacial structure for initial steady state of transient case `wb` on the WASP rig (U_L=0.038 m/s, U_G=5.33 m/s, p=1.06 bar) 199
Figure 4.37 Interfacial structure for initial steady state of transient case `wd` on the WASP rig (U_L=0.034 m/s, U_G=1.30 m/s, p=6.07 bar) 200
Figure 4.38 Interfacial structure for initial steady state of transient case `we` on the WASP rig (U_L=0.025 m/s, U_G=1.32 m/s, p=11.04 bar) 200
Figure 4.39 Axial view of initial steady state of case `wd` on the WASP rig (U_L=0.034 m/s, U_G=1.30 m/s, p=6.07 bar) 201
Figure 4.40 Axial view of steady state flow (U_L=0.015 m/s, U_G=20.0 m/s, p=1.0 bar)... 201
Figure 4.41 Variation of interfacial fluctuation $h_L'(z)$ with transverse position z for initial steady state of transient case `1a` on the low pressure rig (U_L=0.039 m/s, U_G=5.01 m/s, p=1.00 bar)..... 202
Figure 4.42 Influence of time interval over which interfacial fluctuations h_L' are determined for initial steady state of transient case `1c` on the low pressure rig (U_L=0.039 m/s, U_G=7.39 m/s, p=0.99 bar) 202
Figure 4.43 h_L'/D as a function of the holdup ε_L and the gas Reynolds number Re_G^* for results from the low pressure rig 203
Figure 4.44 Plot of $\log_{10}(k_R/D)$ against $\log_{10}(h_L'/D)$ for the experiments from the low pressure rig 203
Figure 4.45 Comparison of pressure gradient calculated with modified PRESBAL with experimental data for U_L=0.04 m/s on the low pressure rig..... 204
Figure 4.46 Comparison of liquid holdup calculated with modified PRESBAL with experimental data for U_L=0.04 m/s on the low pressure rig 204

Figure 4.47 h_L'/D as a function of the holdup ε_L and the gas Reynolds number Re_G^* for results from the low pressure rig and the WASP rig at atmospheric pressure 205
Figure 4.48 h_L'/D as a function of the holdup ε_L and the gas Reynolds number Re_G^* for results from the WASP rig at 6 bar 205
Figure 4.49 h_L'/D as a function of the holdup ε_L and the gas Reynolds number Re_G^* for results from the WASP rig at 1 bar, 6 bar and 11 bar 206
Figure 4.50 Variation of parameter C_s against density ratio ($\rho_G/(\rho_L-\rho_G)$) on WASP 206
Figure 4.51 Comparison of liquid holdup calculated with modified PRESBAL with experimental data from the WASP rig 207

Figure 5.1 Schematic of transient experiment 251
Figure 5.2 Trace of air flow rate U_G for transient case `1c` (U_L=0.039 m/s, $U_{G,1}$=7.39 m/s, $U_{G,2}$=8.08 m/s, p=0.99 bar) on the low pressure rig 251
Figure 5.3 Trace of gas flow rate U_G and liquid flow rate U_L for transient case `wb` (U_L=0.037 m/s, $U_{G,1}$=5.33 m/s, $U_{G,2}$=6.07 m/s, p=1.06 bar) on the WASP rig 252
Figure 5.4 Trace of gas flow rate U_G and liquid flow rate U_L for transient case `wd` (U_L=0.032 m/s, $U_{G,1}$=1.30 m/s, $U_{G,2}$=1.62 m/s, p=6.03 bar) on the WASP rig 252
Figure 5.5 Measured pressure gradient *(dp dx)* for transient case `1c` (U_L=0.039 m/s, $U_{G,1}$=7.39 m/s, $U_{G,2}$=8.08 m/s, p=0.99 bar) on the low pressure rig 253
Figure 5.6 Measured liquid wall shear stress τ_{WL} for transient case `1c` (U_L=0.039 m/s, $U_{G,1}$=7.39 m/s, $U_{G,2}$=8.08 m/s, p=0.99 bar) on the low pressure rig 253
Figure 5.7 Measured gas wall shear stress τ_{WG} for transient case `1c` (U_L=0.039 m/s, $U_{G,1}$=7.39 m/s, $U_{G,2}$=8.08 m/s, p=0.99 bar) on the low pressure rig 254
Figure 5.8 Measured liquid holdup ε_L for transient case `1c` (U_L=0.039 m/s, $U_{G,1}$=7.39 m/s, $U_{G,2}$=8.08 m/s, p=0.99 bar) on the low pressure rig 254
Figure 5.9 Measured liquid phase average velocity u_L for transient case `1c` (U_L=0.039 m/s, $U_{G,1}$=7.39 m/s, $U_{G,2}$=8.08 m/s, p=0.99 bar) on the low pressure rig 255
Figure 5.10 Measured gas phase average velocity u_G for transient case `1c` (U_L=0.039 m/s, $U_{G,1}$=7.39 m/s, $U_{G,2}$=8.08 m/s, p=0.99 bar) on the low pressure rig 255
Figure 5.11 Interfacial fluctuation h_L' for transient case `1c` (U_L=0.039 m/s, $U_{G,1}$=7.39 m/s, $U_{G,2}$=8.08 m/s, p=0.99 bar) on the low pressure rig 256
Figure 5.12 Measured pressure gradient *(dp dx)* for transient case `1f` (U_L=0.058 m/s, $U_{G,1}$=7.07 m/s, $U_{G,2}$=8.75 m/s, p=1.00 bar) on the low pressure rig 256
Figure 5.13 Measured liquid wall shear stress τ_{WL} for transient case `1f` (U_L=0.058 m/s, $U_{G,1}$=7.07 m/s, $U_{G,2}$=8.75 m/s, p=1.00 bar) on the low pressure rig 257
Figure 5.14 Measured gas wall shear stress τ_{WG} for transient case `1f` (U_L=0.058 m/s, $U_{G,1}$=7.07 m/s, $U_{G,2}$=8.75 m/s, p=1.00 bar) on the low pressure rig 257
Figure 5.15 Measured liquid holdup ε_L for transient case `1f` (U_L=0.058 m/s, $U_{G,1}$=7.07 m/s, $U_{G,2}$=8.75 m/s, p=1.00 bar) on the low pressure rig 258
Figure 5.16 Measured liquid phase average velocity u_L for transient case `1f` (U_L=0.058 m/s, $U_{G,1}$=7.07 m/s, $U_{G,2}$=8.75 m/s, p=1.00 bar) on the low pressure rig 258
Figure 5.17 Measured gas phase average velocity u_G for transient case `1f` (U_L=0.058 m/s, $U_{G,1}$=7.07 m/s, $U_{G,2}$=8.75 m/s, p=1.00 bar) on the low pressure rig 259
Figure 5.18 Interfacial fluctuation h_L' for transient case `1f` (U_L=0.058 m/s, $U_{G,1}$=7.07 m/s, $U_{G,2}$=8.75 m/s, p=1.00 bar) on the low pressure rig 259

Figure 5.19 Measured liquid holdup ε_L for transient case wb (U_L=0.037 m/s, $U_{G,1}$=5.33 m/s, $U_{G,2}$=6.07 m/s, p=1.06 bar) on the WASP rig 260
Figure 5.20 Measured liquid phase average velocity u_L for transient case wb (U_L=0.037 m/s, $U_{G,1}$=5.33 m/s, $U_{G,2}$=6.07 m/s, p=1.06 bar) on the WASP rig ... 260
Figure 5.21 Measured gas phase average velocity u_G for transient case wb (U_L=0.037 m/s, $U_{G,1}$=5.33 m/s, $U_{G,2}$=6.07 m/s, p=1.06 bar) on the WASP rig 261
Figure 5.22 Interfacial fluctuation h_L' for transient case wb (U_L=0.037 m/s, $U_{G,1}$=5.33 m/s, $U_{G,2}$=6.07 m/s, p=1.06 bar) on the WASP rig 261
Figure 5.23 Measured liquid holdup ε_L for transient case wd (U_L=0.032 m/s, $U_{G,1}$=1.30 m/s, $U_{G,2}$=1.62 m/s, p=6.03 bar) on the WASP rig 262
Figure 5.24 Measured liquid phase average velocity u_L for transient case wd (U_L=0.032 m/s, $U_{G,1}$=1.30 m/s, $U_{G,2}$=1.62 m/s, p=6.03 bar) on the WASP rig ... 262
Figure 5.25 Measured gas phase average velocity u_G for transient case wd (U_L=0.032 m/s, $U_{G,1}$=1.30 m/s, $U_{G,2}$=1.62 m/s, p=6.03 bar) on the WASP rig 263
Figure 5.26 Interfacial fluctuation h_L' for transient case wd (U_L=0.032 m/s, $U_{G,1}$=1.30 m/s, $U_{G,2}$=1.62 m/s, p=6.03 bar) on the WASP rig 263
Figure 5.27 Measured gas wall friction factor f_G for transient case 1c (U_L=0.039 m/s, $U_{G,1}$=7.39 m/s, $U_{G,2}$=8.08 m/s, p=0.99 bar) on the low pressure rig 264
Figure 5.28 Comparison between measured gas wall friction factor f_G and models for transient case 1c (U_L=0.039 m/s, $U_{G,1}$=7.39 m/s, $U_{G,2}$=8.08 m/s, p=0.99 bar) on the low pressure rig 264
Figure 5.29 Comparison between measured gas wall friction factor f_G and models for transient case 1f (U_L=0.058 m/s, $U_{G,1}$=7.07 m/s, $U_{G,2}$=8.75 m/s, p=1.00 bar) on the low pressure rig 265
Figure 5.30 Measured interfacial friction factor f_i for transient case 1c (U_L=0.039 m/s, $U_{G,1}$=7.39 m/s, $U_{G,2}$=8.08 m/s, p=0.99 bar) on the low pressure rig 265
Figure 5.31 Comparison between measured interfacial friction factor f_i and models for transient case 1c (U_L=0.039 m/s, $U_{G,1}$=7.39 m/s, $U_{G,2}$=8.08 m/s, p=0.99 bar) on the low pressure rig 266
Figure 5.32 Plot of error between measured interfacial friction factor f_i and the new steady state model for transient case 1c (U_L=0.039 m/s, $U_{G,1}$=7.39 m/s, $U_{G,2}$=8.08 m/s, p=0.99 bar) on the low pressure rig 266
Figure 5.33 Comparison between measured interfacial friction factor f_i and models for transient case 1f (U_L=0.058 m/s, $U_{G,1}$=7.07 m/s, $U_{G,2}$=8.75 m/s, p=1.00 bar) on the low pressure rig 267
Figure 5.34 Plot of error between measured interfacial friction factor f_i and the new steady state model for transient case 1f (U_L=0.058 m/s, $U_{G,1}$=7.07 m/s, $U_{G,2}$=8.75 m/s, p=1.00 bar) on the low pressure rig 267
Figure 5.35 Interfacial structure for initial steady state of transient case 1a (U_L=0.039 m/s, $U_{G,1}$=5.01 m/s, $U_{G,2}$=6.46 m/s, p=1.00 bar) on the low pressure rig 268
Figure 5.36 Interfacial structure in the time interval 0-0.6 seconds after the transient change of case 1a (U_L=0.039 m/s, $U_{G,1}$=5.01 m/s, $U_{G,2}$=6.46 m/s, p=1.00 bar) on the low pressure rig 268
Figure 5.37 Interfacial structure in the time interval 1.8-2.4 seconds after the transient change of case 1a (U_L=0.039 m/s, $U_{G,1}$=5.01 m/s, $U_{G,2}$=6.46 m/s, p=1.00 bar) on the low pressure rig 269

Figure 5.38 Interfacial structure in the time interval 29.4-30.0 seconds after the transient change of case 1a (U_L=0.039 m/s, $U_{G,1}$=5.01 m/s, $U_{G,2}$=6.46 m/s, p=1.00 bar) on the low pressure rig 269
Figure 5.39 Interfacial structure for initial steady state of transient case wb (U_L=0.037 m/s, $U_{G,1}$=5.33 m/s, $U_{G,2}$=6.07 m/s, p=1.06 bar) on the WASP rig 270
Figure 5.40 Interfacial structure in the time interval 5.0-5.6 seconds after the transient change of case wb (U_L=0.037 m/s, $U_{G,1}$=5.33 m/s, $U_{G,2}$=6.07 m/s, p=1.06 bar) on the WASP rig 270
Figure 5.41 Interfacial structure in the time interval 15.0-15.6 seconds after the transient change of case wb (U_L=0.037 m/s, $U_{G,1}$=5.33 m/s, $U_{G,2}$=6.07 m/s, p=1.06 bar) on the WASP rig 271
Figure 5.42 Comparison between measured interfacial fluctuation h_L' and new steady state model for transient case 1c (U_L=0.039 m/s, $U_{G,1}$=7.39 m/s, $U_{G,2}$=8.08 m/s, p=0.99 bar) on the low pressure rig 271
Figure 5.43 Plot of error between measured interfacial fluctuation h_L' and the new steady state model for transient case 1c (U_L=0.039 m/s, $U_{G,1}$=7.39 m/s, $U_{G,2}$=8.08 m/s, p=0.99 bar) on the low pressure rig 272
Figure 5.44 Comparison between measured interfacial fluctuation h_L' and new steady state model for transient case 1f (U_L=0.058 m/s, $U_{G,1}$=7.07 m/s, $U_{G,2}$=8.75 m/s, p=1.00 bar) on the low pressure rig 272
Figure 5.45 Plot of error between measured interfacial fluctuation h_L' and the new steady state model for transient case 1f (U_L=0.058 m/s, $U_{G,1}$=7.07 m/s, $U_{G,2}$=8.75 m/s, p=1.00 bar) on the low pressure rig 273
Figure 5.46 Comparison between measured interfacial fluctuation h_L' and new steady state model for transient case wb (U_L=0.037 m/s, $U_{G,1}$=5.33 m/s, $U_{G,2}$=6.07 m/s, p=1.06 bar) on the WASP rig 273
Figure 5.47 Plot of error between measured interfacial fluctuation h_L' and the new steady state model for transient case wb (U_L=0.037 m/s, $U_{G,1}$=5.33 m/s, $U_{G,2}$=6.07 m/s, p=1.06 bar) on the WASP rig 274
Figure 5.48 Comparison between measured interfacial fluctuation h_L' and new steady state model for transient case wd (U_L=0.032 m/s, $U_{G,1}$=1.30 m/s, $U_{G,2}$=1.62 m/s, p=6.03 bar) on the WASP rig 274
Figure 5.49 Plot of error between measured interfacial fluctuation h_L' and the new steady state model for transient case wd (U_L=0.032 m/s, $U_{G,1}$=1.30 m/s, $U_{G,2}$=1.62 m/s, p=6.03 bar) on the WASP rig 275
Figure 5.50 Comparison of calculations with commercial codes with measurement for transient case 1a (U_L=0.039 m/s, $U_{G,1}$=5.01 m/s, $U_{G,2}$=6.46 m/s, p=1.00 bar) on the low pressure rig 275
Figure 5.51 Comparison of calculations with commercial codes with measurement for transient case wa (U_L=0.023 m/s, $U_{G,1}$=5.68 m/s, $U_{G,2}$=6.45 m/s, p=1.07 bar) on the WASP rig 276
Figure 5.52 Comparison of calculations with TRIOMPH with measurement for transient case wb (U_L=0.037 m/s, $U_{G,1}$=5.33 m/s, $U_{G,2}$=6.07 m/s, p=1.06 bar) on the WASP rig 276
Figure 5.53 Comparison of calculations with TRIOMPH with measurement for transient case wd (U_L=0.032 m/s, $U_{G,1}$=1.30 m/s, $U_{G,2}$=1.62 m/s, p=6.03 bar) on the WASP rig 277

Figure 5.54 Stability of stratified flow according to Barnea & Taitel (1994) for air-water flow at atmospheric pressure..... 277

List of Tables

Table 3.1 Minimum velocities in air and water for Pitot tube with a diameter of the interior tube of 3 mm according to British Standard 75
Table 3.2 Air flow rates with 20 mm diameter orifice plate 84
Table 3.3 Typical values for sensor temperature coefficients of resistance α_{20} and sensor resistance R_{20} at 20 °C 88
Table 3.4 Overheat ratios used with the different probes in this study 88

Table 4.1 Flow conditions for steady state experiments 146
Table 4.2 Estimation of hydraulic gradient on the low pressure rig 158
Table 4.3 Values of parameter C_s obtained at different pressures 176
Table 4.4 Results of measured parameters for initial steady states of transient experiments on the low pressure rig 183
Table 4.5 Results of measured parameters for final steady states of transient experiments on the low pressure rig 184
Table 4.6 Results of measured parameters for initial steady states of transient experiments on the WASP rig 186
Table 4.7 Results of measured parameters for final steady states of transient experiments on the WASP rig 187

Table 5.1 Flow conditions of low pressure rig transients chosen for presentation of data 216
Table 5.2 Flow conditions of WASP rig transients chosen for presentation of data 220
Table 5.3 Experimental conditions for transient cases `1a` and `wb` 233
Table 5.4 Conditions of transient experimental cases `1a` and `wa` 239
Table 5.5 Summary of transient tests on the low pressure rig 249
Table 5.6 Summary of transient tests on the WASP rig 250

Chapter 1

Introduction

The research described in this thesis formed part of a project on transient multiphase flow, initiated and supported by the UK Engineering and Physical Sciences Research Council (EPSRC) and by the oil industry and their contractors. Multiphase flows are defined by the flow of two or more distinct phases in systems, such as pipes. A phase is characterized by homogeneous composition and properties and it has clearly defined boundaries.

The main application of multiphase flows nowadays lies in hydrocarbon recovery, both onshore and offshore, where complex mixtures of up to four phases (natural gas, oil, water and solid particles) are transported through pipelines. The mass flow rates in these pipelines are substantial, and improvements in the prediction and the operation of the multiphase systems can result in a significant economic return.

The present study is focused on transient stratified gas-liquid flows in horizontal pipes. A stratified flow is one of the possible flow configurations, called *flow patterns*, that can be distinguished in a horizontal two-phase flow. In this flow pattern the two phases are completely separated from each other and the liquid, which is the denser phase, flows along the bottom of the tube and the gas flows above it. A sketch of a stratified flow is shown in Figure 2.1 at the end of Chapter 2. Many pipelines operate in the stratified flow regime. Gas-liquid stratified flows appear to be simple but they are far from being understood. The complexity of the flow regime stems from the deformable interface, the transition between the two phases. Its shape is mainly determined by the combination of the gas and liquid flow rates in the system. At low gas flow rates the interface is smooth, but at higher gas flow rates it deforms and waves form on top of it. When the gas flow rates are high enough the waves build up and bridge the pipe and transition to another flow pattern, called slug flow, occurs where the two phases are not completely separated any more. Transient stratified flow occurs when the flow is disturbed through operational activities such as changes in the valve openings for the inlet flow rates. After such a disturbance the steady state

stratified flow, where the two phases are in hydrodynamic equilibrium, goes through a transient period before a new steady state is reached.

Stratified flows, both steady state and transient, are commonly modelled in one dimension. Commercial computer codes, such as PLAC, OLGA and TACITE, are based on a transient one-dimensional model and they have become widely used tools in the design of pipeline systems. A widely used type of one-dimensional model is the two-fluid model which is introduced in Section 2.3.2 of this thesis and its set of equations is stated here again to illustrate the subsequent text.

$$\frac{\partial}{\partial t}\left(S_G \rho_G\right) + \frac{\partial}{\partial x}\left(S_G \rho_G u_G\right) = 0 \tag{2.47}$$

$$\frac{\partial}{\partial t}\left(S_L \rho_L\right) + \frac{\partial}{\partial x}\left(S_L \rho_L u_L\right) = 0 \tag{2.48}$$

$$\frac{\partial}{\partial t}\left(S_G \rho_G u_G\right) + \frac{\partial}{\partial x}\left(S_G \rho_G u_G^2\right) + S_G \frac{\partial p_G}{\partial x} = -\tau_i P_i - \tau_{WG} P_G \tag{2.49}$$

$$\frac{\partial}{\partial t}\left(S_L \rho_L u_L\right) + \frac{\partial}{\partial x}\left(S_L \rho_L u_L^2\right) + S_L \frac{\partial p_L}{\partial x} = \tau_i P_i - \tau_{WL} P_L \tag{2.50}$$

The model consists of separate mass continuity and momentum conservation equations for each phase. t is time, x is the position in flow direction, u_L and u_G are the phase velocities in the gas and the liquid, $\partial p_G / \partial x$ and $\partial p_L / \partial x$ are the pressure gradients in the gas and the liquid, S_G and S_L the flow cross sectional areas in the gas and the liquid and P_G, P_L and P_i the wetted perimeters in the gas, the liquid and at the interface. ρ_G and ρ_L are the densities of the gas and the liquid. Important terms in these equations are the wall shear stress in the gas, τ_{WG}, the wall shear stress in the liquid, τ_{WL}, and the interfacial shear stress, τ_i. Models for the shear stresses are needed to close the system of equations.

The question of these shear stresses has been a topic of research for many years. It was found that the shear stresses, especially the interfacial shear stress, result from complex interactions which cannot be represented by analytic solutions which are functions of the primary flow parameters such as liquid height and phase velocities. The complexity of the problem is demonstrated by the large number of relationships for the shear stresses, mainly the interfacial shear stress, which were developed over the years and often presented in the form of correlations based on experimental data.

The research on the shear stresses has so far been limited to steady state flows. Steady state relationships for the shear stresses are nowadays also used in the transient calculations due to a lack of relationships developed for the transient case. It is important to find out if existing steady state models are appropriate for the transient situation or if there are transient effects which are not taken into account by the existing models due to the fact that they were developed for steady state flows. An improvement of the models for the shear stresses for transients is relevant with regard to the calculations of flow transients in pipelines and other multiphase systems.

The present study aimed at a better understanding of phase interactions in both steady state and transient stratified flows. In particular it addressed the question of the shear stresses in steady state and transient stratified flows. The question was tackled by means of experiments. Data for the interfacial shear stress was obtained through the means of the one-dimensional model by using measurements of detailed local parameters. The measurements included the pressure gradient, the liquid height and interfacial structure, wall shear stresses and phase velocities. The presentation of data for interfacial shear stress forms only a small part of the thesis. The measurements of the parameters were interesting in their own right and were discussed in detail. Beside the experimental work some effort was made to use existing one-dimensional transient codes for comparison with the experiments.

The thesis is structured into four main chapters (Chapters 2 to 5) which are followed by a short chapter on conclusions (Chapter 6) where the achievements of the research are summarised and suggestions for possible further work are given.

Chapter 2 presents a review of the relevant literature. It is split into four main parts. The first part comments on the possible flow patterns in horizontal gas-liquid flow. The second part reviews experimental studies of steady state and transient stratified flows. This is followed by a discussion of existing one-dimensional models and of relationships for interfacial and wall shear stresses in stratified flow. A separate section introduces the one-dimensional codes which were used in this study for comparison with the experimental data.

The development of the experimental methods adopted in this study is dealt with in Chapter 3. It started with an evaluation of measurement methods for the input parameters in the one-dimensional model to obtain experimental data for interfacial shear stress. The instrumentation used was built into a specifically designed test spool

which was used on two flow facilities at Imperial College, the low pressure rig and the WASP rig. All the instrumentation was validated in both flow facilities.

Chapter 4 describes steady state data obtained in the experiments on the low pressure rig and the WASP rig. The measurements in two-phase flow are validated versus predictions from computer codes and versus data and models published in the literature. Data for the wall and interfacial shear stresses are compared with steady state models. The interfacial structure is analyzed both qualitatively and quantitatively. Based on the quantitative analysis of the interfacial structure new steady state expressions are developed for interfacial shear stress.

Chapter 5 describes the transient data obtained in the experiments on the low pressure rig and the WASP rig. First, the transient features in the measured parameters are discussed. Then wall and interfacial shear stresses during the transient are compared with predictions from steady state models and the differences are evaluated. Afterwards the interfacial structure is analyzed qualitatively and quantitatively.

Chapter 2

Literature Review

A major focus of research in two-phase flow, particularly in stratified gas-liquid flows, is the improvement of models to predict the key parameters for design of a pipeline system, which are pressure drop and liquid holdup. Steady state stratified flow is commonly modelled using the one-dimensional, two-fluid model (Agrawal et al., 1973; Taitel & Dukler, 1976). In this model the main uncertainties are the closure terms (wall and interfacial shear stresses), which have been a topic of study for many years, and they are addressed in Section 2.3.1. The one-dimensional modelling approach is also used for transient flows. In this case the resulting system of equations is more complex since, in contrast to steady state stratified flow, where the flow parameters can be assumed to be constant along the pipe, the parameters now vary with time and distance along the pipe. A review of studies concentrating on applying the one-dimensional model to transient stratified flows is given in Section 2.3.2. Section 2.4 introduces the one-dimensional codes which have been used in this study for comparison with experimental data.

It is important to back up the modelling work with experiments for two reasons. First, as it is not possible, because of the combined effects of turbulence and the generation of interfacial waves, to describe stratified flows completely analytically experimental data are needed to validate the models. Second, and very importantly, the mathematical models have to represent the physical nature of the two-phase system. An understanding of the physics of the systems can only be achieved through experiments. Therefore the section about one-dimensional modelling is preceded by sections on experimental studies of steady state stratified flows (Section 2.2.1) and transient stratified flows (Section 2.2.2). But to start with, in Section 2.1, some comments are added about flow patterns to place stratified flow in the more general context of two-phase flow in horizontal tubes.

2.1 Flow Patterns in Horizontal Two-Phase Flow

A *flow pattern* or *flow regime* is a term used to describe the distribution of the different phases present in a multiphase system. Flow patterns can be distinguished by visual observation. However, the concept of flow patterns is not just useful to describe the physical appearance of a multiphase system. It is also useful when one wants to model multiphase systems as each flow pattern has its own physics which will determine the behaviour of flow parameters like pressure drop.

Of the possible two-phase flows, gas-liquid flows are the most complex to model because the boundary between the gas and the liquid, the interface, is highly deformable. The flow patterns depend on the angle of inclination of the tube. The flow patterns in a vertical tube are different from those in a horizontal tube. The present study is restricted to flows in horizontal pipes, and flows in inclined or vertical pipes are therefore not addressed.

Hewitt (1982) classified gas-liquid flows in horizontal tubes into six main flow patterns:

- Stratified flow
- Stratified-wavy flow
- Dispersed-bubble flow
- Annular-dispersed flow

and the intermittent flow patterns

- Plug flow
- Slug flow

The flow patterns are exemplified in Figure 2.1. Of direct relevance to this study are the stratified, stratified-wavy and slug flow patterns. Slug flows can be generated from stratified-wavy flows when the gas flow rate is sufficiently increased. The waves then grow and reach the top of the pipe, forming liquid slugs followed by sections where large bubbles of air flow on top of a liquid film.

Transitions from one flow pattern to another have been widely investigated. Transition boundaries are often investigated from experiments but the resulting flow pattern map is then only valid for the system under consideration. Therefore it is desirable to have criteria which can be used more generally. Taitel & Dukler (1976) presented a model for the flow pattern transitions in horizontal gas-liquid flow and

this has been widely used. Their analysis was based on a one-dimensional two-fluid model (see Section 2.3.1) and presented criteria for each of the flow pattern transitions in horizontal and near-horizontal flows. The criteria were based on physical concepts and they expressed the transition from stratified flow to one of the other flow patterns. The transition from stratified-wavy to slug flow, e.g., was assumed to occur from a Kelvin-Helmholtz type instability. The transition from stratified to slug flow would take place if finite-amplitude waves could grow on the stratified surface.

2.2 Experimental Studies

2.2.1 Steady State Stratified Flow

There has been much research on stratified gas-liquid flow both in rectangular and circular channels. Although this system appears to be simple with the two phases flowing separately in the pipe it is highly complex and far from being understood. The subsequent text highlights the complexity of this flow pattern by describing important experimental findings from a selection of the numerous literature sources on stratified gas-liquid flow. The text is subdivided in a section on the characteristics of the interface, one on the flow fields in the gas and the liquid, and one on the wall shear stresses. The sections are related to each other because the structure of the interface influences the flow fields in the phases below and above (Liné et al., 1991). Many of these findings reveal that stratified flows are complex and that the reduction to one dimension which is commonly used for modelling stratified flows (see Section 2.3) is a simplification. Still, one-dimensional models are useful tools as they allow reasonable predictions of two-phase flows with minimum effort.

2.2.1.1 Characterization of the Interface

The complexity of the stratified flow mainly stems from the ability of the gas-liquid interface to deform. In the simplest case of a stratified smooth flow the interface is completely flat. But at higher gas velocities, waves are generated on the interface. The structure of the interface is important when modelling stratified flows. It will dominate the drag between the phases. If a one-dimensional model is used the drag at the interface is expressed in terms of an interfacial friction factor. As a result of the

complexity of the interfacial structure in stratified flow a large number of mathematical relationships have been suggested for interfacial friction (see Section 2.3.1).

Depending on their interfacial structure stratified flows are subdivided into a number of flow patterns. The simplest classification is into two flow regimes, stratified smooth and stratified-wavy flow as suggested by Baker (1954). Stratified-wavy flow can be further subdivided. For example, Andreussi & Persen (1987) distinguished two flow patterns in stratified-wavy flow:

- The 2-D wave regime in which the interface is covered by a continuous 2-D wave structure.
- The large disturbance wave regime in which large disturbances are superposed on the 2-D wave structure.

Even more refined classifications have been suggested. Strand (1993) divided the stratified-wavy regime into six subsections based on a detailed experimental investigation of the gas-liquid interface:

- Small amplitude 2D wave region
- Large amplitude 2D wave region
- 3D wave region
- Pebbly wave region
- Unstable large amplitude 2D wave region

Much of the investigative work done in the context of stratified flow was centred on analyzing the complex structure of the gas-liquid interface and its influence on the flow. Hanratty & McCready (1992) reviewed theoretical work done on the formation of waves. The formation of waves is a very complex process. Linear stability analysis is widely used to describe the wave formation process. Often this is not sufficient and non-linear effects have to be studied. Statistical analysis can be used as a means to distinguish between the different sorts of waves in stratified flow (Andritsos, 1992). The speed of waves can be obtained by cross-correlating measurements of liquid height (or holdup) at two different locations along the pipe. Data using this technique were reported by Roberts (1996) and Strand (1993). Wave speeds were found to grow with increases in gas or liquid flow rate.

The three-dimensionality of the wave field can be characterized by correlating liquid height measurements at several locations in the same cross section. Data for this was presented by Strand (1993). A measure of the non-uniformity of the interfacial roughness in a cross section is the rms (root-mean-square) amplitude. This can be obtained from experimental data of time traces of the liquid height taken at different lateral positions in the same cross section. Data for rms amplitude were discussed by Strand (1993). The distribution of the rms amplitude across the pipe could be divided into four regions for increasing gas flow rate and a fixed liquid flow rate. At low gas flow rates the rms amplitudes were uniformly distributed in a cross section. At increased gas flow rates a region with maximum amplitude occurred towards the wall. At a further increase of the gas flow rate the distribution was again uniform. At even higher gas flow rates a maximum of the rms amplitude appeared towards the middle of the pipe. Additionally higher order statistical moments and spectral analysis were used to characterize the interface.

In the direction normal to the flow another feature of the interface becomes important, its tendency to creep up the tube walls. This deforms the shape of the interface in a cross section from flat into curved. This affects the geometrical parameters which are used in the one-dimensional model (see Figure 2.2). Thus, the gas and liquid wetted perimeters, P_G and P_L, and the length of the interface, P_i, will change from their values for a flat interface. The existence of interfacial curvature was reported by Roberts (1996) for experiments at atmospheric pressure in an acrylic tube. Data on interfacial curvature was derived from measurements of liquid height at several transverse positions in a cross section using twin-wire conductivity probes. Roberts reported that the curvature of the interface increased at higher gas flow rates. A further feature of the interface is a hydraulic gradient (also called interfacial level gradient) which is observed for stratified flows at low gas velocities.

The existence of hydraulic gradients was reported by Strand (1993). In a stratified flow with an interfacial level gradient the pressure drop in the gas and the liquid phases will differ and it will affect the behaviour of the flow (liquid holdup, flow pattern transition) as explained by Bishop & Deshpande (1986).

2.2.1.2 Flow Fields

Some interesting features of stratified flow were demonstrated with detailed measurements of the gas and the liquid flow fields.

Strand (1993) measured the axial and vertical velocity components in a cross section in the liquid using a laser doppler anemometry (LDA) system. The flow conditions were for a fixed liquid superficial velocity and a varying gas velocity. At very low gas velocities the measured axial velocity increased towards the interface in the vertical direction and towards the centre of the pipe in the transverse direction. At higher gas velocities the axial velocities decreased in the upper part of the liquid layer and increased in the lower part of the liquid layer. The fluctuating velocity level was increased due to the occurrence of 2D gravity waves. Transversally, there was a shift in the maximum mean velocity towards the wall. Vertical secondary currents moving downwards in the middle of the liquid phase and upwards towards the wall were observed. At even higher gas velocities the axial velocity in the liquid increased due to increased interfacial drag from the fast moving gas. The fluctuating velocities decreased due to a broadening of the wave spectrum. At these velocities the vertical secondary currents moved upward in one half of the pipe and downwards in the other. Secondary flows in the liquid were also reported by Liné et al. (1991). The source for these secondary flows was believed to be the non-linear interaction between the mean flow and the wave field.

Strand (1993) also performed measurements of the gas flow field using a Pitot tube and LDA for a fixed liquid superficial velocity and different gas superficial velocities. The measured velocity profiles in the vertical direction revealed three different shapes: a symmetrical shape for low gas velocities, a downwardly inclined shape for moderate gas velocities and an upwardly inclined shape for high gas rates. With increasing gas flow rate the profile also became flatter near the maximum velocity. The velocity profiles in the transverse direction were flat for all velocities. The velocity fluctuations in the vertical direction showed minimum values in the core of the gas phase and the highest fluctuations appeared near the interface. The profile of fluctuating velocity in the transverse direction was flat for low gas flow rates, with a sharp increase towards the wall. With increasing gas flow rate the profile changed to one with a maximum level in the centre and two minima located symmetrically on each side of the pipe. At higher gas flow rates the profile became asymmetric with a

minimum near the centre of the tube. The contrast of roughness between the smooth wall and the wavy interface was believed to be the source of secondary flow in the gas phase (Liné et al., 1991).

2.2.1.3 Wall Shear Stresses

Several experimental studies looked at the distribution of wall shear stresses in the gas and liquid phases around the periphery of the pipe (Kowalski, 1987; Rosant, 1994; Espedal, 1998).

Espedal (1998) carried out experiments in stratified flows at small inclinations, performing measurements of the gas wall shear stress at different locations around the circumference using a Preston tube. He found that the angular distribution of the gas wall shear stress was dependent on the wave pattern. For smooth flow the gas wall shear stress was found to be constant from the top of pipe until it started to decrease towards the interface. Where large amplitude waves were present the shear stress was highest at the top of the tube and gradually decreased towards the interface. In the transition zone from small to large amplitude waves irregular waves appeared and the shear stress either decreased midway between the top and the interface before it increased again towards the interface, or the opposite behaviour was observed.

In the work reported by Espedal (1998), liquid wall shear stress was measured at different circumferential positions using a hot-film probe. The distribution of shear stress around the circumference was also found to be dependent on the state of the gas/liquid interface. For the case where the flow was mainly gravity driven the liquid wall shear stress was relatively constant around the bottom of the pipe before it started to decrease towards the gas-liquid interface. The interface was smooth or had small amplitude waves. For high gas flow rates, where large amplitude 3D waves were present, the shear stress was relatively constant around over half of the liquid wetted perimeter before it increased towards the interface. In the transition zone between gravity driven flow and interfacial driven flow the shear stress distribution was found to be dependent on the liquid flow rate.

2.2.2 Transient Stratified Flow

Transient two-phase flow had been a subject of key interest in the nuclear industry before it became a topic of interest in pipeline flows. In water cooled nuclear reactors, transient two-phase flow is very important in the context of loss of coolant accidents (LOCAs). These nuclear studies often formed a basis for the more recent work on pipeline flows. For instance, the commercial code PLAC, which is widely used in the petrochemical industries for modelling transient two-phase flows, was developed from TRAC, which had been used for modelling transients in nuclear systems.

However, there are substantial differences between transients in nuclear systems and those in pipeline systems. The thermodynamic properties of the two phases in nuclear systems (steam-water) are relatively simpler to those in pipeline flows where the liquid is a complex mixture of hydrocarbons. Another difference is the speed at which they occur. Transients in pipeline systems are generally slower than those in nuclear reactors and they can be distinguished into two classes. Slow transients in pipeline systems occur due to changes of the inlet flow rates, changes in outlet pressure and opening and closing of valves. Faster transients in hydrocarbon systems are generated from pipeline rupture and pigging.

One of the significant transients in pipeline systems is transient stratified flow. This type of transient describes the transition from an initial steady state stratified flow to a final steady state stratified flow. As transients in pipeline flows have only become of interest in recent years there is much less published work than on steady state flows. A review of the relevant studies in the field of transient stratified flow is given here.

The first important experimental study of transient stratified flow in pipelines was carried out by Sakaguchi et al. (1973). The test section was a horizontal tube made of acrylic, with 40 mm internal diameter and 8.1 m length.

Sakaguchi et al. investigated characteristics of transient co-current air-water flow, for step changes of the inlet air flow rates or water flow rates. The flow patterns during the transients were visually observed and the dynamic behaviour of the holdup, water velocity and air velocity were measured. Conductance probes were used for the holdup, the air velocity was measured using hot-wire anemometry and the water velocity using impact tubes and static pressure taps.

For a transient produced from an increase in the gas flow rate the waves in the initial steady state stratified flow were observed to increase. When the change in the gas flow rate was large enough the waves could grow and bridge the pipe and one or several liquid slugs could form although the flow patterns of the initial and final steady state were in the stratified regime. The appearance of these temporary slugs was termed "temporary slug flow" and could not be predicted from the steady-state flow regime map. In a stratified smooth flow an increase in the gas flow rate could temporarily generate waves and this was defined as the "temporary wavy flow". The liquid holdup, air and water velocities in the transient from an increase of the gas flow rate first increased and then decreased. The holdup propagated down the tube at nearly a constant velocity. Transients from a reduction of the gas flow rate resulted in smoothing the gas-liquid interface.

In the case of a step increase of the inlet liquid flow rate, the "temporary slug flow" or the "temporary wavy flow" could not be observed. A step increase or decrease of the liquid flow rate resulted in increases or decreases of the measured parameters (holdup and phase velocities). The liquid holdup at position x in the pipe was found to respond to the change in the inlet liquid flow rate after a dead time given by

$$t_d = \frac{x}{\sqrt{gh_L}} \tag{2.1}$$

That means that the change of holdup propagated with the velocity of a gravity wave in the channel with a liquid level h_L.

Sakaguchi et al. (1981) performed a further experimental study of transient stratified flow on the flow facility used by Sakaguchi et al. (1973). They discussed their experimental results in more detail than Sakaguchi et al. (1973) whose findings they confirmed. In addition they noted that the behaviour of the respective phases were interrelated; thus, the response of the gas phase to an increase in the inlet gas flow rate would influence the liquid velocity and also the liquid holdup. They further suggested that the propagation velocity of the hydraulic jump $u_{L,h}$ produced in a transient from an increase in the gas flow rate was given by the following formula:

$$u_{L,h} = u_L + \sqrt{gh_{L,e}} \tag{2.2}$$

where $h_{L,e}$ is an equivalent height of the liquid phase expressed by

$$h_{L,e} = \frac{S_L}{P_i} \tag{2.3}$$

The geometrical parameters can be calculated as suggested in Taitel & Dukler (1976) (see Section 2.3.1). Sakaguchi et al. (1981) included a theoretical analysis which was based on a two-fluid model consisting of mass and momentum equations for the two phases. With the model they were able to qualitatively describe the experimentally determined transient behaviour of the flow parameters.

Minami & Shoham (1994) carried out an extensive experimental program for validation of a new flow pattern prediction model for transient two-phase flows, which was based on the Taitel et al. (1989) model. Taitel et al. had simplified the basic equations (mass and momentum equations for both phases) by assuming a quasi-steady state condition for the gas phase, and local momentum equilibrium considerations. The flow pattern prediction model suggested by Minami & Shoham was based on the stability of the slug flow structure. The experimental data was collected in a 420 m long steel flow loop with an internal diameter of 77.9 mm at Tulsa University. The fluids used were air and kerosene. The measured parameters were pressure and pressure drop, liquid holdup, inlet flow rates and temperature. Four transient experiments were discussed in detail. The transients were generated from changes in the gas or liquid flow rates, from introducing a liquid phase into a pipeline initially flowing single phase gas (termed as liquid buildup transient) and from a liquid blow down, where single-phase gas was fed into a pipeline partially filled with liquid. A transient stratified flow was obtained in the case of a change in gas flow rate. The rapid increase in the gas flow rate caused a temporary pressure drop increase and a temporary intense slugging period that induced high outlet liquid flow rate. The time required to achieve a new steady state condition was fairly long (about 500 seconds). The results from the simplified model used by Minami & Shoham were quite good in most of the cases considered. Unsatisfactory predictions of the model only occurred for the liquid blow down tests.

Vigneron et al. (1995) carried out further transient experiments on the Tulsa University flow loop. Transient stratified flow cases presented were produced from changes in the liquid or gas flow rates.

One transient case where the initial and final steady states were in the stratified flow regime was produced from an increase in the liquid flow rate while the gas flow rate was maintained. After the change in the liquid flow rate the pressure built up gradually as the liquid front advanced through the pipeline. It was estimated that the liquid front traveled with the speed of a continuity shock wave.

Another transient stratified flow experiment reported was produced from an increase of the gas flow rate and the results obtained were in agreement with Minami & Shoham (1994). Immediately after the increase of the gas flow waves were generated at several locations. Some of these waves grew into slugs, which caused the liquid discharge rate to increase. After the intense slugging the liquid discharge rate dropped considerably below the inlet flow rate, before the final steady state was reached.

Sarica et al. (1996) carried out a further study of transient flows on the flow loop at Tulsa University. Their work was limited to transient stratified flow cases which were produced from increases in the inlet gas or liquid flow rate, pipeline start-up and liquid blow out. Their results were in agreement with those by Minami & Shoham (1994) and Vigneron et al. (1995).

Roberts (1996) carried out experiments on transient air-water stratified flow in two test facilities. A set of experiments was run on the Harwell Horizontal Flow Facility, which had a perspex test section of 0.032 m internal diameter and a length of 6 m and was operated at atmospheric pressure. The main aim of the investigation was to study in detail the behaviour of a gas-liquid stratified flow when subject to flow rate transients (increases or decreases in the air or water inlet flow rates). To achieve this, the water level was measured with conductivity probes at different locations along the test section, and videos of the flow behaviour were taken. Conditions investigated were for air superficial velocities between 1.0 and 11.8 m/s and water superficial velocities between 0.0092 and 0.0937 m/s. By cross-correlating signals from axially displaced conductivity probes during a transient, the dominant wave speed could be determined. Steady-state data for wave speed were also collected. The wave speed in air flow rate transients was found to be more closely related to the steady state wave speed of the final steady state than to that of the initial steady state. In water flow rate transients the wave speed however was generally more influenced by the initial steady

state than the final steady state. By analysis of the videos taken during the runs flow regimes were identified, where the stratified regime was split into a number of sub-regimes.

Roberts (1996) also carried out experiments on the WASP facility at Imperial College, which was also used in the present study. Air-water flows up to 10 bar(g) were simulated in a 37 m long steel test section with 0.078 m (3 inch nominal bore) internal diameter. Conditions investigated were for air superficial velocities between 0 and 10.16 m/s and water superficial velocities between 0.003 and 0.58 m/s. As with the Harwell Facility, a wide variety of behaviour was observed during flow rate transients ranging from smooth, gradual changes to the formation of slugs and waves. Trends of the flow structure during transients seemed broadly unaffected by the system pressure. For experiments at atmospheric pressure, wave speeds were determined from axially displaced conductivity probes. For runs at elevated pressure it was not possible to get good cross-correlations and no wave speeds were obtained. The results for wave speed in the transient case at atmospheric pressure were similar to those obtained in the Harwell Facility.

King et al. (1997) studied a wide range of flow rate transients, again using the WASP facility at Imperial College.

King et al. classified three sorts of transients: transients where there was no change of flow pattern before, during and after the transient, transients where the flow pattern temporarily changed during the transient period and transients where the flow pattern change during the transient was preserved in the final steady state. The experiments were carried out at different pressures and the transients were produced from changes (increases or decreases) in the inlet liquid or gas flow rate. The flow rates, the pressures, pressure drop and liquid holdup were sampled.

Though the main emphasis of the work by King et al. (1997) was on transient slug flow, several cases of transient stratified flows were reported. In one case the transient was generated from a decrease in the liquid flow rate and no flow pattern change occurred. The only manifestation of the transient change was a liquid bore which advanced along the pipe. In another case the transient stratified flow was produced from a decrease in the gas flow rate, with no change in flow pattern. Here an interesting feature was observed: after the transient change the liquid holdup first

decreased and finally ended up at a value higher than in the initial steady state. King et al. hypothesised that the dip in liquid holdup was a result of the difference in liquid velocities before and after the transient change. The liquid velocity after the transient change decreased as a result of the lower gas flow rate. The liquid adjusted to the initial gas flow rate would therefore move away from the liquid adjusted to the new, lower gas flow rate.

A further case of transient stratified flow was produced with an increasing gas flow rate. In this experiment two temporary slugs occurred which had been reported in earlier studies (Sarica et al., 1996). King et al. noted that a reason for the formation of temporary slugs in transient stratified flow possibly was the slow change of liquid holdup leading to conditions which can generate a slug flow. In another case a transient stratified flow was produced from an increasing liquid flow rate resulting in a flow pattern change from smooth stratified flow in the initial steady state to wavy-stratified flow in the final steady state. The transient change resulted in the formation of several waves and an overall increase in the liquid holdup.

The prediction of the temporary flow pattern change in a transient from stratified flow to slug flow was addressed by several researchers (Taitel et al., 1978; Minami & Shoham, 1994; Grolman & Fortuin, 1996). It is important to know the flow pattern in the pipeline as it determines significantly the behaviour of the flow parameters. For example, the pressure drop in slug flow will be larger than the pressure drop in a stratified flow.

Taitel et al. (1978) presented a theory to predict flow pattern transitions in transient gas-liquid flows, where the transients were introduced by changing the flow rate of either or both phases. The work was based on Taitel & Dukler's (1976) method for predicting flow pattern transitions in steady state flows. In this method the criteria for calculating flow pattern transitions are all functions of the liquid level in the pipe. The Taitel et al. model took into account that the flow parameters in the transient case varied with distance along the pipe and time. The flow was started off as stratified and flow pattern transition was assumed to occur as soon as one of the steady-state transition criteria was met at any point in the pipe.

Taitel et al. showed that under transient flow conditions, transition from one flow pattern to another could take place at substantially different flow rates than would be observed for steady state flows. For slow changes in the flow rates along a path that crosses several transition boundaries, the sequence of flow patterns observed would be identical to that for steady state flow. However, when the path was traversed rapidly, the transitions took place at different rates, and also flow regimes not expected along the steady state path could appear, e.g. slug flow at the transition between initial and final steady state stratified flows. Predictions from the model were confirmed with experimental data.

Roberts (1996) applied the Taitel et al. method for prediction of temporary slug flow in the transient but found poor agreement with his experimental data.

Minami & Shoham (1994) had confirmed that steady state flow pattern transition criteria (as e.g. the one by Taitel & Dukler, 1976) were not suitable for transient flows. They suggested a flow pattern prediction model for transient flow based on the stability of the slug flow structure and found overall good agreement with their experimental data.

Grolman & Fortuin (1996) further studied the transition from stratified to slug flow in flow rate transients. They developed a model based on Taitel et al. (1978) for predicting the transients and compared them with experiments in two upward inclined glass pipes of 26 mm and 51 mm internal diameter at different inclination angles. In the upward inclined pipeline a slug flow was produced from an initial steady state stratified flow by reducing the gas flow rate. This is different from a horizontal flow where slug flow usually occurs as a result of an increase in the gas or liquid flow rate. Grolman & Fortuin's model was able to predict the experimental traces of holdup and pressure drop, but the transition from wavy to slug flow could not be obtained directly from the transient simulations.

2.3 1D Models

Two-phase flow in a circular pipe is often described using a one-dimensional model. In this model, a single velocity is ascribed to each phase at a given location in the

channel, though the velocities of the respective phases may differ from one another. Separate one-dimensional conservation equations are then written out for each phase. This results in a two-fluid model.

One-dimensional two-fluid models have been widely used in both steady state and transient two-phase flows, and for the cases relevant to stratified flow they are reviewed in the subsequent sections.

2.3.1 Steady State Stratified Flow

The most widely used one-dimensional model for steady state stratified flow is that introduced by Agrawal et al. (1973) and further developed by Taitel & Dukler (1976). Taitel & Dukler used the model to evaluate flow regime transitions in steady state gas-liquid flows. The model uses separate momentum equations for the gas and the liquid phases, which for flow in a horizontal tube are as follows:

$$S_L \frac{dp}{dx} + \tau_{WL} P_L - \tau_i P_i = 0 \qquad (2.4)$$

$$S_G \frac{dp}{dx} + \tau_{WG} P_G + \tau_i P_i = 0 \qquad (2.5)$$

where S_L and S_G are the cross sectional areas occupied by the liquid and gas phases and P_L and P_G the tube peripheries in contact with the respective phases. P_i is the interfacial periphery, dp/dx is the pressure gradient and τ_{WL}, τ_{WG} and τ_i are the liquid/wall, gas/wall and interfacial shear stresses. Both equations contain pressure drop and shear stress terms. The pressure drop was assumed to be the same in both phases. The situation of the flow is shown in Figure 2.2. The shear stresses were evaluated in a conventional manner:

$$\tau_{WL} = f_L \frac{\rho_L u_L^2}{2}; \quad \tau_{WG} = f_G \frac{\rho_G u_G^2}{2}; \quad \tau_i = f_i \frac{\rho_G \left(u_G - u_i\right)^2}{2} \qquad (2.6)$$

where f_L, f_G and f_i are the liquid/wall, gas/wall and gas/interface friction factors respectively and u_G and u_L the gas and liquid velocities. The liquid and gas friction factors are calculated on the basis of relationships commonly used in single phase flows:

$$f_L = C_L \mathrm{Re}_L^{-n} \quad \text{with} \quad \mathrm{Re}_L = \frac{D_L u_L}{\nu_L}$$
$$f_G = C_G \mathrm{Re}_G^{-m} \quad \text{with} \quad \mathrm{Re}_G = \frac{D_G u_G}{\nu_G} \tag{2.7}$$

The following coefficients were utilized: C_G=C_L=0.046, n=m=0.2 for the turbulent flow and C_G=C_L=16, n=m=1.0 for laminar flow. The decision on whether laminar or turbulent flow takes place in each phase was based on the Reynolds numbers defined in equation (2.7).

D_L and D_G in equation (2.7) are the hydraulic diameters evaluated in the manner suggested by Agrawal et al. (1973):

$$D_L = \frac{4S_L}{P_L}; \quad D_G = \frac{4S_G}{P_G + P_i} \tag{2.8}$$

The gas was treated as if it were flowing in a closed channel bounded by the pipe wall and the liquid phase; the liquid phase was treated as though it were an open channel flow, bounded only at its lower surface by the pipe wall.

P_G and P_L are the lengths of the circumference wetted by the gas and liquid phase and P_i is the length of the interface. S_G and S_L are the cross sectional areas of the phases. The geometrical parameters were calculated on the basis of the liquid level h_L in the pipe and its radius R:

$$S_L = R^2\left[\pi - \cos^{-1}\left(\frac{h_L}{R} - 1\right) + \left(\frac{h_L}{R} - 1\right)\sqrt{1 - \left(\frac{h_L}{R} - 1\right)^2}\right] \tag{2.9}$$

$$S_G = R^2\left[\cos^{-1}\left(\frac{h_L}{R} - 1\right) - \left(\frac{h_L}{R} - 1\right)\sqrt{1 - \left(\frac{h_L}{R} - 1\right)^2}\right] \tag{2.10}$$

$$P_L = 2R\left[\pi - \cos^{-1}\left(\frac{h_L}{R} - 1\right)\right] \tag{2.11}$$

$$P_G = 2R\cos^{-1}\left(\frac{h_L}{R} - 1\right) \tag{2.12}$$

$$P_i = 2R\sqrt{1 - \left(\frac{h_L}{R} - 1\right)^2} \tag{2.13}$$

Taitel & Dukler stated that $f_i \cong f_G$ had been established for smooth stratified flow and that the error incurred by using this assumption for stratified wavy flow was small. At the conditions where flow regime transitions were observed to take place, $u_G >> u_L$.

Thus, the gas side interfacial shear stress was evaluated with the same equation as the gas wall shear (i.e. neglecting the interface velocity).

The calculation of interfacial shear is the most significant problem in stratified flow. In most cases the approach used by Taitel & Dukler of modelling interfacial shear stress on the basis of a smooth interface is not appropriate. The topic of interfacial friction in steady state stratified flows has been the focus of much research over the past 20 years and many correlations for interfacial friction have been presented. A number of them are reviewed here.

Sinai (1983) developed relationships for interfacial drag based on estimation of the effective surface roughness in stratified flow. To express the roughness he modified an algebraic relation used in the oceanographic literature. The modified algebraic relation possesses solutions only when the mean gas velocity lies below a certain maximum.

The interfacial friction factor was expressed as a function of mean and friction velocities u_G and u^* (Goldstein, 1965):

$$f_i = \frac{2\tau_i}{\rho_G u_G^2} = 2\left(\frac{u^*}{u_G}\right)^2 \tag{2.14}$$

where the friction velocity u^* is defined as $\sqrt{\tau_i / \rho_G}$. The classical relation between mean and friction velocities for fully-rough internal flow:

$$\frac{u_G}{u^*} = 5.75\log_{10}\left(\frac{R_G}{k_R}\right) + 4.73 \tag{2.15}$$

was used, where R_G is the mean hydraulic radius in the gas:

$$R_G = \frac{2S_G}{P_i + P_G} \tag{2.16}$$

and k_R is the rms (root mean square) roughness scale. Sinai introduced the following expression for an effective roughness, which is a modification of a relationship for roughness used in oceanography (Charnock, 1955):

$$k_{R,eff} = 0.33\frac{C_\xi (u^*)^2}{g}; \quad C_\xi = C_\eta \frac{P_i}{P_i + P_G} \tag{2.17}$$

where C_η is a constant to be determined.

Substitution of equation (2.17) in (2.15) yielded:

$$\frac{u_G}{u^*} = 5.75\log_{10}\left(\frac{20.1\cdot C_\nu{}^2}{C_\xi (u^*)^2}\right); \quad C_\nu{}^2 = gR_G \tag{2.18}$$

For a given value of C_ξ, there is a maximum value of u_G, denoted by $(u_G)_T$, beyond which no solutions of this algebraic equation exist. $(u_G)_T$ was determined by differentiating equation (2.18), finding the solution for $\frac{du_G}{du^*} = 0$ and substituting back into equation (2.18):

$$\left(\frac{u_G}{u^*}\right)_T = 5.0 \tag{2.19}$$

The unknown constant C_η was determined by comparing the expression for $(u_G)_T$, particularised for a rectangular channel, with the Wallis & Dobson (1973) stratified-slug transition correlation. The resulting expression for C_η is:

$$C_\eta = \frac{545\rho_G}{\rho_L - \rho_G} \tag{2.20}$$

Sinai did not compare his theoretical prediction with any experimental data.

Andreussi & Persen (1987) reported measurements of liquid holdup, pressure drop and velocity profiles in the gas phase for air-water stratified flow at atmospheric pressure in a downwardly inclined (0.65 and 2.1°), 5 cm diameter, 26 m long pipeline. τ_{WG} was determined from equations (2.6) and (2.7) and τ_i from the gas-momentum equation (2.5) using measured data for pressure drop and liquid holdup. The law of the wall was used to check these data with measured values for the velocity in the gas phase: velocity measurements relative to the wall region were made dimensionless with respect to the wall friction velocity

$$u_W^* = \sqrt{\frac{\tau_{WG}}{\rho_G}} \tag{2.21}$$

and the measurements taken close to the gas-liquid interface with respect to the interfacial friction velocity

$$u_i^* = \sqrt{\frac{\tau_i}{\rho_G}} \tag{2.22}$$

The dimensionless velocity profiles u_W^+ and u_i^+:

$$u_W^+ = \frac{u_G}{u_W^*}; \quad u_i^+ = \frac{u_G}{u_i^*} \tag{2.23}$$

were in agreement with the law of the wall equations where there is a linear relationship between the dimensionless velocity and the logarithmic dimensionless distance from the wall y_W^+ or the interface y_i^+, respectively:

$$u_W^+ \propto \ln y_W^+; \quad u_i^+ \propto \ln y_i^+ \tag{2.24}$$

This confirmed that τ_{WG} and τ_i could be calculated in the manner adopted and it also supported the hypothesis that there is an analogy between the gas flow over a wavy interface and flow in a rough pipe. Andreussi & Persen pointed out the large dependence of interfacial shear stress on the structure of the interface: at the transition from the stratified smooth to the 2D wave regime, interfacial shear increased greatly, but it didn't change significantly at the transition from the 2D wave regime to the large disturbance wave regime. For the ratio f_i/f_G Andreussi & Persen found the following correlation from best-fit to the experimental data:

$$\frac{f_i}{f_G} = 1 \qquad \mathrm{Fr} \le \mathrm{Fr}_0$$

$$\frac{f_i}{f_G} = 1 + 29.7\left(\mathrm{Fr} - \mathrm{Fr}_0\right)^{0.67}\left(\frac{h_L}{D}\right)^{0.2} \qquad \mathrm{Fr} > \mathrm{Fr}_0 \tag{2.25}$$

$$\mathrm{Fr}_0 = 0.36$$

where Fr is the Froude number, defined as

$$\mathrm{Fr} = u_G\left(\frac{\rho_G}{\rho_L - \rho_G}\frac{\frac{\partial S_L}{\partial h_L}}{S_G}\frac{1}{g\cos\alpha}\right)^{1/2} \tag{2.26}$$

and α is the pipe inclination. Fr_0 is the value at the onset of 2-D waves, i.e. at the transition from stratified-smooth to stratified-wavy flow. Due to the limited set of data on which the correlation was based. Its use for different fluid pairs or flow geometries may lead to appreciable errors.

τ_{WL} was obtained from equation (2.4) using the measured pressure drop and liquid-holdup data and the experimental values for τ_i. The representation of f_L vs. the gas superficial velocity U_G at a given liquid flow rate showed a sharp increase at the onset of 2D waves. However, f_L could well be correlated against Re_L by equation (2.7).

Andritsos & Hanratty (1987) stated that the Taitel and Dukler (1976) model for stratified flow had limitations because of the assumption that drag at the interface, τ_i, was the same as for a flat surface and because the Blasius equation was used to calculate the drag of the wall on the liquid, τ_{WL}. Experiments were therefore performed to determine τ_i and τ_{WL}. These were conducted at atmospheric pressure with horizontal pipelines having diameters of 2.52 and 9.53 cm and with liquid viscosities 1 to 80 cp.

The interfacial stress, τ_i, was calculated from equation (2.5), using measurements of pressure drop, liquid holdup, and the Blasius equation, equation (2.7) for turbulent flow, for f_G. τ_{WL} was calculated from equation (2.4) using experimental data for pressure drop, holdup and τ_i. It was shown that f_i/f_G correlated well with $\Delta h_L/\lambda$ where Δh_L is the amplitude and λ the wavelength of the interfacial waves. Development of this finding led to propose an iterative procedure to calculate frictional pressure losses and h_L/D for stratified flows in horizontal pipelines using the following correlations:

- the equations for f_G from Taitel & Dukler (1976) where the transition from laminar to turbulent flow is defined for Re_G=2000
- for the interfacial friction factor:

$$\frac{f_i}{f_G} = 1 \quad \text{for } U_G \le 5\left(\frac{\rho_{G,atm}}{\rho_G}\right)^{0.5}$$

$$\frac{f_i}{f_G} = 1 + 15\left(\frac{h_L}{D}\right)^{0.5}\left[\frac{U_G}{5}\left(\frac{\rho_G}{\rho_{G,atm}}\right)^{0.5} - 1\right] \quad \text{for } U_G > 5\left(\frac{\rho_{G,atm}}{\rho_G}\right)^{0.5} \tag{2.27}$$

where $\rho_{G,atm}$ is the gas density at atmospheric pressure. $U_G = 5\left(\frac{\rho_{G,atm}}{\rho_G}\right)^{0.5}$ is the superficial gas velocity where large irregular waves appear.

- the liquid wall shear stress τ_{WL} from:

$$\tau_{WL} = \left(\frac{3}{2}\tau_c - \frac{1}{2}\tau_i\right) \Big/ \left(1 - \frac{h_L}{D}\right) \tag{2.28}$$

where τ_c is a characteristic stress in the liquid phase given by:

$$\tau_c = \rho_L\left(\frac{h_L^+ \nu_L}{D}\right)^2\left(\frac{h_L}{D}\right)^{-2} \tag{2.29}$$

where h_L^+ is a dimensionless liquid height given by:

$$h_L^{+} = \left\{ \left(1.082\,\mathrm{Re}_L^{0.5}\right)^5 + \left[0.098\,\mathrm{Re}_L^{0.85} \Big/ \left(1 - \frac{h_L}{D}\right)^{0.5} \right]^5 \right\}^{0.2} \qquad (2.30)$$

A comparison with experimental data showed that the prediction of frictional pressure drop calculated with this model was better than with the Taitel & Dukler (1976) model or than with earlier models.

Kowalski (1987) presented experimental values for the wall and interfacial shear stresses in stratified gas-liquid flow in a horizontal 50.8 mm diameter pipe. Tests for air-water systems were carried out at 2.25 bar and for Freon gas-water flows at 2.25 and 4.2 bar.

The wall shear stresses were measured at different circumferential locations around the pipe, to calculate circumferential average values. Experimental results for f_G agreed reasonably well with equation (2.7) for turbulent flow and with the expression stated in Agrawal et al. (1973):

$$f_G = 0.079\,\mathrm{Re}_G^{-0.25} \qquad (2.31)$$

For wall-to-liquid shear the data were fitted by the following correlation:

$$f_L = 0.263\left[\varepsilon_L\ \mathrm{Re}_L^{+}\right]^{-0.5};\ \ \mathrm{Re}_L^{+} = \frac{U_L D}{\nu_L} \qquad (2.32)$$

where ε_L is the liquid holdup and Re_L^{+} is a Reynolds number based on the liquid superficial velocity and the pipe diameter. The interfacial shear stress was determined in two ways: the first used a combination of the momentum equations, equations (2.4) and (2.5), stated by Taitel & Dukler using experimental values for τ_{WG}, τ_{WL} and void fraction ε_G:

$$\tau_i = \tau_{WL}\frac{P_L}{P_i}\varepsilon_G - \tau_{WG}\frac{P_G}{P_i}\left(1-\varepsilon_G\right) \qquad (2.33)$$

The second method for determining interfacial shear stress was the extrapolation of the gas Reynolds stress profile to the gas-liquid interface. The two methods gave roughly the same results. For wavy stratified flow the following correlation was developed:

$$f_i = 7.5\cdot 10^{-5}\left(1-\varepsilon_G\right)^{-0.25}\left(\mathrm{Re}_G''\right)^{-0.3}\left(\mathrm{Re}_L''\right)^{0.83} \qquad (2.34)$$

for $22600 \le \mathrm{Re}_L'' \le 430600$ and $8800 \le \mathrm{Re}_L'' \le 47800$ with

$$\mathrm{Re}_G" = \frac{u_G D}{\nu_G}; \quad \mathrm{Re}_L" = \frac{u_L D}{\nu_L} \tag{2.35}$$

ε_G is the void fraction. It is to be noted that here that interfacial friction is calculated as a function of the difference between the gas and liquid velocities rather than as a function of the gas velocity only:

$$f_i = \frac{2\tau_i}{\rho_G \left(u_G - u_L\right)^2} \tag{2.36}$$

The presented correlation was in good agreement with Kowalski's data as well as with data from other investigators. For smooth stratified flow the following correlation could be used:

$$f_i = 0.96\left(\mathrm{Re}_G^+\right)^{-0.52}; \ \mathrm{Re}_G^+ = \frac{U_G D}{\nu_G} \tag{2.37}$$

where Re_G^+ is the equivalent of Re_L^+ for the gas phase.

Jayanti (1991) tested three methods for determining interfacial friction, Andritsos & Hanratty (1987), Kowalski (1987) and Sinai (1983), against two independent data sets, which were for air-water flows at near-atmospheric pressure in pipes of fairly large diameters (a hydraulic diameter of 0.13 m for experiments in a rectangular channel and an internal diameter of 0.305 m for experiments in a circular pipe).

This was done by calculating the pressure drop from the gas phase momentum equation, equation (2.5), using the measured liquid height and correlations for interfacial friction and then comparing the prediction against measured pressure drop. For the gas friction factor the standard correlation given by Taitel & Dukler (1976), equation (2.7) for turbulent flow, was used. The reason for using the gas phase momentum equation and not the liquid momentum equation for the analysis was that the prediction of wall shear stress in the gas with the method in Taitel & Dukler (1976) is established whereas for the liquid phase it isn't as was shown e.g. by Kowalski (1987). The Sinai (1983) method was found to yield the best predictions of the data.

Srichai (1994) carried out an experimental study of steady state air-water and air-oil flows on the Imperial College WASP flow facility at pressures of 5, 10 and 15 bar(g).

Liquid holdup and pressure gradient for stratified flow were obtained over the ranges of Reynolds numbers of Re_G = 85840 to 358000 for air, Re_L = 15860 to 73460 for water and Re_L = 112 to 944 for oil. Measured pressure drop was compared with pressure drop calculated from the momentum equations for both phases, equations (2.4) and (2.5), using measured liquid holdup and the suggested relationships for wall and interfacial friction from Taitel & Dukler (1976), Sinai (1983), Kowalski (1987), Andritsos & Hanratty (1987), and Hand (1991). Srichai modified the Hand correlation for interfacial friction to take into account system pressure. The correlation proposed by Andritsos & Hanratty gave a better fit to the data than the others, but it still gave large errors in predicting some of the measured data.

A new correlation was developed based on the experimental data collected by Srichai. For the gas wall friction factor f_G an explicit form of the Colebrook-White formula developed by Eck (1973):

$$f_G = \frac{0.0625}{\left\{\log_{10}\left(\frac{15}{\mathrm{Re}_G} + \frac{k_W / D_G}{3.715}\right)\right\}^2} \qquad (2.38)$$

with a roughness k_W = 0.046 mm yielded the best fit with measured data obtained for single phase air flow. The value found for k_W agreed with tabulated data for roughness of stainless steel, which was the pipe material used in the experiments.

The liquid wall friction factor f_L was expressed as a function of ε_L and Re_L^+ in the manner suggested by Kowalski (1987). The data was best fitted by:

$$f_L = 0.765\left(\varepsilon_L \mathrm{Re}_L^+\right)^{-0.562} \qquad (2.39)$$

For the interfacial friction factor f_i the Sinai method was adopted, equations (2.14) and (2.15), with the difference that the interfacial roughness, k_R, was related to the rms values of the fluctuations in liquid height h_L'

$$\frac{k_R}{D} = 0.1985\left(\frac{h_L'}{D}\right)^{0.0825}$$
$$h_L' = \sqrt{\overline{\left(h_L - \bar{h}_L\right)^2}} \qquad (2.40)$$

where h_L is the instantaneous liquid height and $\bar{h}_L$ the average liquid height. h_L' was found to be a function of the liquid holdup ε_L and Re_G^+, which is the Reynolds

number in the gas phase based on the superficial velocity and the pipe diameter (equation (2.37)):

$$\frac{h_L'}{D} = C_a + C_b\left(\varepsilon_L \mathrm{Re}_G^{+}\right) + C_c\left(\varepsilon_L \mathrm{Re}_G^{+}\right)^2$$

$$C_a = 2.65\cdot 10^{4}\left(\frac{\rho_G}{\rho_L - \rho_G}\right)^{4.517}$$

$$C_b = 8.995\cdot 10^{-10}\left(\frac{\rho_G}{\rho_L - \rho_G}\right)^{-1.22} \qquad (2.41)$$

$$C_c = 1.897\cdot 10^{-13}\left(\frac{\rho_G}{\rho_L - \rho_G}\right)^{-0.925}$$

The coefficients C_a, C_b and C_c take into account the influence of pressure on gas density. The overall predictions of the WASP data by the suggested method were better than those of the others evaluated. The new correlation was also in acceptable agreement with other data reported in the literature.

Spedding & Hand (1997) developed an iterative procedure for the prediction of pressure drop and holdup that incorporated the relationships for the interfacial and wall friction factors suggested by Hand (1991). The gas phase friction factor f_G was calculated using the standard relationship, equation (2.7), suggested by Taitel & Dukler (1976). Because it was under-predicted by the standard formulae used in Taitel & Dukler (1976), the liquid friction factor f_L was calculated as

$$f_L = \frac{24}{\mathrm{Re}_L} \text{ for } \mathrm{Re}_L < 2100$$

$$f_L = 0.0262\left(\varepsilon_L \mathrm{Re}_L^{+}\right)^{-0.139} \text{ for } \mathrm{Re}_L > 2100 \qquad (2.42)$$

with Re_L^{+}, the liquid Reynolds number based on the superficial velocity and the pipe diameter (equation (2.32)).

The interfacial friction factor for air-water systems was calculated as

$$\frac{f_i}{f_{SG}} = 1.76\left(\frac{U_G}{6}\right) + k_i$$

$$k_i = 2.7847\cdot \log_{10}\left(\frac{U_L}{U_L + 6}\right) + 7.8035 \qquad (2.43)$$

where f_{SG} was calculated like f_G, but using the Reynolds number Re_G^{+} based on the superficial gas velocity (equation (2.37)):

$$f_{SG} = \frac{16}{\mathrm{Re}_G^+} \quad \text{for} \quad \mathrm{Re}_G^+ < 2100$$
$$f_{SG} = 0.046\left(\mathrm{Re}_G^+\right)^{-0.2} \quad \text{for} \quad \mathrm{Re}_G^+ > 2100 \tag{2.44}$$

For air-viscous liquid systems the Andritsos & Hanratty (1987) correlations for f_i were suggested.

Predicted pressure drop and liquid holdup were compared with experimental data for air-water stratified flows in pipelines of 0.02515 m ID to 0.0935 m ID obtained by several authors. Predictions were also compared with experimental data for a laminar-turbulent liquid-air system where the liquid phase was a glycerine solution. The model gave good predictions where no interfacial level gradient (see Section 2.2.1.1) was present.

Espedal (1998) made measurements of the shear stresses in the gas and the liquid in a stratified flow at small inclinations. The acrylic test section used had an internal diameter of 60 mm and a length of 18.5 m.

In the gas phase the measured data were best represented by a formula suggested by Biberg (1998) which Espedal modified into an explicit form:

$$\frac{1}{\sqrt{f_G}} = \frac{-3.6\log_{10}\left(\frac{6.9}{\mathrm{Re}_G} + \left(\frac{k_W}{3.7D_G}\right)^{1.11}\right) + 4\log_{10}\left(1+\frac{P_i}{P_G}\right)}{1+4\log_{10}\left(1+\frac{P_i}{P_G}\right)\frac{u_G-u_L}{u_G}\sqrt{f_i}} \tag{2.45}$$

This equation takes into account the two-phase nature of the flow by including the interfacial friction factor. Data for shear stress in the liquid were derived from measured shear stress in the gas, pressure drop and liquid holdup. Of the available models in the literature the relationship suggested in the thesis of Hand (1991), and published by Spedding & Hand (1997), gave the best prediction of the measured liquid shear stress. Espedal developed a new correlation for liquid wall friction which predicted well the data from large amplitude wave experiments:

$$f_L = 0.25\left(1.07 - 7.14\sqrt{0.0225 - 0.0886\,\mathrm{Re}_L^{-0.25}}\right)^2 \tag{2.46}$$

Espedal obtained data for interfacial friction from the one-dimensional momentum equation for the gas phase, equation (2.5), using measured gas wall shear stress, pressure drop and liquid holdup. Of the existing models in the literature, the best

predictions for the experimental data were found with the Hand (1991) and Andreussi & Persen (1987) correlations.

The method of evaluating interfacial shear stress from the gas phase momentum equation, equation (2.5), using measured gas wall shear stress, pressure drop and liquid holdup, and of evaluating liquid wall shear stress from the liquid momentum equation, equation (2.4), using the obtained data for interfacial shear stress, liquid holdup and pressure drop is linked with a considerable experimental uncertainty. Newton & Behnia (1998) found that the uncertainty can go up to 40%. This has to be accounted for when using correlations for interfacial and liquid wall friction which are derived from measurements of gas wall shear stress, liquid holdup and pressure drop.

2.3.2 Transient Stratified Flow

The one-dimensional two-fluid model for steady state conditions presented in the previous section follows from a simplification of the one-dimensional model for the transient situation. The general form of the model for the transient case was stated in Hewitt (1982). Assuming that mass transfer between the phases is negligible the following set of equations is obtained for a horizontal stratified flow:

$$\frac{\partial}{\partial t}\left(S_G \rho_G\right) + \frac{\partial}{\partial x}\left(S_G \rho_G u_G\right) = 0 \tag{2.47}$$

$$\frac{\partial}{\partial t}\left(S_L \rho_L\right) + \frac{\partial}{\partial x}\left(S_L \rho_L u_L\right) = 0 \tag{2.48}$$

$$\frac{\partial}{\partial t}\left(S_G \rho_G u_G\right) + \frac{\partial}{\partial x}\left(S_G \rho_G u_G^2\right) + S_G \frac{\partial p_G}{\partial x} = -\tau_i P_i - \tau_{WG} P_G \tag{2.49}$$

$$\frac{\partial}{\partial t}\left(S_L \rho_L u_L\right) + \frac{\partial}{\partial x}\left(S_L \rho_L u_L^2\right) + S_L \frac{\partial p_L}{\partial x} = \tau_i P_i - \tau_{WL} P_L \tag{2.50}$$

The first two equations are the mass conservation equations, the remaining two equations the momentum conservation equations. The first term in the momentum equations is the time rate of change of momentum per unit volume, the second term is the convective transport of momentum per unit volume. The remaining terms account for the influence of the pressure gradient and the viscous stresses.

If it is assumed that the fluid properties do not change along the pipe the set of equations can further be simplified:

$$\frac{\partial S_G}{\partial t} + \frac{\partial}{\partial x}\left(S_G u_G\right) = 0 \tag{2.51}$$

$$\frac{\partial S_L}{\partial t} + \frac{\partial}{\partial x}\left(S_L u_L\right) = 0 \tag{2.52}$$

$$\rho_G \frac{\partial}{\partial t}\left(S_G u_G\right) + \rho_G \frac{\partial}{\partial x}\left(S_G u_G^2\right) + S_G \frac{\partial p_G}{\partial x} = -\tau_i P_i - \tau_{WG} P_G \tag{2.53}$$

$$\rho_L \frac{\partial}{\partial t}\left(S_L u_L\right) + \rho_L \frac{\partial}{\partial x}\left(S_L u_L^2\right) + S_L \frac{\partial p_L}{\partial x} = \tau_i P_i - \tau_{WL} P_L \tag{2.54}$$

Contrary to steady state flow all the flow parameters, i.e. the phase velocities, the fluid-wall and interfacial shear stresses, pressure drop, and liquid holdup change with time and location along the pipe, and so do the geometrical quantities, S_G, S_L, P_G, P_L, P_i, which are all functions of the liquid height as stated in equations (2.9) to (2.13). As there are no transient models for the shear stresses available steady state models (see Section 2.3.1) are used. The one-dimensional two-fluid model has been widely used in transient simulations. Commercial software packages (OLGA, PLAC) are coded on the basis of this model. Some studies which used the one-dimensional two-fluid model for simulations of transient stratified flow are reviewed here and modifications to the basic equations presented above are discussed.

Taitel et al. (1978) introduced a two-fluid model for prediction of flow patterns in transient flows (see Section 2.2.2). In the liquid phase they used the above mass conservation equation for constant physical properties, equation (2.52), but they modified the momentum equation (2.54) to include a term which accounted for the gravitational influence of the liquid level and assumed that the pressure drop was the same in both phases:

$$\rho_L \frac{\partial}{\partial t}\left(S_L u_L\right) + \rho_L \frac{\partial}{\partial x}\left(S_L u_L^2\right) + S_L \frac{\partial p}{\partial x} + S_L \rho_L g \frac{\partial h_L}{\partial x} = \tau_i P_i - \tau_{WL} P_L \tag{2.55}$$

The Taitel & Dukler (1976) methodology was used to calculate the geometrical parameters S_L, S_G, P_i, P_L, P_G, the hydraulic diameters D_L, D_G, and the wall and interfacial shear stresses. For the gas phase quasi-steady state flow was assumed since the gas velocity was much greater than that of the liquid, and since gas flow rate changes were propagated down the pipe very rapidly compared to the liquid. This resulted in a constant mass flow rate and in a simplified momentum equation:

$$S_G u_G \rho_G = const = \dot{M}_G \tag{2.56}$$

$$\rho_G \frac{\partial (u_G^2 S_G)}{\partial x} = -\tau_{WG} P_G - \tau_i P_i - S_G \frac{\partial p}{\partial x} \tag{2.57}$$

The continuity and momentum equations of both phases were combined into two simultaneous partial differential equations for $h_L(x,t)$ and $u_L(x,t)$:

$$\left[g - \frac{\rho_G}{\rho_L} \left(\frac{\dot{M}_G}{\rho_G S_G} \right)^2 \frac{S_L'}{S_G} \right] \frac{\partial h_L}{\partial x} + \frac{\partial u_L}{\partial t} + u_L \frac{\partial u_L}{\partial x} = -\frac{\tau_{WL} P_L}{\rho_L S_L} + \frac{\tau_i P_i}{\rho_L} \left(\frac{1}{S_L} + \frac{1}{S_G} \right) + \frac{\tau_{WG}}{\rho_L} \frac{P_G}{S_G} \tag{2.58}$$

$$\frac{\partial h_L}{\partial t} + u_L \frac{\partial h_L}{\partial x} + \frac{S_L}{S_L'} \frac{\partial u_L}{\partial x} = 0 \tag{2.59}$$

The derivative of the cross sectional area filled by the liquid S_L' was found by differentiating the expression for S_L, equation (2.9):

$$S_L' = \frac{\partial S_L}{\partial h_L} = 2R \sqrt{1 - \left(\frac{h_L}{R} - 1 \right)^2} \tag{2.60}$$

The Bernoulli term

$$\frac{\rho_G}{\rho_L} \left(\frac{\dot{M}_G}{\rho_G S_G} \right)^2 \frac{S_L'}{S_G} \tag{2.61}$$

was negligible compared to gravity which simplified the momentum equation (2.58):

$$g \frac{\partial h_L}{\partial x} + \frac{\partial u_L}{\partial t} + u_L \frac{\partial u_L}{\partial x} = -\frac{\tau_{WL} P_L}{\rho_L S_L} + \frac{\tau_i P_i}{\rho_L} \left(\frac{1}{S_L} + \frac{1}{S_G} \right) + \frac{\tau_{WG}}{\rho_L} \frac{P_G}{S_G} \tag{2.62}$$

The resulting set of equations, equations (2.59) and (2.62), was solved using finite-difference technique. For the solution procedure a new parameter, called the critical velocity $u_{L,crit}$, was introduced:

$$u_{L,crit} = \sqrt{g H_L} \quad \text{where} \quad H_L = S_L / S_L' \tag{2.63}$$

The solution procedure depended on if the flow was subcritical ($u_L < u_{L,crit}$) or supercritical ($u_L > u_{L,crit}$).

Sakaguchi et al. (1981) developed a further transient two-fluid model for comparison with their experimental results (see Section 2.2.2) and the model predictions agreed qualitatively with the experiments. The model equations were similar to the general

equations for constant fluid properties, equations (2.51) to (2.54), but the analysis was carried out for a rectangular rather than a circular channel.

The set of four equations, two continuity and two momentum conservation equations, was then reduced to a set of two equations in a fashion similar to that in Taitel et al. (1978). To simplify the equations an order of magnitude analysis was carried out based on the conditions for the experiments and the negligible terms in the equations were deleted.

The resulting equations were solved numerically. The boundary conditions at the inlet of the channel were the gas and liquid flow rate. The wall shear stresses in the gas and the liquid were expressed as functions of friction factors in the same way as in Taitel & Dukler (1976). The friction factors in the gas and the liquid were standard friction factors used in the steady state situation, for turbulent flow:

$$f_G = 0.079\,\mathrm{Re}_G^{-0.25}$$
$$f_L = 0.079\,\mathrm{Re}_L^{-0.25} \qquad (2.64)$$

as used by Agrawal et al. (1973), and for laminar flow:

$$f_G = 16/\mathrm{Re}_G$$
$$f_L = 16/\mathrm{Re}_L \qquad (2.65)$$

as used by Taitel & Dukler (1976).

Interfacial shear stress was expressed as a function of the relative velocity between the liquid and the gas rather than of the gas velocity only using equation (2.36) stated by Kowalski (1987). The interfacial friction factor f_i used was not specified.

Taitel et al. (1989) further simplified the model presented by Taitel et al. (1978) in order to provide an easy to use tool for predicting transient gas-liquid flows in pipelines.

The mass continuity equations in both phases were those used by Taitel et al. (1978), equations (2.52) and (2.56), i.e. assuming quasi-steady state for the gas but not for the liquid. For the momentum equations they assumed local equilibrium, i.e. equilibrium at each point in the pipe, that is, in the numerical solution procedure, at each computational grid point. The momentum equations were flow pattern dependent and for horizontal stratified flow the resulting set of equations for both phases would be that given in Taitel & Dukler (1976), equations (2.4) and (2.5). In

these momentum equations Taitel et al. (1989) only modified the fluid-wall friction factors and the interfacial friction factor, and interfacial shear stress was calculated as a function of the difference between the gas and liquid phase velocities, using equation (2.36). The friction factors in the gas and the liquid were calculated using a relationship from Hall (1957):

$$f_G = 0.001375\left[1+\left(2\cdot 10^4\,\frac{k_W}{D_G}+\frac{10^6}{\mathrm{Re}_G}\right)^{1/3}\right]$$
$$f_L = 0.001375\left[1+\left(2\cdot 10^4\,\frac{k_W}{D_L}+\frac{10^6}{\mathrm{Re}_L}\right)^{1/3}\right] \qquad (2.66)$$

where k_W was the pipe roughness and D_G, D_L the hydraulic diameters and Re_G, Re_L the Reynolds numbers used in Taitel & Dukler (1976). The interfacial friction factor was a constant value

$$f_i = 0.0142 \qquad (2.67)$$

suggested by Cohen & Hanratty (1968). The model was used to simulate a hypothetical pipeline. No comparison against field data was made.

Sharma & Brill (1993) used a two-fluid model for simulating transient stratified flows in pipelines which was very similar to the general model presented by Hewitt (1982). The mass conservation equations were identical with equations (2.47) and (2.48). The momentum conservation equations (2.49) and (2.50) were slightly modified to account for the interfacial pressure in the momentum equations of both phases. The resulting momentum equations then became:

$$\frac{\partial}{\partial t}\left(S_G\rho_G u_G\right)+\frac{\partial}{\partial x}\left(S_G\rho_G u_G^2\right)+S_G\frac{\partial p_G}{\partial x}+\left(p_G-p_i\right)\frac{\partial S_G}{\partial x}=-\tau_i P_i-\tau_{WG}P_G \qquad (2.68)$$

$$\frac{\partial}{\partial t}\left(S_L\rho_L u_L\right)+\frac{\partial}{\partial x}\left(S_L\rho_L u_L^2\right)+S_L\frac{\partial p_L}{\partial x}+\left(p_L-p_i\right)\frac{\partial S_L}{\partial x}=\tau_i P_i-\tau_{WL}P_L \qquad (2.69)$$

The Taitel & Dukler (1976) methodology was used to calculate the geometrical parameters S_L, S_G, P_i, P_L, P_G, the hydraulic diameters D_L, D_G, the wall shear stresses τ_{WG} and τ_{WL} and the wall and interfacial friction factors. Only the interfacial shear stress term τ_i was modified and expressed as a function of the relative velocity between the two phases rather than just the gas velocity using equation (2.36).

The gas density was calculated from the equation of state and the liquid was assumed to be incompressible. Interfacial pressure was expressed as being different from the bulk fluid pressures by an amount which represented the gravitational head of the fluid

$$p_L - p_i = \rho_L g h_L$$
$$p_G - p_i = -\rho_G g(D - h_L) \qquad (2.70)$$

The expression for the difference between the pressure in the liquid and at the interface in equation (2.70) is a simplification of the expression stated by Black (1987). The model equations were then numerically solved. The steady state form of the gas phase momentum equation, equation (2.5), and the stratified flow variables predicted from the Taitel & Dukler (1976) model were used as initial conditions. At the inlet of the pipe gas and liquid flow rates were specified, at the outlet pressure was fixed.

The prediction from the simulator was compared with data for a high pressure wet gas condensate pipeline, which had a length of 67 miles and a diameter of 20 inches. The predictions differed greatly from the data. One of the problems was the difference between the measured and predicted pressure at the outlet of the pipe. However, the simulator predicted the general trends of transient responses expected with the type of boundary conditions simulated.

Minami & Shoham (1994) adopted the model suggested by Taitel et al. (1989). They found that the steady state flow pattern criteria were not adequate for transient conditions and therefore developed a new flow pattern prediction method. The method was based on the stability of the slug flow structure. It started from assuming that the slug flow pattern would exist and all the slug flow characteristics were determined using appropriate slug flow equations. The analysis of these characteristics defined the existing flow pattern. With the new flow pattern prediction method the stratified to slug transition occurred at much lower liquid flow rates than in the steady state model developed by Taitel & Dukler (1976).

Minami & Shoham solved their model numerically and compared its predictions with transient experiments, which was described in Section 2.2.2. The simulated results matched the experimental data very well for most of the test runs. The assumption of a quasi-steady state in the gas phase resulted in over-prediction of the measured

pressure drop in transients produced from an increase in the gas flow rate. This behaviour was not observed for transients produced from a change in the inlet liquid flow rate. Unsatisfactory predictions only occurred for liquid blow down tests where the flowing conditions were very close to the stratified to slug flow pattern boundary.

For modelling the stratified wavy to slug transition in transient flows in slightly inclined pipes Grolman & Fortuin (1996) mainly followed the terminology introduced by Taitel et al. (1978). The main modifications to their set of equations was the inclusion of changes in the gas-phase dynamic pressure (Bernoulli effects), the incorporation of a liquid-phase velocity profile factor and the equations used for the frictional contributions to the loss of momentum. The gas phase friction factor f_G was calculated using the formula by Eck (1973) for a smooth pipe:

$$f_G = \frac{0.07725}{\left\{\log_{10}\left[\mathrm{Re}_G / 7\right]\right\}^2} \tag{2.71}$$

The interfacial friction factor f_i was determined from an empirical algorithm based on experimental data for steady state. The liquid phase friction factor f_L for turbulent flow ($\mathrm{Re}_L \geq 2100$) was obtained from the relationship used in Hart et al. (1989), who studied the prediction of pressure gradient and liquid holdup in horizontal pipes with small liquid holdups. For laminar conditions ($\mathrm{Re}_L < 2100$) Grolman & Fortuin modified the formula by Hart et al. The resulting set of equations was numerically solved starting from a steady state situation. The agreement of the model predictions with transient experiments was good.

2.4 1D Codes

One-dimensional models have been widely used in computer codes to simulate transient gas-liquid flows. Several computer codes of this type were used in the present study to compare their predictions with experimental data. The codes are described in the following subsections. Three commercially available codes were used, PLAC, OLGA and TACITE, and also two non-commercial codes, PRESBAL and TRIOMPH, which were developed at Imperial College. Two types of one-dimensional model are used in these codes: the two-fluid model and the drift-flux model. The two-fluid model consists of writing separate mass and momentum

conservation equations for each phase of the form represented by equations (2.47) to (2.50) in this chapter. To close the system of equations suitable closure laws for the wall and interfacial shear stress terms in the momentum equations have to be defined. The drift-flux model consists of separate mass conservation equations and one mixture momentum equation instead of two separate momentum equations as in the two-fluid model. The system of equations is closed with a drift flux closure (Bouré, 1997).

2.4.1 Commercial Codes

As part of the present study, the following codes were made available by their vendors on a confidential basis:

PLAC (AEA Technology plc)

OLGA (IFE/Scandpower)

TACITE (IFP)

The codes were made available on the understanding that results obtained using them would not be specifically ascribed to a given code. The objective, therefore, is not to assess the performance of any given code but, rather, to evaluate in an overall sense the performance of these widely-used group of codes in predicting transient stratified flows. The codes are labelled Code 1, Code 2 and Code 3 but this numerical order does not necessarily correspond to the above order or to, say, alphabetical order! Brief descriptions of the codes are given below, based on published information about them.

2.4.1.1 PLAC (Version 5.3)

The Pipe Line Analysis Code (PLAC) is a code for modelling transient two-phase gas-liquid flows (PLAC User Guide, 1996). It was developed from TRAC (Transient Reactor Analysis Code) which was used to model flow transients in nuclear reactors. PLAC solves a set of six equations of a one-dimensional two-fluid model consisting of the mass, momentum and energy conservation equations for the separate phases. Flow pattern maps and flow pattern-dependent closure relationships are implemented

in the code. The code is semi-implicit and uses a finite difference scheme in the numerical solution procedure.

Fluid properties are calculated from a user-specified composition of the fluid using a PVT package built into PLAC. The pipe geometry can be set up of a number of components such as pipes, tees and valves. Boundary conditions can be specified with two different components: the BREAK component to set pressure boundary conditions and the FILL component to set flow rate boundary conditions.

A PLAC simulation includes three steps: the flow problem is translated into an input file using the PLAC preprocessor. The problem is then solved using the PLAC solver. The simulation generates a graphics file which can be used for visualisation of the results in the PLAC postprocessor, a text file with the results of the various flow parameters and a dump file which can be used for restarting the simulation.

PLAC version 5.3 is now superseded by a new software PROFES which has not been used in the present study.

2.4.1.2 OLGA (Version 3.4)

OLGA is a dynamic one-dimensional modified two-fluid extended model for calculation of two-phase hydrocarbon flow in pipelines and pipeline networks (OLGA User Course, 1997). The set of equations in the OLGA model consists of separate continuity equations for the gas, hydrocarbon liquid film, water film, hydrocarbon liquid droplets and water droplets and two momentum equations, one for the gas and possible liquid droplets, and a separate one for the liquid film. The difference between the velocities of the hydrocarbon film and the water film is calculated from a steady state force balance. The velocity of any entrained liquid droplets in the gas phase is given by a slip relation. It is assumed that hydrocarbon droplets and water droplets have the same velocity. A mixture energy conservation equation is included in the model. Flow pattern-dependent closure relationships are implemented in the code. A finite difference method is used for numerical solution of the model equations. The OLGA code has been extensively tested against experimental and field data.

Fluid properties are calculated from a user-specified composition of the fluid using a PVT package built into OLGA. Boundary conditions can be specified either with fixed pressure or flow rates. Also, initial conditions have to be set for the simulation.

An OLGA simulation includes the following steps: A separate file containing the fluid properties has to be generated using the PVT package in OLGA. The flow problem is then translated into an input file using the OLGA preprocessor. The problem specified by the input and fluid properties files is solved using the OLGA solver. The simulation generates a graphics file which can be used for visualisation of the results in the OLGA postprocessor, a text file with the results of the various flow parameters and a dump file which can be used for restarting the simulation.

OLGA version 3.4 is now superseded by a new code OLGA 2000 which has not been used in the present study.

2.4.1.3 TACITE (Version 4.097)

TACITE is a one-dimensional code which is used to simulate two-phase gas-liquid transient flows in pipelines. It is based on the numerical resolution of a drift-flux type model (Pauchon et al., 1993). The model solves a set of four conservation equations, one for the mass of each phase, one for the mixture momentum and one for the mixture energy. To close the system of equations a separate equation for steady state is incorporated which contains information about the slip between the phases. For separated flow this is a macroscopic momentum balance. Two basic flow patterns are implemented in the code: separated flow (stratified and annular) and dispersed flow. All other flow patterns are expressed as combinations of these two flow patterns. The code has been tested against field data. Boundary conditions are for fixed flow rates at the inlet and for fixed pressure at the pipe outlet.

Data input is specified in seven separate files (Heintzé, 1997): one for the pipe topology, one for the components of the flow line (pipe, inlet, outlet, valve), one for the thermal properties of the flow device, of the fluids and of the environment, one for the spatial discretisation, one for the fluid properties, one for the simulation scenario (including boundary conditions) and one for the output.

TACITE version 4.097 is now superseded by version 4.1 which has not been used in this study.

2.4.2 PRESBAL Code

PRESBAL is a one-dimensional code developed by Khor (1998) at the Department of Chemical Engineering at Imperial College, London. The code is a test bed for closure relationships and it was used to investigate the performance of existing closure relationships in two- and three-phase stratified flow. Two versions of the code exist: one version which is used for calculation of three-phase gas-liquid-liquid stratified flows and one for calculation of two-phase gas-liquid stratified flows. In the present study the two-phase version was used for comparison with steady state experimental data. The code uses the basic one-dimensional two-fluid model for steady state represented by equations (2.4) and (2.5). The set of equations is solved by adjusting the liquid height h_L in steps of $0.00001D$ in the range $0.002D \le h_L \le 0.95D$ until the lowest difference between the pressure gradients in both phases is obtained in the iterative solution procedure. The input data required for calculation of horizontal flow are the superficial velocities, fluid physical properties, interfacial surface tension, pipe diameter and roughness.

For the current study the wall friction factors in the gas and the liquid, f_G and f_L respectively, were calculated from the expression developed by Eck (1973) which was used by Srichai (1994) for the gas phase:

$$f_r = \frac{0.0625}{\left\{\log_{10}\left(\frac{15}{\mathrm{Re}_r} + \frac{k_W / D_r}{3.715}\right)\right\}^2} \tag{2.72}$$

where index r is G or L respectively. The interfacial friction factor f_i was calculated using the methodology by Sinai (1983). Unlike in the methodology developed by Taitel & Dukler (1976) for steady state flows the hydraulic diameters in both phases were calculated for a closed duct:

$$D_r = \frac{4S_r}{P_r + P_i} \tag{2.73}$$

where r is the phase index G or L.

2.4.3 TRIOMPH Code

TRIOMPH is a one-dimensional code developed at the Department of Mechanical Engineering at Imperial College (Issa & Abrishami, 1986). The advantage of the code

is that the computational domain can be subdivided into a much larger number of nodes and therefore much shorter cells than in commercial codes. The governing equations are the two mass and the two momentum equations of the one-dimensional two-fluid model. The liquid is taken to be incompressible, whereas the gas is treated as compressible by employing the perfect gas equation. The flow is assumed to be isothermal. Boundary conditions are a flow rate boundary at the pipe inlet and a pressure boundary at the outlet. The finite volume method is used for the numerical solution.

A number of closure relationships for interfacial and wall shear stress are implemented in the code. For simulations of the turbulent flows in the present study the gas wall friction factor was expressed by equation (2.31) which had also been used by Agrawal et al. (1973). The hydraulic diameters in the gas and liquid phases, D_G and D_L respectively, were expressed for open-channel flow:

$$D_r = \frac{4S_r}{P_r} \tag{2.74}$$

where r is the phase index G or L respectively. The interfacial friction factor f_i was calculated from an expression identical in structure to that for the gas wall friction factor but in terms of a Reynolds number based on the slip velocity between the phases, the gas density and viscosity and a hydraulic diameter D_i for the interface:

$$D_i = \frac{4S_G}{P_G + P_i} \tag{2.75}$$

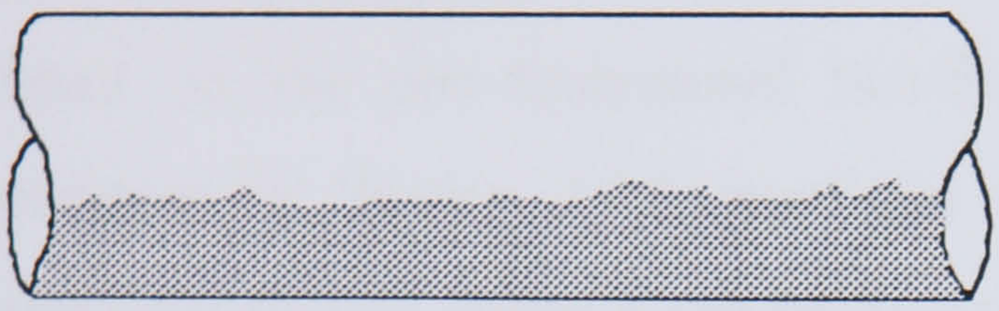
The liquid wall friction factor f_L was calculated with the model by Spedding & Hand (1997) (equation (2.42)).



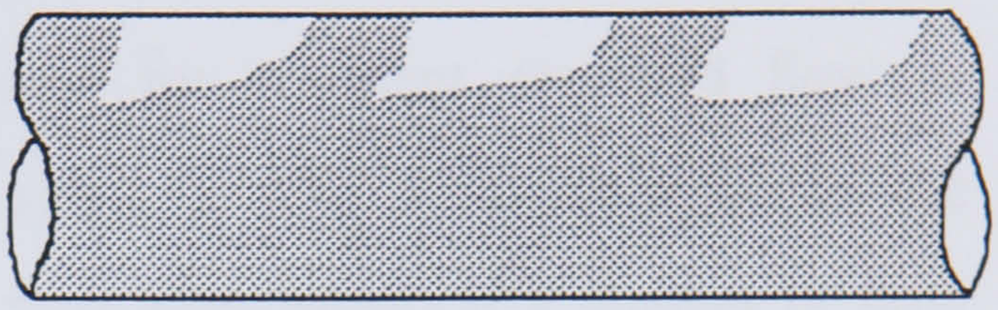
stratified flow



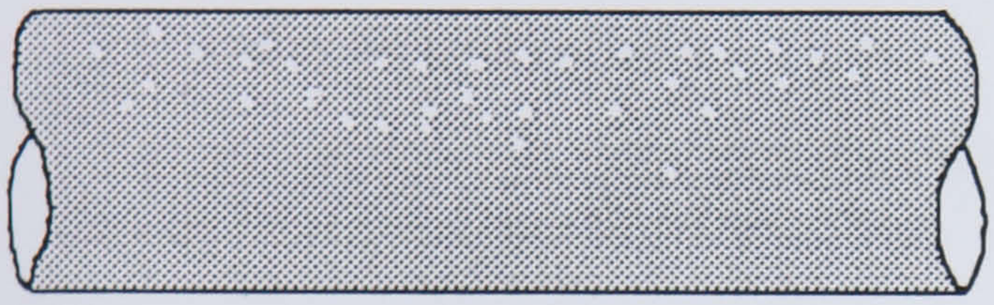
annular-dispersed flow



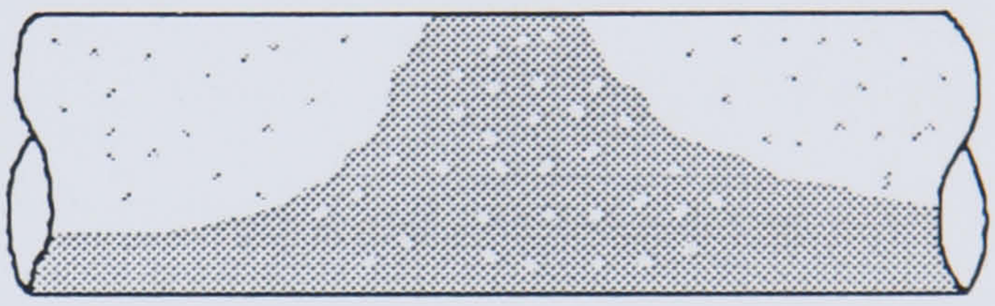
stratified-wavy flow



plug flow



dispersed-bubble flow



slug flow

Figure 2.1 Flow patterns in horizontal flow

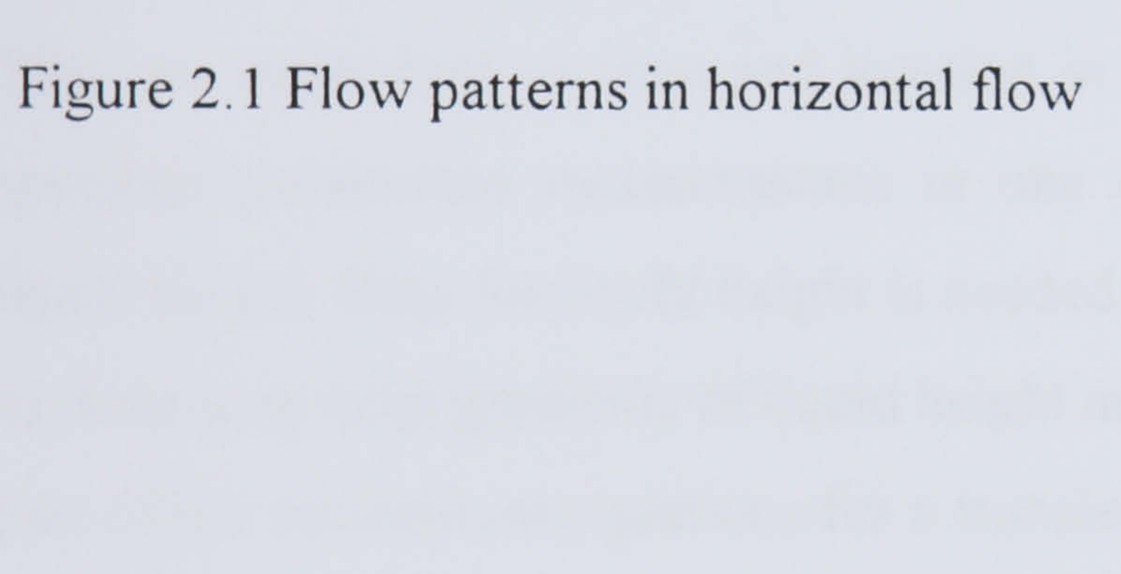


Figure 2.2 Stratified flow in a horizontal pipe

Chapter 3

Experimental Methods

3.1 Introduction

Based on the one-dimensional two-fluid model for transient stratified flow as presented in Section 2.3.2 interfacial shear stress τ_i and as a consequence the interfacial friction factor f_i can be determined from experiments if a number of flow parameters are measured. These are:

- pressure drop dp/dx
- average phase velocities u_G and u_L
- liquid height h_L
- wall shear stresses τ_{WG} and τ_{WL}

They are dependent on time and location in the pipe in a transient flow. For all the specified parameters measurements in one axial location are sufficient except for liquid height. Data for liquid height is needed at two positions along the pipe in order to determine axial gradients of liquid height and of other flow parameters, which form part of the momentum equations for a transient stratified flow. As the structure of the interface is important in the determination of interfacial friction it is useful to additionally record the interfacial characteristics in a cross section of flow. Figure 3.1 represents graphically the parameters to be measured.

The experimental programme for the present study concentrated on measuring the specified parameters simultaneously under steady state and transient conditions. A series of experiments was carried out at atmospheric pressure in a low pressure air-water facility. The practical relevance of this flow facility is limited due to its small length-to-diameter ratio of ~108 and it was therefore used mainly with the intention of validating the experimental techniques. However, a large quantity of data for both steady state and transient flows was obtained from this rig. A further series of experiments was carried out in the Imperial College WASP facility. This flow facility has much more practical relevance than the low pressure rig as its length-to-diameter ratio is much larger, ~470, and it can operate at pressures above atmospheric.

This chapter starts with a review of experimental techniques for measuring the above specified variables (Section 3.2). The review serves as a basis to evaluate the experimental methods to be adopted for this study. The chapter then describes the chosen methods and their implementation in an experimental setup (Sections 3.3 and 3.4). This is followed by a description of the flow facilities used (Section 3.5). Sections 3.6 and 3.7 report on the methods to evaluate fluid properties and on the use of one type of experimental technique, the hot-wire anemometry technique. In Section 3.8 an experimental matrix is presented which was produced to define the range of flow conditions for the experiments of steady state and transient stratified flow. Section 3.9 is devoted to the validation and calibration of the adopted measuring techniques. Section 3.10 describes how local measurements of velocities and liquid heights were transformed into phase average parameters. Section 3.11 reports on the reliability of the various measuring techniques in the two-phase experiments and the consequences for analysis of the data in Chapters 4 and 5.

3.2 Review

Existing experimental methods for measuring wall shear stresses, phase velocities, pressure drop and liquid height (including interfacial structure) were studied in order to evaluate appropriate measuring techniques for the present project.

3.2.1 Wall Shear Stress

Several experimental methods exist for measuring wall shear stress in two-phase flow. The three main types of technique, balancing methods, heat and mass transfer methods and impact probe methods, were reviewed by Hewitt (1978).

In the balancing methods, the total force exerted by the fluid on the channel wall is measured by allowing the whole or part of the channel to 'float' and to measure the force on it. This technique, however, can only operate where the fluid adjacent to the wall is likely to be liquid (e.g. annular flow).

Heat and mass transfer methods are more common for measuring wall shear stress. They are suitable when a localised and continuous measurement of shear stress is required.

In the heat transfer method the shear stress is related to the transfer of heat from a heated film to the fluid. This method has been widely used in two-phase flow. Martin & Whalley (1983), Owen (1986), Govan et al. (1989) and Wolf (1995) employed it to measure liquid wall shear stress in annular gas-liquid flow. Kowalski (1987), Hagiwara et al. (1989), Vlachos et al. (1993), Langsholt et al. (1997) and Espedal (1998) used it for measuring gas and liquid wall shear stresses in stratified gas-liquid flow.

The most commonly used mass transfer technique is the electrochemical method; the mass transfer coefficient is determined for the transport of ions in an electrochemical, conveniently a redox reaction with one of the electrodes built in the wall. This mass transfer coefficient can be related to the liquid wall shear stress. This method has recently been used by Rosant (1994) and Langsholt et al. (1997) for measurements of liquid wall shear stress in stratified flow.

In impact probe methods the velocity profile near the wall is determined by measuring the impact pressure on Preston or Stanton tubes. The shear stress is derived from the measured velocity profile. For this method it is important that the fluid film along the wall is thick compared with the size of the probe. This method was used by Kordyban (1974), Fabre et al. (1981b) and Espedal (1998) for measuring gas wall shear stress in stratified flow.

Of these techniques the heat transfer method was found to be the most practicable solution for this study. Therefore some sources using this technique in stratified gas-liquid flow are reviewed in more detail.

Kowalski (1987) measured the wall shear stresses in the gas and the liquid phases using two flush-mounted hot-film probes, one at the top and one at the bottom of the test section. Experiments were carried out in air-water flows at a pressure of 2.25 bar, and Freon gas-water flows at pressures of 2.25 and 4.20 bar. The probes and the anemometer used were commercially available from Thermo-Systems Inc. (TSI). By rotating the test section around in small steps the wall shear stresses in both phases were measured at different circumferential locations around the pipe.

Hagiwara et al. (1989) used a hot-film sensor flush-mounted at the bottom of the inner wall of an acrylic tube for measurement of liquid wall shear stress. Experiments were carried out in an air-water flow at atmospheric conditions. The hot-film probe

was commercially available, manufactured by TSI Inc. Its sensing element was made of a thin platinum film with dimensions of 1.0 mm x 0.25 mm and coated with a layer of epoxy resin. The hot-film probe was operated by a Kanomax hot-wire anemometer.

Vlachos et al. (1993) used a hot-film probe to measure liquid wall shear stress at two circumferential positions in the liquid film, at 0° and 45° from the pipe bottom. The sensors used were type 55R46 flush-mounted probes manufactured by Dantec Ltd. Its sensing element had a size of 0.2 mm x 0.7 mm and it was protected by a 2 μm quartz coating.

Langsholt et al. (1997) measured wall shear stress in the liquid with a hot-film probe flush-mounted at the bottom of the acrylic test section. The test fluids for the experiments were water and the dense gas sulphur hexafluoride and the system pressure was up to 10 bar. They used the same hot-film probe as Vlachos et al. (1993). The probe was operated by a linearised, constant temperature anemometry system. The measurements with the hot-film probe were backed up with measurements using an electrochemical method, and the results of the two methods were in good agreement.

Espedal (1998) measured the wall shear stress in the liquid at different circumferential positions around the pipe. The type of hot-film probe used was identical with the one in Vlachos et al. (1993). The probe was operated with an anemometer box from TSI Inc. Espedal also tried to use the hot-film probe in the gas phase but abandoned it in favour of the impact probe method.

3.2.2 Phase Velocity

For measuring phase velocities in gas-liquid separated flows three main methods have been used: Pitot tubes, laser Doppler anemometry and hot-wire anemometry.

A Pitot tube determines fluid velocity from the difference between the total and the static pressure in the flow. Pitot tubes were used in studies of steady state stratified flow by Andreussi & Persen (1987), Kang & Kim (1993) and Strand (1993) for measurements in the gas phase. The Pitot tubes were fixed to traversing mechanisms so that it was possible to measure velocity profiles.

Laser Doppler anemometry (LDA) was used by Fabre et al. (1981a), Strand (1993), Paras & Karabelas (1992) to measure liquid velocity. Paras et al. (1998) used LDA for measurements in the gas phase. The principle of operation of this method is based on the Doppler phenomenon, in which the frequency of the scattered light from a moving object differs from that of the incident beam by a value proportional to the velocity of the body. In a moving fluid stream, a particle intercepting a laser beam scatters light which is slightly shifted in frequency by the Doppler effect, depending upon the particle velocity. This change in frequency is detected and related to the flow velocity. LDA is a non-intrusive measuring technique but it requires solid particles added to the fluid for scattering the light. Laser Doppler anemometry is very expensive and difficult to use.

Hot-wire or hot-film probes have also been used for velocity measurements in stratified flow. The difference between the probes is that in hot-wire probes the tiny heated wire (e.g. a Pt-plated Tungsten wire) is unprotected and in direct contact with the fluid, whereas in hot-film probes the metal film is protected by a film of another material, e.g. quartz. Hot-film probes are usually more robust than hot-wires. Hot-wire probes are therefore used in gases only whereas hot-film probes are used in both gases and liquids. With their protection layer on the metal film, hot-film probes are also applicable in conducting liquids. The simplest of these probes are single sensor probes which allow measurement of one velocity component at a time, e.g. the streamwise velocity component. There are more complex probes, incorporating two or three sensors, which then allow simultaneous measurement of two or three velocity components.

Velocity measurements in stratified air-water flows using hot-wire anemometry were reported by Sakaguchi et al. (1973), Fabre et al. (1981a), Sakaguchi et al. (1981), Hagiwara et al. (1989), Murata et al. (1991) and Rosant (1994). In all these studies hot-wire probes were used for measurement of gas velocity. Only Rosant used hot-film probes for measuring the velocities in both phases. The probes were usually fixed to traversing mechanisms to allow the measurement of velocity profiles rather than velocities at one point only.

Of the above methods hot-wire anemometry was considered the most advantageous for the present study. On the one hand it is to be preferred to the Pitot tube method

because it can record data over a large range of frequencies (up to several kHz), on the other hand it is cheaper and easier to use than laser Doppler anemometry.

The use of hot-wire anemometry for velocity measurements in stratified gas-liquid flows is usually reported in less detail than the use of this method for wall shear stress measurement. Only two of the published papers, Hagiwara et al. (1989) and Murata et al. (1991), give detailed descriptions.

Hagiwara et al. (1989) used a hot-wire probe for measurement of gas velocity. The test fluids were air and water at atmospheric pressure. The probe was a 5μm diameter wire and it was fixed to a traversing mechanism. The probe was operated by a Kanomax anemometer.

Murata et al. (1991) used a hot-wire probe for measurement of the gas phase velocity and a hot-film probe for measurement of the liquid velocity. The test fluids used were air and water at atmospheric pressure. The probes were fixed to traversing mechanisms. Commercially available probes were used; the hot-wire probe was supplied by Kanomax, the hot-film probe by TSI Inc. The anemometers used were manufactured by Kanomax.

3.2.3 Pressure Drop

In principle there are two different ways of measuring the pressure difference between two locations in a flow: either by using two separate absolute pressure transducers connected to the system and recording the difference between their simultaneous readings or by using a device which can directly measure pressure differences.

Two types of devices for measuring pressure differences exist: mechanical and electronic devices. Mechanical devices are inclined manometers and micro-manometers. They can measure small pressure differences accurately (down to fractions of 1 mm water). Their disadvantage is that the readings cannot be recorded on-line on a data acquisition system. Electronic devices are also known as DP cells. Their electronic output is usually fairly fast (100 Hz) and they can be connected on-line to data acquisition. DP cells are much more suitable for time-dependent flows than mechanical devices.

When absolute pressure transducers are used two transducers can be connected directly to the two pressure tappings between which the pressure drop has to be

measured. But with this arrangement the accuracy of the pressure difference is determined by the accuracy of the transducers, which in the best case is about 0.1% of their full range. If the actual pressure of the system is e.g. 1 bar the transducers cannot read pressure differences better than 100 Pa and this is too big for stratified flows.

When a DP cell is used for measuring pressure differences the best accuracy is again ~0.1% but this then applies to the pressure difference between the ports which is much lower than the absolute system pressure. In this case one is confronted with the problem of connecting the pressure ports of the device to the pressure tappings using connecting lines. The distance between the tappings and the size of the DP cell decide how long the connecting lines have to be.

Two methods are common for measuring pressure drop in steady state horizontal stratified gas-liquid flow: Andreussi & Persen (1987), Hand (1991), Kang & Kim (1993), Strand (1993), Srichai (1994), Roberts (1996) and Espedal (1998) connected a DP cell to the top of the pipe using air-filled lines, and Paras et al. (1994) measured pressure drop in the liquid phase by connecting a DP cell to the bottom of the pipe using liquid-filled lines. Andritsos & Hanratty (1987) used both methods: at low gas velocities pressure drop was measured in the gas phase, at high gas velocities in the liquid phase. For measurements in the liquid phase it had to be ensured that there were no air bubbles in the connecting lines.

Roberts (1996) used the top-connection method for experiments in transient stratified flow. The use of pipe-top pressure taps is preferable because the static head of the liquid on a DP cell at the tube bottom affects the pressure readings significantly in the range of pressure differences reported for stratified flow. A difference in liquid height of only 1 mm between the two tappings is equal to a pressure difference of 10 Pa. However, the connection of the DP cell at the top can cause problems if liquid blocks the air-filled lines. This can happen due to liquid slugs forming when the stratified flow experiment is being set up, or sometimes even during the experiment.

Srichai (1994) designed a system to keep the connecting lines between the pressure tappings and the manometer liquid free. The manometer was connected to the top of the test section by means of copper tubes. Isolating valves were inserted at the connection of the copper line with the test section. These valves were closed during the setting up of experiments. Stainless steel cylinders with a large inner diameter

compared to the diameter of the copper tube were inserted in the lines to trap any liquid in case that liquid flowed out from the test section while measurements were taken. Liquid blocking the lines was released into the dump tank through vent valves between the cylinder and the pressure tap. Gas-liquid separators connected to the pressure tappings were also used by Hand (1991) to prevent liquid droplets accumulating in the lines.

The pressure drop values reported for stratified flow are very low: Srichai's (1994) values were no higher than 420 Pa/m for air-water and 400 Pa/m for air-oil steady state stratified flows on WASP, operated at 5, 10 and 15 bar(g), and Roberts's (1996) values were less than 350 Pa/m for transient stratified air-water flow in an acrylic tube (3.2 cm internal diameter) at atmospheric pressure.

The measurement of pressure drop in transient stratified flow is additionally difficult for two reasons: the measurement has to be done at a reasonable frequency, e.g. 100 Hz, and the distance between the pressure tappings is a compromise between two constraints. On the one hand the distance between the tappings should be maximised for the low pressure differences present in this flow pattern. But on the other hand the distance should also be kept short in order to be able to track individual features of the flow. Roberts (1996) used a distance of 1.6 m between the two tappings for experiments in an acrylic test section at atmospheric pressure and a distance of 2 m for runs at atmospheric and higher pressures on the WASP rig. A distance of 2 m is also common in steady state stratified flow (Strand, 1993; Srichai, 1994), but also much shorter (0.2 m in the study by Kang & Kim, 1993) and much longer distances (up to 16 m for measurements in the gas phase in the study by Andritsos & Hanratty, 1987) have been used.

3.2.4 Liquid Height and Interfacial Structure

Liquid height in a conducting liquid (e.g. water) can be measured with conductivity probes. The conductivity probe consists of a pair of electrodes which are usually two parallel thin wires mounted normal to the direction of flow and which pass from the top wall of the conduit to the bottom wall. The conductance between the two wires is measured. It depends on the depth of the parallel wire immersed in the liquid. The higher the liquid height, the more the conductance. The measured conductance can be

related to the liquid height by calibration. The measurement with a twin-wire conductivity probe provides data for the liquid height at that location. By placing a number of conductivity probes in one cross section it is possible to get information on the structure of the interface in that cross section. Additionally, the content of liquid in the cross section, i.e. the liquid holdup, is obtained from integration over the individual measurements in a cross section. Twin-wire probes have been widely used in studies of stratified air-water flows (Andreussi & Persen, 1987; Andritsos & Hanratty, 1987; Murata et al., 1991; Strand, 1993; Srichai, 1994; Manolis et al., 1995; Roberts, 1996; Espedal, 1998).

If the material of the pipeline wall is electrically non-conducting, conductivity probes can be directly fixed to the wall. A pair of thin wires is mounted at the top and bottom of the pipeline traversing the inside of the tube and the wires are connected to an electronic circuit outside the pipe (Andritsos & Hanratty, Strand, Roberts, Espedal). However, using an electrically conducting material for the tube wall requires insulation of the wires from the wall. This problem was solved by Manolis et al. and Srichai in different ways, who built conductivity probes into a steel test section. Srichai built his wire probes in between two acrylic rings which fitted together by a tongue and groove mechanism. The two rings were glued together and sandwiched between indented steel flanges. Five pairs of probes were uniformly distributed in a cross section as represented in Figure 3.2. Manolis et al. fixed their probes by means of bosses on the steel test section. A liquid path between the wires of a probe was prevented by means of a silicone rubber disk compressed in the boss.

The thickness of the wires is a compromise between different criteria. The wires have to be strong enough to withstand the flow conditions and they should be thick enough to maximise sensitivity to fluctuations of the liquid height. But they should also be as thin as possible to minimise flow disturbance. 0.5 mm thick platinum wires were used by Srichai and Manolis et al. and a distance of 2 mm was used between the wires of every probe.

3.3 Instrumentation

Experimental methods to measure the various flow parameters introduced in Section 3.1 were evaluated based on the review of existing methods and the adopted methods are described in this section.

3.3.1 Hot-Wire Anemometry

Hot-wire anemometry was chosen for measurement of wall shear stress and phase velocities. There were several reasons which supported this choice:

- The probes used with hot-wire systems are very small. Therefore the disturbance to the flow can be minimised although the technique is intrusive with the probes immersed in the flow.
- The technique allows measurements up to high frequencies (up to several kHz). This makes it applicable in transient flows and it can also be used to capture turbulence characteristics of flows. This is an advantage for this study as the stratified gas-liquid flows with practical relevance are predominantly turbulent.
- Hot-wire anemometry systems are relatively cheap compared to their main competitors, laser Doppler anemometry systems.

There are also some disadvantages with hot-wire systems:

- Hot-wire and hot-film probes are very delicate. The sensing elements in hot-wire probes are thin wires of a few μm thickness. Hot-film probes are usually more robust and the sensitive metal films are coated with a very thin protection layer of e.g. quartz. Both types of probes are very easily damaged from mechanical impact and special care has to be taken in handling the probes. Hot-wire probes can be repaired by replacing the broken wire. However, for broken hot-film probes repair is usually not possible.
- The behaviour of the probe depends on the conditions of the flow where it is immersed. Above all it is sensitive to temperature variations and contamination from particles in the fluid. Variations of the fluid temperature are mainly a problem in liquids where there is a limit to the probe dictated by the need to avoid bubble formation in the liquid. Also contamination is a serious problem when the probes are used in liquids.

3.3.1.1 Operation

The two most useful books about the hot-wire anemometry technique were found to be those of Perry (1982) and Bruun (1995). The latter deals with all important aspects of this technique, and beyond giving essential operating guidelines, it also covers the design of anemometer systems and probes.

The hot-wire anemometer is basically a thermal transducer. The hot-wire or hot-film probe forms one arm of the Wheatstone bridge, which is the main part of the anemometer. An electric current heats the fine filament which is exposed to a cross flow. A variation in the flow rate causes a change in the heat transfer from the filament. The variation of heat transfer from the probe is monitored by various electronic methods which give signals related to the variations in flow velocity or flow temperature. The hot-wire method can therefore be used for measuring instantaneous velocities (and velocity derivatives, such as shear stresses) and temperatures at a point in a flow.

There are two modes of operation of a hot-wire system. The first is the constant current mode (CCA). Here the current in the wire is kept constant and variations in heat transfer cause changes in the probe resistance which are monitored as variations of the voltage drop across the filament. The second mode of operation is the constant temperature mode (CTA). Here the filament is placed in a feedback circuit which maintains the wire at constant resistance and constant temperature. Fluctuations in the cooling of the filament are seen as variations in wire current. Constant current anemometry is laborious to use and susceptible to probe burn-out. It has now been superseded by the CTA mode.

3.3.1.2 The Probes

To measure wall shear stresses and phase velocities, standard hot-wire and hot-film probes supplied by Dantec Electronics Ltd. were used.

For wall shear stress, Type-55R47 glue-on probes were used. A probe of this type is shown in Figure 3.3. The probes are glued to the surface where the shear stress is to be measured. The sensitive part is a nickel film of 0.1 mm x 0.9 mm deposited onto a 0.05 mm thick polyimide foil carrying a 0.5 μm quartz coating. The electrical connection is made by means of very fine (0.1 mm thick) gold-plated copper wires

which are soldered to the probe. The gold protects the copper wire and it has to be removed where electrical connection is to be made to an electronic circuit.

To determine the liquid velocity, a Type-55R42 conical film probe shown in Figure 3.4 was used. The sensitive part is a nickel film deposited onto a conical quartz rod and coated with a quartz layer of 2 μm thickness. The sensor dimensions are 1.4 mm x 0.2 mm. The conical form reduces contamination by particles which might be suspended in the liquid. The probe is supplied with a cable for the electrical connection to the anemometer box. To mount the probe for the experiments it was fixed to a Type- 55H153 mounting tube which was also supplied by Dantec.

To measure air velocity, a Type-55P11 miniature hot-wire probe was used which is shown in Figure 3.5. The sensor is a Pt-plated Tungsten wire of 5 μm thickness and 1.25 mm length spot-welded to stainless steel prongs. The probe body has electrical pins for connection to a cable-equipped Type-55H22 probe support available from Dantec.

In order to correct the anemometer readings for changes in ambient temperature, the temperatures of the gas and the liquid in the pipe were measured using commercially available K-type thermocouples. The temperatures measured with these thermocouples were also used for determination of the fluid properties in the gas and the liquid.

3.3.1.3 The Anemometers

In total four hot-wire/hot-film probes had to be operated simultaneously: two hot-film glue-on probes for measurement of shear stresses in the gas and the liquid, one hot-film probe for measurement of liquid velocity and one hot-wire probe for measurement of gas velocity. For operating each probe an anemometer "box" (containing the associated electronics) was needed. Four anemometer boxes were available for the experimental programme: three DISA Type-55D01 boxes and one DISA Type-55M10 box. Both types of anemometer were operated in the constant temperature mode according to operating manuals which were available with the boxes.

The boxes give a voltage output of 0-10 V which is related to the velocity or shear stress of the fluid depending on which type of probe is used. This is described in detail in Section 3.9.3.

3.3.2 Pressure Transmitter

The two-phase pressure drop was measured by means of a DP cell connected to taps on the top of the test section using air-filled lines. This arrangement was preferred to having a DP cell connected to the bottom of the test section using liquid filled lines because the static head of the liquid would affect the pressure readings significantly in the range of pressure differences reported for stratified flow.

The main concern with the top-connection method was the time needed for a change in pressure to be transmitted through the air-filled lines to the ports of the DP cell. A good time response was required for measurements in transient flows. It was assumed that pressure fluctuations would be transmitted at the speed of sound or an even higher velocity, which under atmospheric conditions would be equivalent to a frequency limit of 300-400 Hz for the measurement. This was found sufficient for the experiments.

For the evaluation of a DP cell two different sets of requirements were identified. For measuring two-phase pressure drop an instrument was required that measured pressure differences of up to 1000 Pa quickly and accurately and that could safely be used up to a working pressure of 30 bar and with the fluids air and water on the WASP facility. For the calibration work an instrument was required that measured up to 200 Pa accurately, with the same requirements on working pressure and fluids. A type 3051CD Smart Pressure Transmitter from Fisher Rosemount Ltd. was chosen for these measurements. This had the advantage of allowing adjustment of the range of pressure drops according to what was required. The chosen pressure transmitter could be adjusted between a minimum range of 200 Pa and a maximum range of 6220 Pa. Its accuracy was 0.1 % over the range set and its frequency response was at least 100 Hz. The pressure transmitter gave an output of 4-20 mA over the range calibrated and it needed an external 24 V dc power supply. A power supply box was built by the Electronics Section of the Department of Chemical Engineering and Chemical Technology at Imperial College. The box also transformed the 4-20 mA

output of the transmitter into a 2-10 V signal which then was directly collected with the data acquisition card.

According to the experimental matrix (Section 3.8) set up for this study, only flow transients without intervening slug flow were to be analyzed. In none of these transients would the air-filled lines be blocked by liquid during an experimental run. But a mechanism had to be implemented to clear the connecting lines when experimental runs were prepared.

The arrangement for pressure drop measurement therefore consisted of small bore 6 mm nylon tubes connecting the tappings on the test section with the ports of the DP cell. Isolating valves were inserted at the junction of the nylon tubes with the pressure tappings. These valves were closed while an experiment was being set up and they were open during an experiment. Purge lines were connected to the drain ports of the transmitter separated by isolating vales. The valves were closed during an experiment to isolate the purging mechanism from the system. The purge system was operated before an experimental run to clear the lines between the pressure tappings and the DP cell of liquid. On the low pressure rig college air supply was used for purging. For runs on the WASP facility, rig pressure was used to clear the lines and the purging then was in the outwards direction. Figure 3.6 shows the arrangement for measuring pressure drop.

3.3.3 Twin-Wire Conductivity Probes

Liquid height and interfacial structure in air-water flows were measured using twin-wire conductivity probes, following Srichai's (1994) design. An array of three conductivity probes was inserted in half a cross section in order not to disturb the probes for velocity measurements, which were placed downstream of these conductivity probes and on the opposite side of the tube (see Section 3.4). The arrangement of the probes is represented in Figure 3.10. The interfacial shape in the cross section could be determined by assuming symmetry of the flow with reference to a vertical plane through the tube centre.

The probes were operated with an electronics box with isolation transformers which had been produced for probes of the type used in the Srichai (1994) study. The

output of each probe was tuned to be in the range of 0-10 V for the range between the pipe empty and fully filled with water.

3.3.4 Pitot Tube

A Pitot tube was used for calibrating the hot-wire/hot-film velocity probes in single phase air and water flows. A Pitot tube consists of a cylindrical head attached perpendicularly to a stem. It is provided with static pressure tapping holes (drilled all around the circumference of the head at one or more cross-sections) and with a total pressure hole (facing the flow direction) at the tip of the axially symmetrical nose of the head. The total pressure is transmitted through a smaller tube inside the Pitot tube and the static pressure through the cavity between the interior and exterior tube to the end of the stem, where a DP cell is connected. A schematic of a Pitot tube is given in Figure 3.7.

The velocity u in a single phase flow is determined from the measured pressure difference between the total pressure hole and the static pressure tapping holes using the following formula in an incompressible flow:

$$u = \sqrt{\frac{2\Delta p}{\rho}} \tag{3.1}$$

where Δp is the measured pressure difference and ρ the density. For water the density is essentially only a function of the temperature while for the air the density is a function of both the pressure and the temperature.

A Pitot tube was designed according to British Standards (BS 1042: Section 2.1: 1983). This states a lower and an upper limit of fluid velocity for the performance of the Pitot tube. Both limits were evaluated for air and water.

The upper limit only applies to compressible fluids and is given by a total Mach number of 0.25. Comparison with the experimental matrix (see Section 3.8) set up for this study showed that the maximum air velocity expected was well below the maximum limit stated by the Standard, which would be about 80 m/s. It can further be assumed that the air for the conditions present in a stratified flow can be treated as incompressible. The lower limit is equivalent to a Reynolds number of 200, the Reynolds number being based on the inner diameter of the interior tube $D_{interior}$, the fluid velocity u and the fluid properties ρ and η:

$$\mathrm{Re}_{Pitot} = \frac{\rho u D_{interior}}{\eta} \qquad (3.2)$$

The lower limit was checked for different diameters of the interior tube. For a fixed Reynolds number and given fluid properties the phase velocity is inversely proportional to the diameter of the interior tube. So to minimise the fluid velocities at which the Pitot tube can be used the diameter of the interior tube had to be maximised. The velocities in both air and water calculated from the lower limit for a diameter of the interior tube of 3 mm are given in Table 3.1 and they were found to satisfy the lowest velocities in the experimental matrix proposed in Section 3.8.

phase	limit from standard/(m/s)
air	1.1
water	0.07

Table 3.1 Minimum velocities in air and water for Pitot tube with a diameter of the interior tube of 3 mm according to British Standard

In agreement with this evaluation a commercial stainless steel tube with 3.97 mm outer diameter was chosen for the interior tube and a stainless steel tube with 7.94 mm outer diameter for the exterior tube. The mechanical strength of the steel tubes was calculated according to British Standards (BS 5500: 1982; paragraph 3.5.1.2). The thickness of the tubes was calculated for a design pressure of 1.5 times the maximum working pressure of 30 bar on WASP. For the exterior tube a minimum wall thickness of 0.1 mm was found, for the interior tube a wall thickness of 0.04 mm. The commercial stainless steel tubing chosen had wall thicknesses which fulfilled these requirements (0.9 mm for the exterior tube and 0.56 mm for the interior tube). Eight static pressure holes of 1 mm diameter were drilled equidistantly around the circumference on the probe head. The overall dimensions of the Pitot tube were 120 mm for the head and 250 mm for the stem.

3.3.5 Data Acquisition

A NAGA PC with a 486 MHz processor and 4 MB of RAM was used for acquisition of the data from the instruments, i.e. from the conductivity probes, the pressure transmitter, the hot-wire and hot-film probes and also from the thermocouples. The voltage output from the electronics boxes which operated the probes was connected

into an A/D converting card. Unused probe channels were grounded. The A/D card was linked with a PC30G data acquisition card (from Amplicon) built into the computer. The PC30G card is equipped with some software packages designed for acquisition of voltage data.

The executable wv.exe from the PC30G card was used for acquisition of the data. This program works with a graphical user interface where the number of channels, the frequency and the sampling time can be set. For saving the data, two methods were used. Small files (obtained, for example, in the calibration procedures) were streamed to the computer memory and then directly saved as files in text-format. The data files obtained from the steady state and two phase transient runs were usually very big so that it would have been time consuming to save them directly as files in the text format. Instead the data was streamed to the harddisk of the acquisition computer which happened virtually instantaneously. After the experiment was finished the data files were reloaded into the graphical user interface and then saved as files in the text-format.

3.4 Design of Test Spool

The aim was to build a test spool which would incorporate all the necessary instrumentation described in the previous section and which could be used on both flow facilities described in Section 3.5, the low pressure flow facility and the WASP rig. The instruments to be built in included: two glue-on hot film probes, one at the top and one at the bottom of the tube, for measuring wall shear stresses in the gas and liquid, three twin-wire conductivity probes in half a cross section for measuring interfacial structure, a hot-wire probe for the gas velocity, a hot-film probe for the liquid velocity, two thermocouples, one at the top and one at the bottom of the tube, a Pitot tube and pressure tappings for connecting the differential pressure transmitter.

There were a number of requirements which had to be taken into account in the design of the test spool:

- The spool had to be designed for a pressure of 30 bar, which is the maximum working pressure for equipment on the WASP facility. For operation on WASP it also needed to be mechanically robust.

- The inside diameter of the test spool had to be 3 inch nominal bore (77.92 mm) to fit the WASP test section. To insert the test section on the low pressure rig, which has an internal diameter of 74 mm, transition sections could be manufactured.
- The conductivity probes could only be used in combination with electrically non-conducting material, and the glue-on probes could not be used with thermally conducting material. The best option was to mount these probes in acrylic sections.
- The instruments for wall shear stress, phase velocity and liquid height had to be arranged close to each other in the axial direction so that it could be justified to assume that all measurements referred to the same axial position.
- Local velocities vary with position inside the test section. It was therefore necessary to use traversing mechanisms with the velocity probes so that it was possible to obtain velocity profiles in both phases which could then be integrated to obtain phase average velocities. Also the wall shear stress around the perimeter varies, but the variation is moderate (Kowalski, 1987; Espedal, 1998). It was therefore decided to measure the wall shear stress in the gas at the top of the tube and the wall shear stress in the liquid at the bottom of the tube only.

A decision was made to build the whole test spool of individual steel and acrylic sections. A sketch showing the assembly of the individual sections is shown in Figure 3.8. The whole test spool had a length of 1.18 m to fit in the space available on the WASP rig.

For the hot-film probes for wall shear stress measurement, a pair of short acrylic thick-wall tube sections fitting together by a tongue and groove mechanism were machined. The rings had the same dimensions as those used by Srichai (1994) for his conductivity probe sections: an outer diameter of 140 mm and an inner diameter of 77.92 mm. The probes were glued on the top and bottom of the inside wall of the upstream ring. The probes were positioned with their wires pointing downstream in order to avoid disturbance of the boundary layer on the probe. In this orientation the sensor was normal to the flow direction. The upstream ends of the probes coincided with the upstream end of the ring. With this arrangement disturbance of the flow passing over the sensor of the glue-on probe was minimised. The probe wires were led between the two acrylic tube sections to the outer periphery, where they were

connected to a BNC socket supported by a metal bracket fixed to the acrylic. The BNC socket provided the electrical contact to the anemometer box. Figure 3.9 shows a view from the horizontal plane in the centre of the tube onto the two acrylic rings and the glue-on probe on the upstream ring.

As described in Section 3.3.3 the design for the conductivity probe holder was that used by Srichai (1994). Three pairs of conductivity probes were placed in half a cross section at equal distance from each other and the centre of the tube. The wires used were Pt-wires (99.99 % purity) with a diameter of 0.5 mm, and the distance between the wires of one pair was 2 mm in accordance with the specifications in Srichai. The arrangement is shown in Figure 3.10. Figure 3.11 shows a length section through the conductivity probe section.

The two acrylic sections for the glue-on and the conductivity probes were separated by a steel flange which was indented on both sides and they were sandwiched between two stainless steel tube sections by means of stainless steel tiebars (see Figure 3.8). The seal between the acrylic sections and the steel flanges was made with O-rings. Both steel tube sections had a rotating flange on the loose end in order to provide flexibility for aligning the test spool.

The downstream steel tube section contained the velocity probes and the thermocouples. The thermocouples were fixed by standard fittings screwed in the wall. There were three openings for the velocity probes: one at the top for the hot-wire probe for gas velocity measurement, one at the bottom for the hot-film probe for liquid velocity measurement and one on the side for the Pitot tube. The openings all had a diameter of 30 mm and they were reinforced with steel pads of 10 mm thickness. The reinforcement of these pads was calculated according to guidelines in British Standards (BS 5500: Section 3.5.4: 1994) for compensation of loss of strength from openings. The openings were located in such a way that the tips of the three probes were at the same axial position when inserted in the test section.

The method of fixing the velocity probes and the Pitot tube in the test spool is schematically represented in Figure 3.12. Each of the velocity probes and the Pitot tube was individually fixed to a traversing slide (with had a leadscrew pitch of 0.5 mm). The probe was held in place by a clamp fixed to the slide and the seal between the probe and the test spool was made by a gland equipped with an O-ring seal. The slide was mounted on an aluminium block, which was machined to fit in the opening

in the wall of the tube for the respective probe. The bottom part of the block was machined with the same curvature as the inner tube. Therefore when inserted the mounting block was flush with the inner wall. The seal between the mounting block and the steel section was made by means of an O-ring and the mounting block was fixed with Allen bolts to the test spool.

The stainless steel tube used for the test spool was 3 inch nominal bore which was identical with that used in the whole WASP test section. All flanges were machined from 3 inch stainless steel blind flanges. The thick-wall acrylic tube sections were machined from an acrylic tube with the required inner (77.92 mm) and outer diameter (140 mm).

After the manufacture of the spool piece was finished it had to be pressure tested to the maximum working pressure of WASP (30 bar) before it could be inserted for any measurements on this rig. For the testing procedure all probes were inserted and the test spool was filled with water and blanked off on both ends using blank flanges. A hydraulic tester was then connected to an opening in one of the flanges. The test was carried out in 10 cycles of applying and releasing the test pressure.

3.5 Flow Facilities

The experimental programme was carried out on two flow facilities which exist at Imperial College: a low pressure rig and the WASP facility.

3.5.1 Low Pressure Rig

Initially, experiments were carried out on the low pressure facility, where air-water flows could be studied at atmospheric pressure.

3.5.1.1 Experimental Setup

The test section had an inner diameter of 74 mm and an overall length of 8 m. It was made up of individual acrylic sections which were connected using tongue-and-groove flanges in order to ensure geometric continuity throughout the test section.

A schematic with the newly designed metal test spool (with inner diameter 77.92 mm and length 1.18 m) inserted in the test section is given in Figure 3.13.

The reference point for the measurements with the instrumentation in the test spool was 5.8 m downstream of the inlet. Two specially designed identical aluminium sections were connected to both ends of the test spool to fit it into the acrylic test section. The aluminium sections, which had a length of 0.1 m served two purposes: they reduced the inner diameter from 77.92 mm (test spool) to 74 mm (acrylic section) and they overcame the differences in the flanges between those of the test spool (which are the same types of flanges used on WASP) and those of the acrylic test section. The inner diameter was reduced at an angle of 2 degrees and it was assumed that this would not significantly disturb the flow. A length section through one of the transition flanges is shown in Figure 3.14.

In addition to the instrumentation built into the test spool there were two separate twin-wire conductivity probes upstream and downstream of the test spool which passed from top to bottom in the centre of the acrylic test section. These probes were built in previous experimental studies on the low pressure rig. They are labelled as cp_us and cp_ds in Figure 3.13. The distance between the upstream probe cp_us and the conductivity probes in the test spool was 0.816 m and the distance between the conductivity probes in the test spool and the downstream conductivity probe cp_ds was 0.704 m. These conductivity probes were used in addition to the conductivity probes in the test spool for determining axial gradients of the liquid height. They were different from those built into the test spool. The flow conditions on the low pressure rig are much less severe than on WASP and therefore it was sufficient to use wires of 0.125 mm thickness as compared to 0.5 mm thick wires used for the conductivity probes on WASP (and in the test spool). The distance between the wires was 2 mm as in the WASP probes. The pressure in the test section was recorded with a pressure transducer built into the test section 1.7 m downstream of the inlet.

The test section was fixed by means of ring supports to a rigid steel framework which could be tilted around a pivot point using the hoist available in the laboratory. With this arrangement the test section could be positioned with an accuracy of 0.02 % using a Roman level. At the end of the test section a cyclone made of PVC was placed. The cyclone was open at the top and the bottom and it was located on top of the water tank.

Figure 3.15 shows a view of the low pressure rig from the inlet. The water enters the test section from the bottom through reinforced plastic tubing, the air is supplied from

the top. The test section ends in the cyclone which is located on top of the water tank. Figure 3.16 shows a photograph of the test spool inserted on the low pressure rig. The flow passes from left to right. The pressure transmitter is held by a bracket on the test spool and its ports are connected to the tappings at the top of the test spool. The thick-wall acrylic sections with the glue-on probes and the twin-wire conductivity probes are sandwiched between the three steel flanges downstream of the pressure transmitter. The mounting mechanisms for the velocity probes at the top and bottom of the spool can be seen; the Pitot tube is at the back of the test spool. The thermocouples are downstream of the mounting mechanisms for the velocity probes. Figure 3.17 shows the acquisition computer and the boxes used to operate the instrumentation. This electronic equipment was located beside and below the test spool which is seen in the upper half of the photograph.

3.5.1.2 Operation

Operation of the low pressure facility is described with reference to Figure 3.13. Water was contained in an acrylic resin tank. From there it was transported to the test line by means of a pump. Its flow rate was measured with a rotameter and could be adjusted by using the valves V5 (on the main line) and V6 (on a bypass line). The air was supplied from the College supply at a pressure of 7 bar. It passed through a pressure regulator, through a critical flow valve V2 and then through a square-edged orifice plate with a D and D/2 tapping arrangement as specified by British Standards BS 1042 (1964) before it entered the acrylic test section. Valve V2 was used to regulate the air flow. A horizontal plate in the inlet section of the acrylic pipe ensured that the two fluids did not mix after entering. This aided development of stratified flow. After passing through the test line the air and the water were separated in the PVC cyclone. The air was vented to atmosphere and the water flowed along the inside wall of the cyclone back into the tank.

The flow rates were calculated on a separate computer, an Amstrad personal computer. The water flow rate was read from the rotameter, and the reading was then transformed into a superficial velocity. For doing the conversion the calibration curve for the rotameter supplied by the manufacturers of the rotameter was used. The range of superficial liquid velocities U_L was 0.04 to 0.58 m/s.

The air flow rate was determined on-line at a frequency of 5 Hz from the measurement of pressure drop across the air orifice section, the pressure upstream of the air orifice section and the pressure in the test section following the calculation method in BS 1042. For the experiments carried out in this study two orifice plates were used: one with an inner diameter of 17.71 mm was used for a range of air superficial velocities U_G of 2 - 5 m/s and an orifice plate with an inner diameter of 22.93 mm was used for a range of air superficial velocities U_G of 5 - 10 m/s.

3.5.2 WASP Facility

The main experimental programme was carried out on the WASP flow facility at Imperial College, where flows of air, oil and water can be studied up to pressures of 30 bar. For the present experiments only air and water were used.

3.5.2.1 Experimental Setup

The test section had a length of approximately 37 m and an internal diameter of 77.92 mm and was made of stainless steel. Two kinds of flanges were used in the test section. On the upstream side, tongue and groove flanges were used to ensure geometrical continuity along the test section. On the downstream side, towards the outlet of the test section, mainly raised face flanges were used.

Most of the test section was located outdoors. Only the downstream end and the slug catcher were located in the WASP control room from where the rig was operated. Because of the number and the delicate nature of most of the instruments (like hot-wire probes) the new test spool was positioned inside the control room. The reference point for the measurements with the instrumentation in the test spool was 33.7 m downstream of the inlet of the WASP test section. A schematic of the WASP rig with the test spool inserted is shown in Figure 3.18.

The test spool was accommodated in the test section together with some equipment already existing on the WASP facility: a thick-wall acrylic visualisation section, a gamma densitometer and Srichai's (1994) additional set of twin-wire conductivity probes for determining axial gradients of the liquid height. The distance between the conductivity probes in the test spool and Srichai's conductivity probe section was 0.579 m. The gamma densitometer was installed and commissioned on WASP by Pan

(1996). It was used for calibrating the conductivity probes. The visualisation section was used for taking videos of the flows. For measuring absolute pressure at the location of the test spool a pressure transducer was connected to a tapping in one of the flanges of the gamma densitometry section. The test spool was located as far upstream as possible in order to minimise effects from where the flow discharges into the slug catcher. A detailed sketch of the downstream end of the test section with the test spool inserted is shown in Figure 3.19.

A photograph of the test spool inserted in the WASP test section is shown in Figure 3.20. The flow direction is from right to left. The conductivity probe section downstream of the test spool is shown at the lower left corner of the photograph together with the electronics box to operate it.

3.5.2.2 Operation

The rig was operated from a computerised control system. This was used to set and maintain the flow rates and, for runs at pressure, the rig pressure and the liquid level in the slug catcher.

The air was supplied from two sources. The college air supply, which was also used for operation of the low pressure rig, supplied air at a pressure of 7 bar and was used to operate the valves on the WASP rig. The air used for the flow experiments was supplied from high pressure tanks in the neighbouring Aeronautics Department, which contained compressed air at about 30 bar. The water was supplied from a separate tank of the WASP rig. For the low flow rates needed to run stratified gas-liquid flows the pump on the water supply line was not used. Instead the water tank was pressurised up to 20 bar(g) with air from the high pressure air supply and the pressure was used to drive the water. The fluids were mixed at the inlet of the test section and then transported through the test section. At the end of the test section the fluids were discharged into the slug catcher. The air was vented off to atmosphere and the liquid was collected in a dump tank from where it was transported back to its supply tank.

The air flow rate was metered by orifice plates with corner tappings designed according to British Standards (BS 1042). The flow was calculated from the measured pressure drop across the orifice and absolute pressure measurement

according to BS 1042. An orifice plate with an inner diameter of 20 mm was used in all the experiments. With this orifice plate the following flow rates depending on the total pressure were obtained:

p/bar	U_G/(m/s)
1	5 - 16
6	1 - 5
11	1 - 4

Table 3.2 Air flow rates with 20 mm diameter orifice plate

The water flow rate was measured with a Danfoss magnetic flow meter, which covered the range 0.02 to 0.7 m/s needed in the experiments. The acquisition of the air and water flow rate was made on a separate acquisition computer.

3.6 Fluid Properties

Properties of air and water were found in the literature. The relationships used to calculate the densities and viscosities of both fluids depending on pressure and temperature are given in the following subsections.

3.6.1 Air Density

The density of the air was calculated based on the assumption of an ideal gas. The density ρ_G at a given pressure, p, and a given absolute temperature, T_{abs}, can then be calculated from a known density, $\rho_{G,ref}$, at pressure, p_{ref}, and temperature, $T_{abs,ref}$, by means of the following relationship:

$$\rho_G = \rho_{G,ref} \frac{p}{p_{ref}} \frac{T_{abs,ref}}{T_{abs}} \tag{3.3}$$

The value of air density, $\rho_{G,ref}$, at temperature $T_{abs,ref} = 273.15$ K and pressure $p_{ref} =$ 1.0 atm (= 1.013 bar) is $\rho_{G,ref} = 1.2928$ kg/m^3 from Perry & Green (1984). When the values for $\rho_{G,ref}$, $T_{abs,ref}$ and p_{ref} are entered in the above formula one finds:

$$\rho_G = 348.5966 \frac{p}{T_{abs}} \tag{3.4}$$

This formula can be used to calculate air density for given pressure, p, in bar and given temperature, T_{abs}, in K.

3.6.2 Air Viscosity

For air viscosity the following correlation was employed (National Research Council, "International Critical Tables of Numerical Data", v. 5, n. 2, McGraw-Hill Book Company, Incorporated, New York, 1928):

$$\eta_G = \left[0.01622 + 2.7083 \cdot 10^{-5}(1.8T + 32)\right] \cdot 10^{-3} \qquad (3.5)$$

where η_G is the gas viscosity in Pa·s and T the temperature in °C.

3.6.3 Water Density

Water density was taken from tabulated data in Perry & Green (1984).

3.6.4 Water Viscosity

For water the following viscosity correlation was used (Van Wingen, 1950):

$$\eta_L = \left\{\exp\left[1.003 - 0.01479(1.8T + 32) + 1.928 \cdot 10^{-5}(1..8T + 32)^2\right]\right\} \cdot 10^{-3} \quad (3.6)$$

where η_L is the liquid viscosity in Pa·s and T the temperature in °C.

3.7 Operation of Hot-Wire Anemometry

Of all the types of instruments used in this study hot-wire and hot-film probes are without doubt the most delicate to operate. Difficulties experienced in operating the probes are reported here.

3.7.1 Mounting of Glue-on Probes

The glue-on probes chosen for measurement of gas and liquid wall shear stresses had to be fixed to the inner wall of the perspex rings which were designed to hold the probes in the test spool.

At the start of the experimental programme ordinary two-component Araldite ® Standard was used to glue the probes. This glue was not found to give satisfactory results as the probes did not stick to the acrylic wall very well. For later probe sections Tensol cement ("perspex glue") was used to glue the probes and these then adhered very well to the wall. Tensol cement had the advantage that it was chemically identical with the substrate, the acrylic, on which it was used. The film of glue

between the probe and the wall was also more uniform when Tensol cement was used. It was important that the probe sat flush on the wall to minimize disturbance to the boundary layer of the flow.

A specially designed metal clamp was used to press the probes against the wall until the cement dried. The part of the clamp which pressed against the probe had the same curvature as the inside wall of the perspex ring. A piece of rubber hose covered with Sellotape was placed between the clamp and the probe to prevent the clamp from damaging the probe. Sellotape did not stick to Tensol cement and it was used so that the clamp could easily be removed after the glue had dried.

The glue-on probes have two sides: the side with the electrical contacts (see Figure 3.3) is the sensitive side whereas the reverse side is more insensitive. For measurements in fluids with a high thermal conductivity, like water, good results are obtained with the glue-on probe mounted with its insensitive side exposed to the flow. For measurements in fluids with low thermal conductivity, like gases, the sensitive side is usually exposed to the fluid in order to enhance probe performance. In this study the probes mounted in this way for measurements in air usually burnt out very quickly although the electrical contacts of the probe were additionally insulated with glue.

Probe burnout was not usually a problem when the probes were mounted in the opposite way, i.e. with the insensitive side exposed to the fluid. It was found that probes mounted in this way gave satisfactory results not just for water, but also for air. This was concluded from comparing the calibration curves in the air for two probes which were mounted differently, one with the sensitive side exposed to the flow, the other with the insensitive side exposed to the flow. Therefore, for the rest of the experimental programme, all glue-on probes for measurements in the liquid and the gas were mounted with the side with the electrical contacts glued onto the wall.

3.7.2 Preparation of Velocity Probes

The hot-wire probe was used together with a Type-55H22 probe support from Dantec. This was an L-shaped metal tube with electrical connections for the Type-55P11 miniature-wire probe. To improve the seal between the ceramic probe body and the probe support some silicone grease was put around that part of the probe

stem which was inserted in the probe support. This ensured watertight mounting especially for application at pressure.

The cable-equipped liquid velocity probe was supported by a Type-55H153 mounting tube from Dantec. The probe body was firmly held by the tip of the mounting tube and the probe cable passed through the tube. For experiments on the low pressure rig the transition between the probe and the mounting tube was sealed with silicone sealant. But for use on WASP the arrangement had to be safe for a pressure up to 30 bar. This was obtained by filling the cavity in the tube with Araldite epoxy resin.

3.7.3 Probe Heating

For heating the probes certain factors have to be considered. The probe temperature should be set as high as possible in order to increase the sensitivity to velocity fluctuations and to reduce the sensitivity to temperature variations (Bruun, 1995). But the temperature up to which the probe can be heated basically depends on two factors:

- The probes must not be heated above a certain temperature which is specified by the probe manufacturer. Above this temperature the heating can damage the probe and destroy it. The maximum temperature is typically about 300 °C for a hot-wire probe, and 150 °C for a hot-film probe.
- The maximum temperature to which the probe can be heated also depends on the fluid in which the measurements are done. In gases the probe temperature is limited by the maximum temperature specified in the previous item. However, in liquids the maximum possible temperature is considerably lower. In liquids, the probe can usually not be heated more than about 20 °C above ambient in order to prevent bubble formation in the liquid. Bubbles around the probe would affect the heat transfer from the probe to the liquid and lead to erroneous readings. This is because the composition of the gas/liquid mixture around the probe would change all the time, and the probe readings could then not be related any more to the calibration relationship which was produced for a particular set of experiments.

Heating of the probe is usually expressed by means of the overheat ratio. This ratio is defined as

$$a = \frac{R_w - R_{20}}{R_{20}} = \alpha_{20}\left(T_w - 20\right) \tag{3.7}$$

where T_w is the temperature of the heated probe, R_w is the resistance of the heated sensor, and R_{20} is the sensor resistance at 20 °C. The sensor temperature coefficient of resistance (TCR) at 20 °C, α_{20}, and the sensor resistance at 20 °C, R_{20}, are supplied with each probe by the probe manufacturer. Typical values for the probes used in this study were:

type of probe	α_{20}/(%/°C)	$R_{20}\,\Omega$
hot-wire probe	0.36	3.3
conical hot-film probe	0.50	10.4
glue-on probe	0.30	11.8

Table 3.3 Typical values for sensor temperature coefficients of resistance α_{20} and sensor resistance R_{20} at 20 °C

Overheat ratios reported in the literature were around 0.05 - 0.1 for probes used in the liquid. 0.4 is common for hot-film probes in the gas flows and 0.8 is usually used for a hot-wire probe in gas (Bruun, 1995).

Typical overheat ratios used in this study are collected in the following table:

fluid	probe	overheat ratio a
water	conical hot-film probe	0.08
	glue-on probe	0.05
air	hot-wire probe	0.8
	glue-on probe	0.35-0.4

Table 3.4 Overheat ratios used with the different probes in this study

The hot-resistance of the probe is set in a procedure which is described in the following subsection.

3.7.4 Probe Setup

The setting up of a hot-wire or hot-film probe for taking measurements involved the following steps:

1. The probe was connected to the anemometer box via a coaxial probe cable. In order to measure the cold resistance of the probe the resistance of the probe cable

had to be compensated for. This was done by replacing the probe at the end of the cable with a short-circuiting probe and by tuning the box to compensate for the cable resistance.

2. The short-circuit probe was then replaced by the proper probe and the resistance measured, R_{tot}, equalled the resistance of the sensor and its leads.
3. In the next step the working resistance of the probe was calculated and set. The hot-resistance was calculated from the following equation

$$R_w = R_{tot} + aR_{20} \tag{3.8}$$

which is a modification of equation (3.7). Once the hot-resistance of the probe was set the electrical circuits were closed. The probe was then heated and ready for measurements.

4. The dynamic response of the anemometer system had to be optimised. For this procedure, which is known as *square wave test*, the probe was exposed to a constant flow and a square wave signal was applied to the system. The system response (i.e. the probe output voltage) was monitored on an oscilloscope and the anemometer was tuned to reduce oscillations of the probe output signal.

These were the main steps in setting up a probe for measurements although the detailed procedures depended on the type of anemometer which was used. Detailed setting up procedures are described in manuals provided by the manufacturers of the anemometer boxes used, DISA 55D01 and DISA 55M10.

3.7.5 Grounding

When hot-film probes are used in conducting liquids the system has to be grounded in order to avoid excessive voltage between the probe and the conducting medium as this would cause the thin protective quartz coating to break.

The two hot-film probes operated in the water were therefore individually grounded. The grounding for the wall shear stress probe was done by connecting an earth wire to one of the bolts which was used to clamp the two acrylic sections in the steel test spool. The liquid velocity probe was grounded by connecting one end of an earth wire to the mounting tube of the probe, which was immersed in the liquid, and the other end to the BNC plug of the probe.

3.7.6 Correction for Temperature

To compensate for the effect of changing ambient temperature on the readings of the hot-wire and hot-film probes, a method introduced by Bearman (1971) was used. Bearman assumed that the coefficients C_M and C_N in the linearised calibration relationship (equation (3.23) in Section 3.9.3.2) were proportional to the temperature difference between the temperature of the heated wire T_w and the ambient temperature:

$$\frac{C(T_1)}{C(T_2)} = \frac{T_w - T_1}{T_w - T_2} \tag{3.9}$$

T_1 and T_2 are two different values for ambient temperature. With this assumption the ratio between the probe output voltages at the two different temperatures became

$$\frac{E(T_1)}{E(T_2)} = \left(\frac{T_w - T_1}{T_w - T_2}\right)^{1/2} \tag{3.10}$$

If the temperature T_1 is taken as a reference temperature of 20 °C and the corresponding voltage is E_C (C for corrected) and if T_2 is the acquisition temperature T_{acq} with the measured voltage E_{acq}, the above relationship becomes:

$$\frac{E_C}{E_{acq}} = \left(\frac{T_w - 20}{T_w - T_{acq}}\right)^{1/2} \tag{3.11}$$

This relationship could further be simplified with equation (3.7) for the overheat ratio a:

$$\frac{E_C}{E_{acq}} = \left(\frac{a}{a - \alpha_{20}\left(T_{acq} - 20\right)}\right)^{1/2} \tag{3.12}$$

where a is the overheat ratio, α_{20} the sensor temperature coefficient of resistance at 20 °C, and T_{acq} the fluid temperature recorded simultaneously with the anemometer output E_{acq}. Equation (3.12) was used to correct the acquired voltages of all the hot-wire and hot-film probes used in this study.

3.7.7 Damaged Probes and Probe Repair

There were two main reasons for probe damage: mechanical impact and probe burnout.

Probe breakage through mechanical impact was a problem, particularly with the hot-wire probes. The probe remained intact as long as the two-phase flow was separated and that the probe was completely immersed in the gas phase. However, if a slug was formed and impacted the probe, the probe became non-operational. Examination under a magnifying glass showed that the wire sensor was torn apart. This experience meant that the hot-wire probe had to be temporarily removed from the test spool whenever a liquid-filled pipe was expected. This was the case when the other (hot-film) probes were calibrated in single phase liquid and when the conditions over which stratified flow existed (both in steady state and during transients) were investigated. A hot-wire probe with a broken wire sensor which was kept as spare served as a dummy probe used for replacing the working hot-wire probe in these cases.

The advantage of the hot-wire probes was that they could be repaired. Some attempts were made to do the repair in-house by soldering a piece of Wollaston wire (silver coated platinum wire) to the prongs of the probe and by then etching the silver sheath away with nitric acid. However, this job was very delicate and in most cases the repair was not successful. The most difficult stage was the soldering on of the tiny wire. Thus, broken probes were sent back to Dantec, where a new Tungsten wire was welded onto the prongs. The repaired probe was then equivalent to a new probe.

Damage of hot-film probes manifested itself in a different manner than damage of hot-wire probes. In the case of the wire probes, the damage was complete and occurred by breaking of the sensor which then resulted in an infinite cold resistance of the probe; damage of the film probes developed gradually and was manifested by a gradual increase of the probe cold resistance from day to day. The probe measurements were considered to be unreliable as soon as the cold resistance of the probe began to increase in this way.

The disadvantage of broken hot-film probes compared to the hot-wire probes was that they could not be repaired. Therefore as soon as damage of a hot-film probe was observed the probe had to be discarded and replaced by a new probe. As described in Section 3.7.1, probe burnout for the glue-on probes mainly was observed when the probes were glued on to the wall with the sensitive side exposed to the flow. Probe burnout was probably caused by the contact of the electrical contacts of the probe with water, an electrical conductor, although the contacts had been insulated with glue. This problem was not observed when the sensitive side of the probe was glued

on to the wall. As the glue-on probes were permanently fixed to acrylic rings the whole unit had to be discarded as soon as a probe broke and it had to be replaced with a new unit with working probes. Usually only one of the two probes built into an acrylic section broke while the other probe still could be operated. Therefore alternative designs were investigated which would have allowed to save the working probe of a unit and to replace only the broken probe. But all these alternative designs were not cost- and time-effective and therefore the original design with two probes permanently fixed to an acrylic unit was kept.

With the conical hot-film probe, damage occurred only once. The problem with this type of probe was that the quartz coating was cracked after a handling mistake (probably the probe accidentally hit the tube wall when it was removed) and it had to be replaced by a new probe.

3.8 Experimental Matrix

Based on the study by Roberts (1996) of transient air-water flows on the WASP rig, an experimental matrix of flow conditions was compiled to cover a wide range of conditions for transient air-water flows where no flow pattern change would occur during the transient.

Roberts studied transient air-water stratified flow at 0, 5 and 10 bar(g). His experiments on WASP aimed at determining wave speeds in this flow regime. Transients were produced by changing liquid and gas superficial velocities, respectively. The flow pattern could change to slug flow during the transient in cases where the change in flow rate was produced by an increase in gas or liquid flow rate. For this study only those transients were considered where Roberts had not reported occurrence of temporary slug flow during the experiment. The conditions for these transients were collected in the matrices presented in Appendix A of this thesis.

3.9 Calibration and Validation

The use of all instrumentation had to be validated. Extensive tests for this were done on the low pressure rig. On the WASP rig, the validation tests were repeated over a smaller range of conditions. All the following subchapters are split in two sections, one for the tests on the low pressure rig and one for the tests on WASP.

For tests with the pressure transmitter and the Pitot tube in single phase flows of air and water, data was acquired at 10 Hz for 30 s. For calibration of the hot-wire and hot-film probes, the conductivity probes and thermocouples data was acquired at 100 Hz for 20 s.

3.9.1 Pressure Drop Measurement

As explained in Section 3.3.2 measurement of pressure gradient was necessary for two separate purposes. Pressure drop measurements in single phase flows of air and water were required for calibration of the glue-on probes (for measurement of wall shear stresses) and for measuring the pressure drop over the Pitot tube which was used for calibrating the velocity probes. Further, pressure drop had to be measured in two phase stratified flow. Validation tests with the Rosemount Smart Pressure Transmitter were done in single phase flows of air and water to find out if the pressure drops measured could be described by the relationships established for single phase flows. For the validation tests and for most of the two-phase experiments the transmitter was ranged to 200 Pa and the accuracy in this range was 0.2 Pa (0.1 %).

3.9.1.1 Pressure Drop in Air

3.9.1.1.1 Pressure Drop in Air: Low Pressure Rig

For a single phase flow through a pipe the momentum balance over a section of tube with length dx yields:

$$\frac{dp}{dx} = 4f\frac{\rho}{2D}u^2 \qquad (3.13)$$

where D is the tube diameter, ρ is the density of the fluid, and u is the mean velocity. f is a friction factor which mainly depends on two factors: on whether the flow is laminar or turbulent and on whether the tube is rough or smooth. All flows investigated in this study were turbulent. For a smooth tube, like acrylic, the friction factor for a turbulent flow was expressed by the Blasius relationship:

$$f = 0.0791\,\mathrm{Re}^{-0.25} \qquad (3.14)$$

where Re is the Reynolds number of the flow defined as:

$$\mathrm{Re} = \frac{\rho u D}{\eta} \qquad (3.15)$$

The fluid properties for air and water were those specified in Section 3.6. For a tube with roughness k_W. Eck (1973) developed an explicit relationship for the friction factor f:

$$f = \frac{0.0625}{\left\{\log_{10}\left(\frac{15}{\mathrm{Re}} + \frac{k_W/D}{3.715}\right)\right\}^2} \qquad (3.16)$$

For his experiments on the WASP rig Srichai (1994) used a value of k_W=4.6·10^{-5} m, which is the roughness of commercial steel tubes. The pressure drops in single phase air predicted from equations (3.13) and (3.14) for a smooth tube and from equations (3.13) and (3.16) for a tube with roughness k_W=4.6·10^{-5} m are represented in Figure 3.21 as "theory smooth" and "theory rough" respectively.

Tests with single phase air were carried out on the low pressure rig over a range of gas superficial velocities of 2-10 m/s. For the first tests the pressure transmitter was connected to the tappings on top of the test spool which were closest to its rotating flanges and which were 0.9 m apart (see Figure 3.8). The reason for using these tappings was to maximise the distance between them which would increase the reliability of the measurement. A micro-manometer with a range of 0-300 Pa and an accuracy of 0.025 % was connected in parallel to the pressure transmitter. The agreement between the pressure transmitter and the micro-manometer readings was very good as Figure 3.21 shows. This proved that the pressure transmitter was reading accurately.

However, the measured data were considerably higher than the predictions for an air flow through a smooth or a rough tube. It was suspected that this was caused by the probe inserts in the test spool across which the pressure drop had been measured. The main blockage in the pipe was due to the Pitot tube with a diameter of its stem of about 1/10 of the internal diameter of the test spool. The velocity probes in the gas and the liquid had been replaced by dummy tubes which only slightly protruded into the test spool. Some minor effects on the pressure drop could have resulted from the conductivity probes traversing from the top to the bottom in the test spool. Therefore the pressure drop was then measured between the tappings upstream of the probe inserts represented in Figure 3.8. The distance between the pressure tappings was then reduced to 0.3 m. The pressure drop measured with the pressure transmitter in this arrangement closely represented the theoretical prediction for a rough tube as

Figure 3.22 shows. It was decided to use these tappings upstream of the probe inserts for any further pressure drop measurement although the distance between the tappings, 0.3 m, was very short.

3.9.1.1.2 Pressure Drop in Air: WASP Rig

The pressure drop in single phase air flow with the pressure transmitter connected to the tappings at the top of the test spool upstream of the probe inserts was also measured on the WASP rig. The range of flow rates covered was 5 - 16 m/s at atmospheric conditions. The results obtained looked very similar to the results from the low pressure rig. The pressure drop was predicted within +/- 10 % of the theoretical curve for a rough tube which was calculated from equations (3.13) and (3.16) and a value for the tube roughness of k_{tt}=4.6·10^{-5} m.

3.9.1.2 Pressure Drop in Water

3.9.1.2.1 Pressure Drop in Water: Low Pressure Rig

Validation of pressure drop measurement in water was important with regard to the calibration of measurement of wall shear stress in the liquid.

An attempt was made to obtain single phase flows of water over the whole range of liquid flow rates possible on the low pressure rig. But only at flow rates higher than 0.35 m/s the straight test line connected to the cyclone was completely filled with liquid; at flow rates below 0.35 m/s the liquid couldn't fill the pipe and a free surface flow formed. Only when the pipe outlet was replaced with an inclined section of pipe (see Figure 3.23) did pipe remain full of water over the whole range of flow rates on the low pressure rig.

For measuring pressure drop in a single phase water flow it was necessary to avoid any air in the lines connecting the pressure transmitter to the pipe. This was not possible when the lines were connected to the tappings at the top of the tube. Therefore the lines were now connected to the tappings at the bottom of the test spool. The tappings upstream of the probe inserts were used because of the disturbance from the probe inserts on the flow which had been identified in Section 3.9.1.1.1 in pressure drop tests in single phase air flow. Filling the lines with liquid

was achieved by running a single phase water flow with the valves on the drain ports of the transmitter open. The valves were closed once the lines were completely filled. The measured pressure drop was plotted in Figure 3.24 together with the prediction for a water flow in a rough pipe. The relationships used for these predictions were the ones from Section 3.9.1.1.1. Appropriate fluid properties for the water were calculated according to Section 3.6.

From the results in Figure 3.24 it is concluded that the theoretical prediction for a rough tube (data set "theory rough" in the figure) under-estimates the real pressure drop in single phase water flow on the low pressure rig by about 15 % in average. From the evaluation of pressure drop measurement in air it would have been expected that the pressure drop in the water would also be represented by the predictions calculated on the basis of a friction factor for a rough tube. However, in the water flow the measured pressure drop was considerably higher than the pressure drop predicted for a pipe with the roughness of a commercial steel tube. It was assumed that the over-prediction was due to the inclined section of pipe at the end. The influence of the inclined section of pipe on the flow was demonstrated in the tests with the Pitot tube in single phase water described in Section 3.9.2.2.1.

3.9.1.2.2 Pressure Drop in Water: WASP Rig

Pressure drop in water was also measured on the WASP rig with the pressure transmitter connected to the tappings at the bottom of the test spool upstream of the probe inserts. In contrast to the low pressure rig single phase flows were obtained with no modification to the exit of the test section over the whole range of liquid flow rates. The pressure drops were measured in a range of $0.1<U_L/(\text{m/s})<0.7$ and they were in reasonable agreement with the predictions for a rough tube (calculated as in Section 3.9.1.1.1) as shown in Figure 3.25.

3.9.2 Pitot Tube

The Pitot tube was used for calibrating the hot-wire and hot-film probes for velocity measurement in air and water. The pressure drop over the Pitot tube was determined with the Rosemount Smart Pressure Transmitter and the fluid velocity was determined with equation (3.1).

On both flow facilities, the low pressure rig and the WASP rig, measurements of local velocities in air and water were done with the Pitot tube at various radial positions in the pipe. Measurements with the Pitot tube were restricted to that half of the cross section which was undisturbed by the upstream twin-wire conductivity probes. For a number of flow rates the Pitot tube was traversed in transverse direction through the tube and measurements were taken at eight equidistant radial positions including the centre of the pipe.

The total flow rate was determined by integration over the measured points and compared with the flow rate obtained from the acquisition systems on the flow facilities. For the integration a numerical method for circular cross sections laid out in the British Standard was used (British Standard BS 1042: Section 2.1: 1983; paragraph 9.1). The Standard for the Pitot tube states a number of effects which can cause measurement errors and which should be corrected for. The three main types of effects were corrected in the evaluation of the Pitot tube data: the stem blockage effect, measuring point position and head loss. The British Standard provides guidelines for calculating these effects.

The stem blockage effect is caused by the size of the Pitot tube: in a conduit the velocity increase when the flow passes between the stem and the walls causes a decrease in the recorded static pressure without affecting the total pressure. The measured pressure difference Δp has to be reduced to take account of the stem blockage effect.

The correction for measuring point position can improve prediction of the flow rate measured with the Pitot tube. In this type of correction Pitot tube measurements recorded at real distances y from the wall are considered for calculation as being carried out at distances $y + \Delta y$, where Δy is a fictitious displacement of the measuring point.

The correction for head loss accounts for the pressure drop in the flow over the distance between the total pressure hole and the static pressure holes. Without the correction the measured differential pressure is over-estimated.

3.9.2.1 Pitot Tube in Air

3.9.2.1.1 Pitot Tube in Air on the Low Pressure Rig

Measurements with the Pitot tube in air were done at six different gas superficial velocities between 2 and 10 m/s. All flows were turbulent, with the Re-number above 2000. The flow profiles were measured in one half of the cross section and the flow rates were determined as described in the previous section. At all velocities the measured profile was in very good agreement with the $1/7^{th}$ power law, given in Hewitt (1990):

$$u(r) = \frac{1}{0.817} u\left(1 - \frac{r}{R}\right)^{1/7} \qquad (3.17)$$

where u is the average velocity in the tube (in a single phase flow identical with the superficial velocity U), r the radial position and R the pipe radius. The measured velocity profile for an air flow rate of 8.2 m/s is compared with the prediction from the $1/7^{th}$ power law in Figure 3.26.

For all the gas flows the flow rates obtained from integration over the measured velocity profiles were compared with the flow rates measured with the rig flow rate acquisition system. The integration was done with and without the corrections for the stem blockage effect, the measuring point position and the friction head loss. The results of the comparisons are represented in Figure 3.27. The results are plotted as the error between the phase velocity determined with the Pitot tube, u(Pitot tube), and the velocity determined from the rig acquisition system, u(rig acquisition):

$$\text{error} = \frac{u(\text{Pitot tube}) - u(\text{rig acquisition})}{u(\text{rig acquisition})} \qquad (3.18)$$

It can be seen that in all the gas flows investigated the Pitot tube over-predicts the flow rate and that the discrepancies between the resulting flow rates from the two methods decrease with increasing gas flow rate. When no corrections were included the error was between 5 - 8 %, but when they were included the error was no higher than 5 %.

3.9.2.1.2 Pitot Tube in Air on the WASP Rig

Tests with the Pitot tube were repeated on WASP in air flows at atmospheric pressure. Traverses with the Pitot tube were done at six different gas superficial

velocities between 5.6 and 15.8 m/s. As on the low pressure rig all flows were turbulent and the $1/7^{th}$ power law gave good predictions of the measured velocity profile at each flow rate. The agreement between the flow rate obtained from integrating over the velocity profiles measured with the Pitot tube and the rig flow rate acquistion was found to be very similar to the results from the low pressure rig. Without corrections the Pitot tube over-predicted the flow rate by about 8 % at all flow rates, with corrections for stem blockage, measuring point position and friction head loss the over-prediction was reduced to 5 %.

3.9.2.2 Pitot Tube in Water

3.9.2.2.1 Pitot Tube in Water on the Low Pressure Rig

As mentioned in Section 3.9.1.2.1 the exit of the test section was replaced by an inclined section of tube to obtain single phase flows of water over the whole range of flow rates on the low pressure rig.

Measurements were done at six different liquid superficial velocities between 0.08 and 0.36 m/s. All flows were turbulent, with the Reynolds number above 2000. At all these flow rates the velocity profiles in one half of the cross section were measured and the flow rates were determined as described in Section 3.9.2. At all velocities the measured profile was in very good agreement with the $1/7^{th}$ power law which was presented in Section 3.9.2.1.1 for air flows. The velocity profiles are exemplified by that for a liquid flow rate of 0.2 m/s in Figure 3.28.

The velocity profiles were integrated and compared with the flow rates obtained from the water rotameter. The integration was done with and without the correction for the stem blockage effect, the measuring point position and the friction head loss and the comparisons for both cases are represented in Figure 3.29. The results are plotted as error defined by equation (3.18). It can be seen that the discrepancies decrease with increasing liquid flow rate as observed for the air flows. The average discrepancies were higher than observed for the air flows. When no corrections were included the error went up to 25 %. When corrections were included the error was still very substantial, between 10% at higher liquid flows and 20 % at lower flow rates.

It was suspected that the high discrepancies resulted from effects of the inclined pipe section at the pipe exit. Therefore tests in single phase liquid were carried out where

the test spool was rotated by 90 ° with the Pitot tube at the bottom of the test spool, and the Pitot was then traversed vertically through the tube. Traverses through the bottom half of the test spool were done for six different liquid flow rates between 0.08 and 0.4 m/s. The agreement with the $1/7^{th}$ power law was as good as for the lateral traverses, but the flow rates obtained from integration over the Pitot tube measurements now compared much better with the flow rates obtained from the rotameter. This is represented in Figure 3.30. The error was within +/- 5 % with and without corrections.

The tests with the lateral and vertical traverses with the Pitot tube in single phase water flow on the low pressure rig showed that the inclined section of pipe at the outlet of the duct influences the velocity measurements in the test spool. From the comparisons in Figure 3.29 it is concluded that also local velocity measurements taken with the Pitot tube in single phase water will over-predict the real value by an average of ~15 %.

3.9.2.2.2 Pitot Tube in Water on the WASP Rig

Pitot traverses were done at atmospheric pressure at two liquid superficial velocities on WASP, U_L=0.16 and U_L=0.55 m/s. These values were representative for the range of liquid flow rates used in this study. At both flow rates the measured profile was reasonably well predicted by the $1/7^{th}$ power law. The deviations between the flow rates obtained from integration over the velocity profiles measured with the Pitot tube and the flow rates obtained from the rig flow rate acquisition were similar to those obtained in the tests in air on WASP. Without corrections the Pitot tube over-predicted the flow rate by about 8 % at each flow rate, with corrections for stem blockage, measuring point position and friction head loss the over-prediction was reduced to 5 %.

3.9.3 Hot-wire and Hot-film Probes

The calibration of hot-wire and hot-film probes is usually done in a single phase flow of the fluid in which the probe is used. The reason for this is that single phase flows can be described using simple well-established relationships while for multiphase flows these simple relationships do not apply. Sometimes it is not possible to cover

the whole range of velocities present in each phase of a multiphase system in single phase flows of the respective fluids on the same experimental facility. Alternative possibilities for calibration are reported here based on experimental studies where hot-film probes for wall shear stress measurement were used.

One way to overcome the problem of a limited range of fluid velocities on the flow facility is to carry out the calibration on a separate facility where the required flow rates can be obtained in single phase flows. This procedure was used by Langsholt et al. (1997). The disadvantage of this method is that, after calibration, the probe has to be transferred back to the flow facility which is used for the main set of experiments. An alternative way is to do the calibration on the same facility where the main set of experiments is done and by extrapolating from the range over which the probe was calibrated. This of course can lead to large errors and is not advisable.

Sometimes it is possible to extend the range of velocities of single phase flows on the experimental flow facility used for the main set of experiments. Hagiwara et al. (1989) adjusted the range of velocities in single phase flow by inserting a rod into the test section and by carrying out probe calibration in single phase flow in the annulus between the rod and the wall of the test section. Wolf (1995) solved the problem of a restricted range of single phase flows by carrying out the calibration in a two-phase system. He calibrated his wall shear stress probe in vertical annular two-phase flow by using a simplified momentum balance for the vertical two-phase flow.

In this study the ranges of single phase flows of air and water on both flow facilities, the low pressure rig and the WASP rig, were found sufficient to calibrate the hot-wire and hot-film probes for measurement in stratified air-water flows.

3.9.3.1 Calibration of Glue-On Probes

The following equation is the one commonly used to relate the anemometer output voltage E of a hot-film probe to the measured wall shear stress τ_W (see Kowalski, 1987; Hagiwara et al., 1989; Vlachos et al., 1993; Langsholt et al., 1997; Espedal, 1998):

$$E^2 = C_A + C_B \tau_W^{1/3} \tag{3.19}$$

where C_A and C_B are calibration constants. The equation follows from an analysis of the heat transfer from the flush-mounted hot-film sensor under the condition that the

thermal boundary layer developing above the sensor is entirely contained within the viscous sublayer of the turbulent boundary layer (Bruun, 1995). The calibration constants are determined from a plot of E^2 versus $\tau_W^{1/3}$. Instead of using correction methods to account for changes of the calibration constants with time it is advised to frequently calibrate the probes.

The above relationship does not take account of a change in the voltage at no flow E_0=$E(u$=0). However, it was found in this study that E_0 could significantly vary over an experimental day compared to the range of voltages over which the probe was used. In order to eliminate influences of E_0 on the measurement it was decided to use a relationship for the calibration which takes account of E_0:

$$E^2 = 0.8E_0^2 + C_B\left(\tau_W\right)^n \tag{3.20}$$

It differs from equation (3.19) by replacing calibration constant C_A by an expression in E_0 and by introducing a new unknown in the power of τ_W. The use of the constant $0.8 \cdot E_0^2$ and of the more general power n was based on studies of calibration relationships for hot-wire probes for velocity measurements in Bruun (1995). The unknowns C_B and n are found when data from a single phase calibration is plotted in a logarithmic form of equation (3.20):

$$\log_{10}\left(E^2 - 0.8E_0^2\right) = \log_{10}\left(C_B\right) + n\log_{10}\left(\tau_W\right) \tag{3.21}$$

Power laws are also often used for calibration of hot-wire and hot-film probes for velocity measurement (see equation (3.23)). Bruun (1995) reported an accuracy better than 1 % for this type of calibration relationship when used for velocity measurements. Using a power law of the form as given in equation (3.19) for calibration of glue-on probes will have a reduced accuracy, maybe 3 - 5 %. The reason for this is that, unlike a velocity probe, the glue-on probe is not completely surrounded by the fluid. Only one side of the probe is in the fluid whereas the other side is fixed to a solid wall. As stated in Bruun a substantial part of the heat from the probe is conducted into the substrate, and therefore only a small proportion of the measured probe signal is flow dependent.

3.9.3.1.1 Calibration of Glue-on Probe in Air

3.9.3.1.1.1 Calibration of Glue-on Probe in Air on Low Pressure Rig

The calibration of the wall shear stress probe in the gas phase was done by relating the probe output voltage E to gas wall shear stress τ_{WG} for a range of gas velocities. The wall shear stress at these flow rates was obtained from an established relationship in single phase flow:

$$\tau_{W} = -\frac{D}{4}\frac{dp}{dx} \qquad (3.22)$$

The pressure drop in the equation was calculated from equation (3.13) using the friction factor for a rough tube, equation (3.16) and a roughness k_W=4.6·10^{-5} m. As demonstrated in Section 3.9.1.1.1 this calculation provided very good estimates of the pressure drop in tests with single phase air.

The gas wall shear stress probe was calibrated in the range of gas flow rates of $5<U_G/(m/s)<10$ which could be produced with the biggest orifice plate used on the rig. The range of gas flow rates was expected to cover the whole range of gas phase average velocities expected in the two-phase flows on the low pressure rig. The resulting range of shear stresses was $0.10<\tau_{WG}/Pa<0.34$ in the single phase air flows. A typical calibration curve obtained on the low pressure rig is shown in Figure 3.31. The value for n in equation (3.20) obtained from this graph was ~0.15 and therefore substantially lower than the standard value of n=1/3 in equation (3.19). However, if the same experimental data was plotted in the standard form, equation (3.19), good fit of E^2 versus $\tau_{WG}^{1/3}$ was obtained.

As the probes were calibrated each day the drift of probe readings between days did not have to be studied. But a test of the probe drift on the same experimental day was carried out by comparing a calibration curve produced at the start of the experimental day with a calibration curve from the end of the same experimental day. Over the day the value of τ_{WG} measured with the probe drifted by about 2 %.

3.9.3.1.1.2 Calibration of Glue-on Probe in Air on WASP Rig

The principle of calibration on the WASP facility was the same as that followed on the low pressure rig. The wall shear stress in single phase air was calculated in the same way. Values for the wall shear stress were calculated with equation (3.22).

using equation (3.13) for pressure drop and equation (3.16) with k_{II}=4.6·10^{-5} m for the friction factor. As discussed in Section 3.9.1.1.2 the calculated pressure drop gave very good predictions.

For the experiments at atmospheric pressure the gas wall shear stress probe was calibrated in the range of gas flow rates of 5<U_G/(m/s)<15 to cover the whole range of gas phase average velocities expected in the two-phase flows on the WASP facility. The resulting range of shear stresses was 0.10<τ_{IIG}/Pa<0.77 in the single phase air flows.

The calibrations of the gas wall shear stress probe for the runs at higher than atmospheric pressure on WASP were repeated at the pressures of the two-phase experiment. For the runs at 6 bar the gas wall shear stress probe was calibrated in a range of gas velocities of 0.1<U_G/(m/s)<3.4 and the resulting range of shear stresses was 0.02<τ_{IIG}/Pa<0.22. For the runs at 11 bar the probe was calibrated in a range of gas velocities of 0.8<U_G/(m/s)<3.3 and the resulting range of shear stresses was 0.03<τ_{IIG}/Pa<0.35.

At all pressures good fit of the calibration data was found with equation (3.20) which had also been used for calibrations on the low pressure rig.

3.9.3.1.2 Calibration of Glue-on Probe in Water

3.9.3.1.2.1 Calibration of Glue-on Probe in Water on Low Pressure Rig

The calibration of the wall shear stress probe in the liquid phase was done in a manner analogous to the gas phase. Values for the wall shear stress were calculated with equations (3.22), using equation (3.13) for pressure drop and equation (3.16) with k_{II}=4.6·10^{-5} m for the friction factor. As discussed in Section 3.9.1.2.1 the calculated pressure drop under-predicted the real pressure drop as a result of the inclined section of pipe fixed at the outlet of the test section.

The liquid wall shear stress probe was calibrated over the whole range of liquid flow rates which could be produced on the low pressure rig. This range was 0<U_L/(m/s)<0.58 and the resulting range of shear stresses was 0<τ_{IIL}/Pa<0.96 in the single phase flows. The calibration curves were expressed by means of equation (3.20) as for the air flows. A typical calibration curve obtained on the low pressure rig is shown in Figure 3.32.

A test of the probe drift on the same experimental day was carried out by comparing a calibration curve produced at the start of the experimental day with a calibration curve from the end of the same experimental day. Over the day the value of τ_{liL} measured with the probe drifted by about 5 %, slightly more than in the gas phase.

3.9.3.1.2.2 Calibration of Glue-on Probe in Water on WASP Rig

The principle of calibration of the glue-on probe for liquid wall shear stress measurement on the WASP facility was the same as that followed on the low pressure rig. The wall shear stress in single phase water flow was calculated as described for the low pressure rig. Values for the wall shear stress were calculated with equation (3.22), using equation (3.13) for pressure drop and equation (3.16) with $k_{li}=4.6\cdot10^{-5}$ m for the friction factor. As discussed in Section 3.9.1.2.2 the calculated pressure drop gave good predictions.

The liquid wall shear stress probe was calibrated over the whole range of single phase liquid flows obtainable on WASP. The flow rates covered a range of $0<U_L/(\mathrm{m/s})<0.7$. The resulting range of shear stresses was $0<\tau_{liL}/\mathrm{Pa}<1.4$ in the single phase water flows. The calibration data was again well fitted by equation (3.20).

3.9.3.2 Calibration of Velocity Probes

The standard relationship to relate the anemometer output voltage E of a velocity probe to the velocity of the fluid u_{local} to which the probe is exposed is given by the following equation:

$$E^2 = C_M + C_N\sqrt{u_{local}} \qquad (3.23)$$

where C_M and C_N are calibration constants. The equation follows from the heat balance of a hot-wire probe and is known as King's law (Bruun, 1995). It cannot only be used for hot-wire probes but also for hot-film probes which are used for velocity measurements. In addition to the power law relationship in equation (3.23) several other types of mathematical relationships can be used to represent the calibration data. One possible method presented in Bruun is a polynomial curve where the velocities are fitted by a polynomial in the probe output voltage E. A modified form of this method was adopted for the present study. The velocity was expressed as a polynomial function of the difference between the probe voltage E at a given velocity

u and the voltage E_0 at no flow. With this method changes of the probe voltage at no flow were compensated for. The calibration curve therefore was of the type:

$$u_{local} = g(E - E_0) \tag{3.24}$$

where g was a second or third order polynomial function obtained from best fit to E-E_0.

The accuracy of polynomial functions used as calibration curves in velocity measurements with hot-wire instruments was discussed in Bruun (1995). For a second order polynomial the accuracy is about 3 %, whereas for a third order polynomial it is better than 1 %.

3.9.3.2.1 Calibration of Velocity Probe in Air

3.9.3.2.1.1 Calibration of Velocity Probe in Air on Low Pressure Rig

Equation (3.17) shows that if the $1/7^{th}$ power law can be used to describe the velocity distribution in a single phase flow, the local velocity measured at a fixed radial position r is a linear function of the average velocity. The Pitot tube was fixed at a radial position of 0.01 m from the pipe centre and the relationship between the local velocity measured with the Pitot tube and the air superficial velocity U_G, was obtained over the range of gas flow rates which were covered for the validation of the Pitot tube. Readings for the Pitot tube were corrected for the stem blockage effect, for measuring point position, and for head loss. As stated in Section 3.9.2.1.1 measurements with the Pitot tube gave good predictions for the flow rate.

The measured points were very well fitted by a straight line as suggested by equation (3.17). This curve was used for calibrations of the hot-wire probe. The hot-wire probe was placed at a radial distance of 0.01 m above the pipe centre and the probe output voltage was recorded for the same range of flow rates which was used for calibration of the wall shear stress probe, $5<U_G/(m/s)<10$. The calibration curve for the hot-wire probe was well fitted by a second order polynomial when the local velocity was plotted versus the difference E-E_0 as suggested in equation (3.24). A typical calibration curve is represented in Figure 3.33.

A test of the probe drift on the same experimental day was carried out by comparing a calibration curve produced at the start of the experimental day with a calibration

curve from the end of the same experimental day. Over the day the value of the gas velocity $u_G(r=0.01$ m) measured with the probe drifted by only about 1 %.

3.9.3.2.1.2 Calibration of Velocity Probe in Air on WASP Rig

For the tests on the WASP rig the experiment on air flows at atmospheric pressure with the Pitot tube placed at a radial position of 0.01 m from the pipe centre was repeated. The range of gas flow rates covered was the same which was used in the validation of the Pitot tube on the WASP rig. The linear relationship between the local velocity measured with the Pitot tube and the gas flow rate was identical with that obtained from the low pressure rig. It was also found that excluding the corrections for the stem blockage effect, for measuring point position, and for head loss did not alter this relationship significantly. As stated in Section 3.9.2.1.2 measurements with the Pitot tube gave good predictions for the flow rate.

For the runs at the higher pressures, 6 bar and 11 bar, the test with the Pitot tube was repeated over the range of flow rates which was used for calibration of the gas wall shear stress probe on WASP. For each pressure a relationship of the local velocity measured with the Pitot versus the gas flow rate was obtained which was very well fitted by a straight line. As a consequence of the test at atmospheric pressure no corrections for stem blockage, etc were applied to the Pitot tube readings at elevated pressures.

At all pressures the calibration curve for the hot-wire probe was well fitted by a second order polynomial of the type given by equation (3.24).

3.9.3.2.2 Calibration of Velocity Probe in Water

3.9.3.2.2.1 Calibration of Velocity Probe in Water on Low Pressure Rig

The calibration of the liquid velocity probe was carried out in the same manner as the calibration of the gas velocity probe. In an initial test, where the Pitot tube was placed at a lateral position 0.01 m away from the centre of pipe, a linear relationship between the local velocity at the position of the Pitot tube and the liquid superficial velocity U_L was obtained as suggested by equation (3.17). For this test the same range of liquid flow rates was covered which was used in the validation of the Pitot tube (see Section 3.9.2.2.1). Readings for the Pitot tube were corrected for the stem blockage effect.

for measuring point position, and for head loss. As stated in Section 3.9.2.2.1 measurements with the Pitot tube over-predicted the velocity.

The calibration curve for the Pitot tube at r=0.01 m was used for calibrations of the hot-film velocity probe. The hot-film probe was placed at a radial distance of 0.01 m below the pipe centre and the probe output voltage was recorded for the same range of flow rates which was used for calibration of the liquid wall shear stress probe, $0<U_L/(\text{m/s})<0.58$. The calibration curve for the hot-film probe was well fitted by a second or third order polynomial when the local velocity was plotted versus the difference E-E_0 as suggested in equation (3.24). A typical calibration curve is represented in Figure 3.34.

A test of the probe drift on the same experimental day was carried out by comparing a calibration curve produced at the start of the experimental day with a calibration curve from the end of the same experimental day. Over the day the value of the liquid velocity u_L(r=0.01 m) measured with the probe drifted by 1.5 %.

3.9.3.2.2.2 Calibration of Velocity Probe in Water on WASP Rig

For the tests on the WASP rig the experiment in water flows at atmospheric pressure with the Pitot tube placed at a radial position of 0.01 m from the pipe centre was repeated. The range of liquid flow rates covered was the same which was used in the validation of the Pitot tube on the WASP rig. The plot of local velocity measured with the Pitot tube versus the liquid flow rate was fitted by a straight line as given by equation (3.17). As for the tests with the Pitot tube in air flows on WASP the measured velocities in the liquid were not corrected for any of the effects, like stem blockage etc. As stated in Section 3.9.2.2.2 measurements with the Pitot tube gave good predictions for the flow rate.

For all tests on the WASP rig the calibration curve for the hot-film probe was well fitted by a third order polynomial when the local velocity was plotted versus the difference E-E_0 as suggested in equation (3.24).

3.9.4 Thermocouples

The two thermocouples for measurement of the temperatures in the gas and the liquid were calibrated outside the test spool in water baths of different temperatures versus a reference thermometer (Tempmaster-100 from Labfacility Ltd.).

The two K-type thermocouples were operated by electronics boxes which had an output of 0-10 V between 0 and 50 °C.

Initially, a calibration was carried out before the experiments on the low pressure rig. For both thermocouples the calibration curves were straight lines as shown in Figure 3.35 for the thermocouple for the gas phase. The calibration was checked once during the experimental campaign on the low pressure rig, and the curves proved to be very stable. The calibration was repeated before the experiments on the WASP rig.

3.9.5 Conductivity Probes

As explained in Section 3.3.3 local liquid heights were recorded using twin-wire conductivity probes. The probes were operated from existing electronics boxes. The accuracy of the experimental method was mainly determined by the electric circuits and it was estimated to be around 1 %.

3.9.5.1 Calibration of Conductivity Probes on Low Pressure Rig

On the low pressure rig there was a total of five pairs of conductivity probes to be calibrated: there were three probes in the same cross section in the test spool (see Figure 3.10) and two conductivity probes built into the centre of the acrylic tube sections upstream and downstream of the test spool (see Figure 3.13).

When the original electronics box for the probes built into the acrylic test section was used, the probes interfered with the steel test spool as the box had no isolating transformers. When the box was replaced with one with isolating transformers the probes behaved normally.

The calibration procedure of the probes was carried out as follows: the cyclone at the end of the test section was disconnected and a weir was fixed to the end of the pipe instead. This allowed the pipe to be filled with liquid up to above the middle of the pipe. An opening at the bottom of the weir allowed draining of the liquid to any desired level. The calibration then consisted of recording the probe output voltages

for different levels of static liquid in the pipe. The liquid level was read on the outside of the acrylic test section with a plastic ruler (with subdivisions of 1 mm) fixed normal to a spirit level. With this arrangement the liquid level in the pipe could be determined within +/- 0.5 mm.

All liquid heights were related to the bottom inside wall of the test spool. As this study was concerned with stratified flows the highest level recorded was equal to about $0.7 \cdot D$ where D was the inner diameter of the test spool.

For the probes in the test spool which were all placed off the pipe centre (see Figure 3.10) the minimum liquid height with reference to the tube centre at which the probe started to read was limited by the curvature of the inner wall of the test section. This minimum liquid height was taken into account to interpret the probe readings.

From visual inspection of the water level in the acrylic test section it was found that the liquid level was 3 mm higher at the tube wall than at the centre of the pipe due to adhesion of the water to the acrylic. The precise liquid height for each of the three off-centre probes in the test spool was then determined from fitting a second order polynomial curve between the pipe centre and the pipe wall accounting for the observed increase of liquid height towards the wall.

The calibration points for each probe in the test spool were very well represented by second order polynomial curves as shown in Figure 3.36. The labels for the individual probes were identical with those in Figure 3.10. The probes in the centre of the acrylic test section upstream and downstream of the test spool gave calibration curves which could be represented by straight lines as shown in Figure 3.37. The probe labels were those used for the schematic of the low pressure rig in Figure 3.13.

At the start of the experimental programme on the low pressure rig full calibrations were done on each day, but it was found that only minor changes occurred from day to day. Later on calibrations were done at weekly intervals.

3.9.5.2 Calibration of Conductivity Probes on WASP Rig

On the WASP rig conductivity probes were used at two axial positions: there were the three conductivity probes in the same cross section in the test spool as represented in Figure 3.10 and downstream of this there was Srichai's (1994) conductivity probe section with a total of five conductivity probes (see Figure 3.2). Three of Srichai's

probes were operated: the centre probe and the two probes in the same half of the cross section as the conductivity probes in the test spool. These probes were labelled cp_s3, cp_s4 and cp_s5 in Figure 3.2. By using these probes only, the influence of flow disturbances of the upstream probe inserts was avoided as much as possible.

Calibration of the conductivity probes on the WASP rig was versus the gamma densitometer downstream of the conductivity probes. The gamma densitometer was first calibrated with an empty tube (calibration with air) and then with a tube full of water. The calibration procedure of the probes versus the gamma densitometer was as follows: the test section was statically filled with liquid up to a certain level. With a centre pipe scan of the gamma the liquid height in the centre of the test section was measured and this liquid level was related to the voltage outputs recorded for the conductivity probes. It was assumed that, as on the low pressure rig, the liquid level was 3 mm higher at the tube wall than at the centre of the pipe due to adhesion of the water to the acrylic. The precise liquid height for each of the three off-centre probes in the test spool and in Srichai's (1994) probe section was then determined from fitting a second order polynomial curve between the pipe centre and the pipe wall.

For the probes in the test spool and for the two probes cp_s4 and cp_s5 in Srichai's (1994) conductivity probe section which were all placed off the pipe centre the minimum liquid height with reference to the tube centre at which the probe started to read was limited by the curvature of the inner wall of the test section. As described for the low pressure rig this minimum liquid height was taken into account to interpret the probe readings.

The calibration data for each probe in the test spool and in Srichai's section were very well represented by second order polynomial curves of the type shown in Figure 3.36 for the low pressure rig.

One full calibration of all the probes was done at the beginning of the experimental campaign on WASP. The probe outputs were then checked each day for one liquid level and compared with the calibration curve produced at the start of the campaign. The changes were found to be negligible, therefore the calibration curve from the start of the campaign was used for the whole campaign.

3.10 Transformation of Local Measurements into Phase Average Parameters

3.10.1 Liquid Holdup

The liquid holdup in the test spool was evaluated by numerically integrating over the liquid heights measured with the three conductivity probes in half a cross section (see Figure 3.10). Figure 3.38 represents the procedure schematically. The liquid heights measured with the three probes cp_ts1, cp_ts2 and cp_ts3 are denoted $h_{L,z1}$, $h_{L,z2}$ and $h_{L,z3}$ in the figure. Symmetry with respect to the pipe centre was assumed. As indicated in the figure the liquid heights between two positions of measurement in the transverse, z, location were extrapolated linearly. It was assumed that the liquid height in the centre of the pipe was identical with the one measured with probe cp_ts1 and the liquid height at the wall of the tube was taken to be that measured by probe cp_ts3. The mean liquid height h_L related to this holdup could then be obtained from the measured value for liquid holdup ε_L by using equation (2.9) for the liquid phase area S_L in chapter 2:

$$\varepsilon_L = \frac{S_L}{\pi R^2} = \frac{1}{\pi}\left[\pi - \cos^{-1}\left(\frac{h_L}{R} - 1\right) + \left(\frac{h_L}{R} - 1\right)\sqrt{1 - \left(\frac{h_L}{R} - 1\right)^2}\right] \qquad (3.25)$$

3.10.2 Phase Average Velocities

Local velocities in the gas and liquid phases were measured using the hot-wire probe in the gas and the conical hot-film probe in the liquid. These local measurements had to be transformed into phase average velocities which were needed to derive interfacial shear stress under transient conditions from the one-dimensional model equations (see Section 2.3.2).

In single phase flows obtaining phase average velocities from local measurements is straightforward as the flows are axisymmetrical. The velocity has a maximum in the centre of the pipe and is zero at the pipe wall. In this case it would be possible to fit measured local velocities in a vertical plane through the centre of the tube with an established velocity profile (second order polynomial curve for laminar flow or power law profile for turbulent flow) and then to obtain the mean velocity from integration over the fitted curve and dividing by the flow cross sectional area.

Obtaining phase average velocities in a separated two-phase flow is a much more complex task, for two main reasons. The flow in each phase is not axisymmetrical and the velocities on the boundaries of each phase are not zero everywhere: the velocities are zero at the tube wall, but they are non-zero at the fluid-fluid interface. The fluid velocity at the interface is not a priori known and it would be very difficult to determine this due to the complex structure of the interface.

In principle accurate determination of phase average velocities from local velocities in the case of a separated two-phase flow would necessitate measurement of local velocity at each point in the phase and then integrating over these measurements. Of course this would mean a lot of effort for each measurement. Also, in the experimental setup of the present study the positions of the velocity probes in both phases are restricted to vertical traverses through the centre of the tube. In principle it would be possible to rotate the complete test spool to traverse the velocity probes at an angle with reference to the vertical but by rotating the test spool also all the other probes (conductivity probes, pressure transmitter, wall shear stress probe) would be displaced from the position in which they have to be placed for measurements. Furthermore, the position of the velocity probes closest to the phase boundaries is limited. Due to their own size the probes could not be positioned closer to the tube wall than about 5 mm and they also had to be kept some distance away from the interface. The gas velocity probe would be destroyed if it was hit by a wave of liquid and the liquid velocity probe would read unphysical values if it was placed in the interfacial area where it would be exposed to a mixture of the two fluids.

For the present study a method had to be evaluated by means of which the phase average velocities could be obtained from traversing each velocity probe vertically through the bulk of the respective phase. The method is discussed for the gas and liquid phases separately in Sections 3.10.2.1 and 3.10.2.2.

One further difficulty for the present study was the transient nature of the experiment. In steady state the flow rates can be set to what is required and measurements with both velocity probes can then be taken at different positions by traversing the probes through the tube. This procedure is not possible in the transient case. In the transient experiment both probes have to be placed in fixed positions and in order to obtain data for local velocities at other positions the transient experiment has to be repeated. Obtaining phase average velocities in the transient case therefore needed repetitive

transients at given conditions with the velocity probes in different positions in each repeat. The phase average velocities could then be obtained by combining the velocity traces of each probe over the repeated runs. This procedure would, of course, only work if the transients were reasonably repeatable and this was discussed in Chapter 5 where the transient data is presented.

3.10.2.1 Phase Average Velocities in Gas Phase

Determination of phase average velocity in the gas was based on measurements of the local gas velocity at three positions as represented in Figure 3.39.

The analysis was started by assuming a $1/7^{th}$ power law distribution in the transverse, z, direction (see Hewitt, 1990):

$$u_G(y,z) = u_G(y,z=0)\left(1-\frac{z}{z_{max}}\right)^{1/7} \tag{3.26}$$

where $u_G(y,z=0)$ is the velocity in the centre of the pipe and z_{max} is the distance of the pipe wall from the pipe centre at the given vertical position y. A power law was assumed as all flows in the present study were turbulent. This type of law had been established in measurements with the Pitot tube (see Section 3.9.2.1). The integration in transverse direction assuming zero velocity at the pipe wall and symmetry with respect to a vertical plane through the centre of the pipe gave:

$$u_G(y) = \frac{1}{z_{max}}\int_0^{z_{max}} u_G(y,z)dz = \frac{7}{8}u_G(y,z=0) \tag{3.27}$$

This expression for $u_G(y)$ could then be used to integrate in the vertical direction in the gas phase to obtain the phase average velocity u_G:

$$u_G = \frac{1}{S_G}\int_{h_L}^{D} u_G(y)dS = \frac{1}{S_G}\frac{7}{8}\int_{h_L}^{D} u_G(y,z=0)dS \tag{3.28}$$

where S_G is the flow cross sectional area of the gas phase and dS as a function of y can be derived from equation (2.9):

$$S(y) = R^2\left[\pi - \cos^{-1}\left(\frac{y}{R}-1\right)+\left(\frac{y}{R}-1\right)\sqrt{1-\left(\frac{y}{R}-1\right)^2}\right] \tag{3.29}$$

Equation (3.28) was used to obtain phase average velocities from local measurements of the gas velocity along the vertical plane through the centre of the tube. The

measured velocities represented discrete values of the function $u_G(y;z=0)$ in the equation and the phase average velocity was obtained from numerical integration over these points. It was assumed that the velocity at the top wall (at $y=D$) was zero and linear interpolation was used in between the measured points.

This method of deriving phase average velocity was evaluated for measurements of the local gas velocity from the low pressure rig. For a given flow (given U_L, U_G) the integration was carried out over the three velocities measured at 0, 15 and 30 mm above the pipe centre. No measurements below the centre of the pipe were included. Phase average velocities were obtained for different combinations of gas and liquid superficial velocities with U_L=0.04, 0.06, 0.08 m/s and $5<U_G/(\text{m/s})<10$. These were then compared with the gas phase average velocities obtained from the measured holdup ε_L and the superficial gas velocity U_G obtained from the rig flow rate acquisition:

$$u_G = \frac{U_G}{1-\varepsilon_L} \tag{3.30}$$

Results of this comparison are presented in Figure 3.40. The agreement between the data obtained with the two different methods, i.e. the integration over measurements with the hot-wire probe on the one hand and the method of deriving the phase average velocity from the holdup and the superficial gas velocity on the other hand, was very good.

3.10.2.2 Phase Average Velocities in Liquid Phase

Determination of phase average velocity in the liquid was based on measurements of the local liquid velocity at three positions as represented in Figure 3.41. The analysis of the liquid phase was done in a manner analogous to the gas phase.

As in the gas phase, a $1/7^{th}$ power law distribution in the transverse, z, direction was assumed and integration in vertical direction in the liquid phase resulted in a relationship analogous to equation (3.28) for the gas phase:

$$u_L = \frac{1}{S_L}\int_0^{h_L} u_L(y)dS = \frac{1}{S_L}\frac{7}{8}\int_0^{h_L} u_L(y,z=0)dS \tag{3.31}$$

where S_L is the flow cross sectional area of the liquid phase and dS as a function of y is given by equation (3.29).

Equation (3.31) was used to obtain phase average velocities from local measurements of the liquid velocity. The measured velocities gave discrete values of the function $u_L(y,z=0)$ in the equation and the phase average velocity was obtained from numerical integration over these points. It was assumed that the velocity at the bottom wall (at $y=0$) was zero and linear interpolation was used in between the measured points.

This method of deriving phase average velocity was evaluated for local measurements of liquid velocity from the low pressure rig. For a given flow (given U_L, U_G) the integration was done over the measurements at three positions. The positions depended on the flow conditions. At a combination of high gas flow rate/low liquid flow rate the liquid level in the pipe would be much smaller compared to a case with a small gas flow rate and high liquid flow rate. The position nearest to the interface was determined from measurements of the mean liquid height h_L. The probe position nearest to the interface was e.g. 16 mm in a case with a high holdup and 9 mm in a case with a very low holdup. The probe position nearest to the wall was ~ 5 mm.

Phase average velocities were obtained for different combinations of gas and liquid superficial velocities with U_L=0.04, 0.06, 0.08 m/s and $5<U_G/(m/s)<10$. These were then compared with the liquid phase average velocities obtained from the measured holdup and the superficial liquid velocity obtained from the rig flow rate acquisition:

$$u_L = \frac{U_L}{\varepsilon_L} \tag{3.32}$$

Results for this are presented in Figure 3.42. The agreement between the data obtained with the two different methods was around +/- 10 %.

3.11 Performance of Instrumentation Methods in Two-Phase Flow

As was described in Section 3.9, the instruments were checked or calibrated in single phase flows or, in the case of the holdup measurements, calibrated in static conditions either visually or against a gamma densitometer. It is obvious that operation of the instruments under two-phase flow conditions represents a more serious challenge. Before proceeding to the presentation and analysis of the data in Chapters 4 and 5 (for the steady state and transient situations respectively) it is important to make an objective assessment of the performance of the instruments so that meaningful

conclusions can be drawn from the analysis of the data. The assessment was based on experimental data from the main series of experiments in this study, the experiments on transient stratified flow (Chapter 5). Each transient experiment was run three times with the velocity probes in different positions in order to determine phase average velocities using the methods presented in Section 3.10.2. The following assessments were made of the various instruments:

(1) **Liquid level (h_L)/holdup (ε_L).** The measurement of liquid level using the conductance probes was found to be highly repeatable and robust in all the tests. Repeatability for a given set of conditions was around +/- 2 % on the low pressure facility and around +/- 10 % on the WASP facility. The *fluctuations* of liquid level (h_L') were also quite repeatable. Thus, it is concluded that all of the data for liquid height/holdup can be used for further analysis.

(2) **Gas velocity (u_G).** The *precision* of a given measurement of the gas velocity would be expected to be better than +/- 5 %. As was explained above, three successive measurements were made for each transient in which the hot-wire probe was placed in a different position. The data from the three successive runs could then be processed to predict the instantaneous mean gas velocities. In steady state flows, these instantaneous means could be used together with the holdup data to obtain the total gas volumetric flow which could then be compared with that obtained from the rig flow meters. The comparisons for the gas volumetric flows were within about +/- 10 % which was encouraging. It is concluded, therefore, that the gas flow rates can be used in further analysis.

(3) **Liquid velocity (u_L).** The hot-film probe for liquid velocity measurements was found to perform much less well than did the hot-wire probe for the gas velocity measurements. Specifically, there was a noticeable temperature drift and reproducibility was relatively poor. When the data for the three successive runs (with the hot-film probe in three different positions) were combined with the holdup data to give average liquid volumetric flows, typical discrepancies with the rig flow meters were of the order of +/- 30 %. Thus, a procedure of *normalization* was implemented in which the velocities observed in the initial steady state period (i.e. before the transient) were multiplied by the ratio of the rig flow rate to the determined averaged flow rate. The normalization factor was retained throughout

the transient and in the final steady state period. In the latter period, the velocities agreed to better than +/- 10 % indicating that the normalization procedure was performing reasonably. This procedure was adopted and the data used (though with some caution).

(4) **Gas wall shear stress (τ_{WG}).** Reproducibility of the gas wall shear stress measurement between the three runs on the low pressure rig was around +/- 15 % and reproducibility for the runs on the WASP facility was around +/- 10 %. Temperature drift would be less serious for the gas measurement because the over-temperature is much greater and the effect of small changes in temperature therefore much smaller. Thus, the data for gas wall shear stress were accepted as being reasonably sound and, certainly in the case of the low pressure facility results, were used in further analysis.

(5) **Liquid wall shear stress (τ_{WL}).** The liquid wall shear stress measurement was much more difficult than that of the gas wall shear stress since the overheat was much smaller and the sensitivity to temperature drifts in the system much greater. Reproducibility between the successive experiments under nominally the same conditions was around +/- 20 % in the low pressure rig and around +/- 30 % in the WASP facility. This made it difficult to make conclusive comparisons with the various models for liquid wall shear stress. However, since the gas wall shear stress is evidently reasonably reliable, a feasible approach is to use the other parameters (total pressure gradient and hydraulic gradient where appropriate) to normalize the data for liquid wall shear stress based on the initial steady state period. This approach was followed for the case of the low pressure data. Unfortunately, it was not possible to do this in the case for the WASP data for which, as will be explained below, the pressure gradient measurements could not realistically be used.

(6) **Pressure gradient (dp/dx).** Measurement of pressure gradient in stratified multiphase flows presents a significant difficulty because of the very small differential pressures involved. Typically, these were of the order of 10 Pa in the low pressure facility and 2 Pa in the WASP facility, measured over a distance (see Figure 3.8) of 0.3 m. In previous experiments on the WASP facility, Srichai (1994) measured pressure gradients in stratified flow using an inclined

manometer. This approach was not appropriate in the present experiments since the pressure gradient needed to be measured in the transient whereas Srichai was measuring in purely steady state flow. Furthermore, since Srichai was measuring over a total distance of 2 m and over a range of gas flow rates significantly higher than those in the present experiments, the range of pressure drops measured was much higher (100-400 Pa). The Rosemount Smart Pressure Transmitter used in the present experiments is capable, in principle, of measuring the very small pressure differences. Thus, its precision is around +/- 0.2 Pa which would represent around +/- 10 % accuracy in pressure gradient in the experimental range covered here. However, the pressure gradients are so small that this kind of accuracy can only be obtained under rather ideal conditions. The conditions in the low pressure experiments were reasonably ideal; the experiments were conducted at approximately equilibrium atmospheric temperatures and it was possible to carry out detailed checks on the instrumentation at all stages. Thus, despite the significantly new challenge of measuring such small pressure differences, it is believed that the measurements in the low pressure facility are reasonably accurate, probably better than +/- 2 % (estimated in terms of the reproducibility between the three successive runs). However, in the more demanding conditions in the WASP facility, where the pressures were higher for most of the runs and where much more industrial-type conditions persisted, it was found impossible to obtain consistent pressure drop data. Thus, the data obtained for two-phase flow were often *lower* than for the same gas flow in the channel. This, of course, is completely inconsistent and indicates that some error has crept in in this application. The availability of time on the WASP facility prevented extensive work being done on addressing this problem. It was concluded, therefore, that the pressure difference data should not be used in further analysis as reported in Chapters 4 and 5. As a consequence of the absence of the pressure drop data, the normalization of the liquid wall shear stress probes could not be carried out (see (5) above) for the case of the WASP facility data and further analysis of this wall shear stress data has been deferred.

Despite the difficulties mentioned above, it has been felt important to put *all* the data obtained in the main set of experiments, the transient tests, into a retrievable form. This has been done in the form of CD ROMs which are included in a separate data

report (Shaha & Hewitt, 1999). This report lists the data on the CD ROMs and gives an indication of how to retrieve it.

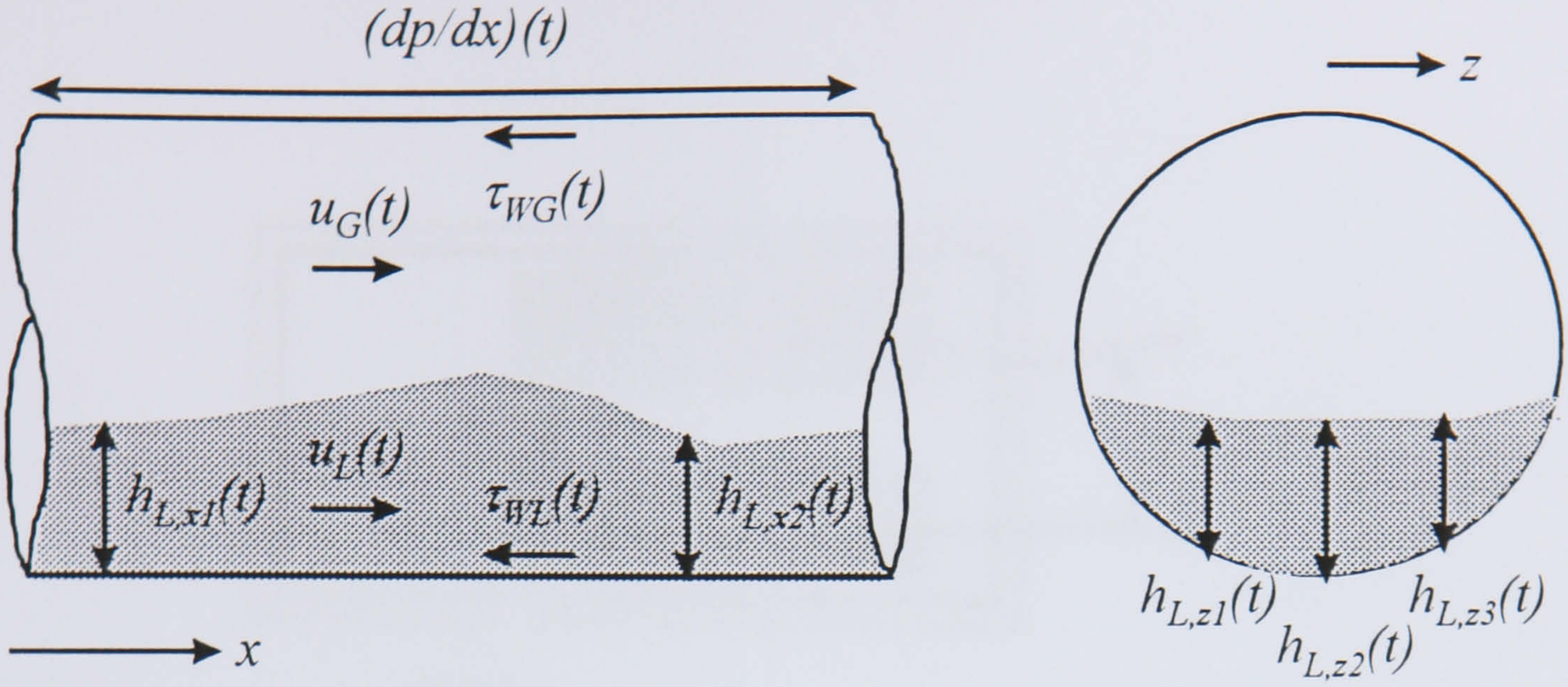


Figure 3.1 Measured parameters

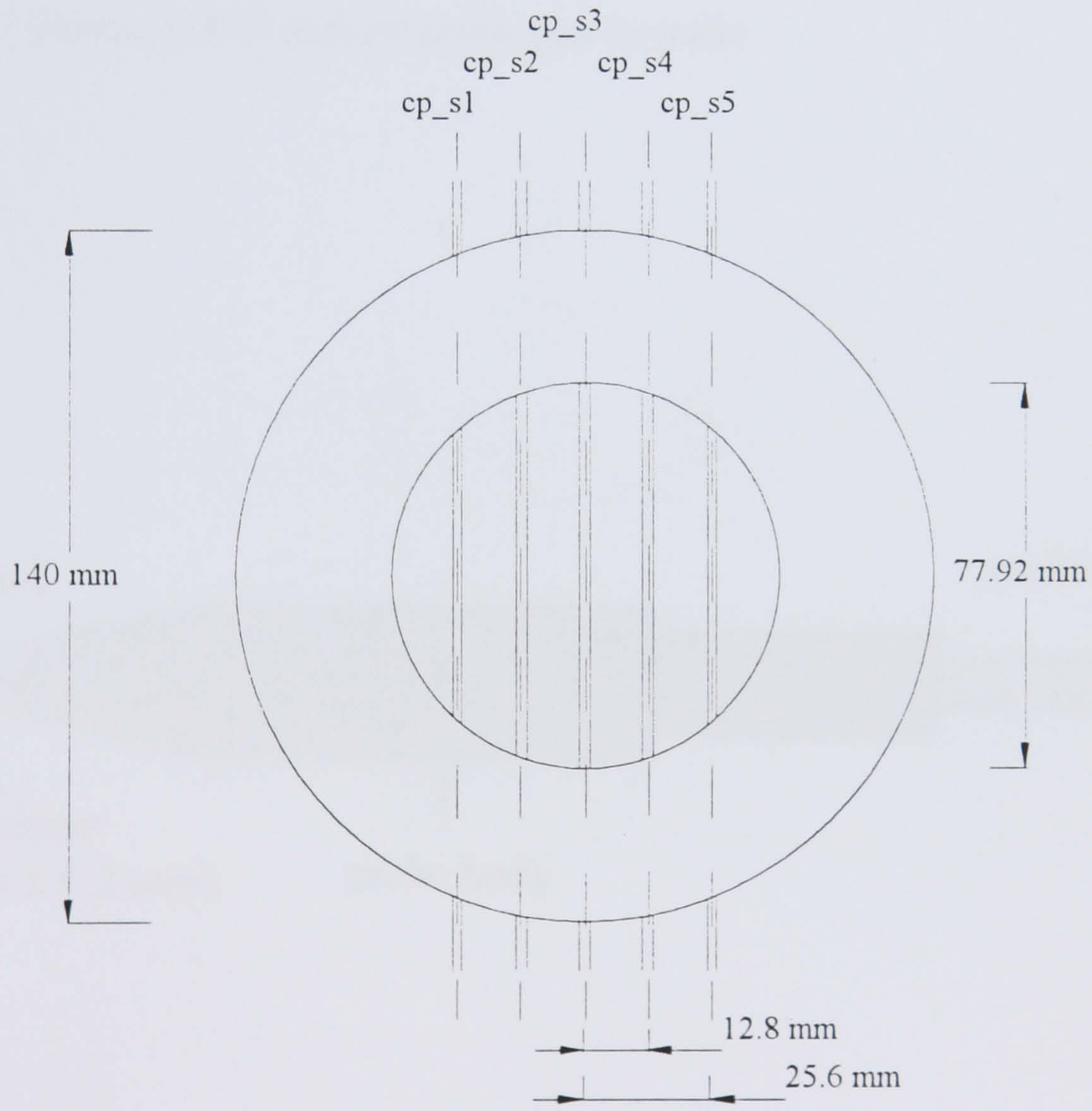


Figure 3.2 Srichai's (1994) conductivity probe section (to scale)

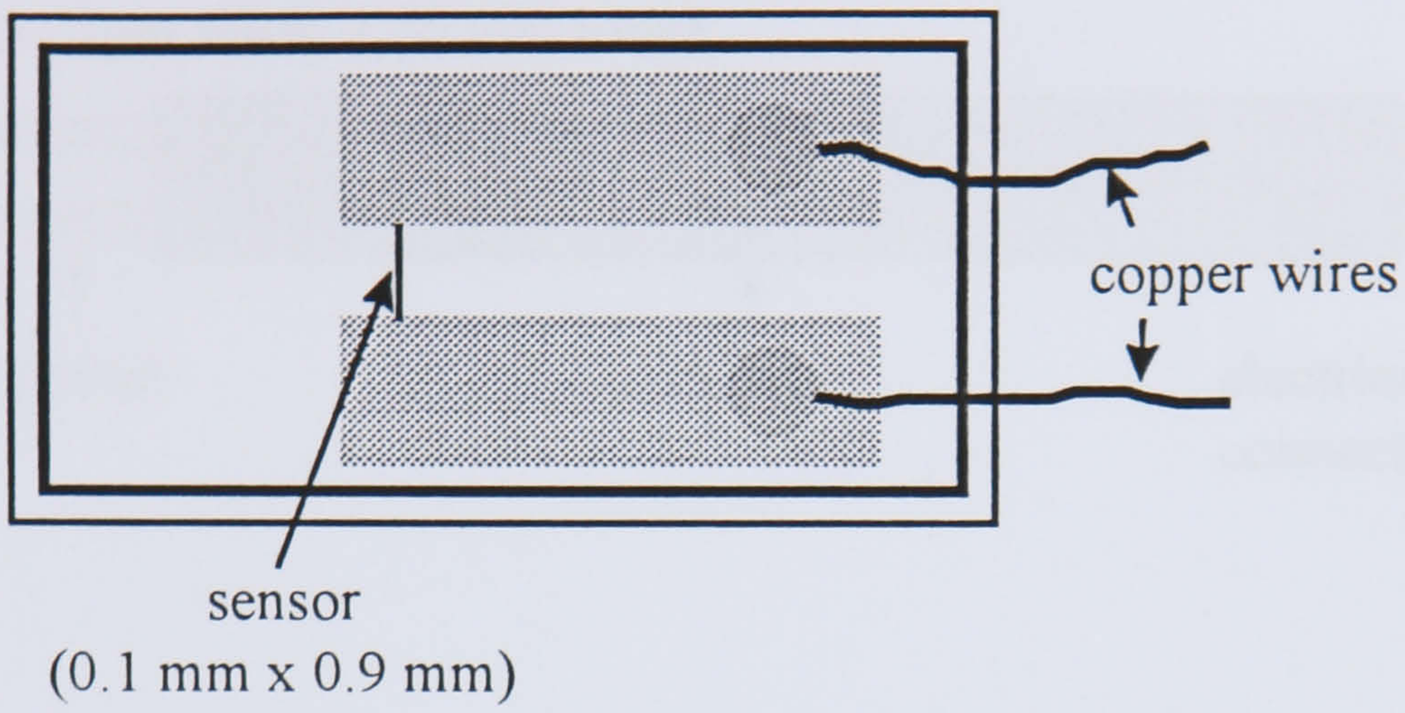


Figure 3.3 Dantec 55R47 glue-on probe (not to scale)

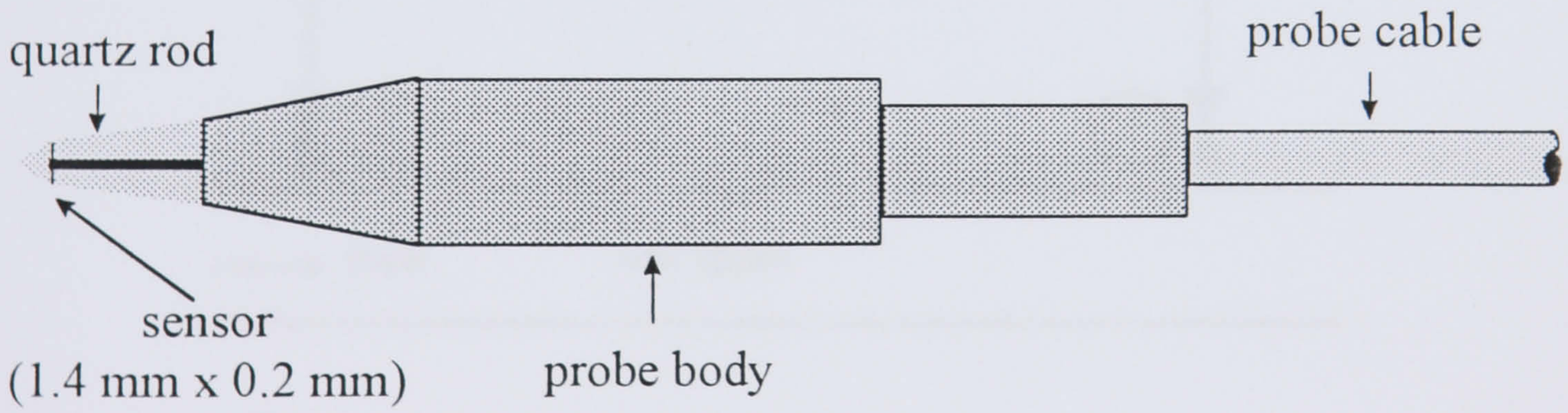


Figure 3.4 Dantec 55R42 conical hot-film probe (not to scale)

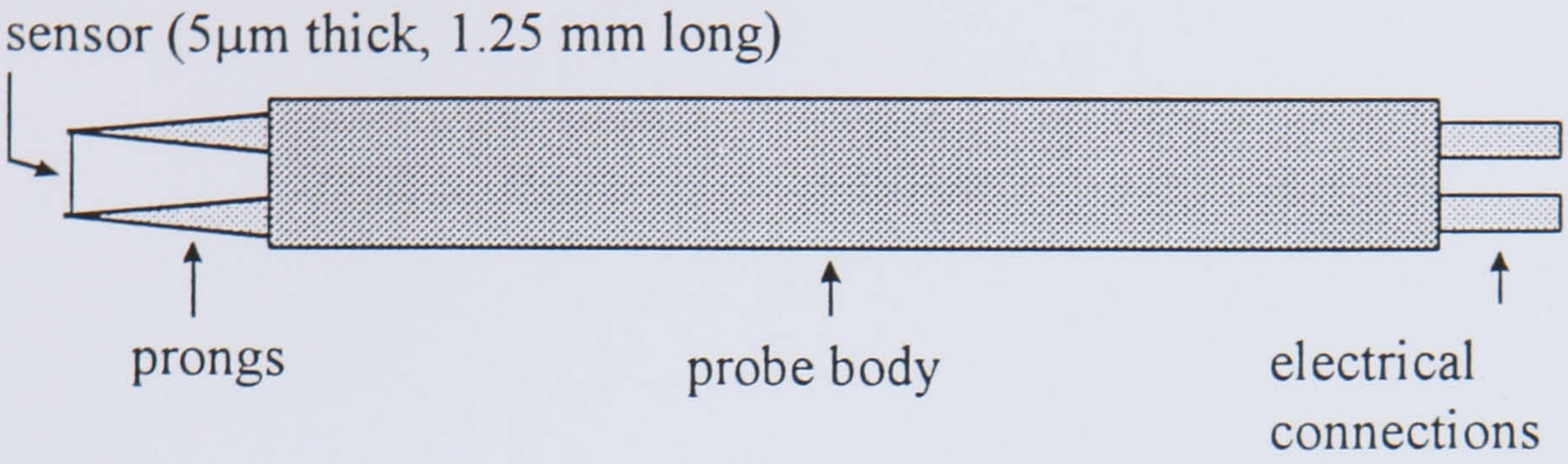
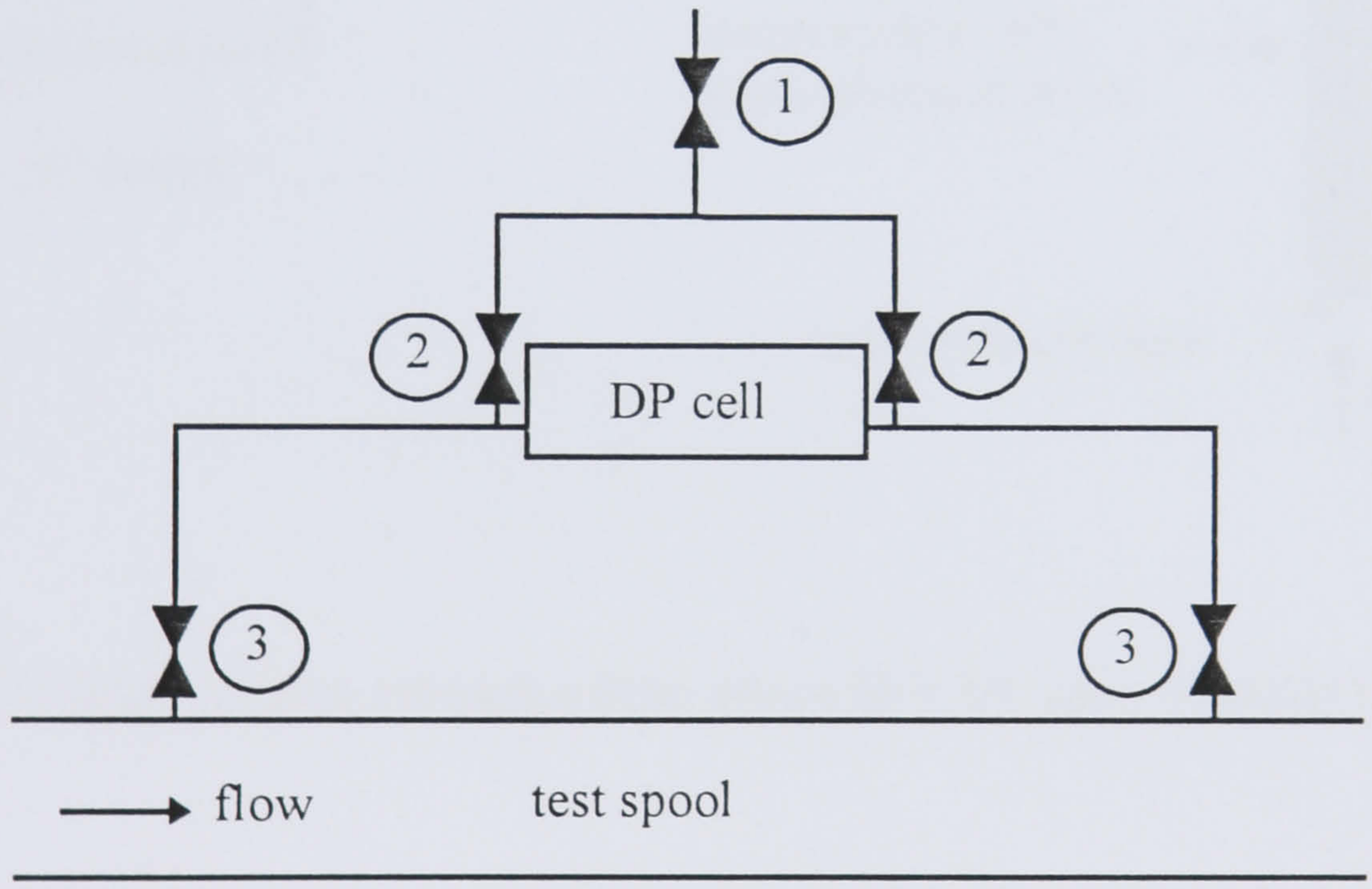


Figure 3.5 Dantec 55P11 miniature wire probe (not to scale)



1 isolating valve on purge line

2 isolating valves on drain ports of dp cell

3 isolating valves on pressure tappings

Figure 3.6 Arrangement for measuring pressure drop

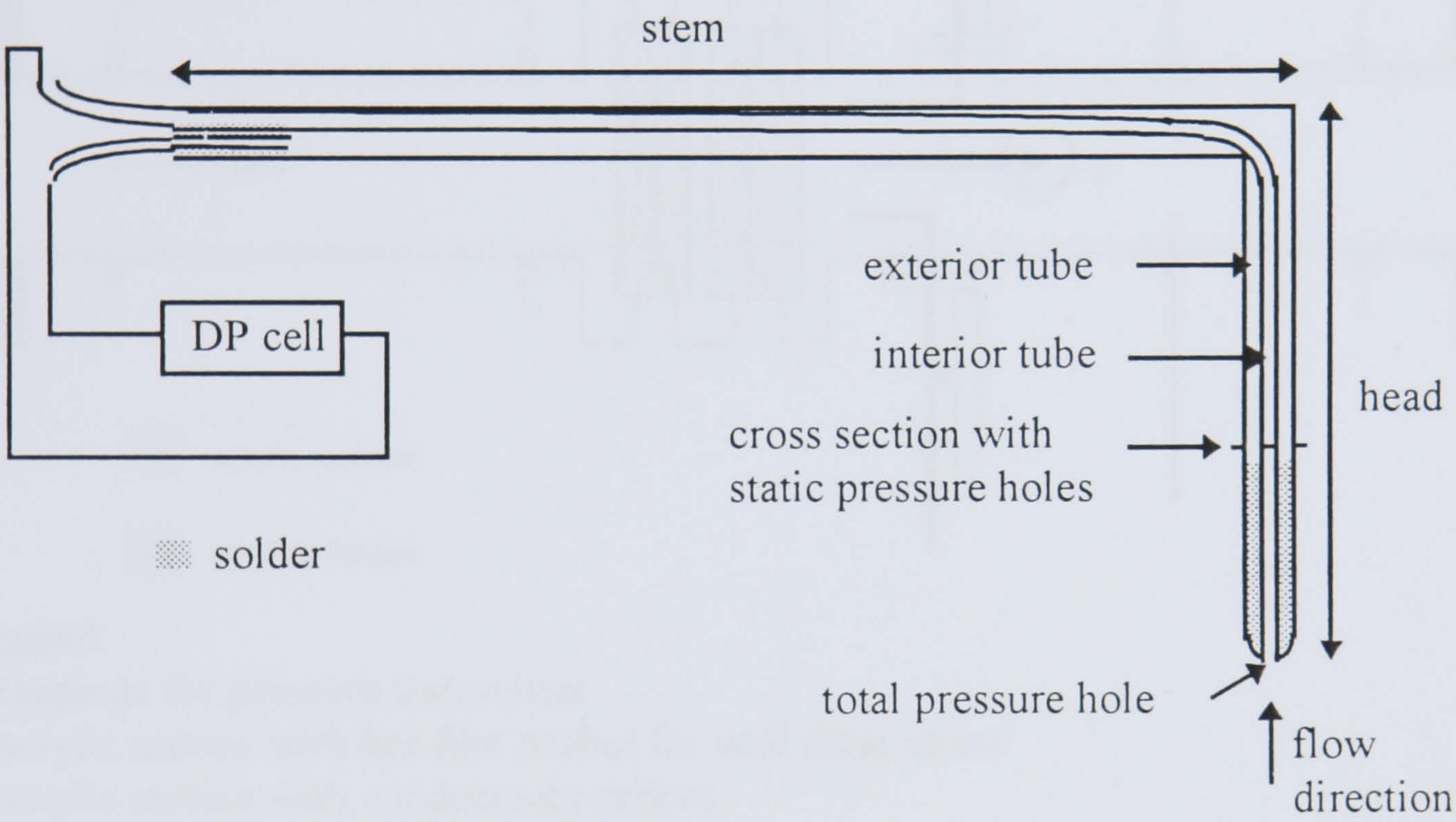
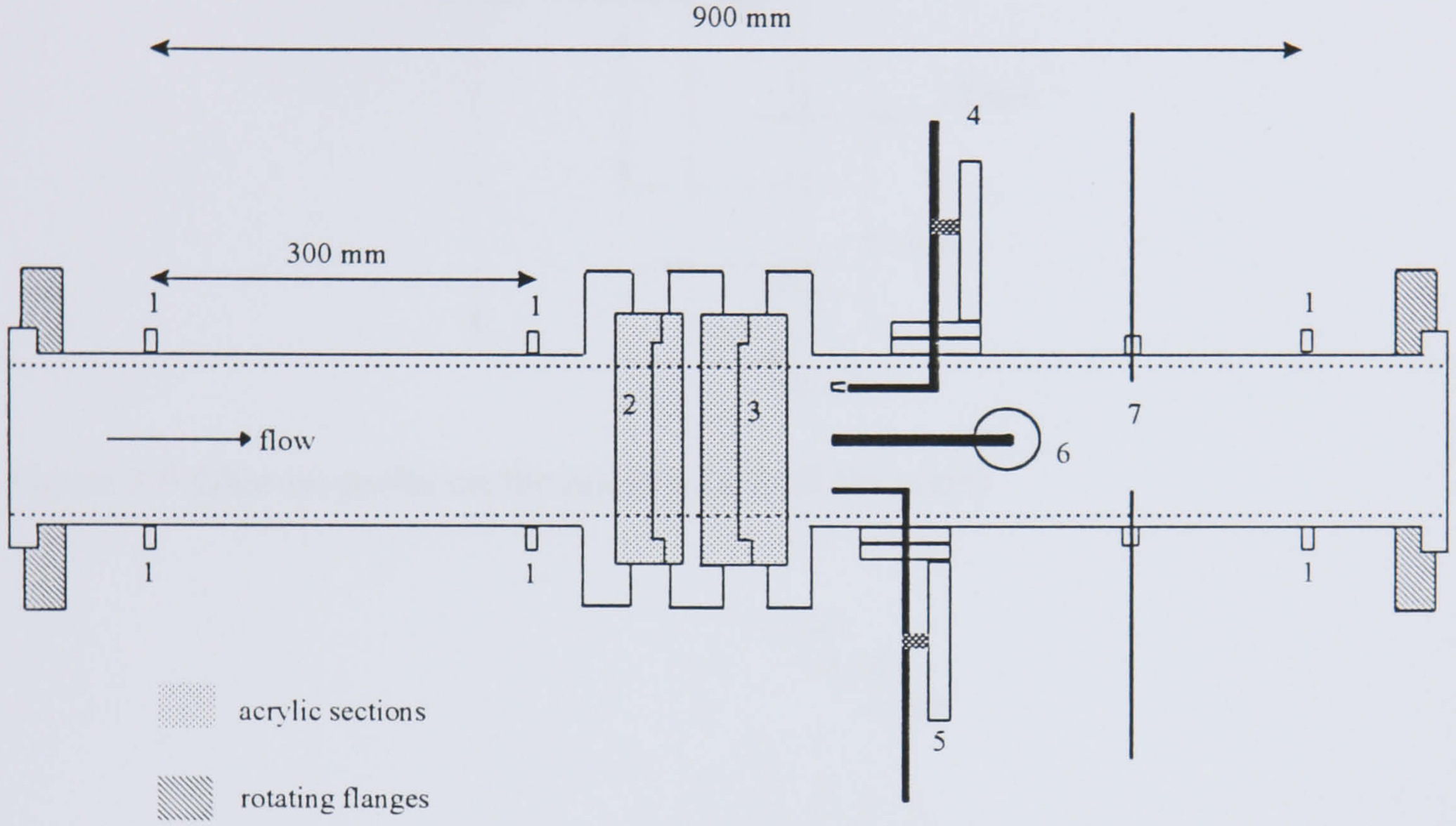


Figure 3.7 Length section through a Pitot tube with a DP cell connected (not to scale)



Legend:
1 tappings for pressure transmitter
2 acrylic section with hot-film probes for wall shear stress
3 acrylic section with conductivity probes
4 traversing hot-wire probe for gas velocity
5 traversing hot-film probe for liquid velocity
6 traversing Pitot tube
7 thermocouples

Figure 3.8 Length section through test spool (not to scale)

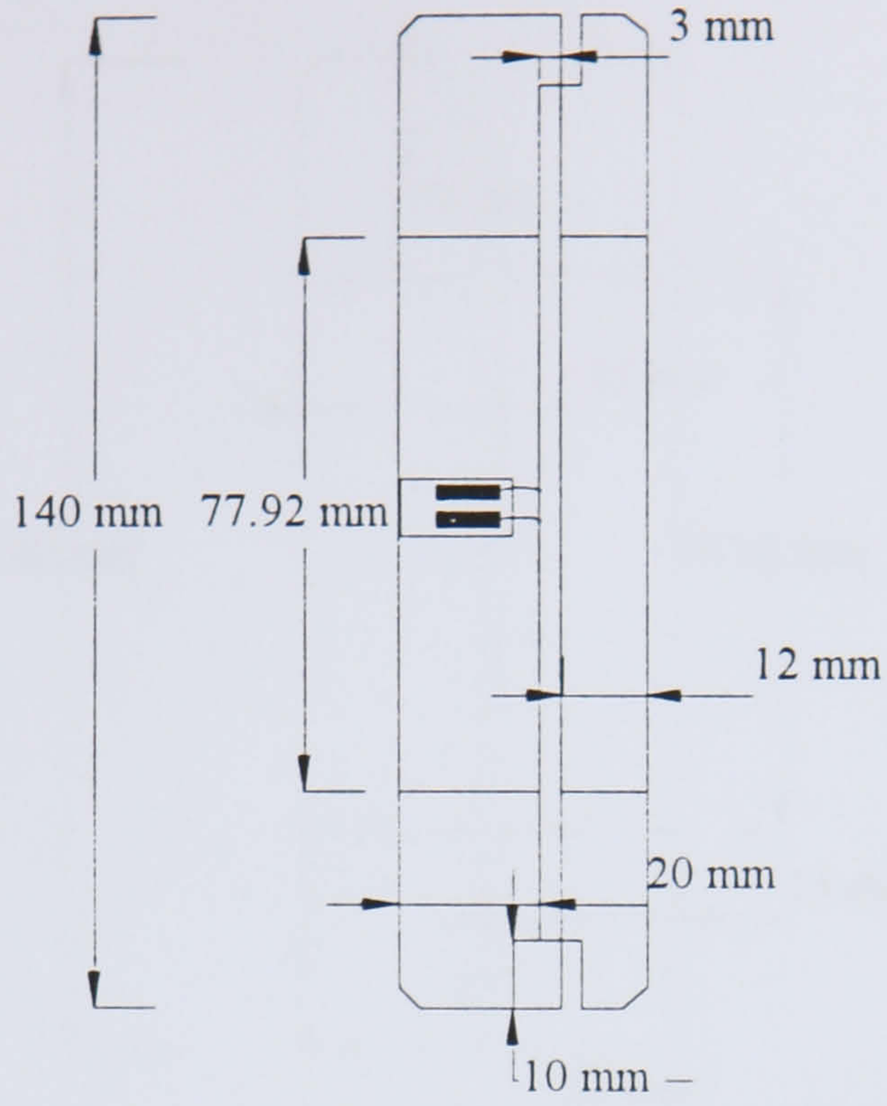


Figure 3.9 Glue-on probe on the inside tube wall (to scale)

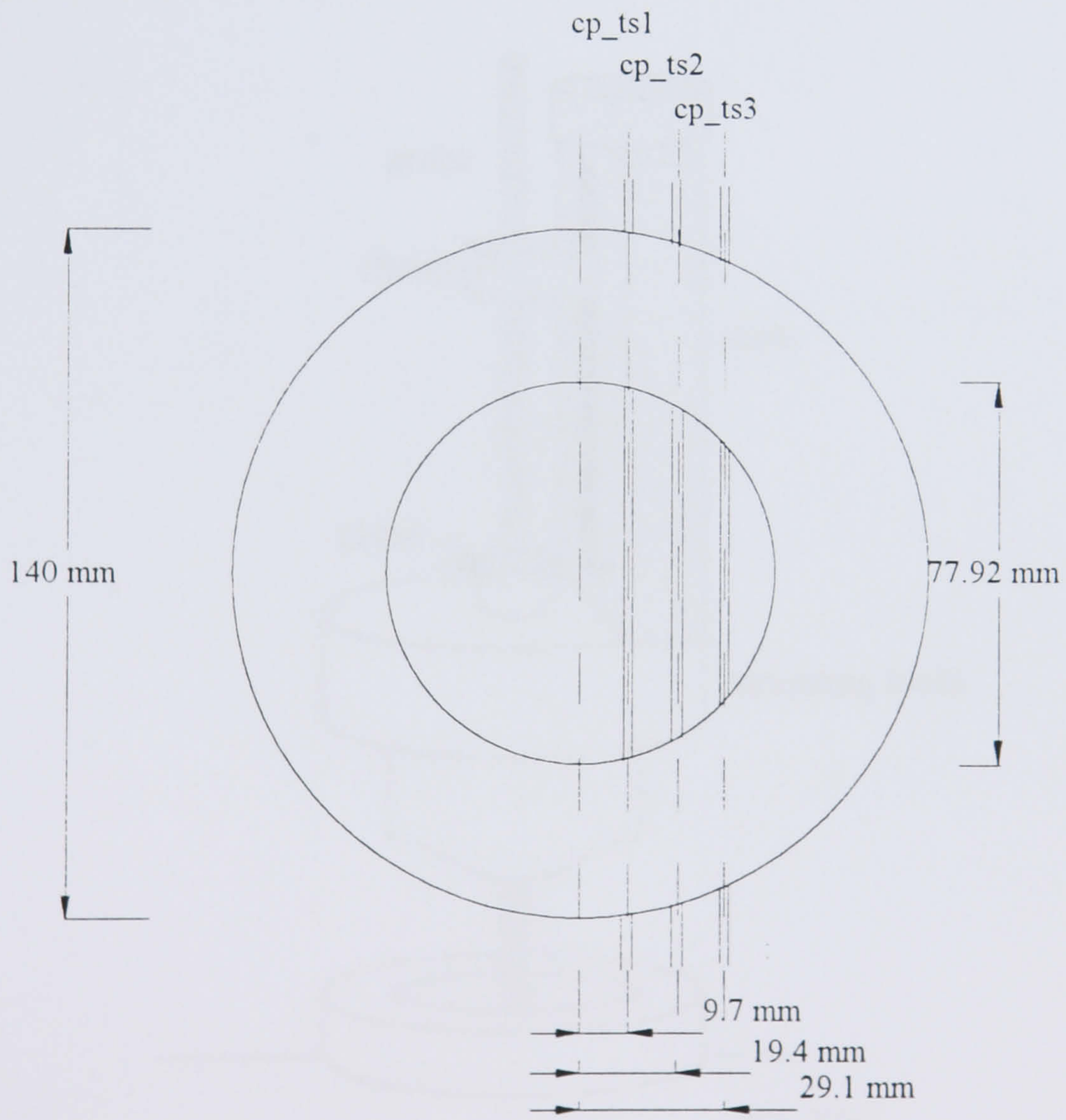


Figure 3.10 Representation of conductivity probes in the cross section facing the flow (to scale)

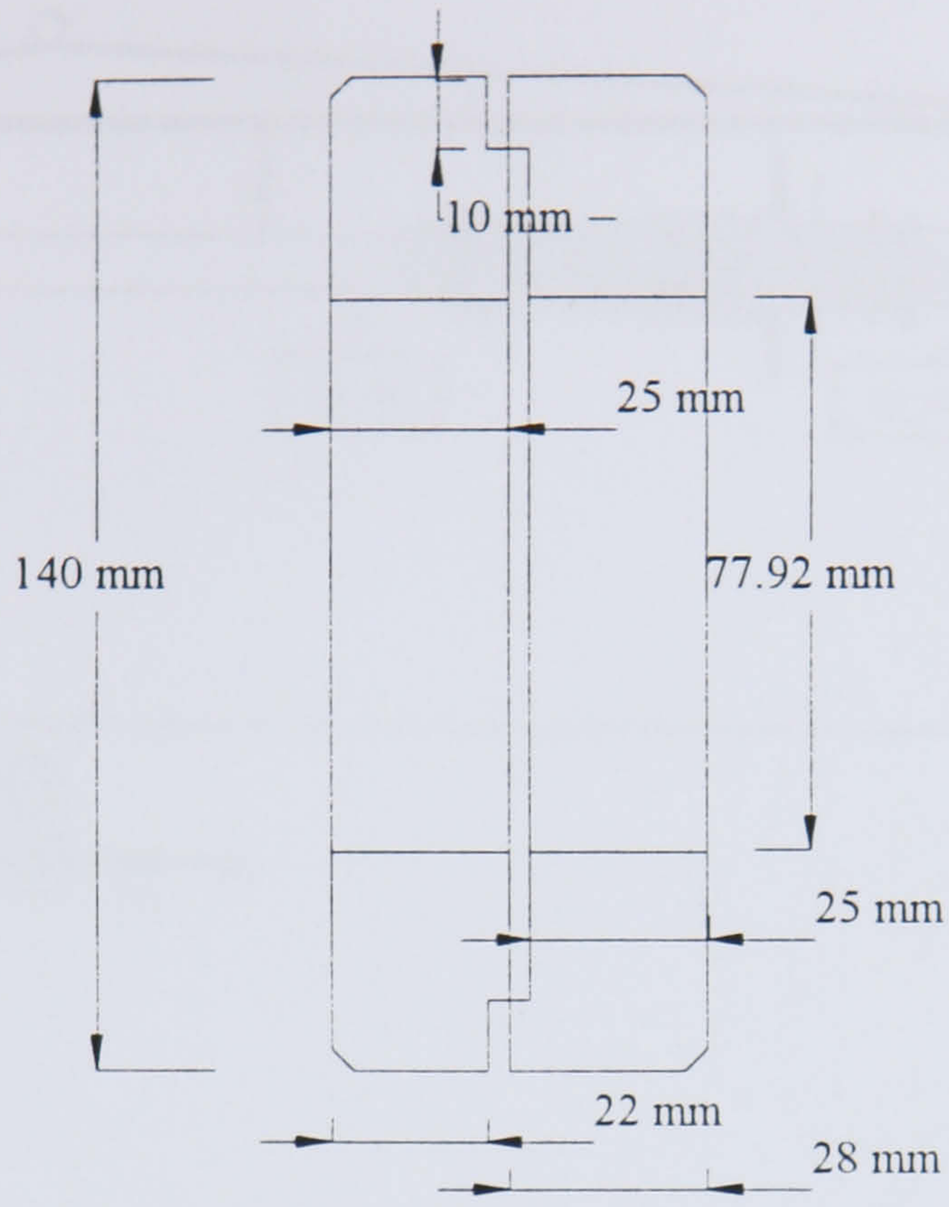


Figure 3.11 Length section through conductivity probe section (to scale)

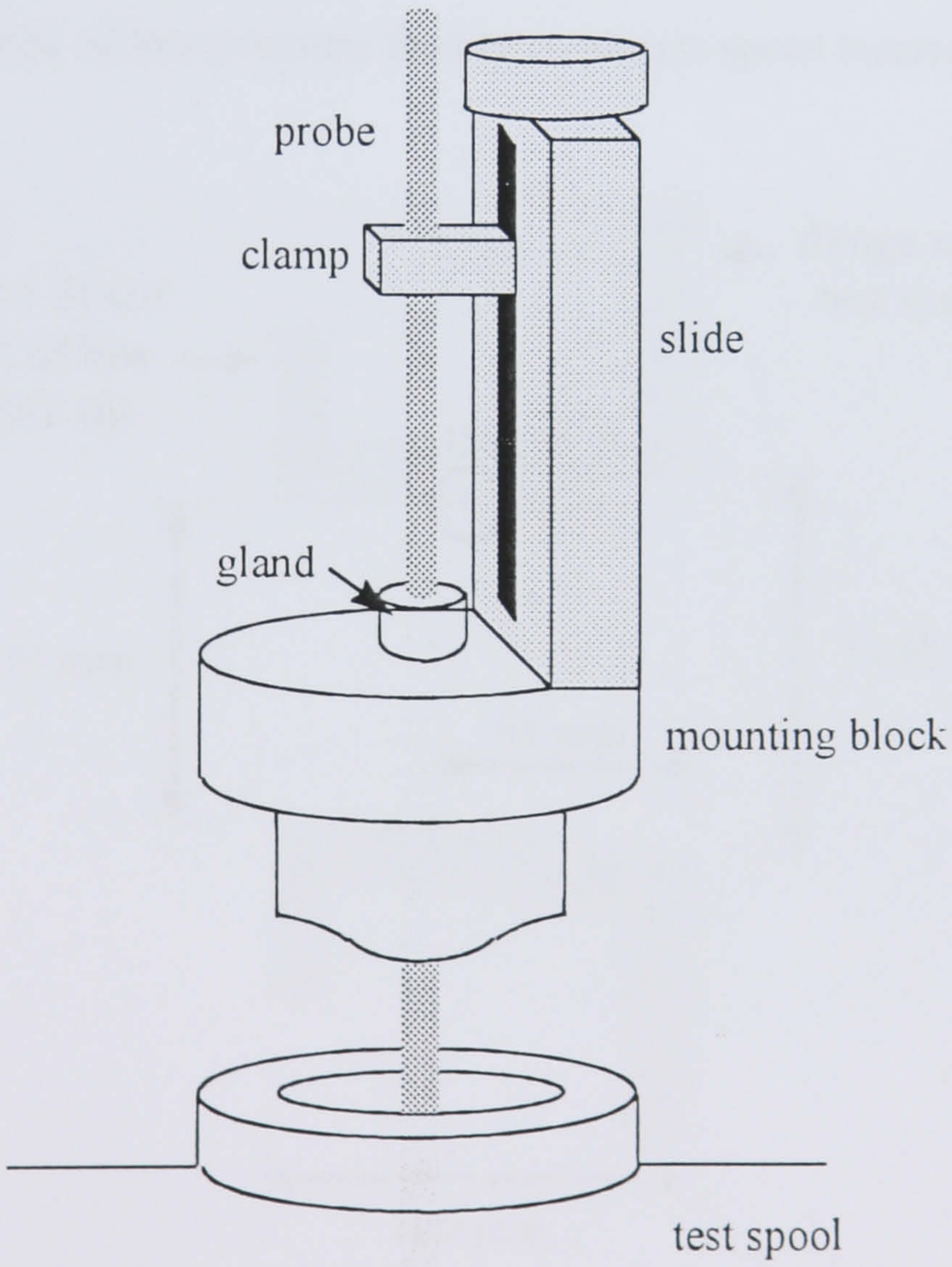


Figure 3.12 Velocity probe held by a slide on a mounting block and partly inserted in the test spool (not to scale)

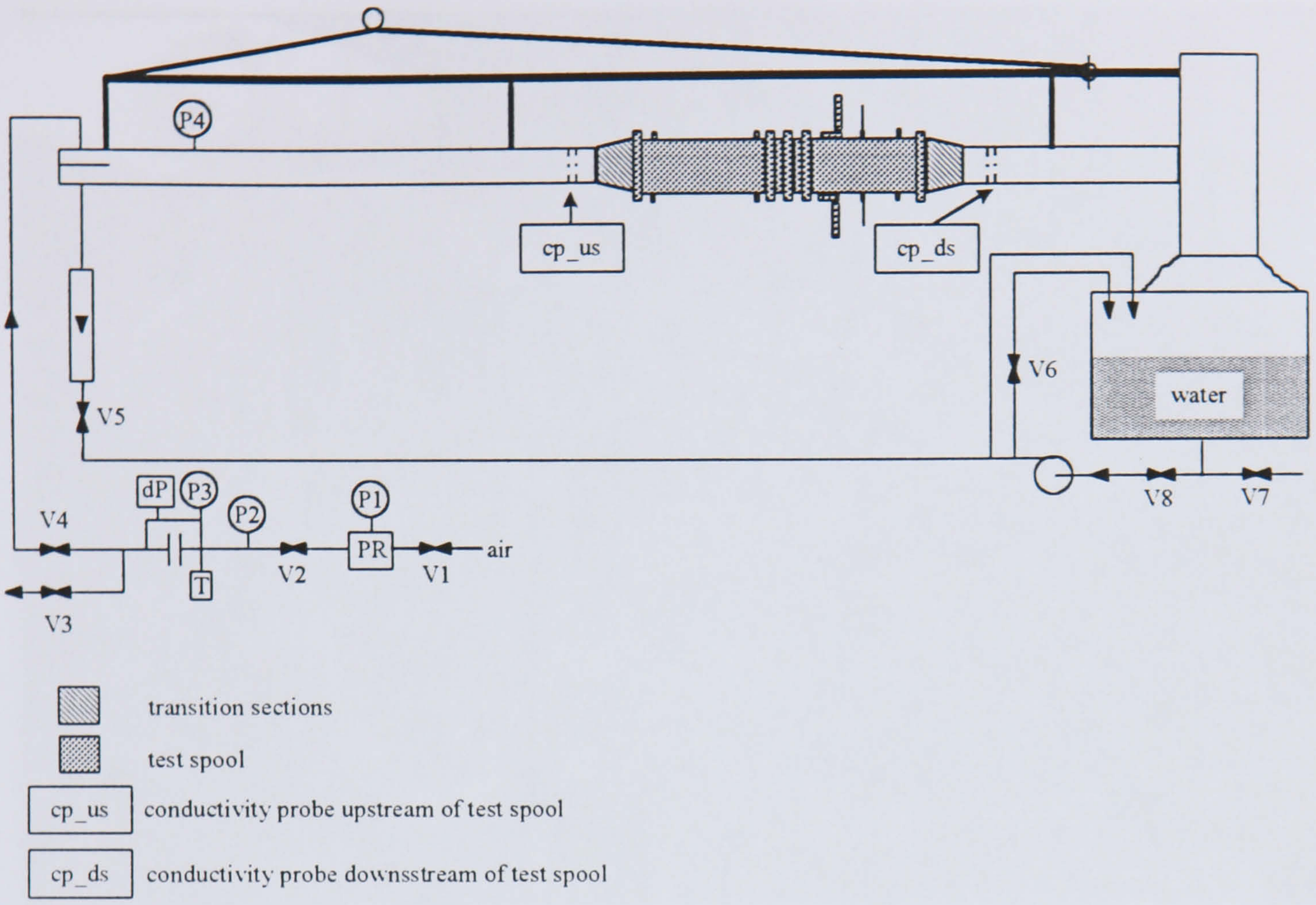


Figure 3.13 Schematic of low pressure facility (with test spool inserted)

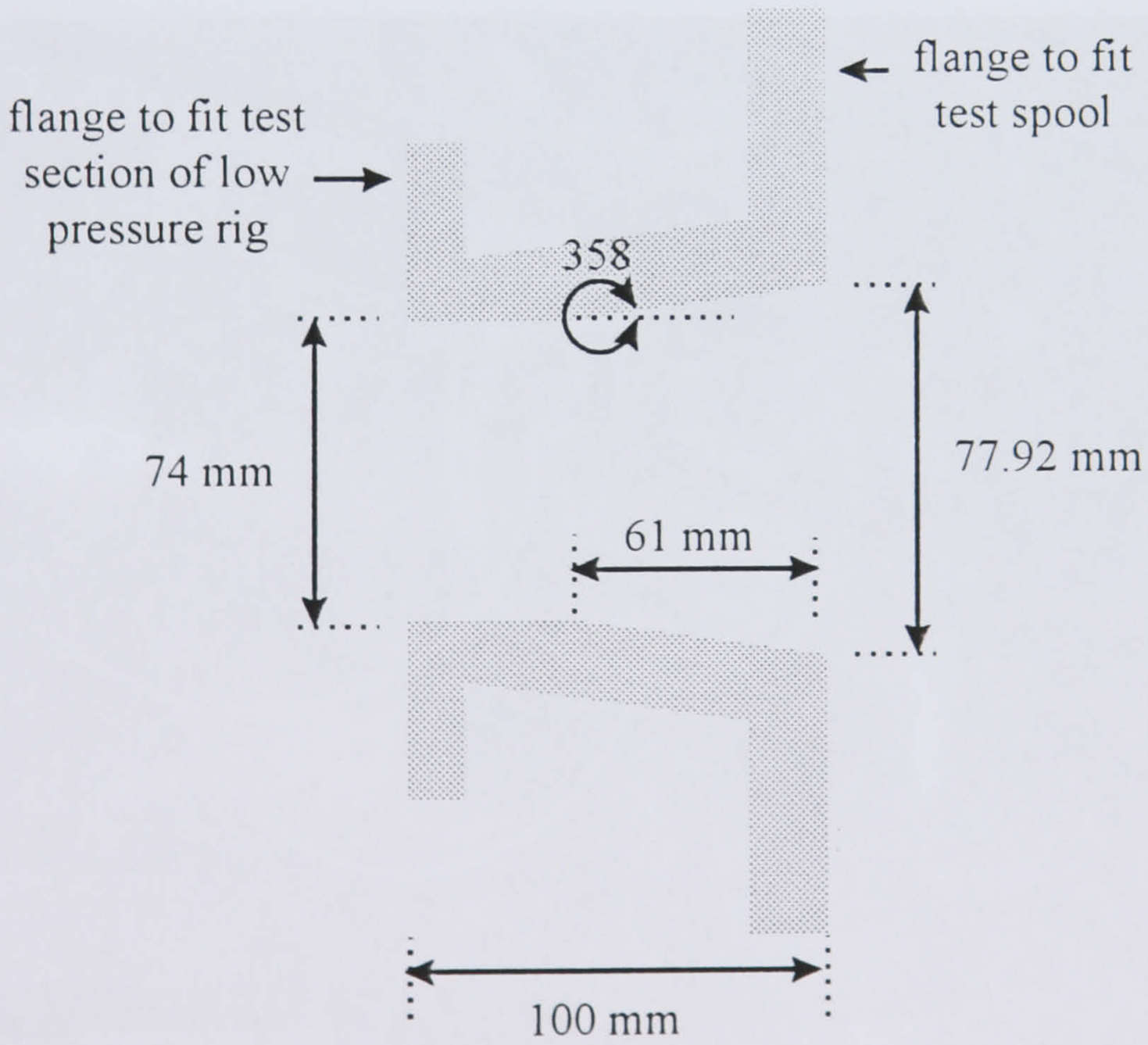


Figure 3.14 Length section through transition flange used for inserting test spool on the low pressure rig (not to scale)

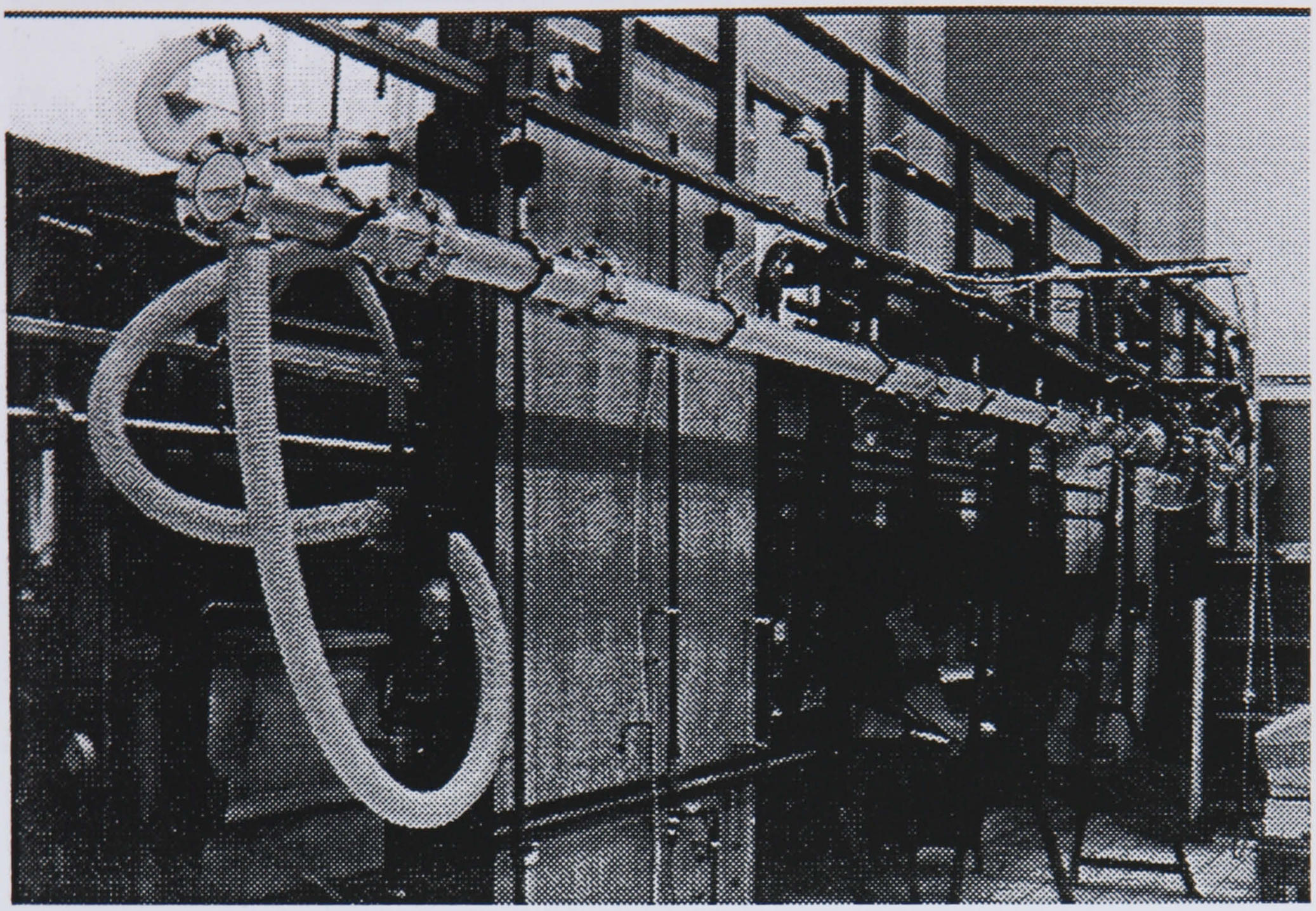


Figure 3.15 View of low pressure rig from inlet section

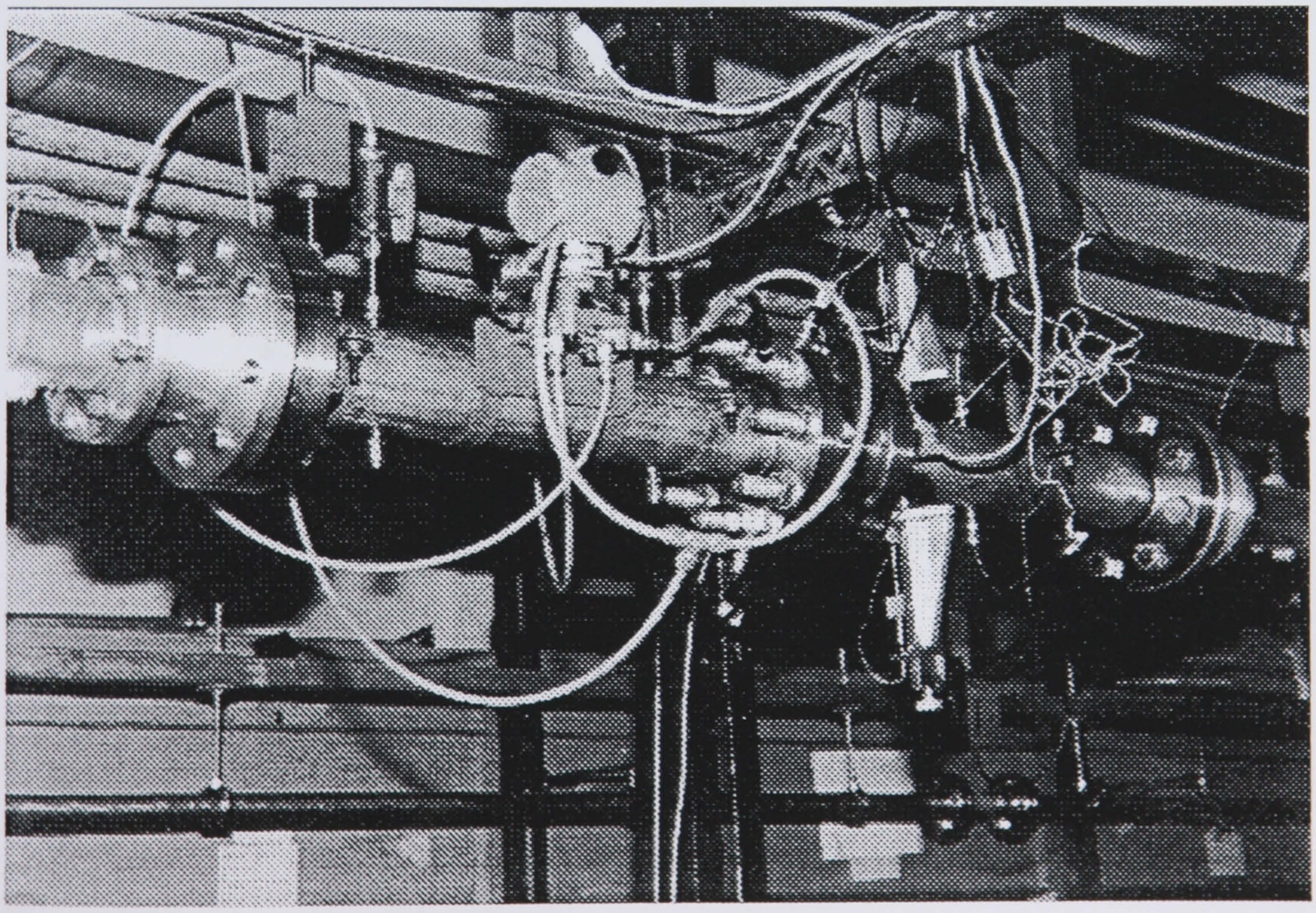


Figure 3.16 Test spool inserted in low pressure rig

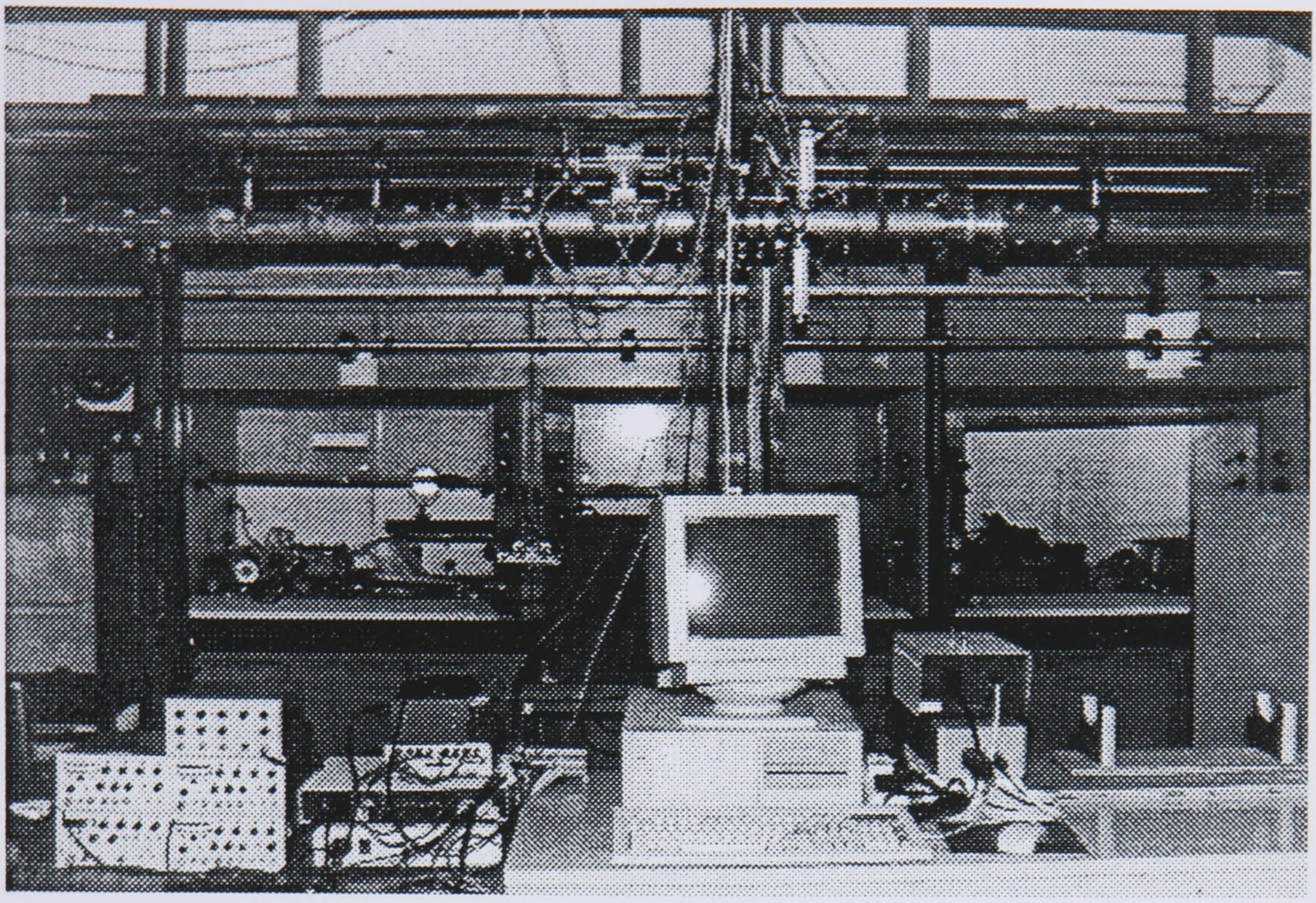


Figure 3.17 Acquisition system and electronics boxes

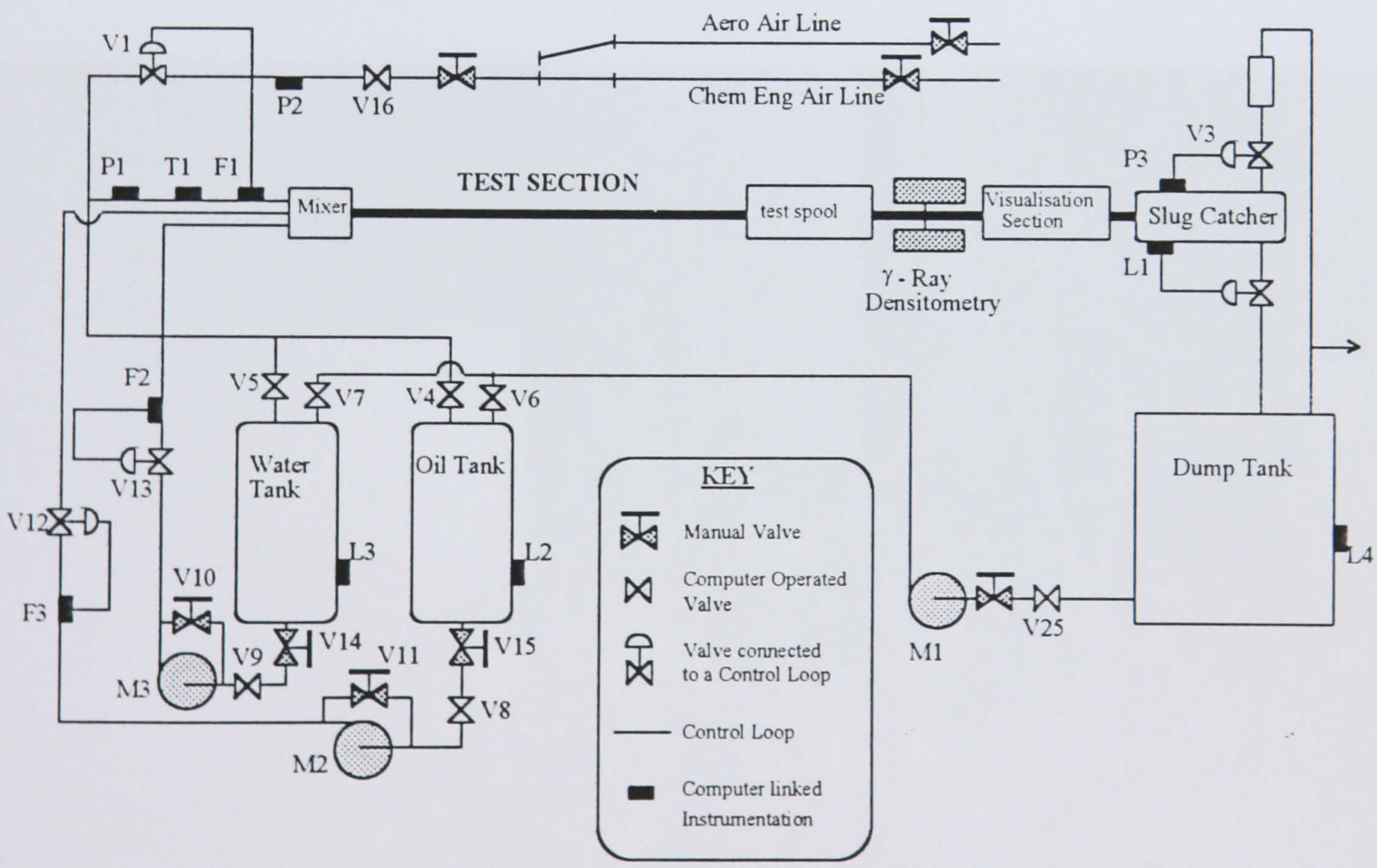


Figure 3.18 Schematic of WASP rig

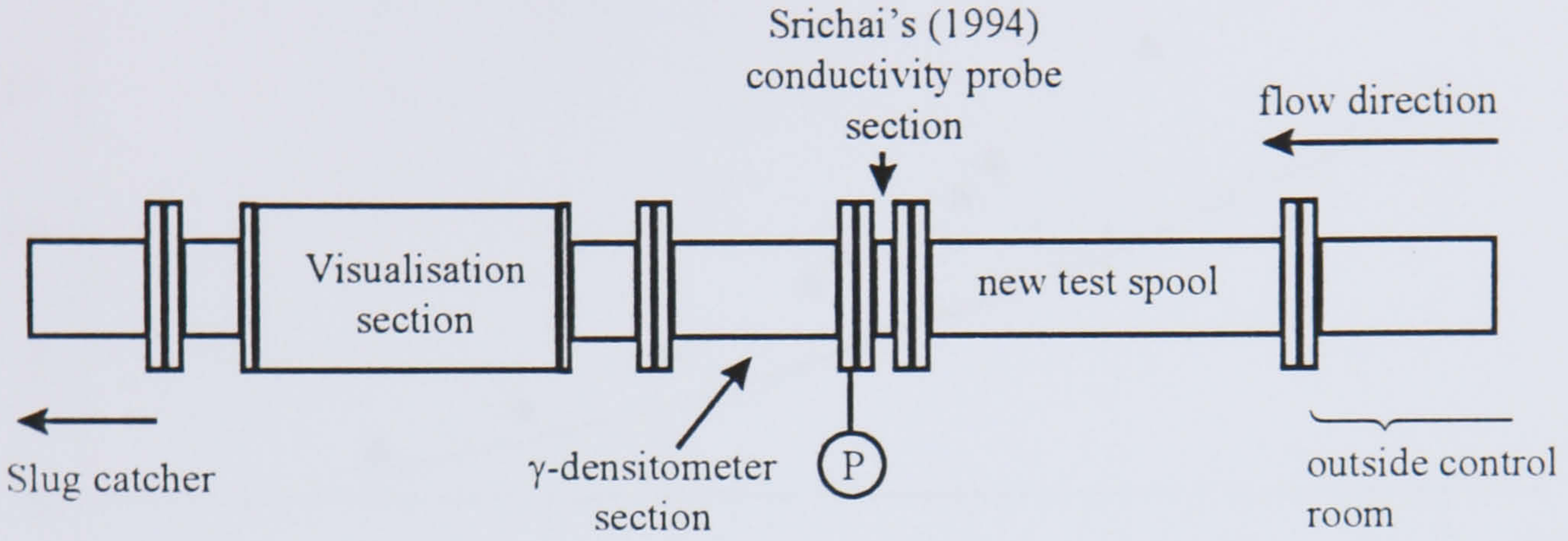


Figure 3.19 Detailed schematic of downstream end of WASP test section with test spool inserted (not to scale)

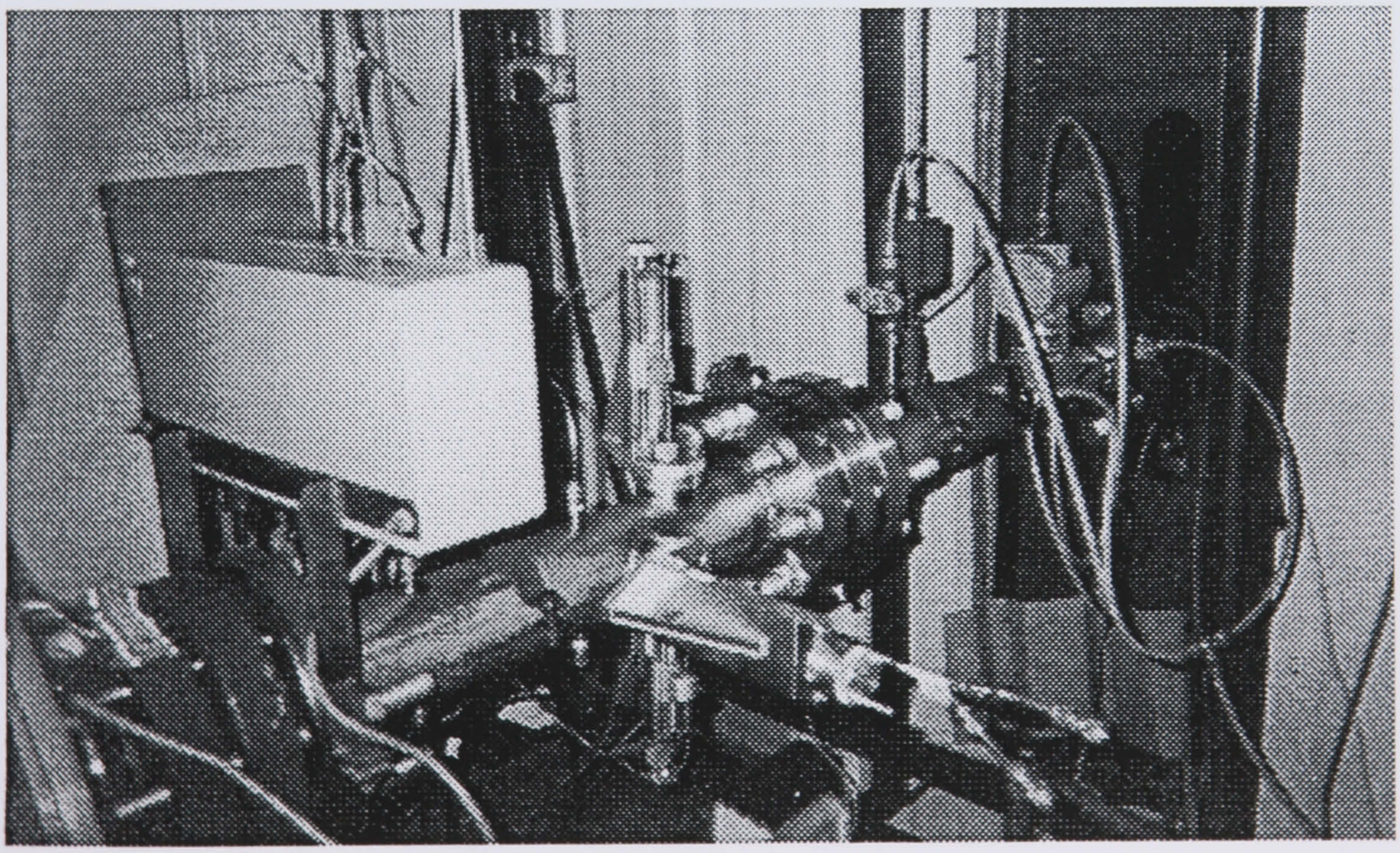


Figure 3.20 Test spool inserted in WASP test section

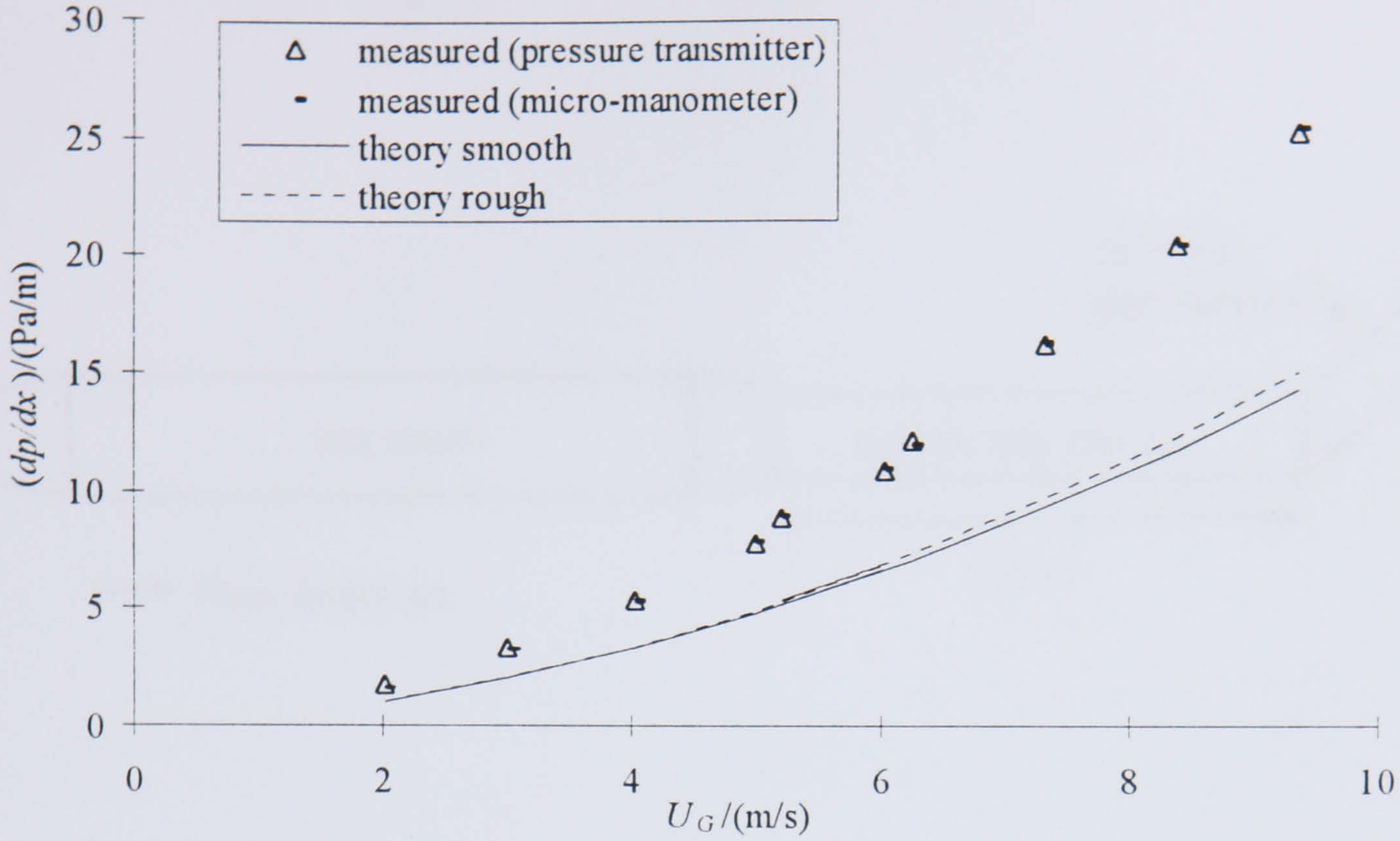


Figure 3.21 Pressure drop in single phase air flow across test spool on the low pressure rig

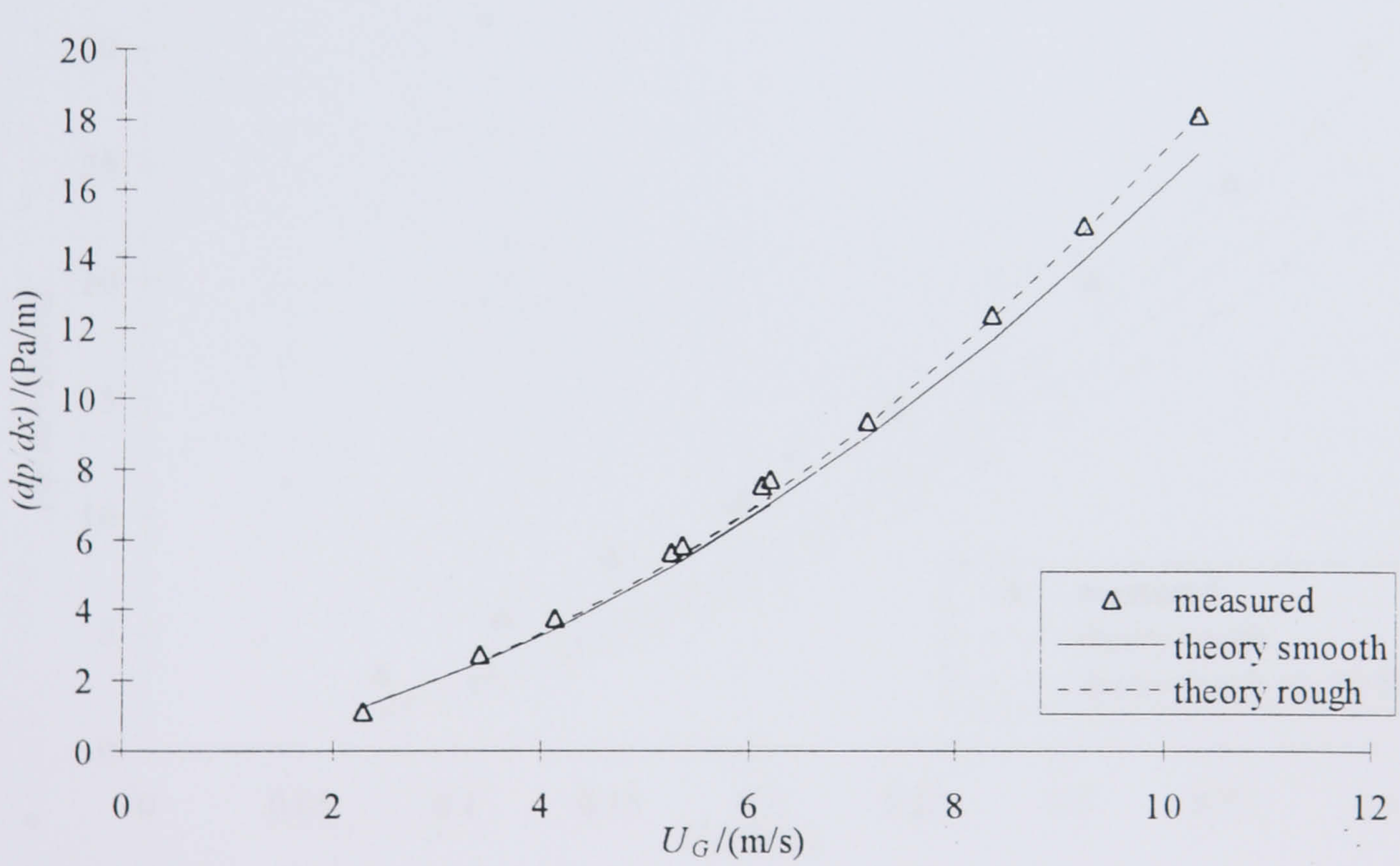


Figure 3.22 Pressure drop in single phase air flow in test spool upstream of probe inserts on the low pressure rig

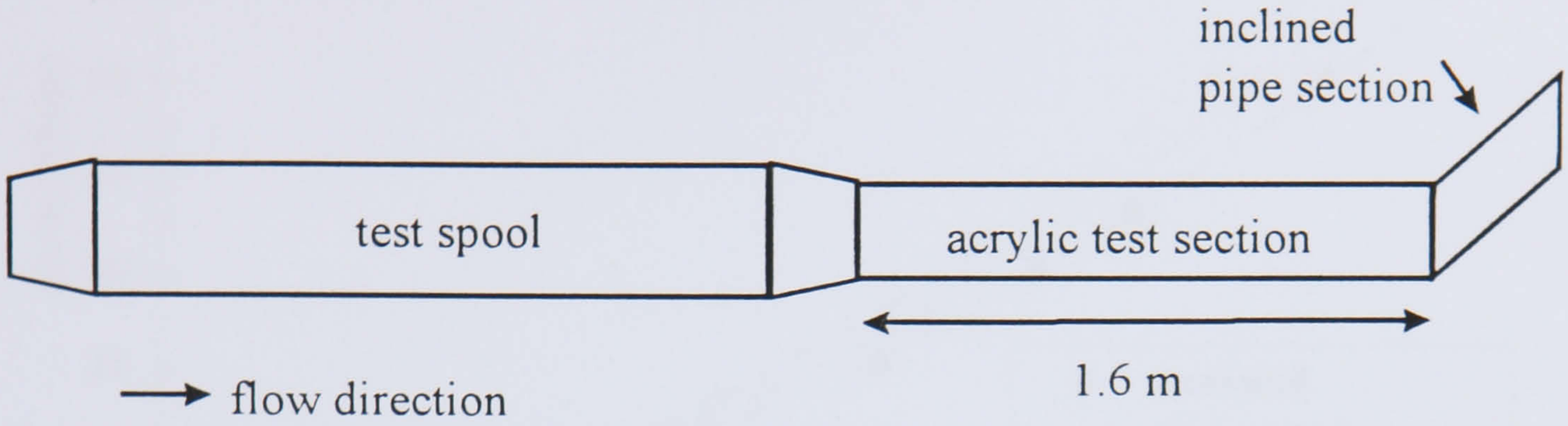


Figure 3.23 Test section on the low pressure rig modified with inclined pipe section at exit

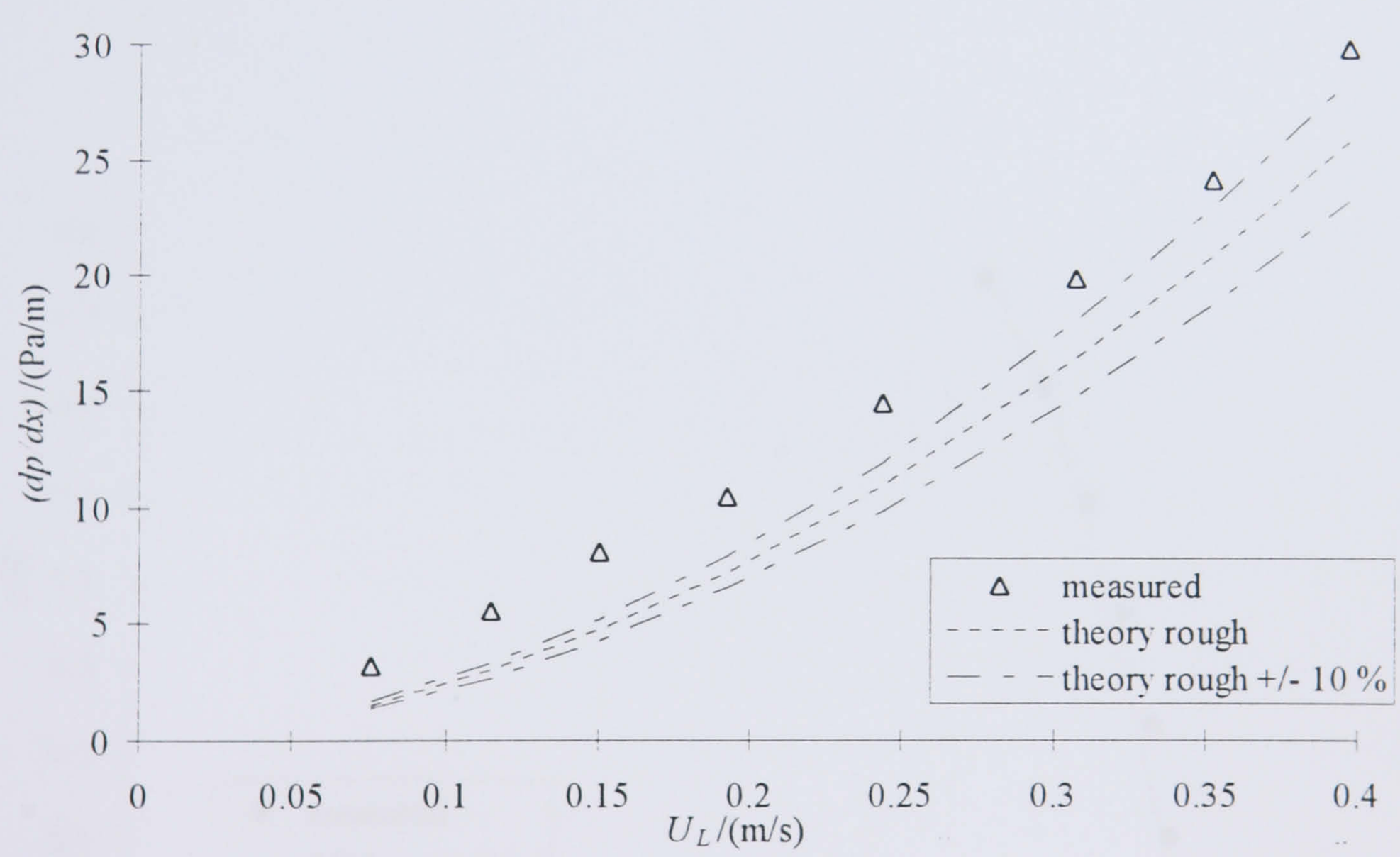


Figure 3.24 Pressure drop in single phase water flow in test spool upstream of probe inserts on the low pressure rig

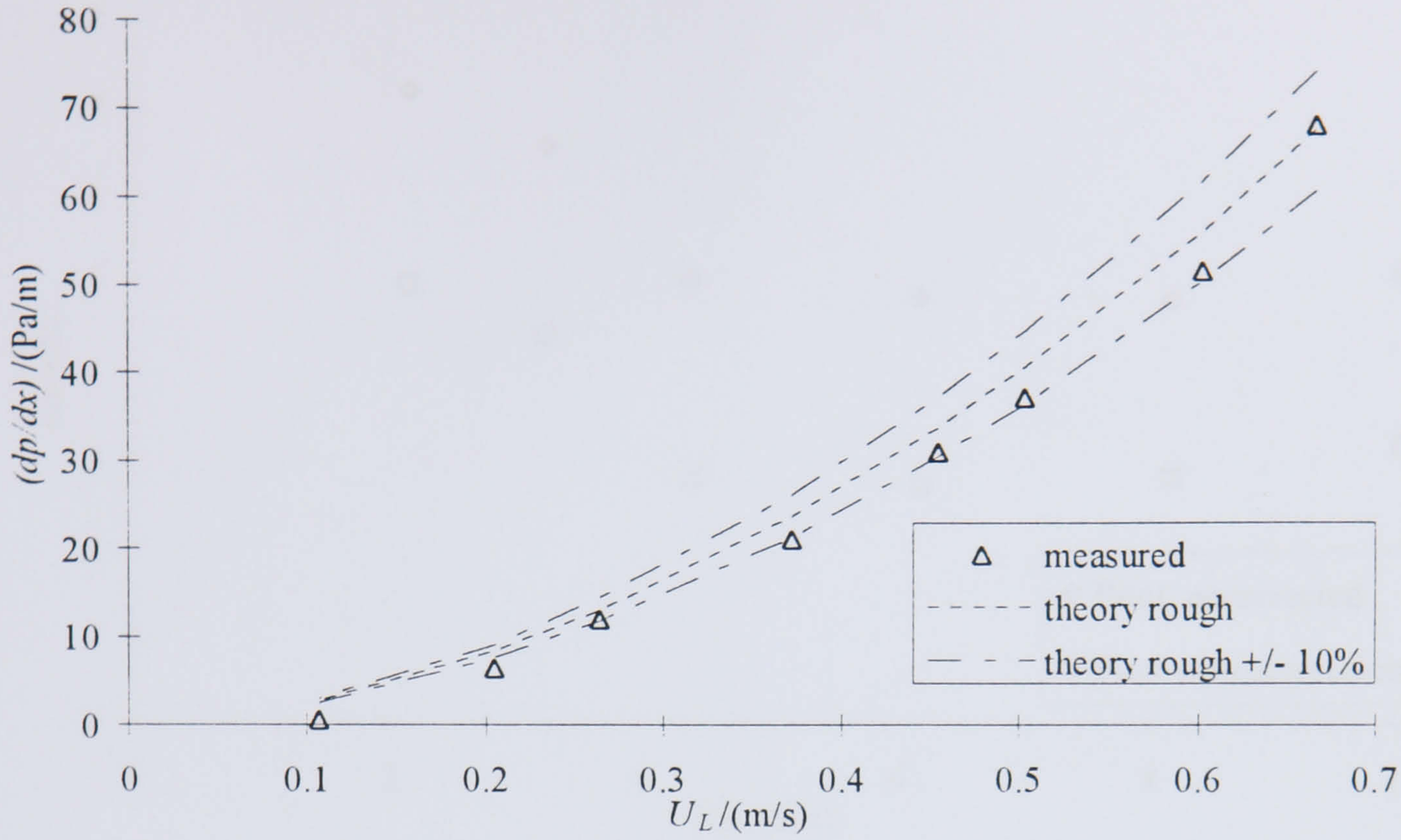


Figure 3.25 Pressure drop in single phase water flow in test spool upstream of probe inserts on the WASP rig

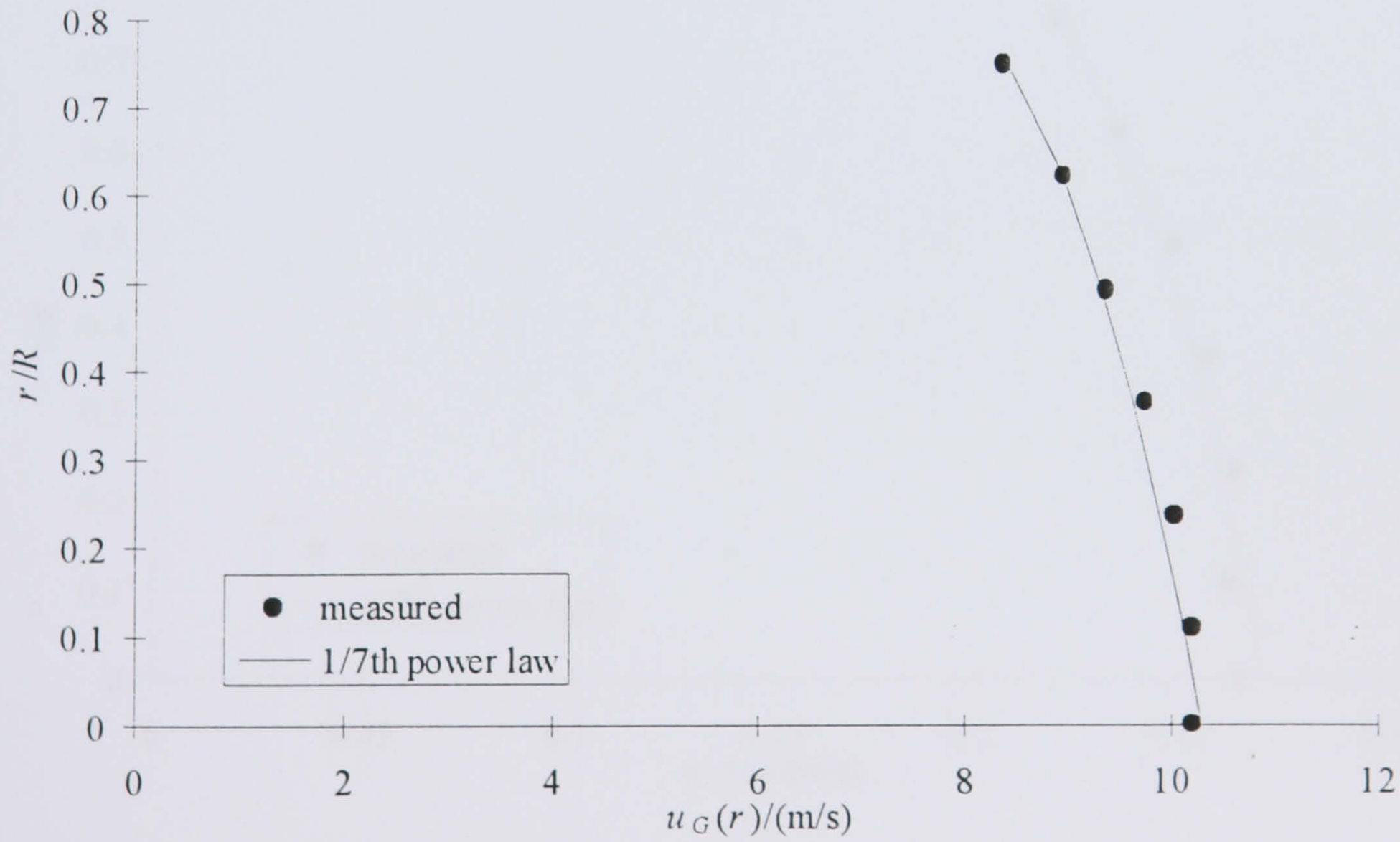


Figure 3.26 Velocity profile for air (U_G=8.2 m/s) measured with Pitot tube on the low pressure rig

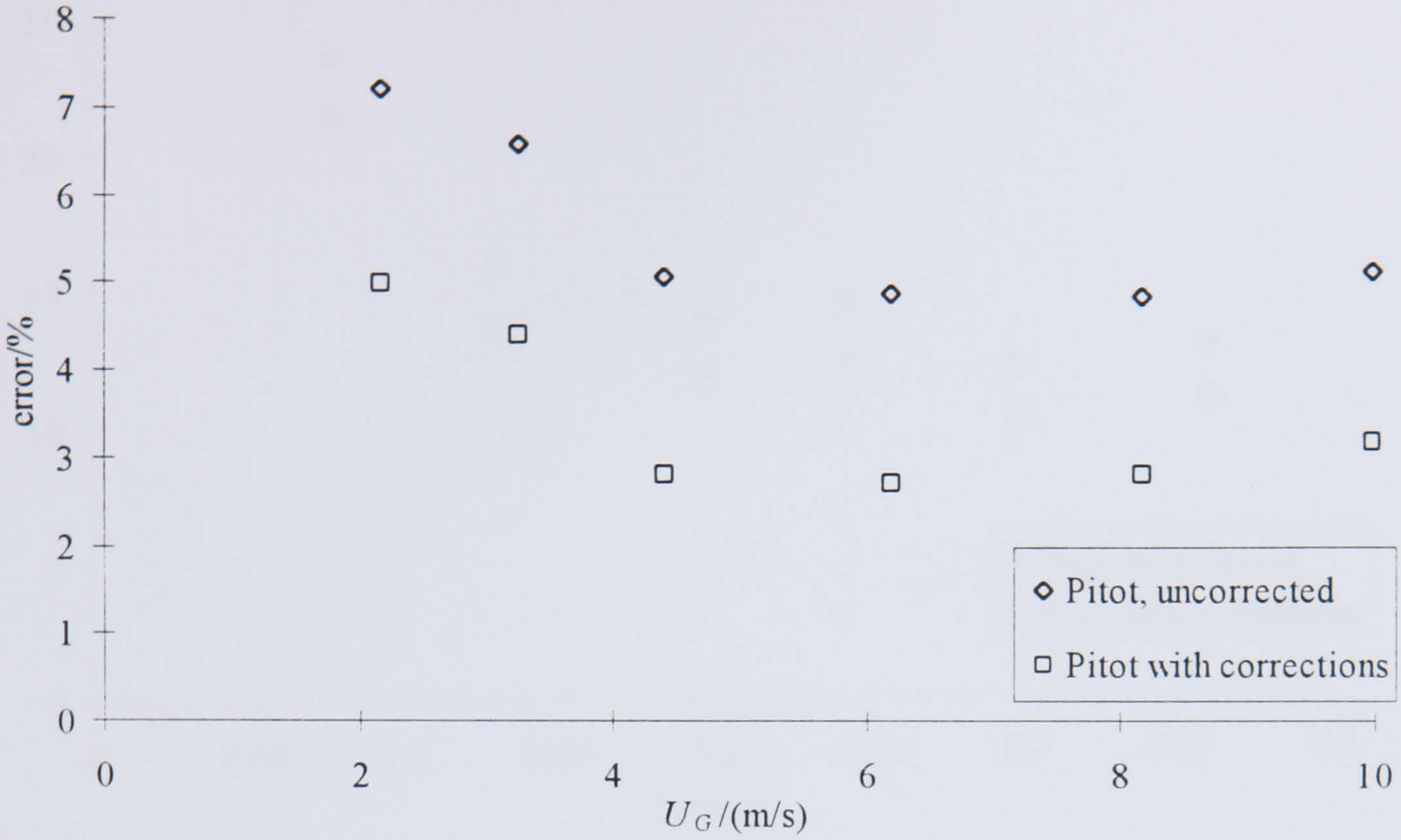


Figure 3.27 Discrepancy between flow rate measured with Pitot and rig flow rate acquisition for air on the low pressure rig

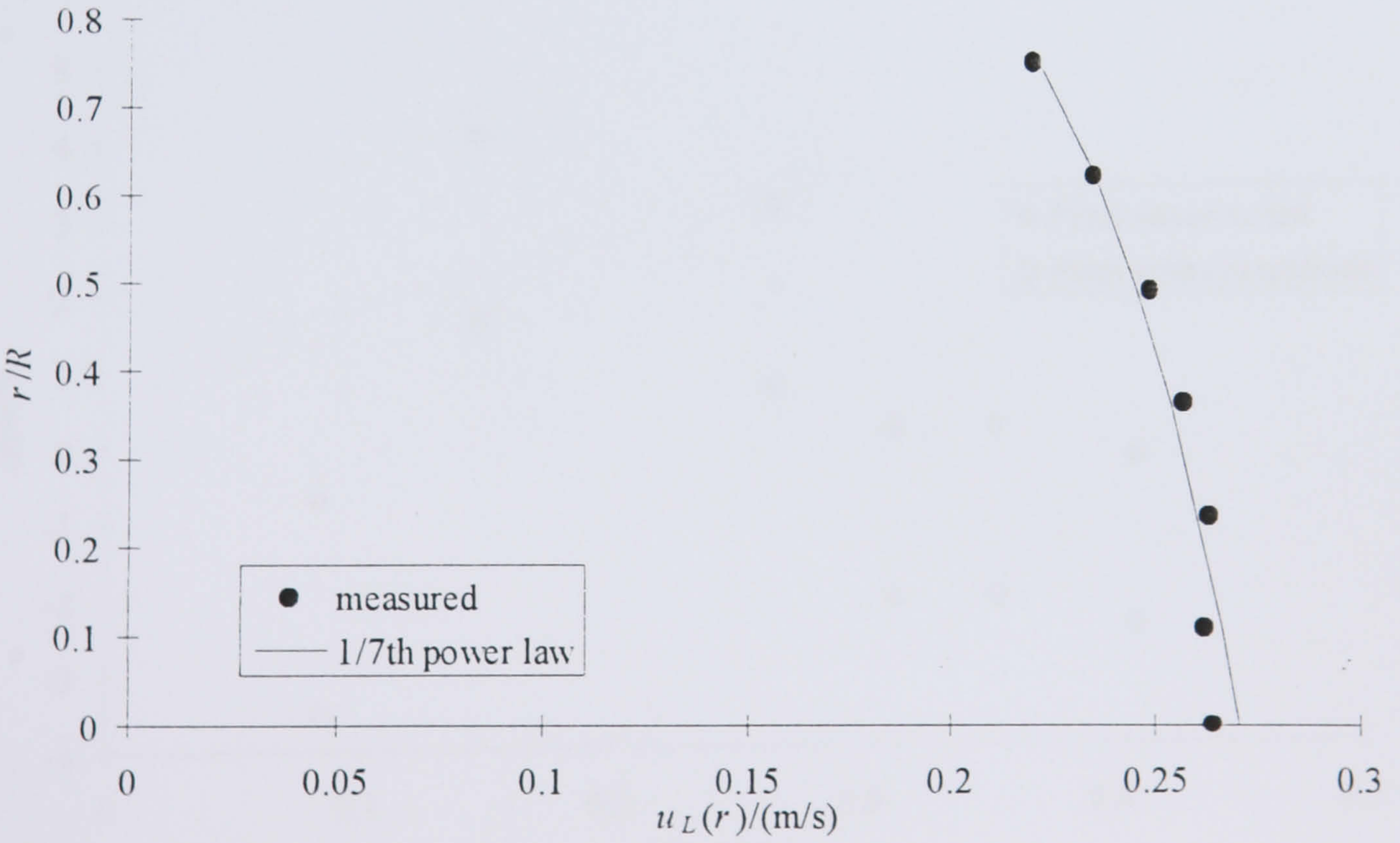


Figure 3.28 Velocity profile for water (U_L=0.2 m/s) measured with Pitot tube on the low pressure rig

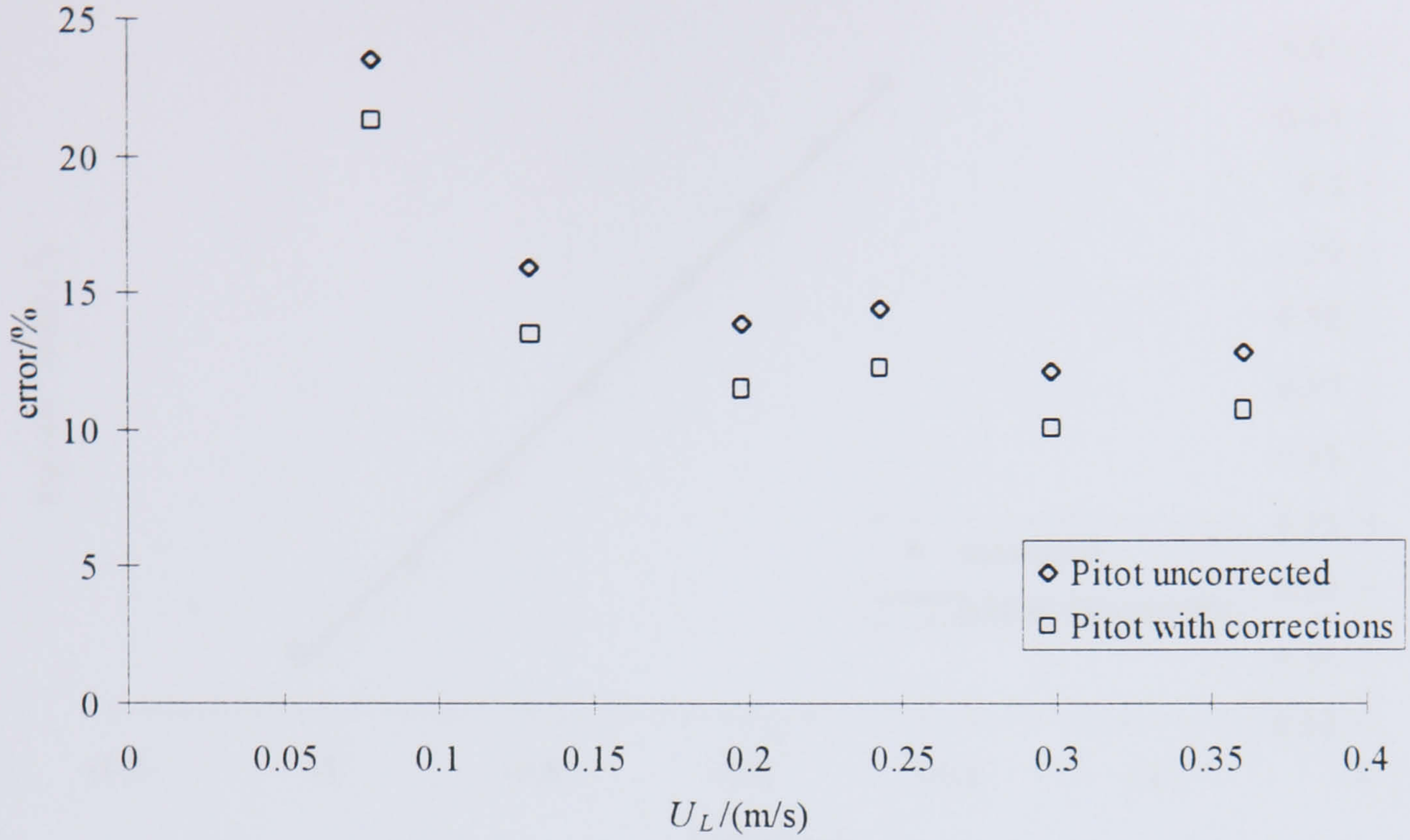


Figure 3.29 Discrepancy between flow rate measured with Pitot and water rotameter on the low pressure rig

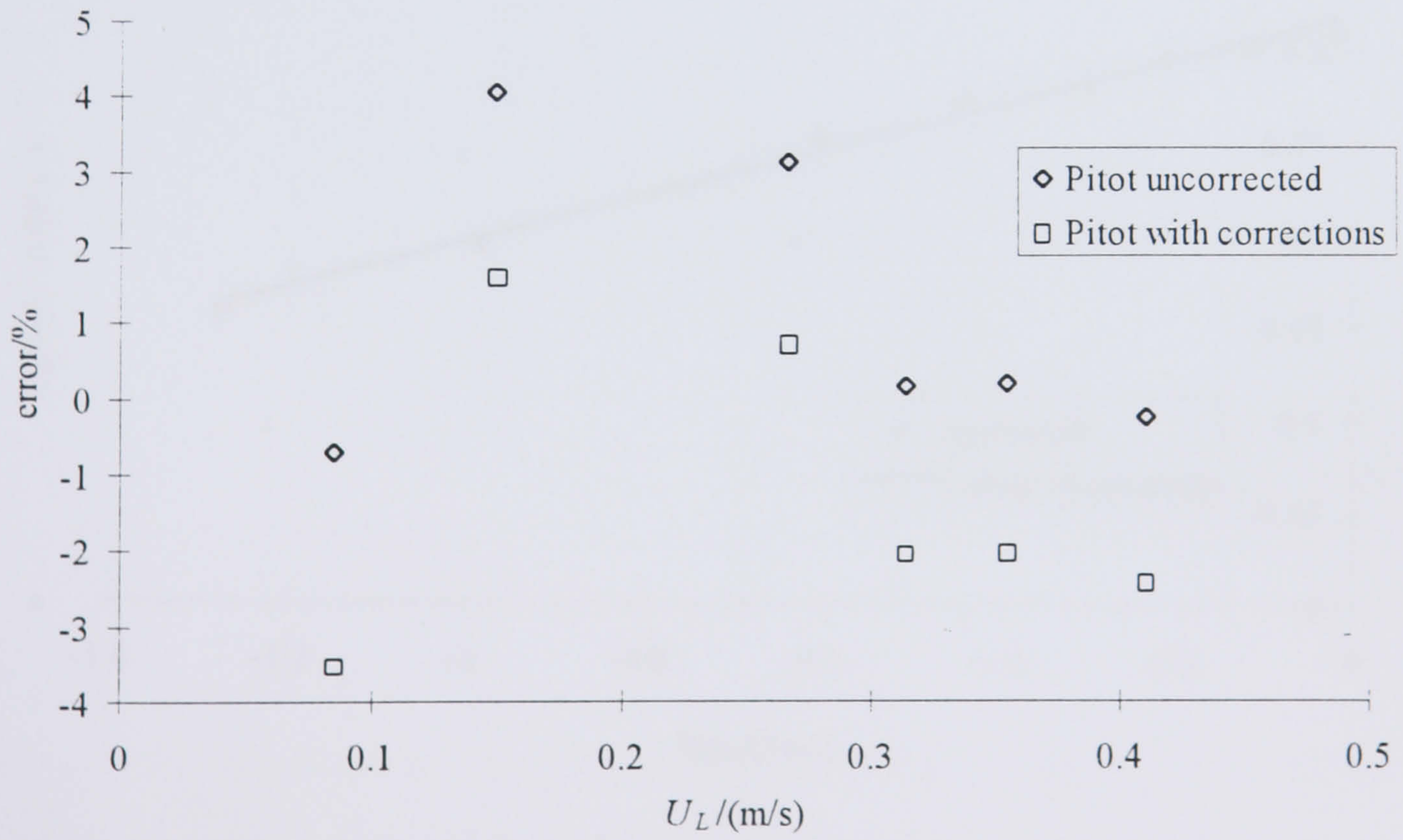


Figure 3.30 Discrepancy between flow rate measured with Pitot and water rotameter on the low pressure rig for traverses of the Pitot from the tube bottom

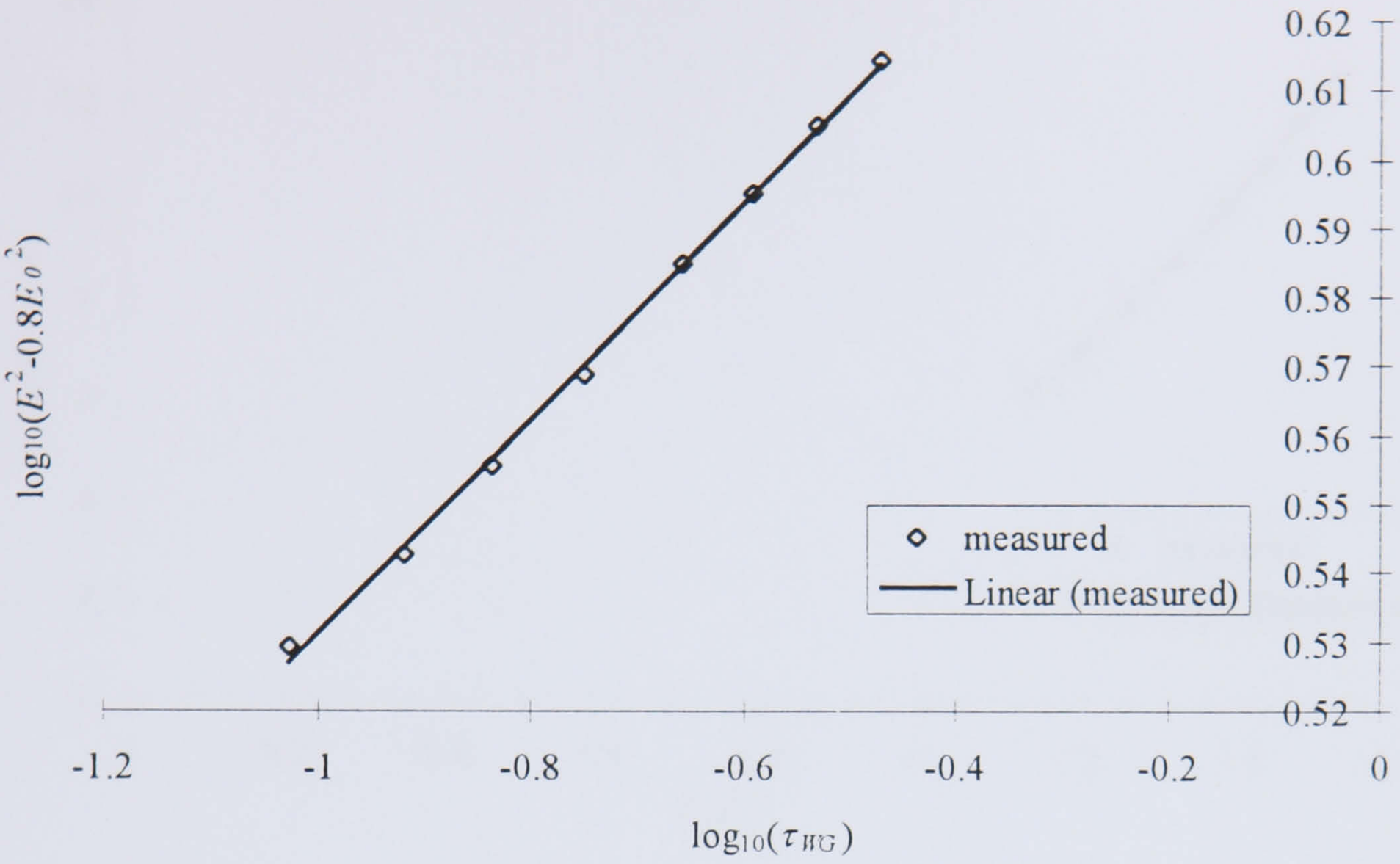


Figure 3.31 Calibration curve for glue-on probe for measurement of gas wall shear stress on the low pressure rig

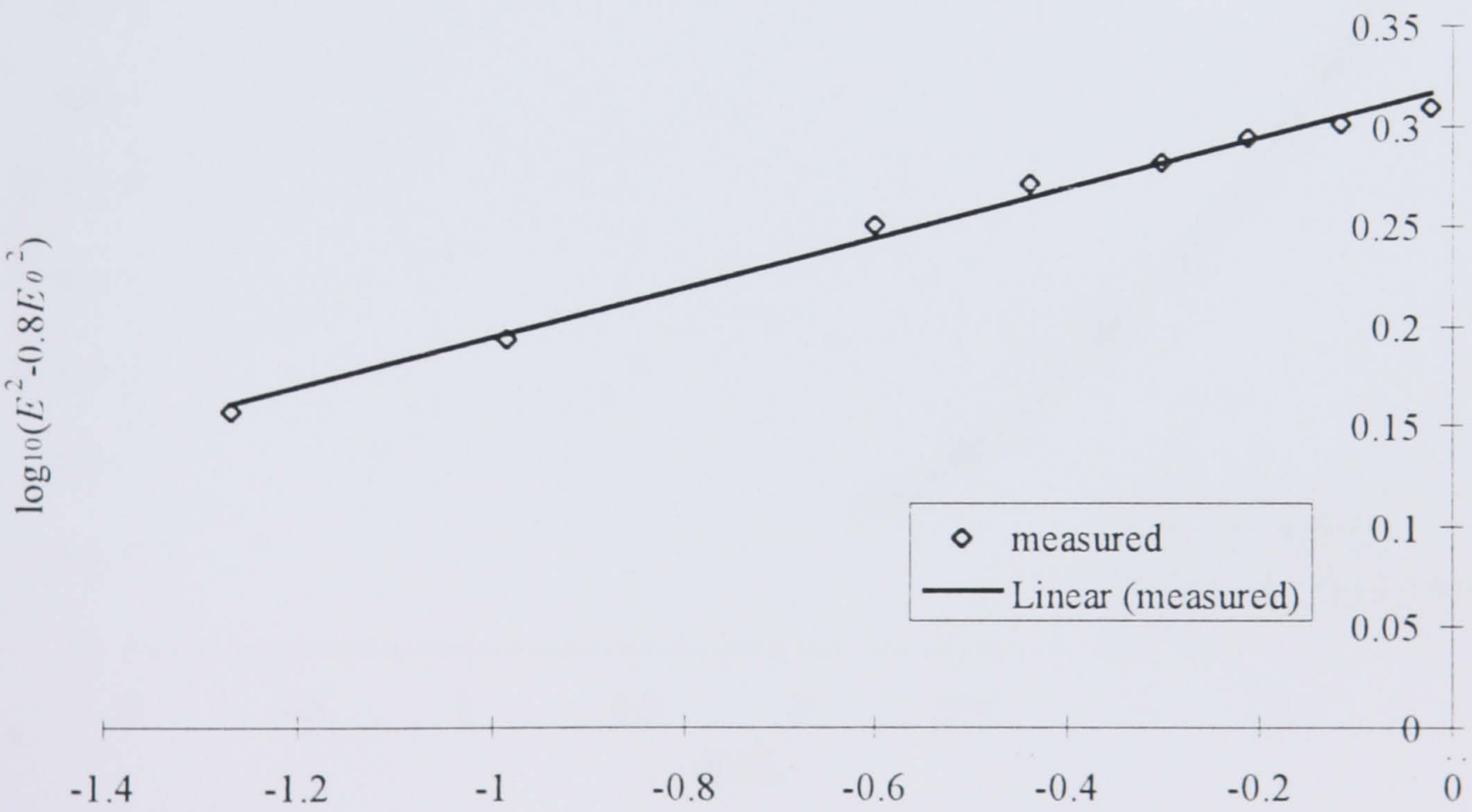


Figure 3.32 Calibration curve for glue-on probe for measurement of liquid wall shear stress on the low pressure rig

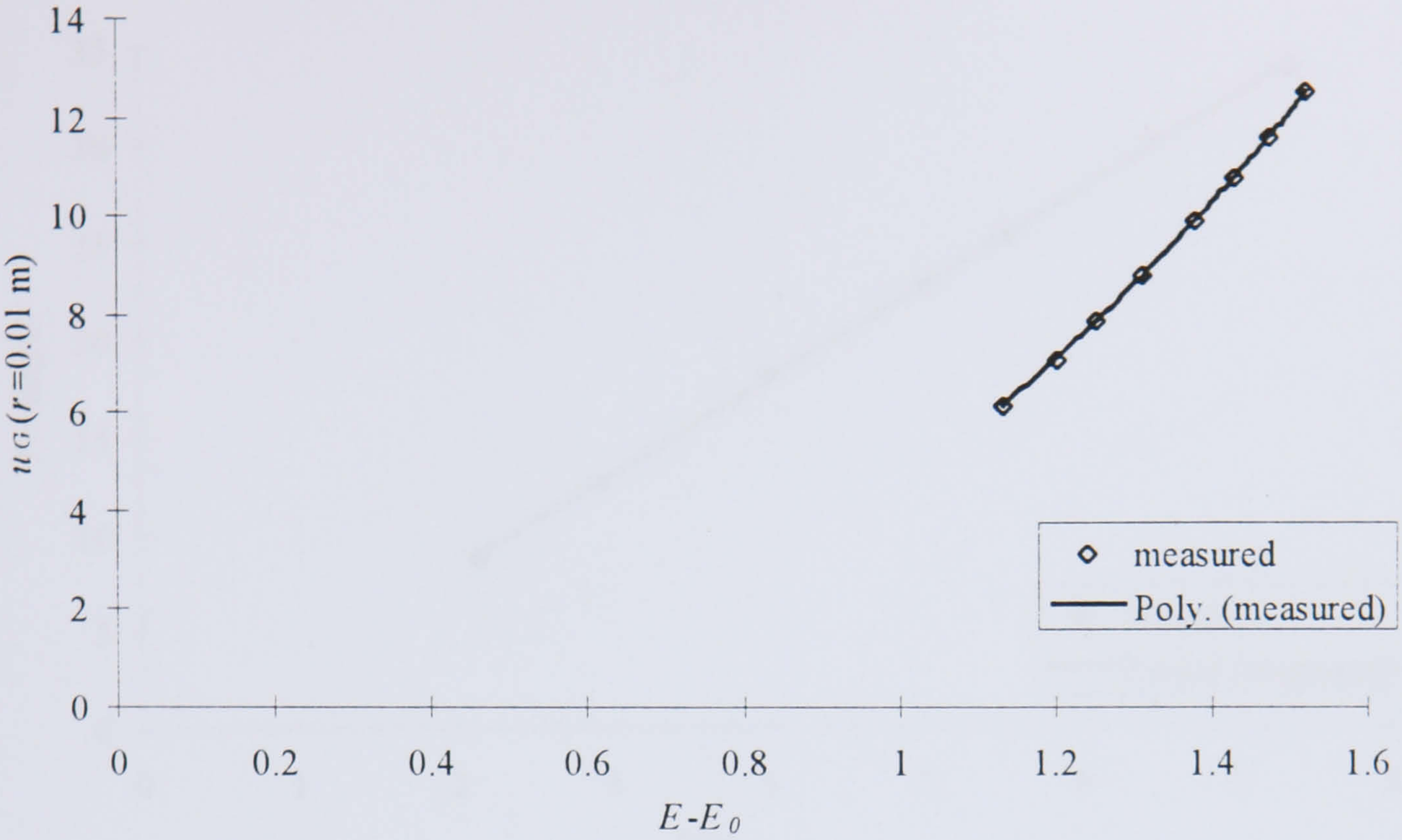


Figure 3.33 Calibration curve for hot-wire probe for measurement of gas velocity on the low pressure rig

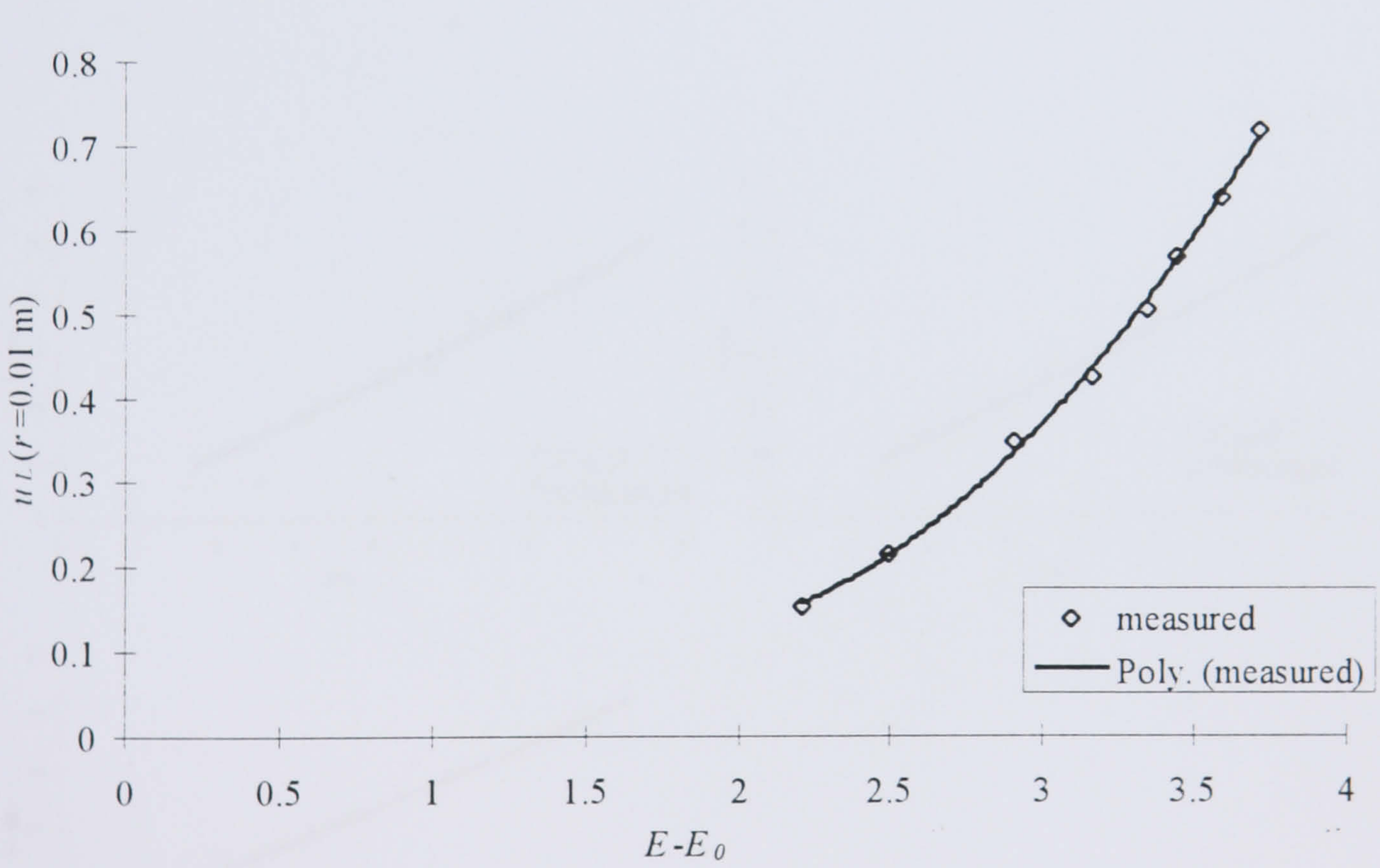


Figure 3.34 Calibration curve for hot-film probe for measurement of liquid velocity on the low pressure rig

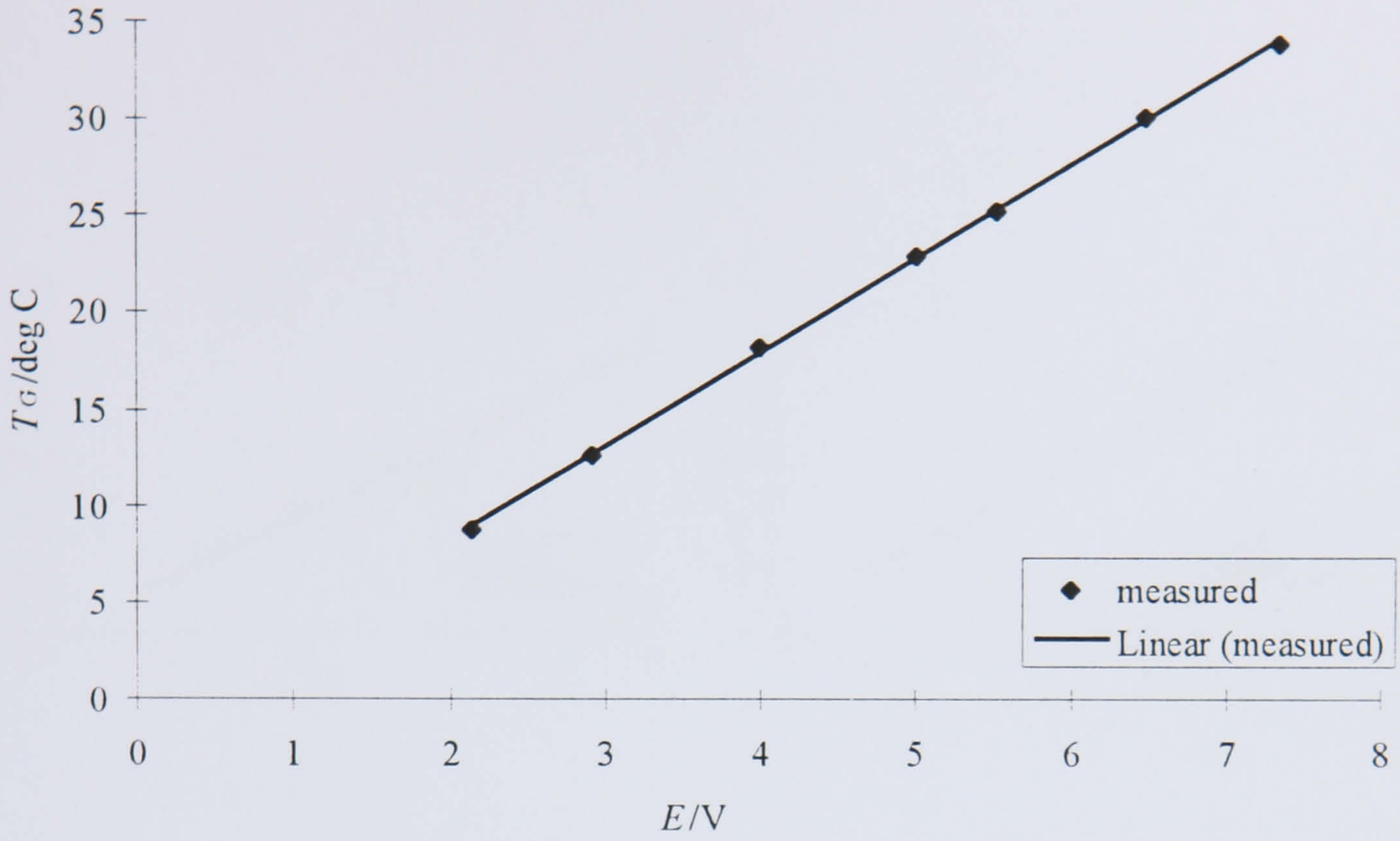


Figure 3.35 Calibration curve for thermocouple for gas temperature for experiments on the low pressure rig

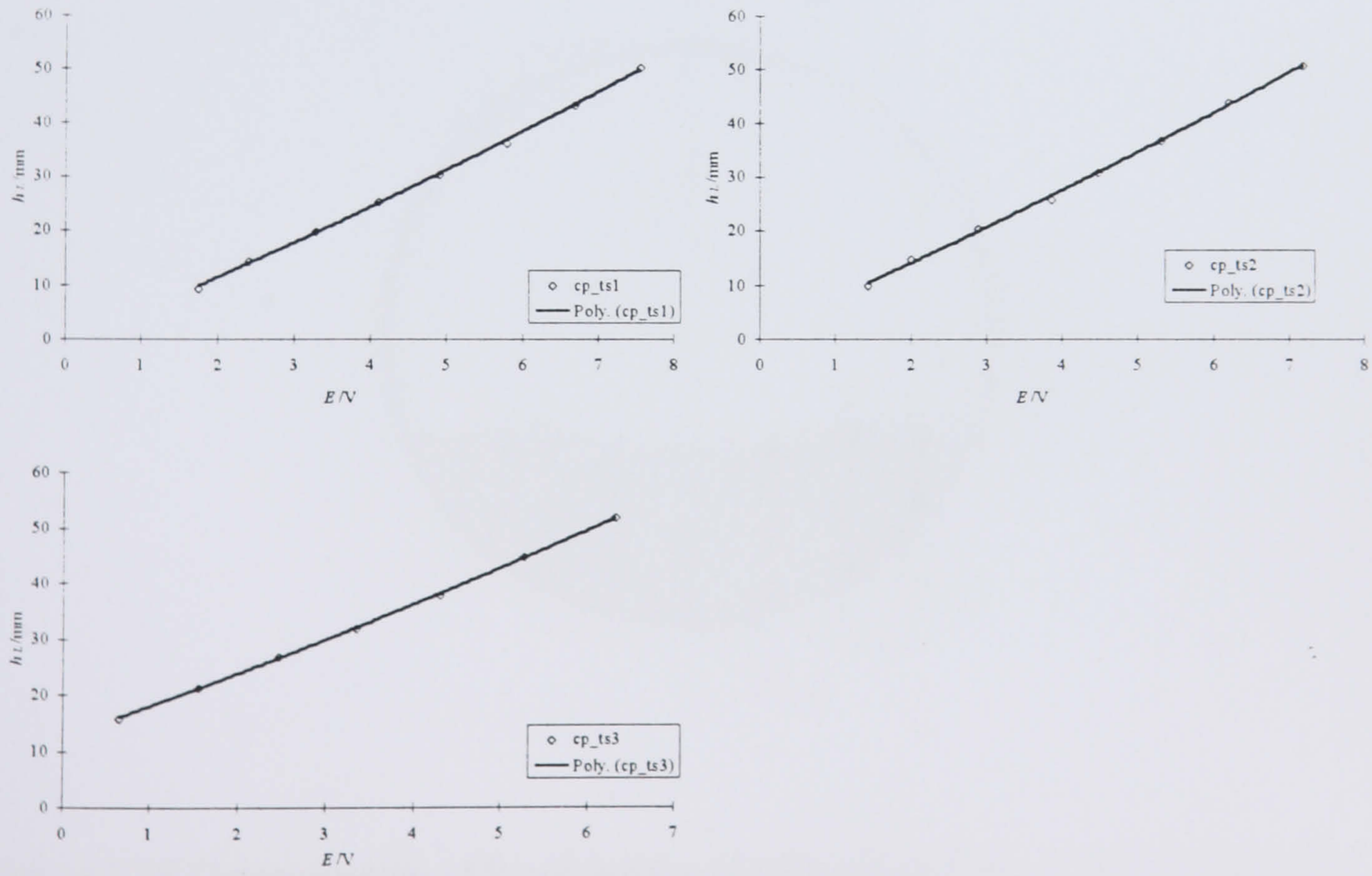


Figure 3.36 Typical calibration curves for conductivity probes in test spool on the low pressure rig

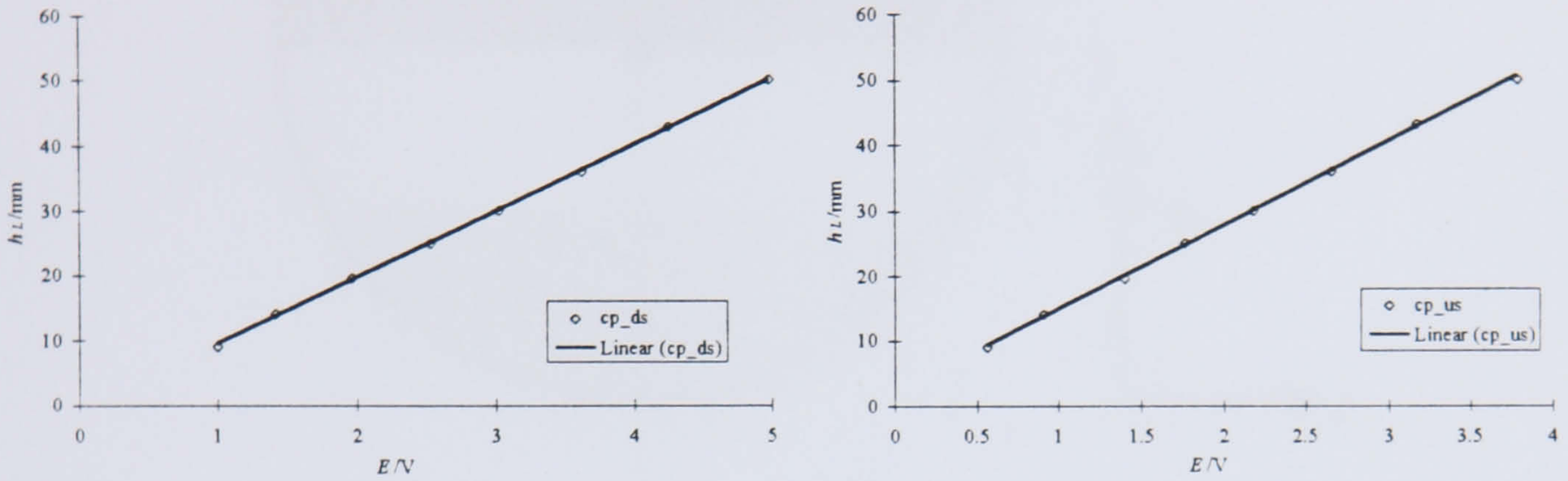


Figure 3.37 Typical calibration curves for conductivity probes upstream and downstream of test spool on the low pressure rig

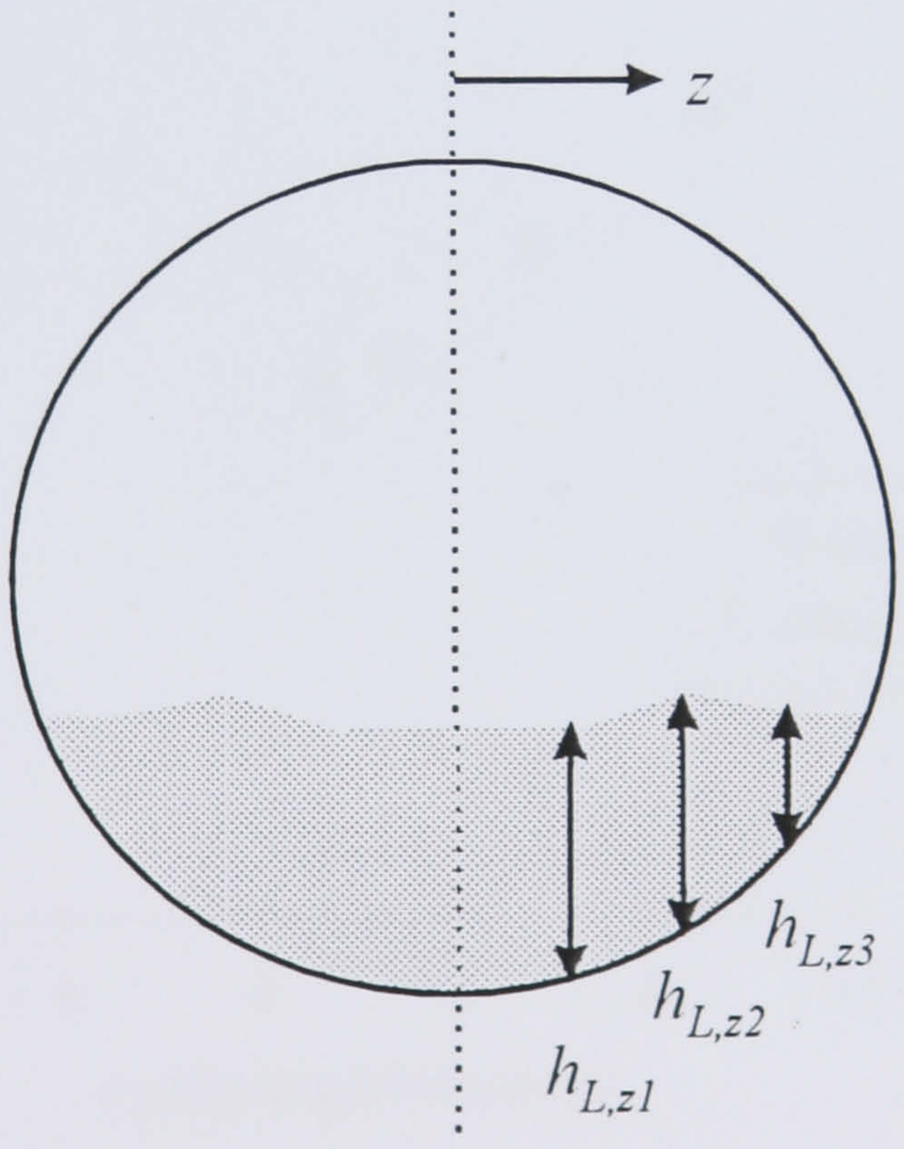


Figure 3.38 Determination of liquid holdup in the test spool from measurement of liquid height at three positions in half a cross section, assuming symmetry with respect to tube centre

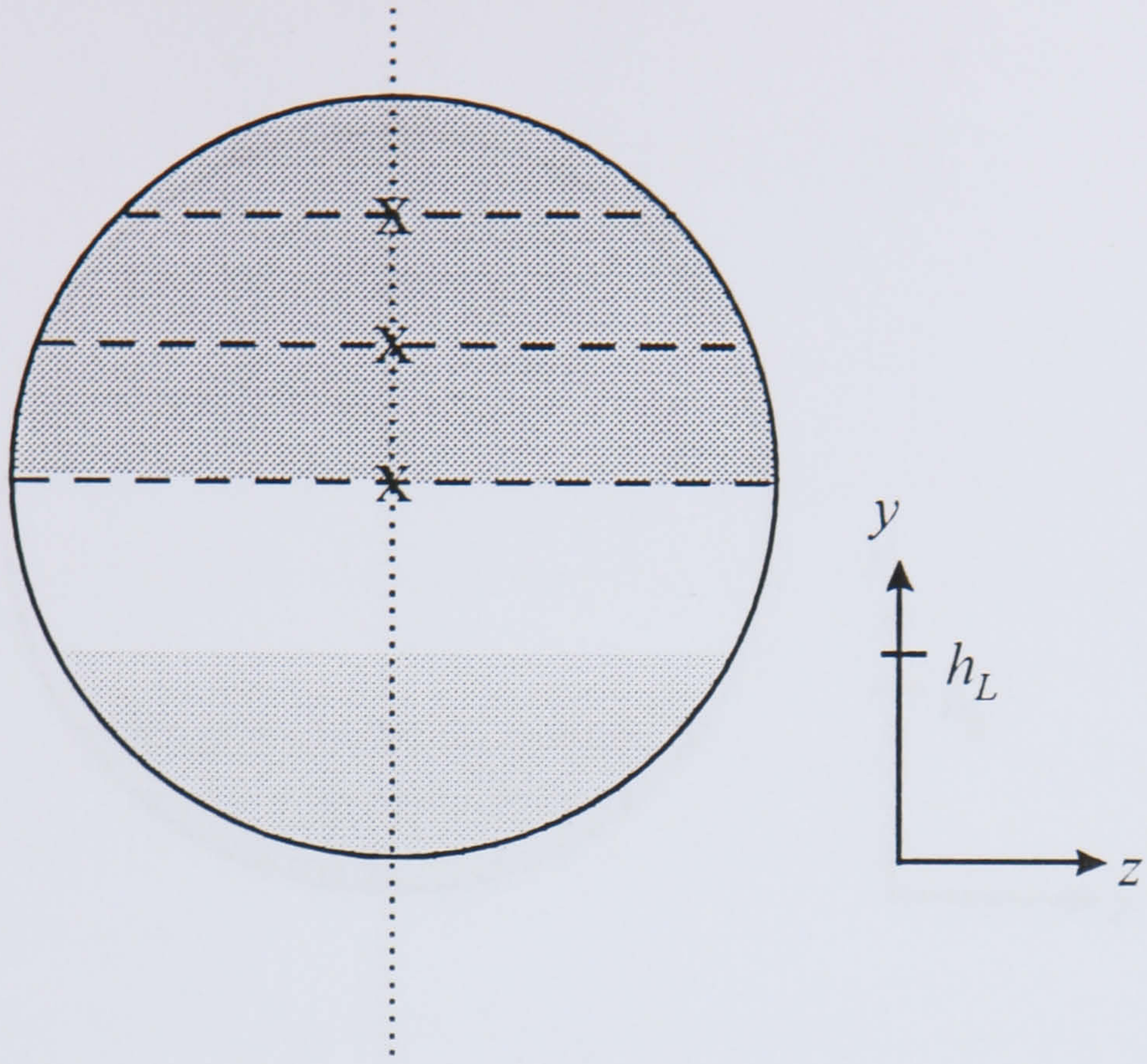


Figure 3.39 Obtaining phase average velocity from three local measurements of velocity in the gas phase

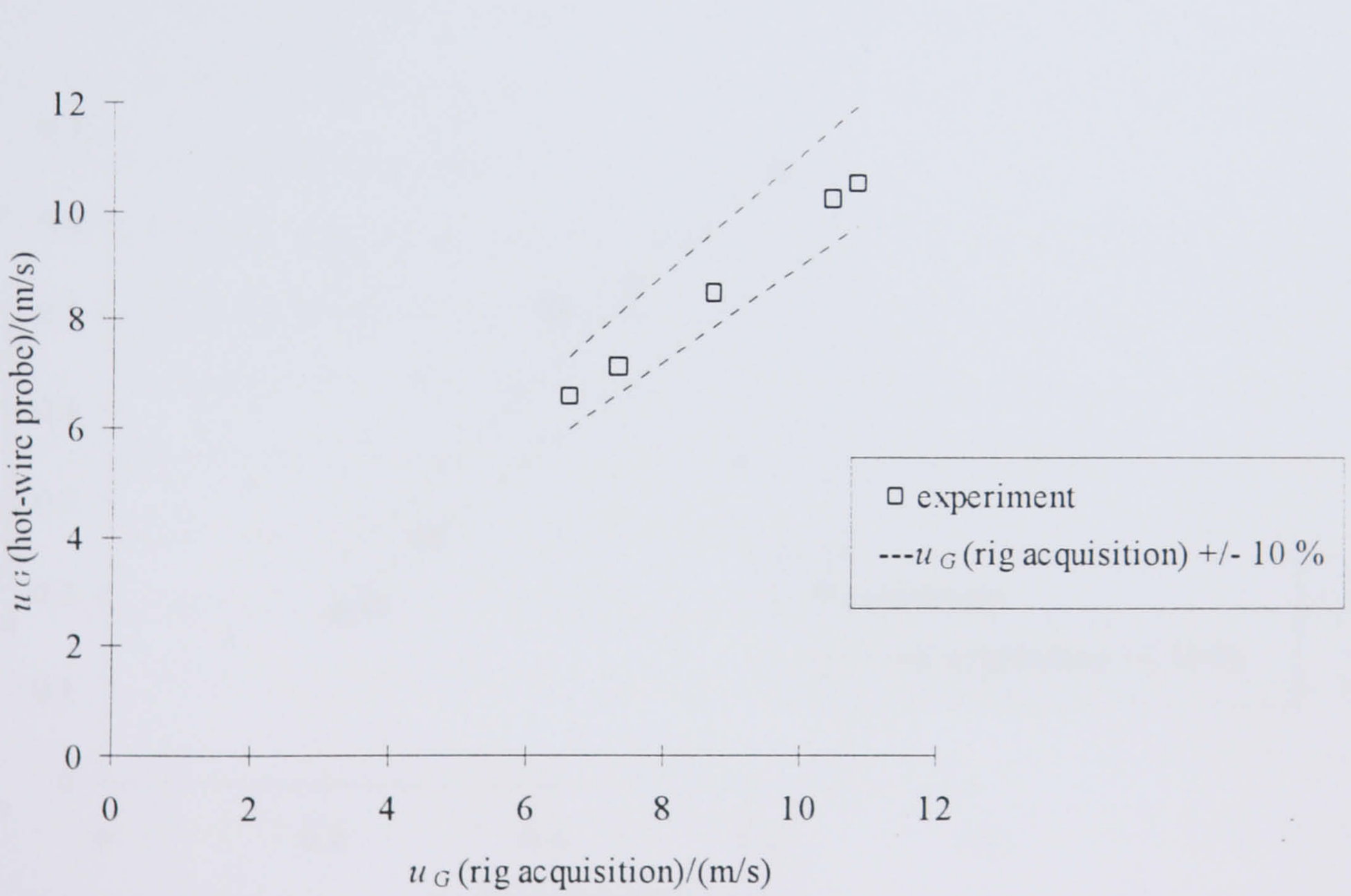


Figure 3.40 Agreement of phase average velocity in gas phase obtained from measurements with hot-wire probe (u_G(hot-wire probe)) with phase average velocity obtained from rig flow rate acquisition (u_G(rig acquisition)) on the low pressure rig

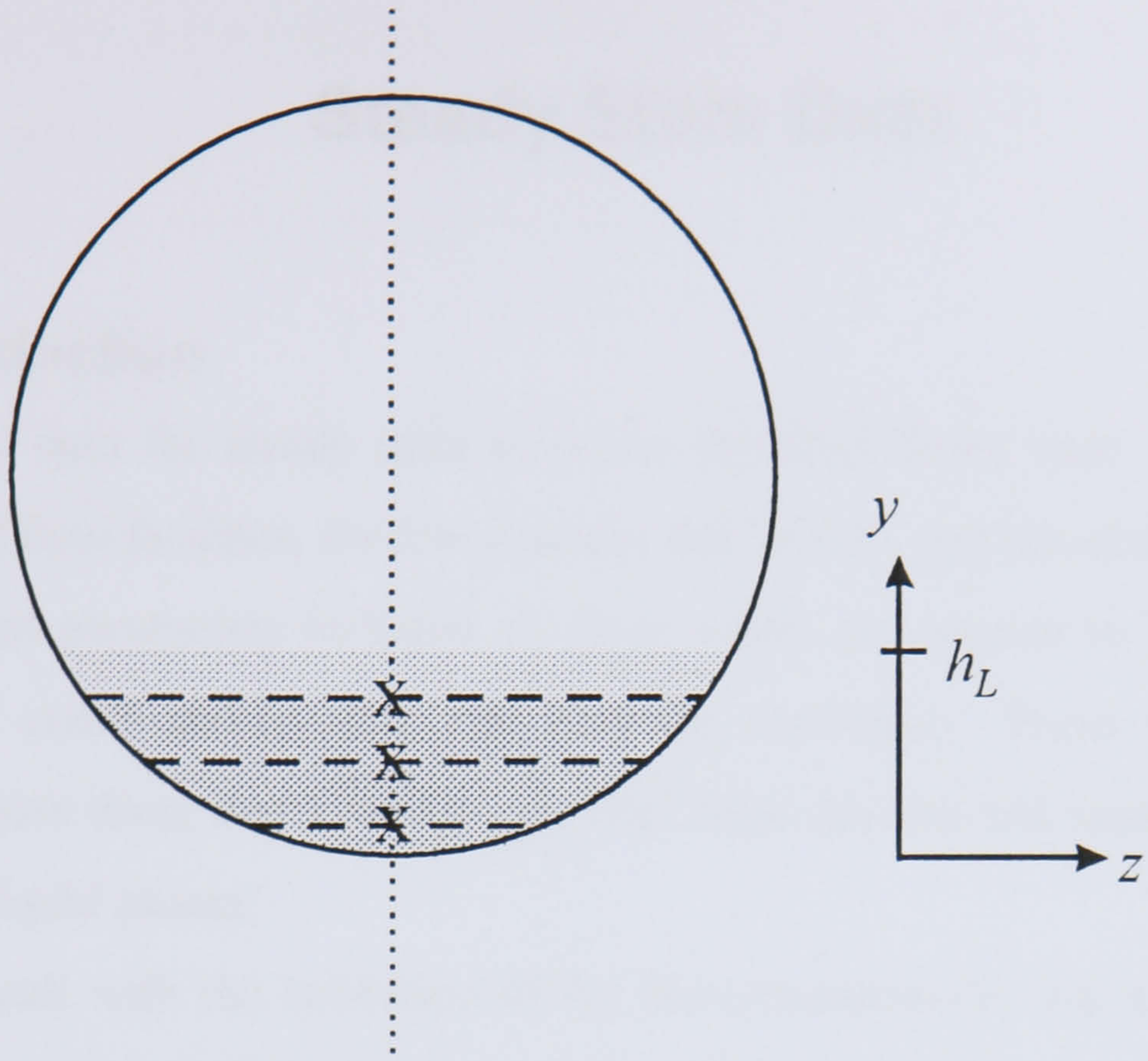


Figure 3.41 Obtaining phase average velocity from three local measurements of velocities in liquid phase

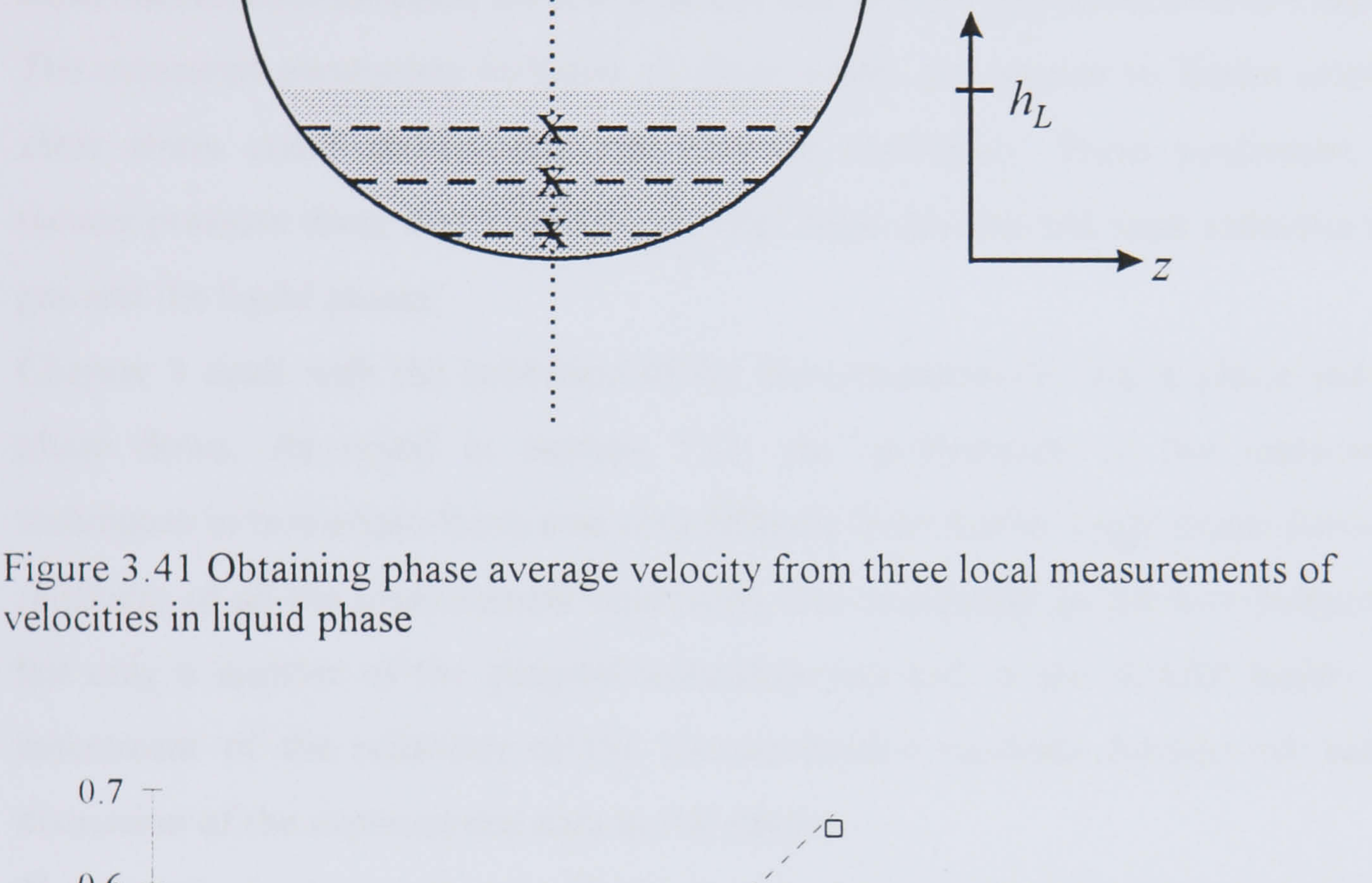


Figure 3.42 Agreement of phase average velocity in liquid phase obtained from measurements with hot-film probe (u_L(hot-film probe)) with phase average velocity obtained from rig flow rate acquisition (u_L(rig acquisition)) on the low pressure rig

Chapter 4

Steady State Data

4.1 Introduction

Experimental data for steady state air-water stratified flows were collected on two experimental flow facilities, the low pressure and WASP rigs introduced in Chapter 3. The measured parameters included all those which are needed to derive interfacial shear stress under steady state and transient conditions. These parameters were namely pressure drop, liquid holdup, gas wall shear stresses and local velocities in the gas and the liquid phases.

Chapter 3 dealt with the validation of the instrumentation in single phase and two-phase flows. As noted in Section 3.11, the performance of the measurement techniques in two-phase flows was very different from that in single phase flows. The reliability of all the measurement techniques was acceptable on the low pressure rig, but only a number of the adopted techniques worked on the WASP facility. This assessment of the reliability of the instrumentation methods formed the basis of discussion of the experimental data in this chapter.

The experimental programme of this study was started on the low pressure rig. Initially, steady state experiments were run which aimed at establishing the use of the adopted measurement techniques in two-phase flow. Later, a series of transient experiments was run. Steady state data from these transient experiments was obtained from the initial and final steady states of the transients.

The experiments on the WASP facility were of interest for two reasons. The WASP rig has a larger length-to-diameter ratio than the low pressure rig. Additionally, experiments on the WASP rig are not restricted to atmospheric pressure. Flows can also be studied at higher pressures. On WASP, only transient experiments were carried out and no separate steady state experiments were run. Steady state data from the WASP runs was obtained from the initial and final steady states of the transient runs.

Chapter 4 is split into several subsections which deal separately with the characteristics of the steady state flows relevant to this study. In Section 4.2 sample

results are presented from the tests from the low pressure facility and the WASP rig. In Sections 4.3, 4.4 and 4.5 data for the phase velocities, pressure gradient and liquid holdup is presented. The data of liquid holdup and pressure gradient is tested against predictions from the one-dimensional computer codes introduced in Section 2.4 of Chapter 2. Section 4.6 shows an evaluation of the hydraulic gradient of the flows. Section 4.7 presents an analysis of the wall shear stress and Section 4.8 an analysis of the interfacial shear stress based on measurements on the low pressure facility. Section 4.9 then deals with a more detailed analysis of the interfacial structure of stratified flows. The behaviour of the gas-liquid interface is analysed both qualitatively and quantitatively. Finally, the conclusions drawn from the presented results are summarised.

4.2 Sample Results

As noted in Chapter 3 two experimental flow facilities were used for measurements with the instrumentation developed: a low pressure facility and the WASP facility. In this section details of the experimental programme are given and sample results are presented for the two rigs separately.

4.2.1 Results from the Low Pressure Rig

4.2.1.1 Transient Tests

The main series of experiments on the low pressure rig were the transient tests. The transient runs were carried out at eight different combinations of liquid and gas flow rates in the range of conditions used in the initial steady state experiments (see Table 4.1). The sampling frequency was 500 Hz in all the runs. Each of the eight transient experiments was repeated three times with the velocity probes in different positions and the details of these runs are collected in Table 5.5 in Chapter 5. The flow rates in both phases were very stable over the three repeats at given conditions, the discrepancy of the flow rates being within +/- 1 % between the repeats. The data acquisition in these experiments lasted for a total of 300 seconds, the transient change was imposed 30 seconds after the data acquisition was started. Steady state data was obtained from the first 20 seconds (initial steady state) and the last 20 seconds (final steady state) of each run.

The data from these transient test was put onto CD ROMs which were distributed with a separate data report (Shaha & Hewitt, 1999). The reliability of the instrumentation in these transient tests was discussed in Section 3.11 of Chapter 3 and is briefly summarised here. Reliable measurements excluding corrections were obtained with the conductivity probes, the pressure transmitter, the gas wall shear stress probe and the hot-wire probe for gas velocity. The measurements with the liquid wall shear stress probe and the liquid velocity probe were made reliable by means of a normalization procedure. For further processing of the data from the transient tests the following decisions were made:

- Data for the pressure gradient and the measurement of liquid height varied less than 10 % over the three repeats for a given transient experiment and data for these parameters was therefore taken only from that repeat where the velocity probes were positioned closest to the wall (see Table 5.5 in Chapter 5).
- Variation of wall shear stresses in the gas and in the liquid was usually more than 10 % over the three repeats of a transient. The variation between the runs was random and no pattern such as drift in a certain direction with time could be identified from the data. The collected data was therefore averaged over the three repeats of a transient.
- The data for the phase average velocities was obtained from a combination of the data traces from the three repeated runs using the methods presented in Chapter 3.10.2.

Sample results are presented for the initial steady state of transient case `1c` (see Table 5.5 in Chapter 5) in Figures 4.1 to 4.7. For producing the plots, the original 500 Hz data was reduced to 5 Hz by averaging over 100 consecutive data points. In addition to the parameters discussed above (pressure gradient, wall shear stresses, liquid holdup, phase velocities), rms (root mean square) fluctuations h_L' are plotted. These were defined by equation (2.40) and Srichai (1994) had used this parameter for characterization of the interfacial structure. The data for h_L' was obtained from an arithmetic average over the h_L' values measured with each of the three conductivity probes in the test spool.

The traces of all the measured parameters are stable with time: the mean value of the parameter is constant over the time interval in the plots. All the parameters show

random fluctuations which arise from the turbulent nature of the flow. The fluctuations with respect to the time mean average value of a given parameter are smaller in the gas phase than in the liquid phase.

The data from the initial and final steady states of the transient runs on the low pressure facility described in Table 5.5 of Chapter 5 is presented in Table 4.4 and Table 4.5. The mean liquid height in the test spool, h_L(test spool), was determined from the measured liquid holdup using equation (3.25) in Chapter 3. In addition to the above stated parameters the mean liquid height downstream of the test spool, h_L(downstream), is given which was measured with the conductivity probe cp_ds (see Figure 3.13 in Chapter 3) in the centre of the test section at a distance of 0.704 m downstream of the conductivity probes in the test spool. The results tables also include the flow conditions (gas and liquid flow rates, pressure and temperatures of gas and liquid).

4.2.1.2 Steady State Tests

At the beginning of the experimental programme steady state stratified flows were studied. These initial experiments were mainly intended to validate the experimental techniques in stratified gas-liquid flow under stationary conditions.

These steady state experiments were carried out at three different liquid flow rates and a range of gas flow rates as represented in the following table:

U_L/(m/s)	U_G/(m/s)
0.04	5-10
0.06	5-10
0.08	5-10

Table 4.1 Flow conditions for steady state experiments

Data from these experiments are not separately presented here in the form of tables but they were incorporated in various sections of this chapter. The data in Table 4.4 and Table 4.5 taken from the initial and final steady states of transient experiments serve as a reference set of steady state results from the low pressure facility.

4.2.2 Results from the WASP Rig

The only experiments carried out on the WASP facility were transient tests. One further system parameter became important in these experiments: the pressure in the test section. Transient runs were carried out at six different combinations of liquid and gas flow rates and system pressure. Three values of the system pressure were investigated: 1, 6 and 11 bar. At each of the pressures two transient conditions were studied. The sampling frequency was 500 Hz in all the runs. Each of the six transient experiments was repeated three times with the velocity probes in different positions and the details of these runs are collected in Table 5.6 in Chapter 5. The agreement of the flow rates for repeated runs at one condition was significantly less than for the experiments on the low pressure rig. In the gas phase the flow rates varied by +/- 3 % over the repeats, and in the liquid the variation was in average +/- 15 % over the repeats. The data acquisition in these experiments lasted for a total of 300 seconds, the transient change was imposed 30 seconds after the data acquisition was started. Steady state data was obtained from the first 20 seconds (initial steady state) and the last 20 seconds (final steady state) of each run.

The data from these transient test was put onto CD ROMs which were distributed with a separate data report (Shaha & Hewitt, 1999). The reliability of the instrumentation in these transient tests was discussed in Section 3.11 of Chapter 3 and is briefly summarised here. The experimental measurements of the pressure gradient in two-phase flow were clearly too low. The measured gas wall shear stress data proved to be much more scattered than on the low pressure rig. Because the data for pressure gradient could not be relied upon it was not possible to normalize the measurements of the liquid wall shear stress in the same way as on the low pressure rig. Based on this evaluation of the performance of the instrumentation techniques on the WASP facility the decision was taken to discard measurements of the pressure gradient and wall shear stresses for further analysis.

Reliable measurements were obtained with the conductivity probes and the gas velocity probe. The measurements of liquid velocity were made reliable with a method of normalization. For further processing of the data from the transient tests the following decisions were made:

- The measurement of liquid height varied about 10 % over the three repeats at one transient condition and data for this parameters was therefore taken only from that repeat where the velocity probes were positioned closest to the wall (see Table 5.6 in Chapter 5).
- The data for the phase average velocities was obtained from a combination of the data traces from three repeated runs using the methods presented in Chapter 3.10.2.

Sample results are presented for the initial steady state of transient case wb (see Table 5.6 in Chapter 5) in Figures 4.8 to 4.11. For producing the plots the original 500 Hz data was reduced to 5 Hz by averaging over 100 consecutive data points. In addition to the parameters discussed above (liquid holdup, phase velocities) also rms (root mean square) fluctuations h_L' are plotted. The data for h_L' was obtained in the same way as described in Section 4.2.1.1.

The traces of all the measured parameters are stable with time: the mean value of the parameter is constant over the time interval used in the plots. The fluctuations with respect to the time mean average value of a given parameter are much smaller than in the case presented for the low pressure rig. This is consistent with the fact that the gas flow rate in the case from WASP is lower than in the case presented for the low pressure rig.

The data from the initial and final steady states of the transient runs on the WASP facility is presented in Table 4.6 and Table 4.7. In addition to the above stated parameters, data for the liquid holdup downstream of the test spool, h_L(downstream), is given. These values were determined from measurements with Srichai's (1994) conductivity probes cp_s3, cp_s4, cp_s5 (see Figure 3.2 in Chapter 3) at a distance of 0.579 m downstream of the conductivity probes in the test spool. The liquid holdup with these probes was calculated from integrating over the local measurements similar to the procedure for obtaining liquid holdup in the test spool described in Section 3.10.1. In the results tables also the flow conditions (gas and liquid flow rates, pressure and temperatures of gas and liquid) are given.

4.3 Velocities

As a basis to the method developed in Section 3.10.2 for determining phase average velocities from local velocity measurements the qualitative features of the velocity profiles in the gas and liquid phases were investigated. Local velocities in both phases were measured at a number of vertical positions in steady state experiments. The obtained velocity profiles and the profiles of the velocity fluctuations in both phases are presented here and compared with literature data.

As discussed in Chapter 3 hot-wire and hot-film probes would only give physical readings if they were used in the phase in which they were calibrated because the heat transfer from the probe to the flow depends on the fluid in which the probe is set. In all the tests it therefore had to be ensured that the velocity probes were always in the phase for which they were set up.For the gas velocity probe it was additionally important to keep it always in the gas phase as a liquid flow would break the fine wire filament. The probe positions were determined based on the measurements of mean liquid height. The liquid velocity probe was never set above the position representing the mean liquid height for given flow conditions. On the other hand the gas velocity probe was kept well above this position.

4.3.1 Liquid Velocities

Profiles of the measured local liquid velocities are presented for two liquid superficial velocities U_L of 0.04 m/s and 0.08 m/s and a range of gas flow rates in Figure 4.12 and Figure 4.13. The measurements were carried out in steady state experiments on the low pressure rig. The data was acquired at 100 Hz during 20 seconds.

Some qualitative features of the velocity profiles are noticeable from the figures. With increasing gas flow rate the measured liquid velocities at a given superficial liquid velocity increase as a result of the increased drag of the gas on the liquid. In order to ensure liquid mass continuity the mean liquid height is reduced. Due to the reduction of the mean liquid height the range is reduced over which the liquid velocity probe can be traversed through the test spool. The growth of the velocities towards the interface becomes more dominant for higher gas superficial velocities whereas at lower gas flow rates the velocity profiles are fairly flat. These velocity profiles are in good qualitative agreement with Strand (1993) who measured liquid velocities with a

laser doppler anemometer for a liquid superficial velocity U_L=0.1 m/s over a range of gas flow rates similar to those used in the present study.

rms fluctuations of the liquid velocities were derived from the sampled data in the way defined in equation (2.40) for the liquid height:

$$u_L' = \sqrt{\overline{\left(u_L - \overline{u}_L\right)^2}} \qquad (4.1)$$

Profiles of the fluctuating parts of the liquid velocities are given in Figure 4.14 and Figure 4.15. For U_L=0.04 m/s the quantities of the fluctuations are strongly dependent on the gas flow rate. For the lower gas flow rates the measured profiles of the fluctuations are fairly uniform whereas at the higher gas flow rates the fluctuations clearly increase towards the interface. At the higher liquid superficial velocity (U_L =0.08 m/s) the same qualitative behaviour of the velocity profiles is observed but the fluctuations are quantitatively less influenced by the gas flow rate. These observations are in qualitative agreement with the findings by Strand (1993). The magnitude of the fluctuations reported in his study were generally lower than those found in the present study: the fluctuations reported by Strand for U_L=0.1 m/s were quantitatively very similar to those found in the present study for U_L=0.04 m/s. Additionally, Strand observed that the fluctuations of the liquid velocities increased very near the bottom wall. This effect was clearly seen only in very few cases in the present measurements (for conditions U_L =0.04 m/s at U_G=5.9 m/s and for U_L =0.08 m/s at U_G =5.7 m/s). In the other cases investigated in the present study the effect was probably not seen as measurements of the liquid velocity were not taken closer than ~ 5 mm from the wall.

4.3.2 Gas Velocities

Profiles of the measured local gas velocities are presented for two liquid superficial velocities U_L of 0.04 m/s and 0.08 m/s and a range of gas flow rates in Figure 4.16 and Figure 4.17. These measurements were taken in steady state experiments on the low pressure rig. The data was acquired at 500 Hz for 30 seconds.

With increasing gas flow rate the measured gas velocities at a fixed superficial liquid velocity increase to conserve gas mass continuity. For a fixed gas flow rate the local velocities are slightly higher for the higher liquid flow rate case due to the smaller area for the gas caused by the higher liquid holdup. The velocity profiles at different gas flow rates vary in shape. For a gas flow rate of 5.6 m/s the maximum velocity is

slightly shifted downwards. For a gas flow rate of around 7.5 m/s the maximum velocity is slightly shifted upwards and for a gas flow rate of around 9.5 m/s the maximum is again shifted downwards. These observations are in good qualitative agreement with Strand (1993) who measured gas velocities with a Pitot tube and a laser doppler anemometer for a liquid superficial velocity U_L=0.1 m/s over a range of gas flow rates similar to those used in the present study.

rms fluctuations of the gas velocities were derived from the sampled data in the way defined in equation (4.1) for the liquid velocity:

$$u_G' = \sqrt{\overline{\left(u_G - \bar{u}_G\right)^2}} \tag{4.2}$$

Profiles of the fluctuating parts of the gas velocity are shown in Figure 4.18 and Figure 4.19. The fluctuations grow with gas flow rate, but they are not much influenced by the liquid flow rate: the profiles for the same gas flow rate but different liquid flow rates (U_L =0.04 and 0.08 m/s) are very similar. All profiles of the velocity fluctuations in the gas exhibit a minimum in the core of the gas phase, i.e. where the gas velocity is highest. The fluctuations increase towards the wall and the interface. The highest fluctuations appear near the interface. These findings are in good qualitative and quantitative agreement with Strand (1993) who measured fluctuations of gas velocities with a laser doppler anemometer for a liquid superficial velocity U_L=0.1 m/s over a range of gas flow rates similar to those used in the present study.

4.4 Pressure Gradient

The measurement of pressure gradient on the low pressure facility was found to be reliable over the whole series of experiments. In a first section comparisons of data from different experimental series are shown and the qualitative behaviour of the pressure gradient is discussed. In a separate section the measurements of pressure gradient are quantitatively investigated through comparisons with predictions from one-dimensional two-phase flow simulators.

4.4.1 Pressure Gradient: Qualitative Discussion

Data for pressure drop measured in the gas phase is presented in Figure 4.20 and Figure 4.21 for two liquid superficial velocities of 0.04 m/s and 0.08 m/s. Data from

steady state and for the steady state initial and final conditions in the transient experiments were used in the plots. The results from a series of steady state experiments are labelled "steady state runs", those from the initial and final steady states of the transient experiments are labelled as "transient runs". The reproducibility of the pressure gradient over the three repeats of each transient run was determined to be +/- 2 %.

As can be seen from the graphs the data for pressure gradient is well repeated over the different experimental series. The graphs show the expected qualitative behaviour. As in single phase flow, an increase in the gas flow causes a rise in the frictional pressure losses. But, in contrast to single phase flow, some of the increase in pressure drop is caused by the higher interfacial activity. By comparing the data for the two liquid flow rates, U_L=0.04 m/s and U_L=0.08 m/s, it is found that at a fixed gas flow rate pressure drop increases with increasing liquid flow rate. The reason for this is that with increasing liquid flow rate at a given gas flow rate the liquid holdup rises and therefore the gas phase average velocity grows.

4.4.2 Pressure Gradient: Quantitative Discussion

Data for pressure gradient from the low pressure rig was compared with model predictions from PRESBAL. The software was introduced in Section 2.4.2 and solves the one-dimensional two-fluid model for steady state. The version of PRESBAL used for this comparison assumed that the pressure gradients in the gas and liquid phases were the same and the closure relationships were that by Eck (1973) (see equation (2.72)) for the gas and liquid wall shear stresses and the model by Sinai (1983) for the interfacial shear stress. The predictions with PRESBAL were obtained with the following input which had to be specified in addition to the closure relationships: the gas and liquid superficial velocities U_G and U_L from the experiments, the pipe diameter D (D=0.07792 m), the pipe-wall roughness k_W (k_W=4.6·10^{-5} m had been established in single phase tests of this study) and the angle of inclination (0 deg for horizontal tube).

The experimental data used for the comparison were the initial and final steady state values of the transient experiments for a liquid flow rate U_L=0.04 m/s. The results of the comparisons are shown in Figure 4.22. The data is plotted as the ratio between

predicted and measured pressure drop. The figure shows that PRESBAL under-predicts the experimental data by an average of about 20 %. The difference between prediction and experiment is not surprising as the discussion of the interfacial and wall shear stress data in Sections 4.7 and 4.8 will show. There are considerable differences between the various models for each of the individual friction factors f_G, f_L and f_i, and these differences will accumulate when combinations of the friction factors are used in the one-dimensional model to predict other flow parameters, such as pressure drop.

4.5 Holdup

The discussion of the data for liquid holdup is presented in a similar way to the pressure gradient data. The measurement of liquid holdup was found to be reliable on both experimental facilities, the low pressure rig and WASP. First, comparisons of data from different experimental series on the low pressure rig are shown and the qualitative behaviour of the holdup is discussed. In a separate section the measurements of liquid holdup from both flow facilities, the low pressure rig and the WASP rig, are quantitatively investigated through comparisons with predictions from one-dimensional two-phase flow simulators.

4.5.1 Holdup: Qualitative Discussion

The qualitative discussion is based on data of the mean liquid height determined from the measured holdup using equation (3.25). Data for mean liquid height is presented in Figure 4.23 and Figure 4.24 for two liquid superficial velocities of 0.04 m/s and 0.08 m/s. Data from steady state and for the steady state initial and final conditions in the transient experiments were used in the plots. The results from a series of steady state experiments are labelled "steady state runs", those from the initial and final steady states of the transient experiments are labelled as "transient runs". The reproducibility of the liquid holdup over the three repeats of each transient run was determined to be +/- 2 %.

As can be seen from the graphs the data for liquid level is well repeatable over the different experimental series. The data in the two figures shows the expected behaviour. When the liquid flow rate is kept constant the liquid level decreases with increasing gas flow rate. As discussed in Section 4.3.1 a higher gas flow rate

increases the drag on the gas liquid interface and overall increases the velocities in the liquid phase. The equilibrium liquid level at given liquid flow rate therefore has to decrease so that mass is conserved. By comparing the data for the two liquid flow rates, U_L=0.04 m/s and U_L=0.08 m/s, it is found that at a fixed gas flow rate the mean liquid height increases with increasing liquid flow rate which is also a direct consequence of mass continuity.

4.5.2 Holdup: Quantitative Discussion

Data for liquid holdup from the low pressure rig and the WASP rig were compared with model predictions from the one-dimensional code PRESBAL. The version of PRESBAL used was described in the discussion of the data for pressure gradient in Section 4.4.2.

For the case of the low pressure rig the same experimental data set was used which formed the basis in the comparison of experimental data with code predictions for pressure drop. The data set consisted of the initial and final steady state values of the transient experiments for a liquid flow rate of U_L=0.04 m/s. The results of the comparisons are shown in Figure 4.25. The data is plotted as the ratio between predicted and measured liquid holdup. The agreement between the measured and predicted holdup is good. PRESBAL tends to underpredict the measured data, but no more than 15 %. The deviations between predictions and measurements decrease towards higher gas flow rates.

For the WASP rig the data used for the comparisons were the initial and final steady states of the transient runs at 1 bar and 6 bar. The experiments at higher pressure were carried out at considerably smaller flow rates than those at 1 bar (see Table 4.6 and Table 4.7). As the liquid flow rates were in the same range in all the experiments the liquid holdups in the runs at pressure were considerably higher than in the atmospheric runs. The results of the comparisons are shown in Figure 4.26. The data is plotted as the ratio between predicted and measured liquid holdup. The runs at the two pressures can easily be identified in the figure: the four data points at low gas flow rates are from the 6 bar runs, whereas the other four points belong to the atmospheric runs. PRESBAL considerably underpredicts the data in all the cases. The deviation between experiment and prediction is about 30 % in the atmospheric runs.

The agreement between the predictions and the experiments is slightly better in the runs at 6 bar.

Also entered in Figure 4.25 and Figure 4.26 are predictions from the three commercial codes PLAC, OLGA and TACITE (labelled as Code 1, Code 2 and Code 3 without identifying which is which) and, in the case of the WASP data, predictions from TRIOMPH. The predictions from these codes were obtained from the initial (first 20 seconds) and final steady states (last 20 seconds) of the transient simulations which are described in Chapter 5. Details of all the codes were given in Section 2.4 of Chapter 2.

For the low pressure rig data predictions with PLAC, OLGA and TACITE were obtained for one transient experiment and these predictions are included in Figure 4.25. The predictions from the three codes are scattered around the predictions from PRESBAL, but there are significant differences between the code predictions themselves of up to 20 %. The differences in predictions between the three codes can be explained as resulting from the different closure laws implemented in the codes.

In the case of the WASP data, predictions with the three commercial codes were calculated for one transient case at 1 bar and included in Figure 4.26. The range of predictions covered by the codes is of the same magnitude as in the case of the low pressure rig. As in the case of PRESBAL, all three codes underpredict the experimental holdup. Calculations with TRIOMPH were run for two transient cases, one at 1 bar and one at 6 bar and they are also included in the figure. It appears that TRIOMPH produces the best predictions of the experimental holdup data. The reason for this is that the input specification in TRIOMPH includes the liquid holdup and the value supplied for this was that from the initial steady state of the transient experiment.

4.6 Hydraulic Gradient

Significant interfacial level gradients can exist in a gas-liquid stratified flow with a high viscosity liquid and low gas velocities (Bishop & Deshpande, 1986). The existence of an interfacial level gradient, which indicates non-uniform stratified flow, will affect the holdup of the flow and delay the transition to other flow patterns, such

as slug flow. It will also cause a difference between the pressure gradient in the gas and liquid phases.

Experimental data for interfacial level gradient was reported by Strand (1993) who measured liquid levels at three different positions along his 35 m long acrylic test section: at 15 m, 23 m and 29.3 m downstream of the inlet. The reported hydraulic gradients were of the order of a few mm. The hydraulic gradient decreased with increase in the gas flow rate. At low gas flow rates, U_G of the order of 1 m/s or lower, the hydraulic gradient increased with increasing liquid flow rate, but at higher gas flow rates the hydraulic gradient was independent of the liquid flow rate.

In the present study the existence of hydraulic gradients was evaluated separately for the experiments on the low pressure facility and WASP. The experimental data used for the evaluation was taken from the initial and final steady states of the transient runs. The analysis of the data is presented in two separate Sections 4.6.1 and 4.6.2.

In the presence of an interfacial level gradient the separate momentum equations for fully developed separated flow, equations (2.4) and (2.5) in Chapter 2, are no longer valid. A more appropriate set of equations to describe the system with hydraulic gradient can be found by starting from the mass and momentum conservation equations for transient flow with constant fluid properties, equations (2.51) to (2.54) in Chapter 2. By neglecting the time dependent terms (terms of nature $\partial/\partial t$) the following momentum equation is obtained from the combination of the gas mass and momentum conservation equations (2.51) and (2.53):

$$-\rho_G u_G^2 S_G' \frac{\partial h_L}{\partial x} + S_G \frac{\partial p_G}{\partial x} + \tau_i P_i + \tau_{WG} P_G = 0 \qquad (4.3)$$

The equation is different from the momentum equation (2.5) by the first term on the right hand side which represents the change of the momentum flux due to the hydraulic gradient. The term is a function of the density ρ_G, of the velocity of the gas phase u_G, of the liquid level gradient $\partial h_L/\partial x$ and of the change of the area of flow for the gas phase S_G with respect to the liquid height S_G' which is found from equation (2.10) in Chapter 2:

$$S_G' = \frac{\partial S_G}{\partial h_L} = -2R\sqrt{1-\left(\frac{h_L}{R}-1\right)^2} \qquad (4.4)$$

By doing a similar analysis in the liquid phase using equations (2.52) and (2.54) the following momentum equation for the liquid is obtained:

$$-\rho_L u_L^2 S_L' \frac{\partial h_L}{\partial x} + S_L \frac{\partial p_L}{\partial x} - \tau_i P_i + \tau_{WL} P_L = 0 \qquad (4.5)$$

where

$$S_L' = \frac{\partial S_L}{\partial h_L} = 2R\sqrt{1-\left(\frac{h_L}{R}-1\right)^2} \qquad (2.60)$$

was presented as equation (2.60) in the review of Taitel et al. (1978). Explanations for the liquid phase are equivalent to those given above for the gas phase.

In the presence of hydraulic gradient the pressure gradients in the gas and liquid phases are not the same. The pressure gradient in the liquid is greater than the pressure gradient in the gas by a term which equals the hydrostatic head between the liquid levels at two positions along the pipeline. If the pressure gradient in the gas is expressed as $\partial p_G/\partial x$ then the pressure gradient in the liquid phase can be calculated as:

$$\frac{\partial p_L}{\partial x} = \frac{\partial p_G}{\partial x} + \rho_L g \frac{\partial h_L}{\partial x} \qquad (4.6)$$

4.6.1 Hydraulic Gradient: Low Pressure Rig

On the low pressure rig measurements of the mean liquid height at three positions in the test section were compared: measurements in the test spool, h_L(test spool), were compared with measurements of the liquid height downstream, h_L(downstream), taken with the conductivity probe cp_ds, and with measurements of the liquid height upstream, h_L(upstream), taken with the conductivity probe cp_us (see Figure 3.13 in Chapter 3). The distance between the upstream probe and the probes in the test spool was 0.816 m, the distance between the downstream probe and the probes in the test spool was 0.704 m. The analysis of the data served two purposes. By comparing the measurements at the three positions it could be established if the test spool or the instrumentation built into it significantly disturbed the flow. From the measurements also an estimation of the hydraulic gradients of the flow was obtained.

Figure 4.27 compares measurements of mean liquid height in the test spool with those upstream of the test spool. It can be seen that the liquid height upstream of the test spool, h_L(upstream), is in average higher than the liquid height in the test spool,

h_L(test spool). Similar behaviour is seen for the liquid height between the test spool and downstream of it in Figure 4.28. The liquid height in the test spool is in average higher than downstream of it. The hydraulic gradient $\partial h_L / \partial x$ between the holdup measurements at two positions along the pipe was estimated by dividing the average of the differences between the mean liquid heights at the two positions by the distance between the probes. The results are collected in the following table:

	Δh_L/mm	Δx/m	$\partial h_L / \partial x$
between test spool and upstream probe	-0.41	0.816	$5.02 \cdot 10^{-4}$
between test spool and downstream probe	-0.39	0.704	$5.54 \cdot 10^{-4}$

Table 4.2 Estimation of hydraulic gradient on the low pressure rig

Both hydraulic gradients are very similar. This indicates that the disturbance from the probe inserts is negligible and the values in Table 4.2 represent hydraulic gradients which are intrinsic to the nature of the flow.

As the low pressure rig data showed that hydraulic gradient was present in these experiments, the set of momentum equations derived in this section, equations (4.3) and (4.5), is used for further analysis of the data from this flow facility instead of the simpler momentum equations (2.4) and (2.5).

4.6.2 Hydraulic Gradient: WASP Rig

The measurements of the mean liquid heights determined with the conductivity probes in the test spool and the conductivity probes in Srichai's (1994) section were compared to check the existence of hydraulic gradient. Srichai's section was placed 0.579 m downstream of the conductivity probes in the test spool. The data is compared in Figure 4.29. Most of the data points agree within +/- 10 %. No obvious pattern can be derived from the figure. It is concluded that hydraulic gradients on WASP were negligibly small in the tests performed.

As the WASP data showed no significant hydraulic gradient it was assumed that the set of momentum equations (2.4) and (2.5) was suitable to model the steady state cases from this flow facility.

4.7 Wall Shear Stress

Although all the measured data on wall shear stress have been stored for possible future analysis, for the reasons outlined in Section 3.11, only the data from the low pressure rig were analysed as part of the present project.

4.7.1 Variation with Position

In the test spool the hot-film probes for measurement of the gas and liquid wall shear stresses were mounted opposite each other. During an experiment they were kept in a fixed position which usually was the bottom of the test spool for the liquid wall shear stress probe and the top of the test spool for the gas wall shear stress probe. In between experiments the position of the probes around the circumference could be changed by undoing the flanges of the test spool and rotating it to a new position. To reduce the effort spent on the experiments it was desirable to only do the measurements with the probes in one position without the need to repeat the experiments with the probes in different positions. This required an assessment of the validity of the assumption that average values could be represented by local measurements of wall shear stresses at top and bottom of the test spool only.

There have been several studies of the variation of shear stress around the perimeter and a summary of these studies is given in Section 2.2.1.3 of Chapter 2. Experimental studies by Kowalski (1987) and Espedal (1998) showed that the variation of the local shear stresses in both phases around the inner pipe wall was relatively small except in the region near the interface. Based on their data the error by using the gas wall shear stress measured at the top of the tube instead of the phase average shear stress in the gas phase was estimated to be about +/- 5 % in horizontal flow. The error by using the liquid wall shear stress measured at the bottom of the tube instead of the phase average shear stress in the liquid phase was estimated to be about +/- 10 % for horizontal flow.

As part of the two-phase steady state experiments on the low pressure rig liquid wall shear stress was measured at different circumferential positions to determine the variation of the wall shear stress in the experiments. The measurements were carried out at two different positions, at the bottom of the test spool (0 deg) and at an angle of 45 deg from the pipe bottom by turning the test spool in the clockwise direction. A

sketch of the measurement positions around the circumference is shown in Figure 4.30. Data from these experiments is presented in Figure 4.31 for a range of gas flow rates and a liquid flow rate U_L=0.08 m/s. Measurements of the liquid height at these conditions indicated that the wall shear stress probe was completely wetted in all the tests.

Over the whole range of gas flow rates the shear stress is about 20 % higher at the position "+45 deg" than at the bottom of the tube. These results suggest that the liquid wall shear stresses measured at the bottom of the tube give reasonable estimates of the liquid phase average wall shear stress which is needed as an input parameter in the one-dimensional model. Therefore it was sufficient to only measure liquid wall shear stress at the bottom of the test section in all further experiments. From the literature data it is assumed that also in the gas phase the wall shear stress over the circumference only varies moderately, and that the measurement of the gas wall shear stress at the top of the tube gives a good estimate of its phase average value.

4.7.2 Gas Wall Shear Stress

For quantitative analysis of the steady state measurements of the gas wall shear stresses the gas wall friction factor f_G was derived from the experimental data and the results were compared with predictions given in the published literature.

Experimental data for the gas wall friction factor f_G were calculated from equation (2.6) using measurements of gas wall shear stress τ_{WG} and gas phase average velocity u_G taken from the initial and final steady states of the transient runs on the low pressure rig:

$$f_G = \frac{2\tau_{WG}}{\rho_G u_G^2} \tag{4.7}$$

This data was compared with three different models described in Chapter 2: the models by Taitel & Dukler (1976), Eck (1973) and Espedal (1998). These models were chosen for the following reasons:

- The Taitel & Dukler model (equation (2.7)) is the simplest expression and is the generally accepted model for expressing f_G. For the flow conditions of this study the model for f_G for turbulent flow applied. The Taitel & Dukler model was used

by Andreussi & Persen (1987), Andritsos & Hanratty (1987) and many other researchers who investigated the gas-liquid interaction in steady state gas-liquid stratified flows. The model is valid for smooth tubes, e.g. acrylic tubes, where the wall roughness is negligible.

- Eck's model (equation (2.38)) is one of the very few models suggested in the literature which accounts for the pipe wall roughness. Srichai (1994) used this type of model because his experiments were carried out in a steel test section where the wall roughness is significant. Similar to the formula suggested by Taitel & Dukler the model suggested by Eck is also mainly a function of the gas Reynolds number.
- The most complex model for the gas wall friction factor was proposed by Espedal, equation (2.45). It does not just account for the behaviour of the gas phase only but also includes the interaction of the gas-liquid interface as it is a function of the difference between the gas and liquid phase average velocities and the interfacial friction factor. The prediction from this model will therefore depend on the values which are inserted for f_i. In Section 4.8 it will be shown that the model by Spedding & Hand (1997) gave the best predictions of the data for interfacial friction of this study, and this model was adopted to calculate values for the interfacial friction factor f_i used with Espedal's model for the gas friction factor.

The model predictions were calculated using experimental data of the required parameters. For the Taitel & Dukler and the Eck model data for liquid height h_L and gas phase average velocity u_G were sufficient. For the Espedal model (with the interfacial friction factor f_i predicted from Spedding & Hand) data for the liquid phase average velocity u_L was additionally needed. Where required, gas and liquid superficial velocities U_G and U_L were calculated from experimental data for liquid holdup and phase average velocities using equations (3.30) and (3.32) in Chapter 3. The values for the superficial velocities obtained in this way were in agreement with the values recorded with the rig flow rate acquisition system.

The comparisons of these three models with the experimental data are shown in Figure 4.32. All three models give predictions which are quantitatively only slightly different from each other. For a given experiment the difference between the highest and the lowest prediction is about 20 %. In each experiment the lowest predicted values are obtained with the Taitel & Dukler model, slightly higher predictions are

given by the Eck model and the highest predictions are obtained with the Espedal model. The explanation for this behaviour is straightforward. The main difference between the Taitel & Dukler and the Eck model is the inclusion of a term to account for the pipe wall roughness. The Eck model yields higher values of the gas wall friction factor than Taitel & Dukler because the measurements in the present study were carried out in a steel test spool. The roughness of the tube was determined in single phase tests as k_R=4.6·10^{-5} m (see Section 3.9.1.1 in Chapter 3). The Espedal model yields even higher predictions as it not just accounts for the pipe wall roughness but also for the interfacial structure. As shown in the sample results of liquid holdup (Figure 4.4) and interfacial fluctuations (Figure 4.7) for experiments on the low pressure rig the structure of the interface is wavy which leads to an increase of f_G in the predictions with Espedal's model.

Both Espedal's and Eck's model agree well with the experimental data. Larger discrepancies between the experimental data and predictions are observed for the Taitel & Dukler model. Also included in the graph are the lines to indicate the variation of +/- 15 % in the repetitive measurements of gas wall shear stress in the transient experiments. It is seen that most of the deviation between Espedal's model and the experiment and also most of the deviation between Eck's model and the experiment is not significant compared with the experimental error.

4.7.3 Liquid Wall Shear Stress

For quantitative analysis of the steady state measurements of the liquid wall shear stresses the liquid wall friction factor f_L was derived from the experimental data and the results were compared with predictions given in the published literature.

Experimental data for the liquid wall friction factor f_L were calculated from equation (2.6) using measurements of the liquid wall shear stress τ_{WL} and liquid phase average velocity u_L from the initial and final steady states of transient runs on the low pressure rig:

$$f_L = \frac{2\tau_{WL}}{\rho_L u_L^2} \tag{4.8}$$

This data was compared with four different models described in Chapter 2: the models by Taitel & Dukler (1976), Andritsos & Hanratty (1987), Srichai (1994) and Spedding & Hand (1997). These models were chosen for the following reasons:

- The Taitel & Dukler model for f_L (equation 2.7) is equivalent to their model suggested for expressing the gas wall friction factor f_G. For f_L this type of relationship is not as widely accepted as in the gas phase. The reason for this is that the wavy structure of the interface leads to an increase in the liquid wall shear stress which is not taken account of in the Taitel & Dukler model.
- The Andritsos & Hanratty model takes into account the behaviour of the gas-liquid interface in the calculation of f_L. Equation (2.28) demonstrates that f_L is calculated on the basis of the interfacial shear stress and a characteristic shear stress which both take into account the interfacial structure. Calculation of the interfacial shear stress in this model is dealt with in more detail in Section 4.8.
- The model for f_L by Srichai, equation (2.39), is a function of the liquid holdup and the Reynolds number in the liquid phase based on the liquid superficial velocity and the diameter of the pipe. An expression of this type for f_L was first introduced by Kowalski (1987). The models by Kowalski and Srichai only differ by the numerical coefficients employed in the expression for f_L.
- The model for f_L by Spedding & Hand, equation (2.42), is dependent on the Reynolds number in the liquid phase. For Re_L<2100 the flow is considered laminar and the expression for f_L is very similar to that in Taitel & Dukler for a laminar flow. For Re_L >2100 the expression for f_L is of the same type as in Srichai. For the experimental conditions of this study only the latter expression applied as Re_L was greater than 2100 in all the experiments.

The model predictions were calculated using experimental data of the required parameters. For the models by Taitel & Dukler, Srichai and Spedding & Hand, data for liquid height h_L and liquid phase average velocity u_L were sufficient. For the Andritsos & Hanratty model data for the gas phase average velocity u_G was additionally needed. Where required, gas and liquid superficial velocities U_G and U_L were calculated from experimental data for liquid holdup and phase average velocities using equations (3.30) and (3.32) in Chapter 3. The values for the superficial

velocities obtained in this way were in agreement with the values recorded with the rig flow rate acquisition system.

Comparisons of the four models with experimental data are shown in Figure 4.33. The model predictions for f_L cover a much wider range than those presented for f_G in Figure 4.32. In a given experiment the highest predictions (Srichai's model) are about a factor four higher than the lowest predictions (Taitel & Dukler's model). The model predictions by Andritsos & Hanratty and Spedding & Hand are in between the two extremes and yield similar values.

The Taitel & Dukler model clearly underpredicts the experimental data. This can be understood as this model does not account for the wavy structure of the interface which has an important influence in the liquid phase. The model by Srichai overpredicts the experimental data clearly. There are two possible reasons which can explain the discrepancies. Srichai developed his relationship for experiments on the WASP facility which is much longer than the low pressure rig and which has a steel test section of the same dimensions as used for the test spool in the present study, but which is different from the acrylic test section on the low pressure rig. Also, Srichai only carried out experiments at elevated pressures (6 bar or higher) and this will have an influence on the interfacial structure. Andritsos & Hanratty and Spedding & Hand worked at experimental conditions which were similar to the ones on the low pressure rig. Their model predictions were developed for gas-liquid flows in acrylic test sections at atmospheric pressure. The two models by Andritsos & Hanratty and Spedding & Hand yield similarly good predictions of the experimental data of this study, the model by Spedding & Hand appears to perform slightly better. Also with these two models there are significant differences to some of the experimental data with the model predictions being outside the range of f_L (+/- 20 %) given by the variation of the liquid wall shear stress between repeats of the transient run.

4.8 Interfacial Shear Stress

In principle data for interfacial shear stress τ_i, and as a consequence data for the interfacial friction factor f_i, can be derived from experiments in the gas and liquid phases separately using the momentum equations of the one-dimensional model. Following the discussion of the sample data in Section 4.2 reliable measurements of

the necessary parameters were only obtained on the low pressure rig. The measurements in the gas phase proved to be more reliable than those in the liquid phase and the discussion is therefore restricted to the set of interfacial shear stress data derived from measurements in the gas phase on the low pressure rig.

In the analysis of the data for the low pressure rig, a significant hydraulic gradient had been found and the set of momentum equations valid under these conditions is given by equations (4.3) and (4.5). Experimental data for interfacial shear stress τ_i was obtained from re-arranging the momentum equation for the gas phase, equation (4.3):

$$\tau_i = \frac{1}{P_i}\left[\rho_G u_G^2 S_G' \frac{\partial h_L}{\partial x} - S_G \frac{\partial p_G}{\partial x} - \tau_{WG} P_G\right] \qquad (4.9)$$

The input parameters used were the pressure drop measured in the gas phase at the top of the test spool, the measured gas wall shear stress and the gas phase average velocity. The value for the hydraulic gradient $\partial h_L/\partial x$ was found in Section 4.6.1 and quantified as $5.54 \cdot 10^{-4}$. The mean liquid height, calculated from the liquid holdup in the test spool with equation (3.25), was used to calculate the geometrical parameters S_G, P_G, P_i, S_G' by means of equations (2.10), (2.12), (2.13) and (4.4). Interfacial curvature was not taken into account in calculating these parameters because an evaluation of the influence of interfacial curvature in the experimental data on the geometrical parameters and on the data for f_i had a negligible influence. The interfacial friction factor f_i was then calculated from equation (2.6) using the liquid phase average velocity u_L as input for the interfacial velocity u_i:

$$f_i = \frac{2\tau_i}{\rho_G\left(u_G - u_L\right)^2} \qquad (4.10)$$

The experimental data was compared with predictions from the same models as those used in the liquid wall shear stress analysis. These were Taitel & Dukler (1976), Andritsos & Hanratty (1987), Srichai (1994) and Spedding & Hand (1997).

- The model by Taitel & Dukler presents the simplest approach to modelling the interfacial friction factor. It assumes that f_i is the same as the gas wall friction factor f_G. As discussed in Chapter 2 this assumption is acceptable for a smooth flow, but not in cases where the interfacial activity is significant through the formation of waves. In these cases the Taitel & Dukler model significantly underpredicts f_i.

- The Andritsos & Hanratty model, equation (2.27), calculates f_i in two different ways depending on the value of the gas superficial velocity U_G. If the gas superficial velocity is lower than a value $U_{G,t}$, which is defined as:

$$U_{G,t} = 5\left(\frac{\rho_{G,atm}}{\rho_G}\right)^{0.5} \tag{4.11}$$

the interface is considered smooth and the model for f_i is the same as that in Taitel & Dukler. The value of $U_{G,t}$ at atmospheric conditions is about 5 m/s. For values of U_G greater than $U_{G,t}$ the interface becomes highly deformed and f_i is then calculated from a more complex expression. In the experiments carried out on the low pressure rig the gas flow rate was higher than the limit defined in equation (4.11) and only the expression for f_i from Andritsos & Hanratty applied where the ratio f_i/f_G was greater than 1.

- The model by Srichai (equations (2.40) and (2.41)) was developed from his own experimental data at elevated pressures, 5, 10 and 15 bar(g) and Strand's (1993) data at atmospheric pressure. Based on Sinai's (1983) work f_i is calculated from the ratio of the gas mean and friction velocities, which is a function of the rms roughness scale k_R of the interface. k_R is calculated from correlations in the values of the liquid level fluctuations h_L' which Srichai developed from his experiments.
- The model by Spedding & Hand for f_i (equation (2.43) and (2.44)) is a function of the gas and liquid superficial velocities. The values of f_i are computed with reference to a friction factor in the gas which is based on the gas Reynolds number calculated from the gas superficial velocity and the tube diameter, rather than the Reynolds number based on the hydraulic diameter in the gas and the gas phase average velocity as was the case in Taitel & Dukler.

The model predictions were calculated using experimental data for the required parameters. For the Taitel & Dukler, Andritsos & Hanratty and Srichai model data for liquid height h_L and gas phase average velocity u_G were sufficient. For the Spedding & Hand model data for the liquid phase average velocity u_L was additionally needed. Where required, gas and liquid superficial velocities U_G and U_L were calculated from experimental data for liquid holdup and phase average velocities using equations (3.30) and (3.32) in Chapter 3. The values for the superficial

velocities obtained in this way were in agreement with the values recorded with the rig flow rate acquisition system.

Comparisons of the experimental data with the four models are shown in Figure 4.34. The differences between the model predictions are even greater than for the liquid wall friction factor but the pattern of the performance of the different models has the same structure as for the liquid wall friction factor. The Taitel & Dukler model under-predicts the experiment, the Srichai model over-predicts the experiment, the models by Andritsos & Hanratty and Spedding & Hand are in between the other two models. The Taitel & Dukler model under-predicts the data because it doesn't account for the wavy structure of the interface which is clearly shown by the sample result for liquid holdup, Figure 4.4. Predictions with the models by Andritsos & Hanratty and Spedding & Hand are better than the other two because they were developed under conditions similar to the low pressure rig. For smaller values of the interfacial friction factor both models appear to perform similarly well, but at higher values of f_i the Spedding & Hand model is clearly better.

4.9 Interfacial Structure

The understanding of stratified gas-liquid flow is closely linked with the structure of the interface. As noted in the literature review (Chapter 2) and in the discussion of the experimental data in this chapter the interaction between the two phases has a major effect on all the flow parameters. In the first part of the present section the interfacial structure in the experiments performed in this study is qualitatively discussed. In a separate section a quantitative description of the interaction between the two phases is derived.

4.9.1 Qualitative Behaviour

4.9.1.1 Interfacial Structure in Three Dimensions

In the discussion of the experimental data so far the flow was treated as one-dimensional, or in the case of the velocities, as two-dimensional. To analyse the structure of the gas-liquid interface in more detail the extension to three dimensions is useful.

Three-dimensional representations of the gas-liquid interface in steady state stratified flow were presented by Strand (1993) and Srichai (1994). These graphs were obtained by plotting simultaneous time traces of the measurements taken with an array of twin-wire conductivity probes in the same cross section. Strand used the time traces of four probes in half a cross section, Srichai all five of his probes distributed equally over the cross section. Strand presented data for different combinations of gas and liquid flow rates ($2.5<U_G/(m/s)<7.75$ and $0.03<U_L/(m/s)<0.13$) at atmospheric pressure, Srichai showed graphical results for a range of gas flow rates U_G between 1.6 and 5.7 m/s and a liquid superficial velocity U_L=0.15 m/s at 11 bar.

In the present study graphical representations of the three-dimensional interfacial structure were obtained from the simultaneous time traces of the three conductivity probes in half a cross section of the test spool, cp_ts1, cp_ts2 and cp_ts3 as represented in Figure 3.10. The locations of the probes were z=9.7, 19.4 and 29.1 mm in the lateral direction z where z=0 was the centre of the test spool. Data for the other half of the test spool was obtained by assuming symmetry of the measured traces with respect to the vertical plane through the centre of the tube. The figures contain instantaneous data sampled at 500 Hz and the measured data points are connected with straight lines.

4.9.1.1.1 Interfacial Structure at Atmospheric Pressure

In this section the interfacial structure of an experiment from the low pressure rig is compared with an experiment from the WASP rig carried out under similar conditions. For both flow facilities the data for comparison was taken from the initial steady state of transient experiments carried out at atmospheric pressure: for the low pressure rig this was transient case `1a` and for the WASP rig this was case `wb`. The specification of the runs was given in the data tables of Section 4.2 and is listed here again:

- Low pressure rig (case `1a`): U_L=0.039 m/s, U_G=5.01 m/s, p=1.00 bar
- WASP rig (case `wb`): U_L= 0.038 m/s, U_G=5.33 m/s, p=1.06 bar

The results of the low pressure rig case are plotted in Figure 4.35, the results from the WASP case are plotted in Figure 4.36 for a duration of 0.6 seconds before the transient change. The interface in the experiment on the low pressure rig is covered

with small amplitude waves. The wave pattern is slightly irregular; the amplitude of the waves is non-uniform in the axial direction but it doesn't change in transverse direction. The amplitude of the larger waves is around 2 mm. The interface is slightly curved in a cross section with the liquid height increasing towards the wall. Like on the low pressure rig the interface in the WASP experiment is covered with waves but their amplitude is much smaller. The largest amplitudes are around 1 mm. The structure of the interface appears slightly irregular as the amplitude of the waves varies in the axial direction. The liquid height in a cross section is uniform. The mean liquid height compares well between the experiments on the two flow facilities.

The comparison of the two figures shows that the interfacial activity is greater in the case of the low pressure rig than for WASP under very similar flow conditions. The major differences between the two flow facilities are the length and material of their test sections. The length of the low pressure rig is only about 8 m compared to 36 m for WASP. On WASP, measurements with the test spool were taken much further away from the inlet of the test section than on the low pressure rig. One likely explanation for the different interfacial behaviour in the two experiments is that there are entrance effects which influence the flow at the measuring position on the low pressure rig, but which have died out before they reach the measuring position on the WASP rig. But also, the material of the test section could have an influence on the interfacial structure. The inside of the acrylic test section on the low pressure rig is smooth compared to the inside of the steel test section on WASP. Due to the roughness of the wall the drag between fluid and wall will be increased on the WASP facility and this could perhaps cause a reduction in the interfacial activity.

4.9.1.1.2 Interfacial Structure at High Pressure

In the case of the WASP experiments the influence of the system pressure on the interfacial structure could be studied. The data from two runs with similar flow rates but substantially different pressures was compared. The data was taken from the initial steady states of cases wd and we, which were performed at 6 and 11 bar system pressure. The specification of the runs was given in the data tables of Section 4.2 and is listed here again:

- 6 bar (case wd): U_L=0.034 m/s, U_G=1.30 m/s, p=6.07 bar

- 11 bar (case we): U_L=0.025 m/s, U_G=1.32 m/s, p=11.04 bar

The results of the 6 bar case are plotted in Figure 4.37, the results from the 11 bar case are plotted in Figure 4.38 for a duration of 0.6 seconds before the transient change. The liquid level in the 6 bar run is very high, around 30 mm. The interface is covered with regular waves with a small amplitude of around 1 mm. The amplitude does not vary in the transverse direction. The graph is dominated by the fact that the highest liquid level is measured with the probe cp_ts2 which is the middle probe in the array of three probes built into half a cross section of the test spool. But the variation of the liquid height in the transverse direction is moderate, about 2 mm. In the graph of the 11 bar case, the qualitative behaviour of the interface is similar to the 6 bar case. The interface is also covered with small amplitude waves which have an amplitude of around 1 mm like at 6 bar. But the variation of the liquid level in the transverse direction is much less dominant than at 6 bar, only around 1 mm. The liquid level in the 11 bar run is lower than in the 6 bar run, but this is mainly attributed to the lower liquid flow rate in the 11 bar case.

4.9.1.2 Axial View Pictures

In stratified gas-liquid flow, the two phases are not always completely separated. This is only the case at low enough gas flow rates. At high gas flow rates the gas picks up liquid droplets from the interface and entrains them. Droplet entrainment is an effect which is not taken account of by the models presented in Section 2.3 of this thesis. Of the three commercial codes used in this study, PLAC, OLGA and TACITE, only the OLGA code calculates a separate droplet field. The question of whether there was droplet entrainment in the experiments of this study was experimentally investigated.

The experiment to address this question consisted of taking axial view pictures of the flows. An axial viewing system for the WASP rig at Imperial College was developed by a student colleague, Shahrokh Badie, and his help in obtaining axial view pictures of the experimental runs in this study is greatly appreciated. The views were taken with the axial viewer connected to the end of the test section and by looking in the upstream direction of the flow. The views were recorded on ordinary video tape.

An axial view of an instant during the initial steady state of transient case wd on the WASP rig is presented in Figure 4.39. The flow conditions of this case were:

U_L=0.034 m/s, U_G=1.30 m/s, p=6.07 bar. The figure shows the liquid flowing at the bottom of the test section. The gas-liquid interface is smooth and flat. The two phases are completely separated and the gas phase is free from any liquid as far as the picture shows. To prove that droplets can be seen with the axial viewer if there are any a view was taken for a case with a much higher gas flow rate than in any of the experiments investigated for this thesis. A picture from a flow with conditions U_L=0.015 m/s, U_G=20.0 m/s, p=1.0 bar is shown in Figure 4.40. The figure shows that the phases are not well separated any more and that a large number of liquid droplets are dispersed in the gas phase.

The axial view pictures presented in this section proved that under the experimental conditions used in this study no droplet entrainment occurred and this issue therefore didn't need to be addressed in the further course of this study.

4.9.2 Quantitative Analysis

As discussed in Section 4.2.2 the only reliable parameters in the WASP experiments were the liquid height and the gas and liquid phase velocities. With this set of data it was not possible to derive the interfacial shear stress in the way followed for the low pressure rig, where values for interfacial shear stress were obtained from measurements of the pressure gradient in the gas phase, the gas wall shear stress, the gas velocity and the liquid level. Therefore an alternative route was followed to derive interfacial shear stress from measurements of the interfacial structure with the three conductivity probes distributed in half a cross section in the test spool.

Srichai (1994) had quantified the interfacial friction factor in terms of the rms fluctuations of the liquid level h_L' as defined by equation (2.40):

$$h_L' = \sqrt{\overline{\left(h_L - \bar{h}_L\right)^2}} \qquad (2.40)$$

where h_L is the instantaneous liquid height and $\bar{h}_L$ is the average liquid height. To calculate the interfacial friction factor Srichai used the methodology by Sinai (1983), equations (2.14), (2.15) and (2.16), to link his experimental data for f_i to the interfacial roughness k_R and he developed an empirical relationship between k_R and h_L' based on experimental data, which was presented in the form of equation (2.40). h_L' was correlated to the product of the liquid holdup ε_L and the gas Reynolds number Re_G^* defined in equation (2.37) accounting for the system pressure.

The method of relating the rms fluctuations of liquid height h_L' to the interfacial friction factor was evaluated in the present study for the experiments on the low pressure and the WASP rig separately and the analysis is presented in Sections 4.9.2.1 and 4.9.2.2.

4.9.2.1 A New Model for Interfacial Shear Stress for the Low Pressure Rig

Measurements of the instantaneous liquid height in the test spool were carried out at three transverse locations in the same cross section using the conductivity probes cp_ts1, cp_ts2 and cp_ts3 represented in Figure 3.10 of Chapter 3. The fluctuations of the liquid height for the three probes are represented in Figure 4.41 for the initial steady state of transient case `1a` (U_L=0.039 m/s, U_G=5.01 m/s, p=1.00 bar). The figure shows a variation of interfacial fluctuation with transverse position z and therefore the decision was taken to evaluate the values of h_L' for further data analysis from arithmetic averaging over the fluctuations from the three separate probes.

Values of h_L' were derived from the measurements with the array of conductivity probes in the test spool during the initial steady state (first 20 seconds) and the final steady state (final 20 seconds) of the transient runs on the low pressure rig. h_L' was determined over the total period of 20 seconds. The influence of the time interval on the result of h_L' was investigated for one case: for 20 seconds of steady state data h_L' was determined over different time intervals of 0.2, 2.0 and 20.0 seconds. The results of the initial steady state of transient case `1c` (U_L=0.039 m/s, U_G=7.39 m/s, p=0.99 bar) are presented in Figure 4.42. The result of h_L' is not significantly influenced by the time interval over which it is determined.

The steady state data from the low pressure rig was then used to develop a new relationship for the interfacial friction factor in analogy to the route followed by Srichai (1994). The data for h_L' from the present study was plotted in dimensionless form (h_L'/D) versus the product $\varepsilon_L \mathrm{Re}_G^{-}$. This is graphically represented in Figure 4.43. The experimental data shows the expected behaviour: the fluctuations of the liquid level increase towards higher gas flow rates due to larger interfacial activity. The trend of the data is reasonably well described by the predictions from Srichai which are calculated from equation (2.41). The input data for atmospheric pressure used by Srichai to develop his correlation for h_L'/D (given by equation (2.41)) was taken from

Strand (1993) who carried out measurements of stratified flow in an acrylic test section of 0.1 m inner diameter. An improvement in predicting the data for h_L' from the present study is obtained with the following relationship

$$\frac{h_L'}{D} = 6.2153 \cdot 10^{-6}\left(\varepsilon_L \, \mathrm{Re}_G^+\right) - 0.0098 \qquad (4.12)$$

which is found from best fit of a straight line to the data in Figure 4.43.

As a next step, the relationship between the interfacial roughness k_R and the rms fluctuations of the liquid height h_L' had to be developed. First the values of the interfacial friction factor f_i were derived from the measurements in the gas phase as described in Section 4.8 accounting for the influence of the hydraulic gradient. These values of f_i were used to determine the values for interfacial roughness k_R from equations (2.14), (2.15) and (2.16) developed by Sinai (1983). The values of k_R were plotted in logarithmic dimensionless form as $\log_{10}(k_R/D)$ against the logarithm of dimensionless fluctuations of liquid height $\log_{10}(h_L'/D)$ shown in Figure 4.44. The following relationship was found from best fit to the data:

$$\log_{10}\left(\frac{k_R}{D}\right) = 0.6273 \log_{10}\left(\frac{h_L'}{D}\right) - 0.0031 \qquad (4.13)$$

or in exponential form

$$k_R = D \cdot 0.9929\left(\frac{h_L'}{D}\right)^{0.6273} \qquad (4.14)$$

To summarise the set of equations proposed to calculate the interfacial friction factor in the low pressure rig are as follows:

$$f_i = 2\left(\frac{u^*}{u_G}\right)^2 \qquad (2.14)$$

$$\frac{u_G}{u^*} = 5.75 \log_{10}\left(\frac{R_G}{k_R}\right) + 4.73 \qquad (2.15)$$

$$R_G = \frac{2S_G}{P_i + P_G} \qquad (2.16)$$

$$k_R = D \cdot 0.9929\left(\frac{h_L'}{D}\right)^{0.6273} \qquad (4.14)$$

$$\frac{h_L'}{D} = 6.2153 \cdot 10^{-6}\left(\varepsilon_L \, \mathrm{Re}_G^+\right) - 0.0098 \qquad (4.12)$$

The PRESBAL code (see Section 2.4.2) was modified to validate this new model for f_i against the experiments on the low pressure rig. The model equations from above for the calculation of f_i were implemented in PRESBAL. For the gas wall friction factor and the liquid wall friction factor the models were used which were evaluated in Section 4.7 to give the best predictions of the measured data from the low pressure rig. The models used were that by Eck (1973) (equation (2.38)) for f_G and that by Spedding & Hand (1997) (equation (2.42) for the turbulent case) for f_L. The set of momentum equations (2.4) and (2.5) was replaced by the momentum equations (4.3) and (4.5) to account for the influence of the hydraulic gradient. The comparisons of code predictions with experimental data are shown in Figure 4.45 for the pressure drop and in Figure 4.46 for the liquid holdup. By comparing the predictions for pressure drop with the new set of relationships (Figure 4.45) with the predictions obtained with the standard set of relationships described in Section 2.4.2 (Figure 4.22) it is clear that the new set of relationships provides slightly better predictions of the pressure gradient. The same comparison for liquid holdup (Figure 4.46 with Figure 4.25) shows that both sets of closure relationships produce very similar predictions for this parameter.

4.9.2.2 A New Model for Interfacial Shear Stress for the WASP Rig

The analysis of the data of h_L' was carried out separately for the WASP experiments. Values of h_L' on the WASP rig were derived from the measurements with the array of conductivity probes in the test spool during the initial steady state (first 20 seconds) and the final steady state (final 20 seconds) of the transient runs. Following the procedure in Section 4.9.2.1 values of h_L' were obtained from arithmetic averaging over the fluctuations from the three separate probes taken over a time interval of 20 seconds.

From the discussion in Section 4.9.1 it was clear that the interfacial structure is influenced by the type of the flow facility and by the system pressure. To start with, data for h_L' from the atmospheric runs on the WASP rig were compared with data from the low pressure rig to evaluate the differences. The comparison is shown in Figure 4.47 in terms of the dimensionless fluctuations $h_L' D$ versus the product of liquid holdup ε_L and the gas Reynolds number Re_G^* defined by equation (2.37). The

data from the low pressure rig was already presented in Figure 4.43. It is evident that the values for h_L' at similar flow conditions are much smaller on WASP than on the low pressure rig although the experimental setup for measurement of h_L' was identical on both flow facilities. Possible reasons for the difference in interfacial activity on the low pressure and the WASP rig were discussed in Section 4.9.1.1.1.

Srichai had obtained his own experimental data for h_L' on the WASP rig at pressures of 6, 11 and 16 bar, but not at atmospheric pressure. Data from the present study for experiments on WASP at 6 bar and 11 bar should therefore be comparable with predictions from Srichai's correlation for h_L', equation (2.41). Experimental data for the interfacial fluctuations for 6 bar from the present study is compared with predictions from Srichai in Figure 4.48. It is seen that both data sets agree reasonably well but that Srichai's values are generally slightly higher. This behaviour can be explained with the influence of the transverse location in the cross section of flow on the measurement of h_L' which was demonstrated in Figure 4.41. The values of h_L' were determined differently in Srichai's study and in the present study. Srichai used an array of five twin-wire conductivity probes equally distributed across a cross section (see Figure 3.2) whereas in the present study a different array of three conductivity probes in half a cross section was used (see Figure 3.10).

As a next step, the data for h_L' at the three different pressures 1, 6 and 11 bar was quantitatively analysed. All steady state data collected in the experiments on WASP in this study are shown graphically in Figure 4.49. It is obvious from the graph that the interfacial fluctuations for a given liquid holdup ε_L and gas Reynolds number Re_G^+ decrease with increasing pressure. This feature was also observed by Srichai. At all three pressures the relation between the dimensionless fluctuations $h_L' D$ and the product $\varepsilon_L \mathrm{Re}_G^+$ can be expressed by straight lines through the origin of the form

$$\frac{h_L'}{D} = C_s\left(\varepsilon_L \, \mathrm{Re}_G^+\right) \tag{4.15}$$

where the parameter C_s depends on the pressure. Srichai had fitted his data for h_L' with polynomials instead of straight lines. By determining the value for C_s at each pressure the relationship between C_s and pressure can be quantified. The values for C_s determined at each of the pressures are collected in the following table:

p/bar	$C_s/10^{-7}$
1	6.459
6	4.169
11	2.606

Table 4.3 Values of parameter C_s obtained at different pressures

Srichai used the density ratio

$$\frac{\rho_G}{\rho_L - \rho_G} \tag{4.16}$$

as a parameter to account for the system pressure. The same parameter is used in the present study for analysis of the data. Figure 4.50 shows the result of plotting the parameter C_s from Table 4.3 versus the density ratio for the three different pressures. From this graphical representation the following polynomial is derived from best fit to the data:

$$C_s = 9.9917 \cdot 10^{-4}\left(\frac{\rho_G}{\rho_L - \rho_G}\right)^2 - 4.558 \cdot 10^{-5}\left(\frac{\rho_G}{\rho_L - \rho_G}\right) + 7 \cdot 10^{-7} \tag{4.17}$$

A separate relationship between the interfacial roughness k_R and the interfacial fluctuations h_L' cannot be derived for the WASP facility due to lack of reliable measurements of key parameters such as pressure drop and wall shear stress. It is assumed that the relationship for k_R developed for the low pressure rig, equation (4.14), is also valid for WASP. This is believed to be justified as the measurements on the two flow facilities were done with the same test spool. To summarise the suggested route for calculating the interfacial friction factor f_i for the WASP experiments is as follows:

$$f_i = 2\left(\frac{u^*}{u_G}\right)^2 \tag{2.14}$$

$$\frac{u_G}{u^*} = 5.75\log_{10}\left(\frac{R_G}{k_R}\right) + 4.73 \tag{2.15}$$

$$R_G = \frac{2S_G}{P_i + P_G} \tag{2.16}$$

$$k_R = D \cdot 0.9929 \left(\frac{h_L'}{D} \right)^{0.6273} \tag{4.14}$$

$$\frac{h_L'}{D} = C_s \left(\varepsilon_L \, \mathrm{Re}_G^{-} \right) \tag{4.15}$$

$$C_s = 9.9917 \cdot 10^{-4} \left(\frac{\rho_G}{\rho_L - \rho_G} \right)^2 - 4.558 \cdot 10^{-5} \left(\frac{\rho_G}{\rho_L - \rho_G} \right) + 7 \cdot 10^{-7} \tag{4.17}$$

The PRESBAL code (see Section 2.4.2) was modified to validate this new model for f_i against the experiments on the WASP rig. The model equations from above for the calculation of f_i were implemented in PRESBAL. For the gas wall friction factor and the liquid wall friction factor, the models were used which were evaluated in Section 4.7 to give the best predictions of the measured data from the low pressure rig. The models used were that by Eck (1973) (equation (2.38)) for f_G and that by Spedding & Hand (1997) (equation (2.42) for the turbulent case) for f_L. The set of momentum equations (2.4) and (2.5) was kept unchanged as, unlike on the low pressure rig, there was no significant hydraulic gradient in the WASP runs. The comparisons of code predictions with experimental data are shown in Figure 4.51 for the liquid holdup. The PRESBAL predictions for liquid holdup with this new set of relationships for WASP are consistent with the predictions obtained with the standard set of relationships described in Section 2.4.2 (Figure 4.26).

4.10 Conclusions

The main conclusions drawn from the analysis of steady state experimental data are as follows:

- Steady state data on detailed local parameters were obtained with the instrumentation described in Chapter 3 in gas-liquid two-phase stratified flow on two experimental flow facilities, a low pressure rig and the WASP rig. On the low pressure rig reliable data were obtained at atmospheric pressure for the pressure gradient in the gas phase, the liquid holdup and the interfacial structure, the velocities and the wall shear stresses in the gas and the liquid phases. On the WASP rig, where measurements were performed at a range of pressures (1, 6 and 11 bar) the reliable data included liquid holdup and the interfacial structure, the gas and liquid velocities in both phases.

- Data on mean and fluctuating velocities in the gas and liquid phases collected on the low pressure rig were compared with published data by Strand (1993). The experimental data from this study showed good qualitative agreement with Strand's data.
- The measurements of pressure gradient on the low pressure rig were analysed. As expected the measured pressure gradient increased with the gas and liquid flow rates. The measurements were compared with predictions from the one-dimensional steady state solver PRESBAL. The code under-predicted the measurements by 20 % on average.
- Measurements of liquid holdup/mean liquid height from the low pressure rig and the WASP rig were compared with predictions from a number of one-dimensional computer codes: PRESBAL and the commercial codes PLAC, OLGA and TACITE. The codes underpredicted the data from the low pressure rig by 15 %. The predictions for the WASP rig were lower than the experiment by 30 %. The predictions from the various codes were also different between themselves: for a given experiment the predictions differed by 20 %. The data from WASP was additionally compared with predictions from TRIOMPH. The agreement of TRIOMPH with the experiment was better than with any of the other codes because the experimental data for holdup was used as input in TRIOMPH.
- Measurements of liquid height at different positions along the test section were used to investigate if hydraulic gradients existed in the experiments. On the low pressure rig a small hydraulic gradient was established and modified momentum equations were derived to properly account for the influence of the hydraulic gradient in both phases. On the WASP rig no significant hydraulic gradient was established.
- Gas and liquid wall shear stresses were measured at the top and the bottom of the test spool on the low pressure rig. In initial tests the variation of the wall shear stresses with position around the pipe circumference was found to be moderate and the values of the shear stresses measured at top and bottom of the test spool were taken to represent the phase average values. The shear stress data were interpreted in terms of friction factors f_G and f_L and compared with published models. The best agreement of the data in the gas phase was found with the

models by Eck (1973) and with the model by Espedal (1998). The data in the liquid phase was best predicted by the model by Spedding & Hand (1997).

- Data for interfacial shear stress was derived from measurements in the gas phase on the low pressure rig. The data was interpreted in terms of the interfacial friction factor f_i and compared with different models published in the literature. The best agreement of the data was found with predictions from the Spedding & Hand (1997) model.

- Information on the interfacial structure was derived from measurements with the array of conductivity probes in the test spool on the low pressure rig and the WASP rig. The qualitative discussion of the data was based on a comparison of two similar experiments from the two flow facilities and on a comparison of two experiments at different pressures on the WASP facility. The interfacial activity under similar conditions was greater on the low pressure rig than on the WASP rig. This was believed to result from the differences in the test sections on the two flow facilities. The comparison of the two runs at different pressures showed that increasing pressure attenuated interfacial activity.

- The information on interfacial structure from the two flow facilities was also quantitatively analysed. The analysis was based on data for the rms fluctuations of the liquid height, h_L'. The discussion of the data, following the route described in Srichai (1994), resulted in new models for the interfacial friction factor f_i for the two flow facilities. The experimental data were compared with predictions from PRESBAL, using the new models for f_i and the models for the wall friction factors which were found to best predict the measurements of wall shear stress on the low pressure rig (Eck (1973) for f_G and the model by Spedding & Hand (1997) for f_L). The comparisons showed about the same level of agreement between prediction and experiment as those where PRESBAL was operated with a standard set of closure relationships.

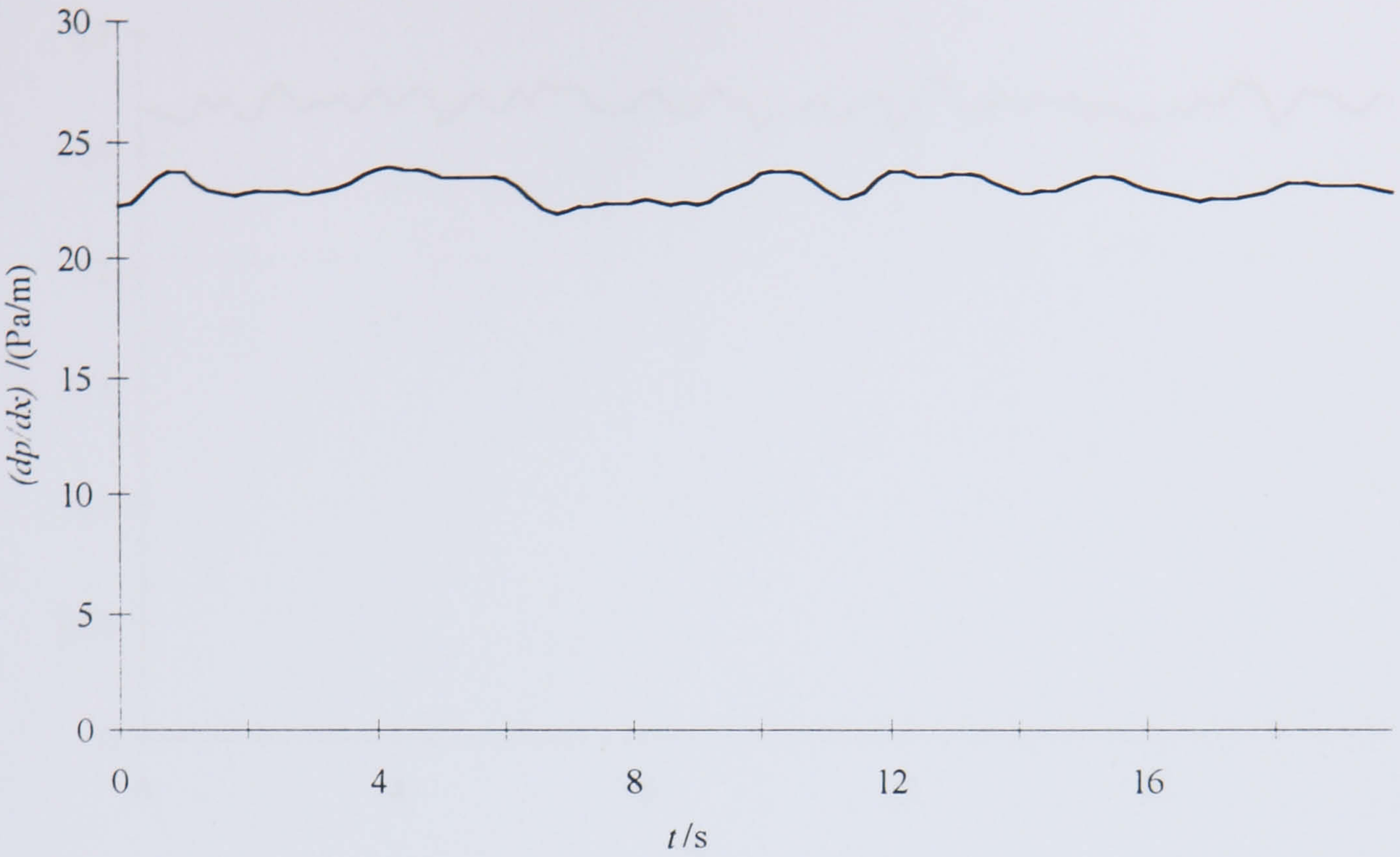


Figure 4.1 Measured pressure gradient *(dp/dx)* for initial steady state of transient case `1c` of the low pressure rig (U_L=0.039 m/s, U_G=7.39 m/s, atmospheric pressure)

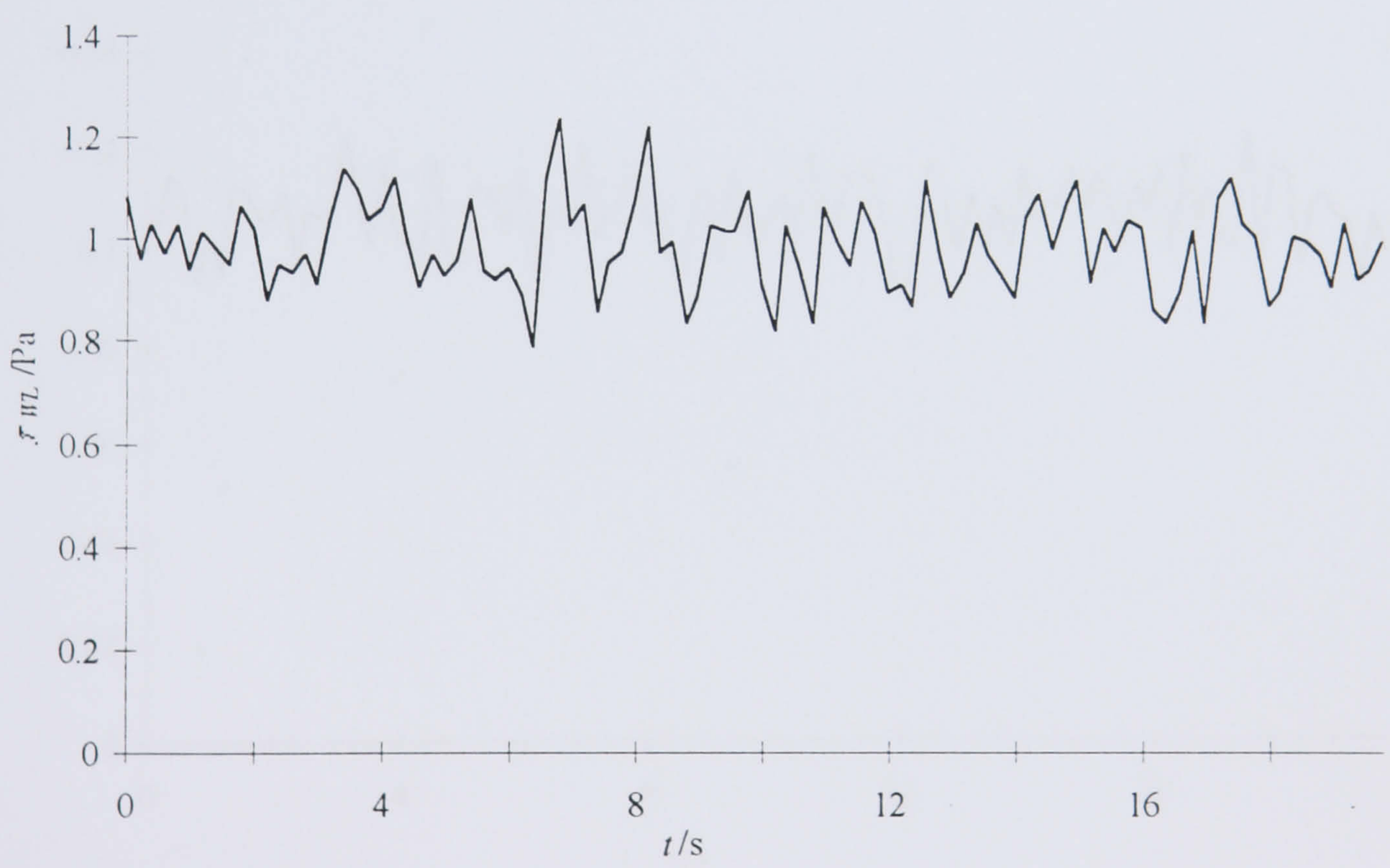


Figure 4.2 Measured liquid wall shear stress τ_{wL} for initial steady state of transient case `1c` of the low pressure rig (U_L=0.039 m/s, U_G=7.39 m/s, atmospheric pressure)

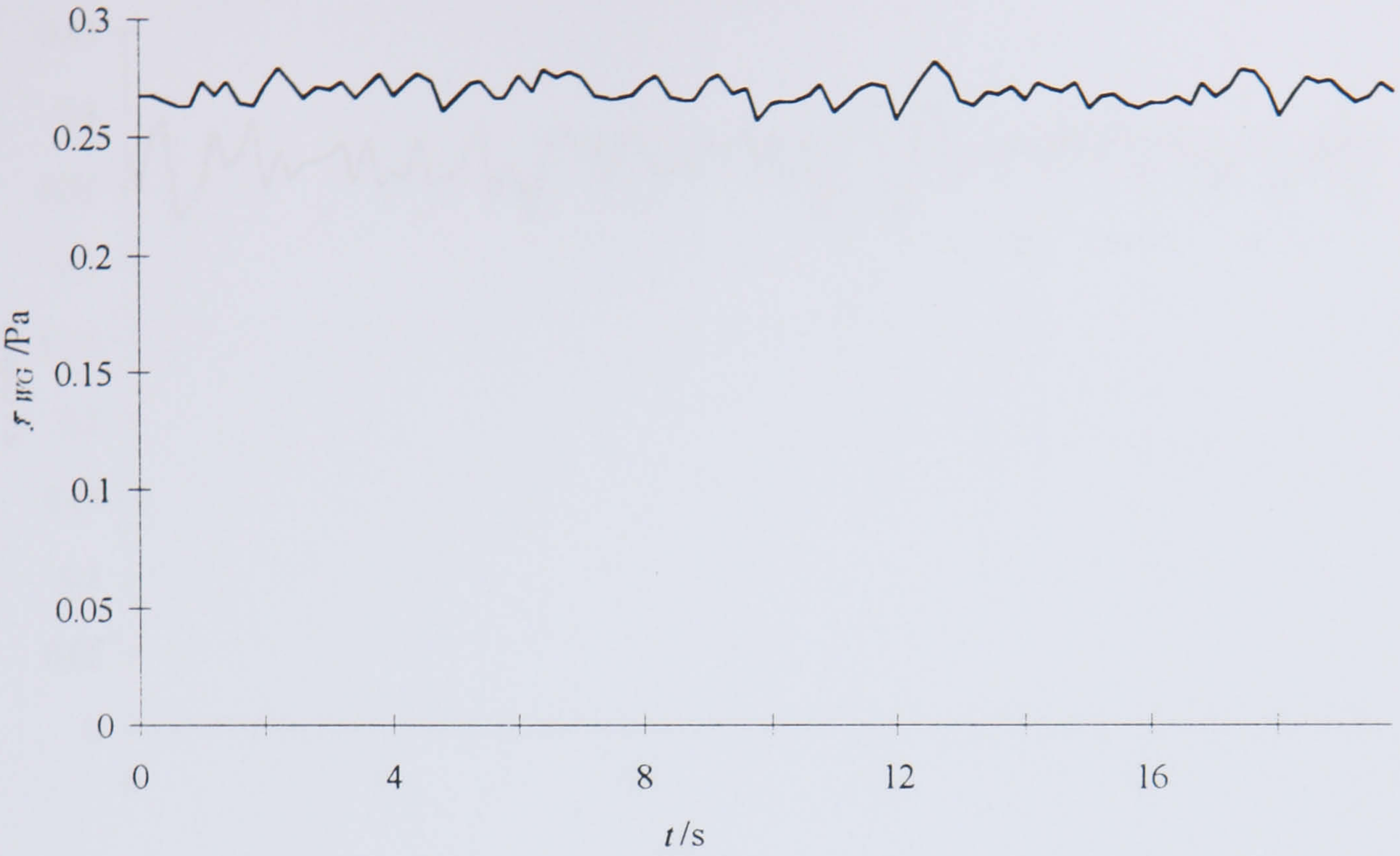


Figure 4.3 Measured gas wall shear stress τ_{WG} for initial steady state of transient case `1c` of the low pressure rig (U_L=0.039 m/s, U_G=7.39 m/s, atmospheric pressure)

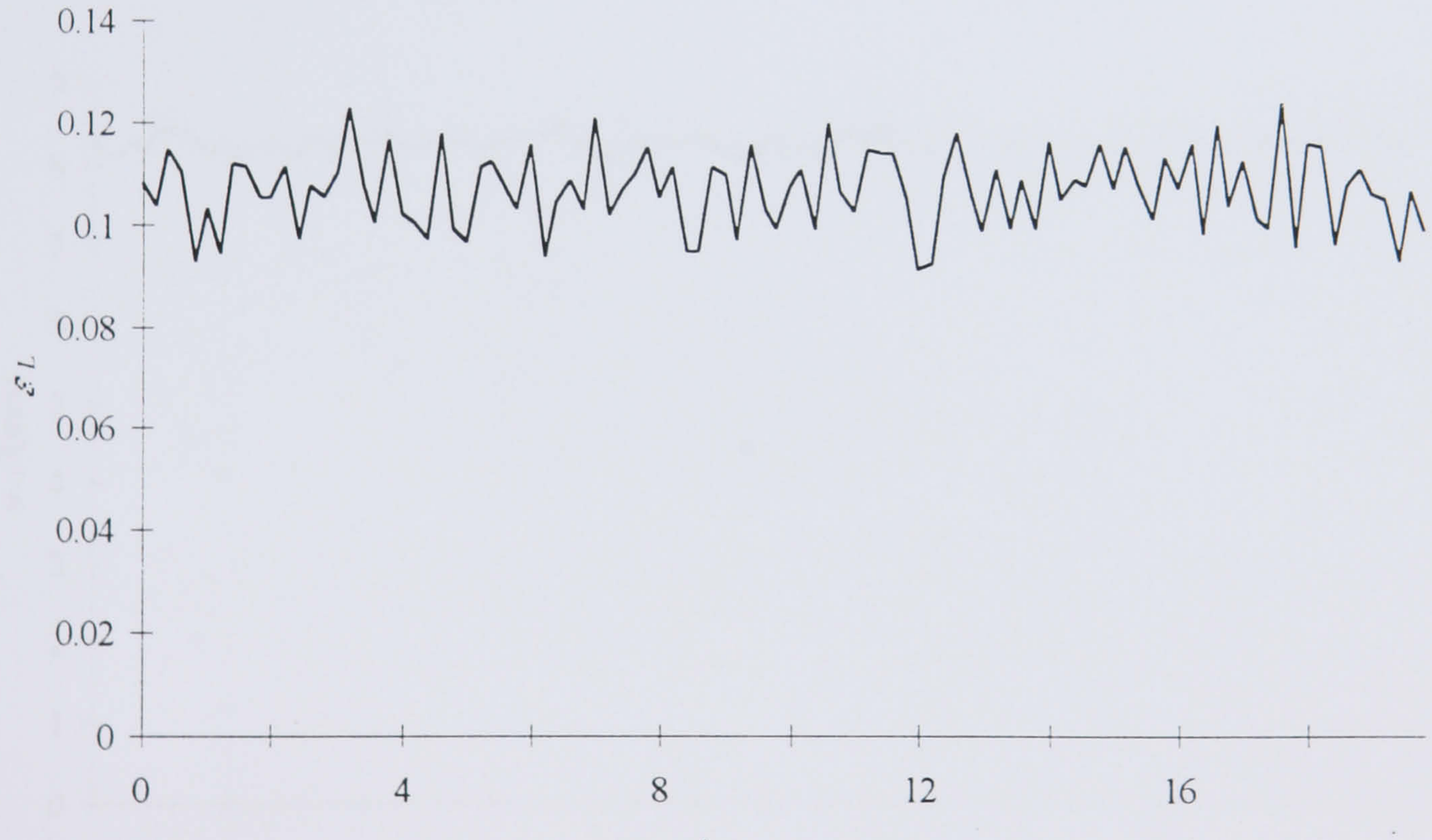


Figure 4.4 Measured liquid holdup ε_L for initial steady state of transient case `1c` of the low pressure rig (U_L=0.039 m/s, U_G=7.39 m/s, atmospheric pressure)

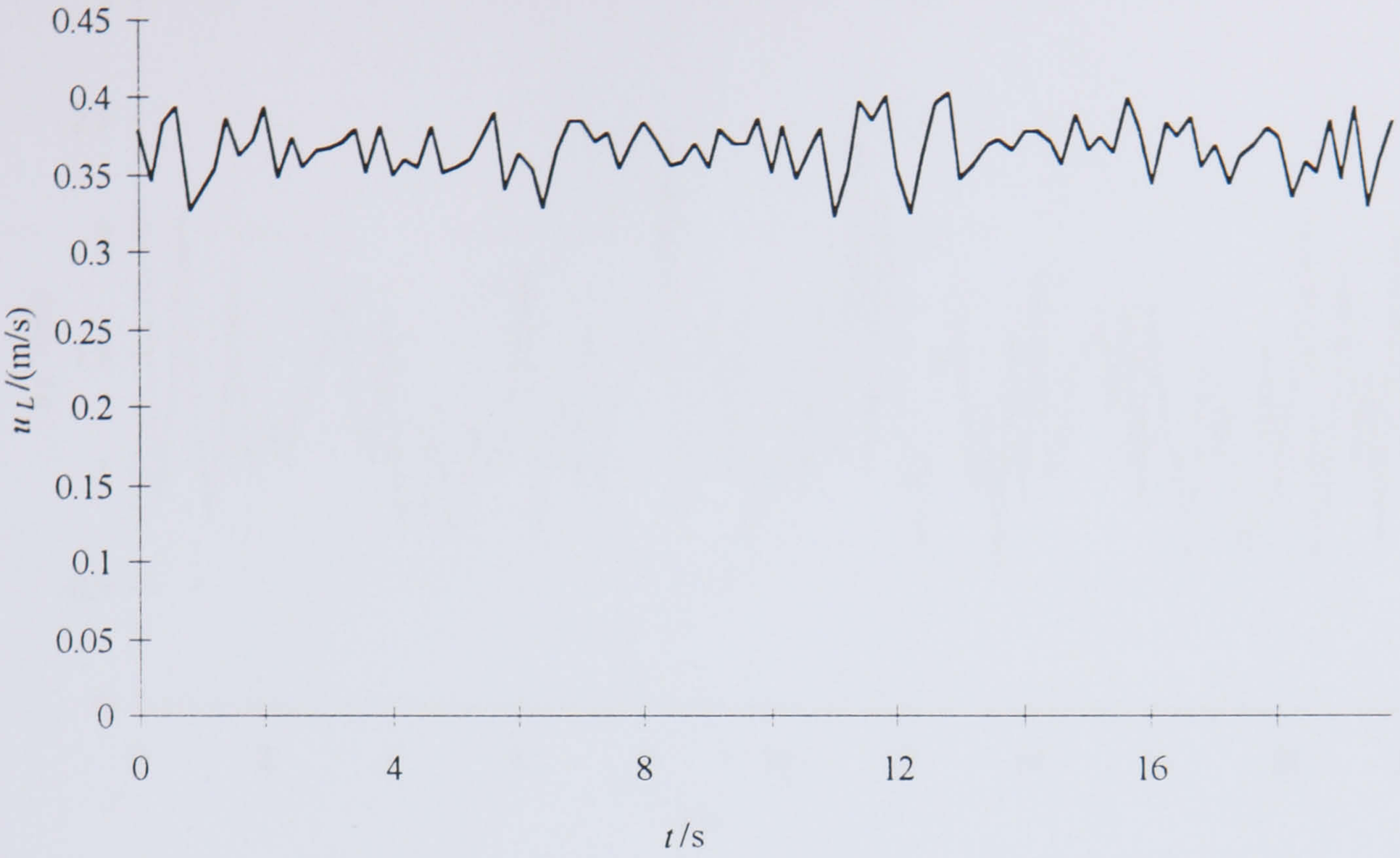


Figure 4.5 Measured liquid phase average velocity u_L for initial steady state of transient case `1c` of the low pressure rig (U_L=0.039 m/s, U_G=7.39 m/s, atmospheric pressure)

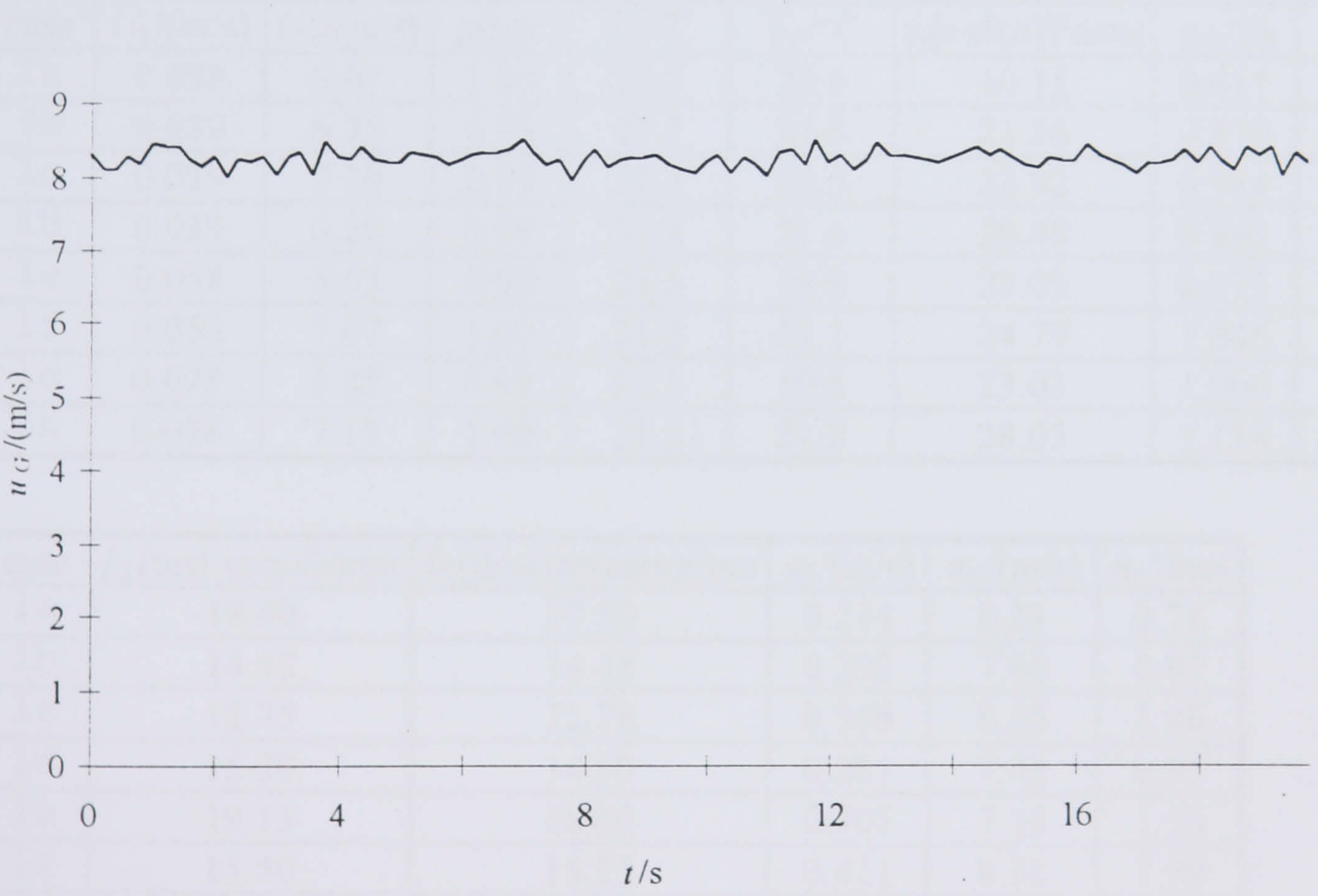


Figure 4.6 Measured gas phase average velocity u_G for initial steady state of transient case `1c` of the low pressure rig (U_L=0.039 m/s, U_G=7.39 m/s, atmospheric pressure)

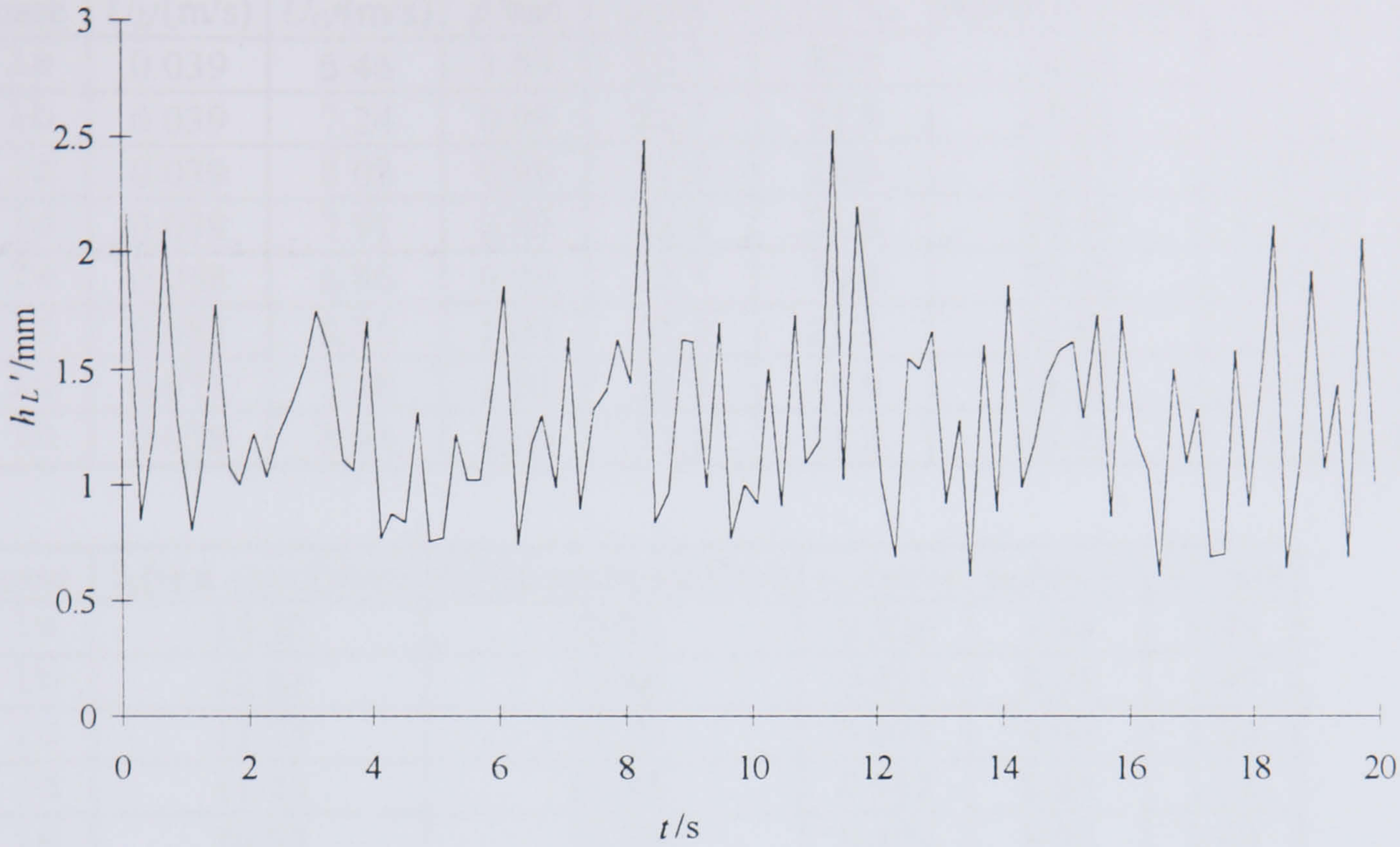


Figure 4.7 Interfacial fluctuation h_L' for initial steady state of transient case `1c` of the low pressure rig (U_L=0.039 m/s, U_G=7.39 m/s, atmospheric pressure)

case	U_L/(m/s)	U_G/(m/s)	p/bar	T_L/°C	T_G/°C	(dp/dx)/(Pa/m)	τ_{WL}/Pa	τ_{WG}/Pa
`1a`	0.039	5.01	1.00	22.7	22.6	10.15	0.411	0.124
`1b`	0.039	6.35	0.99	21.7	21.8	21.16	0.879	0.243
`1c`	0.039	7.39	0.99	21.5	22.0	22.92	0.984	0.268
`1d`	0.039	6.20	0.99	21.4	21.6	20.48	0.845	0.235
`1e`	0.058	5.63	0.99	21.5	19.8	23.05	0.973	0.221
`1f`	0.058	7.07	1.00	21.2	21.1	24.79	1.045	0.270
`1g`	0.078	5.42	0.99	21.5	19.6	23.03	1.006	0.175
`1h`	0.078	7.15	1.00	21.2	21.2	28.65	1.134	0.325

case	h_L(test spool)/mm	h_L(downstream)/mm	u_L/(m/s)	u_G/(m/s)	h_L'/mm
`1a`	18.60	17.50	0.214	6.21	0.78
`1b`	14.92	14.48	0.292	7.62	0.97
`1c`	12.75	12.78	0.366	8.25	1.46
`1d`	15.30	14.50	0.281	7.43	0.95
`1e`	19.13	18.00	0.305	7.15	1.56
`1f`	15.50	15.25	0.411	8.31	1.99
`1g`	22.32	20.60	0.330	7.04	2.30
`1h`	16.97	16.75	0.488	8.65	2.33

Table 4.4 Results of measured parameters for initial steady states of transient experiments on the low pressure rig

case	U_L/(m/s)	U_G/(m/s)	p/bar	T_L/°C	T_G/°C	(dp/dx)/(Pa/m)	τ_{WL}/Pa	τ_{WG}/Pa
la	0.039	6.46	1.00	22.7	22.6	22.33	1.161	0.180
lb	0.039	7.24	0.99	21.7	21.8	22.43	1.322	0.287
lc	0.039	8.08	0.99	21.5	22.0	26.57	1.333	0.314
ld	0.039	7.91	0.99	21.4	21.6	25.49	1.774	0.327
le	0.058	6.86	0.99	21.5	19.8	23.42	1.602	0.283
lf	0.058	8.75	1.00	21.2	21.1	35.64	1.644	0.380
lg	0.078	7.18	1.00	21.5	19.6	28.65	2.038	0.255
lh	0.078	8.94	1.00	21.2	21.2	42.22	1.597	0.457

case	h_L(test spool)/mm	h_L(downstream)/mm	u_L/(m/s)	u_G/(m/s)	h_L'/mm
la	15.30	15.71	0.320	7.48	1.45
lb	12.83	12.86	0.425	8.28	1.49
lc	11.77	11.79	0.433	9.03	1.20
ld	11.93	11.88	0.512	8.85	1.31
le	16.23	15.69	0.459	8.02	2.04
lf	12.88	12.91	0.577	10.00	1.64
lg	16.86	16.80	0.562	8.37	2.51
lh	14.72	14.19	0.616	10.36	2.06

Table 4.5 Results of measured parameters for final steady states of transient experiments on the low pressure rig

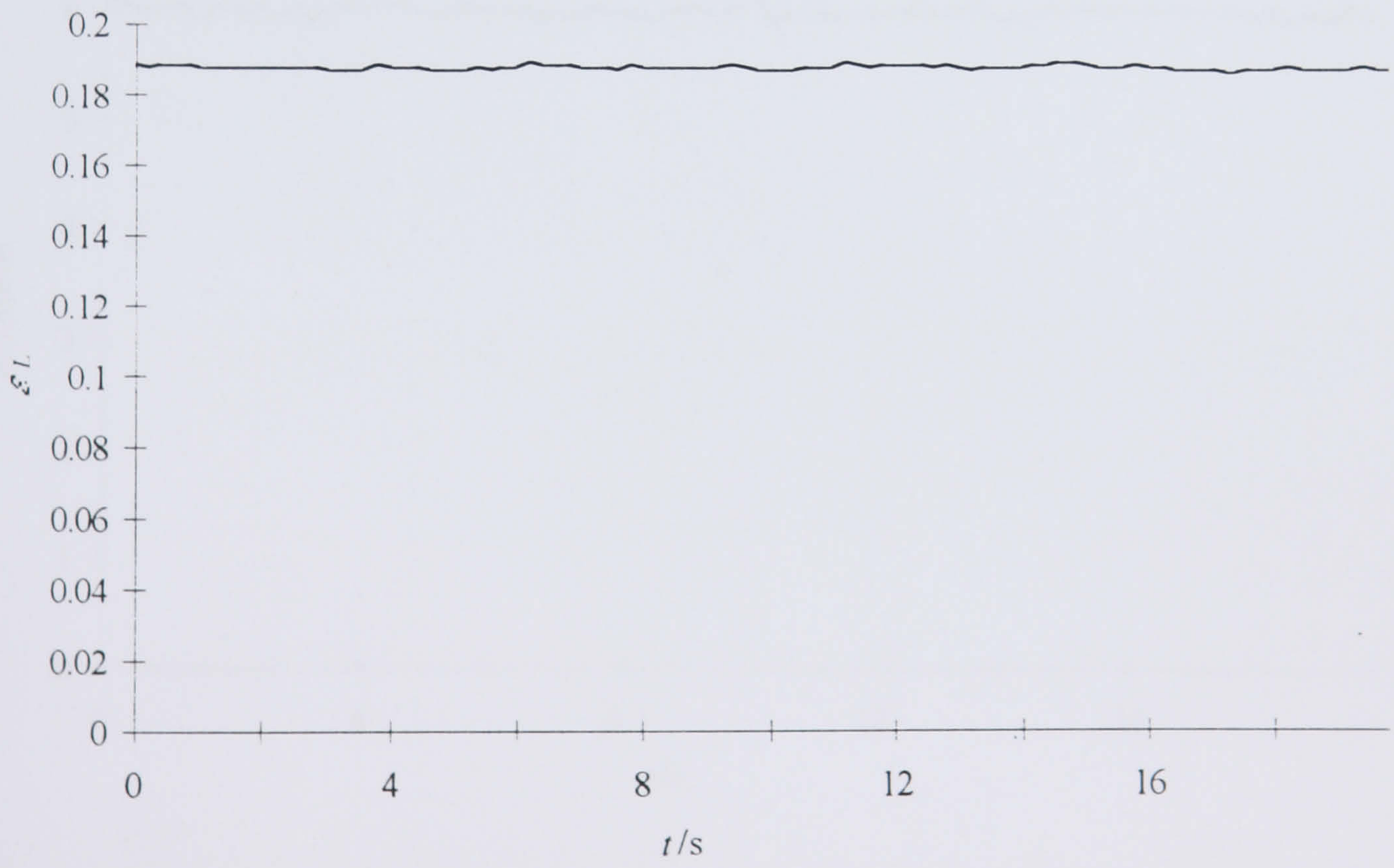


Figure 4.8 Measured liquid holdup ε_L for initial steady state of transient case wb of the WASP rig (U_L=0.038 m/s, U_G=5.33 m/s, atmospheric pressure)

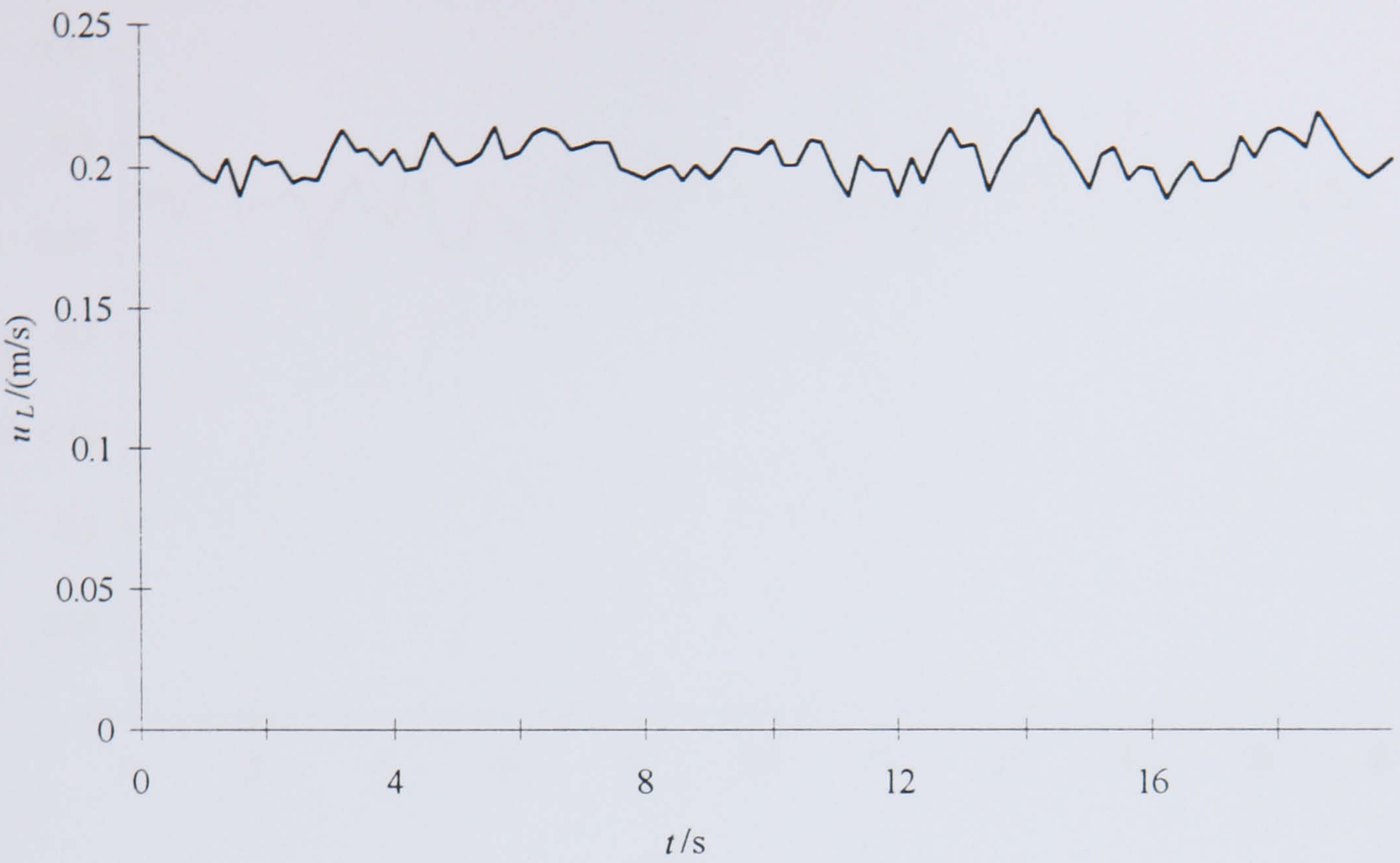


Figure 4.9 Measured liquid phase average velocity u_L for initial steady state of transient case wb of the WASP rig (U_L=0.038 m/s, U_G=5.33 m/s, atmospheric pressure)

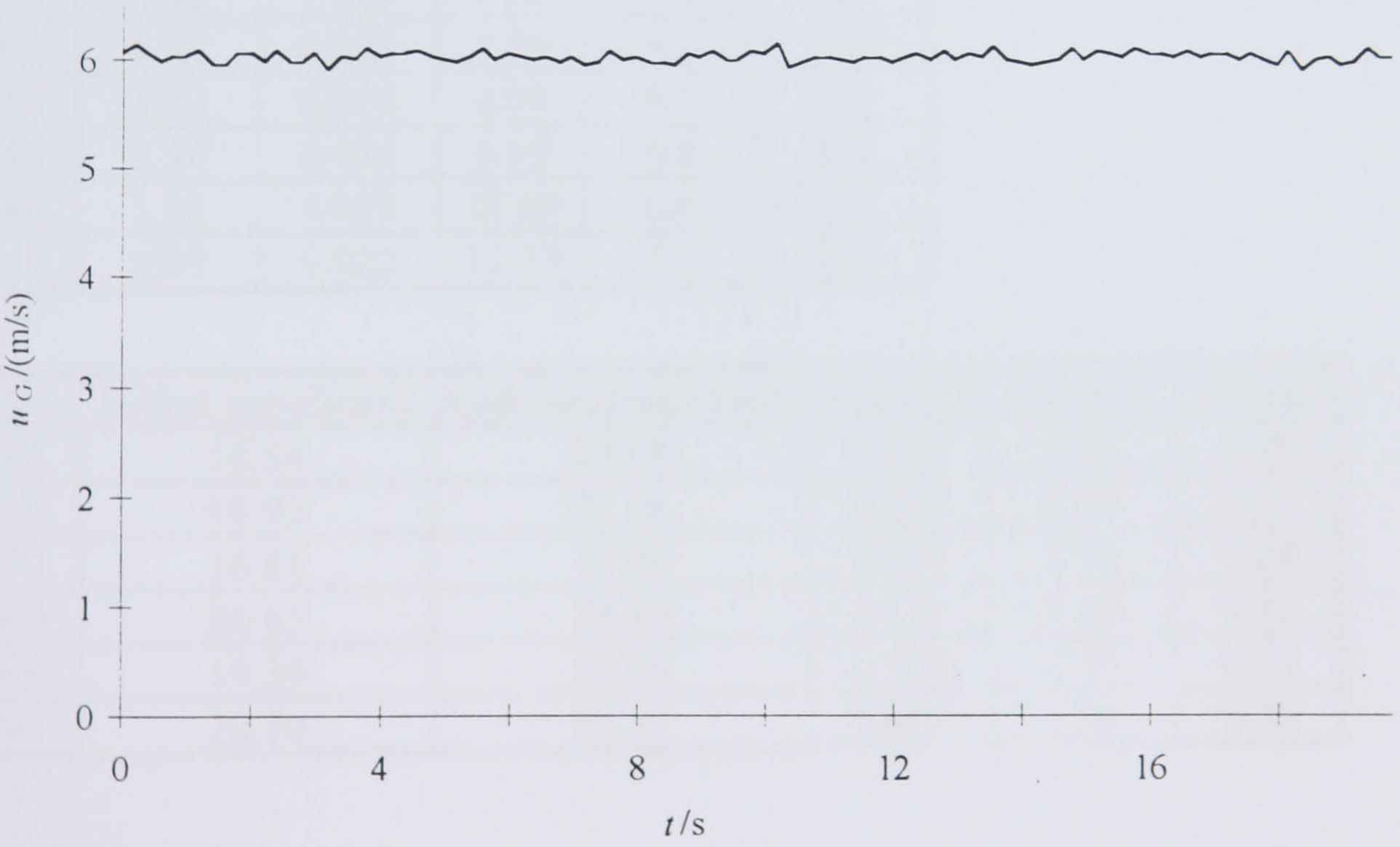


Figure 4.10 Measured gas phase average velocity u_G for initial steady state of transient case wb of the WASP rig (U_L=0.038 m/s, U_G=5.33 m/s, atmospheric pressure)

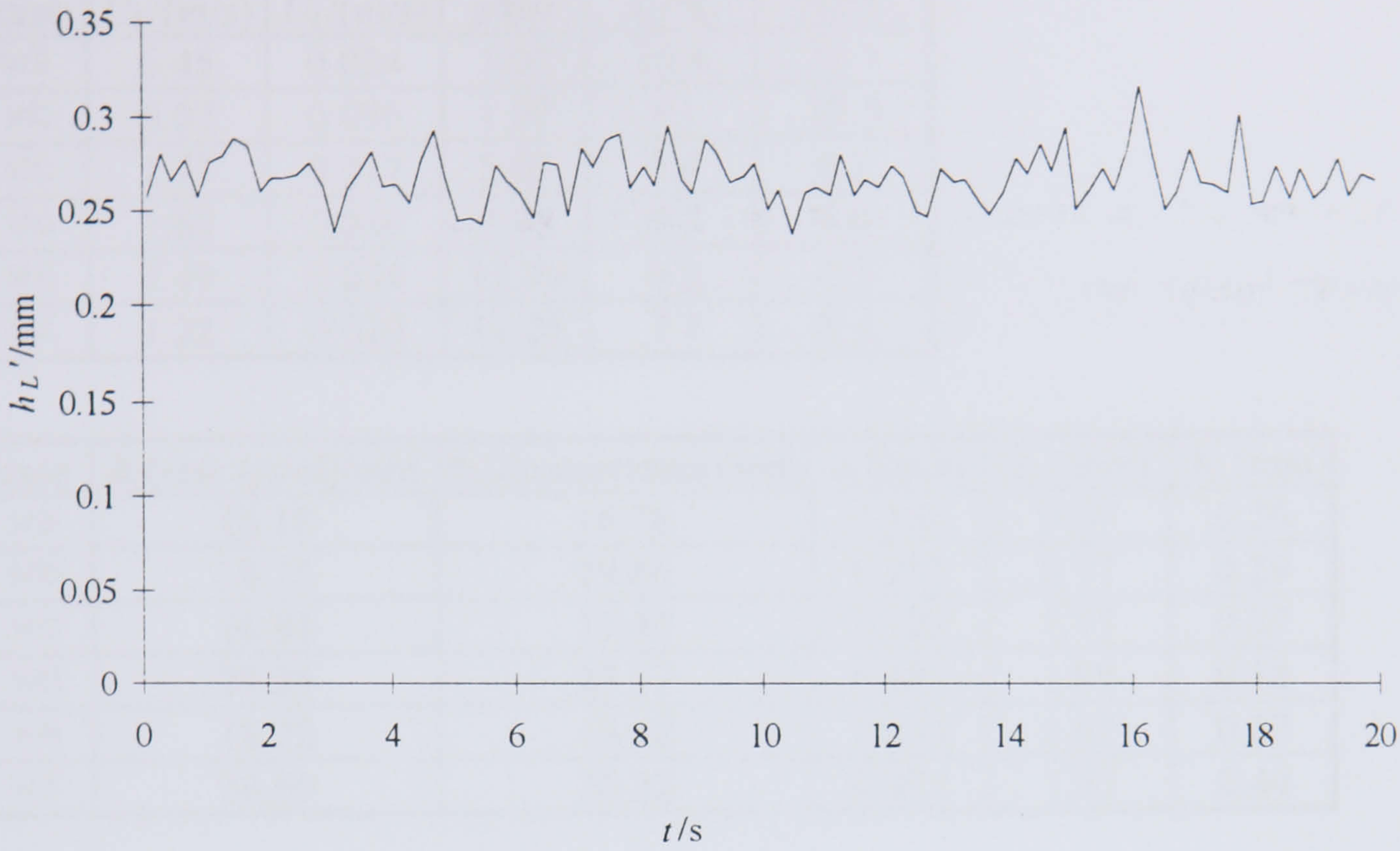


Figure 4.11 Interfacial fluctuation h_L' for initial steady state of transient case wb of the WASP rig (U_L=0.038 m/s, U_G=5.33 m/s, atmospheric pressure)

case	U_G/(m/s)	U_L/(m/s)	p/bar	T_L/°C	T_G/°C
wa	5.68	0.023	1.07	10.5	11.7
wb	5.33	0.038	1.06	9.1	10.8
wc	1.50	0.016	6.01	5.3	6.3
wd	1.30	0.034	6.07	6.8	8.8
we	1.32	0.025	11.04	6.0	6.8
wf	0.97	0.022	11.37	7.7	8.9

case	h_L(test spool)/mm	h_L(downstream)/mm	u_L/(m/s)	u_G/(m/s)	h_L'/mm
wa	16.64	17.68	0.147	6.33	0.25
wb	18.93	21.68	0.202	6.02	0.27
wc	16.81	17.39	0.102	1.54	0.24
wd	26.65	28.80	0.113	1.67	0.42
we	19.34	19.78	0.130	1.55	0.28
wf	28.70	27.53	0.064	1.30	0.39

Table 4.6 Results of measured parameters for initial steady states of transient experiments on the WASP rig

case	U_G/(m/s)	U_L/(m/s)	p/bar	T_L/°C	T_G/°C
wa	6.45	0.024	1.07	10.4	11.5
wb	6.07	0.036	1.07	9.1	10.5
wc	1.77	0.017	6.03	5.4	6.3
wd	1.62	0.030	5.99	6.7	8.0
we	1.49	0.024	11.00	6.2	6.7
wf	1.22	0.020	11.25	7.7	8.4

case	h_L(test spool)/mm	h_L(downstream)/mm	u_L/(m/s)	u_G/(m/s)	h_L'/mm
wa	16.18	16.76	0.162	7.07	0.26
wb	18.75	19.86	0.213	6.77	0.29
wc	16.81	17.42	0.123	1.77	0.27
wd	25.25	27.37	0.121	1.95	0.38
we	18.72	19.52	0.134	1.67	0.27
wf	26.69	26.22	0.071	1.55	0.44

Table 4.7 Results of measured parameters for final steady states of transient experiments on the WASP rig

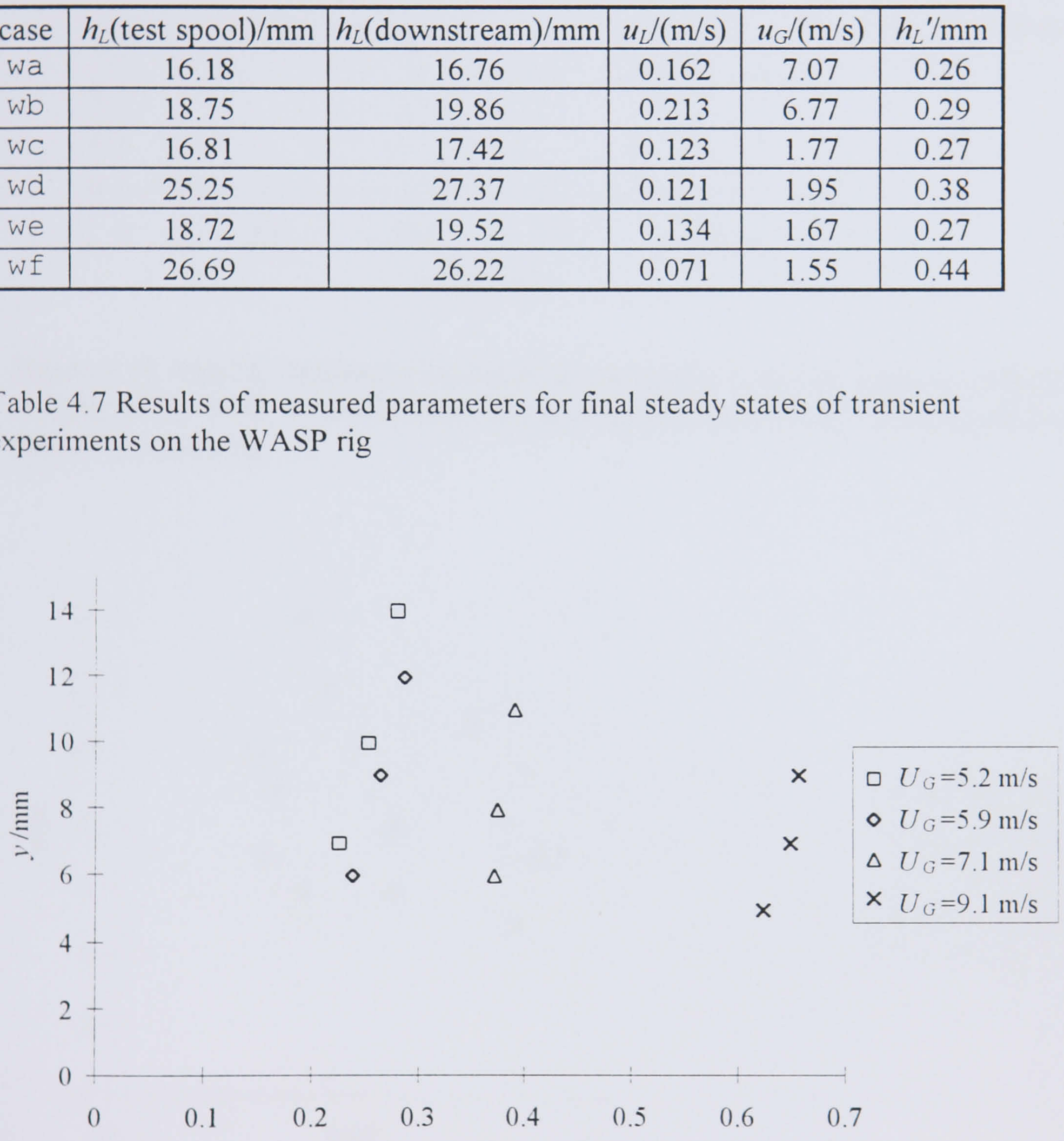


Figure 4.12 Velocity profiles in the liquid phase $u_L(y)$ for a given liquid superficial velocity of U_L=0.04 m/s and a range of gas superficial velocities U_G (see legend) on the low pressure rig

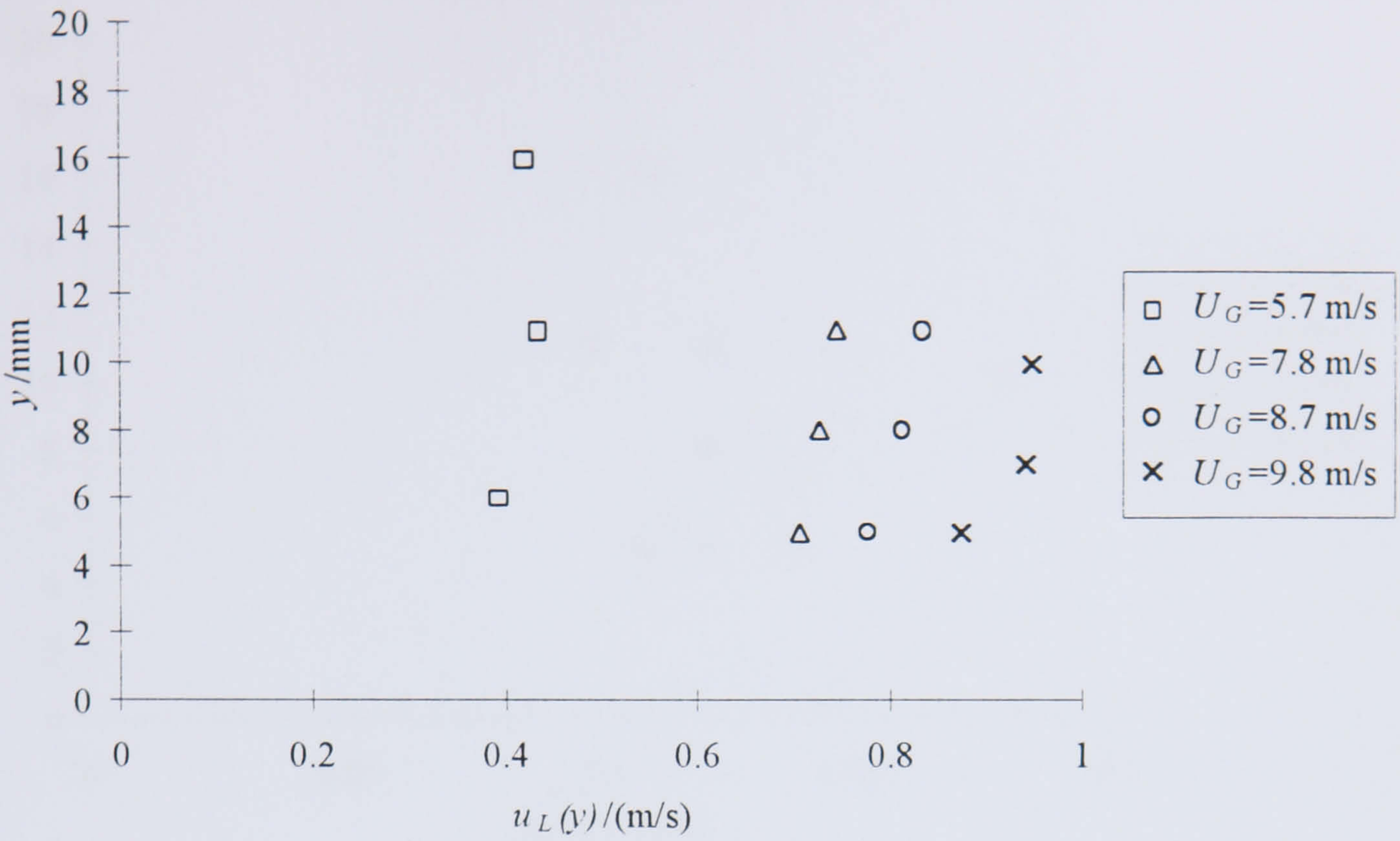


Figure 4.13 Velocity profiles in the liquid phase $u_L(y)$ for a given liquid superficial velocity of U_L=0.08 m/s and a range of gas superficial velocities U_G (see legend) on the low pressure rig

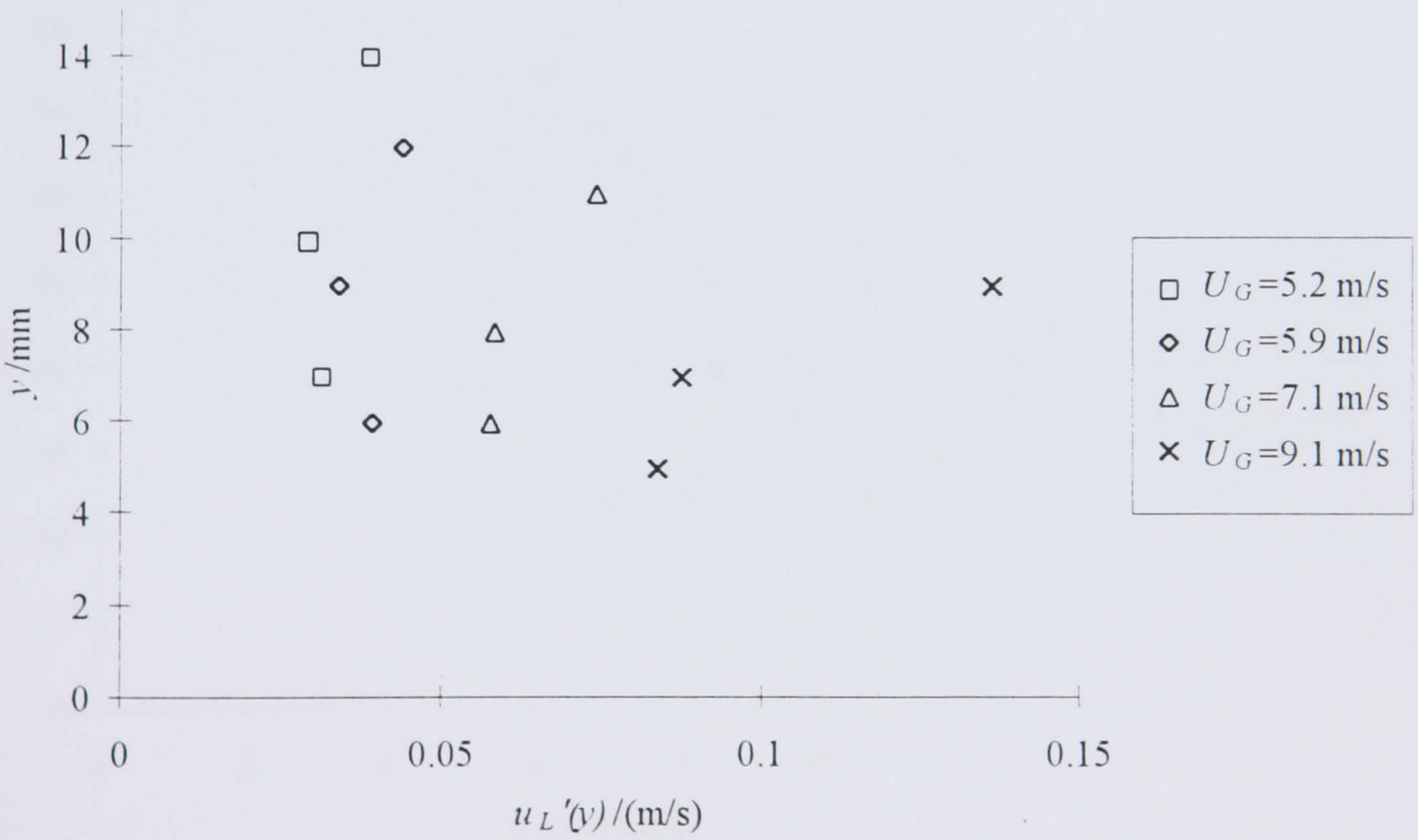


Figure 4.14 Profiles of fluctuations of liquid velocities $u_L'(y)$ for a given liquid superficial velocity of U_L=0.04 m/s and a range of gas superficial velocities U_G (see legend) on the low pressure rig

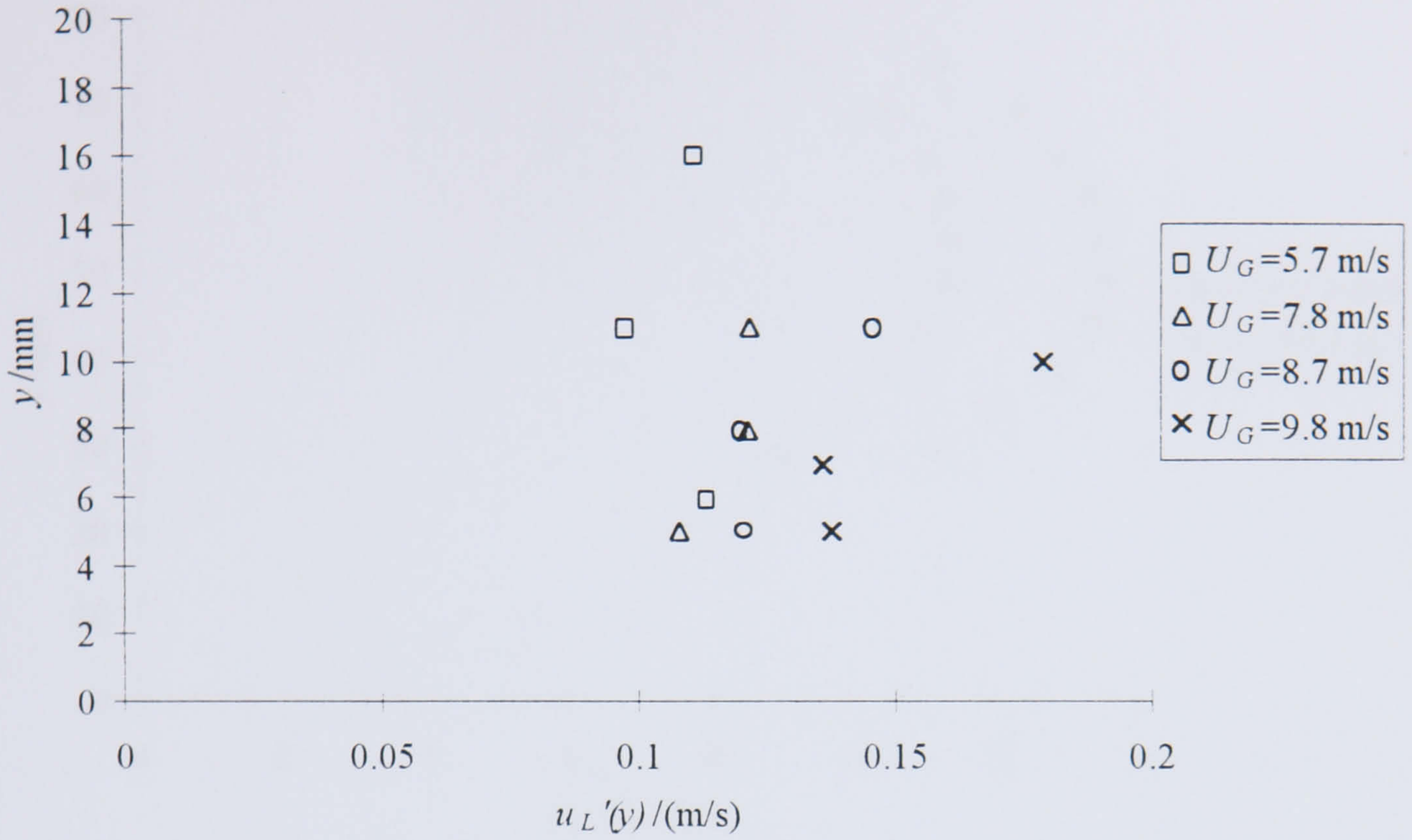


Figure 4.15 Profiles of fluctuations of liquid velocities $u_L'(y)$ for a given liquid superficial velocity of U_L=0.08 m/s and a range of gas superficial velocities U_G (see legend) on the low pressure rig

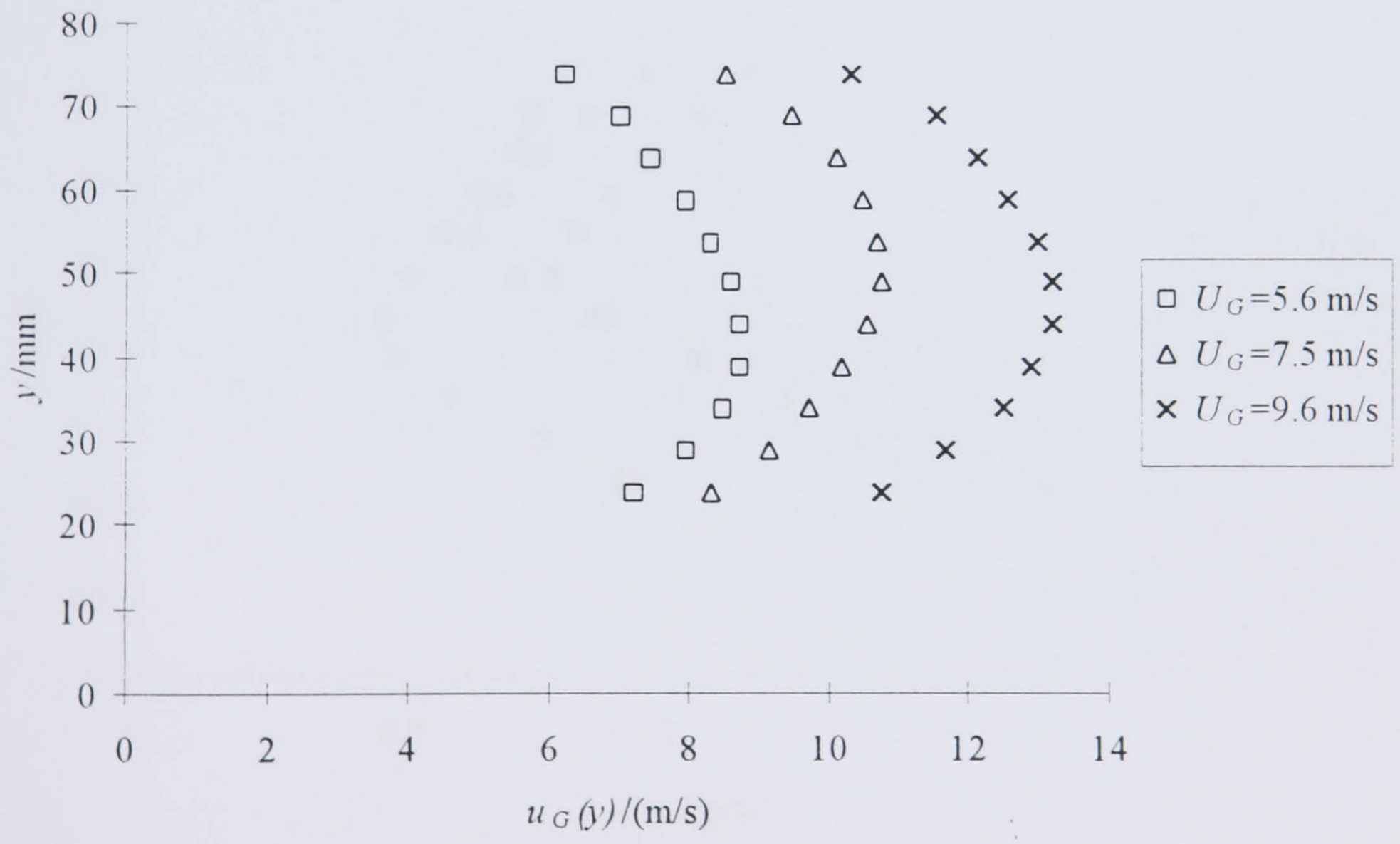


Figure 4.16 Velocity profiles in the gas phase $u_G(y)$ for a given liquid superficial velocity of U_L=0.04 m/s and a range of gas superficial velocities U_G (see legend) on the low pressure rig

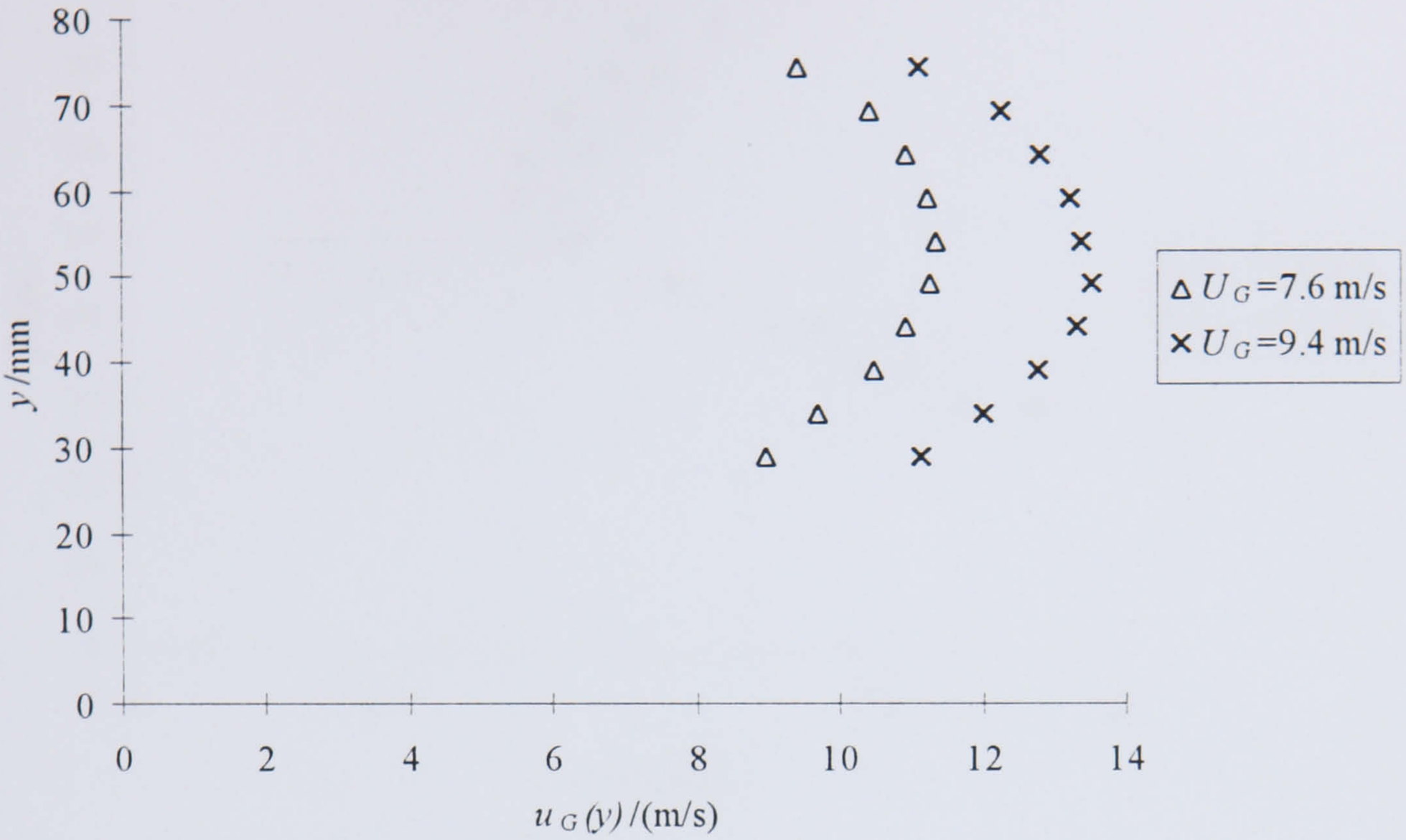


Figure 4.17 Velocity profiles in the gas phase $u_G(y)$ for a given liquid superficial velocity of U_L=0.08 m/s and a range of gas superficial velocities U_G (see legend) on the low pressure rig

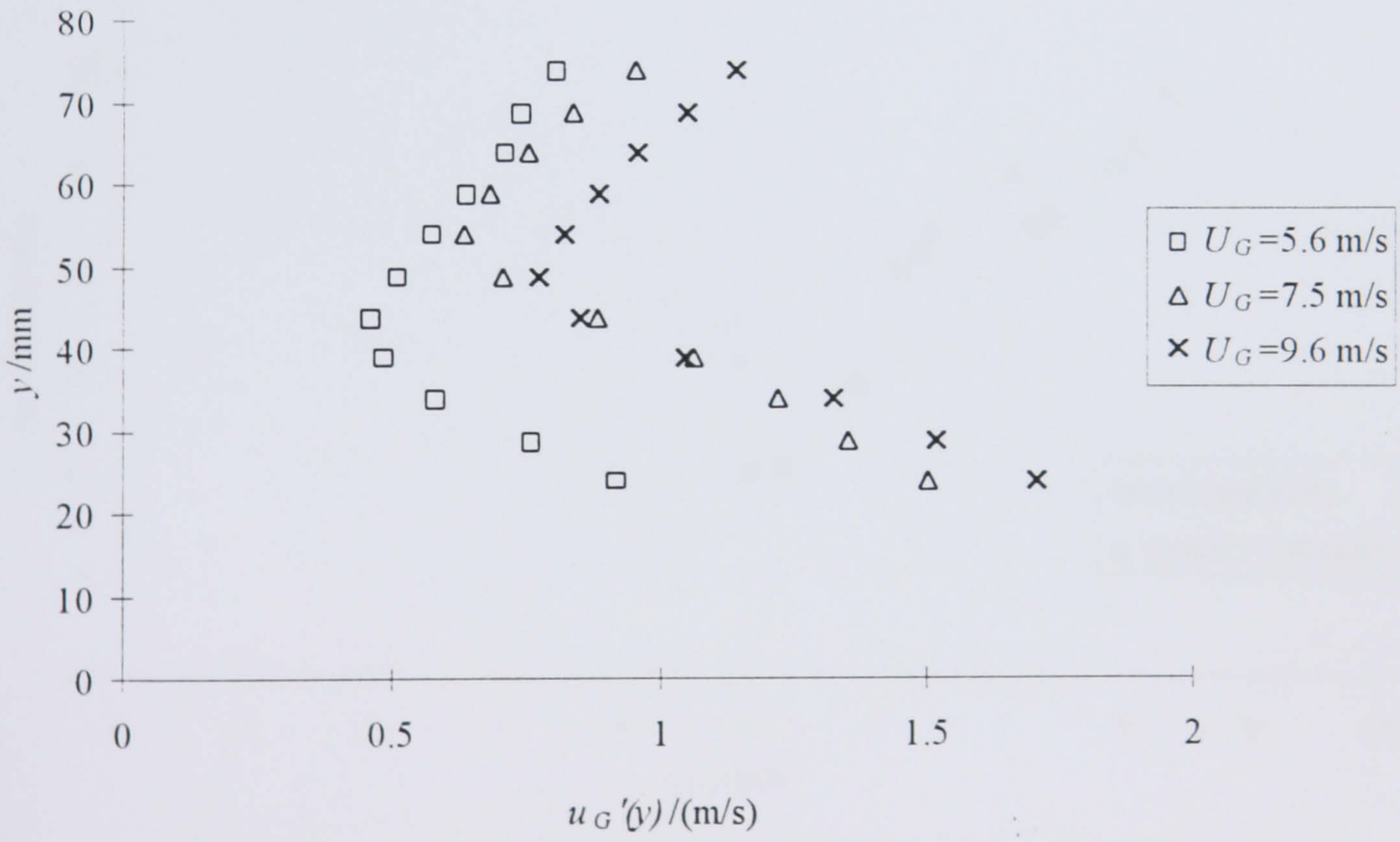


Figure 4.18 Profiles of fluctuations of gas velocities $u_G'(y)$ for a given liquid superficial velocity of U_L=0.04 m/s and a range of gas superficial velocities U_G (see legend) on the low pressure rig

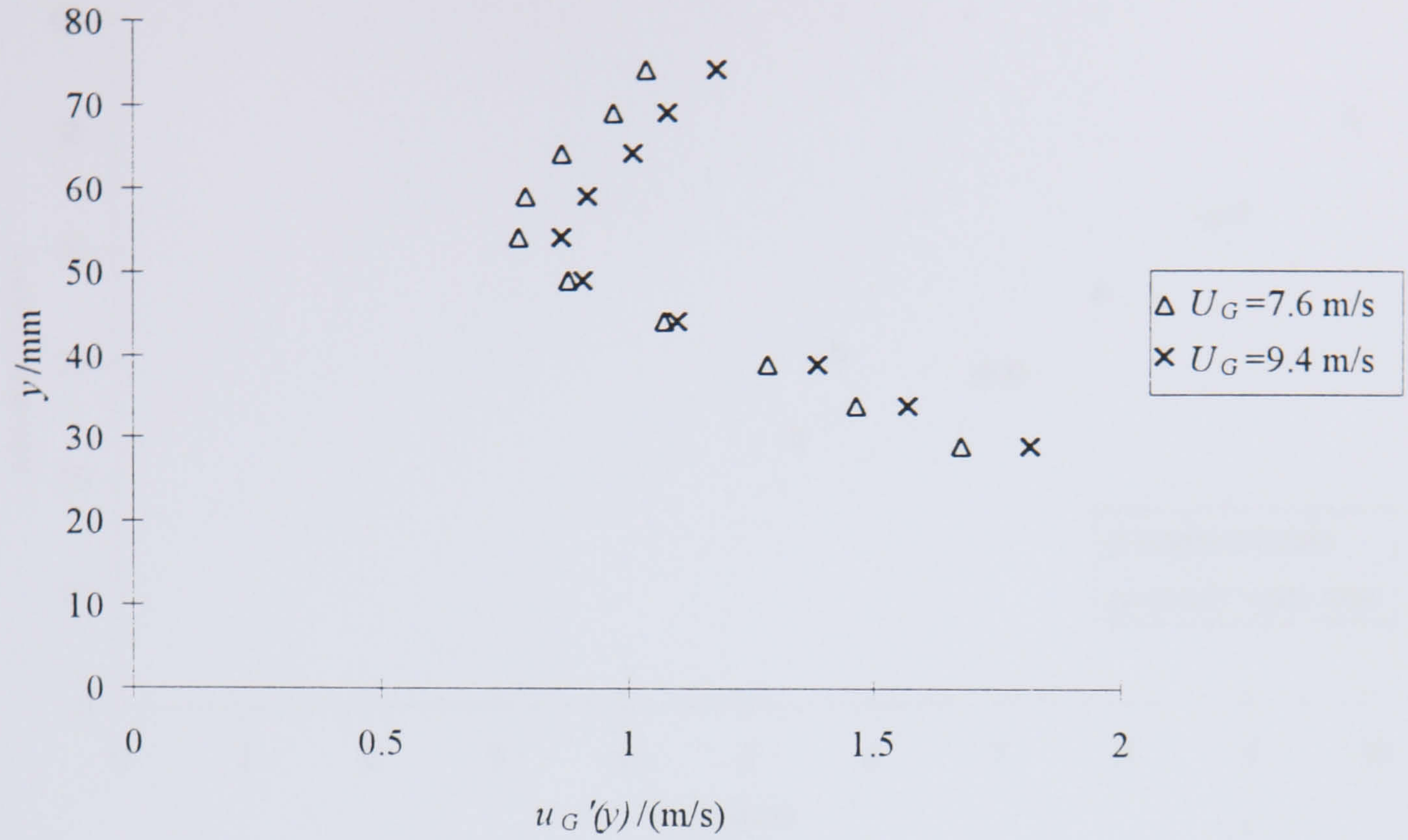


Figure 4.19 Profiles of fluctuations of gas velocities $u_G'(y)$ for a given liquid superficial velocity of U_L=0.08 m/s and a range of gas superficial velocities U_G (see legend) on the low pressure rig

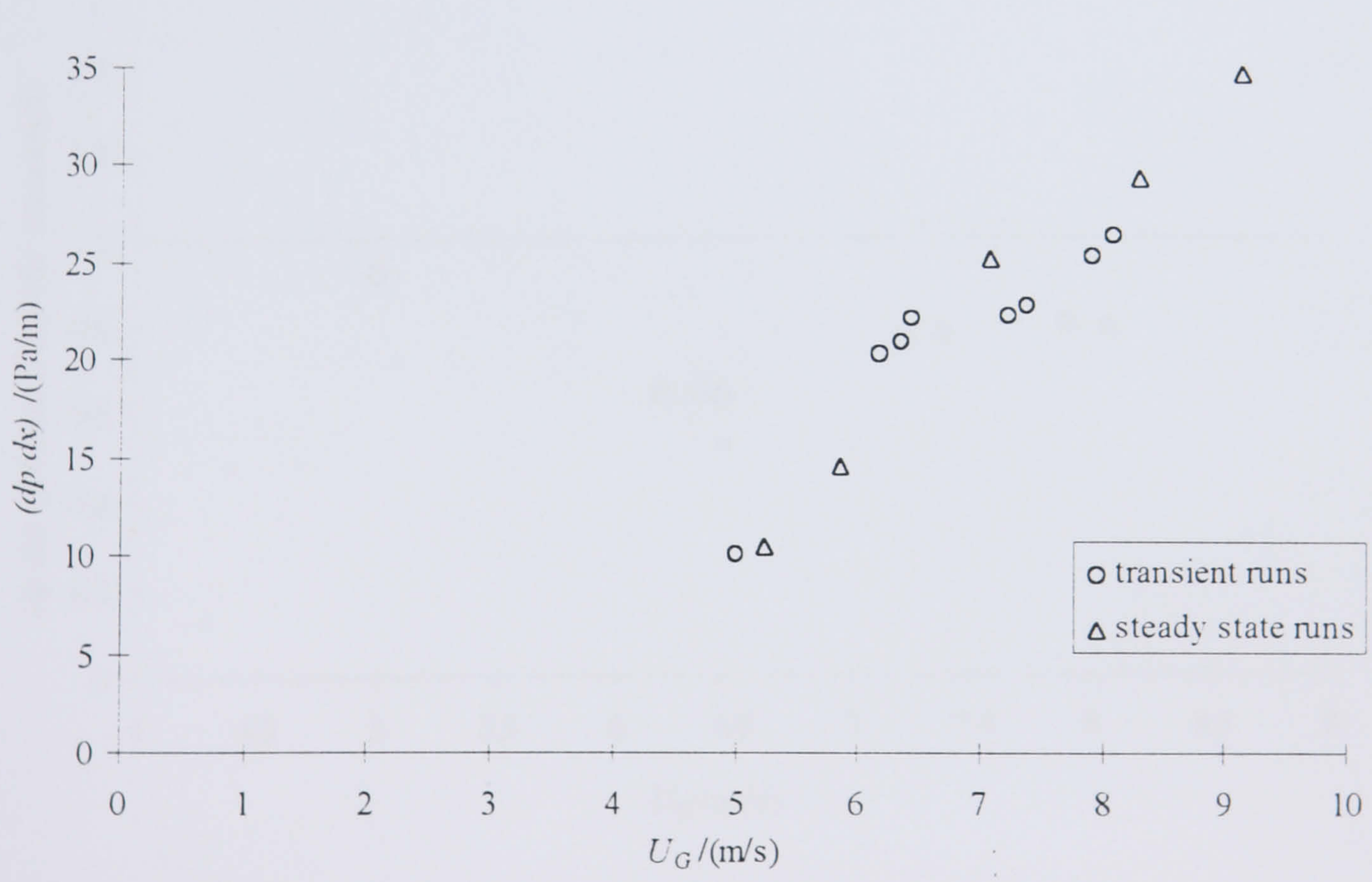


Figure 4.20 Pressure drop *(dp/dx)* as a function of gas superficial velocity for a given liquid superficial velocity of U_L =0.04 m/s on the low pressure rig

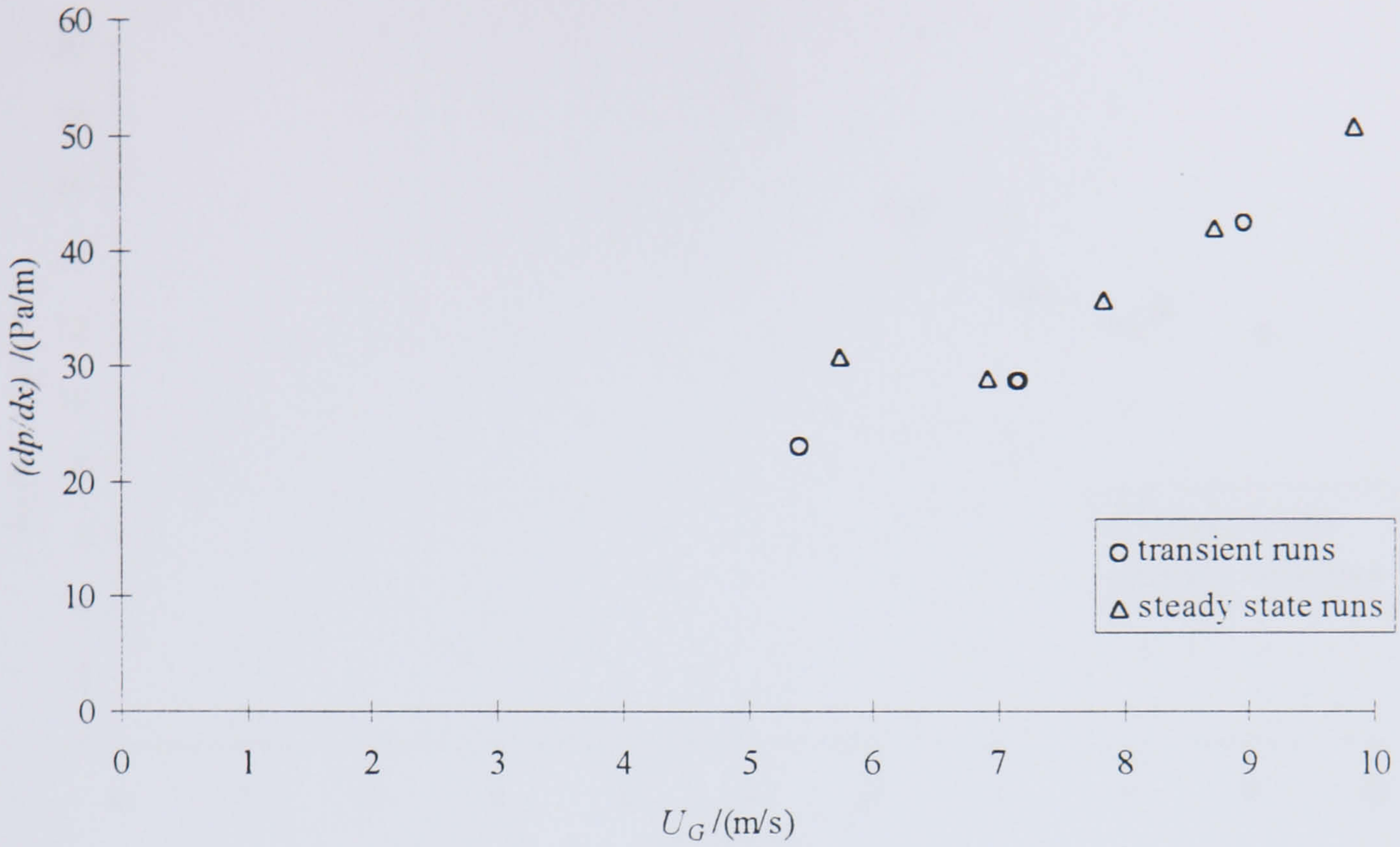


Figure 4.21 Pressure drop *(dp/dx)* as a function of gas superficial velocity for a given liquid superficial velocity of U_L =0.08 m/s on the low pressure rig

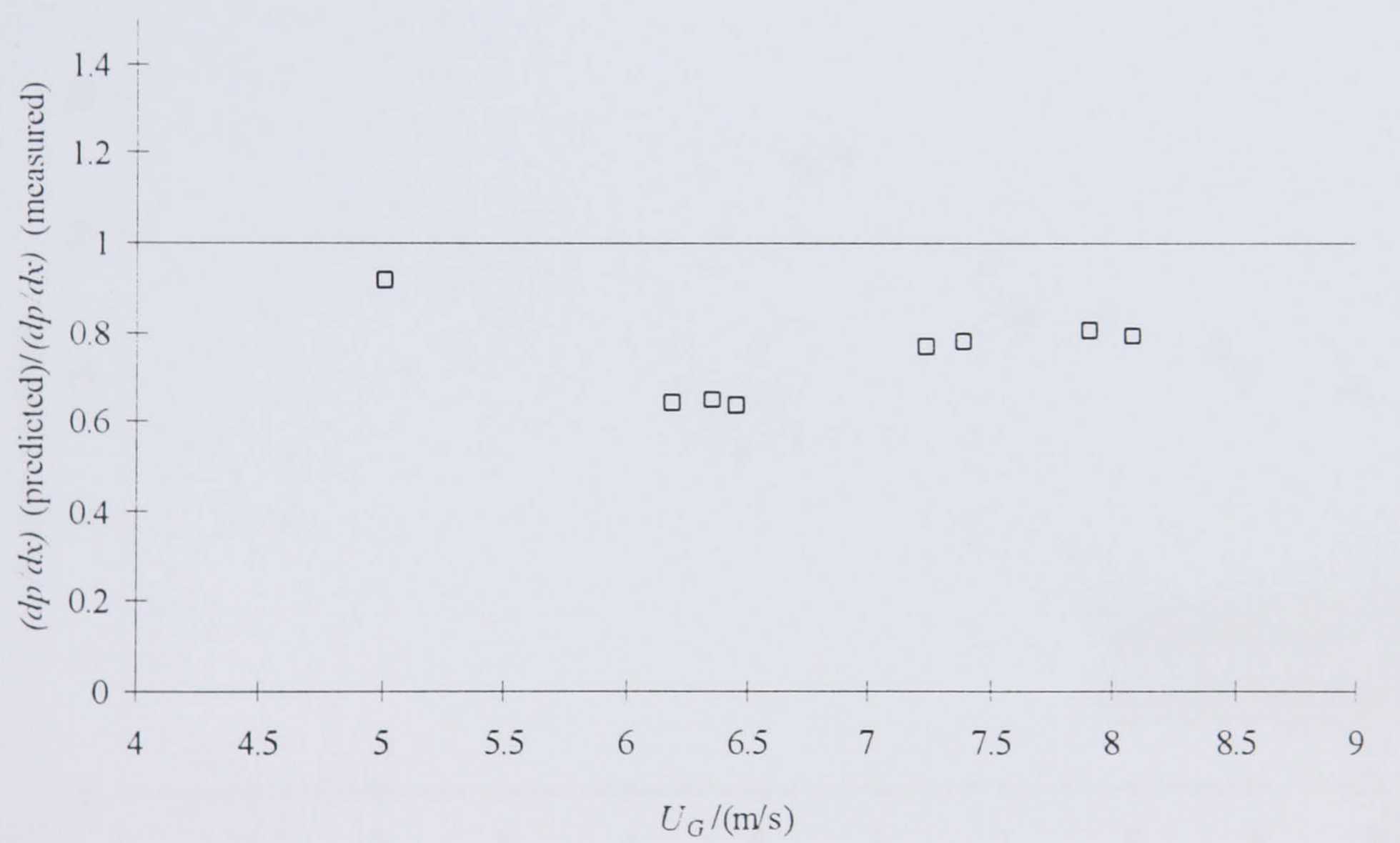


Figure 4.22 Comparison of pressure gradient calculated with PRESBAL with experimental data for U_L=0.04 m/s on the low pressure rig

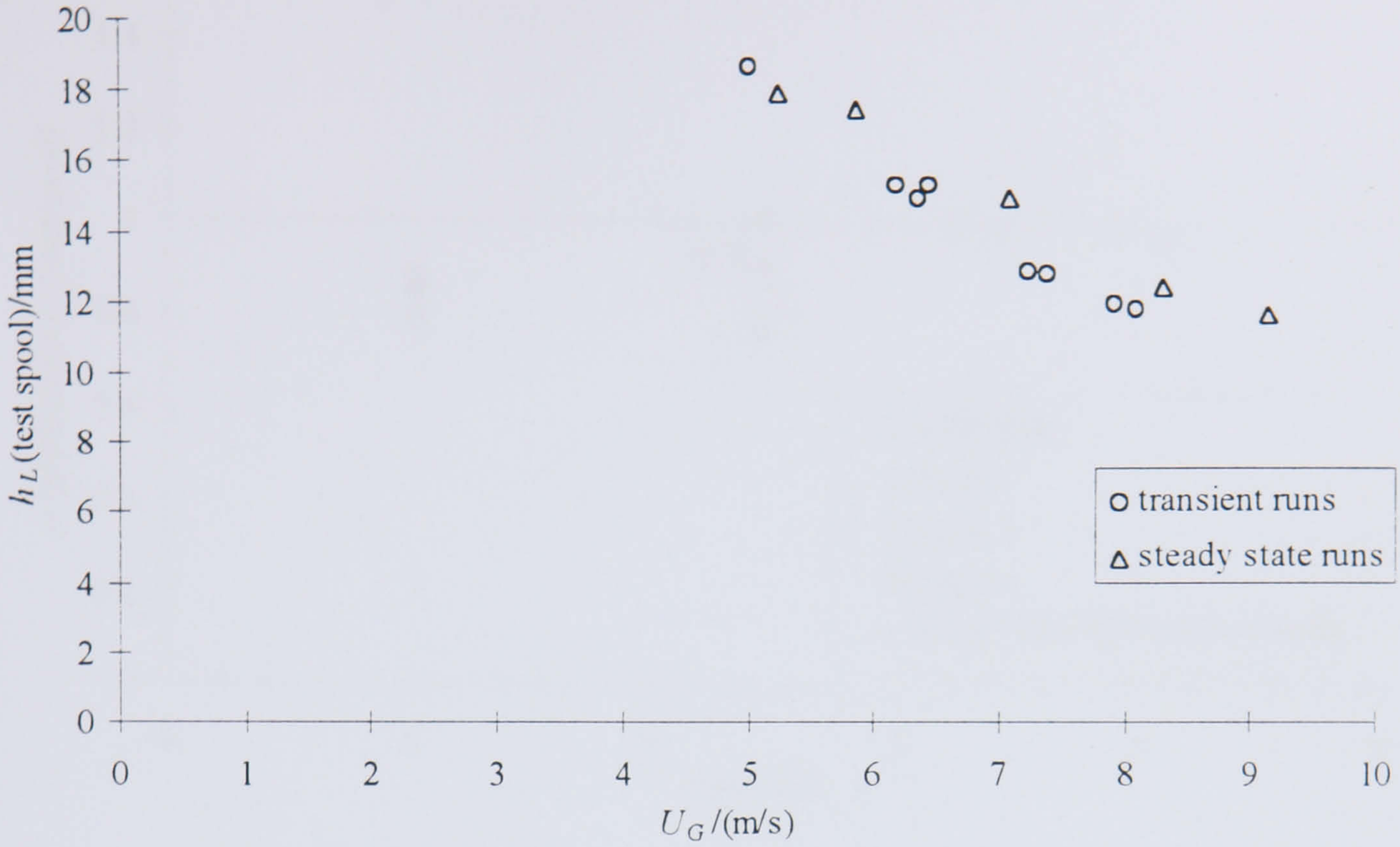


Figure 4.23 Mean liquid height in test spool, h_L(test spool), as a function of gas superficial velocity for a given liquid superficial velocity of U_L =0.04 m/s on the low pressure rig

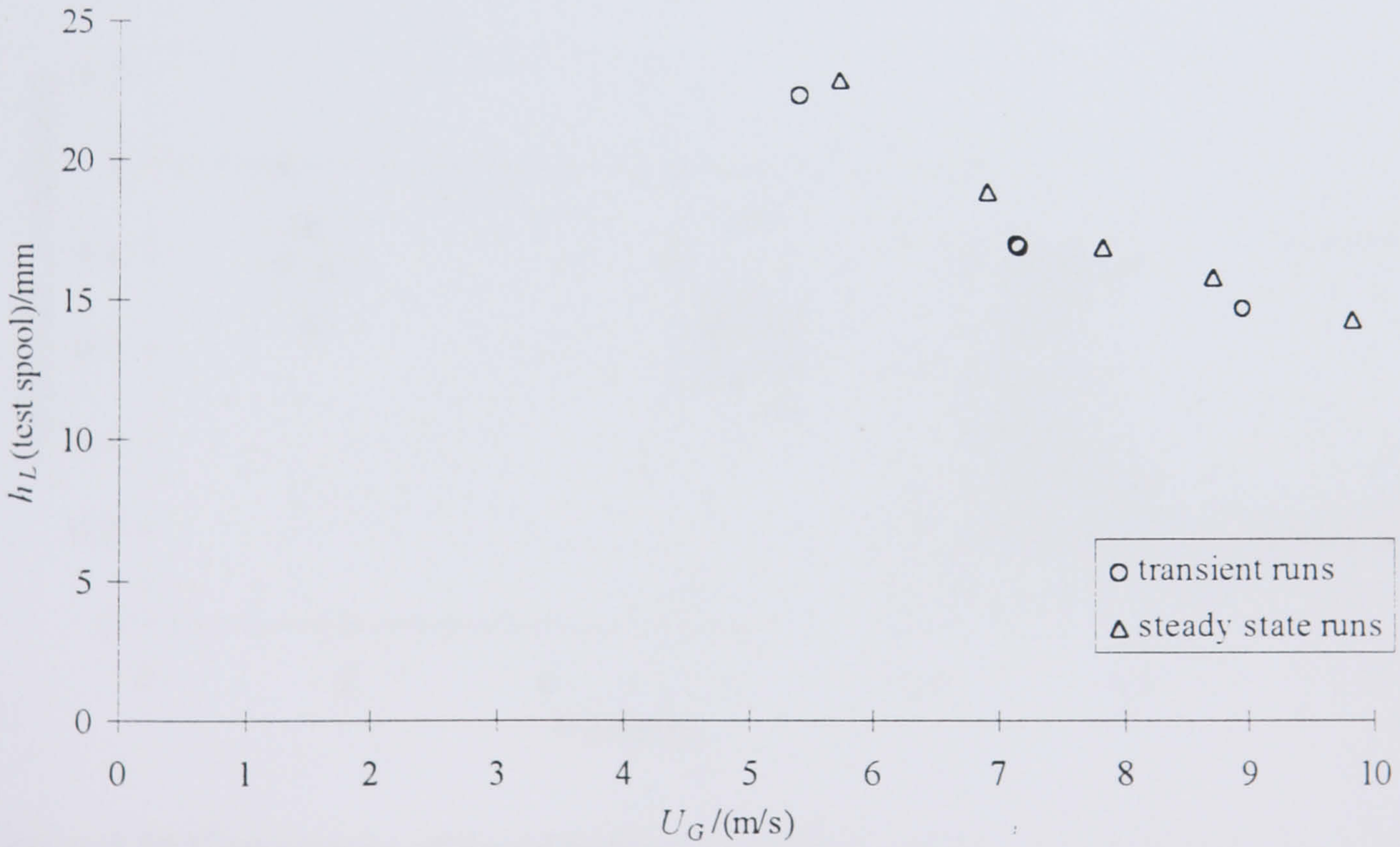


Figure 4.24 Mean liquid height in test spool, h_L(test spool), as a function of gas superficial velocity for a given liquid superficial velocity of U_L =0.08 m/s on the low pressure rig

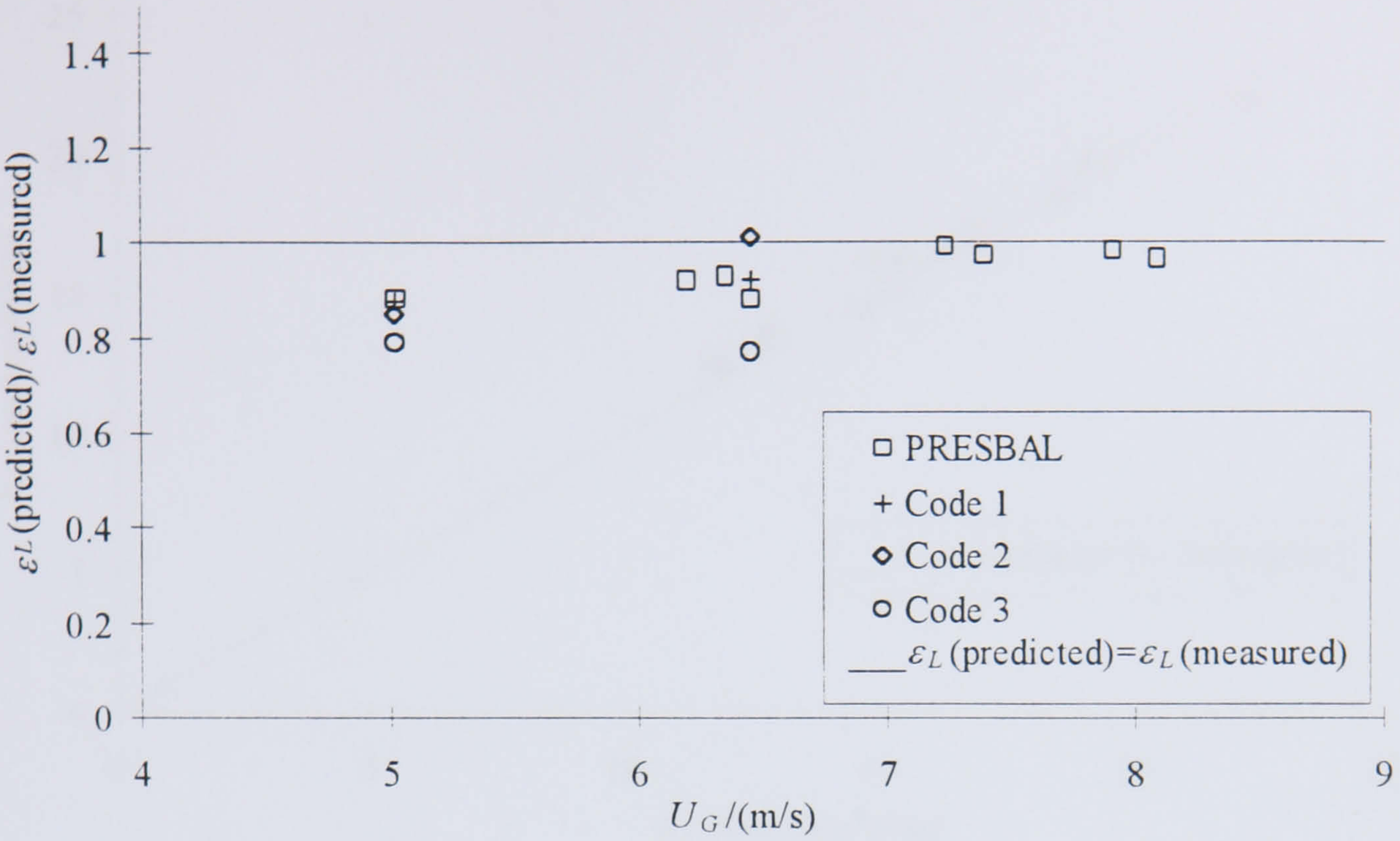


Figure 4.25 Comparison of liquid holdup calculated with one-dimensional codes with experimental data for U_L=0.04 m/s on the low pressure rig

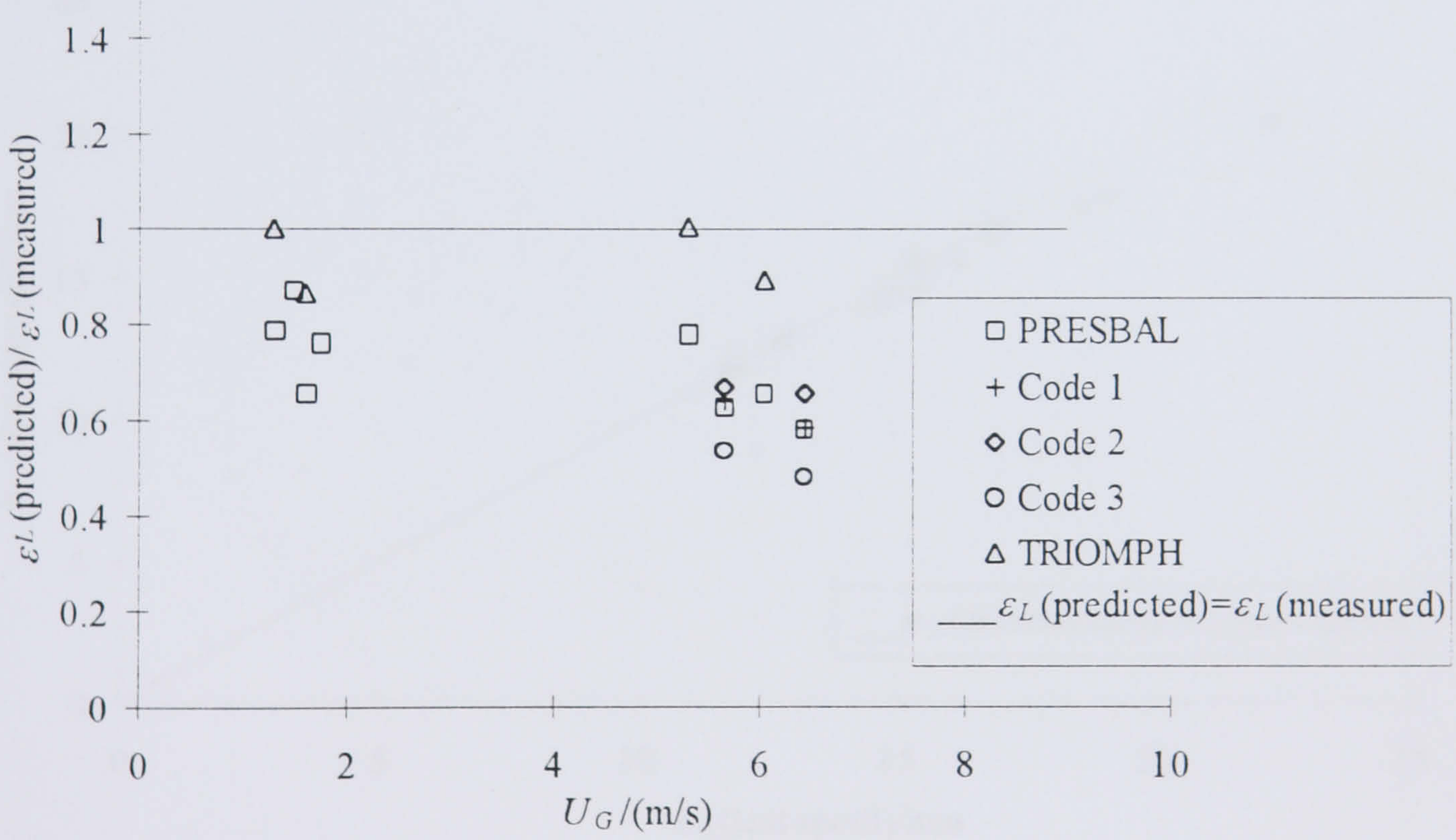


Figure 4.26 Comparison of liquid holdup calculated with one-dimensional codes with experimental data for 1 bar and 6 bar from the WASP rig

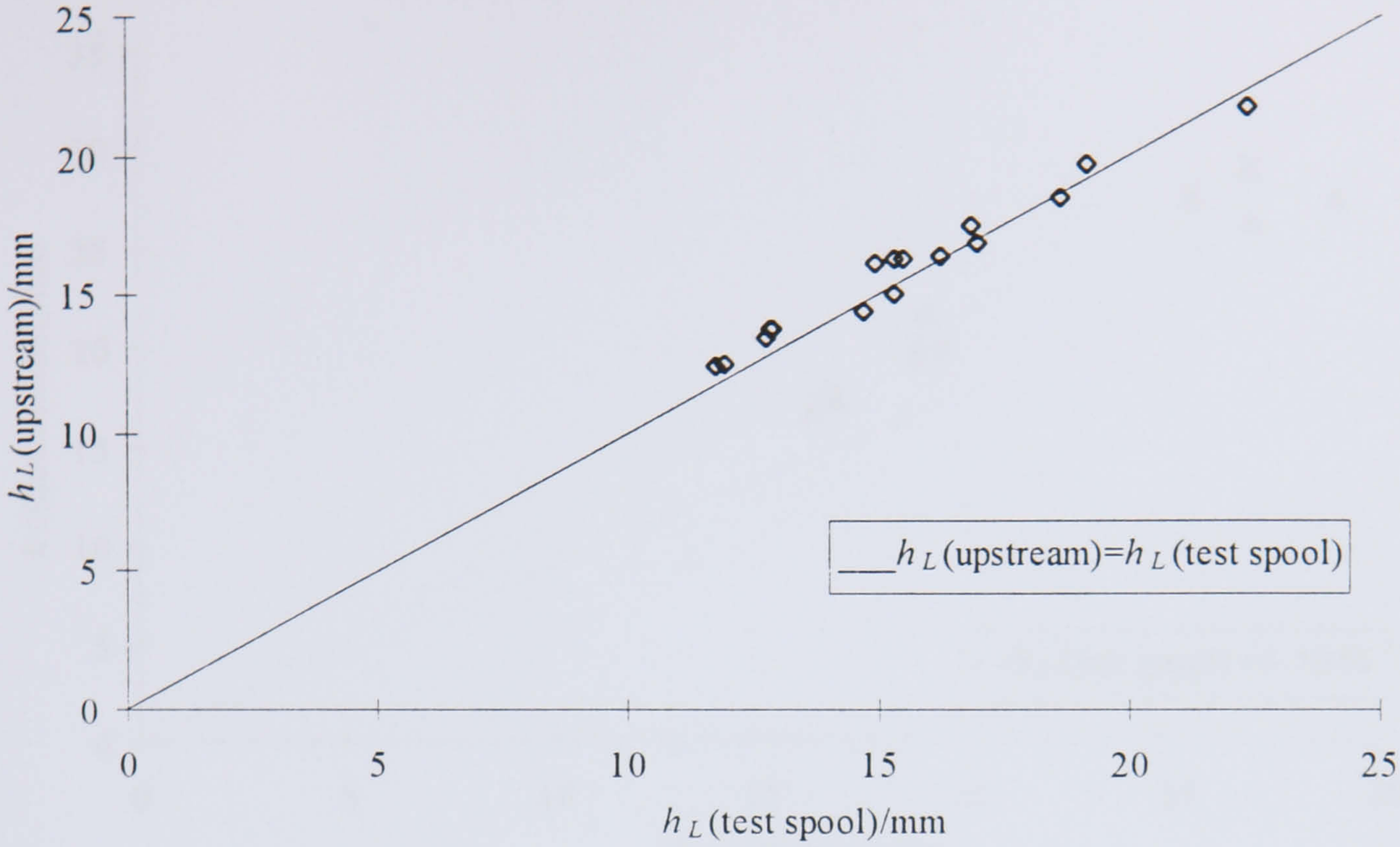


Figure 4.27 Comparison of mean liquid height in test spool, h_L(test spool), with mean liquid height upstream of test spool, h_L(upstream) on the low pressure rig

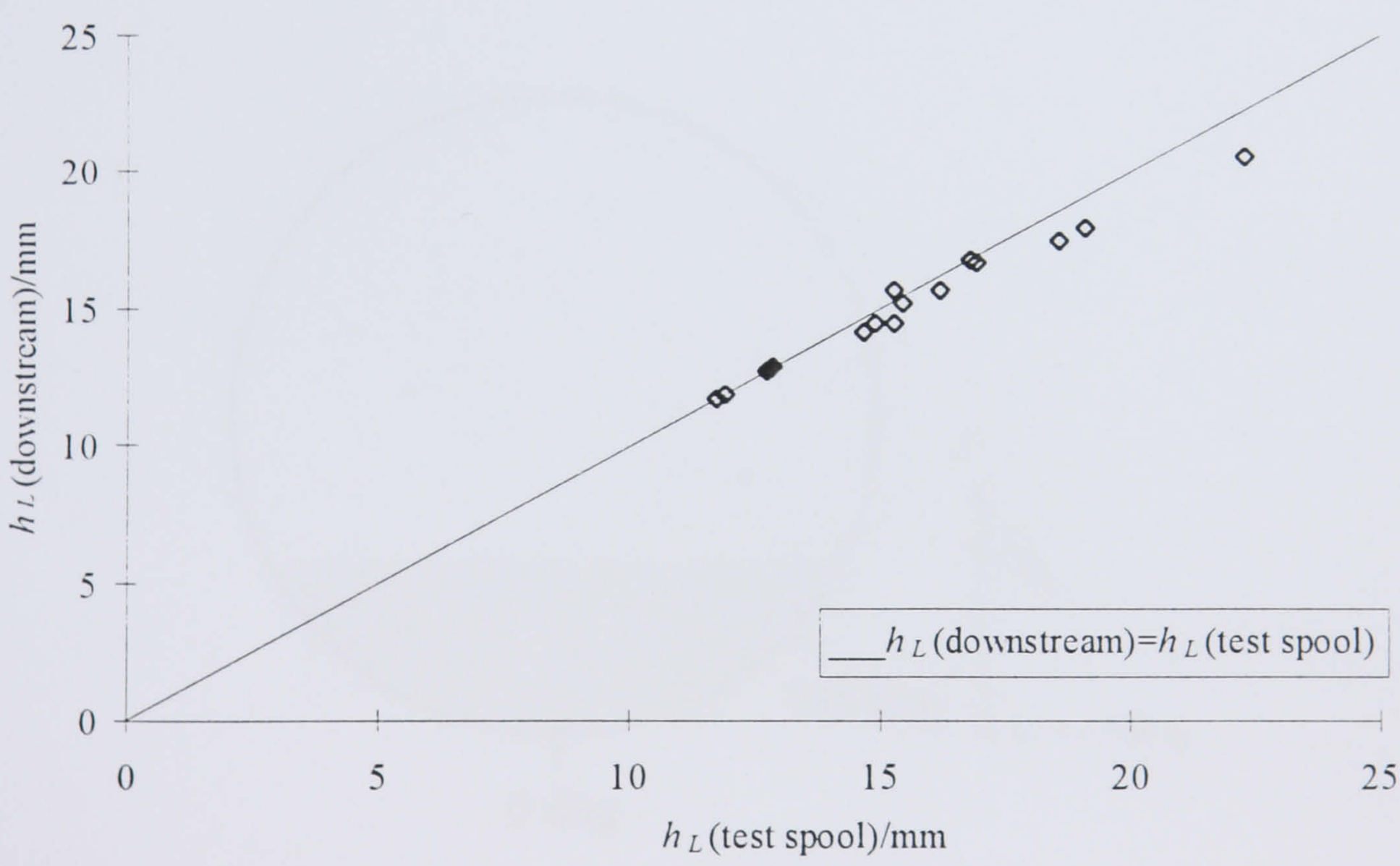


Figure 4.28 Comparison of mean liquid height in test spool, h_L(test spool), with mean liquid height downstream of test spool, h_L(downstream) on the low pressure rig

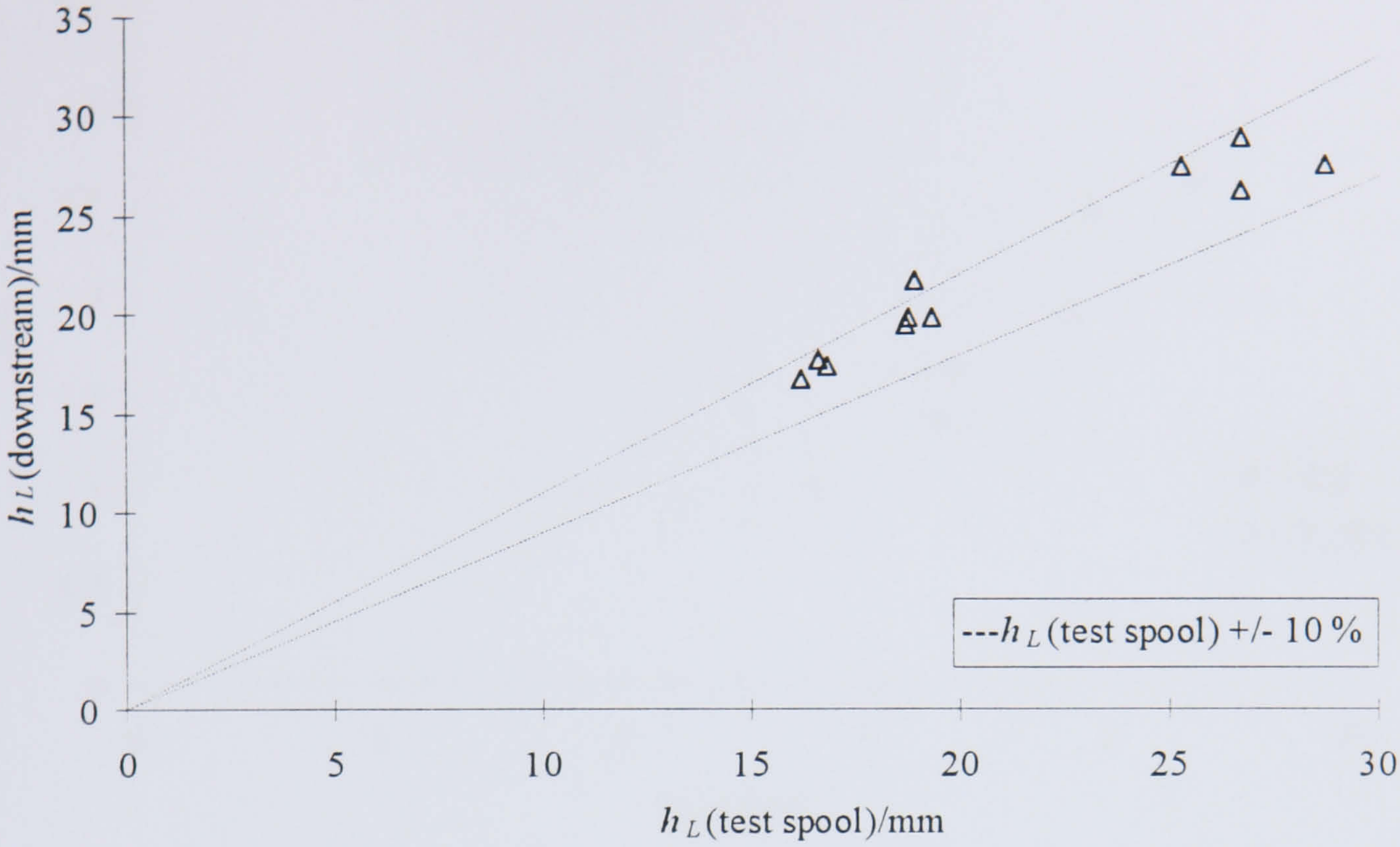


Figure 4.29 Comparison of mean liquid height in test spool, h_L(test spool), with mean liquid height downstream of test spool, h_L(downstream) on WASP

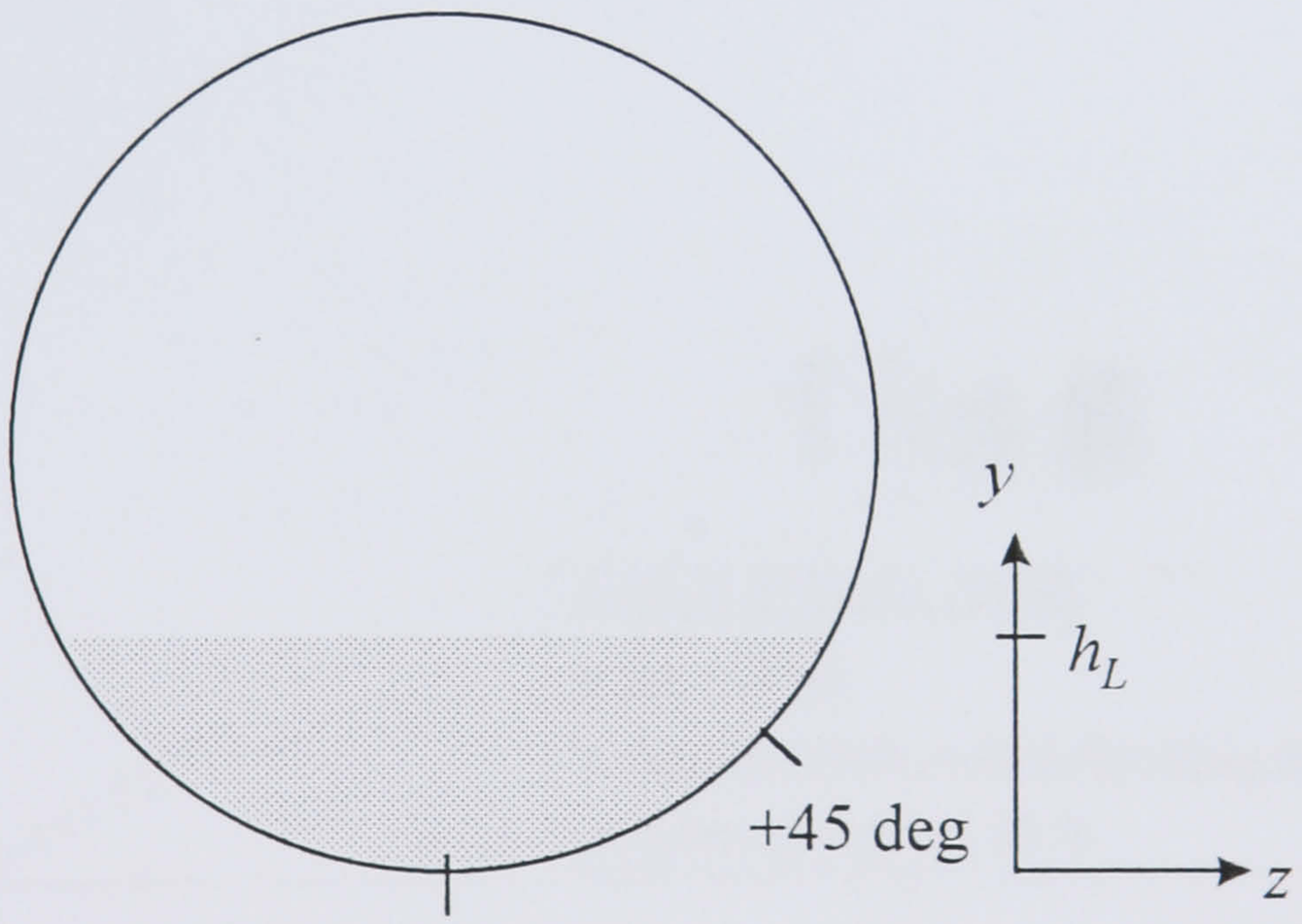


Figure 4.30 Circumferential variation of liquid wall shear stress measurement

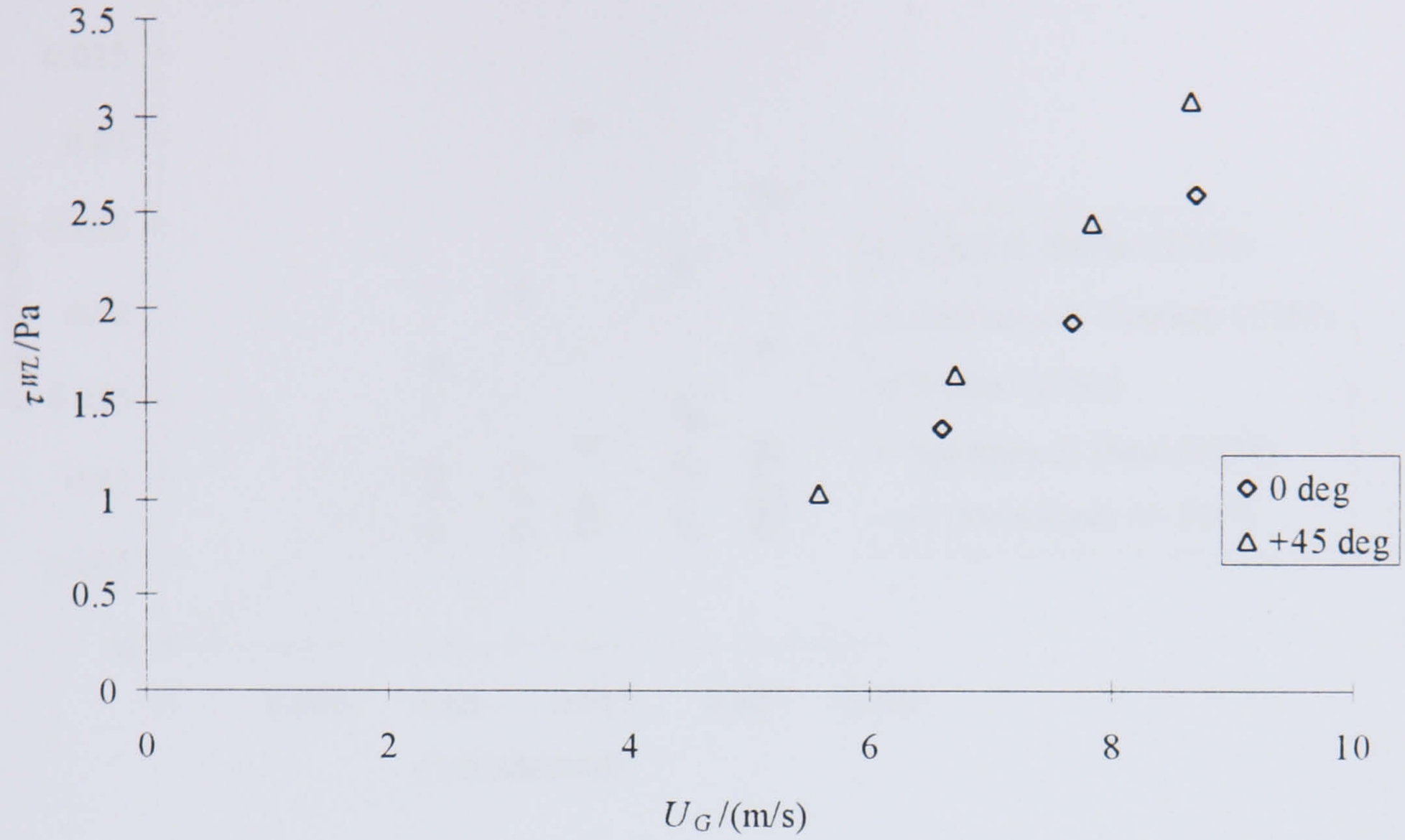


Figure 4.31 Circumferential variation of liquid wall shear stress over a range of gas flow rates at U_L=0.08 m/s on the low pressure rig

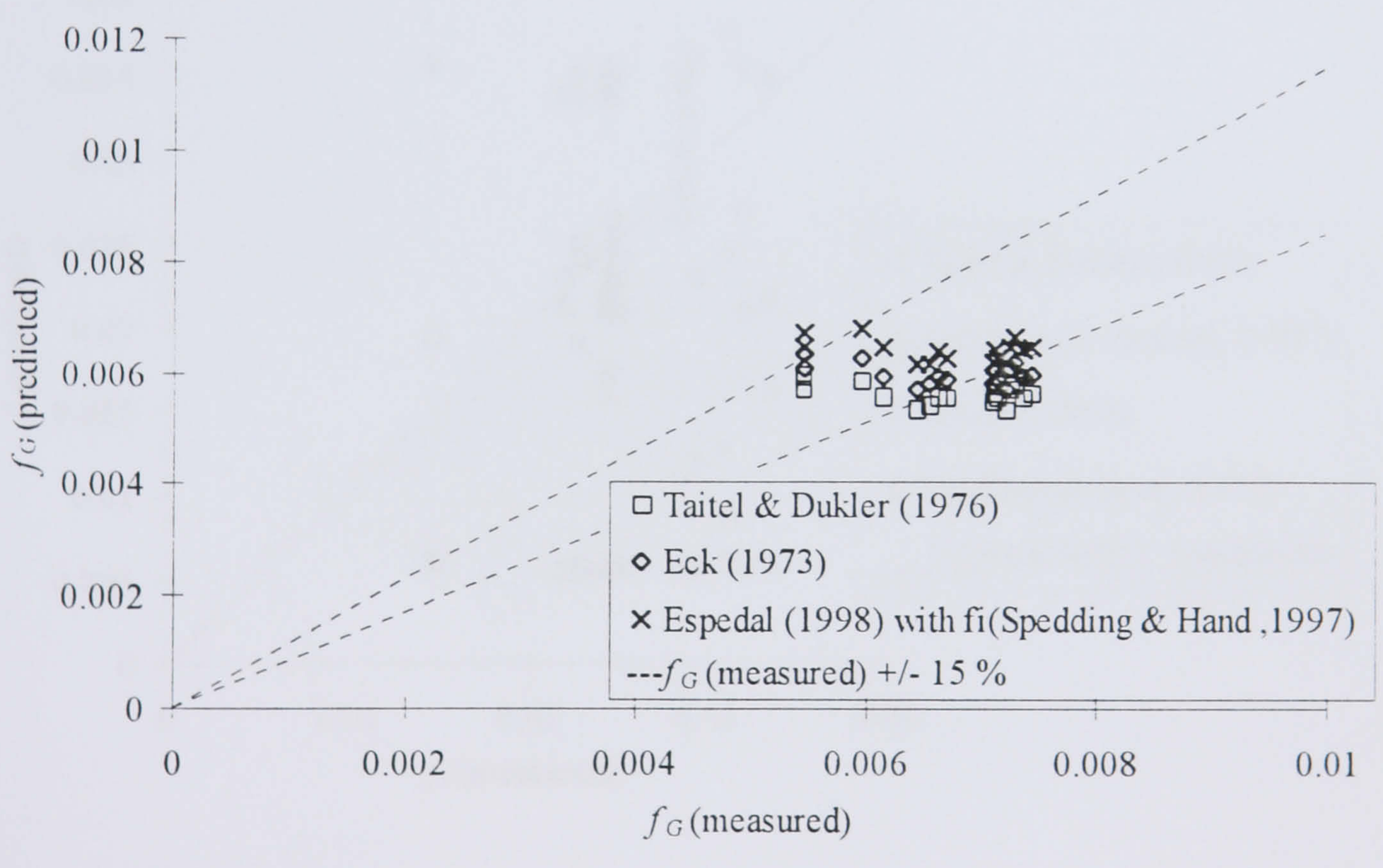


Figure 4.32 Comparison of gas wall friction factor f_G from experiments on the low pressure rig with different models

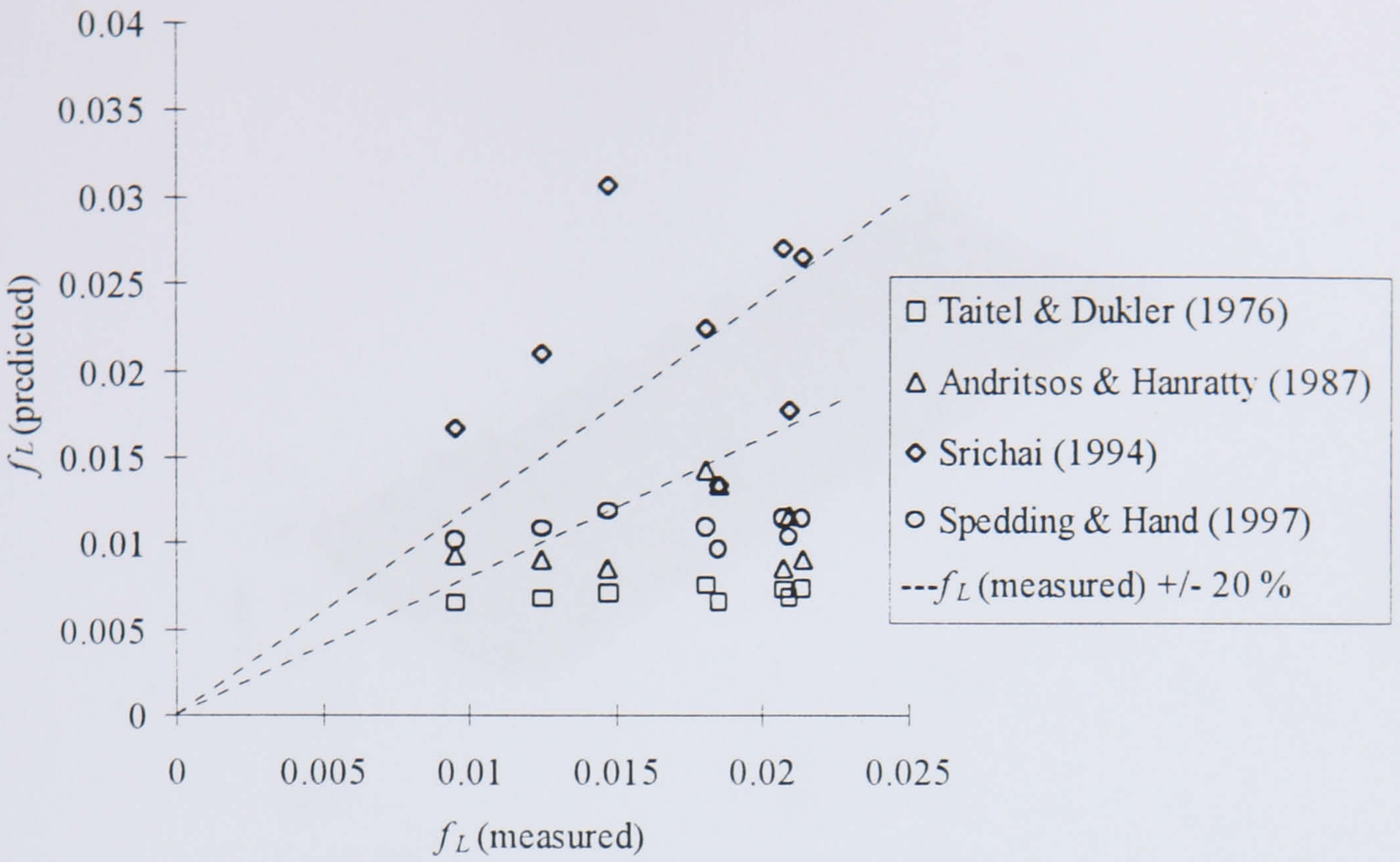


Figure 4.33 Comparison of liquid wall friction factor f_L from experiments on the low pressure rig with different models

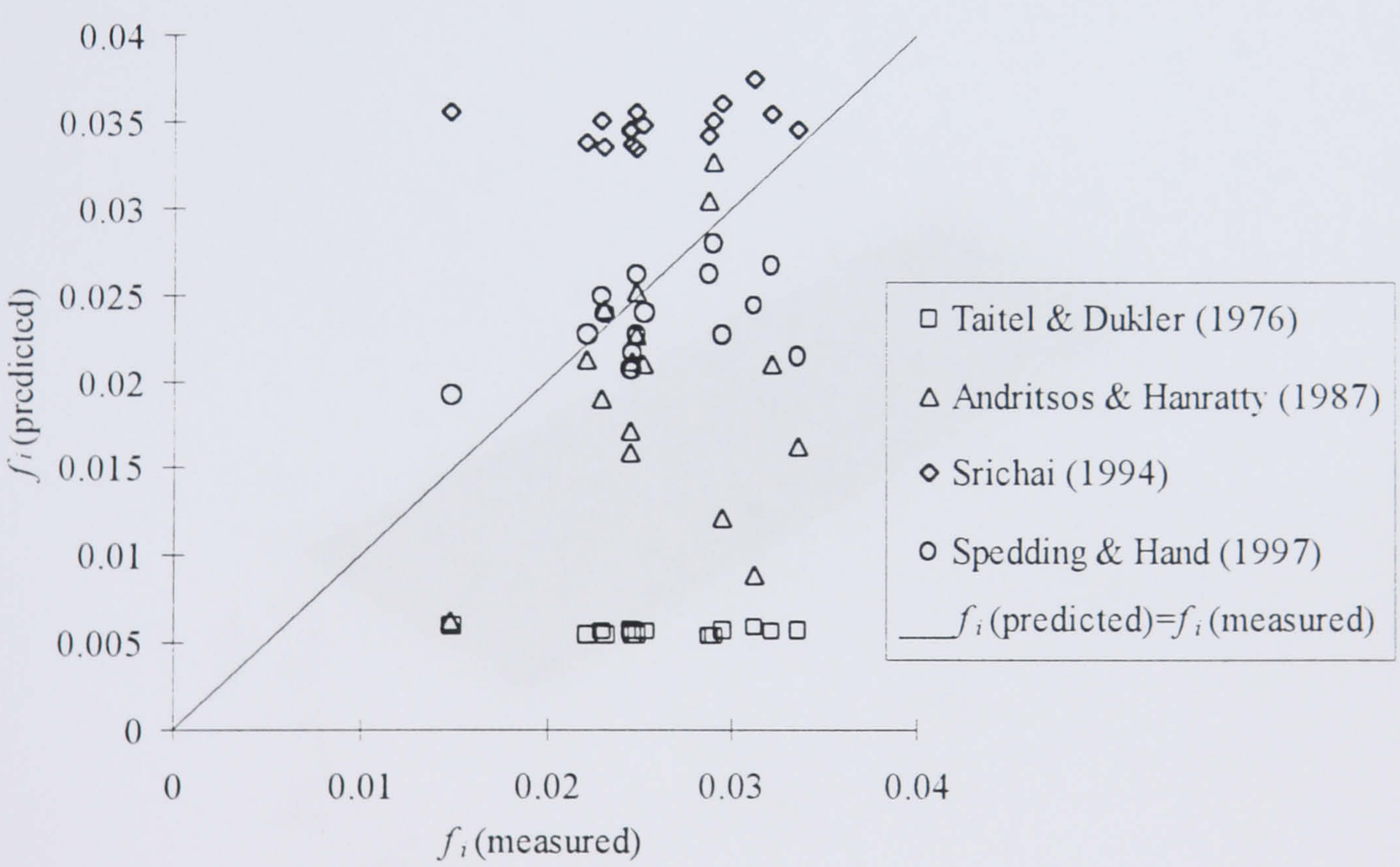


Figure 4.34 Comparison of interfacial friction factor f_i derived from experiments on the low pressure rig with different models

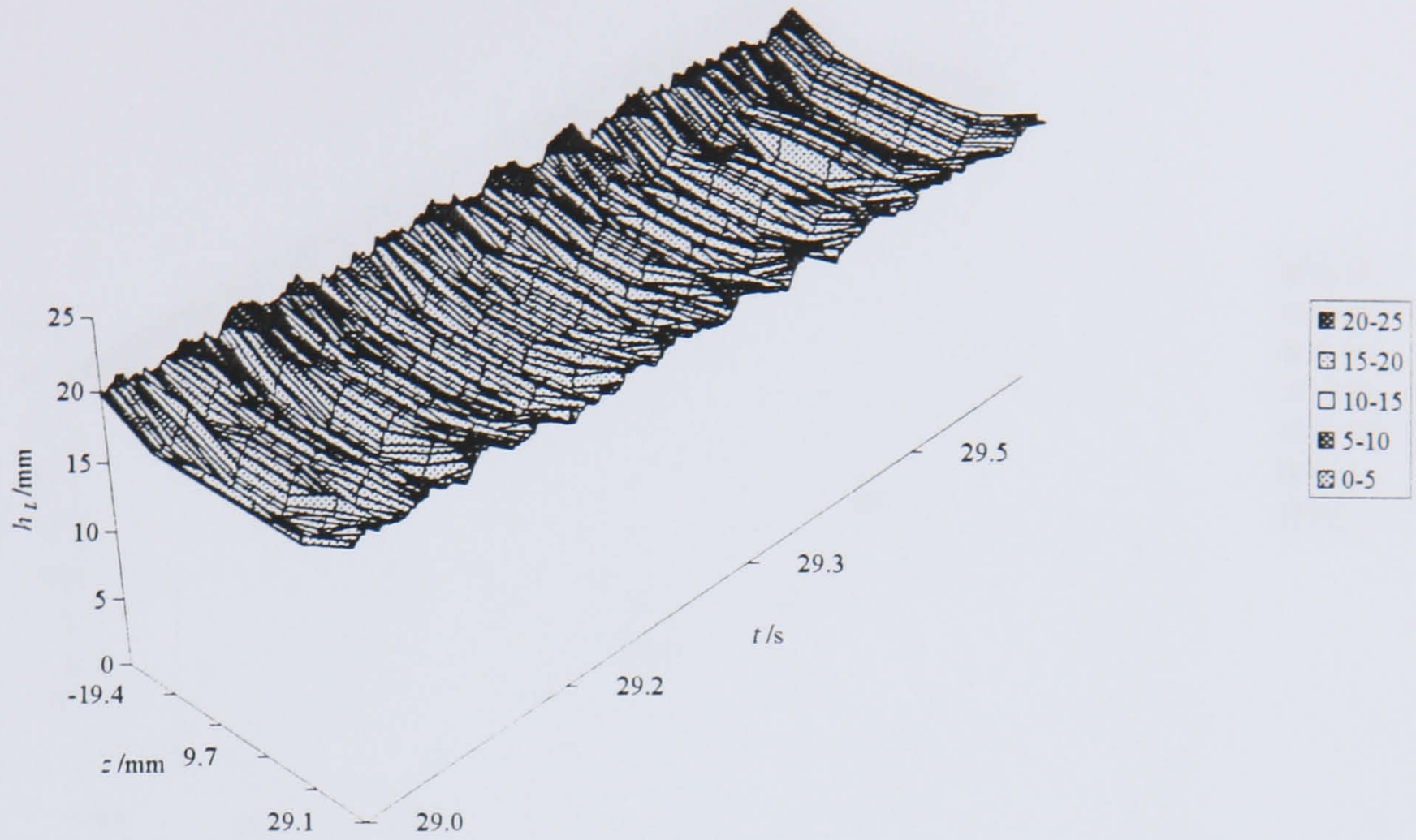


Figure 4.35 Interfacial structure for initial steady state of transient case `1a` on the low pressure rig (U_L=0.039 m/s, U_G=5.01 m/s, p=1.00 bar)

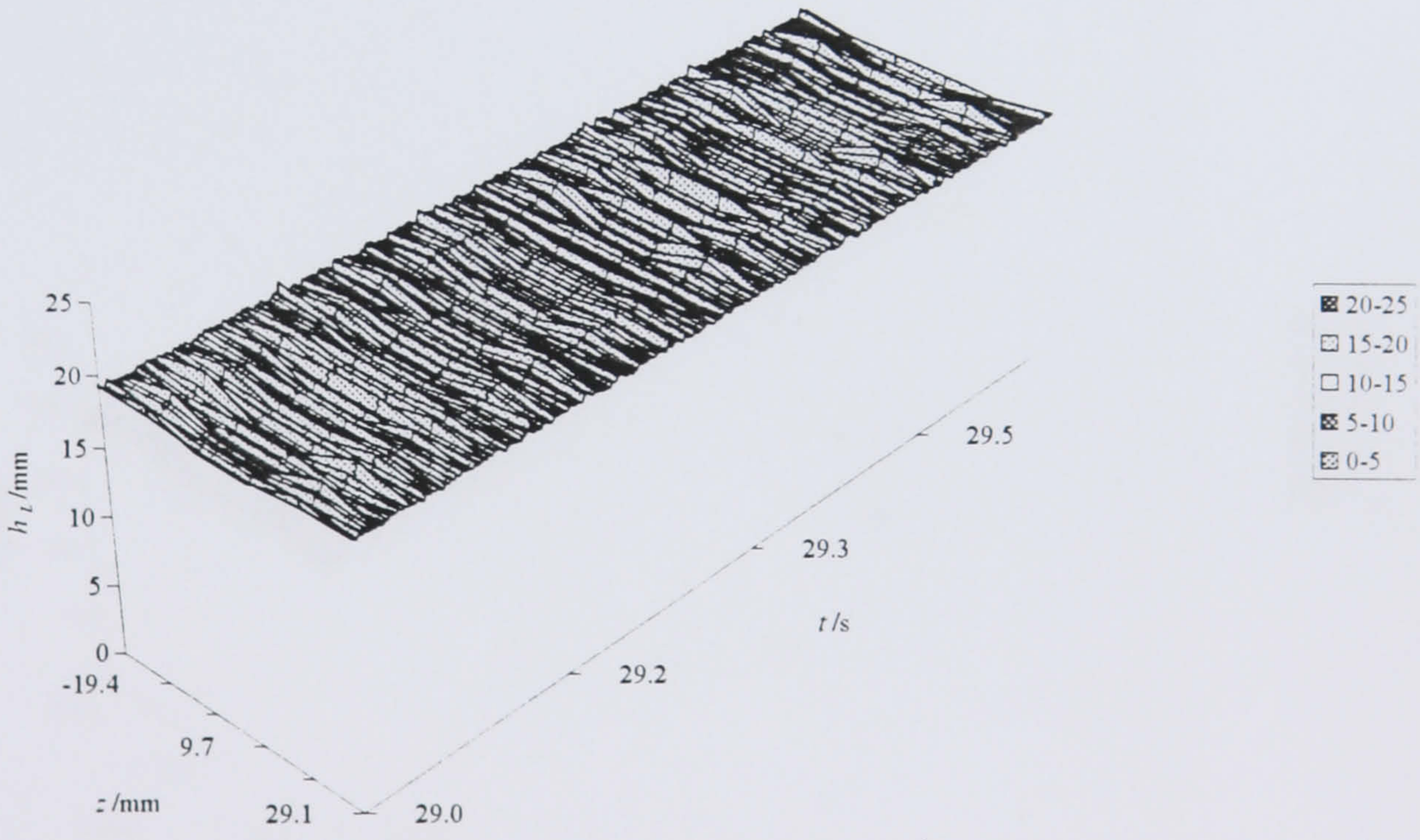


Figure 4.36 Interfacial structure for initial steady state of transient case `wb` on the WASP rig (U_L=0.038 m/s, U_G=5.33 m/s, p=1.06 bar)

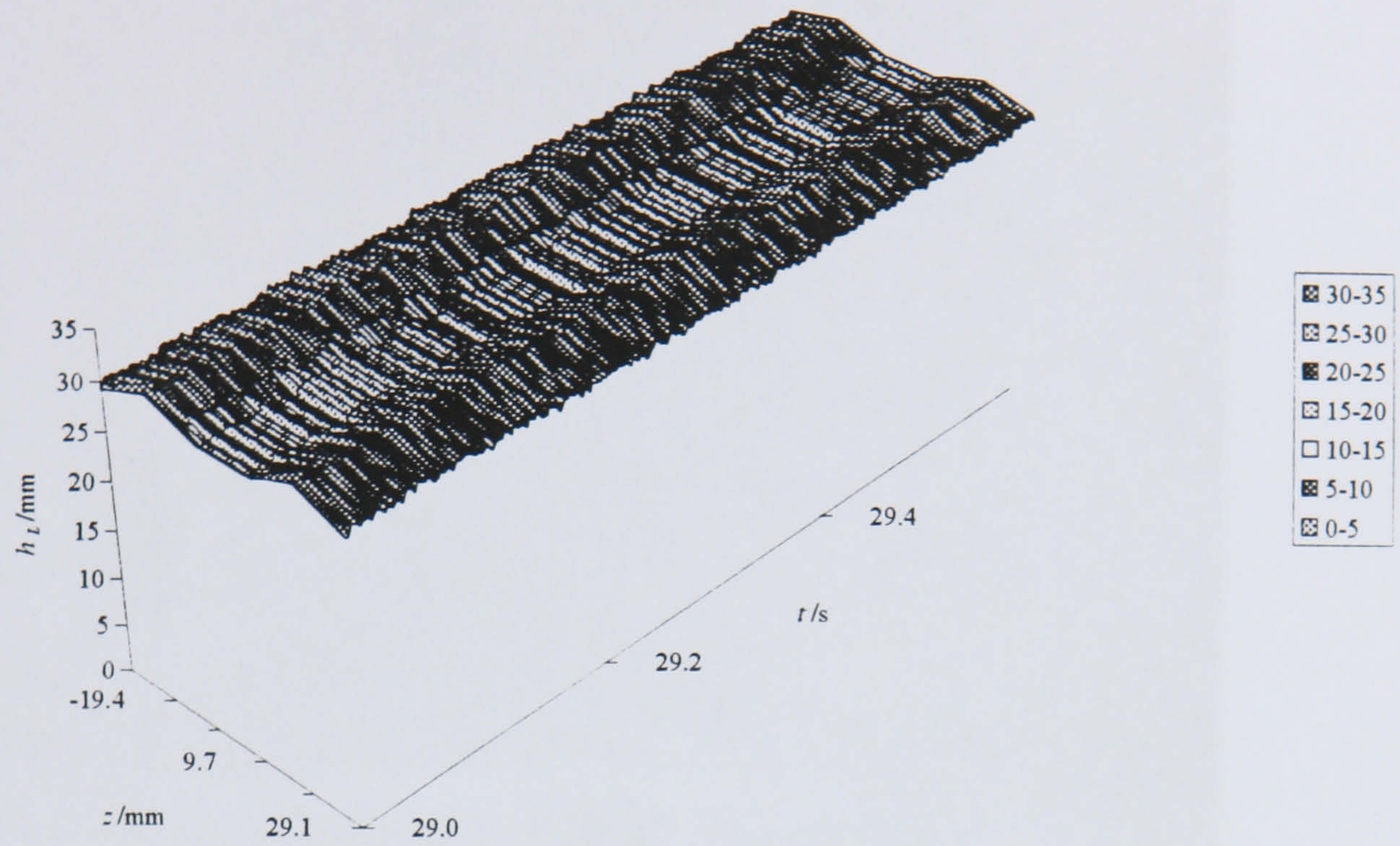


Figure 4.37 Interfacial structure for initial steady state of transient case wd on the WASP rig (U_L=0.034 m/s, U_G=1.30 m/s, p=6.07 bar)

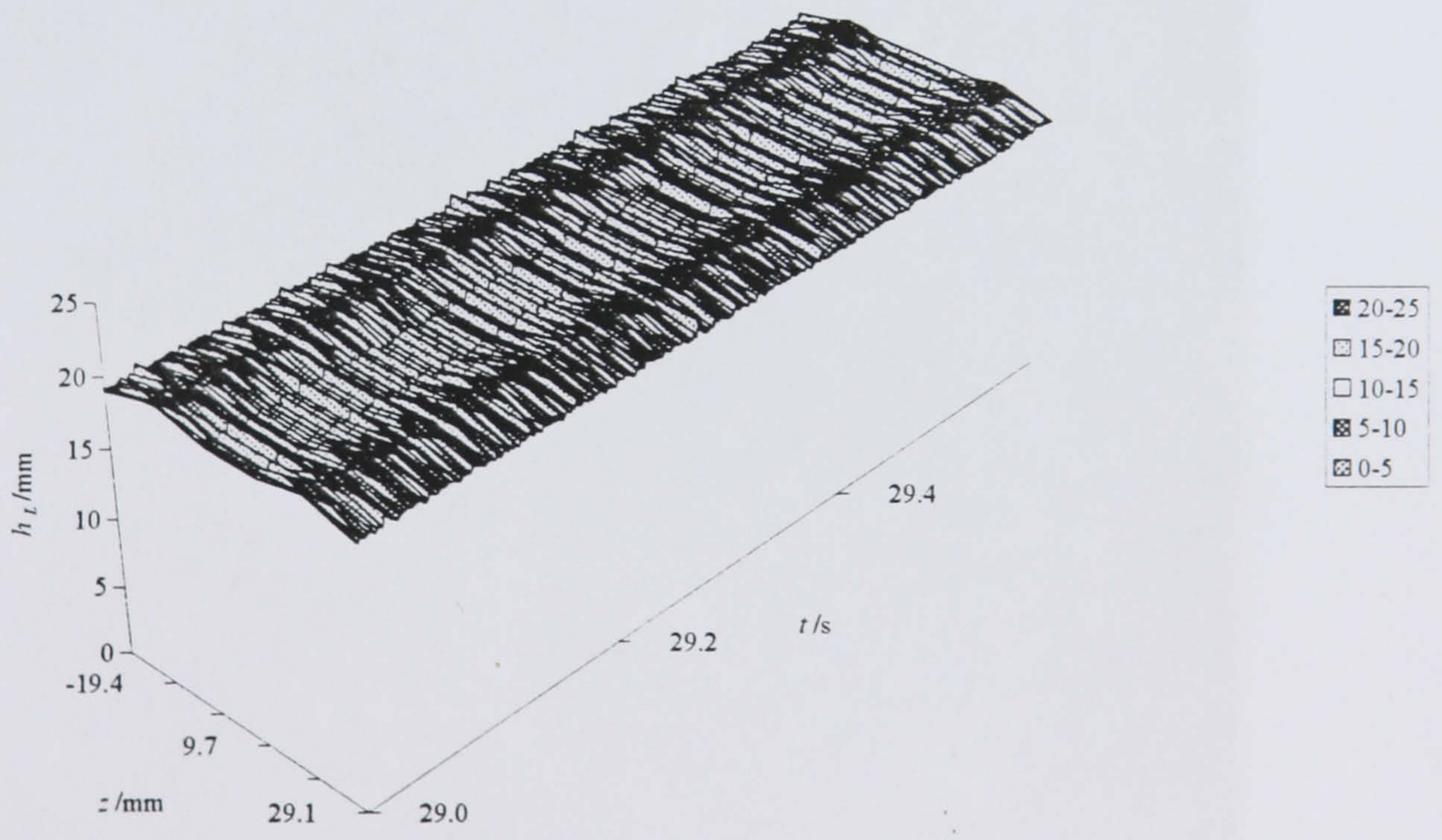


Figure 4.38 Interfacial structure for initial steady state of transient case we on the WASP rig (U_L=0.025 m/s, U_G=1.32 m/s, p=11.04 bar)

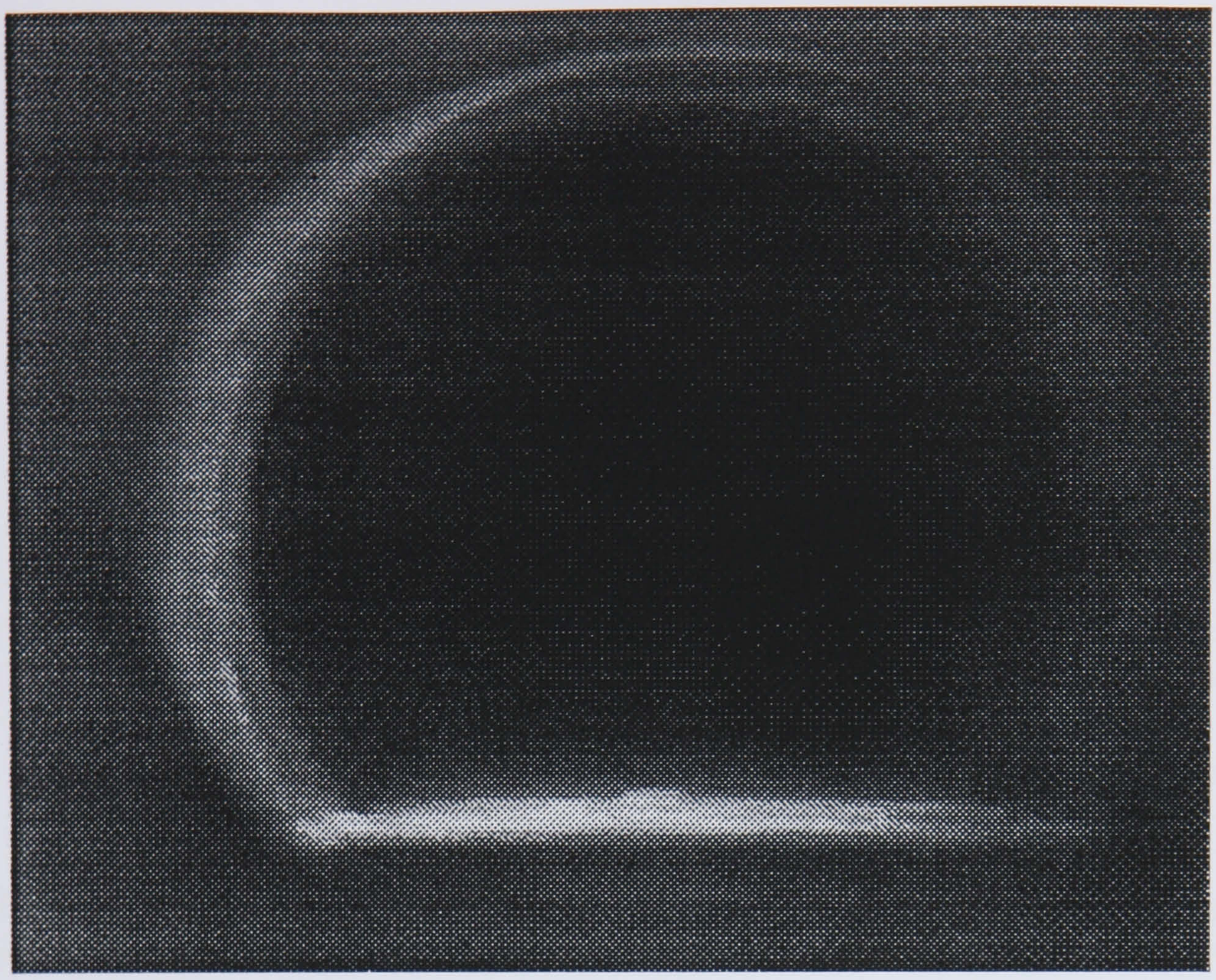


Figure 4.39 Axial view of initial steady state of case wd on the WASP rig (U_L=0.034 m/s, U_G=1.30 m/s, p=6.07 bar)

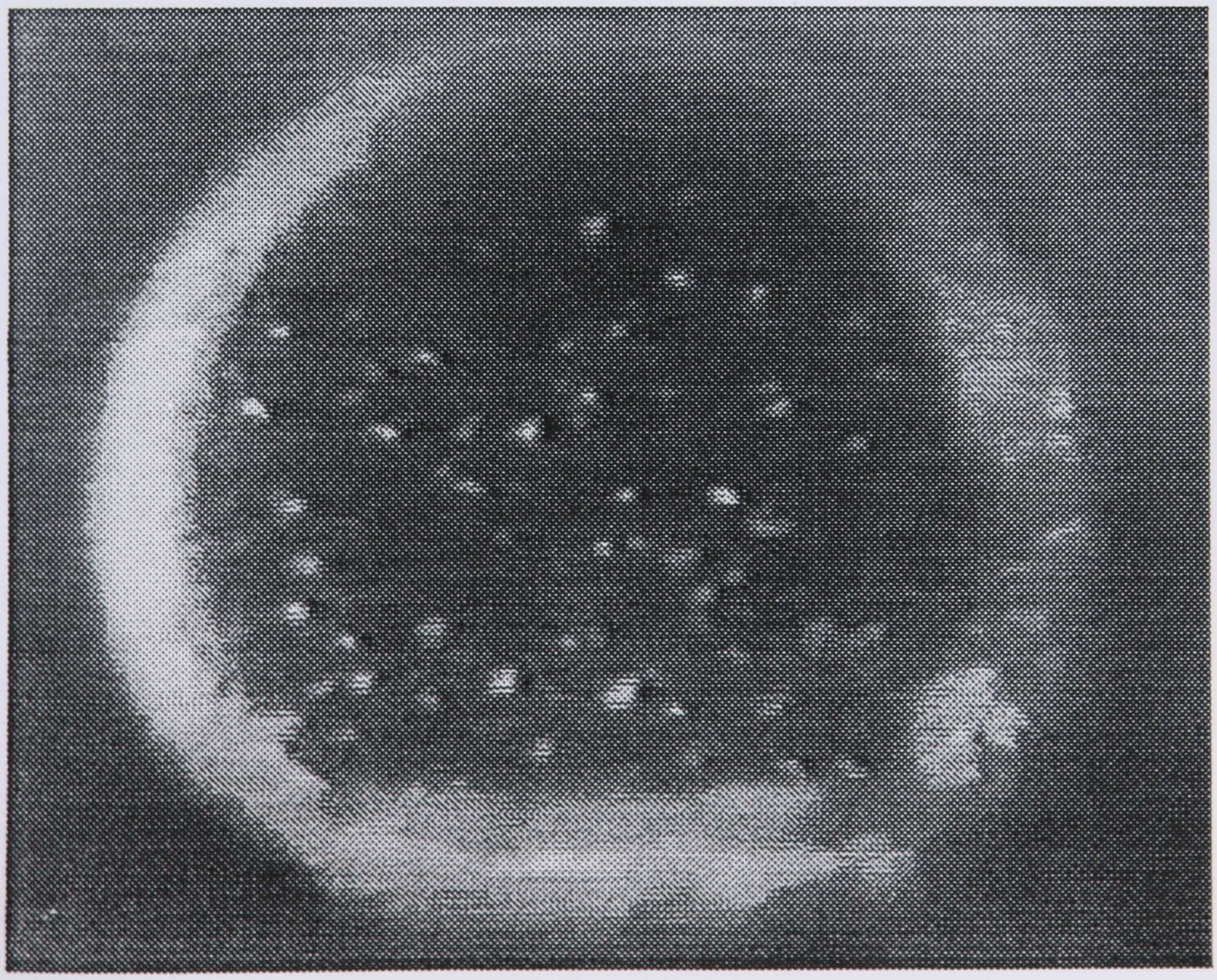


Figure 4.40 Axial view of steady state flow (U_L=0.015 m/s, U_G=20.0 m/s, p=1.0 bar)

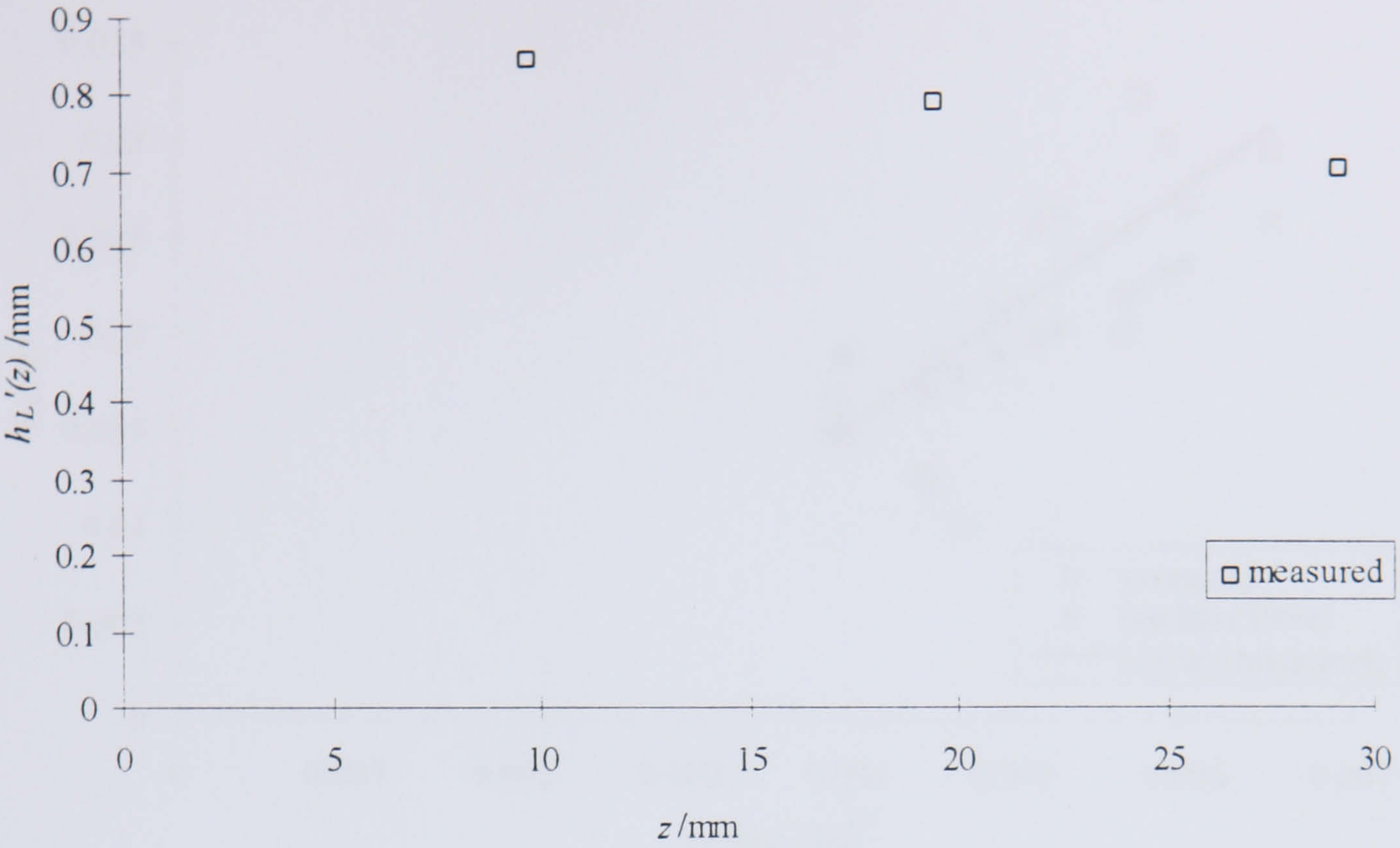


Figure 4.41 Variation of interfacial fluctuation $h_L'(z)$ with transverse position z for initial steady state of transient case `1a` on the low pressure rig (U_L=0.039 m/s, U_G=5.01 m/s, p=1.00 bar)

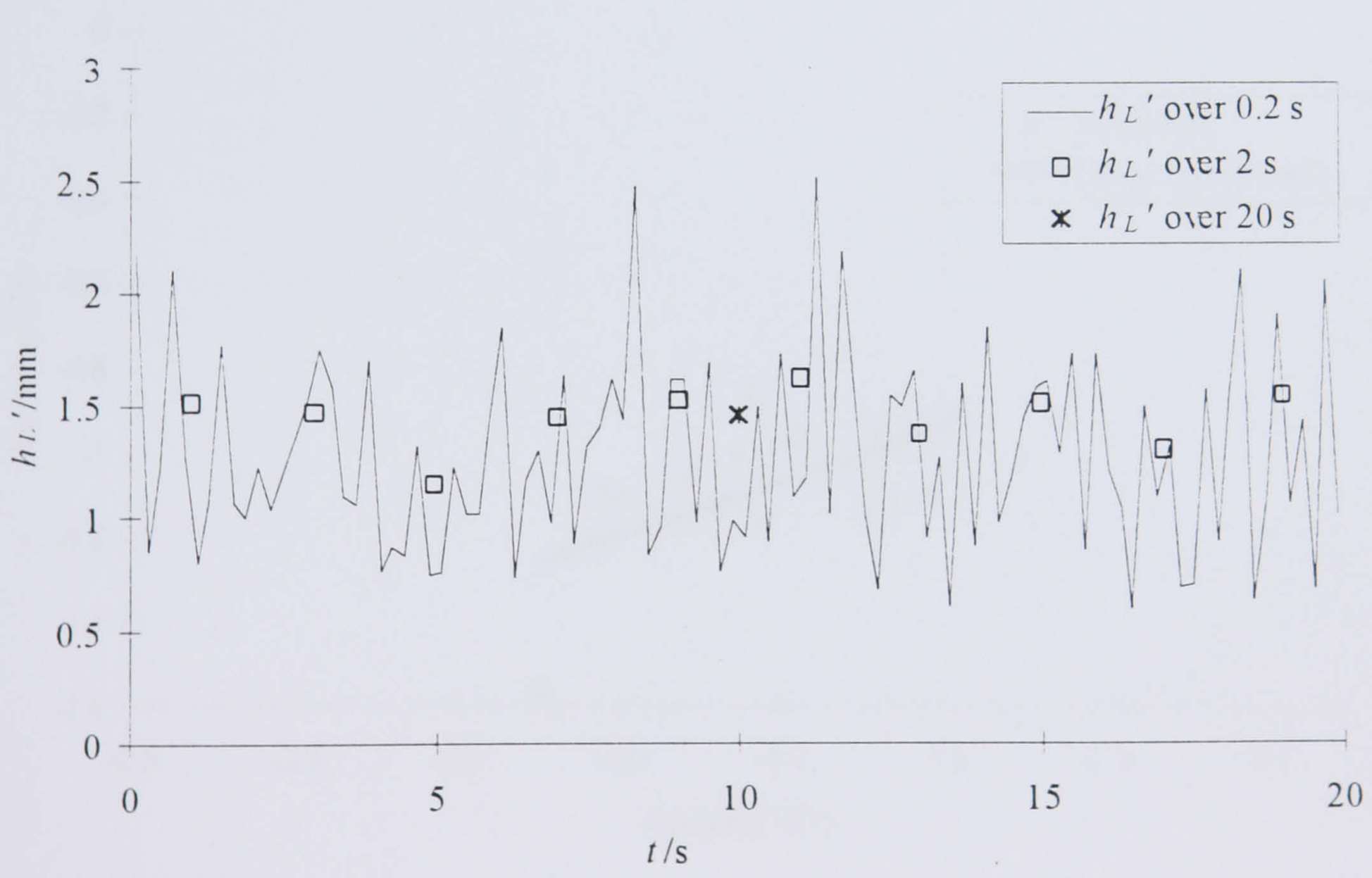


Figure 4.42 Influence of time interval over which interfacial fluctuations h_L' are determined for initial steady state of transient case `1c` on the low pressure rig (U_L=0.039 m/s, U_G=7.39 m/s, p=0.99 bar)

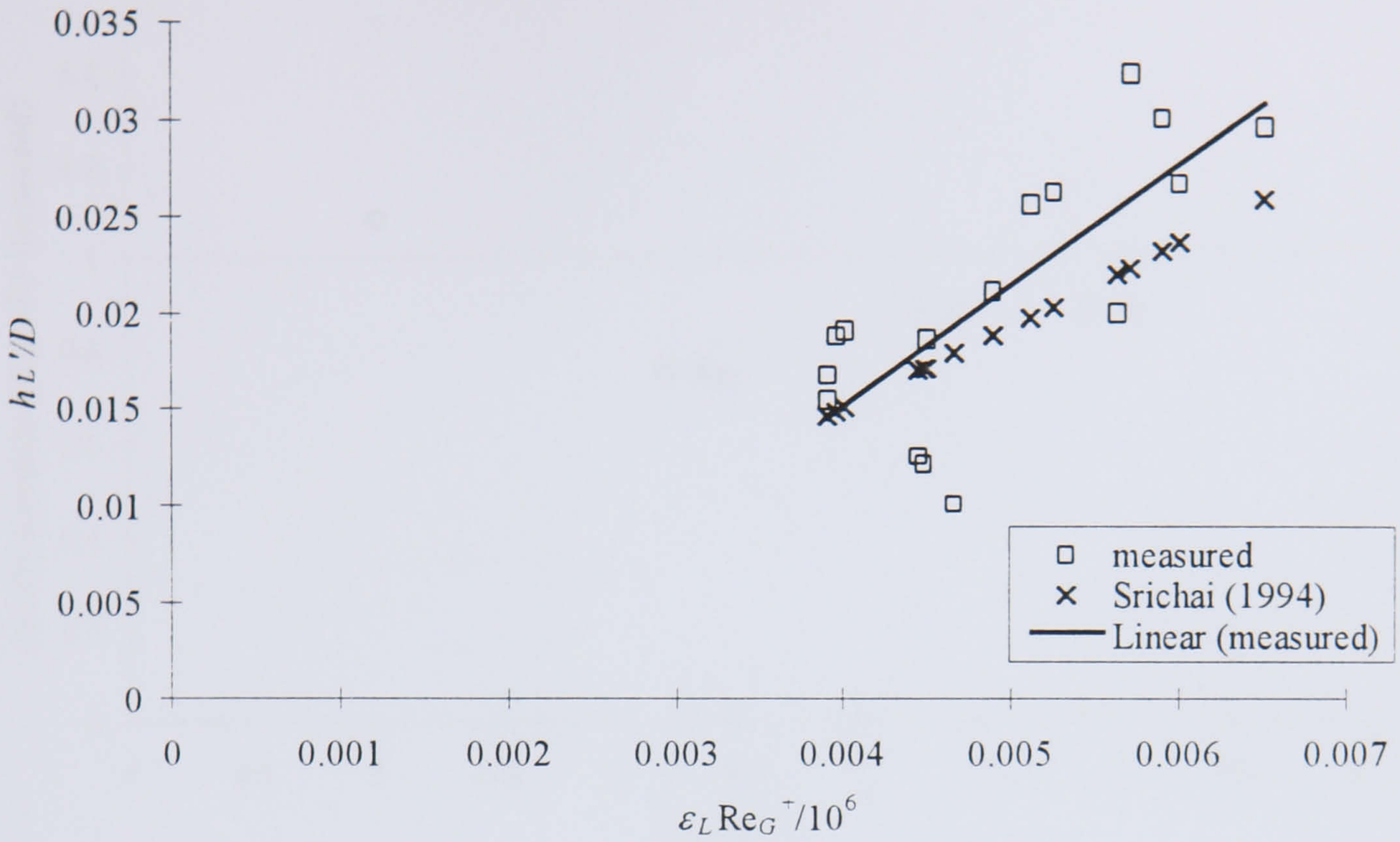


Figure 4.43 h_L'/D as a function of the holdup ε_L and the gas Reynolds number Re_G^{+} for results from the low pressure rig

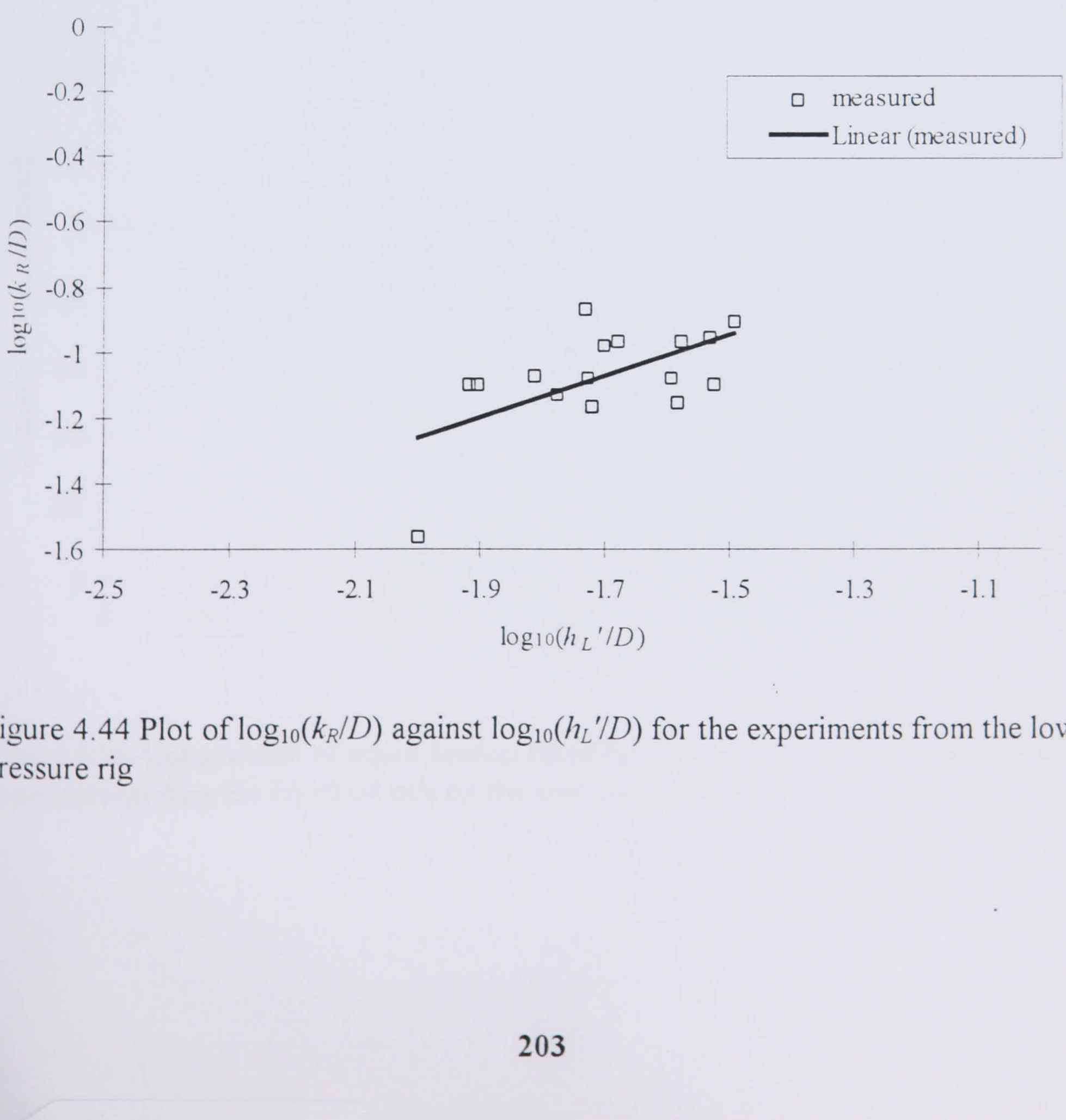


Figure 4.44 Plot of $\log_{10}(k_R/D)$ against $\log_{10}(h_L'/D)$ for the experiments from the low pressure rig

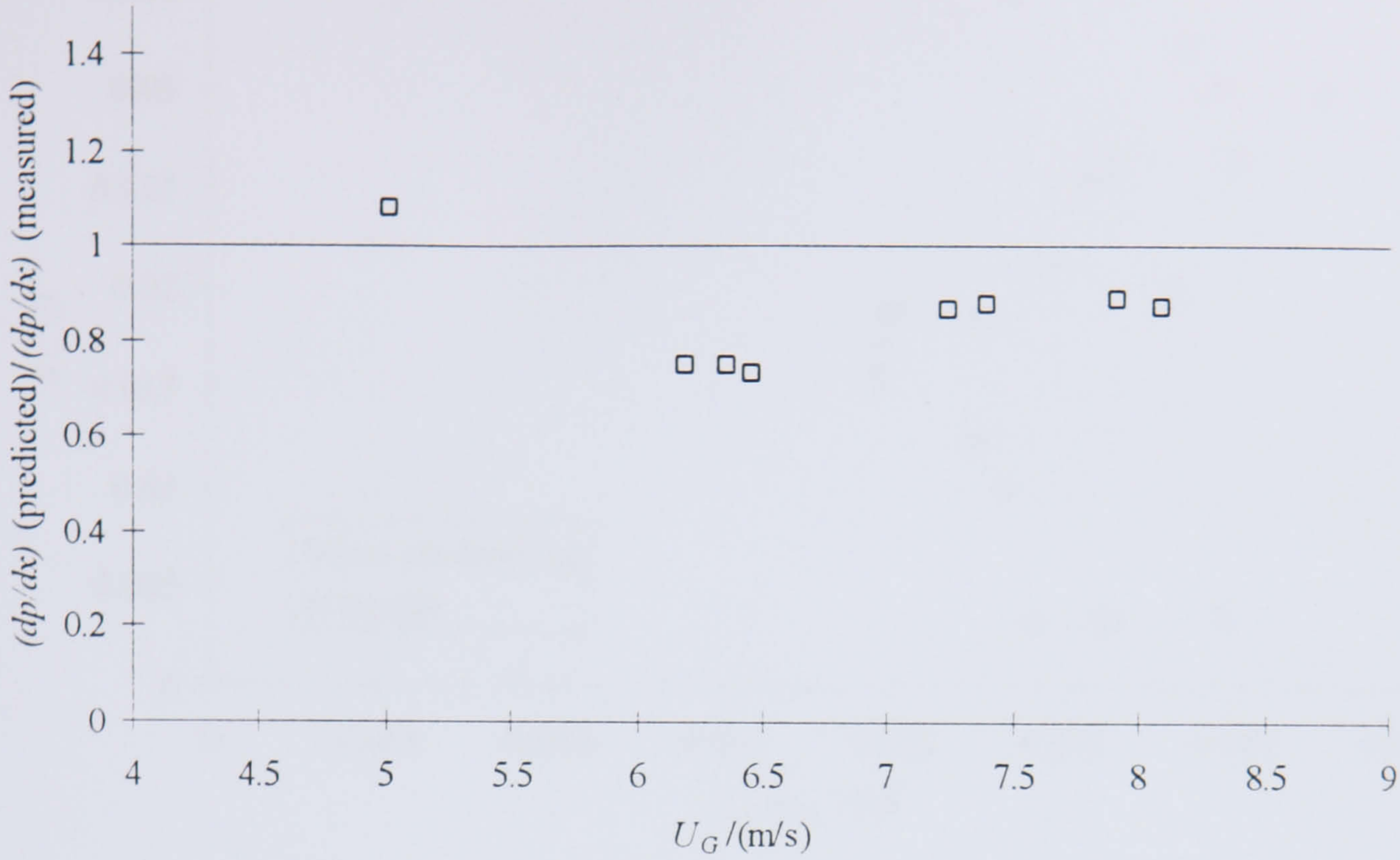


Figure 4.45 Comparison of pressure gradient calculated with modified PRESBAL with experimental data for U_L=0.04 m/s on the low pressure rig

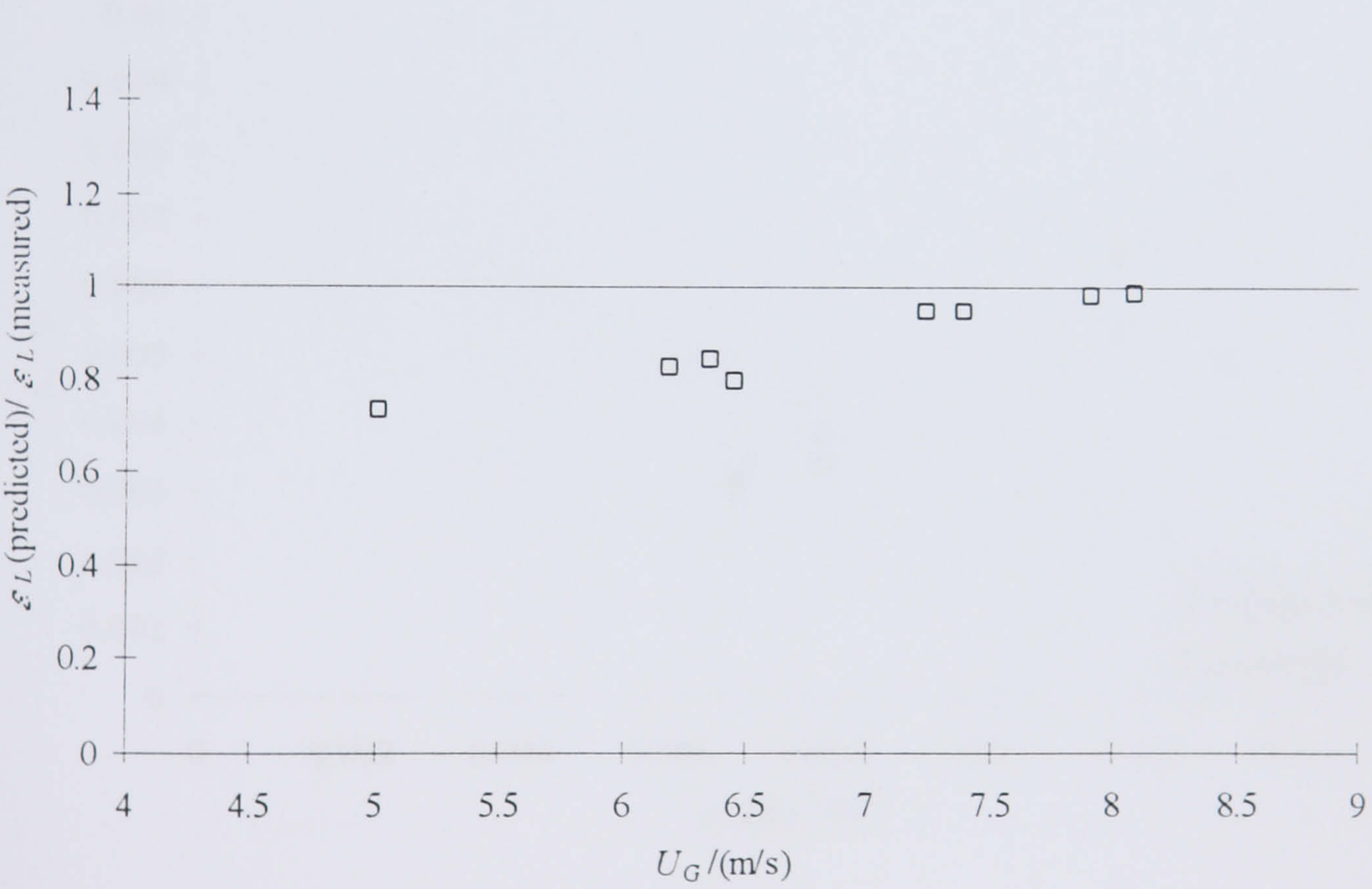


Figure 4.46 Comparison of liquid holdup calculated with modified PRESBAL with experimental data for U_L=0.04 m/s on the low pressure rig

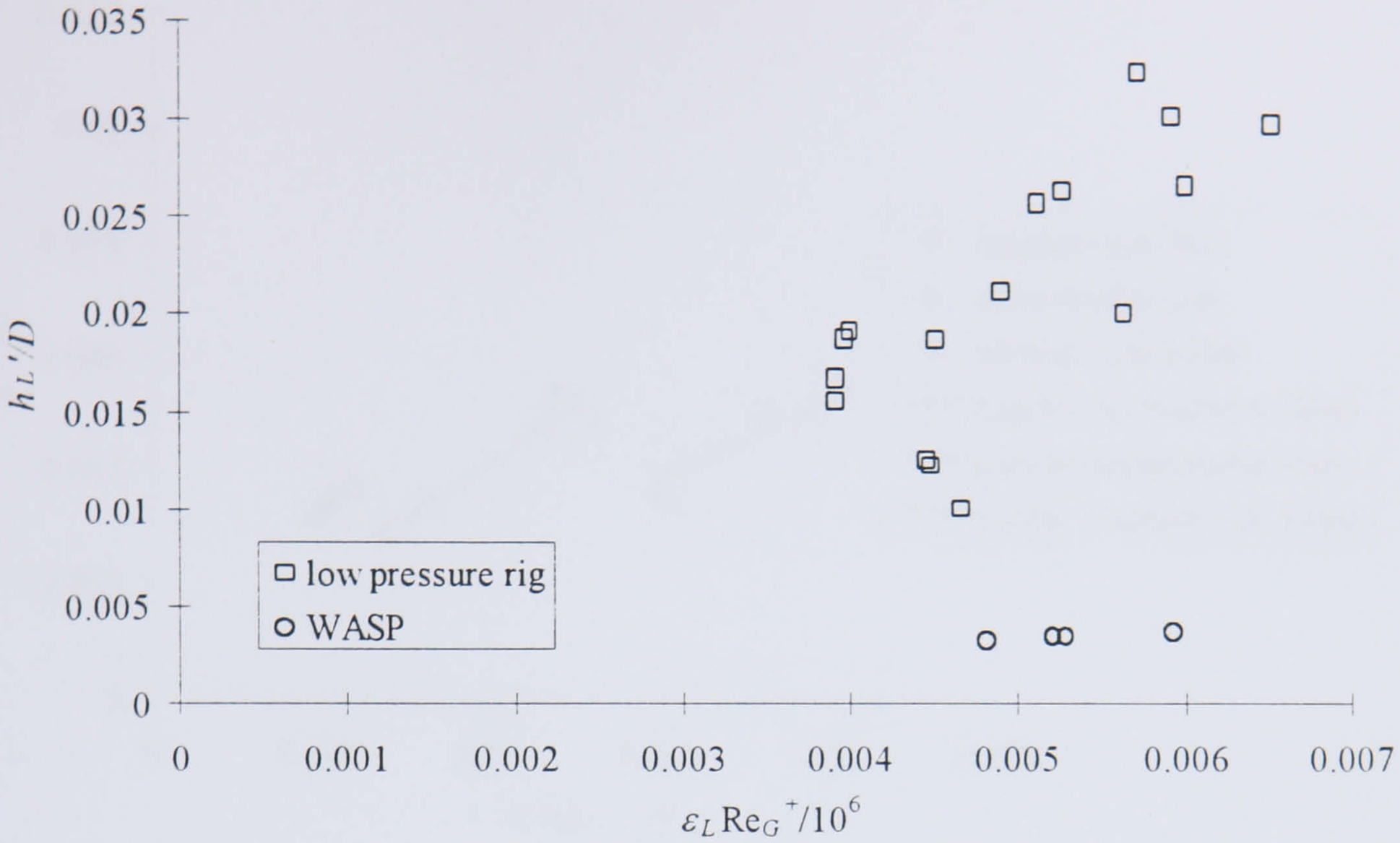


Figure 4.47 h_L'/D as a function of the holdup ε_L and the gas Reynolds number Re_G^{+} for results from the low pressure rig and the WASP rig at atmospheric pressure

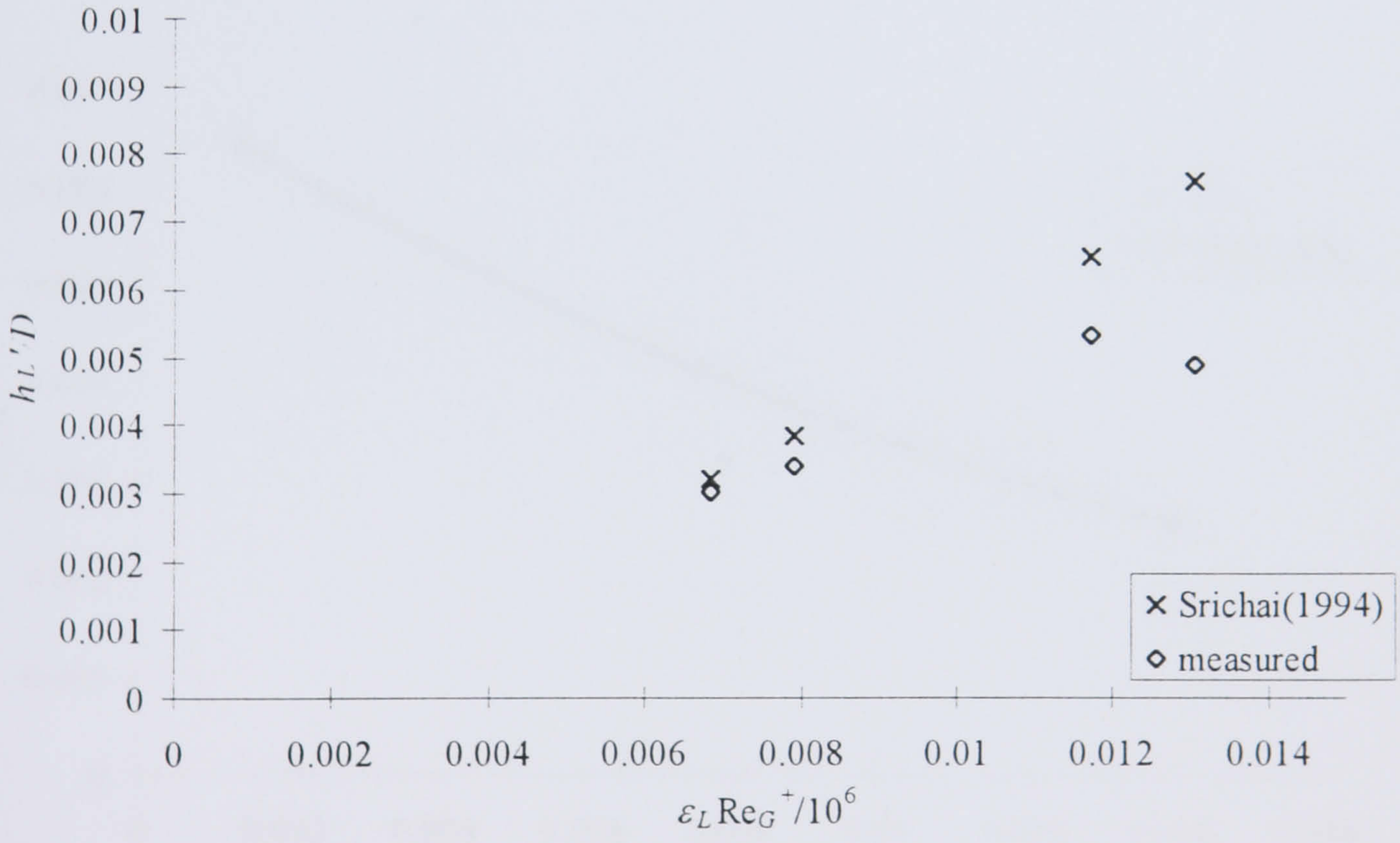


Figure 4.48 h_L'/D as a function of the holdup ε_L and the gas Reynolds number Re_G^{+} for results from the WASP rig at 6 bar

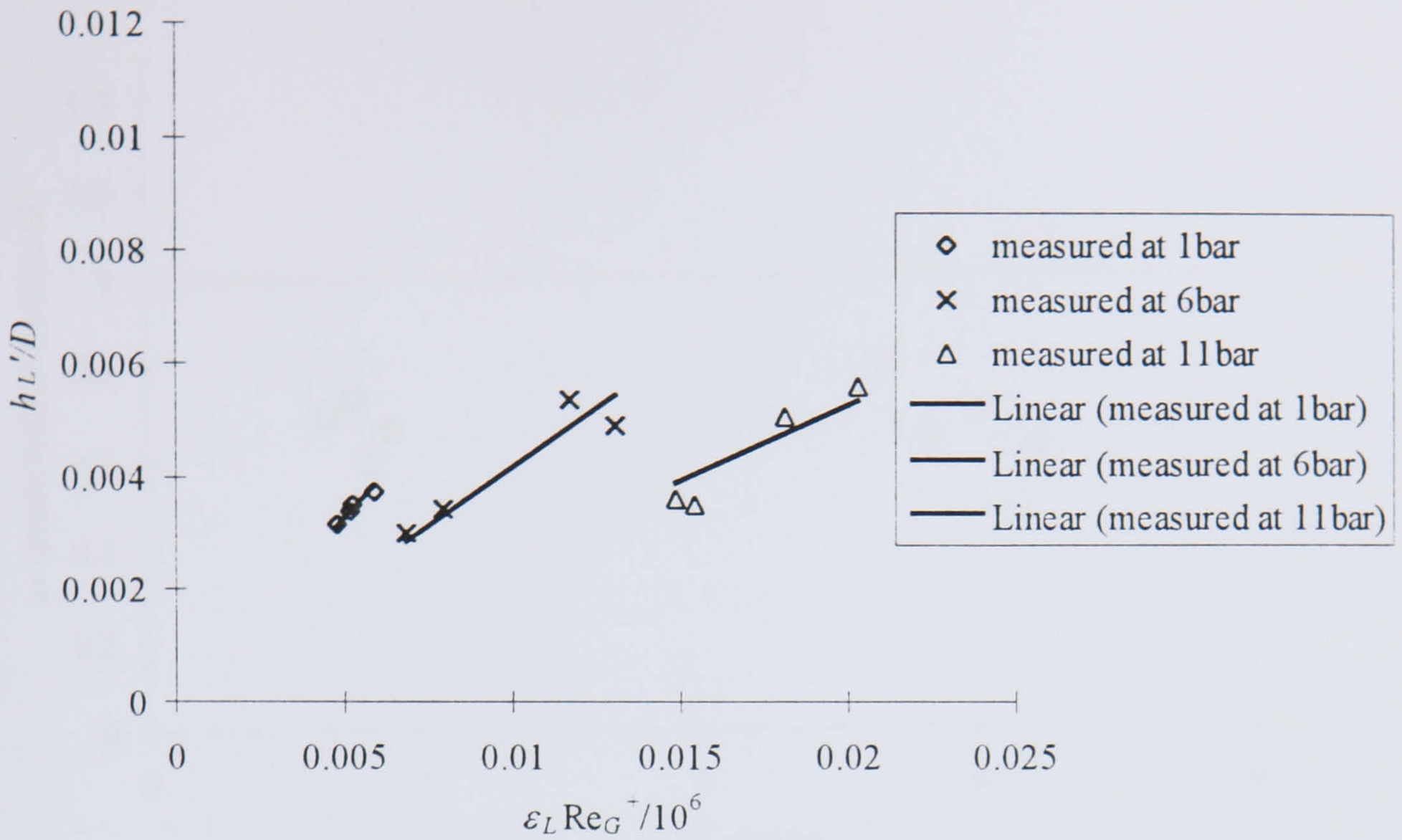


Figure 4.49 h_L'/D as a function of the holdup ε_L and the gas Reynolds number Re_G^{+} for results from the WASP rig at 1 bar, 6 bar and 11 bar

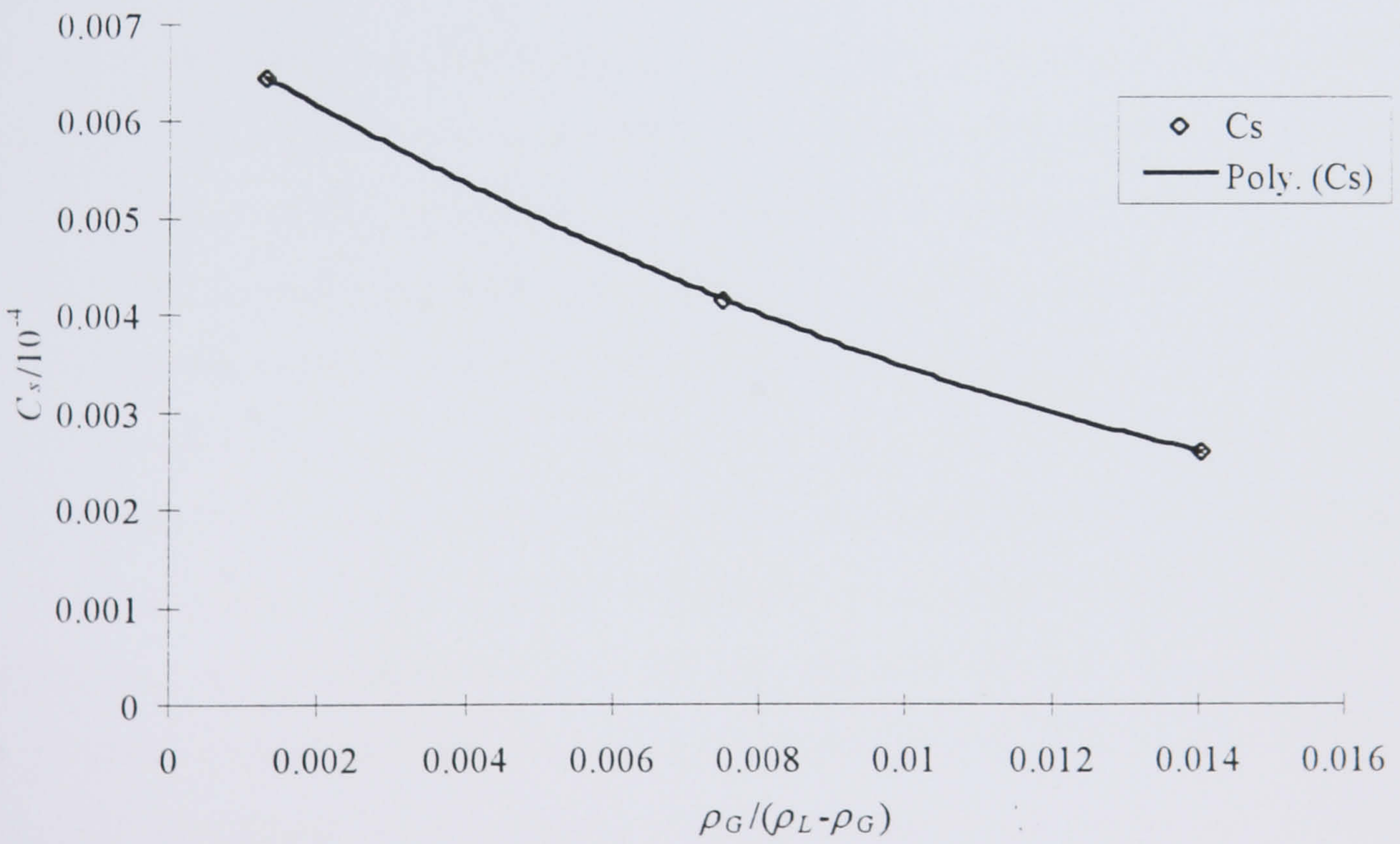


Figure 4.50 Variation of parameter C_s against density ratio ($\rho_G/(\rho_L-\rho_G)$) on WASP

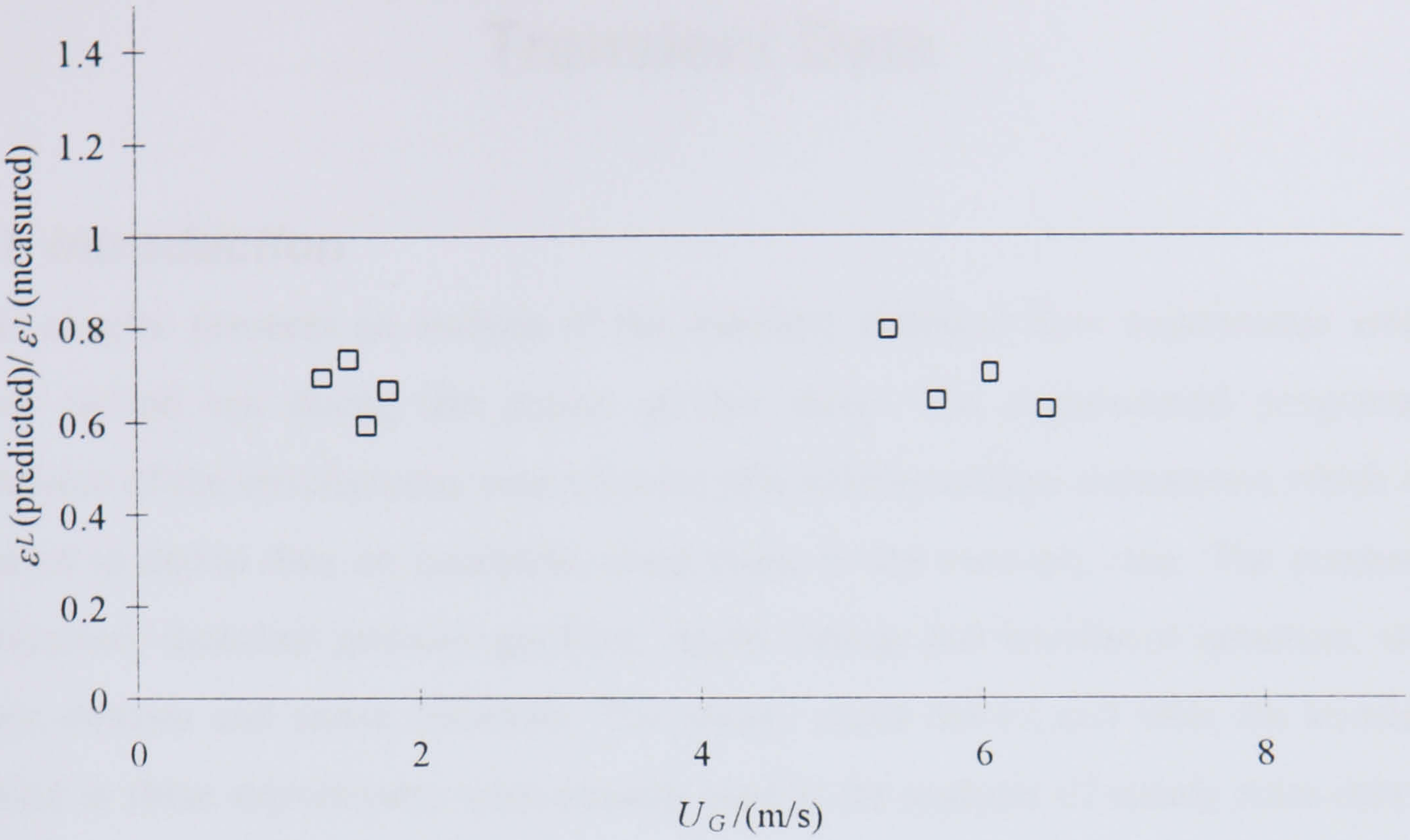


Figure 4.51 Comparison of liquid holdup calculated with modified PRESBAL with experimental data from the WASP rig

Chapter 5

Transient Data

5.1 Introduction

This chapter presents an analysis of the transient stratified flow experiments which were carried out during the course of this study. The experimental programme consisted of the simultaneous measurement of a number of flow parameters which are needed to derive data on interfacial shear stress in the transient case. The measured parameters included pressure gradient, liquid holdup and interfacial structure, wall shear stresses and phase velocities. The steady states before and after the transient period in these experiments were already used in the analysis of steady state data in Chapter 4. The current chapter focuses on the time-dependent characteristics of the transient experiments.

The measurements were carried out with the instrumentation described in detail in Chapter 3. The experiments were carried out on two flow facilities: the low pressure rig and the WASP rig which were both described in Chapter 3. In terms of practical relevance, the results from the WASP rig are probably more interesting. The WASP test section has a greater length-to-diameter ratio than the low pressure rig and it can run flows at a range of pressures whereas the low pressure rig is limited to atmospheric pressure. However, the complete set of the adopted measurement techniques only worked on the low pressure rig whereas only a few of the techniques worked on WASP.

The chapter is split into a number of subsections which follow on from the discussion of the steady state data in Chapter 4. In Section 5.2 the experimental programme carried out on both flow facilities, the low pressure rig and the WASP rig, is presented in detail. In Section 5.3 data for the measured parameters obtained on both flow facilities under various experimental conditions is presented and discussed. Section 5.4 presents an analysis of the wall shear stress during the transient period by comparing the experiment with predictions from a number of steady state models. In Section 5.5 the analysis is presented for interfacial shear stress: experimental data for interfacial shear stress is compared with predictions from a number of steady state

models. In Section 5.6 the qualitative and quantitative discussion of the interfacial structure introduced in Section 4.9 of Chapter 4 is extended to the transient case. In Section 5.7 comparisons of experiments with a number of one-dimensional transient computer codes are presented and the ability of the codes to model the transient features is discussed. The chapter ends with a section on conclusions.

5.2 Experimental Programme

The experimental matrix presented in Section 3.8 of Chapter 3 was prepared for six different sorts of transients. These could be produced from increases or decreases in the flow rate of one phase while the flow rate of the other phase was kept constant or by simultaneous increases or decreases of the flow rates of both phases. Due to time constraints the time available for the experimental programme on transient stratified flow in the present study was limited. It was therefore decided to only look at one possible type of transient. The most interesting transient was that produced by a step increase in the gas flow rate as this causes the most significant transient changes in the flow. During such transients the flow pattern can change either temporarily or permanently from stratified to slug flow, as first reported by Sakaguchi et al. (1973). In this study care was taken in producing the transients to avoid these flow pattern changes and to keep the flow stratified at all times.

Figure 5.1 schematically represents the transient experiment. Initially, a steady state flow was set up with fixed gas and liquid superficial velocities, $U_{G,1}$ and U_L. When the flow was stationary (after 5 minutes) acquisition of data from the instrumentation in the test spool was started. After a fixed time interval of 30 seconds the gas flow rate was increased to a new known value, $U_{G,2}$, while the liquid flow rate was kept constant at its initial value. The increase in the gas flow rate caused a disturbance to the flow. Gradually a new steady state flow was formed as a result of interactions between the gas and liquid phases.

Transient experiments of this type were carried out on the low pressure rig and the WASP rig and they are separately described in more detail in Sections 5.2.1 and 5.2.2. All data from the transient experiments was put onto CD ROMs which were distributed with a separate data report (Shaha & Hewitt, 1999).

5.2.1 Experimental Programme on the Low Pressure Rig

The ranges of flow rates for the initial and final steady states of the transient were obtained by comparing the flow conditions for atmospheric pressure stated in the experimental matrix of Section 3.8 with the flow conditions studied in steady state experiments on the low pressure rig, which were reported in Table 4.1 of Chapter 4. Conditions for possible transient experiments at a range of liquid flow rates, U_L=0.04, 0.06 and 0.08 m/s, and for different changes of the gas flow rate to produce the transients were tested. It was ensured that in all of the cases the flow remained stratified with no slug formation.

The conditions used for the series of transient stratified flow experiments are summarised in Table 5.5. The table lists the liquid flow rate U_L, the initial steady gas flow rate ($U_{G,1}$), the final steady gas flow rate ($U_{G,2}$) and the pressure p in the experimental runs. In the last two columns the positions of the velocity probes in the tests are entered. Four of these transient experiments were run at U_L=0.04 m/s and two each at U_L=0.06 m/s and 0.08 m/s. Each transient test was repeated three times with the velocity probes in different positions in order to apply the methods introduced in Section 3.10.2 of Chapter 3 to calculate phase average velocities in the gas and liquid phases by combining three local velocity measurements per phase. The positions for the velocity probes were determined from measurements of the liquid level in steady state experiments at the conditions of the initial and final steady states of the transient runs. It was ensured that the gas velocity probe was always placed above the gas-liquid interface and the liquid velocity probe below it. Table 5.5 shows that the gas velocity probe was traversed between the same three positions in the upper half of the test spool in all the tests whereas the positions for the liquid velocity probe were varied between the experimental conditions. The probe positions in the liquid phase were chosen to traverse the probe over most of the liquid layer, which at a combination of low gas velocity/high liquid flow rate was considerably higher than at a combination of high gas velocity/low liquid flow rate.

In each of the transient runs all of the instrumentation systems described in Chapter 3 were operated. These instruments were the conductivity probes (for measuring liquid level and interfacial structure), the pressure transmitter, the wall shear stress probes and the velocity probes. Except for the velocity probes, all other instruments were kept in the same position for all the tests. The gas wall shear stress probe was always

placed at the top of the test spool, the liquid wall shear stress probe at the bottom. As explained in Section 3.11 of Chapter 3 the measurements with the wall shear stress probe and the velocity probe in the liquid had to be normalized in order to obtain reliable data. Considering the variation of the measurements between the transient repeats the following decisions were taken for further processing of the data:

- Data for the pressure gradient and the liquid height varied less than 10 % between the repeats at given experimental condition and data for these parameters were therefore taken from the test where the velocity probes were positioned closest to the tube wall (see Table 5.5).
- Variation of the wall shear stresses in both phases was usually more than 10 % (typically 15 % in the gas phase and 20 % in the liquid phase) between the three repeats of a transient. The variation between the runs was random and no pattern such as drift in a certain direction with time was identified. The measurements in both probes were therefore averaged over the three repeats of a transient.

At the start of each experiment a steady state stratified flow was set up with the conditions stated in Table 5.5. When stationary flow conditions were obtained (after about 5 minutes) data acquisition from the instruments was started. 30 seconds after the start of the data acquisition the transient was produced by a step change of the inlet gas flow rate from a swift manual change of the valve position for the initial gas flow rate to the valve position of the final gas flow rate. Measurements were taken throughout the transient experiment. The data logging was stopped after 300 seconds from the start of the data acquisition. The frequency chosen for data logging was 500 Hz. Details of the experimental procedure of the flow rate transients on the low pressure rig are given in Appendix B.

The flow rates in both phases were very stable over the transient repeats. The water flow rates in the initial and final steady states of the three repeats of a transient experiment were identical. The variation of the gas flow rate in the initial and final steady states of the transient repeats at given experimental conditions was within +/- 1 % between the repeats as shown in Table 5.5. The water flow rate controlled with a valve on the water rotameter was kept constant during the transient. A sample trace for the gas flow rate during transient experiment `1c` is shown in Figure 5.2. The

figure shows that the gas flow rate is kept reasonably constant before and after the transient change and that the transient change is realised virtually instantaneously.

5.2.2 Experimental Programme on the WASP Rig

The evaluation of the flow rates for the transient experiments on the WASP rig was carried out similarly to their evaluation on the low pressure rig. The flow rates complied with the experimental matrix which was presented in Section 3.8 of Chapter 3. It was also necessary to ensure that, at the given conditions, the flow pattern remained stratified throughout the course of the transient. In addition to the tests on the low pressure rig the matrix of tests on the WASP facility also needed to cover a range of pressures. Preliminary transient cases were run at four different liquid velocities, U_L= 0.02, 0.04, 0.06, 0.08 m/s, and the three pressures 1, 6, 11 bar. At the higher flow rates, U_L=0.06 and 0.08 m/s slug flow occurred, sometimes only temporarily during the transient, but sometimes the slugs were preserved in the final steady state. In order to eliminate the problem of the flow pattern changes the transients were restricted to liquid flow rates of U_L=0.02 and 0.04 m/s.

The conditions used in the transient stratified flow experiments are summarised in Table 5.6. The table lists the liquid superficial velocity U_L, the initial ($U_{G,1}$) and final ($U_{G,2}$) gas superficial velocity and the pressure p used in the experimental runs. In the last two columns the positions of the velocity probes in the tests are entered. The matrix of tests covers the three pressures 1, 6 and 11 bar with two transient experiments per pressure. In the case of 1 bar and 6 bar system pressure experiments were carried at two different liquid flow rates whereas at 11 bar both experiments were run at the same liquid flow rate. The gas flow rates were much lower in the experiments at elevated pressure than at atmospheric pressure, consistent with the experimental matrix presented in Section 3.8.

Each transient test was repeated three times with the velocity probes in different positions in order to apply the methods introduced in Section 3.10.2 of Chapter 3 to calculate phase average velocities in the gas and liquid phases by combining three local velocity measurements per phase. The positions for the velocity probes were determined from measurements of the liquid level in the initial and final steady states of the preliminary transient runs on the WASP rig. It was ensured that the gas

velocity probe was always placed above the gas-liquid interface and the liquid velocity probe below it. Table 5.6 shows that the gas velocity probe was traversed between the same three positions in the upper half of the test spool in most cases. Only where the liquid holdup was very high the position closest to the interface was moved higher up in the test spool. The positions for the liquid velocity probe were varied between the different experiments. The probe positions in the liquid phase were chosen to traverse the probe over most of the liquid level, which at a combination of low gas velocity/high liquid flow rate was considerably higher than at a combination of high gas velocity/low liquid flow rate. All of the instrumentation described in Chapter 3, except for the gas wall shear stress probe, were operated in all the runs. The gas wall shear stress probe was broken during the three repeats of cases wa and wc and at these conditions, tests with the gas wall shear stress probe only were run separately as shown in Table 5.6.

An assessment of the performance of the measuring techniques on the WASP facility was given in Section 3.11 of Chapter 3. Reliable measurements were obtained with the conductivity probes (for measuring liquid level and interfacial structure) and the gas velocity probe. Measurements with the liquid velocity probe were corrected. The measurement of liquid height varied about 10 % over the three repeats at one transient condition. For further processing of the measurements data for this parameter was taken only from that repeat where the velocity probes were positioned closest to the wall (see Table 5.6).

At the start of each experiment a steady state stratified flow was set up with the conditions stated in Table 5.6. When stationary flow conditions were obtained (after about 5 minutes) data acquisition from the instruments was started. 30 seconds after the start of the data acquisition the transient was produced by a step change of the inlet gas flow rate from a swift change of the valve position for the initial gas flow rate to the position of the final gas flow rate. Measurements were taken throughout the transient experiment. The data logging was stopped after 300 seconds from the start of the data acquisition. The frequency chosen for data logging was 500 Hz. Details of the experimental procedure of the flow rate transients on the WASP rig are given in Appendix C.

The flow rates in both phases were not as stable as in the experiments on the low pressure rig. The variation of the gas flow rate in the initial and final steady states of the transient repeats at given experimental condition was within +/- 3 % between the repeats. The variation of the liquid flow rate between the repeats of a transient experiment was considerably higher, +/- 15 %. The gas and liquid flow rate traces for one transient experiment at atmospheric pressure, case wb, are shown in Figure 5.3. The fluctuations in the gas phase are larger than on the low pressure rig. The increase in the gas flow rate to produce the transient is clearly seen in the figure. It seems from the graph that the change in the gas flow rate is not as instantaneous as on the low pressure rig. But this is more a fact of the sampling frequency of the flow rates on WASP which was only 0.4 Hz. Roberts (1996) had done a test with the air flow rate being sampled at a much higher frequency than usually used on WASP and confirmed that the response of the air flow rate was close to step-like behaviour. The mean value of the liquid flow rate is stationary over the whole time but there are large fluctuations on its signal. In Figure 5.4 the flow rate traces are shown for a transient case at a pressure of 6 bar, case wd. The fluctuations on the signal for the air flow rate are smaller than in the atmospheric run on WASP but there is a periodic pattern in the trace which is not seen at atmospheric pressure. This kind of pattern is probably a result of the way in which the WASP rig operates at pressure: pressure and air flow rate in the test section are maintained by balancing the inflow of air versus its loss at the outlet. The liquid velocity shows fluctuations of similar magnitude to those observed in the atmospheric runs. But it is also clear from the figure that in this experiment the mean liquid flow rate slightly decreases as time progresses. The reason for this is as follows: for the low liquid flow rates used in this study the liquid tank was pressurised to 20 bar and this pressure was used to drive the liquid. The liquid level in the tank decreased with time and with this the pressure in the liquid tank became lower. The tanks were frequently repressurised but in the experiments at elevated pressure the decrease in pressure in the liquid tank during an experiment could still significantly affect the liquid flow rate.

5.3 Presentation of Data

In this section data for the flow parameters measured in the transient tests on the two flow facilities, the low pressure rig and the WASP rig, are presented in graphical form and discussed. The measurements on both flow facilities were taken at 500 Hz for a total of 300 seconds with the transient change (the increase in gas flow rate) being set 30 seconds after data acquisition was started. For the visual presentation in this section the collected data was reduced to 5 Hz by taking time averages over 100 consecutive data points.

Beside the directly measured parameters, such as pressure gradient and holdup, also data for the rms fluctuations of liquid height h_L', which were defined by equation (2.40), are presented. Following the presentation of steady state data in Section 4.9, the values for h_L' were determined from arithmetic averages over the measurements with the three conductivity probes in half the cross section of the test spool. The values for h_L' were calculated over sets of 100 consecutive data points which was equivalent to a duration of 0.2 seconds in the measurements at 500 Hz. An interval of 0.2 seconds had been evaluated in the steady state analysis of the results for the low pressure rig (Section 4.9.2.1) to produce reliable data for h_L'. A detailed analysis of the parameter h_L' during the transient is given in Section 5.6.

5.3.1 Data for Low Pressure Rig

The transients on the low pressure rig are determined by two system parameters: the liquid flow rate and the gas flow rate. Beside the values of the flow rates in both phases it is also the change in the gas flow rate to produce the transient which will dominate the behaviour of the flow. In order to show the influence of the flow conditions on the transient two cases from the low pressure rig are chosen for presentation. The two transient cases are labelled as case `1c` and case `1f` in Table 5.5. The flow conditions of these transients are summarised in the following table where U_L is the liquid flow rate and $U_{G,1}$ and $U_{G,2}$ are the gas flow rates of the initial and final steady states and p the system pressure.

case	U_L/(m/s)	$U_{G,1}$/(m/s)	$U_{G,2}$/(m/s)	p/bar
`1c`	0.039	7.39	8.08	0.99
`1f`	0.058	7.07	8.75	1.00

Table 5.1 Flow conditions of low pressure rig transients chosen for presentation of data

The two cases cover a similar range of gas flow rates, but the change in the gas flow rate between initial and final steady state is about the double in case `1f`. The liquid flow rate is 50 % higher in case `1f` than in case `1c`. The measured parameters are presented for both cases separately below.

5.3.1.1 Case `1c` (For conditions see Table 5.1)

The results from this case are presented in Figure 5.5 to Figure 5.11. Comments are given here for every measured parameter separately.

Pressure gradient (dp dx) (Figure 5.5): The mean value of the pressure gradient in the final steady state is higher than in the initial steady state due to the higher gas flow rate in the final steady state. There are random (turbulent) fluctuations on the steady state signal which are slightly higher in the final steady state compared to the initial steady state.

The transient change is very well discernible from the turbulent fluctuations in the initial and final steady states. When the gas flow rate is changed after 30 seconds the pressure gradient reacts instantaneously. It steeply rises to a maximum value and then gradually decreases to a new steady state above the initial steady state. From the figure the time scale of the transient change of the pressure drop is estimated to be of the order of 20-30 seconds.

The behaviour of the pressure drop during the transient can be understood by combining the results for the liquid holdup and the gas phase average velocity discussed below. The velocity in the gas phase increases without delay to the transient change to its new steady state value while the liquid holdup only gradually decreases to its final steady state value. The pressure drop in the gas phase is dominated by the flow area in the gas phase and by the gas velocity. A steep increase in the gas flow rate at a given liquid holdup leads to a steep increase in pressure drop. The pressure

drop then gradually decreases to its new steady state value due to the decrease in liquid holdup which causes an increase of the gas phase area at a given gas flow rate.

Liquid wall shear stress τ_{WL} (Figure 5.6): As a consequence of the increase in the liquid phase velocity (discussed below) the mean value of the liquid wall shear stress is higher in the final steady state than in the initial steady state. Also the fluctuations on the signal grow between the initial and final steady state.

The transient change in liquid wall shear stress is apparent from the figure. As soon as the transient change is produced the fluctuations on the signal decrease and the mean value of the parameter starts to rise gradually until the final steady state value is reached. The time interval over which the liquid wall shear stress rises is short: the final steady state is reached about 10 seconds after the transient change is set.

Gas wall shear stress τ_{WG} (Figure 5.7): The mean value of gas wall shear stress is higher in the final steady state than in the initial steady state. The fluctuations on the signal are similar in both steady states.

The transient change is obvious. As a result of the increase in the gas flow rate the gas wall shear stress instantaneously responds and increases to its value in the final steady state.

Liquid holdup ε_L (Figure 5.8): Due to the increase in gas flow rate while the liquid flow rate is maintained the liquid holdup is reduced by about 10 % in the final steady state. The fluctuations in the steady states before and after the transient are about the same. A more detailed discussion of the fluctuations of the liquid height is presented in terms of rms fluctuations h_L' below.

When the transient change is produced after 30 seconds the mean liquid holdup doesn't immediately change. Only the fluctuations of liquid holdup slightly increase. A few seconds after the transient change the mean liquid holdup starts to gradually decrease to a new value below the initial steady state. From the figure the time scale of the transient change of liquid holdup is estimated to be of the order of 30 seconds. The behaviour of the liquid holdup is a consequence of the transient change in the gas flow. An increase in gas flow accelerates the liquid already in the channel. This results

in higher fluctuations of liquid holdup but the holdup remains the same until this initial liquid passes out of the channel. The combination of a new, higher gas flow rate with the same liquid flow rate as in the initial steady state results finally in a decrease in holdup. However, the response in holdup is slower than that of the liquid velocity (see below).

Liquid phase average velocity u_L (Figure 5.9): The mean value of the liquid velocity is higher in the final steady state than in the initial steady state but the fluctuations are about the same in both steady states.

The transient change of liquid velocity can be very well seen from the figure. The liquid velocity immediately begins to respond to the sudden change in the gas flow rate. The fluctuations on the signal decrease and the velocity gradually increases to its new steady state value. The time for the transient change is estimated from the figure to be about 10 seconds.

The response of the liquid velocity is a direct consequence of the sudden increase in gas flow rate. As soon as the gas flow rate is changed the liquid is accelerated. However, the time scale of the transient change in the liquid phase is slower than in the gas. The liquid needs time to respond as the increased drag from the gas is only transmitted gradually through the liquid phase.

Gas phase average velocity u_G (Figure 5.10): The fluctuations of the gas velocity are similar in the steady states before and after the transient. The transient change is apparent. When the gas flow rate is changed the gas phase velocity instantaneously responds and increases to its value in the final steady state.

Fluctuations of liquid height h_L' (Figure 5.11): Large random variations are seen in the value of h_L', the rms variation of liquid height measured over 100 successive samples at 500 Hz. These variations are quantitatively similar to the mean values of the signal. In this example the mean values of h_L' are about the same in the steady states before and after the transient although the gas flow rate is higher after the transient. However, the dependence of h_L' on the gas flow rate was established in the discussion of steady state data in Section 4.9 of Chapter 4. The graph does not show a transient behaviour which is clearly different from that in the steady states.

5.3.1.2 Case 1f (For conditions see Table 5.1)

The results from this case are presented in Figure 5.12 to Figure 5.18. The responses in this case are quantitatively different from case 1c, where the liquid flow rate was lower and the range over which the gas flow rate was increased in the transient was smaller. However, much of the qualitative description given above for case 1c is true and the description in this section concentrates on the differences between the two cases.

For the measurements of pressure gradient, liquid wall shear stress and liquid velocity no changes occurred to the qualitative behaviour described for case 1c. All other parameters are discussed here.

Gas wall shear stress τ_{WG} (Figure 5.14): As found in the previous case the gas wall shear stress responds instantaneously to the change in the gas flow rate. Unlike in the description for case 1c, the final steady state value is not reached immediately after the change in the gas flow rate. A slight "overshoot" is observed in the signal: for a period of about 10 seconds after the transient is set the wall shear stress has a value which is about 10 % higher than the final steady state value. This is the same kind of behaviour that is observed for the gas phase velocity. A description of the feature is given in the discussion of the data for gas velocity below.

Liquid holdup ε_L (Figure 5.15): In case 1c described above an instantaneous response of the liquid holdup caused by the transient change is seen as an increase in holdup fluctuations. The observations for case 1f are different. There is no immediate effect from the transient. The holdup fluctuations increase after about 5 seconds. However, the reduction of the mean holdup caused by the higher gas flow rate then also begins to happen much more quickly than in case 1c: within about 5 seconds the holdup is reduced from its value in the initial steady state to the value in the final steady state.

Gas phase average velocity u_G (Figure 5.17): As observed in case 1c, the response of the gas phase velocity is instantaneous to the change in the gas flow rate. However, a

new feature is seen in the graph which was also observed for the gas wall shear stress. The final steady state value is not reached immediately after the change in the gas flow rate. A slight "overshoot" is observed in the signal: for a period of about 10 seconds after the transient is set the gas velocity has a value which is a few percent higher than the final steady state value. This can be understood from the discussion of the liquid holdup given above. The gas phase velocity, which is linked with holdup and gas flow rate through equation (3.30), rises to a maximum after the transient change as long as the liquid holdup is maintained at its initial steady state value. Then the gas velocity decreases slightly while the liquid holdup adjusts to its final steady state.

Fluctuations of liquid height h_L' (Figure 5.18): In contrast to case `1c` the behaviour of h_L' is clearly different in the initial and final steady states. The random variations on the trace are considerably lower in the final steady state than in the initial steady state. In the transient period a transition is seen from the large variations of h_L' in the initial steady state to the smaller variations in the final steady state. Also, the mean value of h_L' seems to slightly increase during the transient before it decreases again to reach the final steady state.

5.3.2 Data for WASP Rig

The transients on the WASP facility are characterized by three system parameters: the liquid flow rate, the gas flow rate and the pressure. Out of the six transient cases run on WASP, two for different pressures are chosen for presentation of the data. These are the transient cases `wb` and `wd` listed in Table 5.6. The flow conditions of these transients are summarised in the following table where U_L is the liquid flow rate and $U_{G,1}$ and $U_{G,2}$ are the gas flow rates of the initial and final steady states and p the system pressure.

Case	U_L/(m/s)	$U_{G,1}$/(m/s)	$U_{G,2}$/(m/s)	p/bar
wb	0.037	5.33	6.07	1.06
wd	0.032	1.30	1.62	6.03

Table 5.2 Flow conditions of WASP rig transients chosen for presentation of data

Case wb was run at atmospheric pressure, case wd at 6 bar. The liquid flow rates are similar in both cases, but the gas flow rates and their transient changes were much lower in all runs at elevated pressure than in the atmospheric runs.

As noted in Section 5.2 not all measurements were reliable on WASP. The presentation of the transients of WASP therefore only includes liquid holdup, phase average velocities in gas and liquid and liquid level fluctuations. This data is presented for both cases wb and wd separately below.

5.3.2.1 Case wb: 1.06 bar (For conditions see Table 5.2)

The results from this case are presented in Figure 5.19 to Figure 5.22. The results in each of the figures are discussed separately here.

Liquid holdup ε_L (Figure 5.19): The increase in gas flow rate during the transient results in only a marginal overall decrease of the holdup in the final steady state compared to the holdup in the initial steady state. The short term fluctuations in the signal are of similar magnitude in both steady states, but there is a distinct difference between the initial and the final steady state. The mean value in the initial steady state is stationary whereas there is a periodic behaviour in the holdup trace in the final steady state. Since (in contrast to the high pressure cases - see Figure 5.3) there was no periodic pattern in the gas flow rate, the periodic variation in the liquid holdup in the final steady state represents a physical effect associated with the transient. This is supported by the fact that the holdup at the end of the data collection is only very slightly smaller than the holdup of the initial steady state.

The response to the change in the air flow rate to produce the transient is very noticeable and clearly different from what was observed in the cases for the low pressure rig. In contrast to the observations on the low pressure rig, the fluctuations of the holdup seem to be unaffected first, they only slightly grow as time advances. The mean liquid holdup nearly instantaneously responds to the change in the gas flow rate. Instead of decreasing immediately the holdup first rises to a value which is about 10 % higher than in the initial steady state. It then slightly decreases, then forms a second peak, until it gradually drops down to reach final steady state. The time

interval over which this liquid surge is seen is quite long: it happens over about 110 seconds after the gas flow rate is changed.

A possible explanation for the transient behaviour is as follows. In the initial steady state the two phases are in hydrodynamic equilibrium. When the gas flow rate is increased the gas accelerates the liquid which results in an overall reduction of holdup in the final steady state where the gas phase which flows faster than in the initial steady state is in equilibrium with the original water flow rate. The decrease in holdup is reached by discharging the excess liquid from the pipe which is seen as a large liquid surge in the liquid holdup trace.

Liquid phase average velocity u_L (Figure 5.20): The mean value of the liquid velocity is higher in the final steady state than in the initial steady state but the fluctuations are similar in both steady states.

The transient change of liquid velocity is clearly seen from the figure. The liquid velocity rapidly responds to the sudden change in the gas flow rate. The fluctuations on the signal decrease and the velocity gradually increases to a maximum value which is little higher than the final steady state value. The time interval over which the liquid velocity changes is much shorter than for the liquid holdup, only about 20 seconds.

The response of the liquid velocity is a direct consequence of the sudden increase in gas flow rate. As soon as the gas flow rate is changed the liquid is accelerated. However, the time scale of the transient change in the liquid phase is slower than in the gas. The liquid needs time to respond as the increased drag from the gas is only transmitted gradually through the liquid phase.

Gas phase average velocity u_G (Figure 5.21): The fluctuations of the gas velocity are similar in the steady states before and after the transient. The transient change is apparent. When the gas flow rate is changed the gas phase velocity responds virtually instantaneously in increasing to its value in the final steady state.

Fluctuations of liquid height h_L' (Figure 5.22): The variations in the signal for h_L' are much smaller than on the low pressure rig. For this WASP test, the mean values are similar in the initial and final steady states. In contrast to the results on the low pressure rig the trace for h_L' for WASP shows much clearer transient features. The

behavior of h_L' during the transient is qualitatively similar to that of the liquid holdup. Immediately after the gas flow rate is increased the liquid level fluctuations increase gradually until a peak is reached. The fluctuations then slightly decrease and then start to grow again until a second peak is reached which is lower than the first peak. Afterwards, the fluctuations decrease to a new steady value. The time scale over which the transient behaviour is seen is similar to that in the holdup trace, ~ 100 seconds.

5.3.2.2 Case wd: 6.03 bar (For conditions see Table 5.2)

The results from this case are presented in Figure 5.23 to Figure 5.26. The results in each of the figures are discussed separately here.

Liquid holdup ε_L (Figure 5.23): Due to the increase in gas flow rate, the liquid holdup in the final steady state is clearly lower than in the initial steady state. The high frequency fluctuations are small during the course of the transient. A small but significant periodic feature is observed in the steady state where the holdup slightly grows and drops in cycles of uniform duration. The periodic behaviour stems from the gas flow rate at pressure which was shown in Figure 5.4 and which was believed to be a result of the operations of the rig control system in maintaining rig pressure and flow rate during the experiment.

The behaviour of liquid holdup during the transient is clearly different from the steady states. As the gas flow rate and its change in the transient are much smaller than in the experiment at atmospheric pressure the flow responds with some delay to the transient change. About 5 seconds after the transient is initiated the holdup increases by about 3 %, then slightly drops and then reaches a peak which is nearly 10 % above the initial steady state value. From then on the holdup reduces to its final steady state value. The time over which the transient effects take place is longer than in the atmosheric run, about 150 seconds. A possible explanation for the qualitative features of the holdup trace was presented for case wb of WASP.

Liquid phase average velocity u_L (Figure 5.24): The mean value and the fluctuations of the liquid velocity are higher in the final steady state than in the initial steady state.

As in the case of holdup, a small but significant periodic feature is observed in the steady state where the velocity grows and drops in cycles of uniform duration.
The response of the liquid velocity to the transient is quicker than for the holdup. The liquid velocity steeply rises to a maximum which is only slightly above the mean value in the final steady state. The duration over which the velocity shows a behaviour which is clearly different from steady state is about 60 seconds. The whole transient period is superimposed with the same kind of periodic behaviour which is observed in the steady state and the reason for this was discussed in the presentation of the liquid holdup above.

Gas phase average velocity u_G (Figure 5.25): Due to the increase in the gas flow rate the mean values of the gas velocity are higher in the final steady state than in the initial steady state. The high frequency fluctuations are about the same throughout the transient. A periodic feature is observed for the whole trace of the collected data which is observed in the traces of the other parameters at pressure.
There is a clear transient change. When the gas flow rate is changed the gas phase velocity rapidly responds and increases to its value in the final steady state.

Fluctuations of liquid height h_L' (Figure 5.26): As for case wb of WASP the variations in the signal for h_L' are much smaller than on the low pressure rig. During the transient, the mean value of h_L' slightly decreases. As shown for case wb the curve for h_L' during the transient relates to the liquid holdup measurement in the case presented here, but the transient features are only weakly expressed. The time scale over which the transient behaviour is apparent is shorter to that in the holdup trace, i.e. about 100 seconds.

5.3.3 Discussion of Data

Data was presented for two transient cases from the low pressure facility: cases `1c` and `1f` from Table 5.1. In the latter the liquid flow rate was higher and the transient change in the gas flow rate larger. The following features were observed in both cases:

- All the measured parameters showed clear transient features. The response in the gas phase was quicker than in the liquid phase. The slowest changes were observed for holdup. The time scales of the transient changes were similar in both cases investigated.
- The fluctuations in holdup were slightly increased during the transient which was followed by a decrease in the mean holdup to final steady state.

The main difference between the two cases was, in case `1f`, the occurrence of a maximum value in the signals of the gas velocity and gas wall shear stress during the transient which was higher than the final steady state value.

For the WASP rig results for two transients, case wb at a pressure of 1 bar and case wd at a pressure of 6 bar, were presented. The conditions of these runs are collected in Table 5.2. The liquid flow rates were similar in both cases, but the gas pressure was higher and the gas flow rates and the transient change in the gas flow rate were much lower in case wd. The following features were observed in both cases:

- There was a clear increase of the liquid holdup during the transient before the final steady state holdup was reached. Possibly due to the longer test section, the transient period was much longer than on the low pressure rig.
- There were also clear transient changes in the liquid level fluctuations which were qualitatively related to the behaviour of liquid holdup.

The main difference between the two cases was that, possibly due to the lower gas flow rates, the transient changes were slower in case wd. In runs at pressure, a small but significant periodic behaviour in the signals of all parameters was observed which stemmed from the operation of the WASP rig control system.

This is the first time that such comprehensive measurements have been presented for transient stratified flow. The measurements reported in the open literature for this flow regime only include a few of the parameters measured here. Roberts (1996) only presented measurements of the liquid level whereas King et al. (1997) also included pressure and pressure gradient. Sakaguchi et al. (1973) and Sakaguchi et al. (1981) also reported measurements of the local gas and liquid velocities.

The literature so far has dealt with all classes of possible transients, produced by increases or decreases in either flow rate. The cases presented for increases in the air flow rate often resulted in a period of slugging (Sarica et al., 1996; King et al., 1997) whereas the tests in the present study were restricted to transients without flow pattern change.

For a transient stratified flow with no flow pattern change produced from an increase in the gas flow rate Sakaguchi et al. (1973) showed a peak during the transient period in the measurements of liquid holdup, gas and liquid velocities. As reported above an increase in the liquid holdup during the transient was also found in the transient cases presented in this study, especially in the WASP transients. The peaks in the gas and liquid velocities, if there were any at all, were not so pronounced.

For measurements in a 32 mm acrylic test section Roberts (1996) presented transient data following an increase in gas flow rate where the flow pattern changed from initially smooth to stratified wavy flow. During the transient the holdup fluctuations increased and then the mean holdup decreased to its value in the final steady state. This is in agreement with the observations of the present study in the transient cases on the low pressure rig.

King et al. (1997) presented data for an increasing gas flow rate transient on the WASP facility where two short temporary slugs appeared. If the slugs are ignored, their plot of liquid holdup for the transient agrees qualitatively with the cases from WASP studied in the present project where the liquid holdup was observed to increase during the transient period for some time and then decrease to its value in the final steady state.

5.4 Wall Shear Stress

Reliable measurements of the wall shear stress were obtained on the low pressure rig only. Of the two measured shear stresses, the one in the gas and the one in the liquid, the gas wall shear stress was the more trustworthy. This was also the shear stress from which interfacial friction was evaluated during the transient (Section 5.5). An analysis of the gas wall shear stress measured on the low pressure rig is presented here.

The analysis is carried out in terms of the gas wall friction factor and the results are compared with predictions from published models for steady state. The analysis is presented for the two transient cases `1c` and `1f`, which had also been used in the discussion of the measured parameters in Section 5.3.1. The conditions for these runs were listed in Table 5.1 and are repeated here.

Case	U_L/(m/s)	$U_{G,1}$/(m/s)	$U_{G,2}$/(m/s)	p/bar
`1c`	0.039	7.39	8.08	0.99
`1f`	0.058	7.07	8.75	1.00

Table 5.1 Flow conditions of low pressure rig transients chosen for analysis

For each point of time in the transient the experimental gas wall friction factor f_G was derived from the measurements of the gas wall shear stress τ_{wG} and the gas phase average velocity u_G using equation (4.7).

The calculations were done for averages of the 500 Hz data sampled in the transient experiments. The averaging consisted of taking time averages of each of the measured parameters required in the calculations over 100 consecutive data points, which reduced the frequency of the data down to 5 Hz.

As the result for case `1c` shows (Figure 5.27) there were large fluctuations in the signal which made it difficult to see the transient features. The experimental values for f_G were therefore further averaged by taking rolling averages over two data points before and after each data point. This removed high frequency fluctuations as shown in Figure 5.28. Also shown in this figure are the predictions from the same three models which had been used in the analysis of the steady state data for f_G (see Section 4.7.2). The three models were that by Taitel & Dukler (1976), Eck (1973) and Espedal (1998). The input values for the interfacial friction factor f_i in Espedal's model were calculated from the Spedding & Hand (1997) relationship which was found to best predict the steady state data for f_i.

Figure 5.28 shows that the fluctuations in the model predictions are considerably smaller than in the experiment. The figure makes clear that all three models underpredict the experimental data for f_G for the whole period of time. In the analysis of the steady state data in Section 4.7.2 the differences between the experiment and the Eck and the Espedal model were found to be insignificant compared to the experimental error whereas the Taitel & Dukler model significantly underpredicted

the measurement. All models show a distinct and instantaneous reduction in the value of f_G when the transient change happens, but the drop is only about 3 % of the absolute value of the initial steady state. A clear, but small reduction in the value for f_G is also seen in the experimental trace.

The same comparison between experiment and models is shown in Figure 5.29 for case `1f`. The results are qualitatively very similar to those presented for case `1c`. But the reduction of f_G during the transient in the experiment and in the models is more pronounced than in case `1c`. The reason for the larger reduction is the bigger change in the gas flow rate in transient case `1f`. There is one feature in the prediction by Espedal in case `1f` which was not seen in `1c`. Immediately after the transient is initiated, the gas wall friction factor f_G drops to a minimum but then slightly increases before it reaches final steady state. The increase after the transient stems from the influence of the interfacial friction factor in Espedal's model. However, a clear increase in the value of f_G above that for the final steady state is not seen in the experiment.

The evaluation of the gas wall shear stress data in the transient showed that the transient features observed in the experiment are adequately predicted by steady state models.

5.5 Interfacial Shear Stress

The most reliable measurements in this study were obtained in the gas phase on the low pressure rig. This data was used to derive interfacial shear stress for the transient case.

Experimental data for interfacial friction was derived from the gas mass continuity and gas momentum conservation, equations (2.51) and (2.53) in Chapter 2. The gas mass continuity equation was modified to extract an expression for the axial gradient of the gas phase velocity u_G:

$$\frac{\partial u_G}{\partial x} = -\frac{1}{S_G}\left(u_G \frac{\partial S_G}{\partial x} + \frac{\partial S_G}{\partial t}\right) \tag{5.1}$$

where S_G is the gas flow cross sectional area defined by equation (2.10). Using this expression for $\partial u_G / \partial x$ with the gas momentum equation (2.53) the following term was obtained for interfacial shear stress τ_i:

$$\tau_i = -\frac{1}{P_i}\left[\rho_G\left(S_G\frac{\partial u_G}{\partial t} - u_G\frac{\partial S_G}{\partial t} - u_G^2\frac{\partial S_G}{\partial x}\right) + S_G\frac{\partial p_G}{\partial x} + \tau_{WG}P_G\right] \quad (5.2)$$

where all higher order terms in the derivatives were now eliminated. In this equation P_i and P_G are the perimeters of the interface and of the gas phase, $\partial p_G/\partial x$ is the pressure gradient in the gas phase and τ_{WG} the gas wall shear stress. Derivatives of the gas phase area S_G with respect to time t, $\partial S_G/\partial t$, and location x, $\partial S_G/\partial x$, were modified into derivatives of the liquid height h_L using equation (4.4) in Chapter 4 for S_G' which then resulted in:

$$\tau_i = -\frac{1}{P_i}\left[\rho_G\left(S_G\frac{\partial u_G}{\partial t} - u_G S_G'\frac{\partial h_L}{\partial t} - u_G^2 S_G'\frac{\partial h_L}{\partial x}\right) + S_G\frac{\partial p_G}{\partial x} + \tau_{WG}P_G\right] \quad (5.3)$$

The axial derivative of the liquid height was eliminated using the following conservation:

$$dh_L = \frac{\partial h_L}{\partial x}dx + \frac{\partial h_L}{\partial t}dt = 0 \quad (5.4)$$

which resulted in the following expression:

$$\frac{\partial h_L}{\partial x} = -\frac{1}{u_c}\frac{\partial h_L}{\partial t} \quad (5.5)$$

where

$$u_c = \frac{dx}{dt} \quad (5.6)$$

is the wave celerity which is found from the dominant peak in the cross correlation of the holdup measurements in the test spool and downstream of it. Equation (5.5) for the spatial variation of the film thickness is identical with the expression which Kang & Kim (1992) used under the assumption that the wave was frozen in shape and that the average wave celerity u_c was constant.

By introducing equation (5.5) in (5.3) the following expression for interfacial shear stress was obtained:

$$\tau_i = -\frac{1}{P_i}\left[\rho_G\left(S_G\frac{\partial u_G}{\partial t} + u_G S_G'\frac{\partial h_L}{\partial t}\left(\frac{u_G}{u_c} - 1\right)\right) + S_G\frac{\partial p_G}{\partial x} + \tau_{WG}P_G\right] \quad (5.7)$$

For each point of time the interfacial shear stress τ_i was calculated from equation (5.7) and the interfacial friction factor f_i was calculated from τ_i using equation (4.10) in Chapter 4.

The calculations were done for averages of the 500 Hz data sampled in the transient experiments. The averaging consisted of taking time averages of each of the measured parameters over 100 consecutive data points, which reduced the frequency of the data down to 5 Hz.

The analysis is presented for the two transient cases `1c` and `1f`, which were also used in the discussion of the gas wall friction factor. The conditions for these runs were listed in Table 5.1 and are repeated here.

Case	U_L/(m/s)	$U_{G,1}$/(m/s)	$U_{G,2}$/(m/s)	p/bar
`1c`	0.039	7.39	8.08	0.99
`1f`	0.058	7.07	8.75	1.00

Table 5.1 Flow conditions of low pressure rig transients chosen for analysis

As the result for case `1c` shows (Figure 5.30) there were large fluctuations in the signal which could instantaneously go negative and made it difficult to see the transient features. The reason for the negative values of f_i could be due to the limits of the one-dimensional model to represent the complex two-phase system. The experimental values for f_i were further averaged by taking rolling averages over two data points before and after each data point. This removed high frequency fluctuations as shown in Figure 5.31. In this figure also the predictions from the same four models are plotted which had been used in the analysis of the steady state data for f_i (see Section 4.8). These models were that by Taitel & Dukler (1976), Andritsos & Hanratty (1987), Srichai (1994) and Spedding & Hand (1997). Additionally, the predictions from the new steady state model (labelled "new steady state model" in the figure) developed from the analysis of the interfacial structure in Section 4.9.2.1 are plotted.

Figure 5.31 clearly shows that the fluctuations in the model predictions are much smaller than those in the experimental trace throughout the transient. In the experimental data, the mean value of f_i appears to be invariable with time, but there is a notable increase in the fluctuations of f_i when the transient change is made. The increased fluctuations only cover a time interval of a few seconds. As noted in the discussion of the steady state data for f_i, there are large discrepancies between the models themselves and between the models and the experiment. Reasonable predictions of the steady state and transient experimental data are found with

Andritsos & Hanratty, Spedding & Hand and the new model developed in this study. These three models predict a clear increase in the value of f_i during the transient, which in the case of the Andritsos & Hanratty and the Spedding & Hand models is conserved in the final steady state. The time scale of the transient change predicted with the three models appears to be longer than the transient time scale seen in the experiment. The models by Taitel & Dukler and by Srichai, which do not predict the steady state experimental data well, also show hardly any variation throughout the transient.

The difference between experiment and model is better represented in terms of error against time where the error is defined as:

$$\text{error}(f_i) = \frac{f_i(\text{predicted}) - f_i(\text{measured})}{f_i(\text{measured})} \qquad (5.8)$$

The error between the measurement and predictions from the new steady state model developed in this study is shown in Figure 5.32. The graph shows that the error is about the same during initial and final steady state. There are large fluctuations in the plot which stem from the large fluctuations in the experimental data. When the transient change happens the error clearly increases for a very short time.

The comparisons of the models with the experiment for case `1f` are shown in Figure 5.33. The experimental data are again obtained from rolling averages over two data points before and after each data point. In the experimental data the mean value of f_i is higher in the final steady state. The increase in the mean value of f_i is reached after a transient period where the fluctuations of f_i are clearly bigger than in the steady state. The transient period appears to be slightly longer than in case `1c`. As in case `1c`, the Andritsos & Hanratty, the Spedding & Hand and the new steady state model yield the best predictions. All three models predict clear transient changes. The largest increase between initial and final steady state is shown by the Andritsos & Hanratty model. The transient time scale in the model predictions is similar to that from the experiment.

The error between the measurement and predictions from the new steady state model developed in this study was calculated for case `1f` using equation (5.8) and is shown in Figure 5.34. The error in the final steady state is lower than in the initial steady state. There is a transient period about 10 seconds long where the fluctuations

increase by a factor of eight. The increase in fluctuations during the transient is bigger than observed in case `1c` and this can be attributed to the bigger change in the gas flow rate in transient case `1f`.

The discussion of the data for the interfacial friction factor revealed that the discrepancy between the experiment and the predictions from steady state models increased significantly for a short while during the transient period. It is assumed that the time of increased error between model and experiment is longer for a test section with greater length than that of the low pressure rig. From these comparisons it is concluded that the steady state models do not predict the transient features sufficiently well and that an improvement of the models is necessary with regard to the transient. An improvement of the models is not possible with the limited data set in this study. A substantial improvement of the models would require experimental data for a wider range of experimental conditions.

5.6 Interfacial Structure

Examination of the structure of the gas-liquid interface is central in understanding the phase interactions in stratified flow. In Section 4.9 of Chapter 4, investigations of the behaviour of the interface under steady state conditions were reported; both qualitative and quantitative aspects were discussed. The presentation of data for interfacial structure under transient conditions follows the same structure as in the steady state section. In a first part the development of the interface during the transient is described qualitatively and in a second part the quantitative behaviour is discussed with regard to predictions from the models for the interfacial fluctuations developed in Section 4.9.

5.6.1 Qualitative Discussion

The qualitative aspects of the interfacial behaviour are presented in the form of three-dimensional plots of the gas-liquid interface. Such plots had been presented for steady state in Section 4.9.1.1 of Chapter 4 and for transient conditions they were technically obtained in the same way as for steady state. Three-dimensional representations of the interfacial structure were produced from the simultaneous time traces of the three conductivity probes in half a cross section of the test spool, cp_ts1, cp_ts2 and cp_ts3

as represented in Figure 3.10. The locations of the probes were z=9.7, 19.4 and 29.1 mm in the lateral direction z where z=0 indicated the centre of the test spool. Data for the other half of the test spool was obtained by assuming symmetry of the measured traces with respect to the vertical plane through the centre of the tube. The figures contain instantaneous data sampled at 500 Hz and the measured data points are connected with straight lines.

Sample results are presented for the two transient cases which were used to compare the interfacial structure from an experiment on the low pressure rig with an experiment on the WASP rig under similar conditions in steady state (see Section 4.9.1.1.1 in Chapter 4). The two experimental cases were transient case `1a` from the low pressure rig and transient case `wb` from the WASP rig. The conditions of these cases are collected in the table below:

case	U_L/(m/s)	$U_{G,1}$/(m/s)	$U_{G,2}$/(m/s)	p/bar
`1a`	0.039	5.01	6.46	1.00
`wb`	0.037	5.33	6.07	1.06

Table 5.3 Experimental conditions for transient cases `1a` and `wb`

The results for case `1a` from the low pressure rig for different times around the transient are shown in Figure 5.35 to Figure 5.38. Figure 5.35 is the same plot which was presented in Chapter 4. It shows the interfacial structure during initial steady state. Here, the interface is covered with small amplitude waves. The wave pattern is slightly irregular; the amplitude of the waves is non-uniform in axial direction but it doesn't change in the transverse direction. The amplitude of the waves is around 2 mm. The interface is slightly curved in a cross section with the liquid height increasing towards the wall. An effect from the transient is observed about 0.5 seconds after the change in the gas flow rate as shown in Figure 5.36. The amplitude of the waves starts to grow moderately. In the time interval of 1.8 to 2.4 seconds after the transient change (Figure 5.37) the transient effects are clearly seen. Large waves with amplitudes up to about 5 mm dominate the interfacial structure. The amplitude and frequency of these waves is irregular. The large amplitude waves are separated from each other by an arbitrary number of small amplitude waves. The mean liquid height is still around what it was before the transient. Some 30 seconds after the transient change much of the increased interfacial activity has disappeared (Figure 5.38). The

structure is dominated by long troughs which alternate with small amplitude waves. The frequency between the waves is much smaller than what it was in the initial steady state and the mean liquid height is reduced considerably indicating that the flow is reaching equilibrium at the new combination of gas and liquid flow rate in the final steady state.

The results for case wb from the WASP rig for different times around the transient are shown in Figure 5.39 to Figure 5.41. Figure 5.39 shows the interfacial structure during initial steady state and was already presented in Chapter 4. The interface is covered with small amplitude waves. Their amplitudes are around 1 mm. The structure of the interface appears slightly irregular as the amplitude of the waves varies in the axial direction. The liquid height in a cross section is uniform. In contrast to the transient run presented for the low pressure rig the effect of the transient on the interfacial structure is not obvious. 5 seconds after the transient change (Figure 5.40) the interface appears to be the same what it was before the transient. Also the liquid level is unchanged. After another 10 seconds (Figure 5.41) the interfacial structure still has the same features of the initial steady state but the liquid level is increased. The increase in the liquid level after the transient has already been discussed in Section 5.3.2.1 where the measured parameters for case wb were presented (see Figure 5.19). Overall, from the presentation of data for interfacial structure in Figure 5.39 to Figure 5.41, it is clear that its change during the transient is not obvious for the case from WASP.

5.6.2 Quantitative Discussion

Transient data for the fluctuations of liquid height h_L' were presented together with other measured parameters in Section 5.3. The values for h_L', which are defined by equation (2.40), were determined from arithmetic averages over the measurements with the three conductivity probes in half the cross section of the test spool. The values for h_L' were calculated over sets of 100 consecutive data points which was equivalent to a duration of 0.2 seconds in the measurements at 500 Hz.

In this subsection the data for h_L' obtained from measurements is compared with predictions from steady state relationships developed in Section 4.9 in the chapter on

steady state data, Chapter 4. The comparisons were made with the objective to extract the transient information from the data.

5.6.2.1 Low Pressure Rig

The analysis of data for h_L' is presented for the two transient cases `lc` and `lf`, which were also used for the presentation of the measured parameters and in the discussion of the gas wall and interfacial friction factor. The conditions for these runs were listed in Table 5.1 and are repeated here:

case	U_L/(m/s)	$U_{G,1}$/(m/s)	$U_{G,2}$/(m/s)	p/bar
`lc`	0.039	7.39	8.08	0.99
`lf`	0.058	7.07	8.75	1.00

Table 5.1 Flow conditions of low pressure rig transients chosen for analysis

Experimental data for h_L' was compared with predictions from the relationship developed in Section 4.9.2.1 from steady state data for h_L' from the low pressure rig. This model was obtained as an expression of the diameter of the test section D, the liquid holdup ε_L and the gas Reynolds number Re_G^+ defined in equation (2.37) and is repeated here:

$$h_L' = D\left[6.2153 \cdot 10^{-6}\left(\varepsilon_L \, \mathrm{Re}_G^+\right) - 0.0098\right] \qquad (4.12)$$

Predictions from this model were calculated from experimental data of the relevant parameters which were obtained from time averages over 100 consecutive data points in the measurements. The comparison of the measured data with the predictions for transient case `lc` are shown in Figure 5.42. The experimental data on their own were presented previously as Figure 5.11 and the data was discussed in 5.3.1.1. Large random variations are seen in the signal for the fluctuations of the liquid height h_l'. The graph does not show a transient behaviour which is clearly different from that in the initial steady states. The fluctuations in the model predictions (labelled "new steady state model" in Figure 5.42) are much smaller than in the experiment. The mean value in the prediction increases steeply after the transient change and then reduces to its value in the final steady state.

The difference between experiment and model is better represented in terms of error against time where the error is defined as:

$$\text{error}(h_L') = \frac{h_L'(\text{predicted}) - h_L'(\text{measured})}{h_L'(\text{measured})} \qquad (5.9)$$

In order to reduce the large fluctuations in the experimental trace for h_L' the experimental data was further averaged by taking rolling averages over two data points before and after each data point. The error between these averaged data obtained from the measurements and the predictions from the new steady state model calculated with equation (5.9) is shown in Figure 5.43. The graph shows that the error is about the same during initial and final steady state. When the transient change happens the fluctuations clearly increase by a factor of about 2 for a very short time.

The comparison of the measured data with the predictions for transient case `1f` are shown in Figure 5.44. The experimental data on their own were presented previously as Figure 5.18 and the data was discussed in 5.3.1.2. In contrast to case `1c` the behaviour of h_L' is clearly different in the initial and final steady states. The random variations on the trace are considerably lower in the final steady state than in the initial steady state. In the transient period a transition is seen from the large variations of h_L' in the initial steady state to the smaller variations in the final steady state. The mean value of h_L' slightly increases during the transient before it decreases again to reach the final steady state. The fluctuations in the model predictions (labelled "new steady state model" in Figure 5.44) are much smaller than in the experiment. The mean value in the prediction increases steeply after the transient change and then reduces to its value in the final steady state.

The difference between experiment and model is again represented in terms of error against time using equation (5.9). The large fluctuations in the experimental trace for h_L' were reduced like for case `1c` by taking rolling averages over two data points before and after each data point. The error between these averaged data obtained from the measurements and the predictions from the new steady state model is shown in Figure 5.45. The fluctuations in the error are clearly bigger in the initial than in the final steady state. The consequences from the transient change are seen as an immediate reduction in the fluctuations of the error.

The findings for the transient behaviour of h_L' presented in this subsection are different from the findings of the interfacial friction factor f_i discussed in Section 5.5. For the interfacial friction factor f_i derived from the gas phase the error between the

experiment and the predictions with the new steady state model developed in this study from analysis of the interfacial fluctuations showed a peak during the transient for both cases `lc` and `lf`. The peak was higher in the latter case where the change in the gas flow rate during the transient and the flow rate in the liquid were greater than in case `lc`. On the contrary, the error between the transient data for h_L' and the new steady state model developed in this study only showed a peak for case `lc`, but not for case `lf`. This might indicate differences in the transient behaviour in the two phases, the liquid and the gas phase.

5.6.2.2 WASP Rig

The analysis of data for h_L' is presented for the two transient cases `wb` and `wd`, which were also used for the presentation of the measured parameters. The conditions for these runs were listed in Table 5.2 and are repeated here:

Case	U_L/(m/s)	$U_{G,1}$/(m/s)	$U_{G,2}$/(m/s)	p/bar
wb	0.037	5.33	6.07	1.06
wd	0.032	1.30	1.62	6.03

Table 5.2 Flow conditions of WASP rig transients chosen for analysis

The liquid flow rates are similar in both cases. The principal differences between the two runs were the gas flow rates and the system pressure.

Experimental data for h_L' was compared with predictions from the relationship developed in Section 4.9.2.2 from steady state data for h_L' from the WASP rig. This model was obtained as an expression of the diameter of the test section D, the liquid holdup ε_L and the gas Reynolds number Re_G^+ defined in equation (2.37) and is repeated here:

$$h_L^+ = D C_s \left(\varepsilon_L \, \mathrm{Re}_G^+\right) \tag{4.15}$$

$$\text{with} \quad C_s = 9.9917 \cdot 10^{-4} \left(\frac{\rho_G}{\rho_L - \rho_G}\right)^2 - 4.558 \cdot 10^{-5} \left(\frac{\rho_G}{\rho_L - \rho_G}\right) + 7 \cdot 10^{-7} \tag{4.17}$$

Predictions from this model were calculated from experimental data of the relevant parameters which were obtained from time averages over 100 consecutive data points. The comparison of the measured data with the predictions for transient case `wb` are shown in Figure 5.46. The experimental data on their own were presented

previously as Figure 5.22 and the data was described in Section 5.3.2.1. The variations in the signal for h_L' are much smaller than on the low pressure rig. The trace for h_L' shows clear transient features. Immediately after the gas flow rate is increased h_L' increases gradually until a peak is reached. h_L' then slightly decreases and then starts to grow again until a second peak is reached which is lower than the first peak. Afterwards, h_L' decreases to a new steady value. The predictions from the new steady state model compare very well with the experimental data during the transient.

The difference between experiment and model can be quantified in terms of error against time using equation (5.9) and this is represented in Figure 5.47. The graph shows that the error increases between the initial and final steady state. The effect from the transient is seen as in increase in error which is preserved in the final steady state. The values of error during the transient are in between those of the initial and final steady state.

The comparison of the measured data with the predictions for transient case wd are shown in Figure 5.48. As for case wb of WASP, the variations in the signal for h_L' are much smaller than on the low pressure rig. During the transient the mean value of h_L' slightly increases and then decreases. In the final steady state it is slightly lower than in the initial steady state. The model predictions (labelled "new steady state model" in Figure 5.48) are significantly different from the measured data. h_L' predicted by the model sharply increases during the transient and the predicted h_L' is clearly higher in the final steady state compared to the initial steady state. The small periodic feature in the final steady state results reflects periodic changes in the variables in the model, namely liquid holdup ε_L and gas velocity u_G. These small periodic fluctuations result from operation of the WASP rig control system.

To quantify the difference between experiment and model, equation (5.9) is used. The error for h_L' is shown in Figure 5.49. The graph shows that the error increases instantaneously to its value in final steady state when the transient change is made.

Presentation of data for h_L' for the two cases wb and wd of WASP indicated that during the transient the discrepancies between the measured data and predictions from the new steady state model developed in this study are similar to the

discrepancies in steady state. In other words, in the case of the WASP experiments, the model appeared to be capturing the main features of the transient variations.

5.7 Comparisons with Code Predictions

A number of one-dimensional computer codes were used to simulate the transient experiments. The key parameter in these comparisons was the liquid holdup. In Subsection 5.7.1, simulations with the three commercial computer codes, PLAC, OLGA and TACITE are presented. In a separate subsection the experiments are compared with predictions from the transient code TRIOMPH, which was developed at Imperial College. In a third subsection the limitations of the one-dimensional model in predicting the transient features of the experiment are addressed.

5.7.1 Predictions from Commercial Codes

Results from the transient experiments were compared with predictions from the main proprietary computer codes, namely PLAC, OLGA and TACITE. The comparisons were carried out for transient case `la` from the low pressure rig and for transient case `wa` from the WASP rig. The conditions for these transients are summarised in the following table:

Case	U_L/(m/s)	$U_{G,1}$/(m/s)	$U_{G,2}$/(m/s)	p/bar
`la`	0.039	5.01	6.46	1.00
`wa`	0.023	5.68	6.45	1.07

Table 5.4 Conditions of transient experimental cases `la` and `wa`

Both transients are for atmospheric pressure. The range of gas flow rates is similar in both cases, but the liquid flow rate is smaller in the WASP case.

The simulation procedure was the same for both cases apart from the specifications of the grid. For the transient case from the low pressure rig the computational grid was set up of eight cells of 1 m length with an inner diameter of 0.07792 m. Thus the minor change of inner diameter in the experimental setup from 74 mm in the acrylic test section to 77.92 mm in the test spool was not accounted for. For the WASP case a computational grid of 36 m length with 1 m long cells of 0.07792 m inner diameter was made up. The wall roughness was set as k_{II}=4.6·10^{-5} m. In all three codes the flow rates in both phases were specified at the inlet of the pipe and the system

pressure at the outlet of the pipe. The data for the flow conditions was taken from Table 5.4. The simulations were initiated by obtaining stationary stratified flow over 5 minutes at the conditions of the initial steady state. The transient simulation was then a restart from the solution of the initial steady state. After 30 seconds from the start of the transient simulation the gas flow rate was changed in a step like increase to its value in the final steady state, and the transient simulation was left to run for a total of 300 seconds, as in the experiment.

The results from the simulations for the location in the pipe where the measurements were taken are plotted together with the experimental trace for transient case `1a` in Figure 5.50 and for transient case `wa` in Figure 5.51. The predictions from the codes are shown in the form of an area because, due to commercial security reasons, the individual codes could not be identified. In both cases the graphs exhibit the same characteristic features. All three codes underpredict the experimental values throughout the transient. The underprediction is greater in the case of the WASP experiment. A discussion of the quantitative differences between code predictions and experiment in the initial and final steady states of the transients was given in Section 4.5.2 in Chapter 4. From Figures 5.50 and 5.51 it is very noticeable that the predictions from the three codes cover a large range and this can be attributed to the different closure relationships which are used in the codes.

Concerning the features of the transient the discrepancies between the codes and the experiment are obvious. In both the transient cases (`1a` and `wa`) the codes do not show the characteristic increase in liquid holdup during the transient which is most pronounced in case `wa`, the WASP case investigated here. The time scale of the transient predicted by the codes is reasonably close to the experiment for the case from the low pressure rig, but in the case from the WASP rig the codes predict the transient change over time intervals which are considerably different between the codes themselves and also between the codes and the experiment. The experiment on the low pressure rig shows an increase in interfacial activity during the transient before the mean liquid holdup decreases. This would increase the interfacial friction above that expected from steady state relationships, causing the transient to occur more rapidly than is predicted.

The most significant discrepancy between the codes and the experiment during the transient are the liquid surges which are clearly seen in the experiment but are non-existent in the code predictions. There are two possible reasons why the codes fail to predict these liquid surges. It could either be that the computational grids chosen for the simulations are too coarse or that the surges are due to effects which cannot be predicted on the basis of the one-dimensional model used by the codes. The effect of computational grid size is addressed in Section 5.7.2 below and the question of the limitations in the one-dimensional models is addressed in Section 5.7.3.

5.7.2 Investigations of the One-Dimensional Modelling Approach

In the calculations carried out with the commercial codes, a grid size corresponding to 1 m of pipe length was used. Though this gridding is actually finer than that used in most commercial calculations, it may not be sufficiently fine to avoid numerical damping of incipient waves on the surface. In the one-dimensional model used in the codes, the waves predicted on the interface are of the Kelvin-Helmholtz type. A small perturbation in the liquid interface leads to restriction of the gas flow area, to acceleration of the gas and to a local reduction of pressure. This tends to suck the interface upwards, giving growth of the perturbation if the suction force is greater than the gravitational force tending to flatten the interface (for very small wavelengths, surface tension can also be an important restoring force). Such waves can be predicted analytically through linear perturbation theory. The classical Kelvin-Helmholtz theory was for inviscid flow (see for instance Kordyban & Ranov, 1970). Taitel & Dukler (1976) found that the onset of Kelvin-Helmholtz instability leading to wave growth and slug flow occurred at much lower gas velocities than were predicted from *inviscid* flow theory; they introduced a correction factor for pipe flow which was dependent on the ratio of liquid height to tube diameter. Lin & Hanratty (1986) carried out an analysis based on linear perturbation theory applied to the full (viscous) one-dimensional flow equations. Good agreement was obtained between this *viscous* Kelvin-Helmholtz theory and the experimentally observed transition to slug flow. Barnea & Taitel (1994) used numerical solutions of the one-dimensional equations. To investigate whether the surges observed in the present work could have their origin in Kelvin-Helmholtz instabilities, two approaches were followed:

(1) Calculations were carried out by Dr. Martin Kempf of the Department of Mechanical Engineering, Imperial College (a collaborator in the Transient Multiphase Flow project of which the work described in this thesis formed a part) using the Imperial College TRIOMPH Code (described in Section 2.4.3).

(2) The transients were plotted on stability plots prepared by Mr. Colin Hale of the Department of Chemical Engineering & Chemical Technology, Imperial College (also a collaborator in the Transient Multiphase Flow project). These stability plots were calculated from the numerical model of Barnea & Taitel (1994).

Predictions with the TRIOMPH Code. The TRIOMPH Code was used in the Transient Multiphase Flow project by Issa & Woodburn (1998) as a means of evaluating the performance of one-dimensional codes. Using the very flexible TRIOMPH Code as a benchmark, they were able to establish the following features of one-dimensional predictions relating to Kelvin-Helmholtz instability and the onset of slug flow:

(1) Below the viscous Kelvin-Helmholtz instability limit, the flow was stable over the full range of nodalisation (typically from 10 to 50 nodes per metre).

(2) Above the viscous Kelvin-Helmholtz limit, and below the inviscid limit, the flow was calculated as being unstable provided enough nodes were used in the calculation. Use of a small number of nodes per metre led to stabilization of the interface purely as a result of (artificial) numerical damping of any perturbations. As the number of nodes was increased, the wave growth rate became independent of the number of nodes, indicating *numerical convergence* of the calculations.

(3) Above the inviscid Kelvin-Helmholtz limit, the flow again appeared stable, indicating strong numerical damping, when a small number of nodes was used. As the number of nodes was increased, the interface demonstrated strong instability but in this case, there was no numerical convergence with increasing number of nodes since, beyond the inviscid Kelvin-Helmholtz limit, the equations are ill-posed and there are no solutions to the basic equations.

> Solutions are obtained only if the numerical methods introduce extra terms which make the solutions possible; such solutions are, of course, artificial in nature.

In the commercial codes, the nodes are typically an order of magnitude larger and the numerics would be expected to damp out instabilities of the Kelvin-Helmholtz type, even beyond the inviscid limit where the equations are ill-posed.

The objective of seeking to apply the TRIOMPH Code to the present cases was to confirm that the surges observed in the transients could not be predicted by the one-dimensional method, even with a large number of nodes.

Calculations with TRIOMPH were carried out for comparison with the two transient experimental cases wb and wd from WASP. The conditions of these runs were presented in Table 5.2 in Section 5.3.2 and are summarised here again for convenience:

Case	U_L/(m/s)	$U_{G,1}$/(m/s)	$U_{G,2}$/(m/s)	p/bar
wb	0.037	5.33	6.07	1.06
wd	0.032	1.30	1.62	6.03

Table 5.2 Conditions of transient experimental cases wb and wd of WASP

The two experiments were run at different pressures. The liquid flow rate is similar in both experiments but the gas flow rates at elevated pressure are much smaller than at atmospheric pressure. In both experiments there was a characteristic increase in holdup during the transient period as discussed in Section 5.3.2.

In the simulations with TRIOMPH presented in this section (carried out, as was mentioned above, by Dr. M. Kempf, Department of Mechanical Engineering at Imperial College) the computational grid had the overall dimensions of the WASP test section (length = 36 m, inner diameter = 0.07792 m) and was subdivided into 1250 cells. Flow conditions were specified at the inlet and outlet of the test section. At the inlet the liquid and gas superficial velocities of the initial steady state were set and the split between the two phases was defined by the liquid holdup measured in the initial steady state of the transient experiment. At the outlet the system pressure from the experiment was set. The simulation was run for a total of 300 seconds and, like in the experiment, the gas flow rate was increased to the final steady state value after 30 seconds from the start. The results from TRIOMPH for liquid holdup at the position

of the measurements on WASP, which was 33.7 m downstream of the inlet, were compared with the experimental data.

The comparison for case wb is shown in Figure 5.52, the comparison for case wd in Figure 5.53. Before the transient change the liquid holdup is the same in experiment and simulation because the holdup value of the initial steady state in the experiment was used as input for the simulation. When the transient change is applied the holdup in the experiment increases and only after a considerable period of time decreases and reaches final steady state. In the TRIOMPH simulations no increase in liquid holdup is observed. When the transient change is set the holdup gradually decreases. The decrease is more pronounced than in the experiment. In case wb final steady state is reached about 140 seconds after the transient change, in case wd the total simulation time of 300 seconds is not sufficient to reach final steady state.

These comparisons show the same characteristic features as the comparisons between the experiment and the commercial codes. TRIOMPH doesn't predict an increase in holdup after the transient change. As much smaller computational cells were used in the simulations with TRIOMPH it is concluded that it is not the nodalisation which prevents prediction of the characteristic liquid surge during the transient with the commercial codes. It is more likely that the one-dimensional model is inadequate to model the liquid surge.

Stability plots. The onset of viscous and inviscid Kelvin-Helmholtz instability can be represented on a plot of relative velocity (difference between gas and liquid velocities) and liquid holdup.

A stability map of this form was prepared by Mr. C.P. Hale of the Department of Chemical Engineering & Chemical Technology at Imperial College. As was mentioned above, Mr. Hale is a collaborator in the Transient Multiphase Flow project; his work is concerned with the onset of slug flow and with slug generation. The stability plot was based on an adaptation of the methodology of Barnea & Taitel (1994) and was for atmospheric pressure flow in a 77.92 mm pipe. Lines were calculated for the viscous and inviscid Kelvin-Helmholtz instability and are shown on the plot (Figure 5.54). Also shown are the tracks (in terms of relative velocity and holdup) of the near-atmospheric pressure transients analysed from the present work.

namely cases `lf` and `wb`. As will be seen, both transients lie well below the viscous Kelvin-Helmholtz stability line. Even if it is assumed that the holdup remains constant during the initial rise of velocity, the stability criterion is not breached. This result is consistent with the finding from the TRIOMPH Code calculations referred to above.

It will be seen that the surges observed in the experiments reported here cannot be explained in terms of the Kelvin-Helmholtz instability and, thus, it cannot be calculated from the one-dimensional two-fluid model.

5.7.3 Multi-Dimensional Effects

As was seen from Section 5.7.2, the surges observed in the transient experiments could not be accounted for by the one-dimensional models. Their origin must be a matter of speculation but it may lie in the real multi-dimensional nature of the flow. At gas velocities much below those required for Kelvin-Helmholtz instability, waves are formed on the interface, signalling the transition from smooth-stratified to wavy-stratified flow. These result from energy transport from the gas to the liquid resulting from pressure variations in the gas which are not (as in the case of the Kelvin-Helmholtz instability) 180 ° out of phase with the wave height. There has been extensive work on such waves (Miles, 1957; Benjamin, 1959; Jeffreys, 1925); typically, some form of separation is assumed in the flow over the waves (for example the Jeffreys "sheltering hypothesis"). Taitel & Dukler (1976) used the Jeffreys approach in modelling the transition from smooth to wavy stratified flow. Such effects are not predicted by the one-dimensional models.

As the measurements of h_L' clearly show, waves are formed in the steady state. However, the wave activity during the transient is seen to be anomalous and this might provide a clue as to the surge mechanism. Could it be that a group of waves are formed during the transient which gather together under the action of the increased gas velocity to produce the surge? This must be a matter of speculation but there can be no doubt that the surges observed in the present work are one of the most interesting and potentially important outcomes from the study.

Why are the surges potentially important? Obviously, it is because they are potential slug precursors! If a large enough surge is formed, then closure of the channel leading to slug flow can occur due to the growth of small perturbations on the surface of the

surge (Kordyban, 1977). Once the slug is formed, it may persist and grow despite the fact that the average conditions in the channel are well below those required for Kelvin-Helmholtz instability, as shown by Bendiksen & Espedal (1992).

5.8 Conclusions

The main conclusions which were drawn from the presentation and the analysis of the transient data in this chapter are as follows:

- Transient data of detailed local parameters were obtained with the instrumentation described in Chapter 3 in transient gas-liquid stratified flow on two flow facilities, a low pressure rig and the WASP rig. The transients were produced solely from a step-like increase in the gas flow rate while the liquid flow rate was kept constant. Reliable measurements at atmospheric pressure on the low pressure rig included pressure gradient in the gas phase, liquid holdup and interfacial structure, velocities and wall shear stresses in both phases. On the WASP rig, where measurements were performed at 1, 6 and 11 bar, the reliable data included liquid holdup and interfacial structure, and the velocities in both phases. All measured parameters showed clear temporal changes. Generally, the parameters in the gas phase changed rapidly to the new value in the final steady state, whereas the parameters in the liquid gradually changed to the final steady state value. The measured parameters in the liquid phase took longer to reach final steady state on WASP than on the low pressure rig. This was attributed to the longer test section on WASP. Of all the measured parameters, the liquid holdup showed the longest transient period. On the low pressure rig the transient response of the liquid holdup was seen as an increase in interfacial activity before its value decreased to the final steady state. On the WASP rig a substantial liquid surge was observed before the liquid holdup reached final steady state.

- Transient measurements of the gas wall shear stress on the low pressure rig were analysed in terms of the gas wall friction factor f_G and compared with predictions from a number of steady state models. The experimental data for f_G showed fluctuations much bigger than the model predictions. The transient change was observed as an instantaneous decrease of f_G to the final steady state value both in

the experiment and in the predictions. The transient decrease in f_G was bigger for a greater change of the gas flow rate.

- Transient data of the interfacial friction factor f_i was derived from measurements in the gas phase on the low pressure rig and compared with predictions from a number of steady state models. Also included were predictions from the new steady state model for f_i developed from an analysis of interfacial fluctuations in Chapter 4. The experimental data for f_i showed fluctuations much bigger than the model predictions. The transient change in the experimental data was mainly seen as an increase in the fluctuations of the signal for f_i for a short time. An investigation of the error between the experiment and the new steady state model for f_i developed in this study revealed a clear peak in the error for a short period during the transient. The peak was higher in the case of a greater change of the gas flow rate to produce the transient. As a consequence of the increased error during the transient the need was stated for an improvement of the steady state models for f_i to better represent the transient features.
- Information on the interfacial structure was derived from measurements with the array of conductivity probes in the test spool on the low pressure rig and the WASP rig. The development of the interface during the transient was qualitatively investigated for one case from the low pressure rig and one case from WASP, which were for similar flow conditions. The case from the low pressure rig showed a clear and sudden increase in interfacial activity during the transient which was reduced as time advanced. In the WASP cases the changes in the interfacial structure were consistent with local gas velocity and holdup changes during the surges.
- The interfacial structure was also quantitatively investigated by comparing the measurements of h_L' during the transient with predictions from the new steady state models for h_L' developed in Chapter 4 for the low pressure rig and the WASP rig. The comparisons were analysed in terms of the error between prediction and measurement. Only in one case from the low pressure rig the error showed a peak during the transient above the levels of error in the initial and final steady states. In the other cases, including the ones from the WASP rig, the error between prediction and measurement during the transient was not greater than in the initial

and final steady states. This was in contrast to the observations for the interfacial friction factor f_i derived from measurements in the gas phase on the low pressure rig where discrepancies between experiment and models were clearly different in the transients and steady states.

- Measurements of the liquid holdup for the transient were compared with predictions from the three one-dimensional computer codes, PLAC, OLGA and TACITE. The main consequence for the transient was that none of the codes showed the liquid surges mainly observed in the experiments on the WASP rig. By supplementing the comparisons with predictions from the one-dimensional TRIOMPH code and by plotting the transients on a stability map, it was concluded that it was not the nodalisation of the computational domain which prevented the codes from predicting the liquid surges. It was hypothesized that the liquid surges were complex features which could not be predicted with the existing models in the codes and could possibly arise from complex multi-dimensional effects.

case	U_L/(m/s)	$U_{G,1}$/(m/s)	$U_{G,2}$/(m/s)	p/bar	y(hfp)/mm	y(hwp)/mm
1a	0.039	5.01	6.46	1.00	5	69
	0.039	4.98	6.40	1.00	8	54
	0.039	4.99	6.49	1.00	13	39
1b	0.039	6.35	7.24	0.99	5	69
	0.039	6.35	7.36	1.00	8	54
	0.039	6.32	7.34	1.00	10	39
1c	0.039	7.39	8.08	0.99	5	69
	0.039	7.31	8.09	1.00	8	54
	0.039	7.37	8.25	1.00	10	39
1d	0.039	6.20	7.91	0.99	5	69
	0.039	6.08	7.90	1.00	8	54
	0.039	6.14	7.95	1.00	10	39
1e	0.058	5.63	6.86	0.99	5	69
	0.058	5.62	6.84	1.00	8	54
	0.058	5.67	6.90	1.00	12	39
1f	0.058	7.07	8.75	1.00	5	69
	0.058	7.07	8.83	1.00	8	54
	0.058	7.14	8.79	1.00	10	39
1g	0.078	5.42	7.18	0.99	5	69
	0.078	5.42	7.15	1.00	8	54
	0.078	5.48	7.10	0.99	13	39
1h	0.078	7.15	8.94	1.00	5	69
	0.078	7.15	8.90	1.00	8	54
	0.078	7.06	8.85	1.00	11	39

Legend: U_L = liquid superficial velocity

$U_{G,1}$ = gas superficial velocity for initial steady state

$U_{G,2}$ = gas superficial velocity for final steady state

p = system pressure

y(hfp) = vertical distance of tip of hot-film probe for liquid velocity measurement from the bottom of the tube

y(hwp) = vertical distance of tip of hot-wire probe for gas velocity measurement from the bottom of the tube

Table 5.5 Summary of transient tests on the low pressure rig

case	U_L/(m/s)	$U_{G,1}$/(m/s)	$U_{G,2}$/(m/s)	p/bar	y(hfp)/mm	y(hwp)/mm
wa	0.023	5.68	6.45	1.07	5	69
	0.019	6.02	6.73	1.07	8	54
	0.022	6.09	6.72	1.06	10	39
	0.014	5.46	6.23	1.06	*	*
wb	0.037	5.33	6.07	1.06	5	69
	0.036	5.35	6.11	1.06	9	54
	0.028	5.07	5.86	1.05	13	44
wc	0.016	1.50	1.77	6.02	5	69
	0.012	1.53	1.79	6.12	9	54
	0.011	1.57	1.86	6.08	13	39
	0.016	1.44	1.84	6.10	*	*
wd	0.032	1.30	1.62	6.03	5	69
	0.030	1.33	1.64	6.10	12	54
	0.021	1.23	1.54	5.92	17	44
we	0.024	1.32	1.49	11.02	5	69
	0.012	1.28	1.45	11.16	9	54
	0.019	1.26	1.41	11.15	13	39
wf	0.021	0.97	1.22	11.31	5	69
	0.022	0.98	1.25	11.29	10	54
	0.032	0.95	1.18	11.19	15	44

Legend: U_L = liquid superficial velocity

$U_{G,1}$ = gas superficial velocity for initial steady state

$U_{G,2}$ = gas superficial velocity for final steady state

p = system pressure

y(hfp) = vertical distance of tip of hot-film probe for liquid velocity measurement from the bottom of the tube

y(hwp) = vertical distance of tip of hot-wire probe for gas velocity measurement from the bottom of the tube

* measurement with gas wall shear stress probe only

Table 5.6 Summary of transient tests on the WASP rig

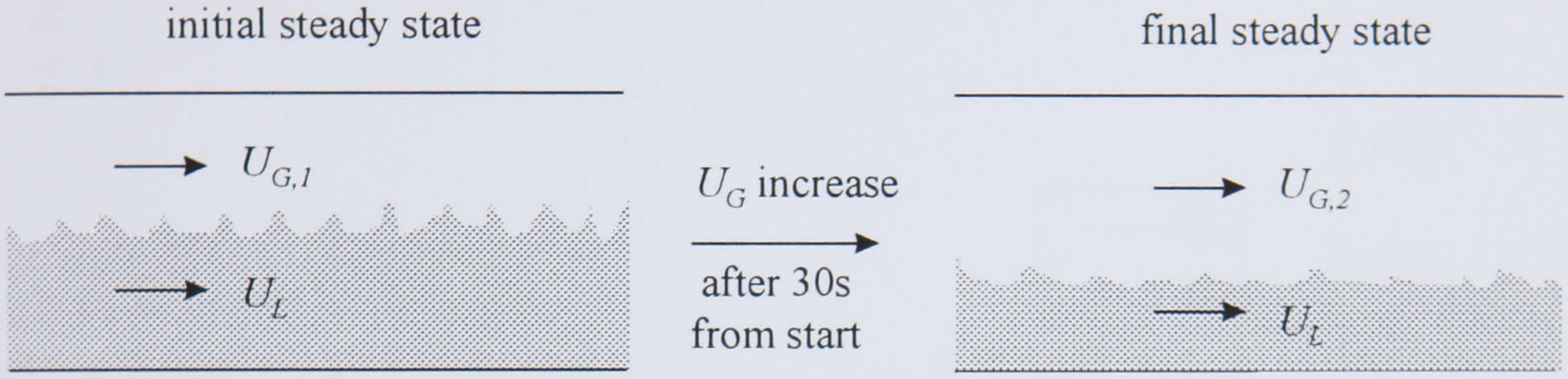


Figure 5.1 Schematic of transient experiment

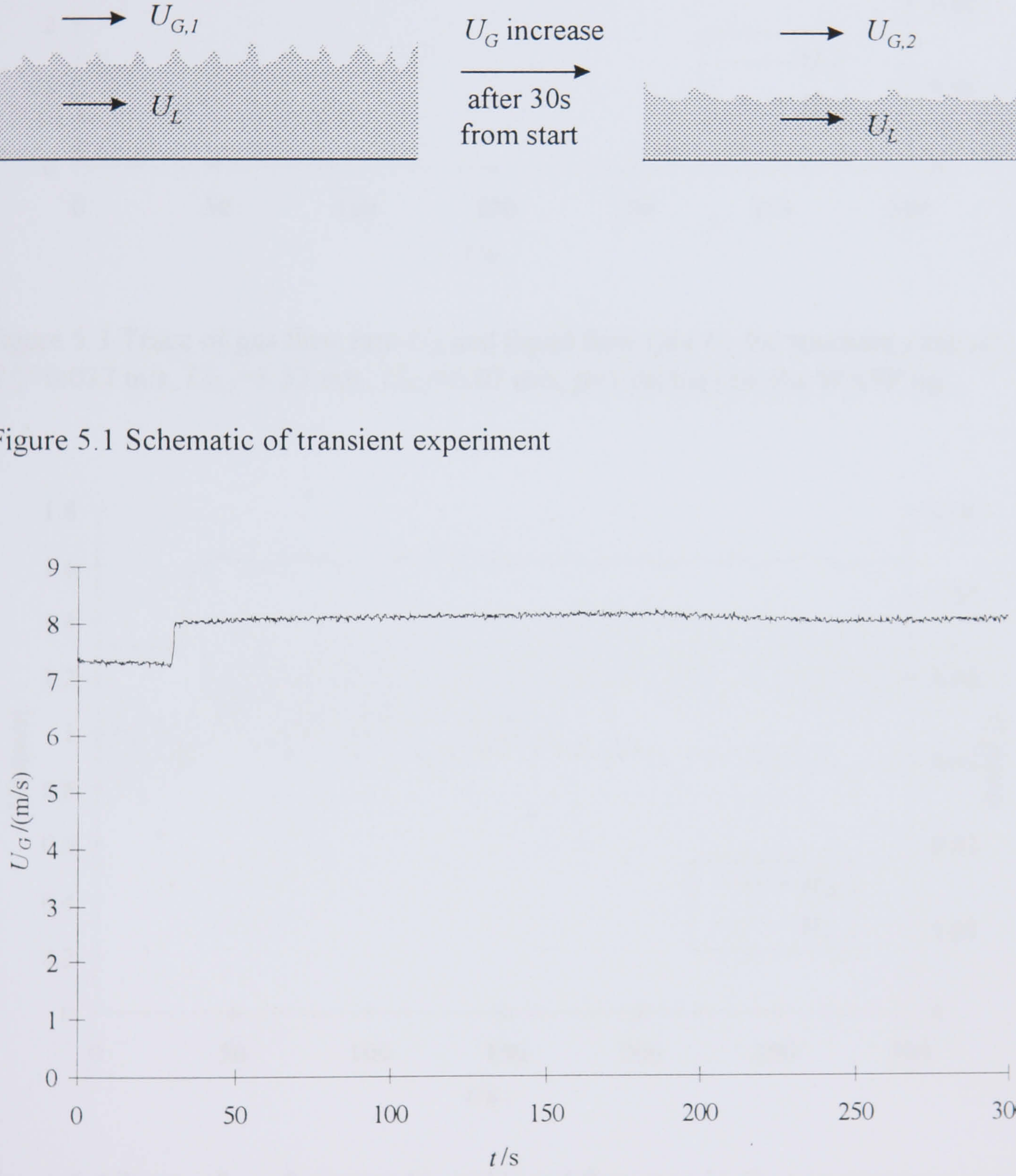


Figure 5.2 Trace of air flow rate U_G for transient case 1c (U_L=0.039 m/s, $U_{G,1}$=7.39 m/s, $U_{G,2}$=8.08 m/s, p=0.99 bar) on the low pressure rig

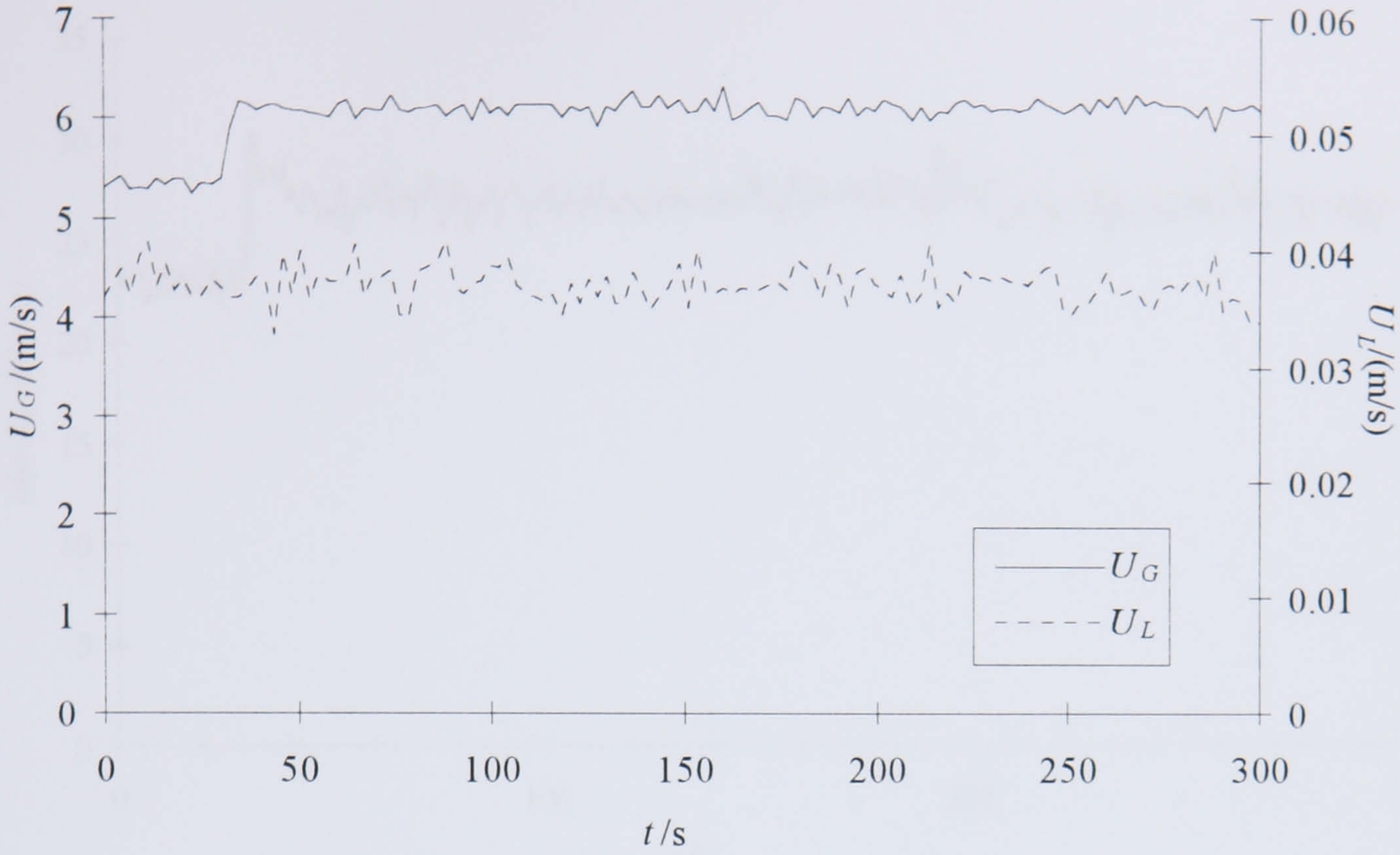


Figure 5.3 Trace of gas flow rate U_G and liquid flow rate U_L for transient case wb (U_L=0.037 m/s, $U_{G,1}$=5.33 m/s, $U_{G,2}$=6.07 m/s, p=1.06 bar) on the WASP rig

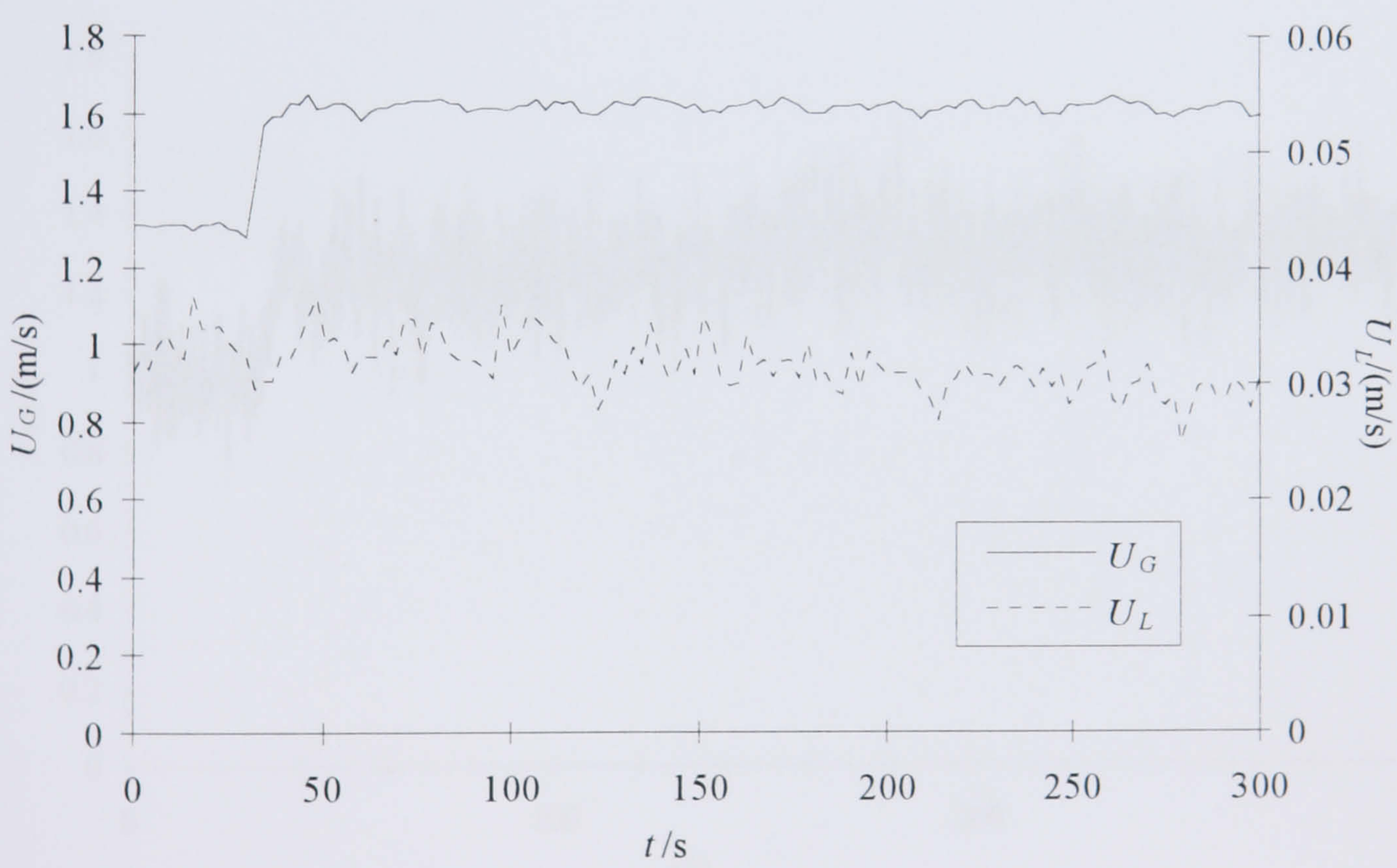


Figure 5.4 Trace of gas flow rate U_G and liquid flow rate U_L for transient case wd (U_L=0.032 m/s, $U_{G,1}$=1.30 m/s, $U_{G,2}$=1.62 m/s, p=6.03 bar) on the WASP rig

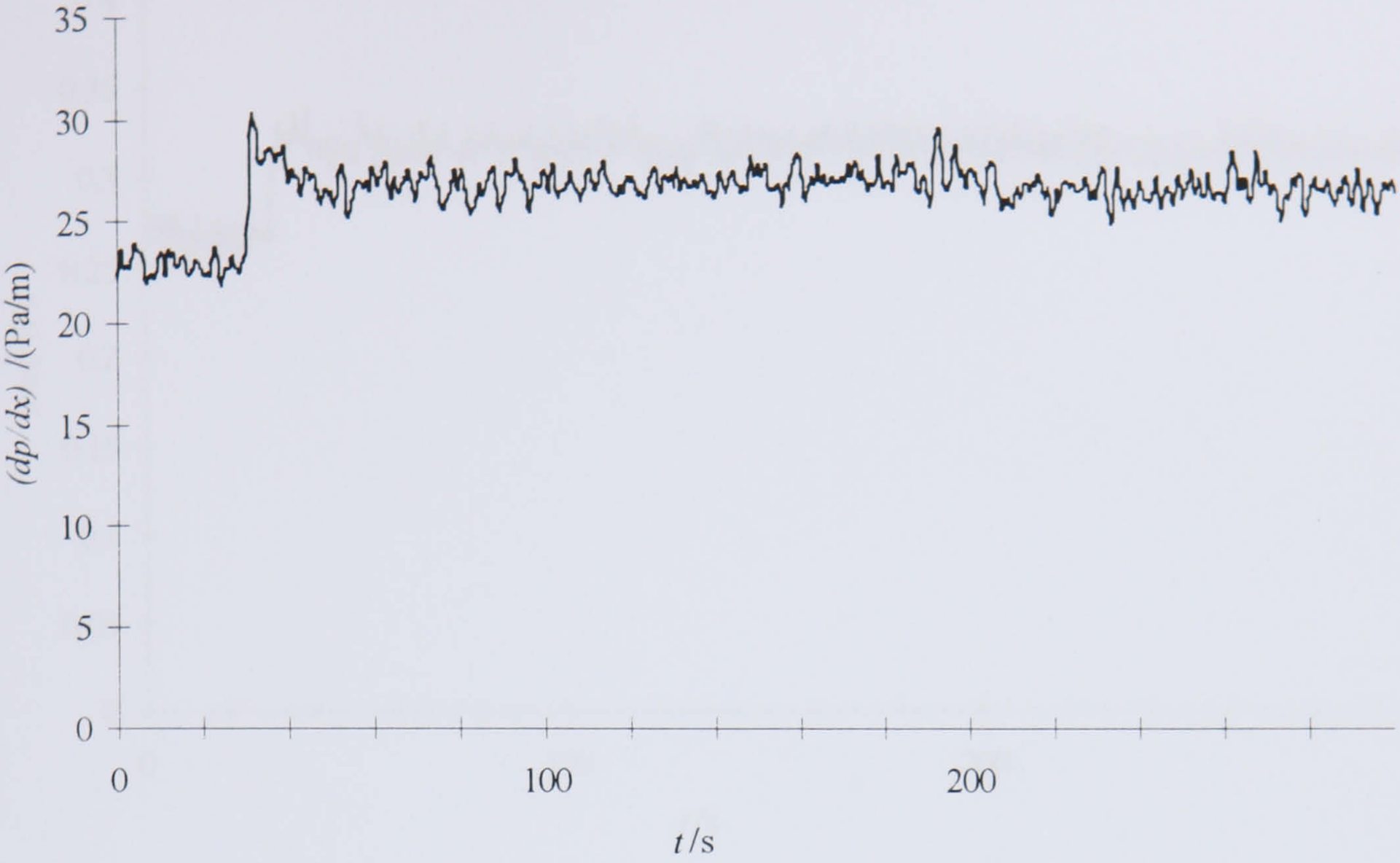


Figure 5.5 Measured pressure gradient *(dp/dx)* for transient case `1c` (U_L=0.039 m/s, $U_{G,1}$=7.39 m/s, $U_{G,2}$=8.08 m/s, p=0.99 bar) on the low pressure rig

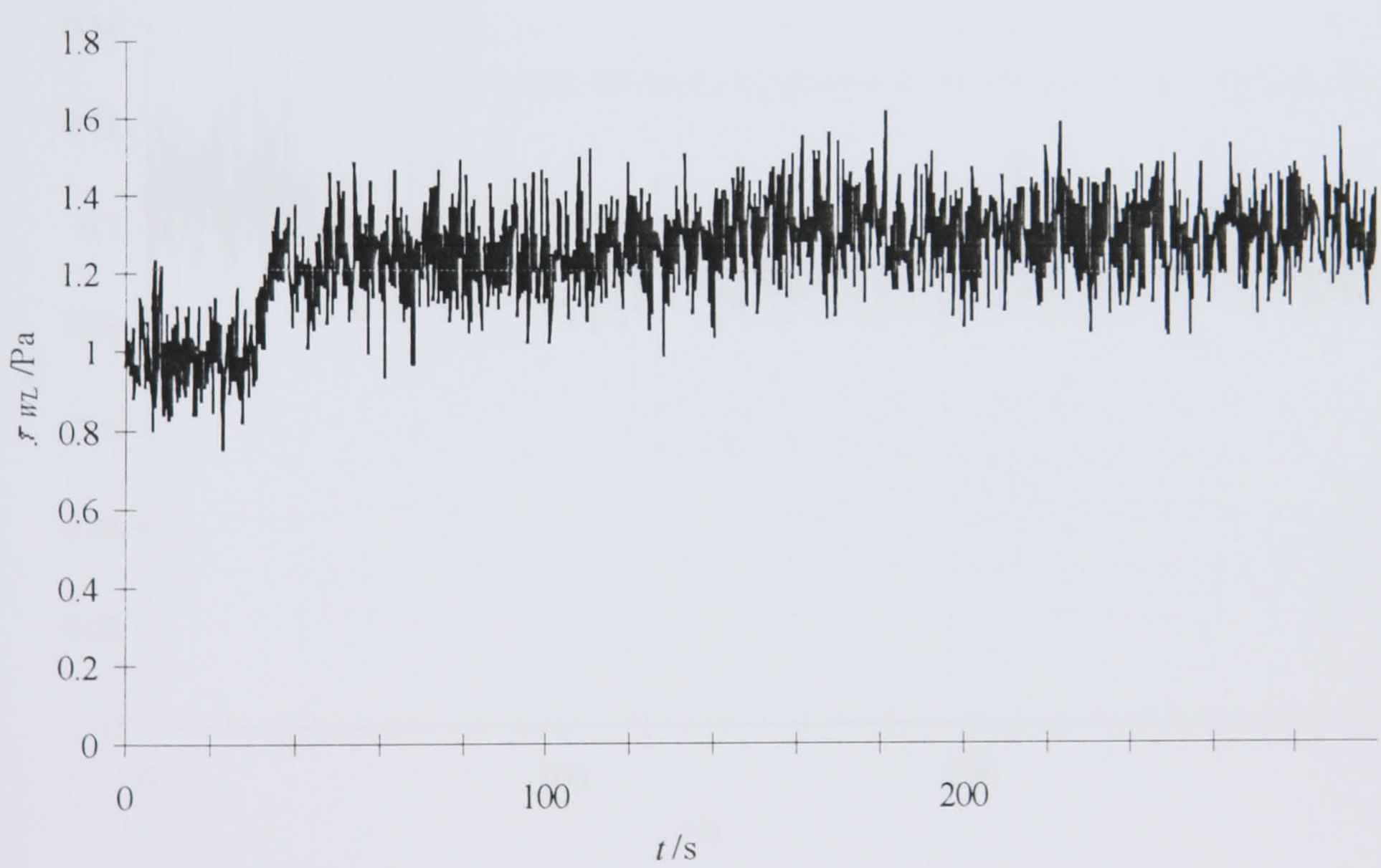


Figure 5.6 Measured liquid wall shear stress τ_{WL} for transient case `1c` (U_L=0.039 m/s, $U_{G,1}$=7.39 m/s, $U_{G,2}$=8.08 m/s, p=0.99 bar) on the low pressure rig

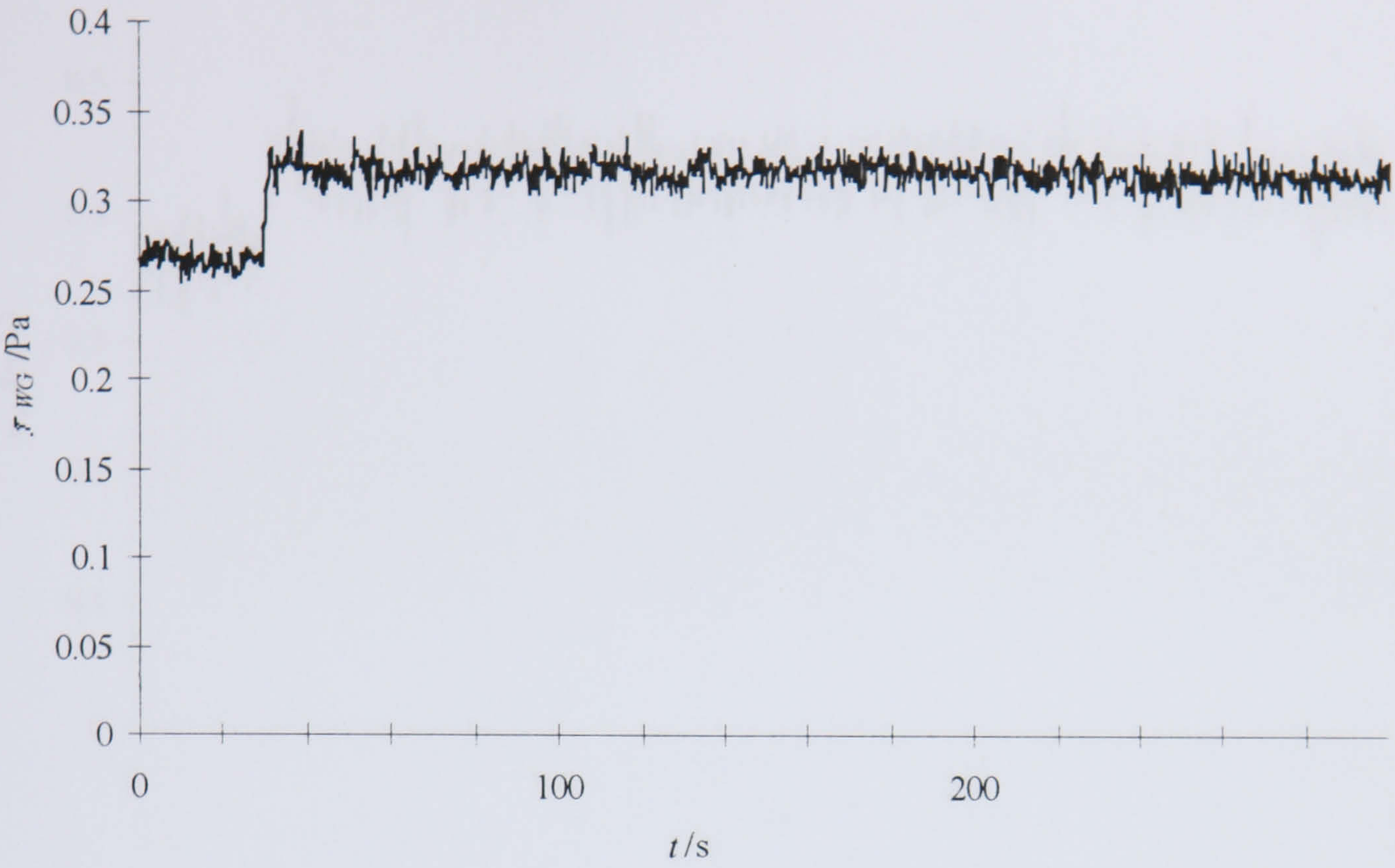


Figure 5.7 Measured gas wall shear stress τ_{WG} for transient case 1c (U_L=0.039 m/s, $U_{G,1}$=7.39 m/s, $U_{G,2}$=8.08 m/s, p=0.99 bar) on the low pressure rig

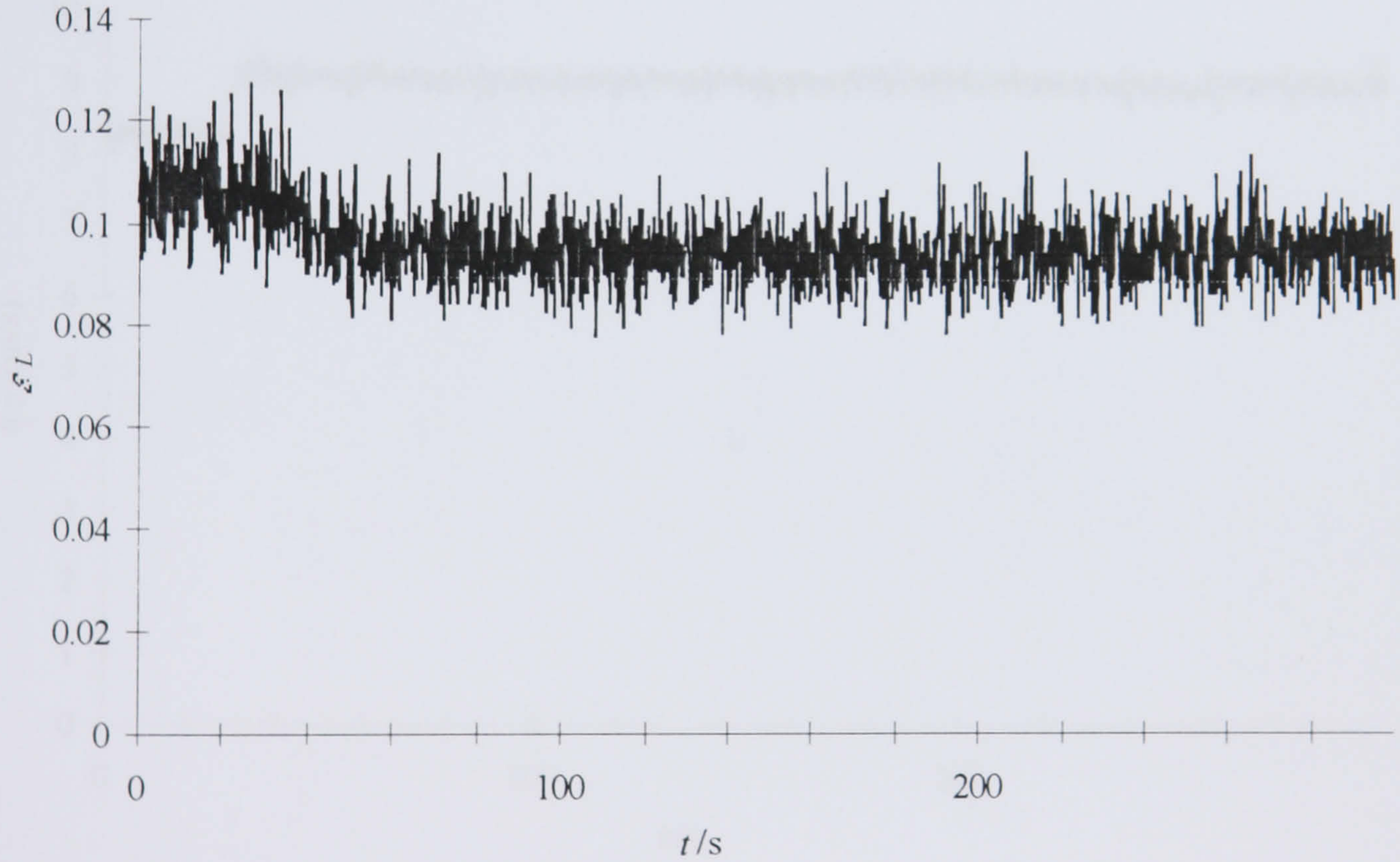


Figure 5.8 Measured liquid holdup ε_L for transient case 1c (U_L=0.039 m/s, $U_{G,1}$=7.39 m/s, $U_{G,2}$=8.08 m/s, p=0.99 bar) on the low pressure rig

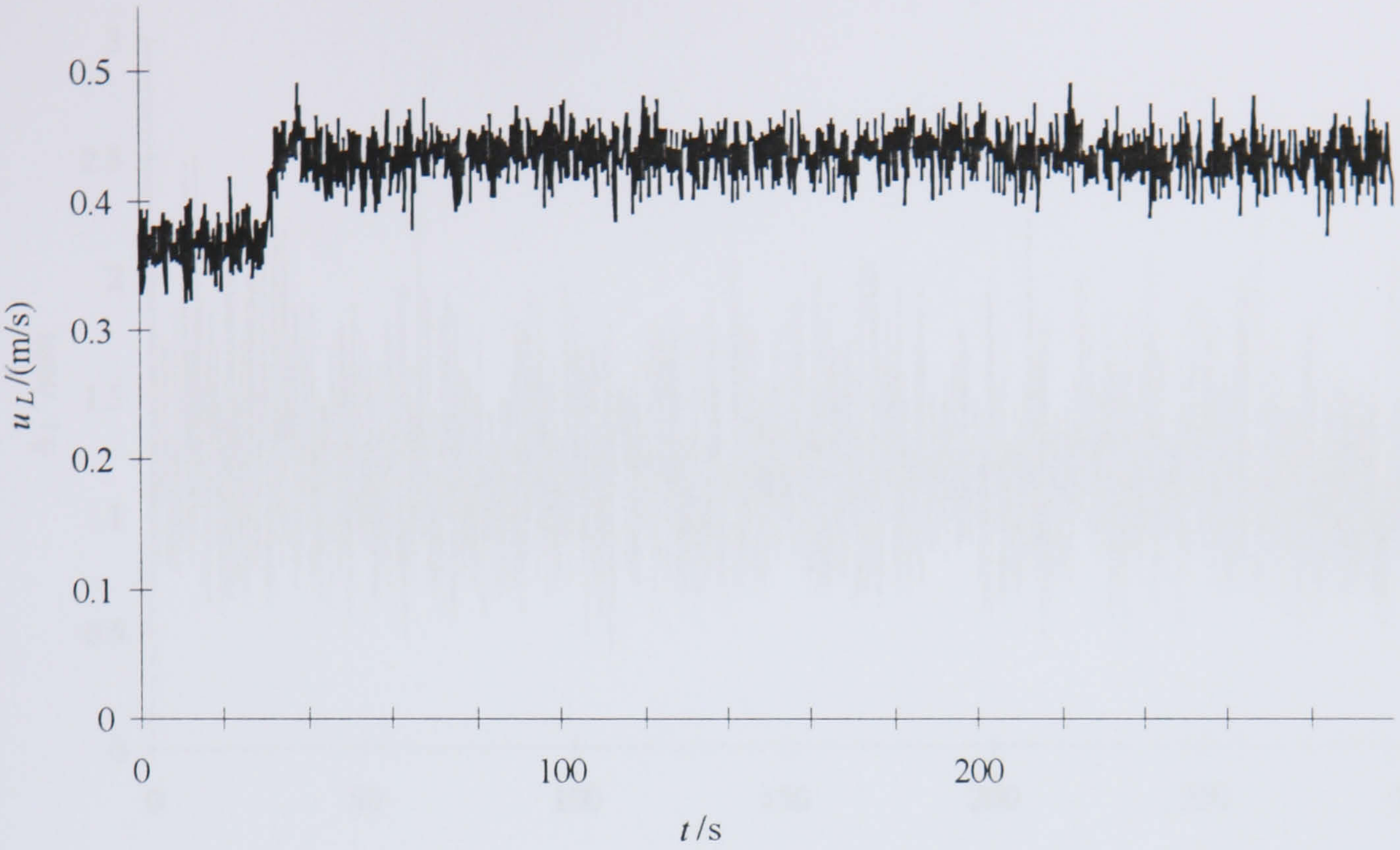


Figure 5.9 Measured liquid phase average velocity u_L for transient case `1c` (U_L=0.039 m/s, $U_{G,1}$=7.39 m/s, $U_{G,2}$=8.08 m/s, p=0.99 bar) on the low pressure rig

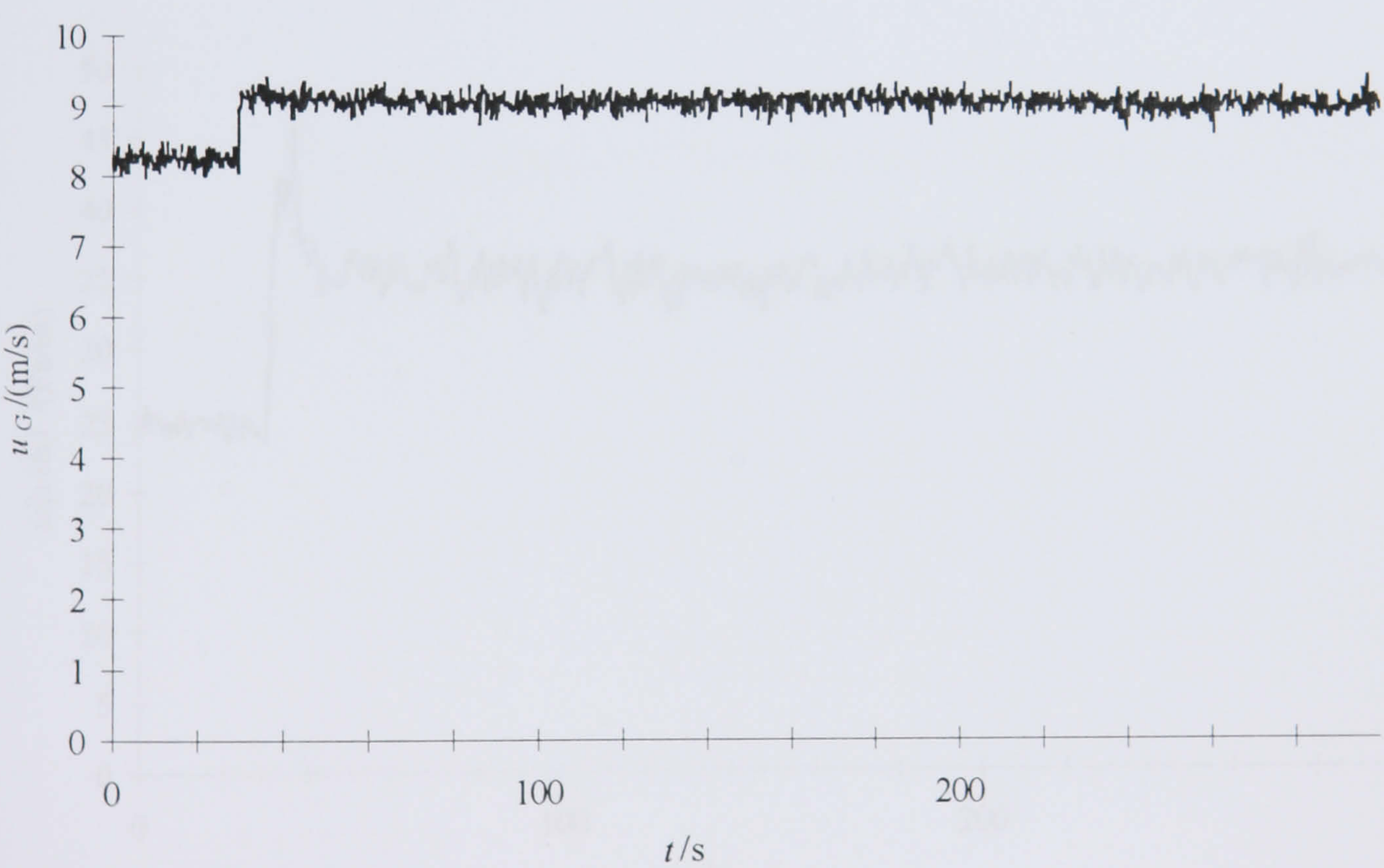


Figure 5.10 Measured gas phase average velocity u_G for transient case `1c` (U_L=0.039 m/s, $U_{G,1}$=7.39 m/s, $U_{G,2}$=8.08 m/s, p=0.99 bar) on the low pressure rig

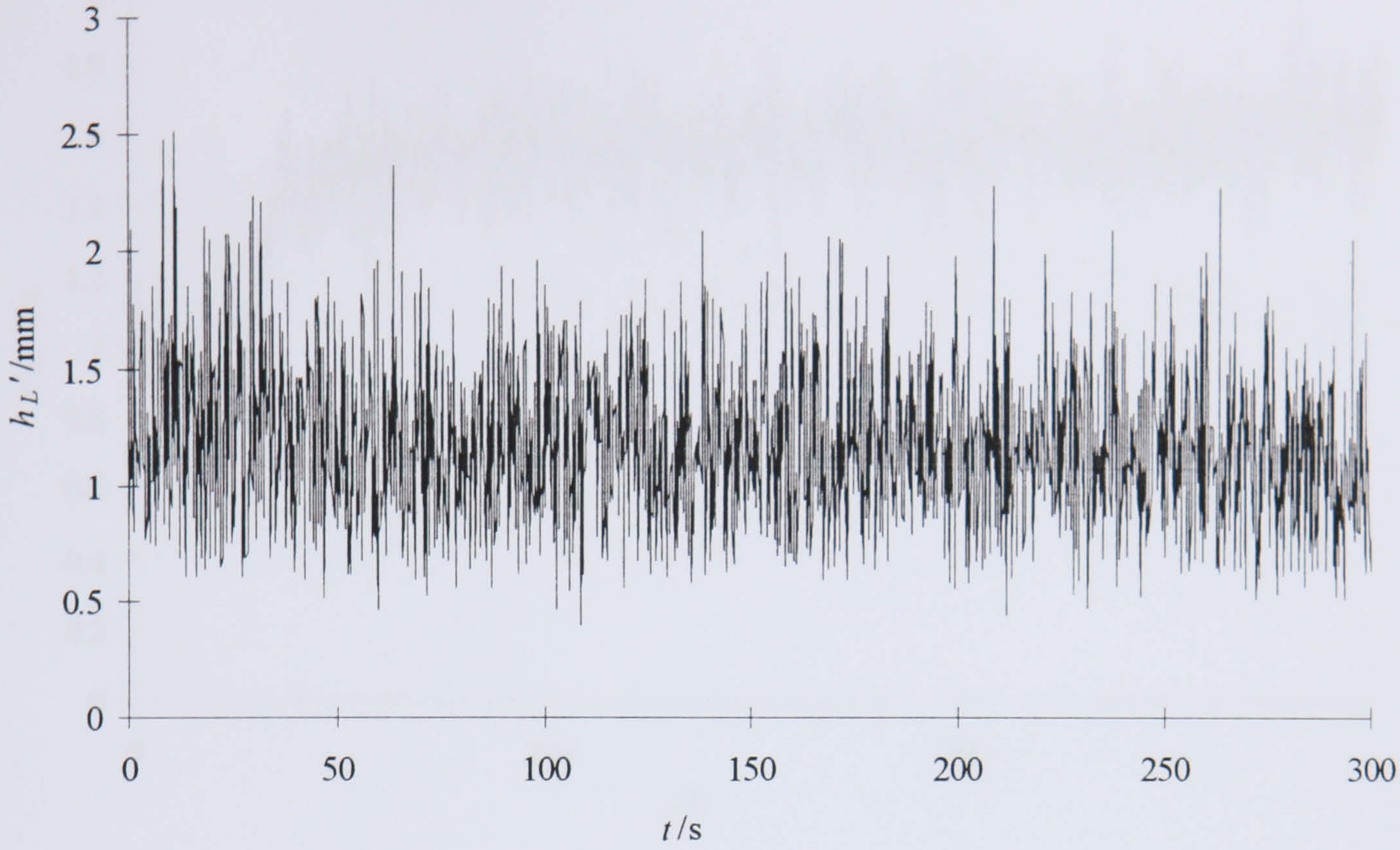


Figure 5.11 Interfacial fluctuation h_L' for transient case `lc` (U_L=0.039 m/s, $U_{G,1}$=7.39 m/s, $U_{G,2}$=8.08 m/s, p=0.99 bar) on the low pressure rig

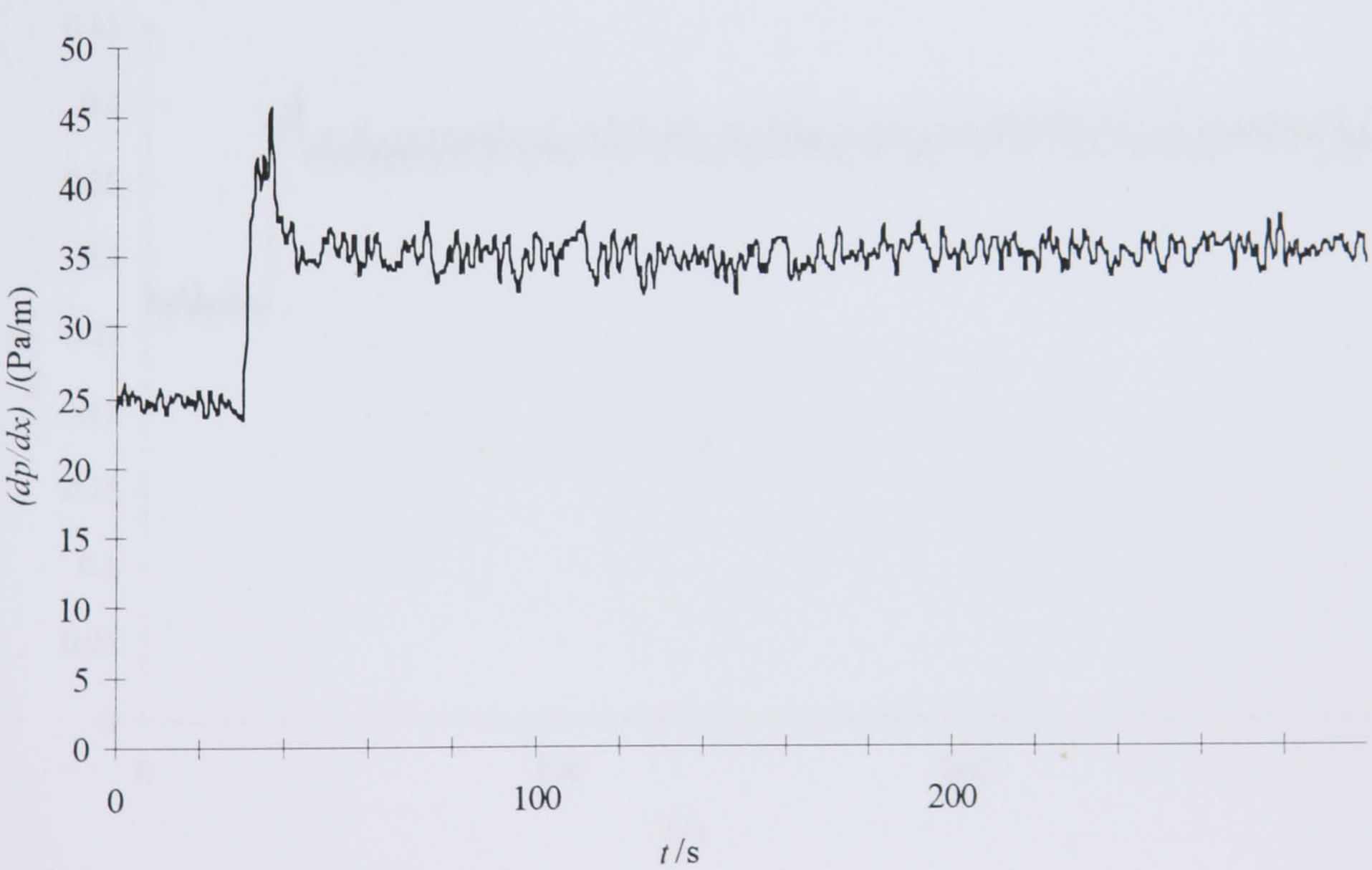


Figure 5.12 Measured pressure gradient *(dp/dx)* for transient case `lf` (U_L=0.058 m/s, $U_{G,1}$=7.07 m/s, $U_{G,2}$=8.75 m/s, p=1.00 bar) on the low pressure rig

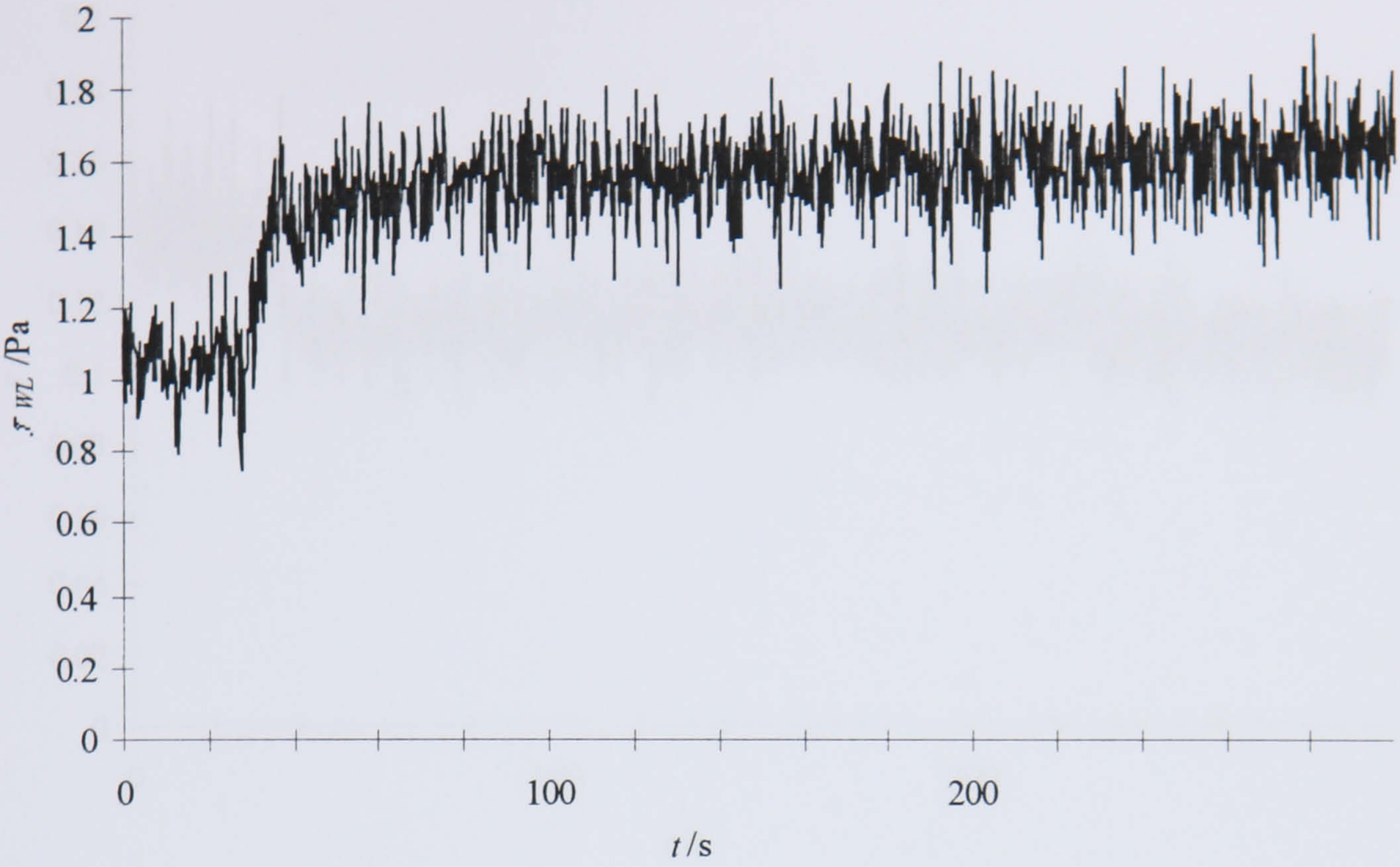


Figure 5.13 Measured liquid wall shear stress τ_{WL} for transient case `lf` (U_L=0.058 m/s, $U_{G,1}$=7.07 m/s, $U_{G,2}$=8.75 m/s, p=1.00 bar) on the low pressure rig

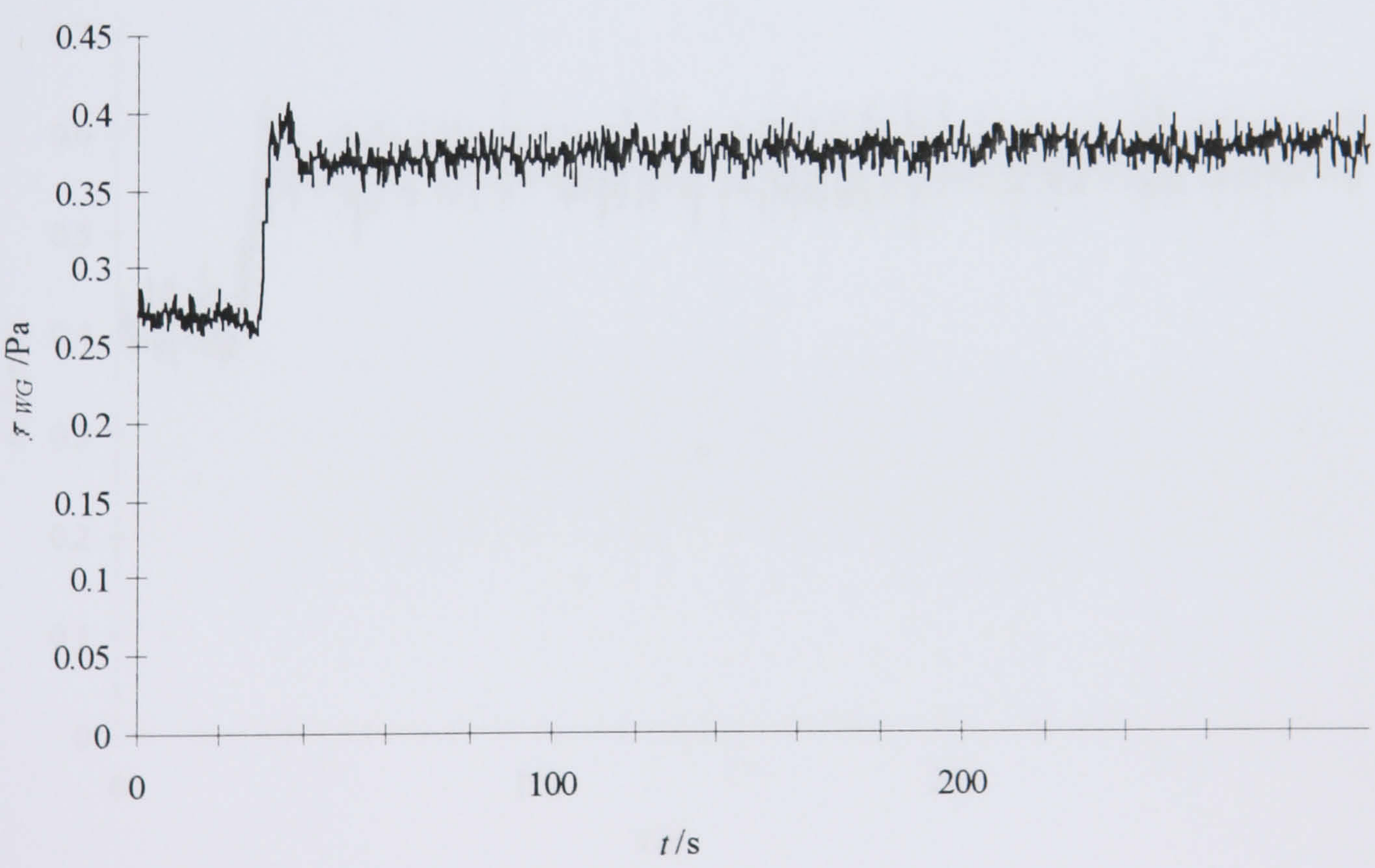


Figure 5.14 Measured gas wall shear stress τ_{WG} for transient case `lf` (U_L=0.058 m/s, $U_{G,1}$=7.07 m/s, $U_{G,2}$=8.75 m/s, p=1.00 bar) on the low pressure rig

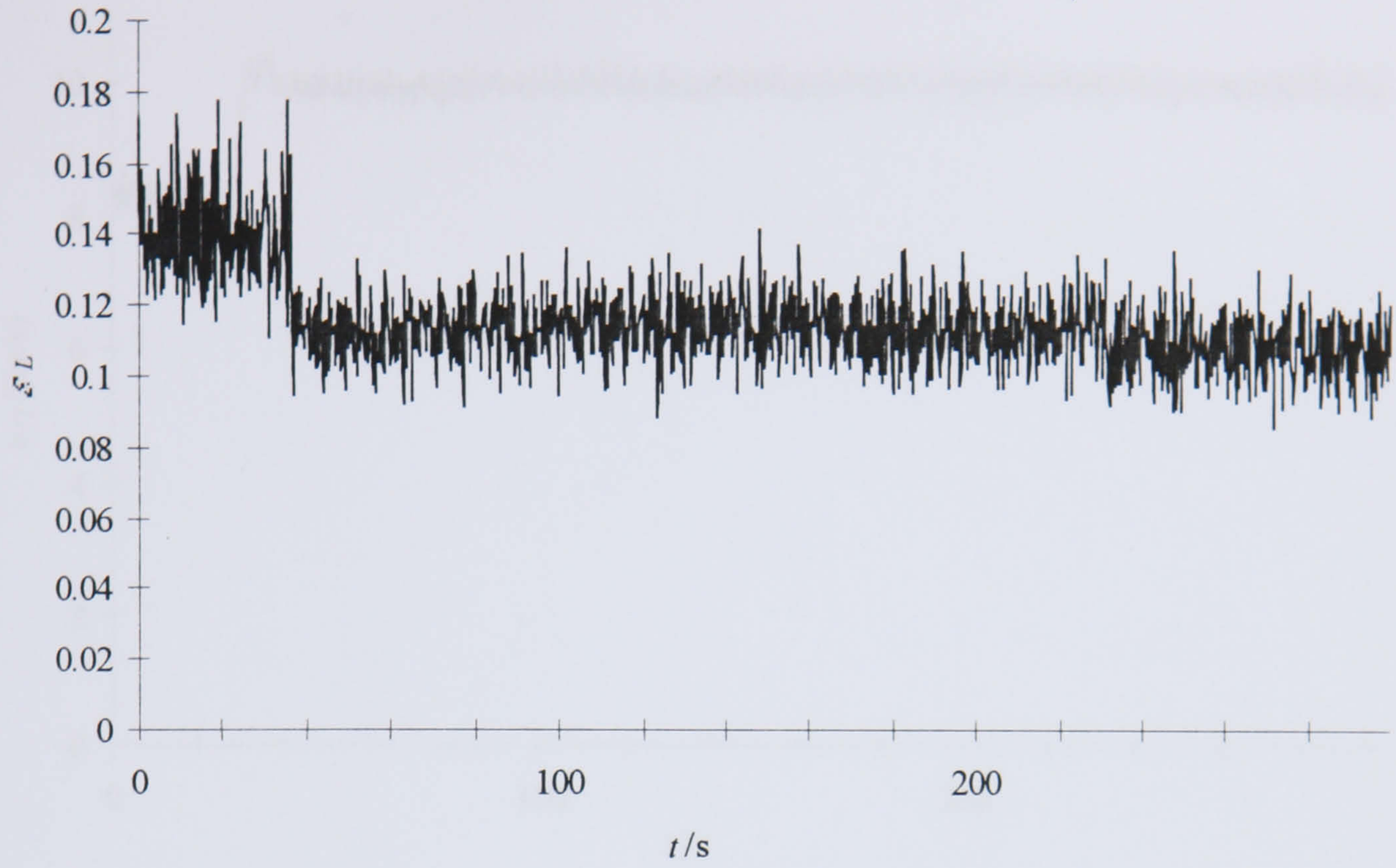


Figure 5.15 Measured liquid holdup ε_L for transient case `lf` (U_L=0.058 m/s, $U_{G,1}$=7.07 m/s, $U_{G,2}$=8.75 m/s, p=1.00 bar) on the low pressure rig

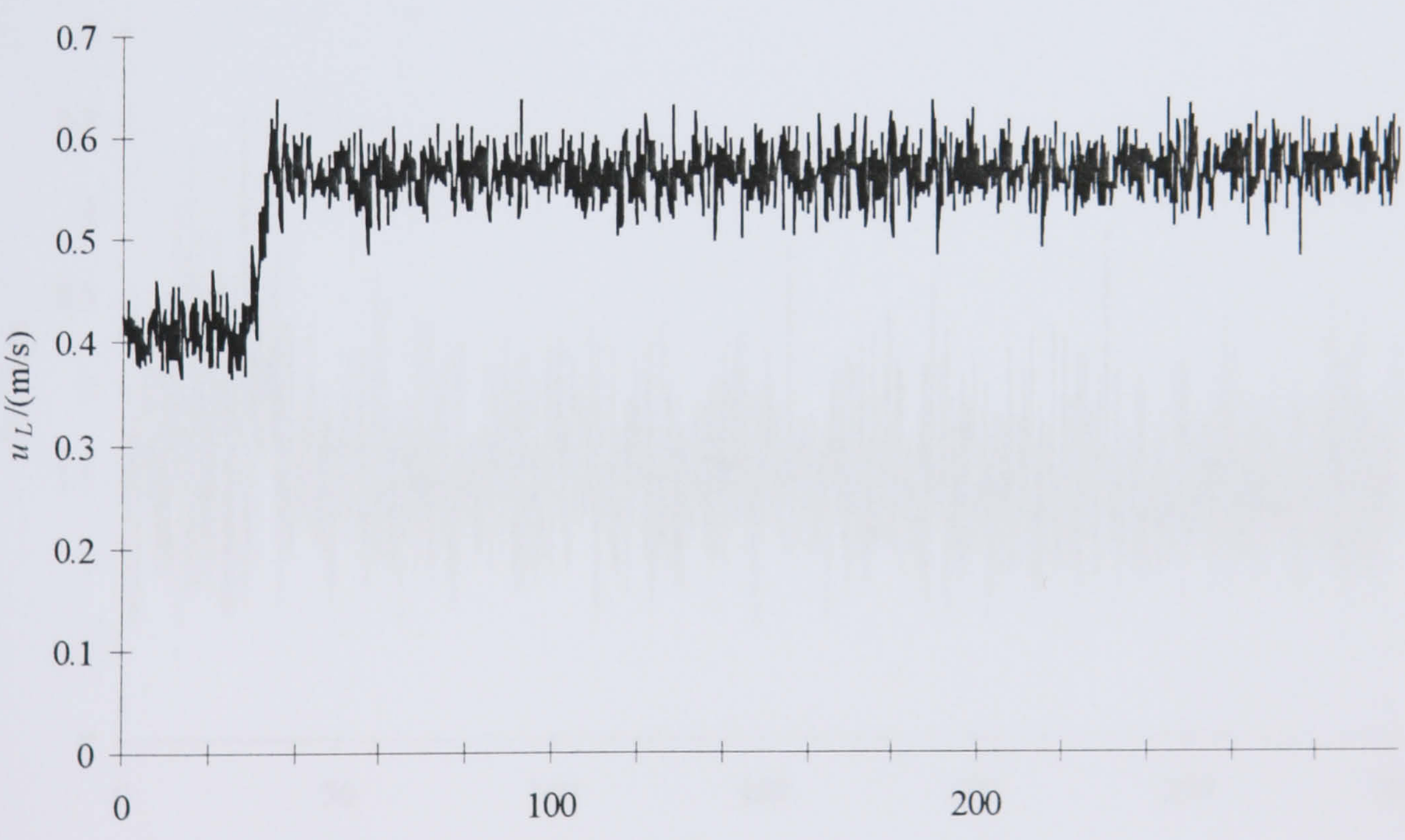


Figure 5.16 Measured liquid phase average velocity u_L for transient case `lf` (U_L=0.058 m/s, $U_{G,1}$=7.07 m/s, $U_{G,2}$=8.75 m/s, p=1.00 bar) on the low pressure rig

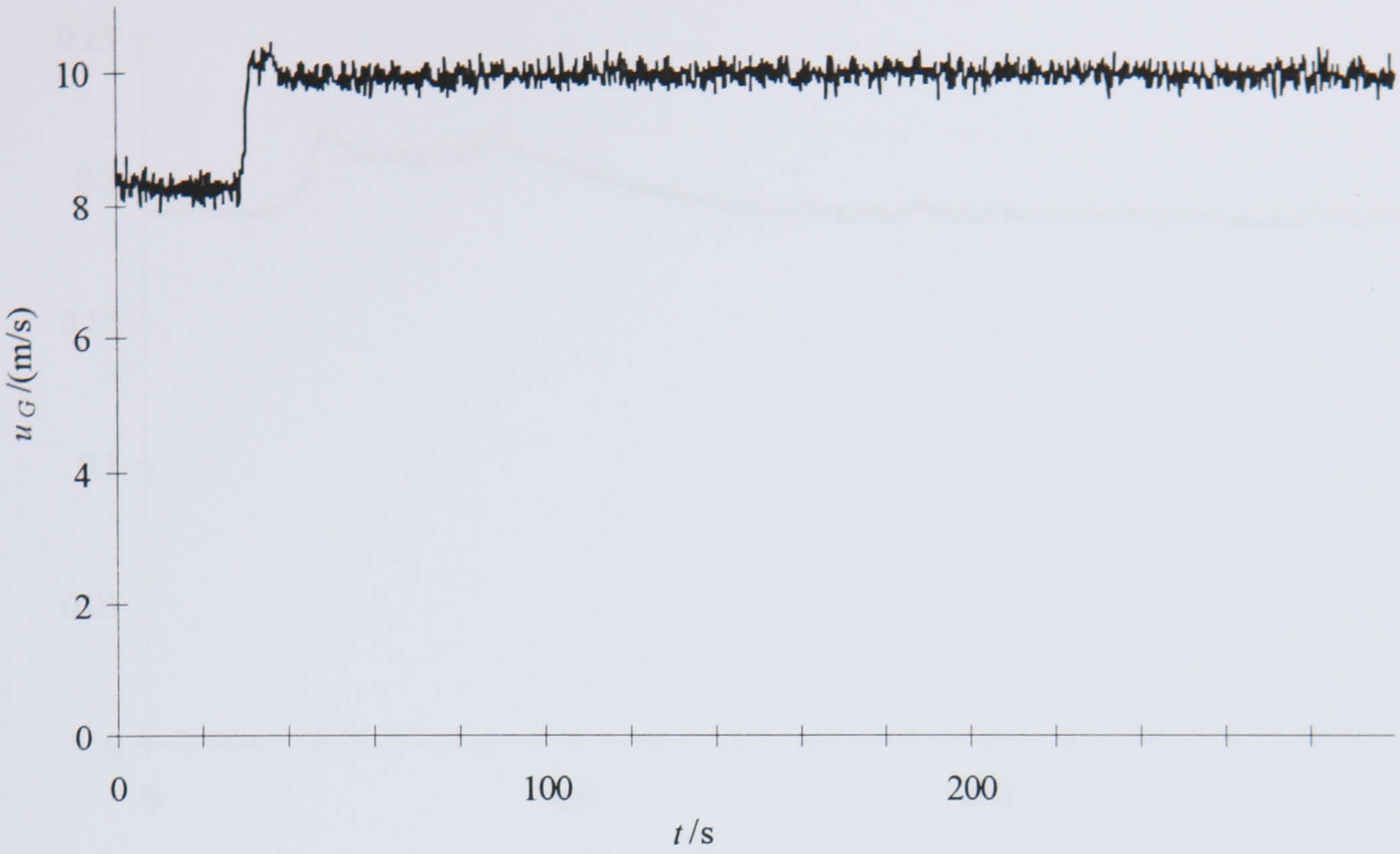


Figure 5.17 Measured gas phase average velocity u_G for transient case `1f` (U_L=0.058 m/s, $U_{G,1}$=7.07 m/s, $U_{G,2}$=8.75 m/s, p=1.00 bar) on the low pressure rig

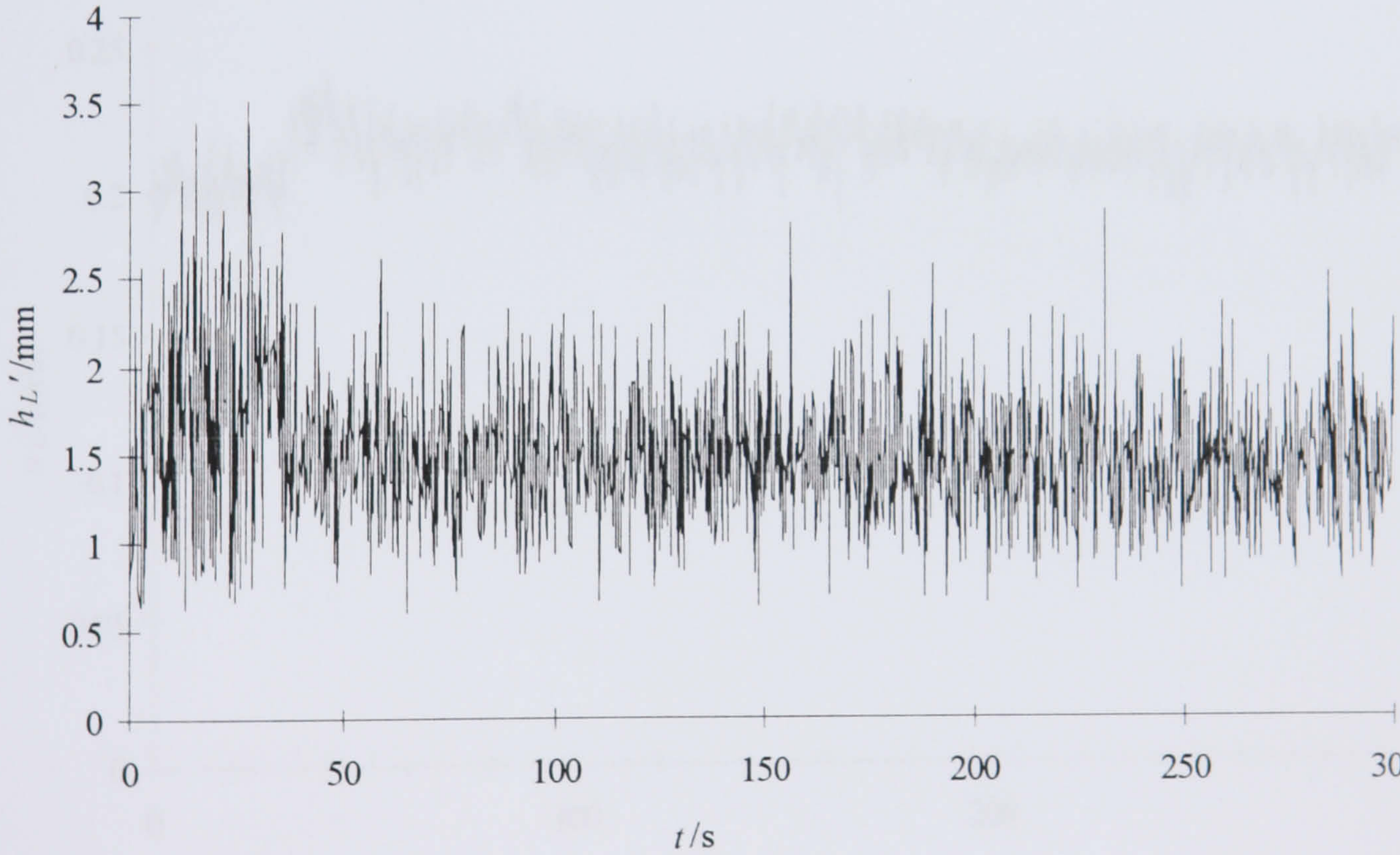


Figure 5.18 Interfacial fluctuation h_L' for transient case `1f` (U_L=0.058 m/s, $U_{G,1}$=7.07 m/s, $U_{G,2}$=8.75 m/s, p=1.00 bar) on the low pressure rig

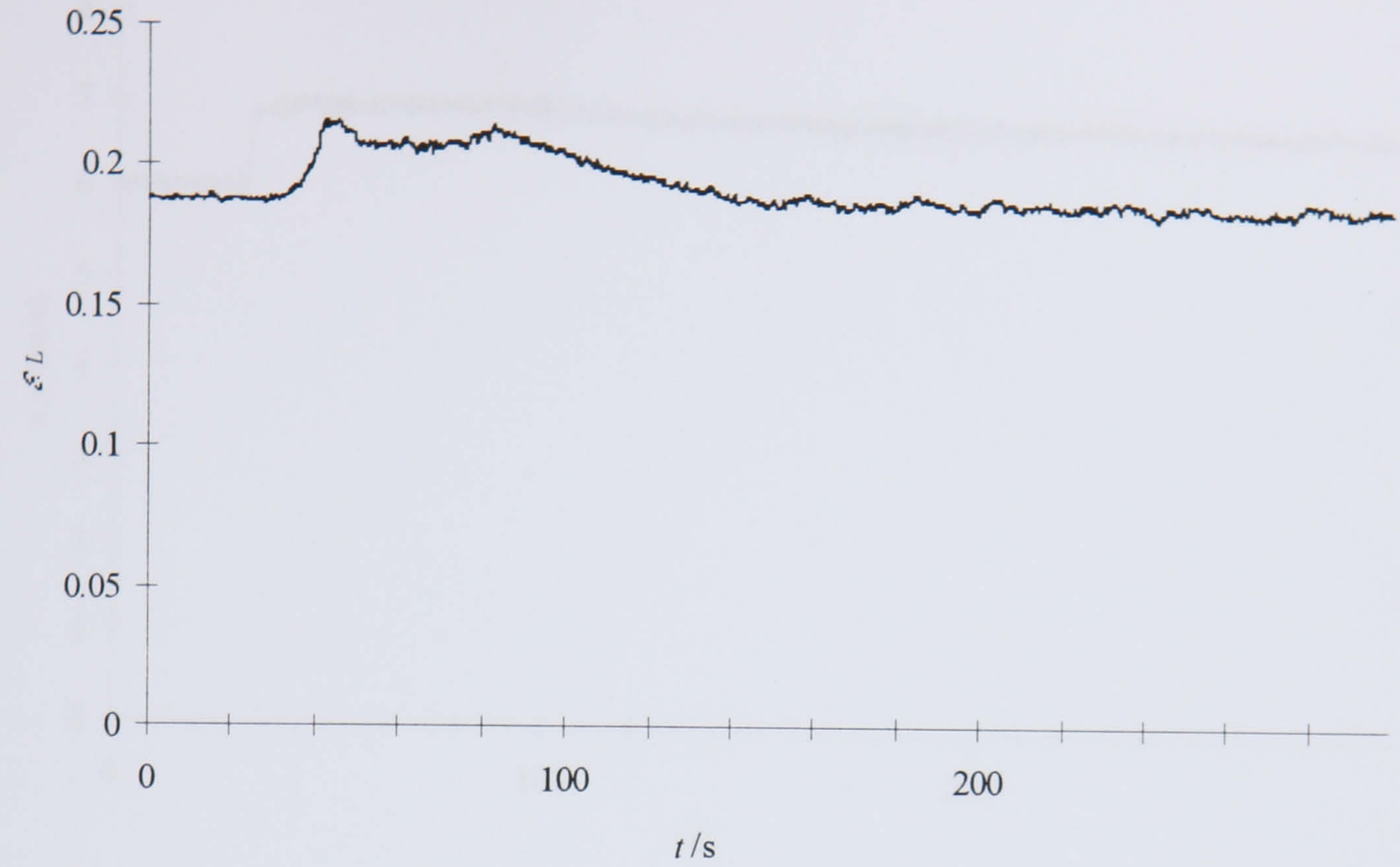


Figure 5.19 Measured liquid holdup ε_L for transient case wb (U_L=0.037 m/s, $U_{G,1}$=5.33 m/s, $U_{G,2}$=6.07 m/s, p=1.06 bar) on the WASP rig

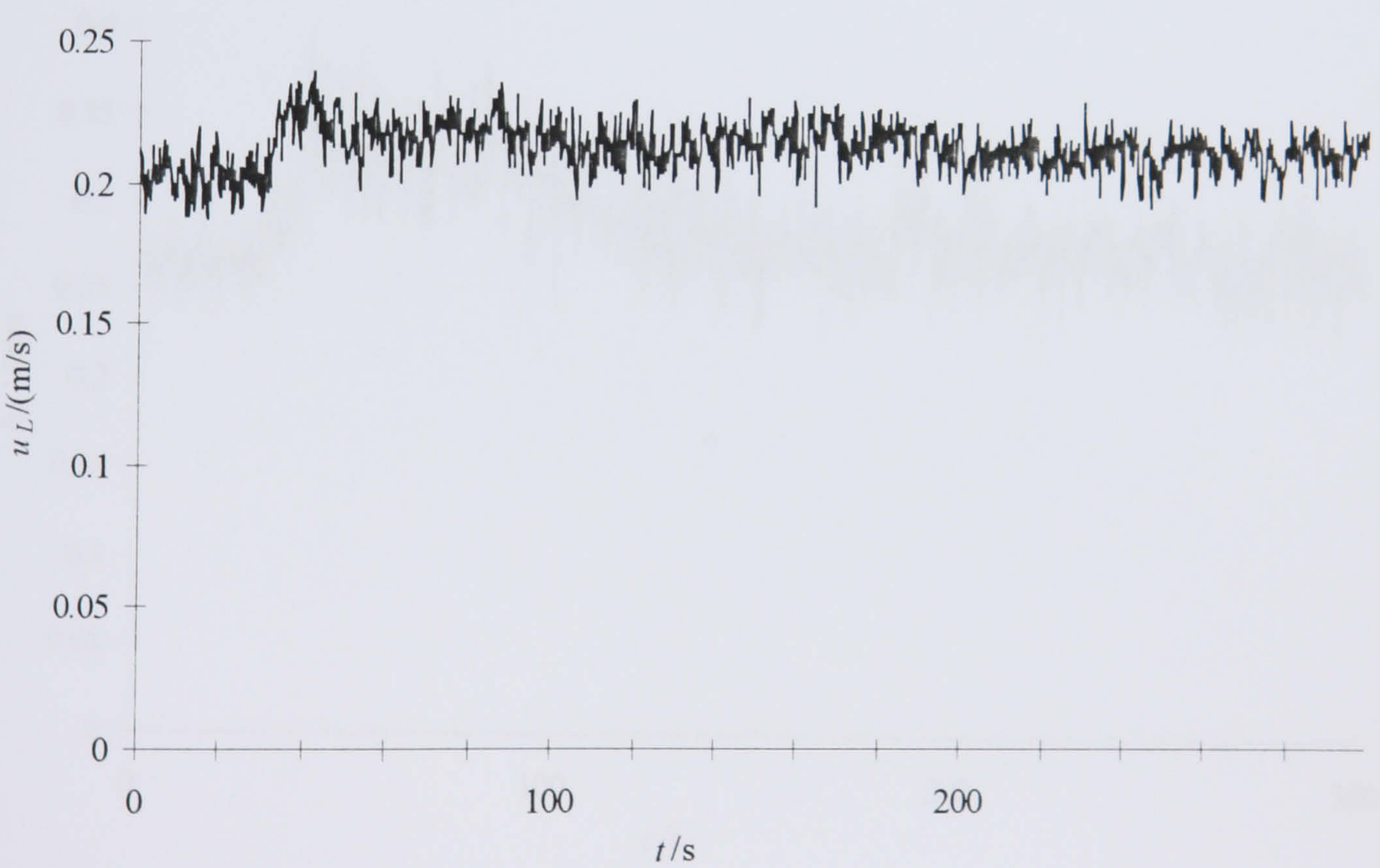


Figure 5.20 Measured liquid phase average velocity u_L for transient case wb (U_L=0.037 m/s, $U_{G,1}$=5.33 m/s, $U_{G,2}$=6.07 m/s, p=1.06 bar) on the WASP rig

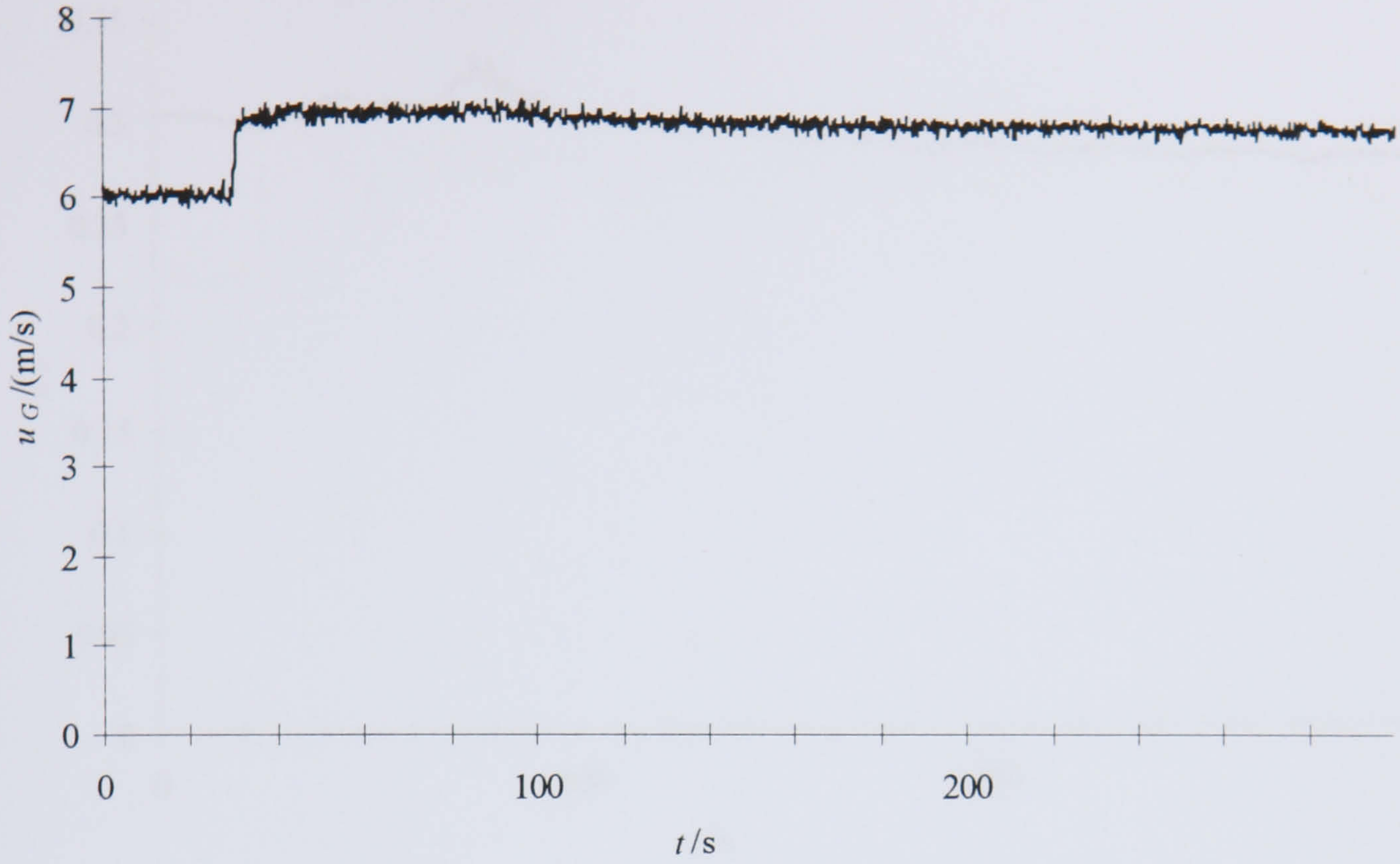


Figure 5.21 Measured gas phase average velocity u_G for transient case wb (U_L=0.037 m/s, $U_{G,1}$=5.33 m/s, $U_{G,2}$=6.07 m/s, p=1.06 bar) on the WASP rig

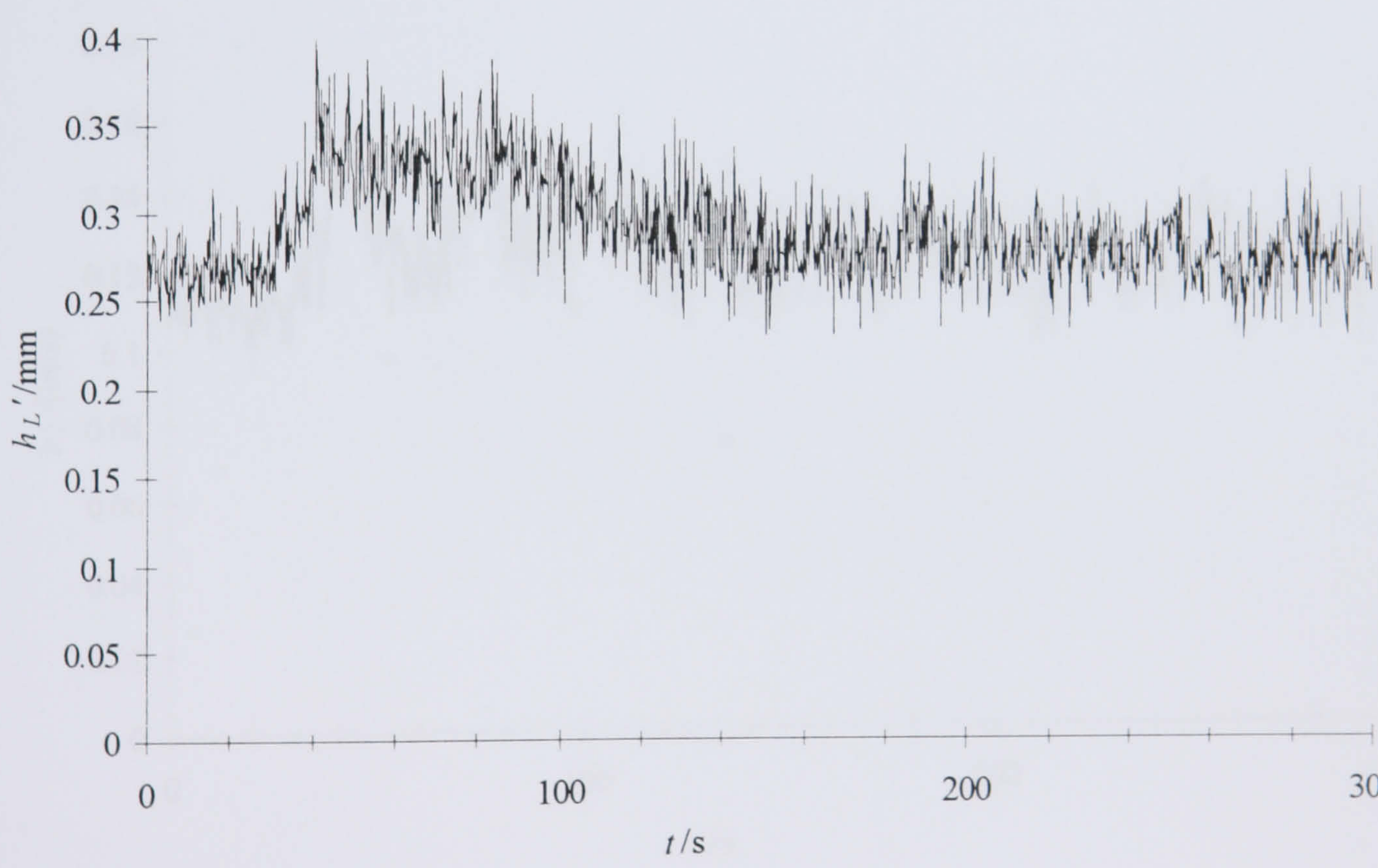


Figure 5.22 Interfacial fluctuation h_L' for transient case wb (U_L=0.037 m/s, $U_{G,1}$=5.33 m/s, $U_{G,2}$=6.07 m/s, p=1.06 bar) on the WASP rig

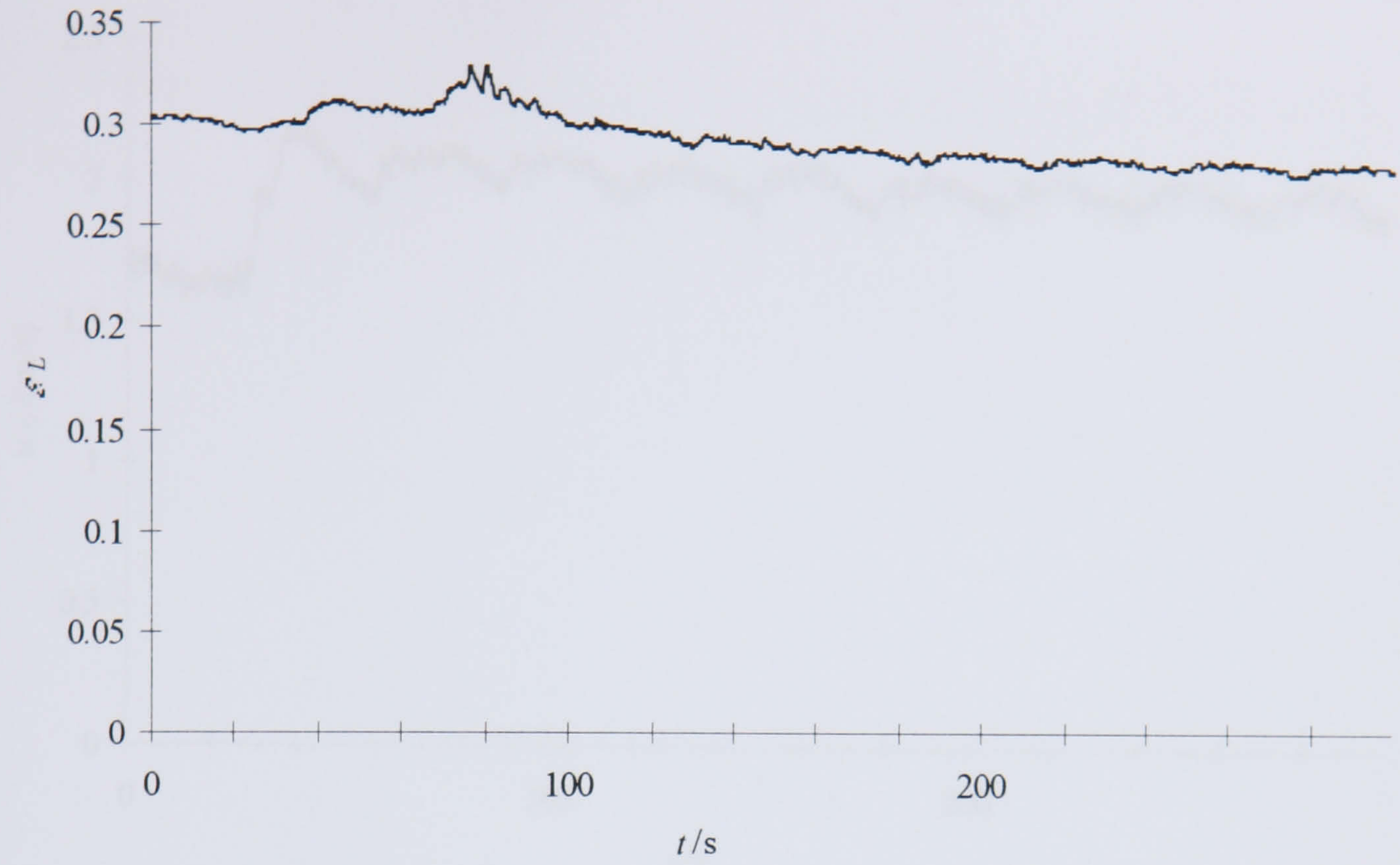


Figure 5.23 Measured liquid holdup ε_L for transient case wd (U_L=0.032 m/s, $U_{G,1}$=1.30 m/s, $U_{G,2}$=1.62 m/s, p=6.03 bar) on the WASP rig

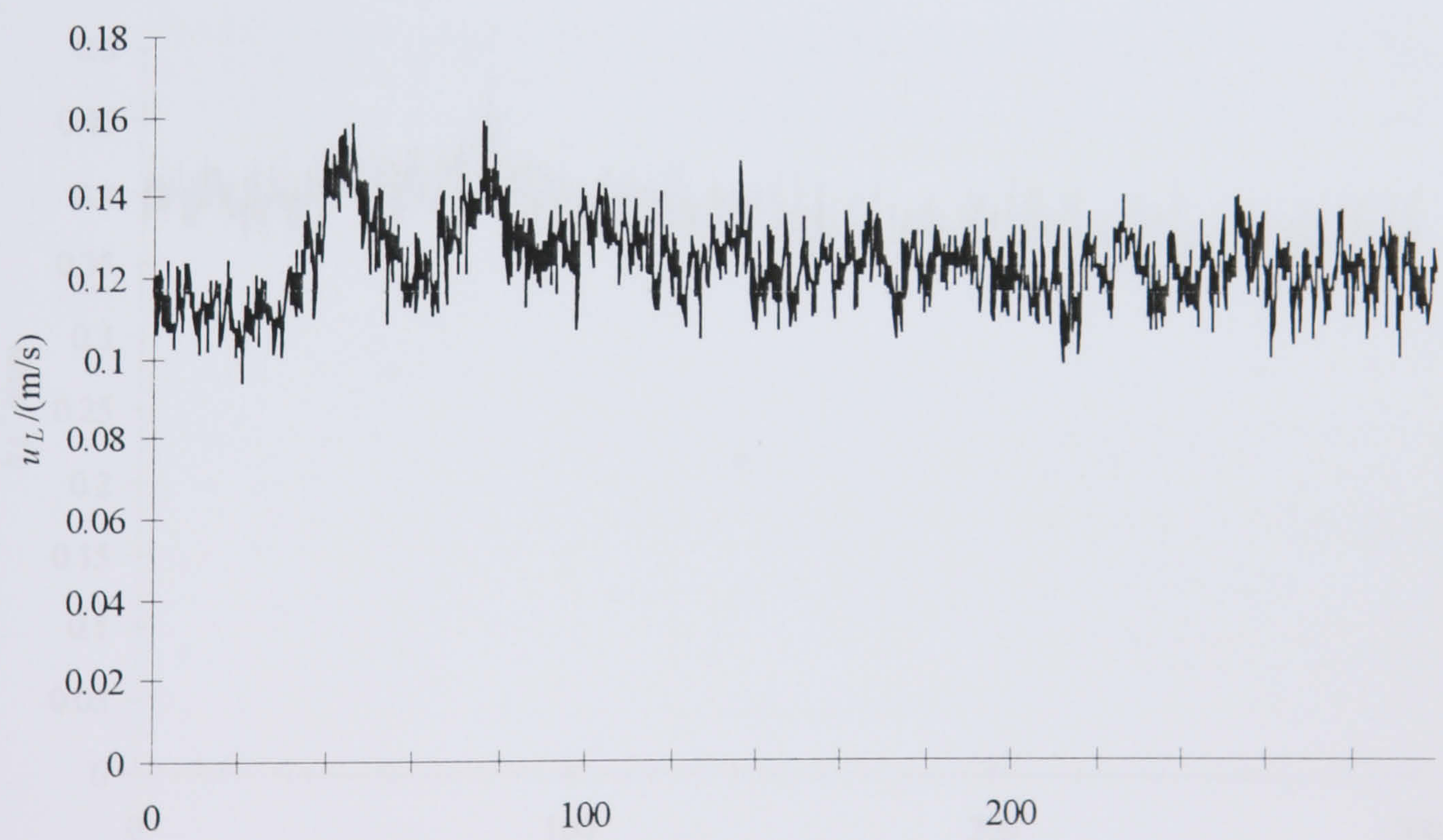


Figure 5.24 Measured liquid phase average velocity u_L for transient case wd (U_L=0.032 m/s, $U_{G,1}$=1.30 m/s, $U_{G,2}$=1.62 m/s, p=6.03 bar) on the WASP rig

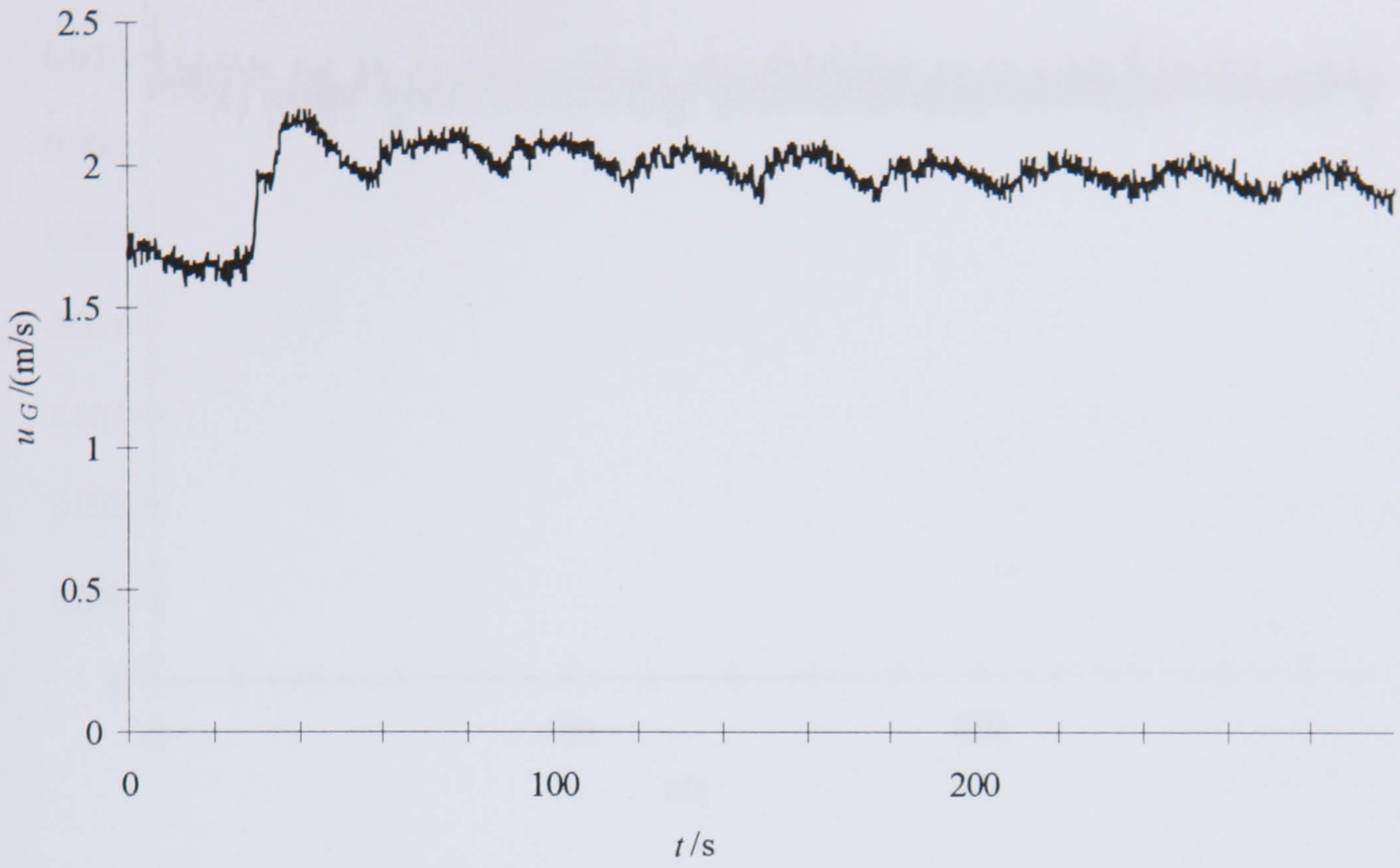


Figure 5.25 Measured gas phase average velocity u_G for transient case wd (U_L=0.032 m/s, $U_{G,1}$=1.30 m/s, $U_{G,2}$=1.62 m/s, p=6.03 bar) on the WASP rig

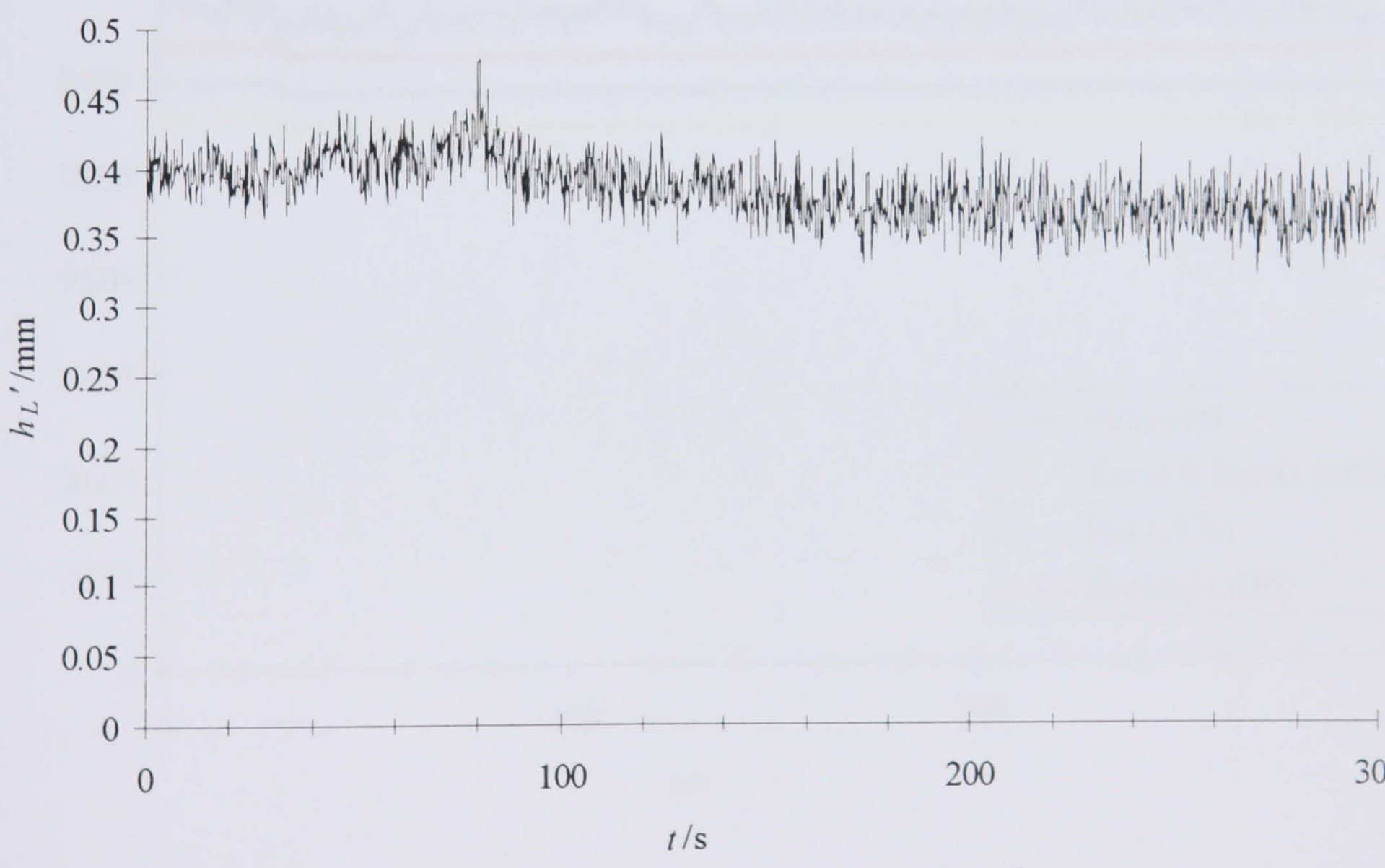


Figure 5.26 Interfacial fluctuation h_L' for transient case wd (U_L=0.032 m/s, $U_{G,1}$=1.30 m/s, $U_{G,2}$=1.62 m/s, p=6.03 bar) on the WASP rig

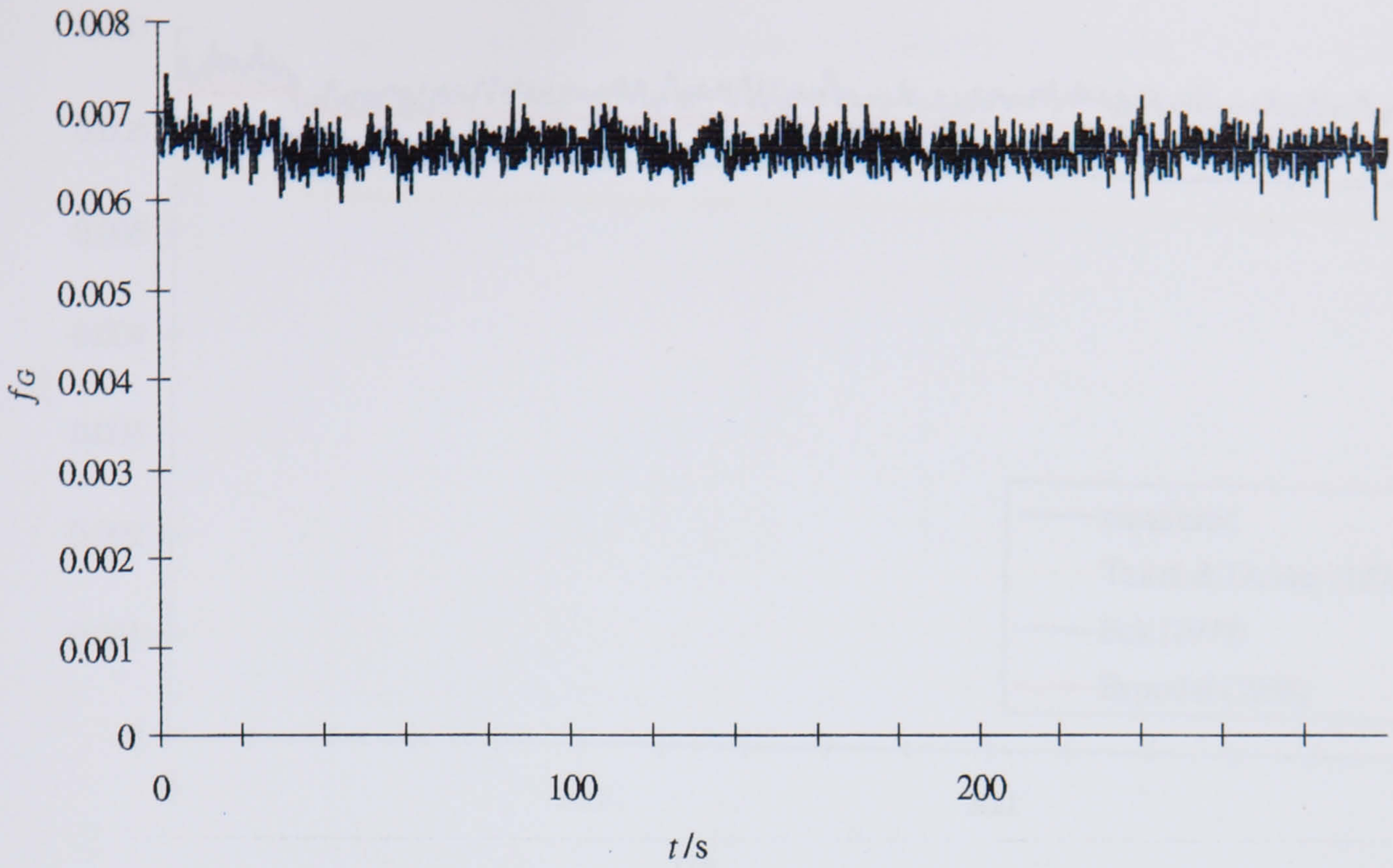


Figure 5.27 Measured gas wall friction factor f_G for transient case `1c` (U_L=0.039 m/s, $U_{G,1}$=7.39 m/s, $U_{G,2}$=8.08 m/s, p=0.99 bar) on the low pressure rig

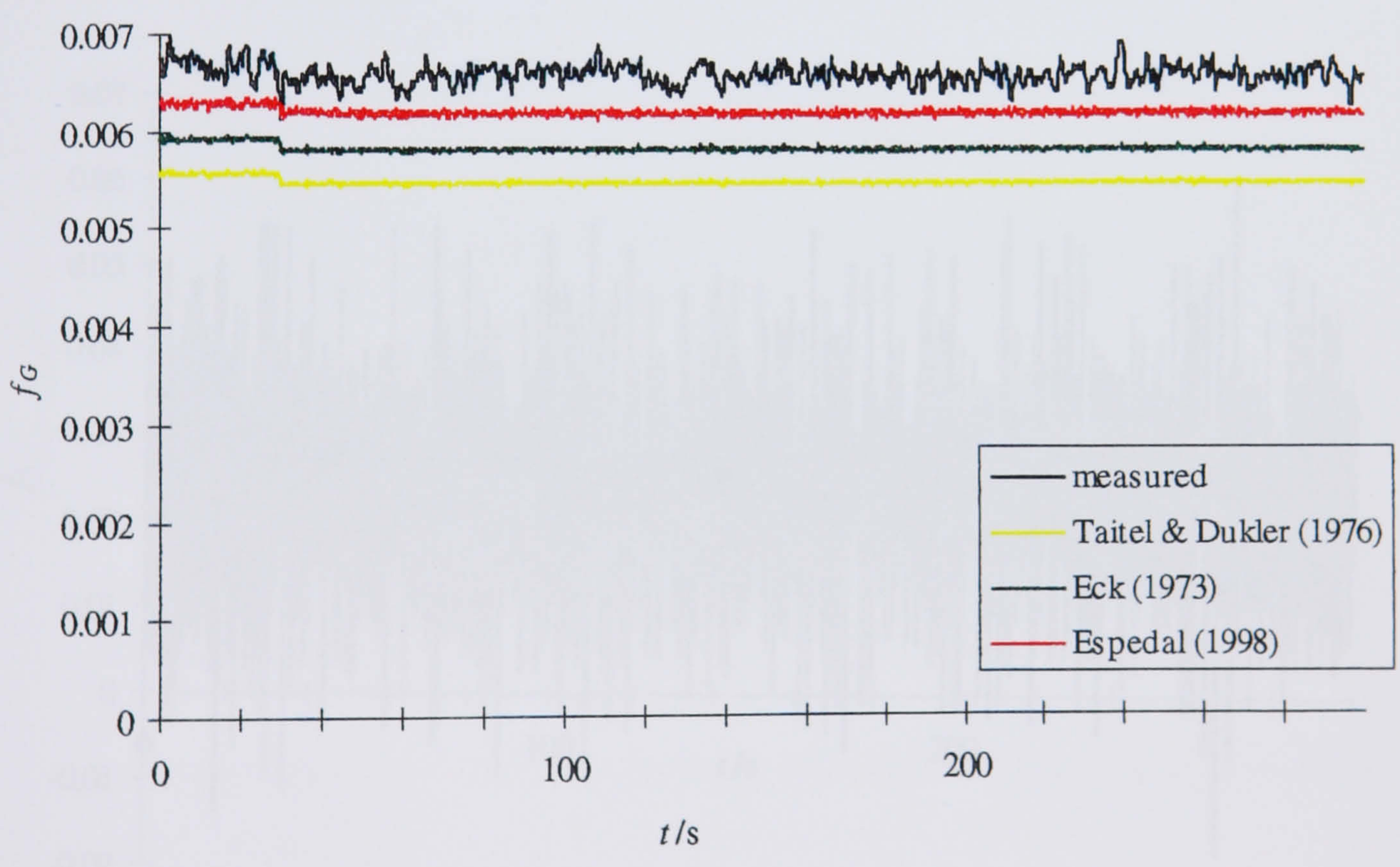


Figure 5.28 Comparison between measured gas wall friction factor f_G and models for transient case `1c` (U_L=0.039 m/s, $U_{G,1}$=7.39 m/s, $U_{G,2}$=8.08 m/s, p=0.99 bar) on the low pressure rig

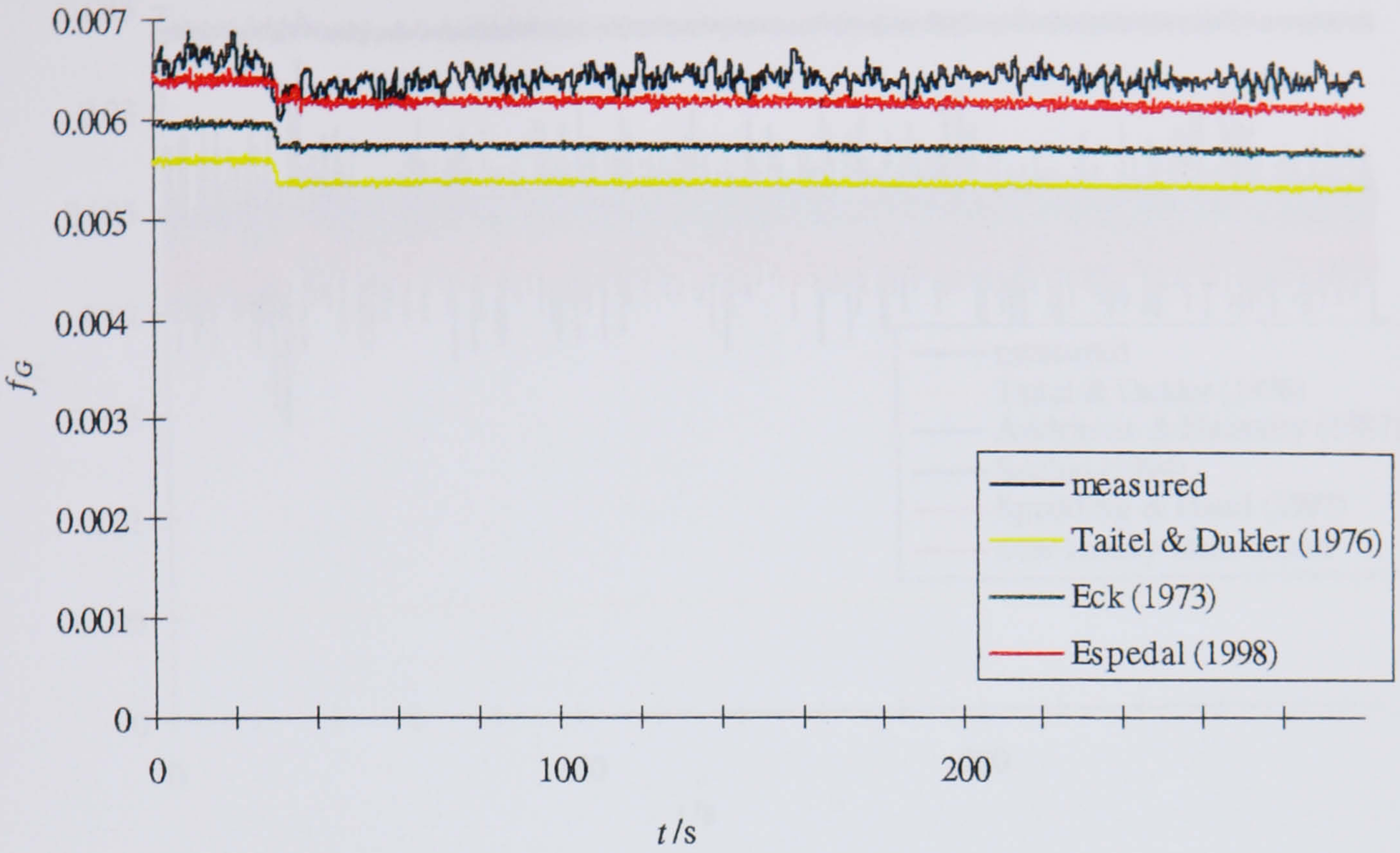


Figure 5.29 Comparison between measured gas wall friction factor f_G and models for transient case `1f` (U_L=0.058 m/s, $U_{G,1}$=7.07 m/s, $U_{G,2}$=8.75 m/s, p=1.00 bar) on the low pressure rig

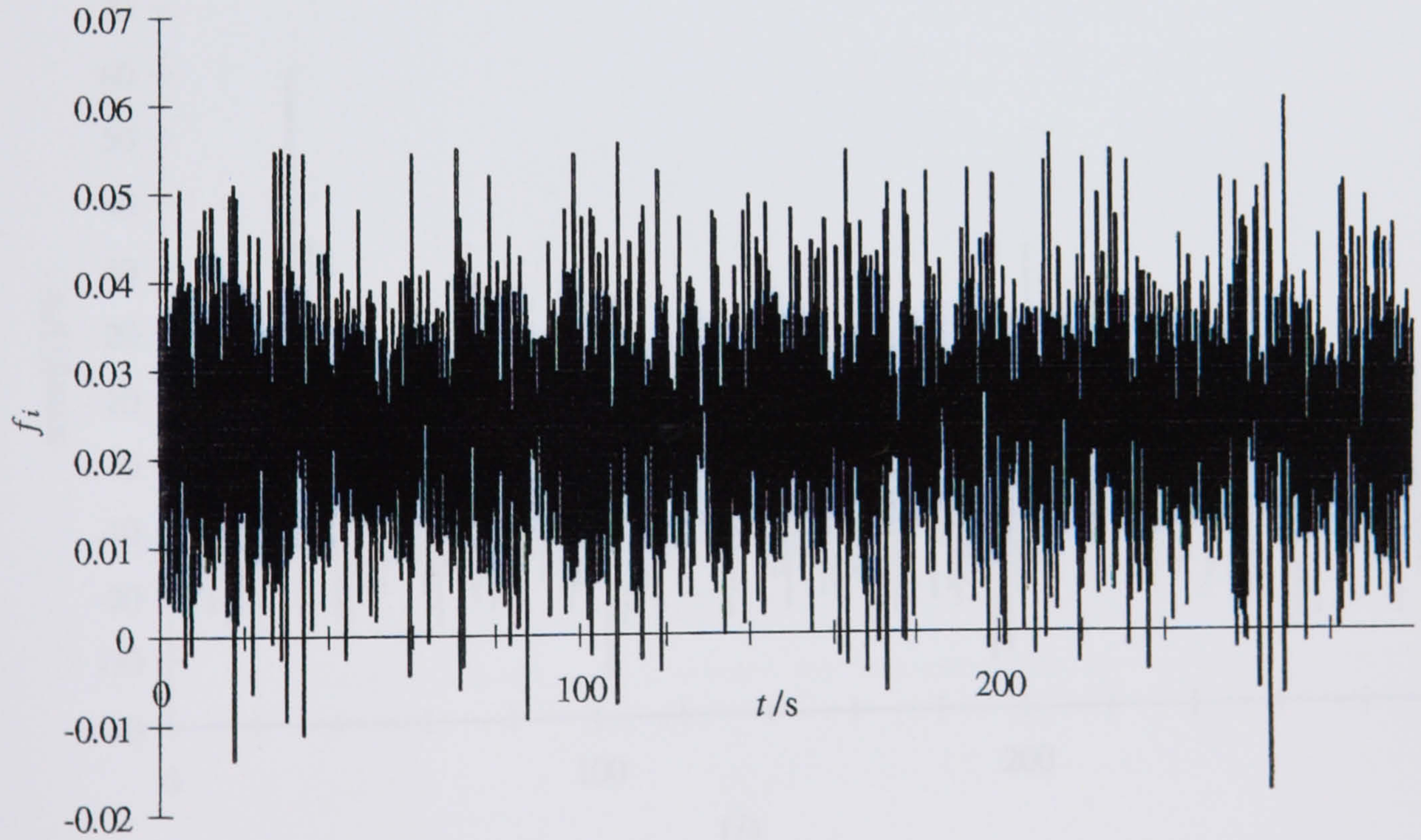


Figure 5.30 Measured interfacial friction factor f_i for transient case `1c` (U_L=0.039 m/s, $U_{G,1}$=7.39 m/s, $U_{G,2}$=8.08 m/s, p=0.99 bar) on the low pressure rig

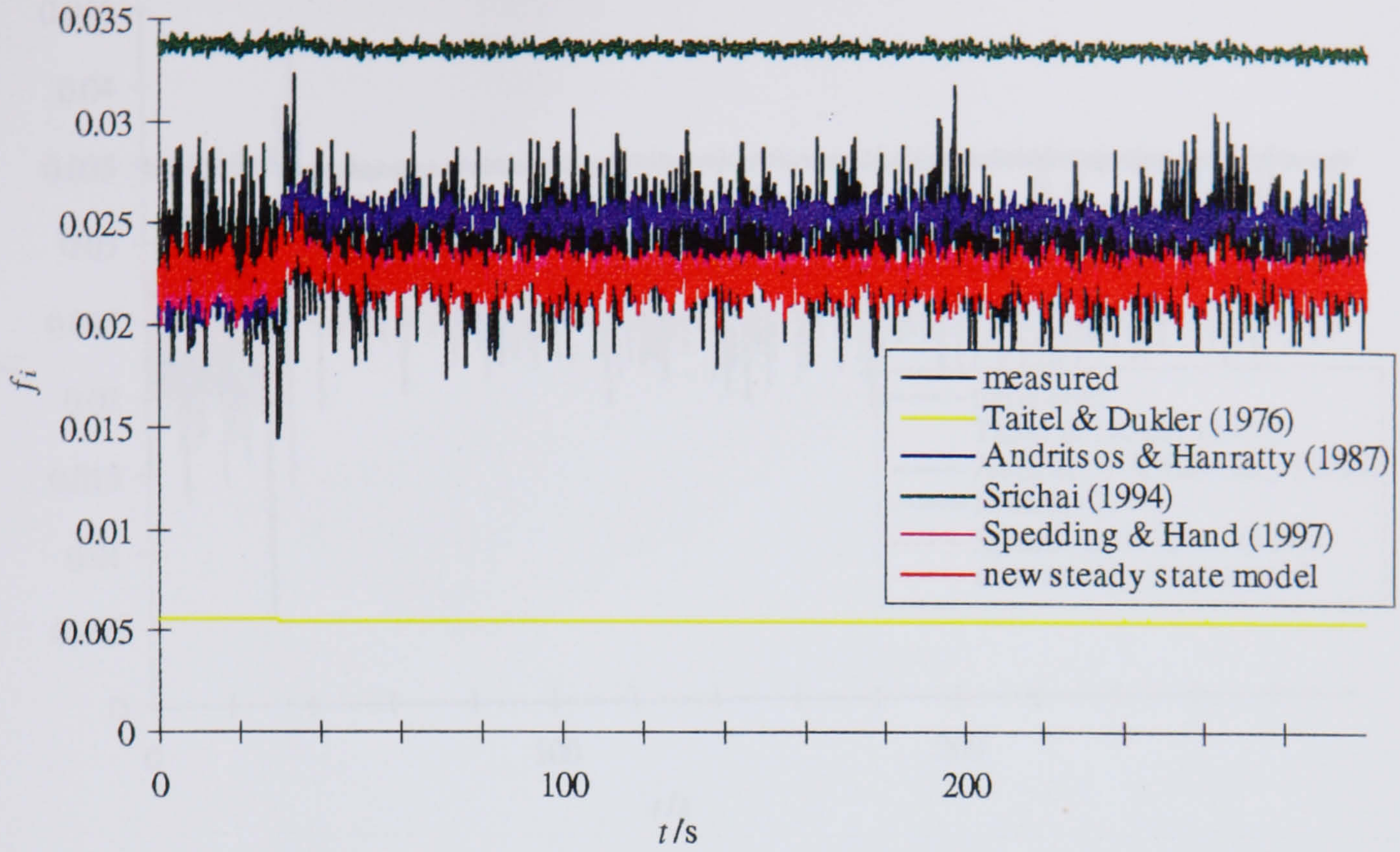


Figure 5.31 Comparison between measured interfacial friction factor f_i and models for transient case `1c` (U_L=0.039 m/s, $U_{G,1}$=7.39 m/s, $U_{G,2}$=8.08 m/s, p=0.99 bar) on the low pressure rig

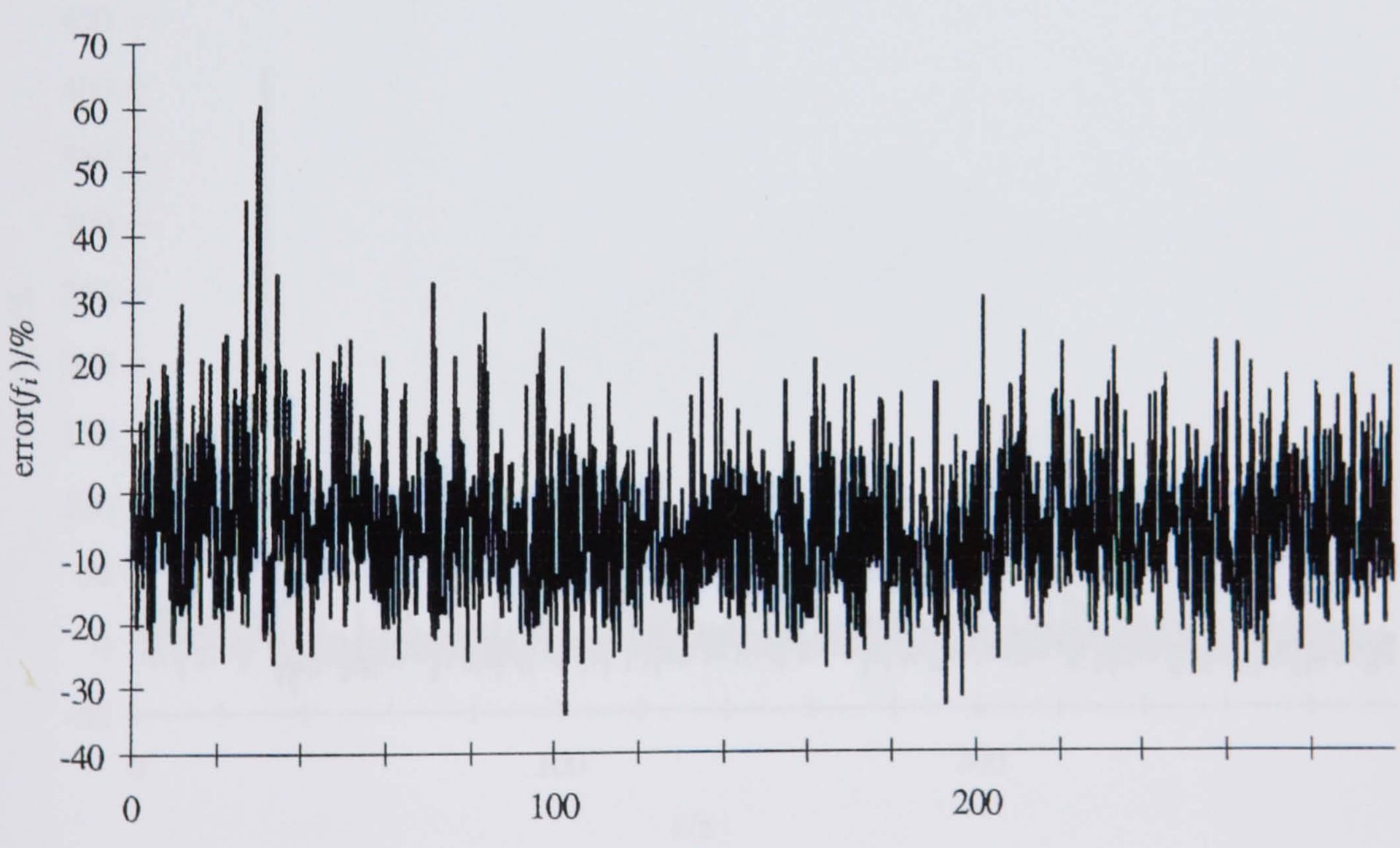


Figure 5.32 Plot of error between measured interfacial friction factor f_i and the new steady state model for transient case `1c` (U_L=0.039 m/s, $U_{G,1}$=7.39 m/s, $U_{G,2}$=8.08 m/s, p=0.99 bar) on the low pressure rig

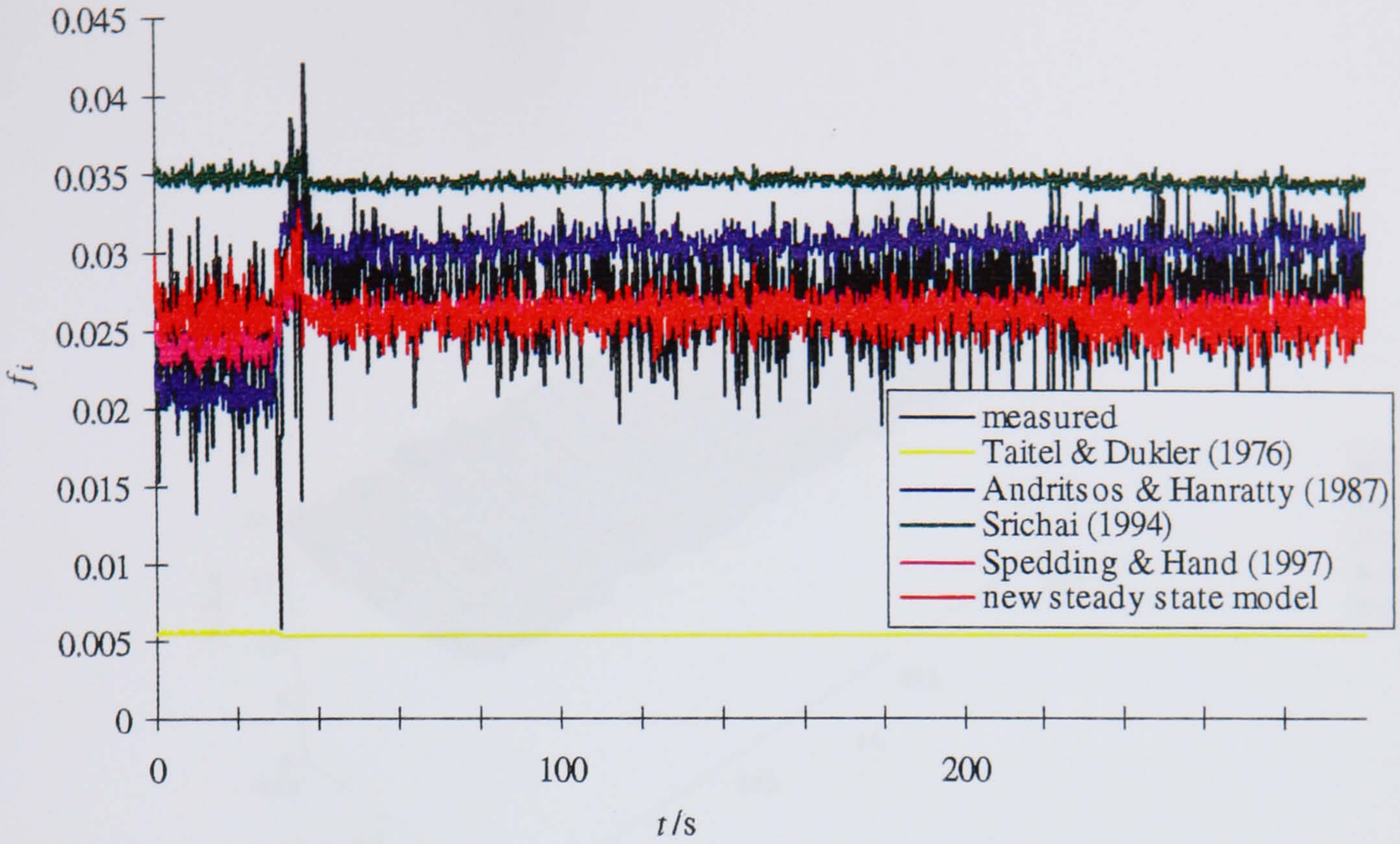


Figure 5.33 Comparison between measured interfacial friction factor f_i and models for transient case `1f` (U_L=0.058 m/s, $U_{G,1}$=7.07 m/s, $U_{G,2}$=8.75 m/s, p=1.00 bar) on the low pressure rig

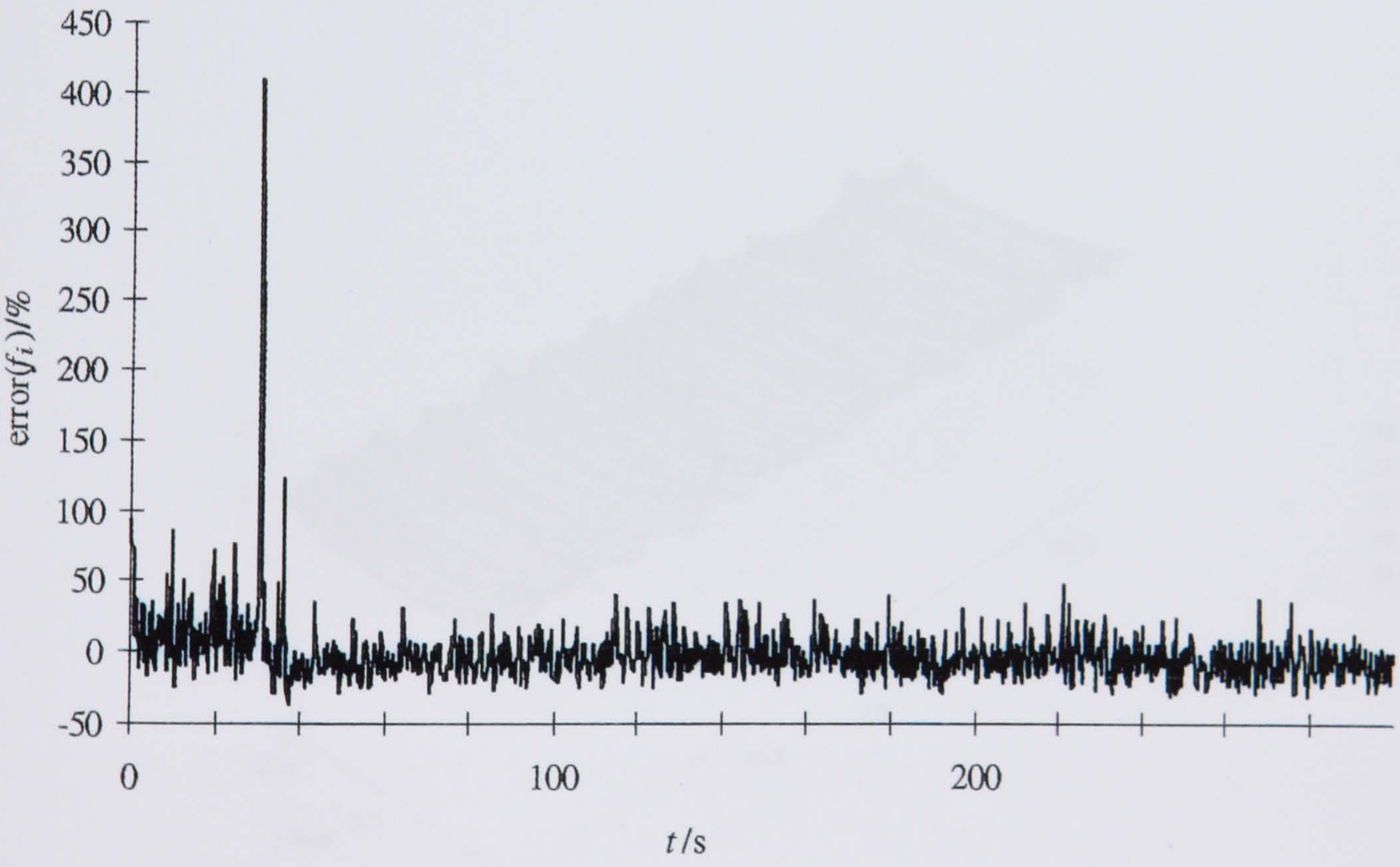


Figure 5.34 Plot of error between measured interfacial friction factor f_i and the new steady state model for transient case `1f` (U_L=0.058 m/s, $U_{G,1}$=7.07 m/s, $U_{G,2}$=8.75 m/s, p=1.00 bar) on the low pressure rig

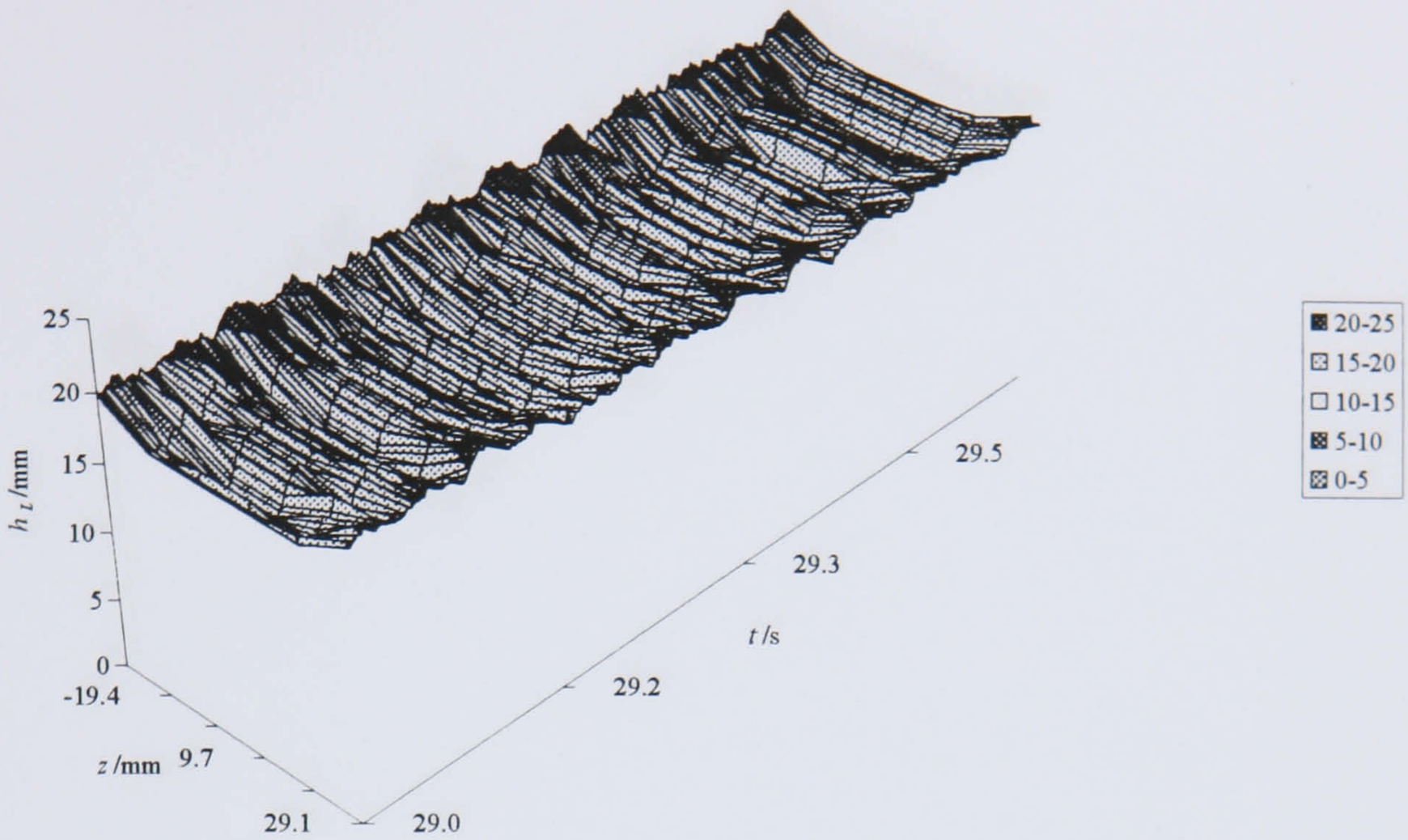


Figure 5.35 Interfacial structure for initial steady state of transient case `1a` (U_L=0.039 m/s, $U_{G,1}$=5.01 m/s, $U_{G,2}$=6.46 m/s, p=1.00 bar) on the low pressure rig

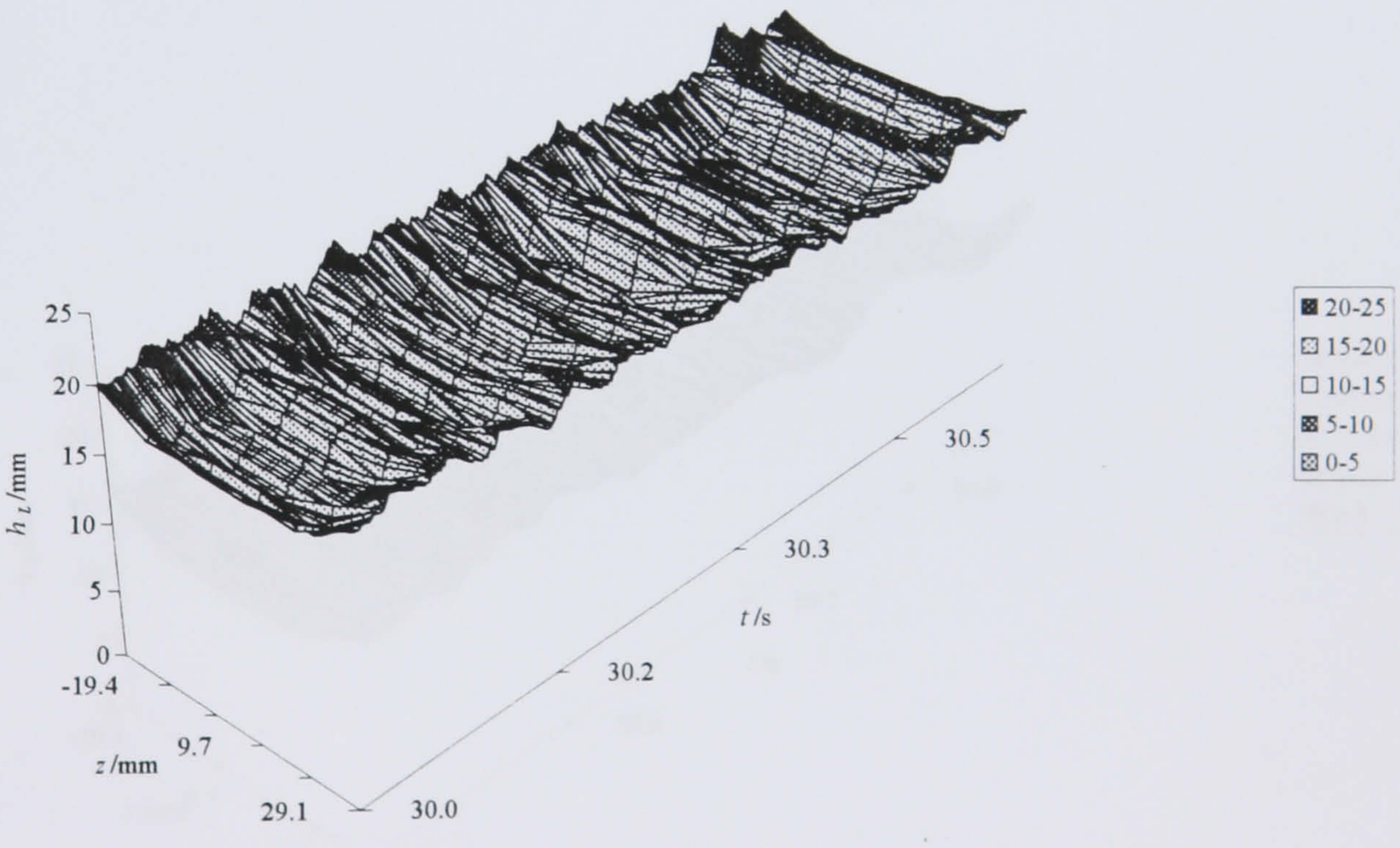


Figure 5.36 Interfacial structure in the time interval 0-0.6 seconds after the transient change of case `1a` (U_L=0.039 m/s, $U_{G,1}$=5.01 m/s, $U_{G,2}$=6.46 m/s, p=1.00 bar) on the low pressure rig

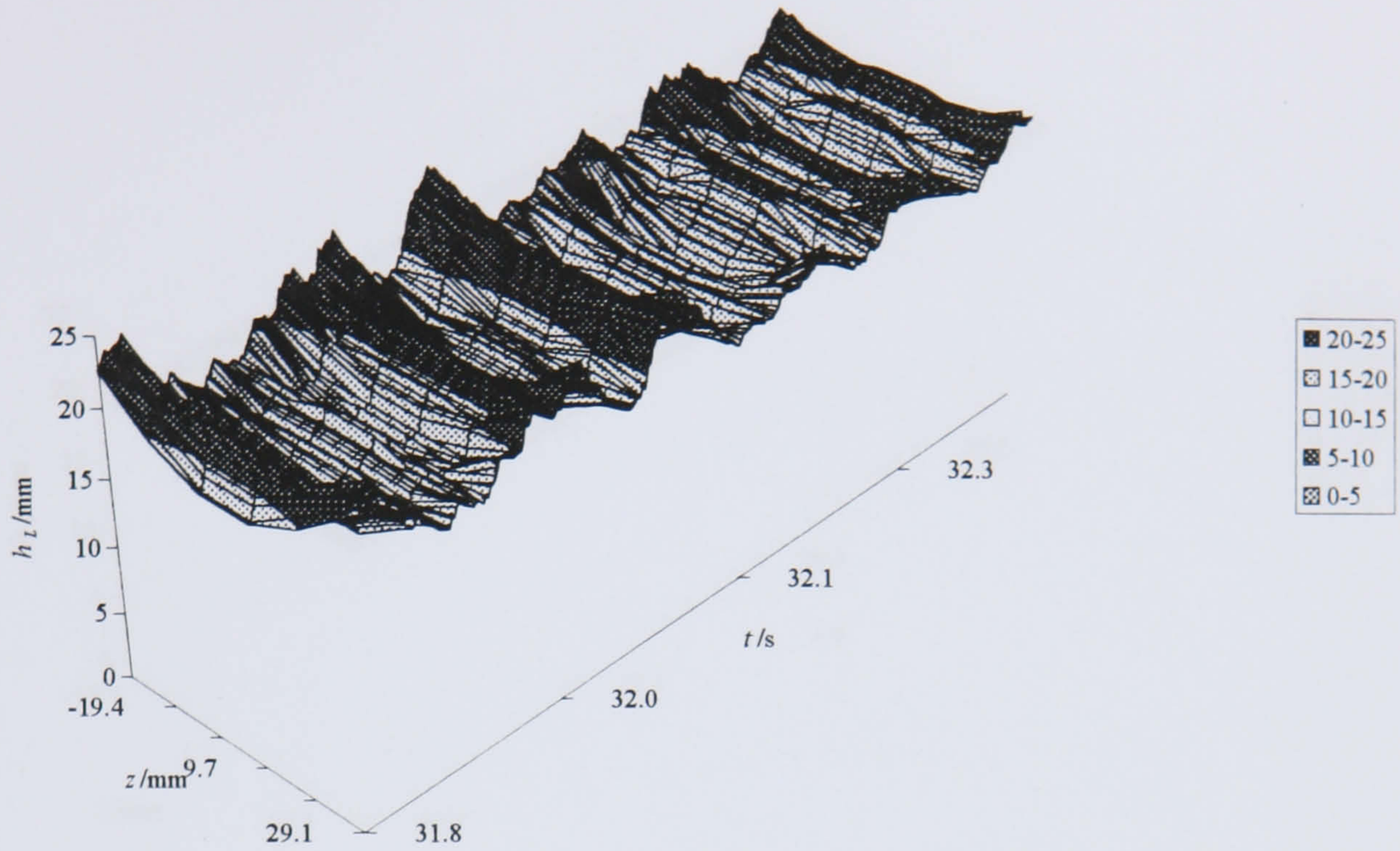


Figure 5.37 Interfacial structure in the time interval 1.8-2.4 seconds after the transient change of case `1a` (U_L=0.039 m/s, $U_{G,1}$=5.01 m/s, $U_{G,2}$=6.46 m/s, p=1.00 bar) on the low pressure rig

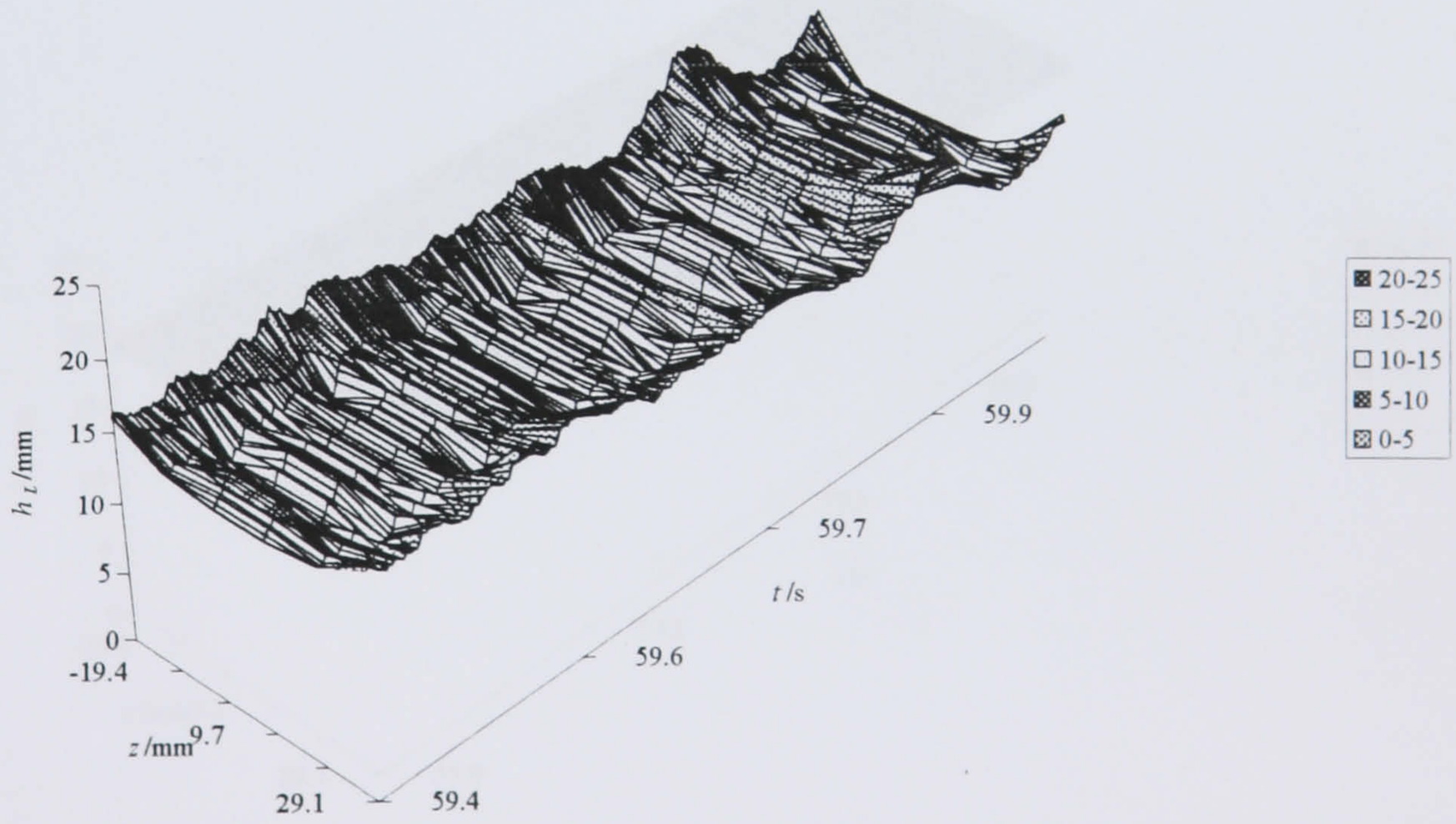


Figure 5.38 Interfacial structure in the time interval 29.4-30.0 seconds after the transient change of case `1a` (U_L=0.039 m/s, $U_{G,1}$=5.01 m/s, $U_{G,2}$=6.46 m/s, p=1.00 bar) on the low pressure rig

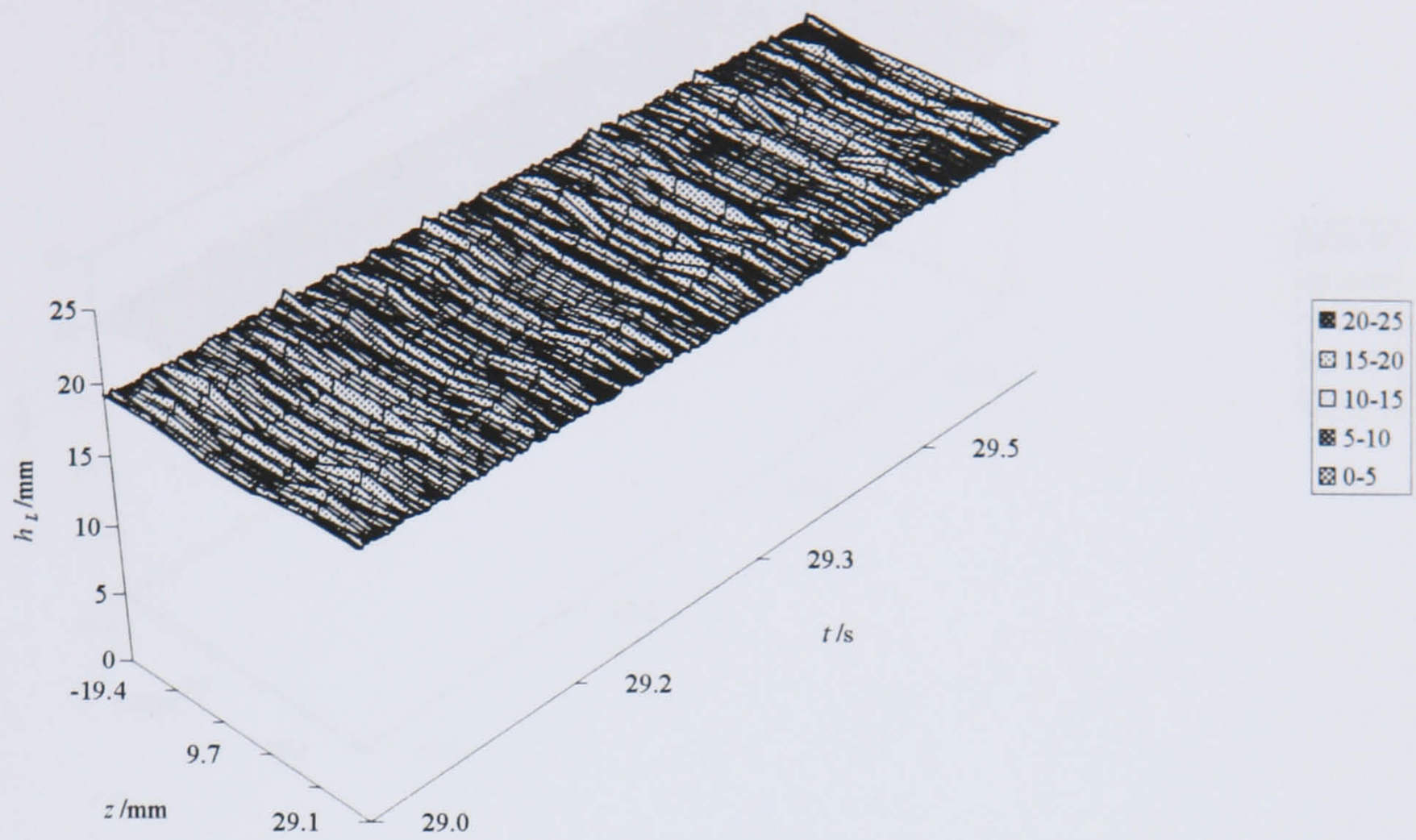


Figure 5.39 Interfacial structure for initial steady state of transient case wb (U_L=0.037 m/s, $U_{G,1}$=5.33 m/s, $U_{G,2}$=6.07 m/s, p=1.06 bar) on the WASP rig

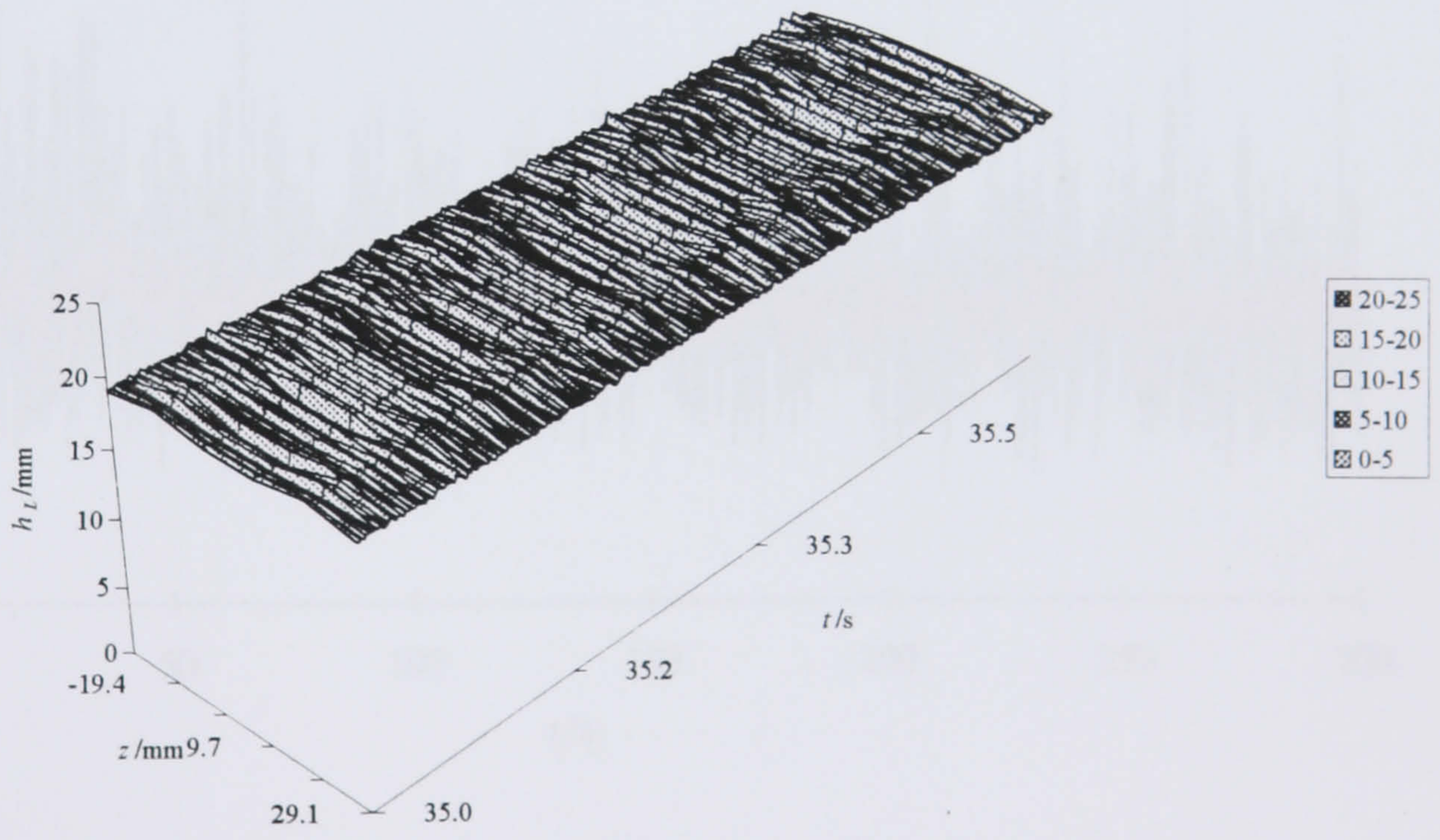


Figure 5.40 Interfacial structure in the time interval 5.0-5.6 seconds after the transient change of case wb (U_L=0.037 m/s, $U_{G,1}$=5.33 m/s, $U_{G,2}$=6.07 m/s, p=1.06 bar) on the WASP rig

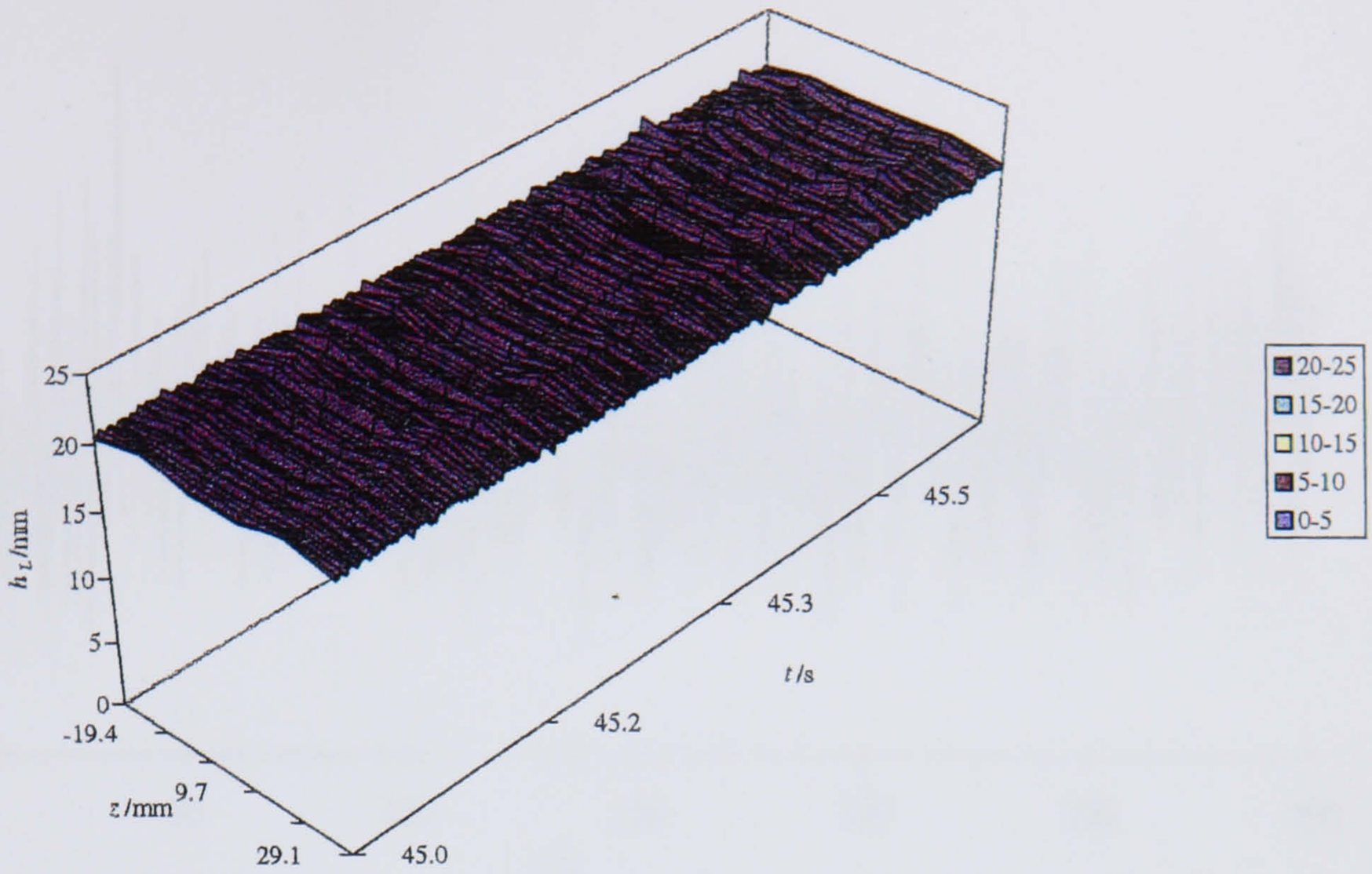


Figure 5.41 Interfacial structure in the time interval 15.0-15.6 seconds after the transient change of case wb (U_L=0.037 m/s, $U_{G,1}$=5.33 m/s, $U_{G,2}$=6.07 m/s, p=1.06 bar) on the WASP rig

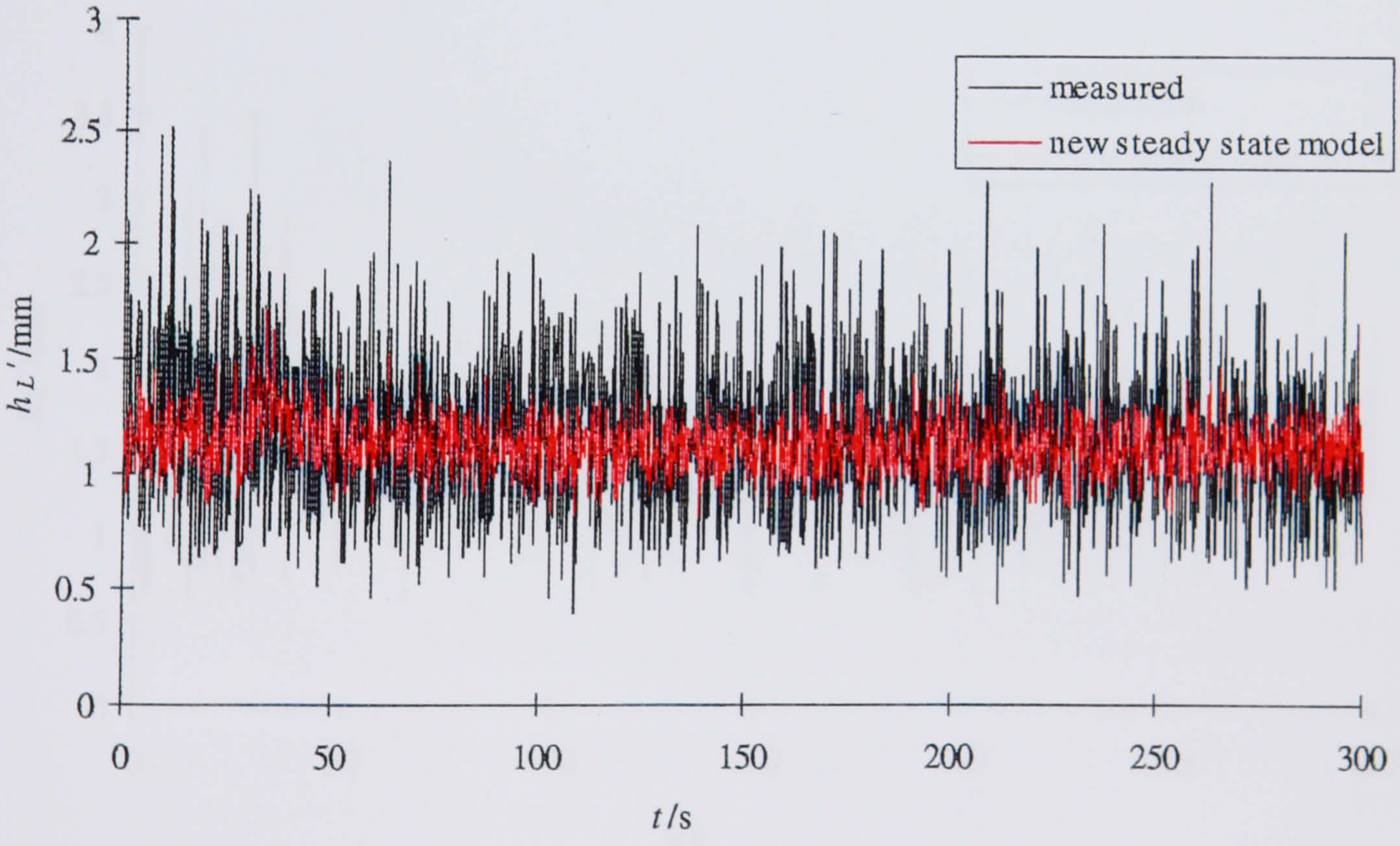


Figure 5.42 Comparison between measured interfacial fluctuation h_L' and new steady state model for transient case lc (U_L=0.039 m/s, $U_{G,1}$=7.39 m/s, $U_{G,2}$=8.08 m/s, p=0.99 bar) on the low pressure rig

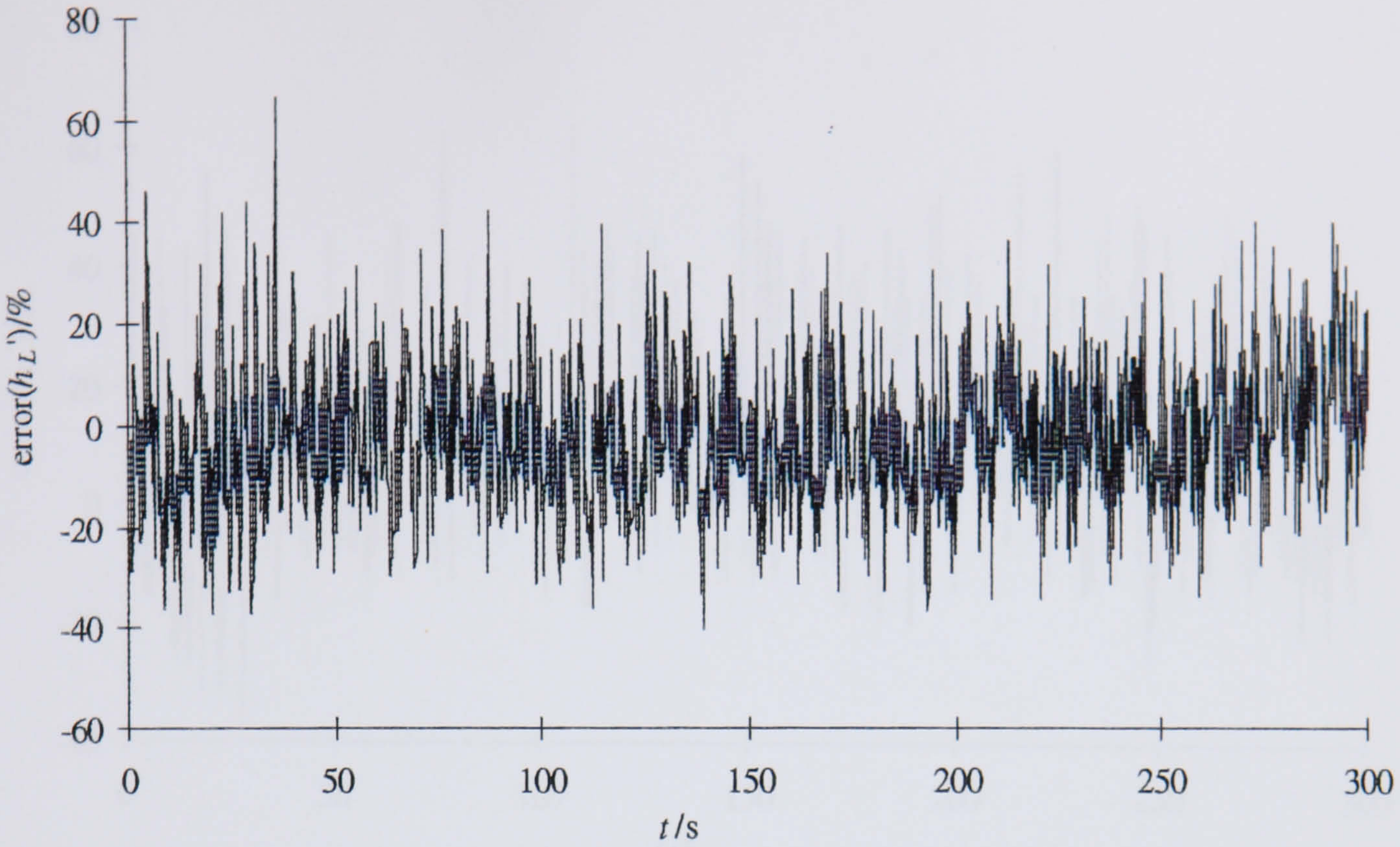


Figure 5.43 Plot of error between measured interfacial fluctuation h_L' and the new steady state model for transient case `1c` (U_L=0.039 m/s, $U_{G,1}$=7.39 m/s, $U_{G,2}$=8.08 m/s, p=0.99 bar) on the low pressure rig

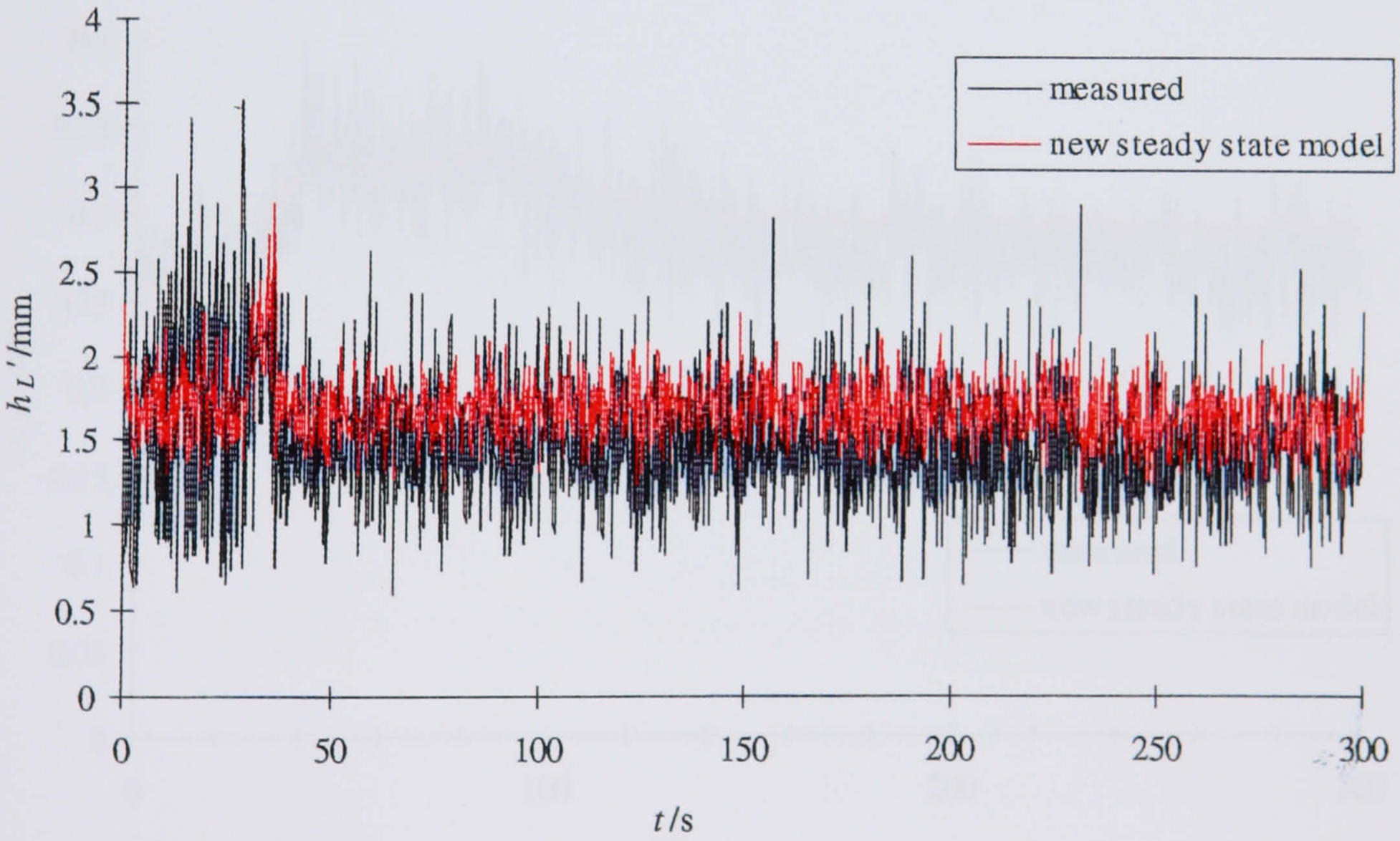


Figure 5.44 Comparison between measured interfacial fluctuation h_L' and new steady state model for transient case `1f` (U_L=0.058 m/s, $U_{G,1}$=7.07 m/s, $U_{G,2}$=8.75 m/s, p=1.00 bar) on the low pressure rig

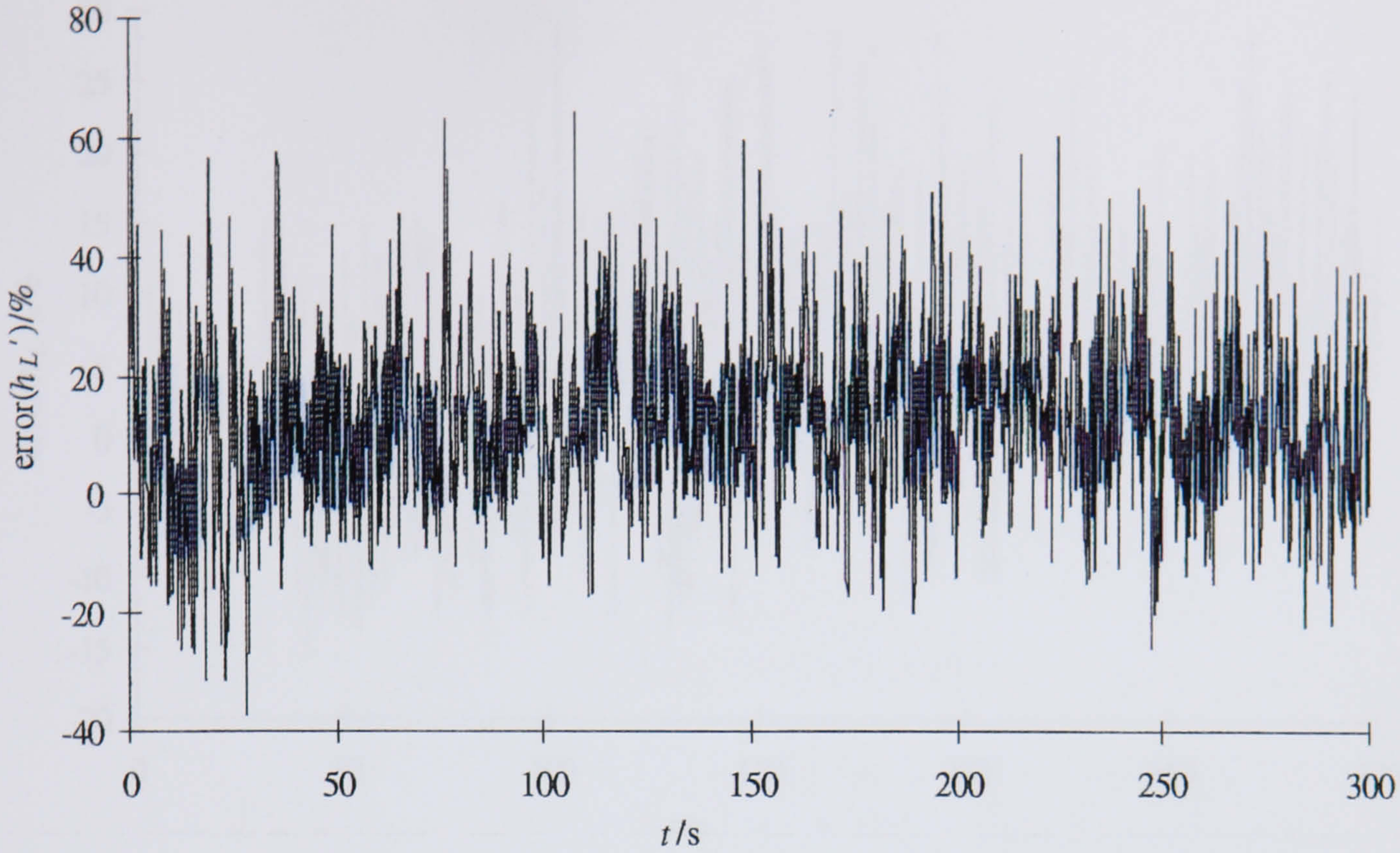


Figure 5.45 Plot of error between measured interfacial fluctuation h_L' and the new steady state model for transient case `lf` (U_L=0.058 m/s, $U_{G,1}$=7.07 m/s, $U_{G,2}$=8.75 m/s, p=1.00 bar) on the low pressure rig

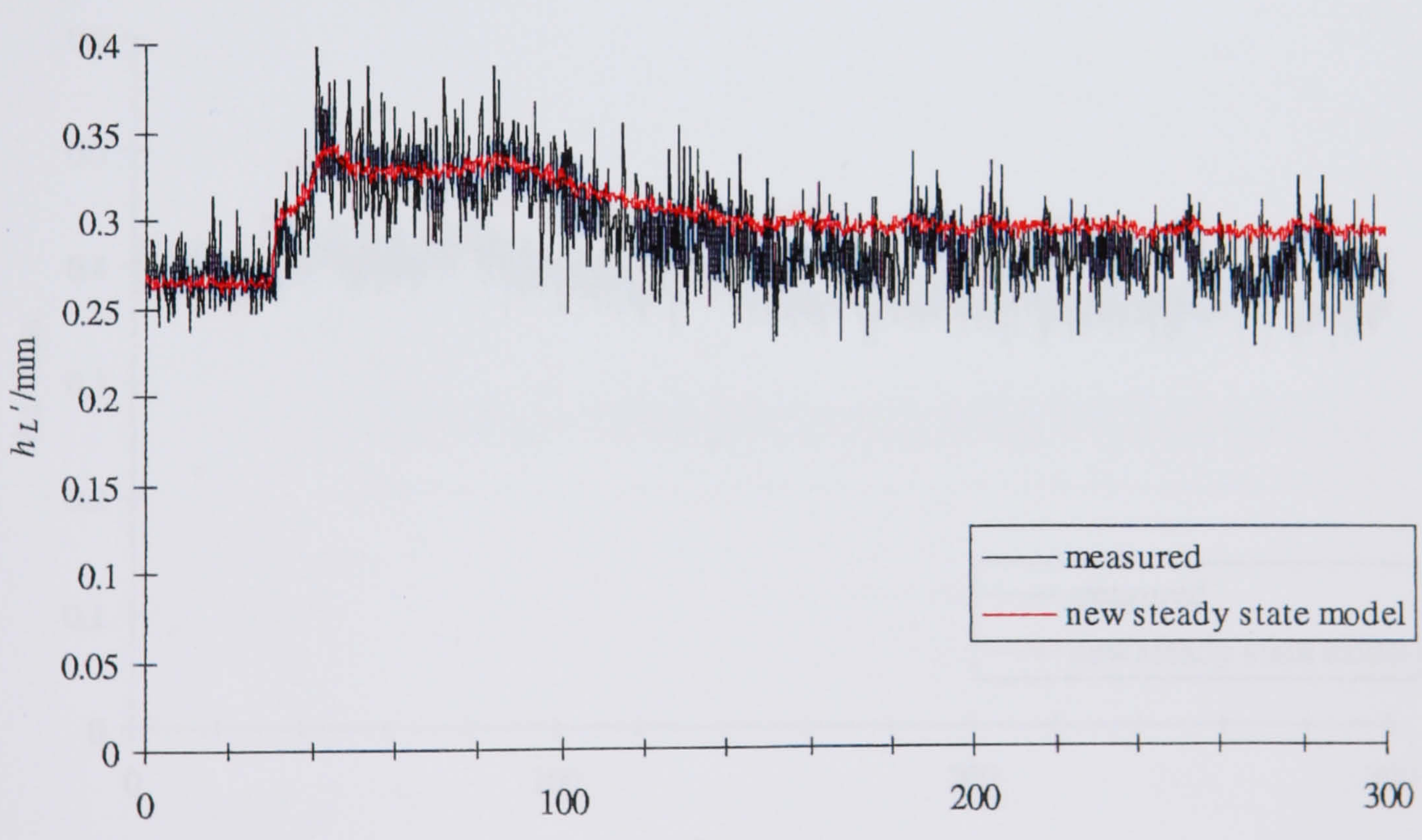


Figure 5.46 Comparison between measured interfacial fluctuation h_L' and new steady state model for transient case `wb` (U_L=0.037 m/s, $U_{G,1}$=5.33 m/s, $U_{G,2}$=6.07 m/s, p=1.06 bar) on the WASP rig

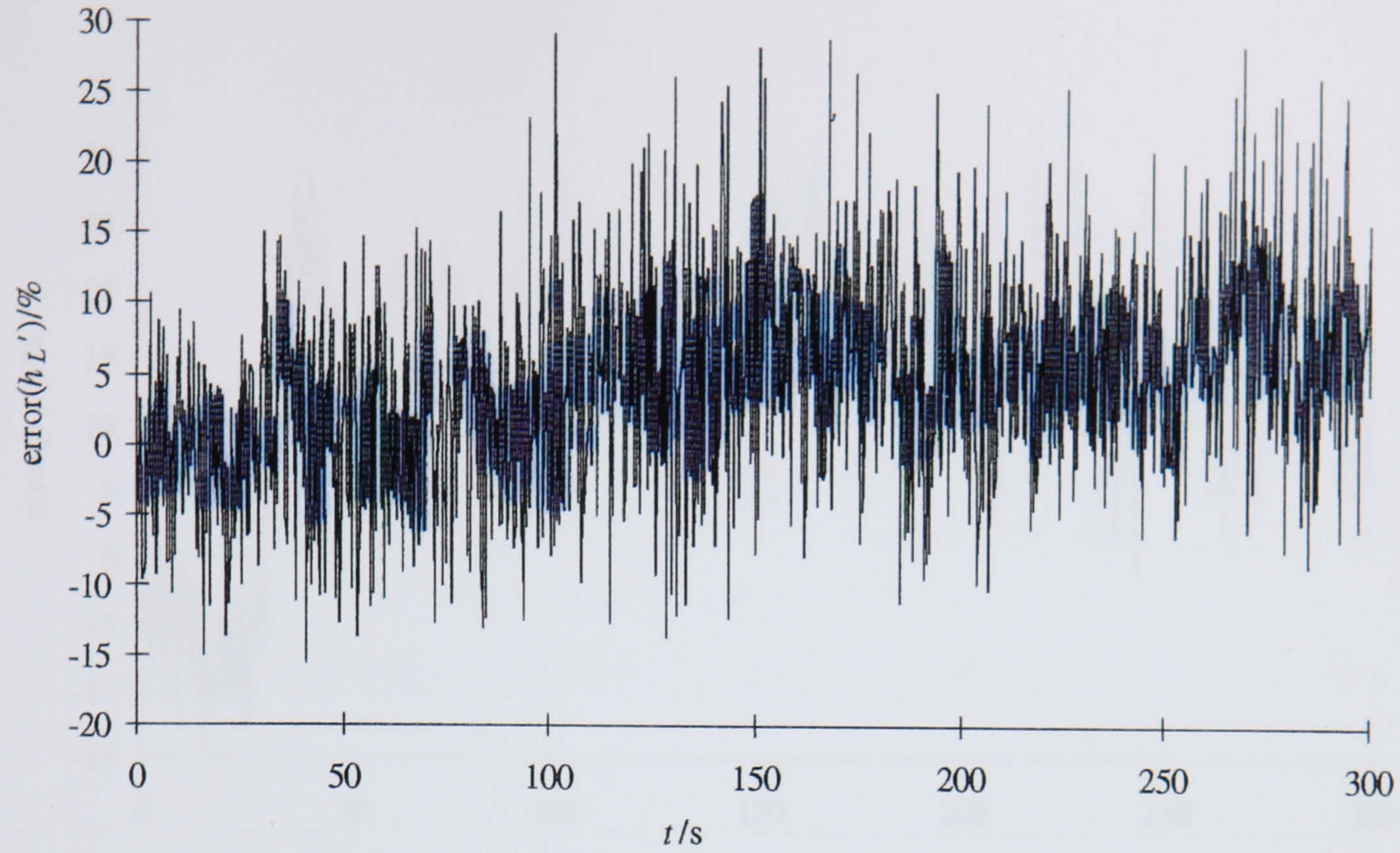


Figure 5.47 Plot of error between measured interfacial fluctuation h_L' and the new steady state model for transient case wb (U_L=0.037 m/s, $U_{G,1}$=5.33 m/s, $U_{G,2}$=6.07 m/s, p=1.06 bar) on the WASP rig

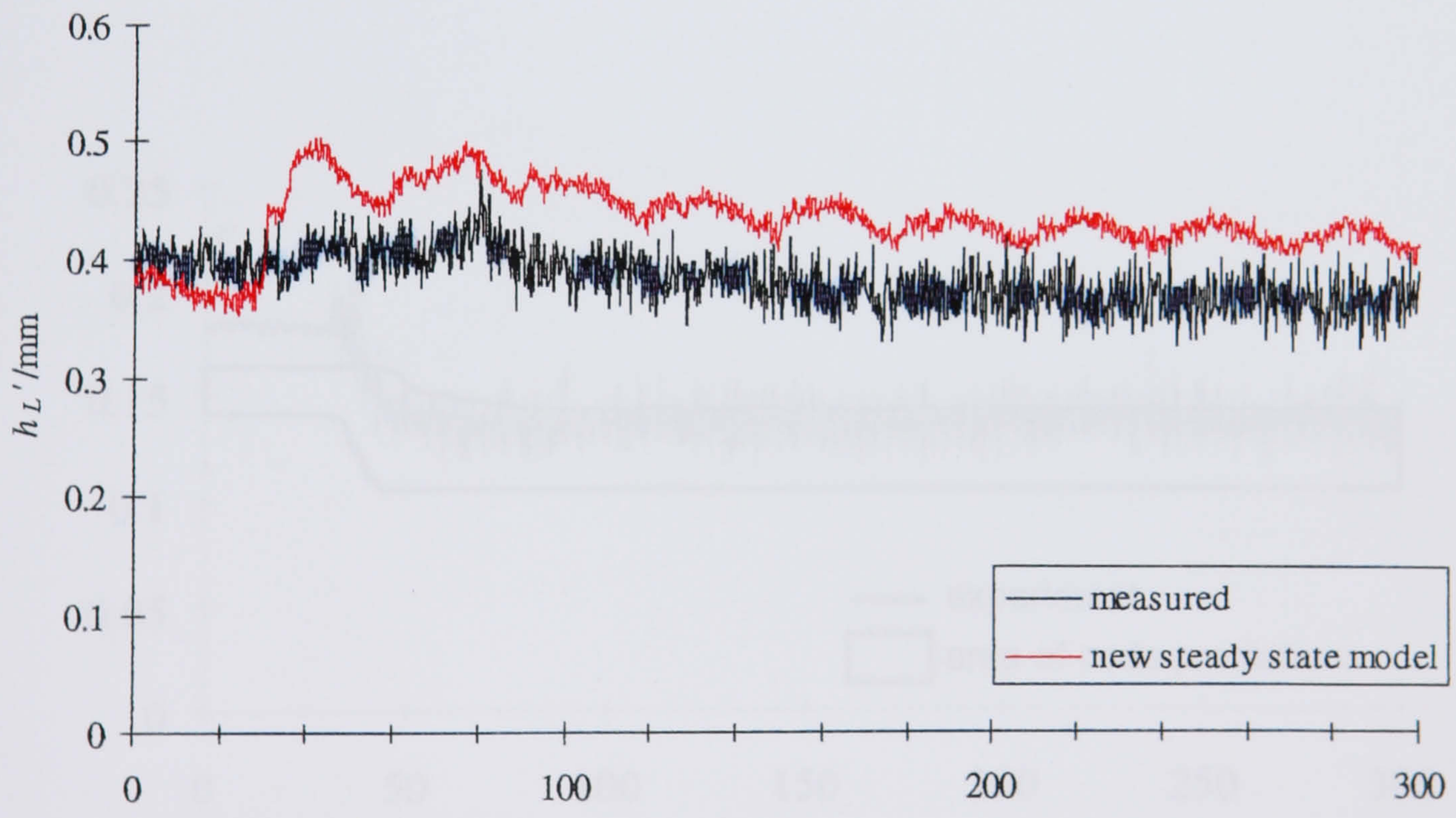


Figure 5.48 Comparison between measured interfacial fluctuation h_L' and new steady state model for transient case wd (U_L=0.032 m/s, $U_{G,1}$=1.30 m/s, $U_{G,2}$=1.62 m/s, p=6.03 bar) on the WASP rig

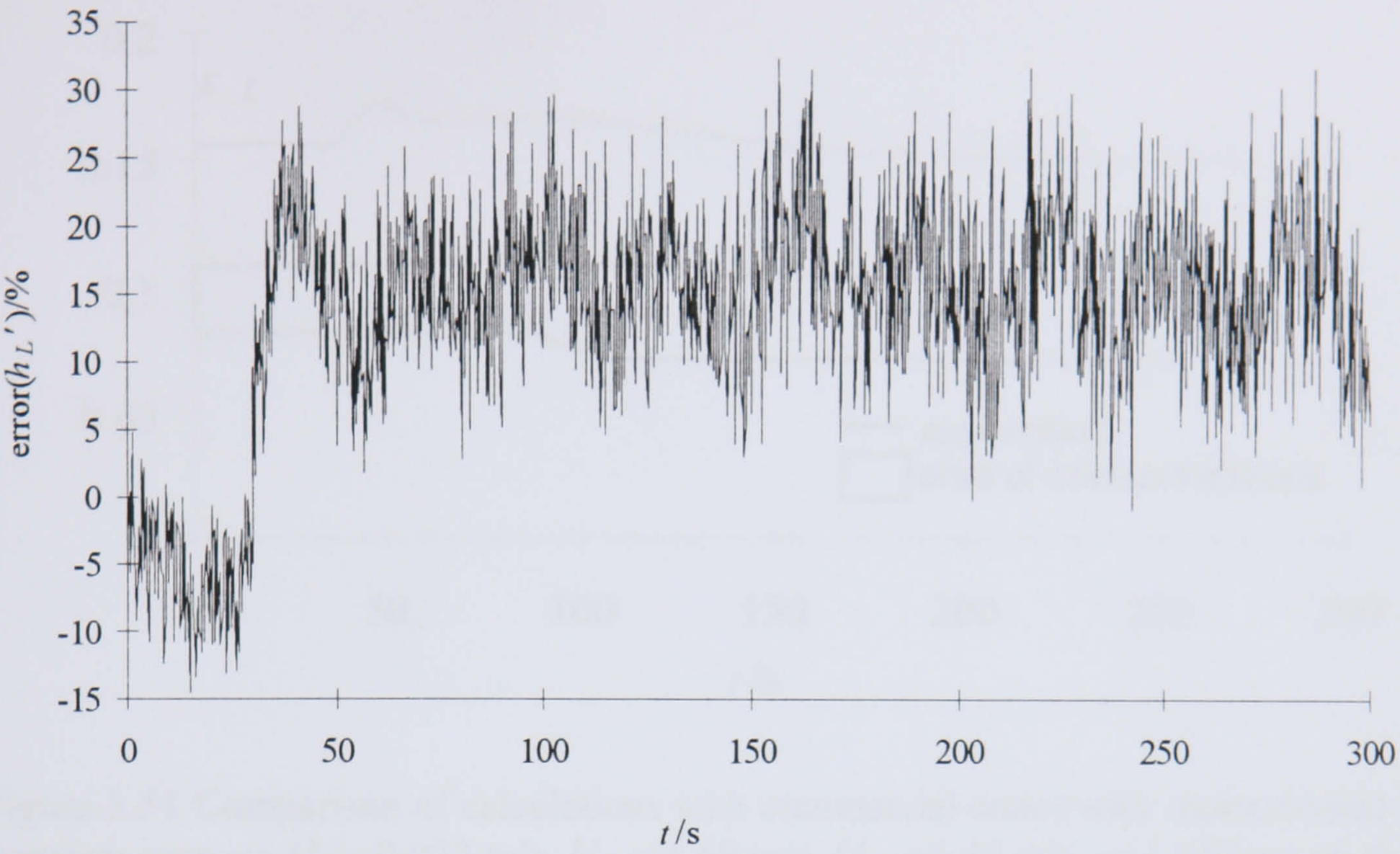


Figure 5.49 Plot of error between measured interfacial fluctuation h_L' and the new steady state model for transient case wd (U_L=0.032 m/s, $U_{G,1}$=1.30 m/s, $U_{G,2}$=1.62 m/s, p=6.03 bar) on the WASP rig

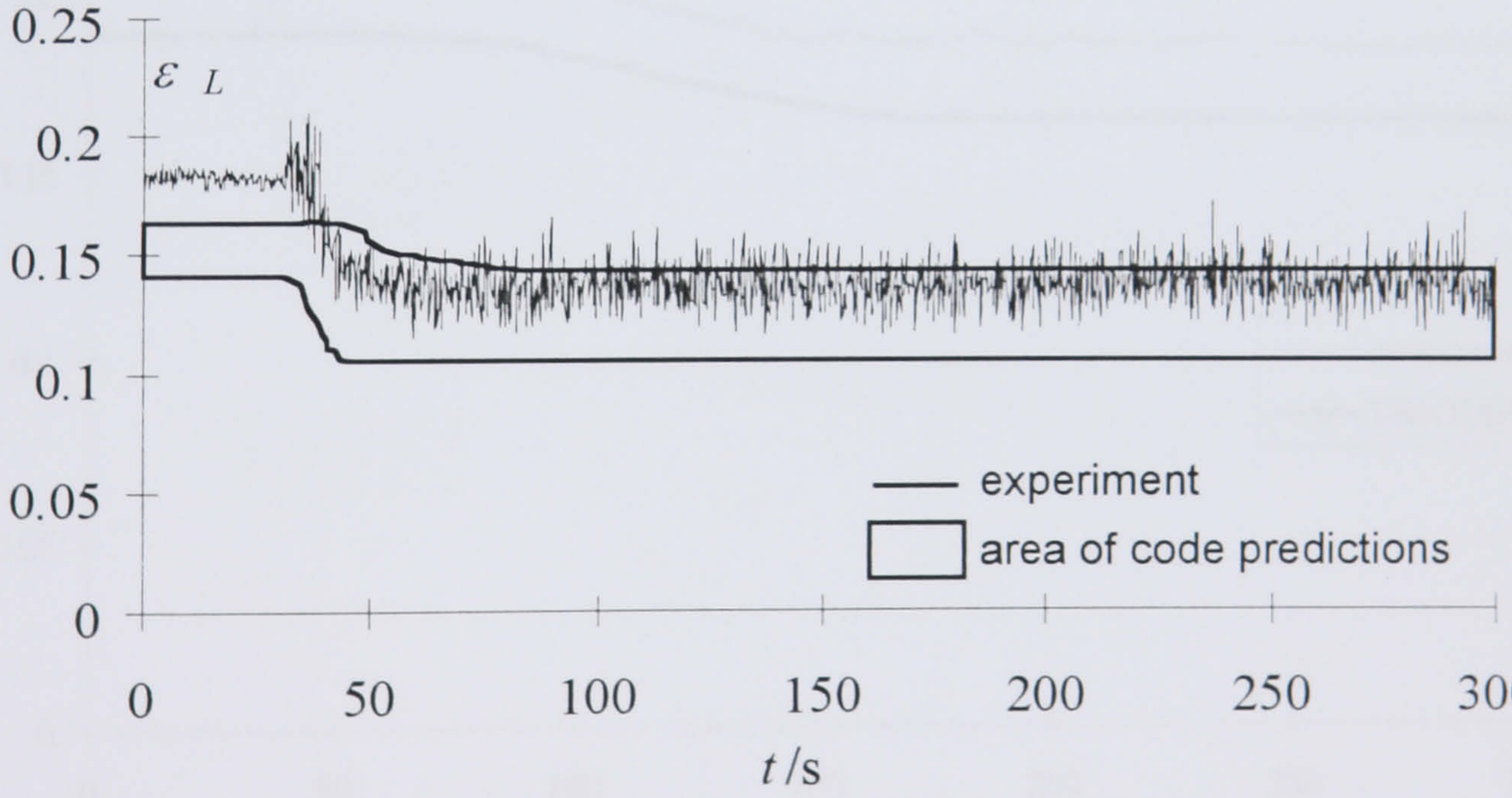


Figure 5.50 Comparison of calculations with commercial codes with measurement for transient case la (U_L=0.039 m/s, $U_{G,1}$=5.01 m/s, $U_{G,2}$=6.46 m/s, p=1.00 bar) on the low pressure rig

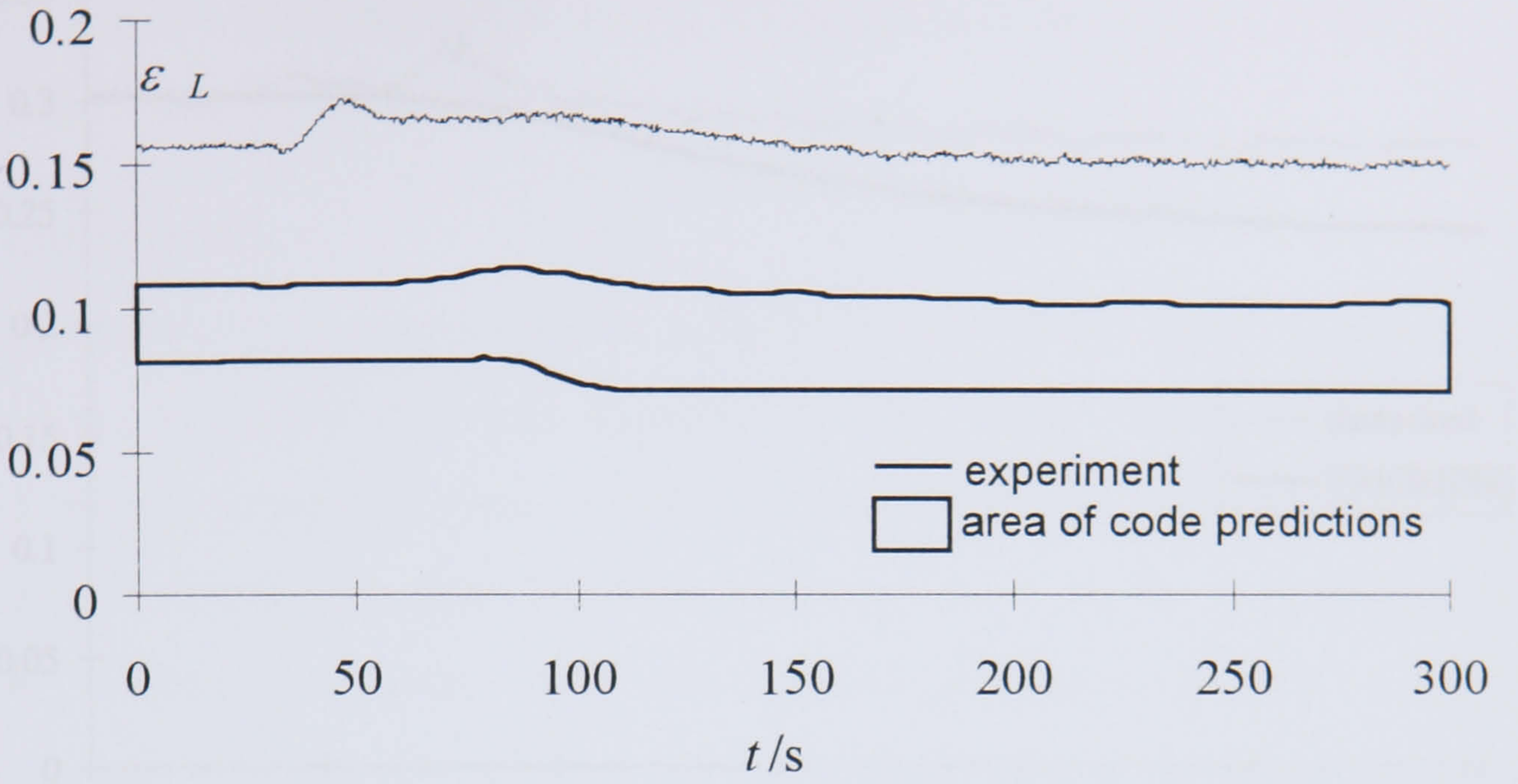


Figure 5.51 Comparison of calculations with commercial codes with measurement for transient case wa (U_L=0.023 m/s, $U_{G,1}$=5.68 m/s, $U_{G,2}$=6.45 m/s, p=1.07 bar) on the WASP rig

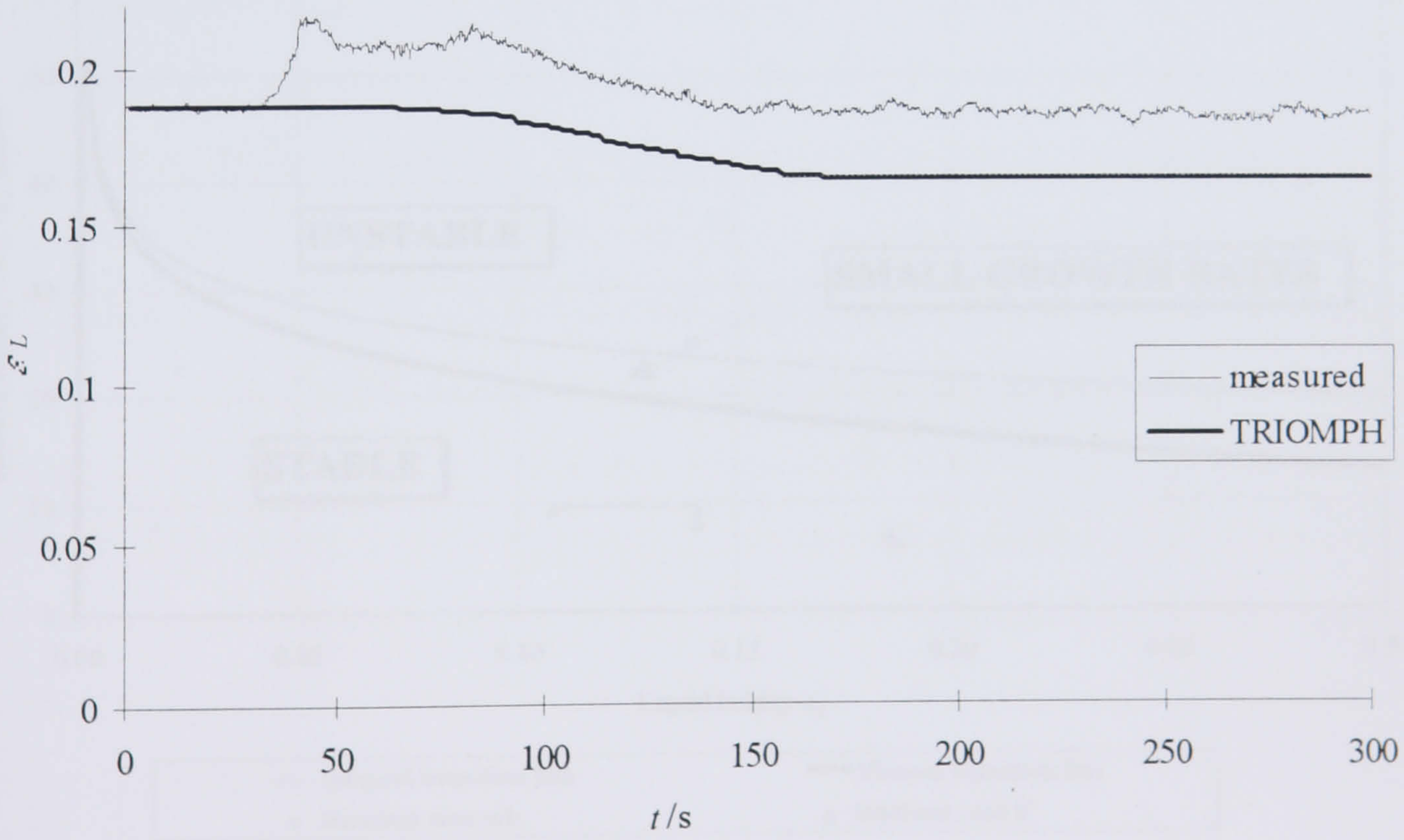


Figure 5.52 Comparison of calculations with TRIOMPH with measurement for transient case wb (U_L=0.037 m/s, $U_{G,1}$=5.33 m/s, $U_{G,2}$=6.07 m/s, p=1.06 bar) on the WASP rig

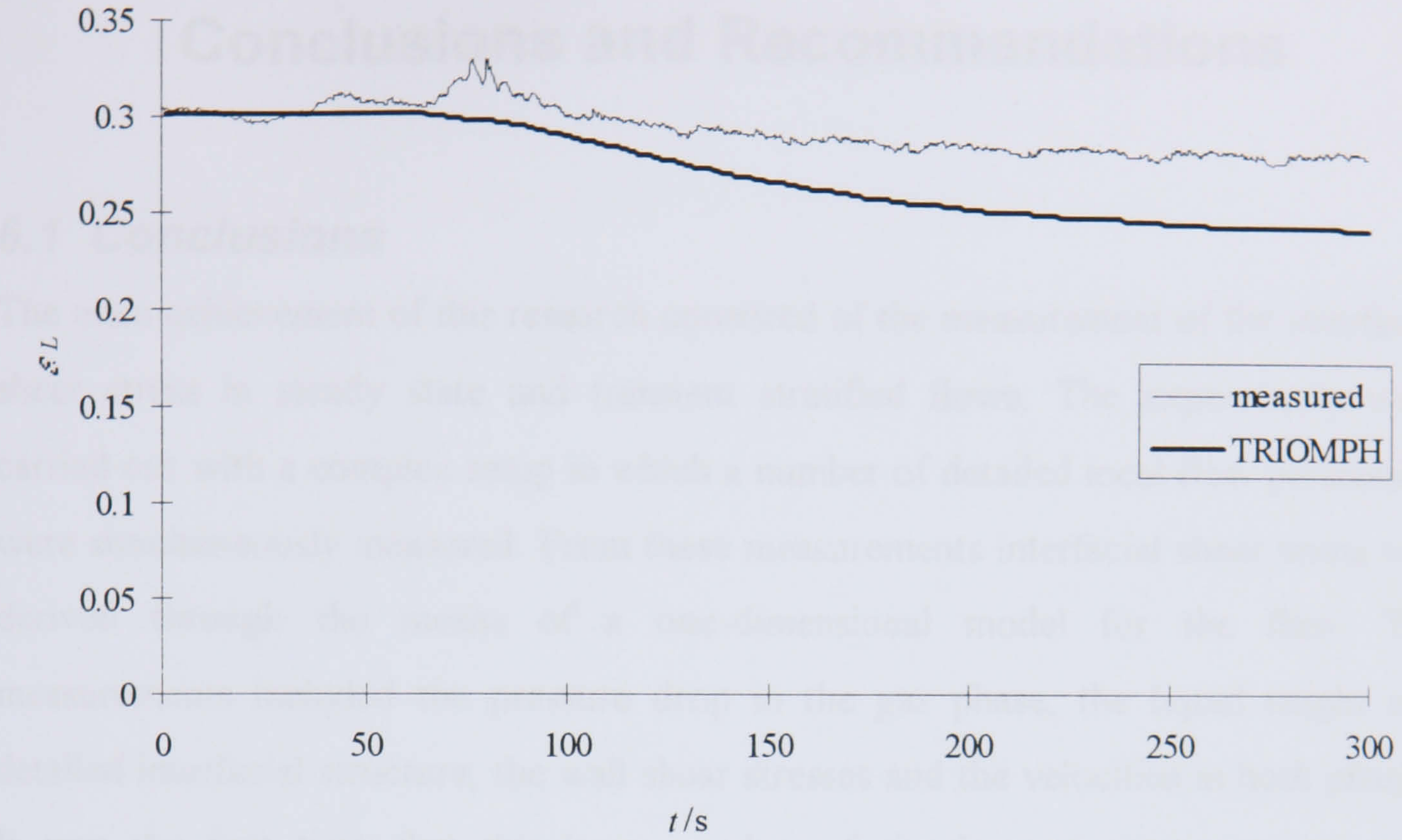


Figure 5.53 Comparison of calculations with TRIOMPH with measurement for transient case wd (U_L=0.032 m/s, $U_{G,1}$=1.30 m/s, $U_{G,2}$=1.62 m/s, p=6.03 bar) on the WASP rig

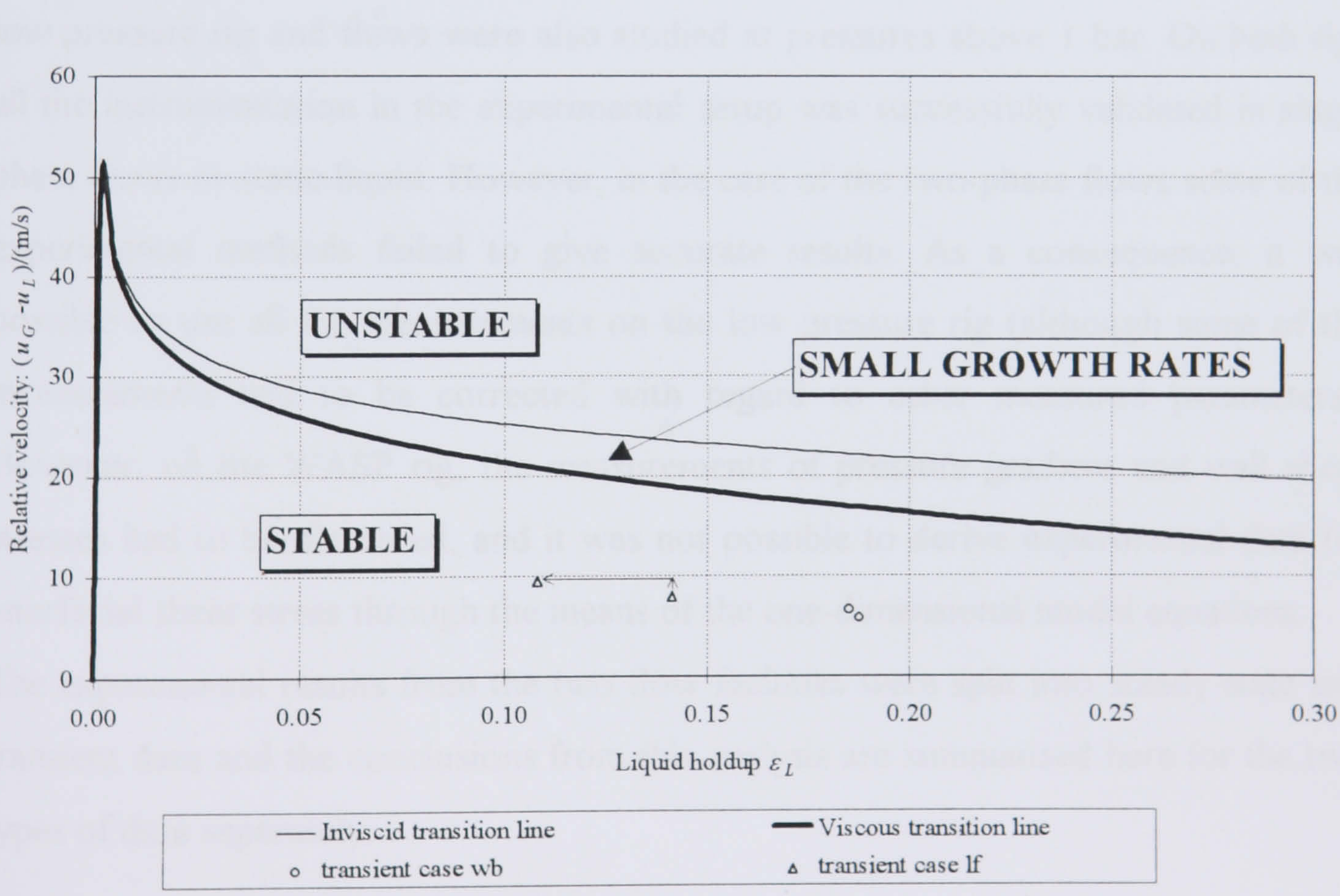


Figure 5.54 Stability of stratified flow according to Barnea & Taitel (1994) for air-water flow at atmospheric pressure

Chapter 6

Conclusions and Recommendations

6.1 Conclusions

The main achievement of this research consisted of the measurement of the interfacial shear stress in steady state and transient stratified flows. The experiments were carried out with a complex setup in which a number of detailed local flow parameters were simultaneously measured. From these measurements interfacial shear stress was derived through the means of a one-dimensional model for the flow. The measurements included the pressure drop in the gas phase, the liquid height and detailed interfacial structure, the wall shear stresses and the velocities in both phases. It was the first time that this large number of simultaneous measurements was performed in separated two-phase flows.

Experiments were carried out on two experimental flow facilities, a low pressure facility and the WASP rig. In the latter the test section was much longer than on the low pressure rig and flows were also studied at pressures above 1 bar. On both rigs all the instrumentation in the experimental setup was successfully validated in single phase flows or static liquid. However, in the case of the two-phase flows some of the experimental methods failed to give accurate results. As a consequence, it was possible to use all the measurements on the low pressure rig (although some of the measurements had to be corrected with regard to other measured parameters). However, on the WASP rig, the measurements of pressure gradient and wall shear stresses had to be discarded, and it was not possible to derive experimental data for interfacial shear stress through the means of the one-dimensional model equations.

The experimental results from the two flow facilities were split into steady state and transient data and the conclusions from this analysis are summarised here for the two types of data separately.

6.1.1 Conclusions from Steady State Data

The analysis of the steady state experimental data was presented in Chapter 4 of this thesis. The chapter was centred around the validation of the measured parameters

through predictions from one-dimensional codes and data published in the literature, and it also had a strong focus on the gas-liquid interaction. The main conclusions from this discussion are summarised here:

- Data of mean and fluctuating velocities in the gas and the liquid from the low pressure rig were in good agreement with data published by Strand (1993).
- Measurements of the pressure gradient and the liquid holdup were compared with predictions from the one-dimensional code PRESBAL (developed at Imperial College), which used a set of standard closure relationships. PRESBAL underpredicted the data but still the agreement with the data was reasonably good. In the case of liquid holdup the experimental data was additionally compared with predictions from the three commercial codes PLAC, OLGA and TACITE, and from the TRIOMPH code developed at Imperial College. The agreement between the code predictions and the experiment was similar to the agreement in the comparisons with PRESBAL. For a given experiment there were considerable discrepancies between the code predictions themselves which were attributed mainly to the different sets of closure relationships used in the codes.
- The question of whether there were hydraulic gradients in the measurements was checked. On the low pressure rig a small hydraulic gradient was established, on the WASP rig no clear hydraulic gradient was found.
- In measurements of the gas and liquid wall shear stresses on the low pressure rig the variation with position around the inner periphery was found to be only modest and the measurements taken at top and bottom of the test section were used as phase average values. The shear stresses were compared with models in the published literature. The data in the gas phase was best predicted by the models of Eck (1973) and Espedal (1998). The liquid wall shear stress was in good agreement with predictions from Spedding & Hand (1997).
- Data for interfacial shear stress was derived from measurements in the gas phase on the low pressure rig. The data was in good agreement with predictions from the model by Spedding & Hand (1997).
- The qualitative behaviour of the interfacial structure was discussed. One experiment from the low pressure rig was compared with one experiment at similar flow conditions from WASP. The interfacial structure was much smoother in the

case of WASP and this was attributed to differences in the test sections on the two flow facilities. The influence of pressure was investigated by comparing two experiments from the WASP rig. With an increase in pressure the interfacial activity was attenuated.

- Data of the interfacial structure was also quantitatively analysed. This resulted in two new models for the interfacial friction factor, one for the low pressure rig and one for the WASP rig. The new models were implemented in the PRESBAL code and the predictions agreed well with the experimental data.

6.1.2 Conclusions from Transient Data

The analysis of the transient experimental data was presented in Chapter 5 of this thesis. The chapter focused on investigating the transient effects in the experiments by means of a qualitative description of the data and also by means of quantitative comparisons with predictions from existing steady state models. An important part in the chapter was dedicated to comparisons between the experiments and transient computer codes which currently use steady state relationships for the closure laws. The main conclusions from the discussion are summarised here:

- Transient stratified flows were produced from step-like increases in the gas flow rate while the liquid flow rate was kept constant. All measured parameters showed clear temporal changes. Generally, the change of the parameters in the gas phase was quicker than the change in the liquid phase. The transients on the WASP rig showed longer transient periods in the measured parameters than the transients on the low pressure rig, which was attributed to the longer test section on WASP. The most interesting features were seen in the response of the liquid holdup. On the low pressure rig the transient response of the holdup was seen as an increase in interfacial activity before its value decreased to the final steady state. On the WASP rig a substantial liquid surge was observed before the liquid holdup reached final steady state.
- Comparisons of transient data for the gas wall shear stress from the low pressure rig with predictions from steady state models showed no significant discrepancies between the experiment and the models. In all cases the gas wall friction factor instantaneously decreased as a result of the increased gas flow rate.

- Experimental data for the interfacial shear stress during the transient was derived from measurements in the gas phase on the low pressure rig and compared with predictions from published steady state models. The new model for the interfacial friction factor in Chapter 4 of this study developed from quantitative analysis of the interfacial structure in steady state was also used in the comparisons. Although some of the steady state models performed fairly well in predicting the experiment there were large differences between predictions and experiment for a short time during the transient period.
- The qualitative behaviour of the interfacial structure during the transient was investigated for one experiment from the low pressure rig and one experiment of similar flow conditions from WASP. The interfacial structure in the experiment on the low pressure rig clearly increased as a result of the change in the gas flow rate whereas the interfacial structure on the WASP rig was consistent with the new model.
- A comparison of data for the fluctuations of the liquid level h_L' with predictions from the new models developed in Chapter 4 of this study revealed not much difference. This was in contrast to the findings for the interfacial friction factor on the low pressure rig where large deviations from the model predictions were observed during the transient (see above).
- Measurements of the liquid holdup in the transient were compared with predictions from the three one-dimensional computer codes, PLAC, OLGA and TACITE. None of the codes showed the characteristic increases of holdup observed in the experiments during the transient. From further comparisons with the one-dimensional code TRIOMPH and from evaluation of stability limits it was concluded that the main discrepancies between the codes and the experiment during the transient are likely to be caused by limitations of the one-dimensional approach per se.

6.2 Recommendations for Future Work

There are two problem areas which evolve from this study and in which further work is needed. The one addresses the limitations of the set of transient data available from

this study, the other one the limitations of existing models to predict transient stratified flows.

6.2.1 Experimental Work

The discussion of the performance of the experimental methods in Section 3.11 of Chapter 3 revealed the limits and problems of the measuring techniques chosen in this study:

- Hot-wire anemometry which was used for measuring wall shear stresses and phase velocities is a difficult experimental technique. When operated in the gas where the probes can be heated much above ambient temperature the probes were usually found to perform well (with the exception of the gas wall shear stress probe on WASP - see below). The operation of the probes in the liquid where the overheat is much lower was less successful. It is believed that the performance of the probes in the liquid could be much improved by looking in more detail at the method to account for a drift in the ambient temperature. The method adopted in the present study (see Section 3.7.6) seemed not to solve completely the problem of temperature drift.
- The data obtained with the gas wall shear stress probe on the WASP facility were found to be far too high (up to a factor of 4) compared to predictions from steady state models. These models had given reasonable predictions for the data on the low pressure rig and were therefore trusted. The data for gas wall shear stress from the WASP facility was therefore not used in the analysis of the data. No sound explanation was found for the misbehaviour of the probe on the WASP rig and this would have to be investigated in later experiments.
- The measurement of the pressure gradient in the gas on WASP was found to be unreliable and was therefore not used in the data analysis. The measured pressure gradients were generally far too low. The most likely reason for the failure of this experiment was the short distance (0.3 m) over which these very small pressure drops were measured. A possible solution to overcome the problem would be to increase the distance between the pressure ports up to 1 - 2 m.

Due to these problems it was not possible to obtain data on interfacial shear stress from direct measurement for the WASP rig. However, for a comprehensive study of

the question of interfacial shear stress in transient stratified flow it is necessary to back up the measurements from the low pressure rig with measurements in a flow facility with more practical relevance, such as WASP. By solving the problems indicated in the above list of items data for interfacial shear stress could be obtained on WASP in the same way as described for the low pressure rig. One of the most interesting findings from the present work was the identification of the surges in holdup resulting from the transients in the WASP facility. Possibly, these surges result from an increase in wave activity (as observed in the shorter low pressure rig test section) with the waves piling up to produce the surge (as observed in the longer WASP test section). It would be a great interest to observe the development of the wave structure over the full length of the WASP facility and it is recommended that such experiments be carried out. This would involve placing conductance probe arrays at frequent intervals along the test section length. It would be advantageous in such tests to operate with a wider range of flow rates to establish under what conditions the surges could develop into slugs.

6.2.2 Improvement of Models

Limitations of closure models for steady state and transient flows have become apparent during the course of this study and they are dealt with in detail in the following list of items.

- Comparisons of steady state experimental data for shear stresses, especially liquid wall shear stress and interfacial shear stress, with existing models showed how much the predictions for given experimental conditions differ between themselves. This indicates the need for more generally valid closure relationships for steady state flow.
- It has become clear from the data analysis that there are limits as to how accurately existing steady state models for the interfacial friction factor can predict the data under transient conditions. The presentation of the data for interfacial shear stress for the low pressure rig revealed that there is a short period during the transient where the discrepancies between model predictions and experiment are much higher than in the steady states. It is believed that the duration of increased error between experiment and models is longer in a test section of greater length but this

hypothesis is subject to an experimental investigation of interfacial shear stress in transient stratified flow in a test section, such as the WASP test section, which is longer than that of the low pressure rig. If these experiments confirm the finding that the available models for interfacial shear stress are inappropriate to model the transient case then there clearly is a need for improved models for the transient.

- The comparison of predictions from one-dimensional transient computer codes, such as PLAC, OLGA and TACITE, with transient experiments showed that there is a need to improve the existing models in the codes. The codes were not able to model characteristic increases in holdup during the transient period which were observed in the experiment. The route for an improvement of the models should start with the relationships for the interfacial friction factor. As stated in the item above, there seems to be a need for improvement of the existing relationships for interfacial friction to model transients. Once such a model exists it could be implemented in the existing codes. If still then the codes fail to predict the liquid surges during the transient it is required to tackle the problem in more than one dimension. Multi-dimensional computations of the flow could become necessary.

References

Agrawal S.S., Gregory G.A. & Govier G.W. 1973 "An Analysis of Horizontal Stratified Two-Phase Flow in Pipes", *Can. J. Chem. Eng.*, Vol. 51, pp. 280-286

Andreussi P. & Persen L.N. 1987 "Stratified Gas-Liquid Flow in Downwardly Inclined Pipes", *Int. J. Multiphase Flow*, Vol. 13, No. 4, pp. 565-575

Andritsos N. & Hanratty T.J. 1987 "Influence of Interfacial Waves in Stratified Gas-Liquid Flows", *AIChE J.*, Vol. 33, No. 3, pp. 444-454

Andritsos N. 1992 "Statistical Analysis of Waves in Horizontal Stratified Gas-Liquid Flow", *Int. J. Multiphase Flow*, Vol. 18, No. 3, pp.465-473

Baker O. 1954 "Simultaneous Flow of Oil and Gas", *Oil Gas J.*, Vol. 53, pp. 185-195

Barnea D. & Taitel Y. 1994 "Interfacial and Structural Stability of Separated Flow", *Int. J. Multiphase Flow*, Vol. 20, Suppl., pp. 387-414

Bearman P.W. 1971 "Corrections for the Effect of Ambient Temperature Drift on Hot-Wire Measurements in Incompressible Flow", *DISA Info*, No. 11, pp. 25-30

Bendiksen K. & Espedal M. 1992 "Onset of Slugging in Horizontal Gas-Liquid Pipe Flow", *Int. J. Multiphase Flow*, Vol. 18, No. 2, pp. 237-247

Benjamin T.B. 1959 "Shearing Flow over a Wavy Surface", *J. Fluid Mech.*, Vol. 6, pp. 161-205

Biberg D. 1998 "A Simple Friction Model for Two-Phase Stratified Pipe Flow", *Third International Conference on Multiphase Flow (ICMF '98)*, Lyon, France, June 8-12

Bishop A.A. & Deshpande S.D. 1986 "Interfacial Level Gradient Effects in Horizontal Newtonian Liquid-Gas Stratified Flow-I", *Int. J. Multiphase Flow*, Vol. 12, No. 6, pp. 957-975

Black P.S. 1987 "Analysis of Horizontal Stratified Two-Phase Flow and Studies using Reactor Safety Codes", PhD thesis, Queen Mary College, University of London

Bouré J.A. 1997 "Wave Phenomena and One-Dimensional Two-Phase Flow Models - Part III: General Case; Generalized Drift Flux Models; Other Two-Fluid Models", *Multiphase Science and Technology*, Vol. 9, pp. 63-107

Bruun H.H. 1995 *"Hot-Wire Anemometry, Principles and Signal Analysis"*, Oxford University Press, New York

Charnock H. 1955 "Wind Stress on Water Surface", *Quart. J. Roy. Met. Soc.*, Vol. 81, p. 639

Cohen L.S. & Hanratty T.J. 1968 "Effect of Waves at a Gas-Liquid Interface on a Turbulent Air Flow", *J. Fluid Mech.*, Vol. 31, Part 3, pp. 467-479

Eck B. 1973 *"Technische Strömungslehre"*, Springer, New York, USA

Espedal M. 1998 "An Experimental Investigation of Stratified Two-Phase Pipe Flow at Small Inclinations", PhD thesis, Department of Applied Mechanics, Norwegian University of Science and Technology (NTNU), Trondheim, Norway

Fabre J., Masbernat L. & Suzanne C. 1981a "Stratified Flow, Part I: Local Structure", Report, Institut de Mecanique des Fluides de Toulouse, France, pp. 285-301

Fabre J., Masbernat L, Fernandex-Flores R. & Suzanne C. 1981b "Stratified Flow, Part II: Interfacial and Wall Shear Stress", Report, Institut de Mecanique des Fluides de Toulouse, France, pp. 302-315

Goldstein S. 1965 *"Modern Developments in Fluid Dynamics"*, Vol. II, Dover Publ., New York

Govan A.H., Hewitt G.F., Owen D.G. & Burnett G. 1989 "Wall Shear Stress Measurements in Vertical Air-Water Annular Two-Phase Flow", *Int. J. Multiphase Flow*, Vol. 15, No. 3, pp. 307-325

Grolman E. & Fortuin J.M.H. 1996 "Transient Gas-Liquid Flow in Upward Sloping Pipes, Approaching the Wavy-to-Slug Flow Transition", *J. Fluids Eng.*, Vol .118, pp. 729-735

Hagiwara Y., Esmaeilzadeh E., Tsutsui H. & Suzuki K. 1989 "Simultaneous Measurement of Liquid Film Thickness, Wall Shear Stress and Gas Flow Turbulence of Horizontal Wavy Two-Phase Flow", *Int. J. Multiphase Flow*, Vol. 15, No. 3, pp. 421-431

Hall N.A. 1957 *"Thermodynamics of Fluid Flow"*, Longmans Green

Hand N.P. 1991 "Gas-Liquid Co-Current Flow in a Horizontal Pipe", PhD thesis, Faculty of Engineering, The Queen's University of Belfast

Hanratty T.J. & McCready M.J. 1992 "Phenomenological Understanding of Gas-Liquid Separated Flows", *Proc. of the 3rd Int. Workshop on Two-Phase Flow Fundamentals*, Imperial College, London, April 1992

Hart J., Hamersma P.J. & Fortuin J.M. 1989 "Correlations Predicting Frictional Pressure Drop and Liquid Holdup During Horizontal Gas-Liquid Pipe Flow with a Small Liquid Holdup", *Int. J. Multiphase Flow*, Vol. 15, No. 6, pp. 947-964

Heintzé E. 1997 "TACITE Version 4.097 USER GUIDE", Institut Français du Pétrole, Rueil Malmaison, France

Hewitt G.F. 1978 *"Measurement of Two Phase Flow Parameters"*, Academic Press Inc. Ltd., London

Hewitt G.F. 1982 "Liquid-Gas Systems", Chapter 2 in *"Handbook of Multiphase Systems"*, ed. G. Hetsroni, Hemisphere Publishing Corporation, New York

Hewitt G.F. 1990 *"Hemisphere Handbook of Heat Exchanger Design"*, Hemisphere Publ. Corp., USA

Issa R.I. & Abrishami Y. 1986 "Computer Modelling of Slugging Flow", Report (Commercial in Confidence), Petroleum Engineering, Imperial College, London

Issa R.I. & Woodburn P.J. 1998 "Numerical Prediction of Instabilities and Slug Formation in Horizontal Two-Phase Flows", *Third International Conference on Multiphase Flow (ICMF '98)*, Lyon, France, June 8-12

Jayanti S. 1991 "Interfacial Friction in Horizontal Stratified Flow", Report MPS/6, Department of Chemical Engineering, Imperial College, London

Jeffreys H. 1925 "On the Formation of Water Waves by Wind", *Proc. Roy. Soc. Lon.*, Vol. A107, pp. 189-206

Kang H.C. & Kim M.H. 1992 "Measurement of Three-Dimensional Wave Form and Interfacial Area in an Air-Water Stratified Flow", *Nuclear Engineering and Design*, Vol. 136, pp. 347-360

Kang H.C. & Kim M.H. 1993 "The Relation between the Interfacial Shear Stress and the Wave Motion in a Stratified Flow", *Int. J. Multiphase Flow*, Vol. 19, No. 1, pp. 35-49

King M.J.S., Hale C.P., Fisher S.A., Lawrence C.J., Mendes-Tatsis M.A., Hewitt G.F. & Roberts I.F. 1997 "Experimental Investigations of Flowrate Transients in Horizontal Pipes", *8th International Conference on Multiphase Production (Multiphase '97)*, Cannes, France, 18-20 June

Khor S.H. 1998 "Three-Phase Liquid-Liquid-Gas Stratified Flow in Pipelines", PhD thesis, Department of Chemical Engineering, Imperial College, London

Kordyban E.S. & Ranov T. 1970 "Mechanism of Slug Formation in Horizontal Two-Phase Flow", *J. Basic Eng.*, Vol. 92, pp. 857-864

Kordyban E. 1974 "Interfacial Shear in Two-Phase Wavy Flow in Closed Horizontal Channels", *J. Fluids Eng.*, Vol. 96, No. 2, pp. 97-102

Kordyban E. 1977 "Some Characteristics of High Waves in Closed Channels Approaching Kelvin-Helmholtz Instability", *J. Fluids Eng.*, Vol. 99, pp. 339-346

Kowalski J.E. 1987 "Wall and Interfacial Shear Stress in Stratified Flow in a Horizontal Pipe", *AIChE J.*, Vol. 33, No. 2, pp. 274-281

Langsholt M., Nordsveen M., Lunde K., Nesic S. & Enerhaug J. 1997 "Wall Shear Stress and Mass Transfer Rates-Important Parameters in CO_2 Corrosion", paper presented at *the 8th International Conference on Multiphase Production (Multiphase '97)*, Cannes, France, 18-20 June

Lin P.Y. & Hanratty T.J. 1986 "Prediction of the Initiation of Slugs with Linear Stability Theory", *Int. J. Multiphase Flow*, Vol. 12, No. 1, pp. 79-98

Liné A., Masbernat L., Miré A. & Soualmia, A. 1991 "Analysis of the Local Structure of Co-Current Stratified Two-Phase Flow", paper presented at *European Two-Phase Flow Group Meeting*, Rome, May 27-29

Manolis I.G., Mendes-Tatsis M.A. & Hewitt G.F. 1995 "The Shedding Rate in Horizontal and Inclined Pipes/"Push-out" Experiments", Report MPS/60 WASP 14, Department of Chemical Engineering, Imperial College, London

Martin C.J. & Whalley P.B. 1983 "Wall Shear Stress Measurements in Annular Two-Phase Flow", *International Conference on the Physical Modelling of Multi-Phase Flow*, Coventry, England

Miles J.W. 1957 "On the Generation of Surface Waves by Shear Flows", *J. Fluid Mech.*, Vol. 3, pp. 185-204

Minami K. & Shoham O. 1994 "Transient Two-Phase Flow Behaviour in Pipelines - Experiment and Modeling", *Int. J. Multiphase Flow*, Vol. 20, No. 4, pp. 739-752

Murata A., Hihara E. & Saito T. 1991 "Turbulent Behavior Below an Air-Water Interface Affected by Wall Bursting, Interfacial Shear Stress, and Interfacial Waves", *JSME International Journal*, Series II, Vol. 34, No. 4, pp. 439-446

Newton C.H. & Behnia M. 1998 "On the Use of the Stratified Momentum Balance for the Deduction of Shear Stress in Horizontal Gas-Liquid Pipe Flow", *Int. J. Multiphase Flow*, Vol. 24, No. 8, pp. 1407-1423

OLGA User Course 1997 Version 3.4, Scandpower A/S, Kjeller, Norway

Owen D.G. 1986 "An Experimental and Theoretical Analysis of Equilibrium Annular Flows", PhD thesis, Department of Chemical Engineering, University of Birmingham

Pan L. 1996 "High Pressure Three-Phase (Gas/Liquid/Liquid) Flow", PhD thesis, Department of Chemical Engineering, Imperial College, London

Paras S.V. & Karabelas A.J. 1992 "Measurements of Local Velocities Inside Thin Liquid Films in Horizontal Two-Phase Flow", *Experiments in Fluids*, Vol. 13, pp. 190-198

Paras S.V., Vlachos N.A. & Karabelas A.J. 1994 "Liquid Layer Characteristics in Stratified-Atomization Flow", *Int. J. Multiphase Flow*, Vol. 20, No. 5, pp. 939-956

Paras S.V., Vlachos N.A. & Karabelas A.J. 1998 "LDA Measurements of Local Velocities Inside the Gas Phase in Horizontal Stratified/Atomization Two-Phase Flow", *Int. J. Multiphase Flow*, Vol. 24, No. 4, pp. 651-661

Pauchon C., Dhulesia H., Lopez D. & Fabre J. 1993 "TACITE: A Comprehensive Mechanistic Model for Two-Phase Flow", paper presented at *6th International Conference on Multi Phase Production*, Cannes, France, 16-18 June

Perry A.E. 1982 *"Hot-Wire Anemometry"*, Oxford University Press, New York

Perry R.H. & Green D. 1984 *"Perry's Chemical Engineers' Handbook"*, 6th Ed., McGraw-Hill Book Company, Singapore

PLAC User Guide 1996 PC Version: 5.3, Process Studies Department, AEA Technology, Harwell, UK

Roberts I. 1996 "Modelling and Experimental Studies of Transient Stratified Multiphase Flows", PhD thesis, Department of Chemical Engineering, Imperial College, London

Rosant J.M. 1994 "Liquid-Wall Shear Stress in Stratified Liquid/Gas Flow", *J. Appl. Electrochem.*, Vol. 24, pp. 612-618

Sakaguchi T., Akagawa K., Hamaguchi H. & Ashiwake N. 1973 "Transient Behavior of Air-Water Two-Phase Flow in a Horizontal Tube", *ASME Paper 73-WA HT-21, Winter Annual Meeting*, Detroit, Michigan, USA

Sakaguchi T., Akagawa K., Hamaguchi H., Ashiwake N. & Imoto M. 1981 "Dynamic Behavior of Flow Characteristics in the Stratified Flow Regime", presented at the *Two-Phase Flow Dynamics Japan-US Seminar*, Kobe, Japan, 31 July - 3 Aug 1979

Sarica C., Vigneron F. & Brill J.P. 1996 "Effects of Inlet Flow Rate Changes on Two-Phase Stratified Flow in Horizontal Pipelines", FED-Vol. 236, 1996 *Fluids Engineering Division Conference*, Volume 1, ASME 1996

Sinai Y.L. 1983 "A Charnock-Based Estimate of Interfacial Resistance and Roughness for Internal, Fully-Developed, Stratified, Two-Phase Horizontal Flow", *Int. J. Multiphase Flow*, Vol. 9, No.1, pp. 13-19

Shaha J. & Hewitt G.F. 1999 "Phase Interactions in Transient Stratified Flow - Distribution of Transient Experimental Data", Report MPS/120 TMF/4, Department of Chemical Engineering, Imperial College, London

Sharma Y. & Brill J.P. 1993 "Simulation of Transient Flow in Gas-Liquid Pipelines Using a Two-Fluid Formulation", *ASME-PD (Petroleum Division): Pipeline Engineering*, Vol. 55, pp. 35-43

Spedding P.L. & Hand N.P. 1997 "Prediction in Stratified Gas-Liquid Co-Current Flow in Horizontal Pipelines", *Int. J. Heat Mass Transfer*, Vol. 40, No. 8, pp. 1923-1935

Srichai S. 1994 "High Pressure Separated Two-Phase Flow", PhD thesis, Department of Chemical Engineering, Imperial College, London

Strand O. 1993 "An Experimental Investigation of Stratified Two-Phase Flow in Horizontal Pipes", PhD thesis, Department of Mathematics, University of Oslo, Norway

Taitel Y. & Dukler A.E. 1976 "A Model for Predicting Flow Regime Transitions in Horizontal and Near Horizontal Gas-Liquid Flow", *AIChE J.*, Vol. 22, No. 1, pp. 47-55

Taitel Y., Lee N. & Dukler A.E. 1978 "Transient Gas-Liquid Flow in Horizontal Pipes: Modeling the Flow Pattern Transitions", *AIChE J.*, Vol. 24, No. 5, pp. 920-934

Taitel Y., Shoham O. & Brill J.P. 1989 "Simplified Transient Solution and Simulation of Two-Phase Flow in Pipelines", *Chem. Eng. Sci.*, Vol. 44, No. 6, pp. 1353-1359

Van Wingen N. 1950 *"Secondary Recovery of Oil in the United States"*, American Petroleum Institute, p. 127

Vigneron F., Sarica C. & Brill J.P. 1995 "Experimental Analysis of Imposed Two-Phase Flow Transients in Horizontal Pipelines", *Proceedings of the 7th International Conference on Multiphase Production*, Cannes, France, June 1995

Vlachos N.A. Paras S.V. & Karabelas A.J. 1993 "Liquid Layer and Wall Shear Stress Characteristics in Stratified/Atomization Flow", *30th Meeting European Two-Phase Flow Group*, Hannover, June 1993

Wallis G.B. & Dobson J.E. 1973 "The Onset of Slugging in Horizontal Stratified Air-Water Flow", *Int. J. Multiphase Flow*, Vol. 1, pp. 173-193

Wolf A. 1995 "Film Structure of Vertical Annular Flow", PhD thesis, Department of Chemical Engineering, Imperial College, London

Nomenclature

Roman Letters

a	overheat ratio	
C_i	constant (with letter index)	
D	pipe diameter	m
D_G	hydraulic diameter in gas phase	m
D_L	hydraulic diameter in liquid phase	m
E	voltage	V
f_i	interfacial friction factor	
f_G	gas-wall friction factor	
f_L	liquid-wall friction factor	
Fr	Froude number	
g	acceleration of gravity	$\frac{\text{m}}{\text{s}^2}$
h_L	height of liquid layer	m
h_L'	rms fluctuations of liquid height	m
Δh_L	wave amplitude	m
h_L^+	dimensionless liquid height	
k_R	rms roughness scale of interface	m
k_W	roughness of pipe wall	m
$\dot{M}_G$	gas mass flow rate	$\frac{\text{kg}}{\text{s}}$
p	system pressure	Pa
p_i	interfacial pressure	Pa
p_G	pressure in gas phase	Pa
p_L	pressure in liquid phase	Pa
P_i	length of interface	m
P_G	tube periphery wetted by gas phase	m
P_L	tube periphery wetted by liquid phase	m
r	radial position	m
R	radius of pipe	m

R_G	mean hydraulic radius in gas phase	m
R_w	resistance of heated probe	Ω
R_{20}	resistance of probe at 20 °C	Ω
R_{tot}	total resistance of probe	Ω
S_G	gas flow cross-sectional area	m^2
S_G'	derivative of S_G with regard to h_L	m
S_L	liquid flow cross-sectional area	m^2
S_L'	derivative of S_L with regard to h_L	m
t	time	s
T	temperature	°C
T_w	temperature of heated probe	°C
T_{abs}	absolute temperature	K
u_c	wave celerity	$\frac{m}{s}$
u_i	interfacial velocity	$\frac{m}{s}$
u_G	gas velocity	$\frac{m}{s}$
u_G'	rms fluctuations of gas velocity	$\frac{m}{s}$
u_L	liquid velocity	$\frac{m}{s}$
u_L'	rms fluctuations of liquid velocity	$\frac{m}{s}$
u^*	friction velocity	$\frac{m}{s}$
U_G	gas superficial velocity	$\frac{m}{s}$
U_L	liquid superficial velocity	$\frac{m}{s}$
x	coordinate in the main flow direction	m
y	coordinate vertically upward in the pipe along the centreline	m
z	coordinate in transverse direction in pipe	m

Phase Reynolds Numbers

$$\mathrm{Re}_G = \frac{D_G u_G}{\nu_G} \qquad \mathrm{Re}_L = \frac{D_L u_L}{\nu_L}$$

$$\mathrm{Re}_G^{+} = \frac{U_G D}{\nu_G} \qquad \mathrm{Re}_L^{+} = \frac{U_L D}{\nu_L}$$

$$\mathrm{Re}_G^{''} = \frac{u_G D}{\nu_G} \qquad \mathrm{Re}_L^{''} = \frac{u_L D}{\nu_L}$$

Greek Letters

α	pipe inclination	°
α_{20}	temperature coefficient of resistance at 20 °C	%/°C
ε_G	void fraction	
ε_L	liquid holdup	
η_G	dynamic viscosity of gas phase	$\frac{\mathrm{kg}}{\mathrm{ms}}$
η_L	dynamic viscosity of liquid phase	$\frac{\mathrm{kg}}{\mathrm{ms}}$
λ	wave length	m
ρ_G	density of gas phase	$\frac{\mathrm{kg}}{\mathrm{m}^3}$
ρ_L	density of liquid phase	$\frac{\mathrm{kg}}{\mathrm{m}^3}$
τ_i	interfacial shear stress	Pa
τ_{WG}	gas-wall shear stress	Pa
τ_{WL}	liquid-wall shear stress	Pa
τ_c	characteristic shear stress	Pa
ν_G	kinematic viscosity of gas phase	$\frac{\mathrm{m}^2}{\mathrm{s}}$
ν_L	kinematic viscosity of liquid phase	$\frac{\mathrm{m}^2}{\mathrm{s}}$

Subscripts

acq	acquired
atm	atmospheric
C	corrected
crit	critical
G	gas
i	liquid-gas interface
L	liquid
r	phase index
ref	reference value
W	pipe surface
0	no flow

Appendix A: Feasible Experimental Matrix

Before the start of the present experimental work, it was important to establish a feasible range of transients which could be covered without changing from stratified into slug flow either temporarily or permanently. Fortunately, reliable data on flow patterns in transients from initially stratified flows had been obtained on the WASP facility by Roberts (1996) and this allowed the establishment of a feasible matrix. As was explained in Chapter 5, only a small part of this matrix was covered in the present work (namely a selection of conditions for increasing gas flow transients). However, it was felt that it would be useful (for future reference) to state the full established matrix in this Appendix. The complete range of conditions for transient stratified flow without change of flow pattern during the transient was evaluated from campaign 2 in Roberts (1996), namely his Tables 5.6 to 5.11.

The number of runs in the first column of the following tables indicates how many transient steps of consecutive ranges of superficial velocities of a phase were necessary to cover the range of flow rates given for that phase. Only for U_L=0.04 and 0.06 m/s would the ranges of gas superficial velocities overlap between the runs. Transients were classified as follows:

AU	increasing air flow rate transient
AD	decreasing air flow rate transient
WU	increasing water flow rate transient
WD	decreasing water flow rate transient

The terms "up to" and "down to" mean that the range of superficial velocity stated is covered by the number of runs indicated in the first column of the table. A hyphen between numbers means a single step change.

p=1 bar

number of runs	U_G/(m/s)	U_L/(m/s)	type of transient
6	5.13 up to 8.74	0.02	AU
7	9.34 down to 3.83	0.02	AD
7	4.96 up to 10.16	0.04	AU
8	10.04 down to 2.39	0.04	AD
6	5.71 up to 10.04	0.06	AU
8	9.95 down to 2.61	0.06	AD
3	5.44 up to 9.95	0.08	AU
4	9.28 down to 2.78	0.08	AD
5	6.4	0.013 up to 0.107	WU
5	6.3	0.101 down to 0.000	WD
5	7.4	0.012 up to 0.098	WU
5	7.2	0.092 down to 0.000	WD

p=5 bar(g)

number of runs	U_G/(m/s)	U_L/(m/s)	type of transient
6	1.06 up to 3.38	0.02	AU
4	3.32 down to 0.90	0.02	AD
4	0.75 up to 2.55	0.04	AU
4	2.53 down to 0.72	0.04	AD

p=10 bar(g)

number of runs	U_G/(m/s)	U_L/(m/s)	type of transient
6	0.71 up to 2.10	0.02	AU
4	2.38 down to 0.79	0.02	AD
4	0.83 up to 1.93	0.04	AU
4	2.18 down to 0.73	0.04	AD

Appendix B: Experimental Procedure for Low Pressure Rig

This appendix describes in detail the procedure for the transient experiments on the low pressure rig.

Preparation of an Experimental Day

Each experimental day started with calibration work. The hot-wire and hot-film probes were calibrated on a daily basis whereas a full calibration of the twin-wire conductivity probes was only done periodically. The calibrations were done in the following sequence:

- With a dummy probe inserted instead of the hot-wire probe for gas velocity and with the isolating valves on the pressure tappings closed the hot-film probes in the liquid (the velocity and the wall shear stress probe) were set up and calibrated in single phase liquid flow.
- This was followed by calibration of the twin-wire conductivity probes.
- Afterwards the hot-wire probe for measurement of gas velocity was inserted and both probes for the gas phase (the hot-wire probe for velocity measurement and the hot-film probe for wall shear stress measurement) were set up and calibrated in single phase air flow.

Experimental Procedure

This part describes in detail the steps of the transient experiment. The transient was produced from a sudden controlled increase in the gas flow rate.

- At the start of the experiment the isolating valves on the pressure tappings were opened and the lines connecting the pressure transmitter to the pressure tappings were purged using mains compressed air. The hot-wire and hot-film probes for measurement in the gas were heated. The output voltages of the pressure transmitter, the gas velocity, the gas wall shear stress probe and the thermocouple in the gas were recorded for no flow in the test section. The velocity probes in the gas and liquid were then placed close to the wall.

- The flow rates for the initial steady state two-phase flow were then set up. In order to avoid formation of slug flow as far as possible the air flow rate was set initially and only then the water supply was gradually opened until its flow rate specified for the experiment was obtained. The flow was left to develop for approximately 5 minutes. The hot-film probes for the liquid phase were heated.
- The velocity probes were placed at the positions specified for the run. When the initial steady state flow was developed the liquid flow rate was read from the water rotameter. Data from the two thermocouples in the test spool was collected for 20s at 100 Hz.
- Acquisition of the air flow rate was then started and the time was noted as time t_{ref}. 30 s later (at time=t_{ref}+30 s) data collection from the conductivity probes, the pressure transmitter and the hot-wire and hot-film probes was started at 500 Hz for a duration of 300 s. The data was directly streamed to the hard disk of the acquisition computer. It was transformed into text format with the software in the acquisition card when the experiment had finished. At time=t_{ref}+60 s the gas flow rate was increased by a controlled change of the position of the valve on the air supply.
- After the data acquisition was finished the anemometer boxes for the gas velocity and the gas wall shear stress probe were set to stand-by and the gas velocity probe was replaced with the dummy probe. The isolating valves on the lines to the pressure transmitter were closed. The output voltages of both hot-film probes in the liquid (the liquid velocity probe and the liquid wall shear stress probe) and the thermocouple in the liquid were collected in a single phase liquid flow with a specified flow rate. The liquid velocity probe for this was placed at a distance of 10 mm below the centre of pipe, i.e. in the same position as during the calibration. The voltages from the instruments were collected to derive their values at no flow. When this was finished the anemometers for the hot-film probes in the liquid were set to stand-by and the liquid velocity probe was positioned close to the bottom tube wall.

Appendix C: Experimental Procedure for WASP Rig

This appendix describes in detail the procedure for the transient experiments on the WASP rig. The procedure was very similar to that noted in Appendix B for the low pressure rig.

Preparation of an Experimental Day

Each experimental day started with calibration work. The hot-wire and hot-film probes were calibrated on a daily basis whereas a full calibration of the twin-wire conductivity probes was only done at the start of the experimental campaign on WASP. The daily calibrations were done in the following sequence:

- With a dummy probe inserted instead of the hot-wire probe for gas velocity and the isolating valves on the pressure tappings closed the hot-film probes in the liquid (the velocity and the wall shear stress probe) were set up and calibrated in single phase liquid flow. As this procedure involved filling the test section with single phase liquid the flows for these calibrations were set by the WASP Safety Officer.
- When the test section was empty from the liquid the hot-wire probe for measurement of gas velocity was inserted and both probes for the gas phase (the hot-wire probe for velocity measurement and the hot-film probe for wall shear stress measurement) were set up and calibrated in single phase air flow. In order to provide a pressure tight seal between the hot-wire probe for gas velocity and its probe support some silicone grease was put around the probe stem before it was inserted.

Experimental Procedure

This part describes in detail the steps of the transient experiment. The transient was produced from a sudden controlled increase in the gas flow rate.

- At the start of the experiment the empty test section was pressurised up to 5 bar and the lines connecting the pressure transmitter to the pressure tappings on the

test spool and the air orifice section for measurement of the air flows were purged using rig pressure. The hot-wire and hot-film probes for measurement in the gas were heated. The output voltages of the pressure transmitter, the gas velocity, the gas wall shear stress probe and the thermocouple in the gas were recorded for no flow in the test section. The velocity probes in the gas and liquid were then placed close to the wall.

- The flow rates for the initial steady state two-phase flow and the pressure for the run were then set up. In order to avoid formation of slug flow as far as possible the air flow rate was set initially and only then the water supply was gradually opened until its flow rate specified for the experiment was obtained. The flow was left to develop for approximately 5 minutes. The hot-film probes for the liquid phase were heated.
- The velocity probes were placed at the positions specified for the run. When the initial steady state flow was developed, data from the two thermocouples in the test spool was collected for 20s at 100 Hz.
- The video camera was started to film the flow. Acquisition of the air and water flow rates was then started and the time was noted down as time t_{ref}. 30 s later (at time=t_{ref}+30 s) data collection from the conductivity probes, the pressure transmitter and the hot-wire and hot-film probes was started at 500 Hz and also data collection with the gamma densitometer. Data was collected for a total of 300 s. The data collected at 500 Hz was directly streamed to the hard disk of the acquisition computer. It was transformed into text format with the software in the acquisition card when the experiment had finished. At time=t_{ref}+60 s the gas flow rate was increased by a controlled change of the position of the valve on the air supply.
- After the data acquisition was finished the fluid temperatures were again collected and the video was switched off. In cases of flows at elevated pressures the pressure was released. Then the anemometer boxes for the gas velocity and the gas wall shear stress probe were set to stand-by and the gas velocity probe was replaced by the dummy probe. The isolating valves on the lines to the pressure transmitter were closed. The output voltages of both hot-film probes in the liquid (the liquid velocity probe and the liquid wall shear stress probe) and the

thermocouple in the liquid were collected in single phase liquid at no flow. When this was finished the anemometers for the hot-film probes in the liquid were set to stand-by and the liquid velocity probe was positioned close to the bottom tube wall.